INDC(JPN)-169/L

JAERI-M
94-019

PROCEEDINGS OF THE 1993 SYMPOSIUM ON NUCLEAR DATA

November 18-19, 1993, JAERI, Tokai, Japan

February 1994

(Eds.) Masayoshi KAWAI* and Tokio FUKAHORI

日本原子力研究所
Japan Atomic Energy Research Institute

JAERI-Mレポートは，日本原子力研究所が不定期に公刊している研究報告書です。
入手の問合わせは，日本原子力研究所技術情報部情報資料課（〒319-11茨城県那珂郡東海村）あて，お申しこしください。なお，このほかに財団法人原子力弘済会資料センター（〒319-11茨城県那珂郡東海村日本原子力研究所内）で複写による実費頒布をおこなっております。

JAERI-M reports are issued irregularly.
Inquiries about availability of the reports should be addressed to Information Division, Department of Technical Information, Japan Atomic Energy Research Institute, Tokai-mura, Naka-gun, Ibaraki-ken 319-11, Japan.

編集兼発行　日本原子力研究所
印　　刷　㈱原子力資料サービス

JAERI-M 94-019

Proceedings of the 1993 Symposium on Nuclear Data November 18-19, 1993, JAERI, Tokai, Japan

(Eds.) Masayoshi KAWAI* and Tokio FUKAHORI

Japanese Nuclear Data Committee
Tokai Research Establishment
Japan Atomic Energy Research Institute
Tokai-mura, Naka-gun, Ibaraki-ken

(Received January 24, 1994)

The 1993 Symposium on Nuclear Data was held at Tokai Research Establishment, Japan Atomic Energy Research Institute (JAERI), on the 18th and 19th of November, 1993. The symposium was organized by Japanese Nuclear Data Committee (JNDC) and Nuclear Data Center, JAERI. Celebrating the 30th anniversary of JNDC, two special sessions were held; the review of foreign activities by inviting foreign scientists and the panel discussion on the future of nuclear data activity. In the oral session, a total of 14 papers was presented under the sessions of foreign activities, JENDL and intermediate energy shielding experiments, nuclear data needs in non-energy applications, and unstable nuclei beam. The panel discussion was held with keynote address and 7 panelists' presentations. In the poster session, presented were 29 papers concerning experiments, evaluations and benchmark tests of nuclear data. All of the 43 papers and the reports in the panel discussion are compiled in this proceedings.

Keywords: Nuclear Data, Symposium, Proceedings, JENDL-3.2, Intermediate Energy, Experiment, Evaluation, Benchmark Test

---

* Toshiba Corporation

JAERI-M 94-019

1993年核データ研究会報文集

1993年11月18日～19日，日本原子力研究所，東海村

日本原子力研究所東海研究所
シグマ研究委員会
（編）川合　將義*・深堀　智生

（1994年1月24日受理）

1993年核データ研究会が，1993年11月18日と19日の両日，日本原子力研究所東海研究所において開催された。この研究会は，日本原子力研究所のシグマ研究委員会（以下「シグマ委員会」と呼ぶ）と核データセンターが主催して開いたものである。シグマ委員会30周年を記念し，国外の研究者を招待して国外の核データ活動レビュー・セッションを，また，わが国の核データ活動の将来についてのパネル討論会を催した。口頭発表では，14件の論文が「各国の核データ活動」，「ＪＥＮＤＬと高エネルギー中性子遮蔽実験」，「新分野からの核データニーズ」，「不安定核ビーム」のセッションで報告された。パネル討論は基調講演および７人のパネリストにより行われた。ポスターセッションでは，核データの測定，評価，積分テストに関する29件の報告があった。このレポートは，全部で43件の論文およびパネル討論の報告をまとめたものである。

東海研究所：〒319－11　茨城県那珂郡東海村白方字白根２－４

＊（株）東芝

Program Committee

Masayoshi KAWAI (Chairman)	(Toshiba Corporation)
Satoshi CHIBA	(Japan Atomic Energy Research Institute)
Tokio FUKAHORI	(Japan Atomic Energy Research Institute)
Kazuki HIDA	(Toshiba Corporation)
Tetsuo IGUCHI	(University of Tokyo)
Hideki IIMURA	(Japan Atomic Energy Research Institute)
Shin IWASAKI	(Tohoku University)
Yutaka NAKAJIMA	(Japan Atomic Energy Research Institute)
Shigeaki OKAJIMA	(Japan Atomic Energy Research Institute)
Makoto SASAKI	(Mitsubishi Atomic Power Industries, Inc.)
Naoki YAMANO	(Sumitomo Atomic Energy Industries, Ltd.)

プログラム委員会

川合　将義（委員長）	((株) 東芝)
千葉　　敏	(日本原子力研究所)
深堀　智生	(日本原子力研究所)
肥田　和毅	((株) 東芝)
井口　哲夫	(東京大学)
飯村　秀紀	(日本原子力研究所)
岩崎　　信	(東北大学)
中島　　豊	(日本原子力研究所)
岡嶋　成晃	(日本原子力研究所)
佐々木　誠	(三菱原子力工業 (株))
山野　直樹	(住友原子力工業 (株))

Contents

1. Preface 1
2. Papers Presented at Oral Session 5
2.1 International Session 7
2.1.1 Nuclear Data Activities in the United States 7
F.M. Mann
2.1.2 Study of Nuclear Data in Indonesia 20
R.S. Lasijo, F. Aziz, B. Santoso and I.R. Subki
2.1.3 Nuclear Data Activities at Khlopin Radium Institute, Russia 25
A.A. Rimski-Korsakov
2.1.4 Recent Nuclear Data Activities in China Related to CENDL-2 28
Zhao Zhixiang and Zhang Jingshang
2.1.5 Status Report EFF/EAF Projects 37
H. Gruppelaar and J. Kopecky
2.1.6 The ITER Blanket and Shield Design Status as of September 1993 42
Y. Gohar
2.1.7 Status of the International Fusion Evaluated Nuclear Data Library (FENDL) 55
A.B. Pashchenko and S. Ganesan
2.2 JENDL and Shielding Experiment for High Energy Neutron 68
2.2.1 JENDL-3 Revision 2 68
T. Nakagawa
2.2.2 Integral Test of JENDL Activation Library for Fusion Applications 79
Y. Ikeda
2.2.3 Shielding Experiments with Quasi-monoenergetic Several Tens MeV Neutrons at 90 MV AVF Cyclotron Facility TIARA . 95
T. Nakamura and Accelerator Shielding Experiment Group
2.3 Nuclear Data Needs from Non-nuclear Engineering Fields 104
2.3.1 Atomic, Molecule's and Nuclear Data for Medical Application 104
S. Iwanami
2.3.2 Theoretical Approach to Proton Upset 113
Y. Shimano

2.3.3 Nuclear Astrophysics and Critical Roles of Nuclear Data .123
Y. Nagai, M. Igashira, T. Shima, T. Ohsaki, T. Irie,
S. Seino, K. Senoo, K. Watanabe, H. Satoh, T.S. Suzuki
and H. Kitazawa
2.4 Beam of Unstable Nuclei 132
2.4.1 Frontiers in Nuclear Physics and Nuclear Astrophysics
with Radioactive Nuclear Beams 132
S. Kubono
3. Panel Discussion for the 30th Anniversary of JNDC
- Nuclear Data Activity being at the Crossroads - 141
3.1 Keynote Address 143
3.1.1 Recollections of JNDC in the Early Stage 143
R. Nakasima
3.2 Panelist Presentation 145
3.2.1 Some Personal Comments on Evaluation and
Measurements of Nuclear Data 145
S. Chiba
3.2.2 Problems in Reactor Physics and Shielding Design 146
A. Zukeran
3.2.3 Nuclear Data Needs for Fusion Reactor Development 149
Y. Seki
3.2.4 Request of Nuclear Data File for Study of New
Application of Transmutation 152
T. Iwasaki
3.2.5 Needs of Atomic, Molecule's and Nuclear Data for
Medical Application in Japan 154
S. Iwanami
3.2.6 Experiments Using Accelerators for Space Application ...158
Y. Shimano
3.2.7 Environment of Nuclear Energy Development and
International Cooperation of Nuclear Data Activity 159
T. Fuketa
3.3 Summary 162
3.3.1 A Review Talk and Panel Discussion on Nuclear Data
Activities at a Turning Point 162
M. Nakazawa
4. Closing Session 165

4.1 Evolution of Data Requirement Since the Early 1980's 167
T. Yoshida
5. Papers Presented at Poster Session 169
5.1 Measurements of Thermal Neutron Cross Section and Resonance Integral for the $^{237}Np(n,\gamma)^{238}Np$ Reaction 171
K. Kobayashi, A. Yamanaka and I. Kimura
5.2 Measurement of Cross Section for $^{241}Am(n,f)$ Reaction between 0.5 eV and 10 keV with Lead Slowing-down Spectrometer 179
K. Kobayashi, M. Miyoshi, S. Yamamoto, Y. Fujita, I. Kimura, I. Kanno and S. Kanazawa
5.3 Spectrometry of Several Tens MeV Neutrons Penetrating through Shields Using Organic Liquid Scintillator at 90 MeV AVF Cyclotron Facility, TIARA 183
N. Nakao, T. Nakamura, M. Takada, M. Baba, Shun-ichi Tanaka, H. Nakashima, Y. Sakamoto, Y. Nakane, Susumu Tanaka, K. Shin and E. Tanabe
5.4 Measurements of Double-differential α-Particle Production Cross Sections Using a Gridded Ionization Chamber - Application of $^{14}N(d,n)^{15}O$ and $^{15}N(d,n)^{16}O$ Neutron Sources - 191
I. Matsuyama, M. Baba, S. Matsuyama, T. Kiyosumi, T. Sanami, N. Hirakawa, N. Ito, S. Chiba, T. Fukahori, M. Mizumoto, K. Hasegawa and S. Meigo
5.5 Characterization and Application of 20-90 MeV $^{7}Li(p,n)$ Neutron Source at TIARA 200
M. Baba, T. Kiyosumi, T. Iwasaki, M. Yoshioka, S. Matsuyama, N. Hirakawa, T. Nakamura, Susumu Tanaka, R. Tanaka, Shun-ichi Tanaka, H. Nakashima and S. Meigo
5.6 Application of Large Volume Liquid Scintillator for Scattering Cross Section Measurements 210
S. Matsuyama, T. Ohkubo, M. Baba, S. Iwasaki, D. Soda and N. Hirakawa
5.7 Measurements of Double Differential α-particle Emission Cross Sections of ^{12}C with 14 MeV Incident Neutrons 220
H. Nishizawa, A. Takahashi and Y. Murakami
5.8 Measurements of the Neutron Scattering Cross Sections for ^{12}C, ^{16}O, ^{40}Ca and ^{56}Fe at 14.2 MeV 230
T. Nishio, S. Shirato and Y. Ando

5.9 Characterization of Neutrons Produced from the $^{1}H(^{11}B,n)^{11}C$ Reaction 243
S. Meigo, S. Chiba and T. Fukahori

5.10 Measurement of Formation Cross Sections Producing Short-lived Nuclei - Mg, S, Ga, Y, Mo, Pd, Sn - 253
K. Yamauchi, Y. Kasugai, H. Yamamoto, A. Takahashi, T. Iida and K. Kawade

5.11 Measurement of Beta-decay Half-lives of Short-lived Nuclei .264
S. Itoh, A. Tanaka, H. Yamamoto, T. Iida, A. Takahashi and K. Kawade

5.12 Measurement of Hyperfine Structure in ^{143}Pr ($T_{1/2}$=13.6d) by Collinear Laser-ion-beam Spectroscopy 271
H. Iimura, M. Kubota, Y. Nakahara, S. Ichikawa and T. Horiguchi

5.13 Reevaluation of FP Nuclear Data for JENDL-3.2 276
M. Kawai and JNDC Fission Product Nuclear Data Working Group

5.14 Evaluation of ^{238}U Inelastic Scattering Cross Section 290
T. Kawano, N. Fujikawa and Y. Kanda

5.15 Evaluation of Neutron Cross Sections of ^{12}C up to 50 MeV ...300
S. Chiba, T. Fukahori, Y. Watanabe and Y. Koyama

5.16 Evaluation of Neutron Dosimetry Cross Sections of ^{59}Co and ^{197}Au up to 50 MeV 310
N. Odano and S. Iwasaki

5.17 Dosimetry Cross-section Evaluation by Cubic-B Spline Fitting 320
S. Iwasaki

5.18 Evaluation of the D(γ,n) Reaction Cross Section 330
T. Murata

5.19 Nuclear Level Density Parameter Systematics Revisited: Nuclear Deformation Effects 337
A. Mengoni and Y. Nakajima

5.20 Shell-pairing Correlations of Nuclear Level Density 342
H. Nakamura

5.21 Comments on ENSDF - from the Evaluator to Dear Bitter Users 346
K. Kitao

5.22 Systematics of the Fragmentation Cross Section for Incident Proton Energies up to 3 GeV 351
N. Shigyo, K. Ishibashi and Y. Wakuta

5.23 Integral Test of Secondary Gamma-ray Production Cross Sections of Iron in JENDL-3 with Continuous Energy Monte Carlo Analysis 362
K. Ueki, A. Ohashi and N. Yamano

5.24 Techniques of Integral Experiment and Methods for Validation of Evaluated Nuclear Data Libraries for Secondary Gamma-ray Data under D-T Neutron Field 369
F. Maekawa and Y. Oyama

5.25 An Index Database of Charged-particle Nuclear Reaction Data .380
M. Chiba and K. Kato

5.26 Sensitivities of Nuclear Data to the Nuclear Equilibrium State 387
H. Nakamura and H. Sekimoto

5.27 Some Subjects in ICF Reactors Requiring Nuclear Data in the Medium Energy Region 397
Y. Nakao, A. Oda and H. Nakashima

5.28 Measurement of the Neutron Capture Cross Section of ^{99}Tc ...403
T. Katoh, Y. Ogata, H. Harada and S. Nakamura

5.29 Nuclear Data Activities in Hungary 408
J. Csikai

目　　次

1. まえがき …… 1
2. 口頭発表論文 …… 5
2.1 国際セッション …… 7
2.1.1 米国における核データ活動 …… 7
F. M. Mann
2.1.2 インドネシアの核データ研究 …… 20
R. S. Lasijo, F. Aziz, B. Santoso and I. R. Subki
2.1.3 クローピン・ラジウム研究所の核データ活動 …… 25
A. A. Rimski－Korsakov
2.1.4 CENDL－2に関連した最近の中国の核データ活動 …… 28
Zhao Zhixiang and Zhang Jingshang
2.1.5 EFFおよびEAF計画の現状 …… 37
H. Gruppelaar and J. Kopecky
2.1.6 ITERのブランケットおよび遮蔽設計の現状 …… 42
Y. Gohar
2.1.7 FENDLライブラリーの現状 …… 55
A. B. Pashchenko and S. Ganesan
2.2 JENDLと高エネルギー中性子遮蔽実験 …… 68
2.2.1 JENDL－3改訂第2版 …… 68
中川　庸雄
2.2.2 核融合のためのJENDL放射化断面積ライブラリーの積分テスト …… 79
池田　裕二郎
2.2.3 90MV AVFサイクロトロン施設TIARAにおける数十MeV準単色中性子による遮蔽実験 …… 95
中村　尚司，加速器遮蔽実験グループ
2.3 新分野からの核データニーズ …… 104
2.3.1 医学用の原子分子および原子核データ …… 104
岩波　　茂
2.3.2 陽子アップセットへの理論的アプローチ …… 113
嶋野　洋介

2.3.3 天体核物理と核データ …… 123
永井 泰樹，井頭 政之，嶋 達志，大崎 敏郎，入江 貴志，
清野 聡，妹尾 賢一，渡辺康太郎，佐藤 尚夫，鈴木 武史，
北沢日出男
2.4 不安定核ビーム …… 132
2.4.1 放射性核種ビームを用いた核物理および核宇宙物理学における
フロンティア …… 132
久保野 茂
3. シグマ委員会30周年記念パネル討論会（岐路に立つ核データ活動） …… 141
3.1 基調講演 …… 143
3.1.1 シグマ委員会30年を振り返って …… 143
中嶋 龍三
3.2 パネリスト発表 …… 145
3.2.1 核データの評価と測定に関する個人的なコメント …… 145
千葉 敏
3.2.2 炉物理・遮蔽に関する問題点 …… 146
瑞慶覧 篤
3.2.3 核融合炉開発のための核データニーズ …… 149
関 泰
3.2.4 新たな消滅処理の応用研究のための核データの要請 …… 152
岩崎 智彦
3.2.5 わが国における医学用の原子分子および原子核データのニーズ …… 154
岩波 茂
3.2.6 宇宙利用のための加速器を用いた実験 …… 158
嶋野 洋介
3.2.7 原子力開発環境および核データ活動の国際協力 …… 159
更田豊治郎
3.3 総 括 …… 162
3.3.1 岐路に立つ核データ活動に関する基調講演およびパネル討論 …… 162
中沢 正治
4. 閉会の辞 …… 165
4.1 1980年代初頭からのデータ要求の発展 …… 167
吉田 正

5. ポスター発表論文 …… 169

5.1 $^{237}Np(n,\gamma)^{238}Np$反応の熱中性子断面積及び共鳴積分の測定 …… 171
小林 捷平，山中 章広，木村 逸郎

5.2 鉛減速スペクトロンメータを用いた0.5 eVから10 keVにおける^{241}Amの核分裂断面積の測定 …… 179
小林 捷平，三好 光晴，山本 修二，藤田 薫顕，木村 逸郎，神野 郁夫，金沢 哲

5.3 90MV AVFサイクロトロン施設TIARAにおける有機シンチレータを用いた遮蔽体を透過した数十MeV中性子のスペクトル測定 …… 183
中尾 徳晶，中村 尚司，高田 真志，馬場 護，田中 俊一，中島 宏，坂本 幸夫，中根 佳弘，田中 進，秦 和夫，田辺 英治

5.4 グリッド電離箱を用いたヘリウム生成二重微分断面積の測定 …… 191
－ $^{14}N(d,n)^{15}O$と$^{15}N(d,n)^{16}O$中性子源の応用 －
松山 勇，馬場 護，松山 成男，清住 武秀，佐波 俊哉，平川 直弘，伊藤 伸夫，千葉 敏，深堀 智生，水本 元治，長谷川和夫，明午伸一郎

5.5 TIARA 20－90 MeV $^{7}Li(p,n)$中性子源の特性測定とその応用 …… 200
馬場 護，清住 武秀，岩崎 智彦，吉岡 正博，松山 成男，平川 直弘，中村 尚司，田中 進，田中 隆一，田中 俊一，中島 宏，明午伸一郎

5.6 大型角柱液体シンチレータを用いた散乱断面積測定法の開発 …… 210
松山 成男，大久保 剛，馬場 護，岩崎 信，曽田 大輔，平川 直弘

5.7 14 MeV中性子による^{12}Cのα粒子放出二重微分断面積の測定 …… 220
西沢 博志，高橋 亮人，村上 喜信

5.8 14.2 MeV中性子による^{12}C，^{16}O，^{40}Ca，^{56}Feの散乱断面積の測定 …… 230
西尾 禎治，白土 釧二，安藤 嘉章

5.9 $^{1}H(^{11}B,n)^{11}C$反応からの生成中性子の特性 …… 243
明午伸一郎，千葉 敏，深堀 智生

5.10 短寿命核生成断面積の測定 － Mg，S，Ga，Y，Mo，Pd，Sn － …… 253
山内 浩司，春日井好己，山本 洋，高橋 亮人，飯田 敏行，河出 清

5.11 短寿命核のベータ半減期の測定 …… 264
伊藤 茂，田中 晶彦，山本 洋，飯田 敏行，高橋 亮人，

河出　清
5.12 コリニアー・レーザー・イオン・ビーム分光による$^{143}Pr(T_{1/2}=13.6d)$の超微細構造の測定 …… 271
飯村　秀紀，久保田正志，中原　嘉則，市川　進一，堀口　隆良
5.13 JENDL－3.2用ＦＰ核データの再評価 …… 276
川合　將義，ＦＰ核データワーキンググループ
5.14 ^{238}U非弾性散乱断面積の評価 …… 290
河野　俊彦，藤川　登，神田　幸則
5.15 50 MeVまでの^{12}C中性子断面積の評価 …… 300
千葉　敏，深堀　智生，渡辺　幸信，小山　佳英
5.16 50 MeVまでの^{59}Coと^{197}Auの中性子ドシメトリ反応断面積の評価 …… 310
小野田直光，岩崎　信
5.17 3次Bスプライン・フィッティング法によるドシメトリ断面積の評価 …… 320
岩崎　信
5.18 D(γ,n)反応断面積の評価 …… 330
村田　徹
5.19 準位密度パラメータ・システマティクス再訪：核変形効果 …… 337
A.Mengoni，中島　豊
5.20 原子核準位密度公式におけるShell－Pairing相関 …… 342
中村　久
5.21 ENSDF評価者からユーザーへのコメント …… 346
喜多尾憲助
5.22 入射陽子エネルギー 3 GeVまでのフラグメンテイション断面積の系統性 …… 351
執行　信寛，石橋　健二，和久田義久
5.23 連続エネルギー・モンテカルロ解析を用いたJENDL－3中の鉄の2次γ線生成断面積の積分テスト …… 362
植木紘太郎，大橋　厚人，山野　直樹
5.24 D－T中性子場における2次γ線の積分実験手法と評価済核データの検証法 …… 369
前川　藤夫，大山　幸夫
5.25 荷電粒子核反応データのインデックスデータベース …… 380
千葉　正喜，加藤　幾芳
5.26 核平衡状態に対する核データの感度係数 …… 387
中村　浩規，関本　博
5.27 中間エネルギー領域の核データを要求する慣性核融合炉における問題点 …… 397
中尾　安幸，小田　明範，中島　秀紀

5.28 ^{99}Tcの中性子吸収断面積の測定 …… 403
加藤 敏郎，緒方 良至，原田 秀郎，中村 詔司
5.29 ハンガリーの核データ活動 …… 408
J. Csikai

1. Preface

The 1993 Symposium on Nuclear Data was held at Tokai Research Establishment, Japan Atomic Energy Research Institute (JAERI), on 18th and 19th of November, 1993. The symposium was organized by Japanese Nuclear Data Committee (JNDC) and Nuclear Data Center, JAERI. The program of the symposium is listed below. In this symposium, there are two special sessions celebrating the 30th anniversary of JNDC. One is the international session in which 10 scientists from various countries, who attended the IAEA specialist meeting held before the symposium at JAERI, participated with a speaker specially invited from Indonesia and total 7 papers were presented emphasizing the nuclear data activities in each country or organization. The other is the panel discussion entitled with "Nuclear Data Activity Being at the Crossroads". In the other oral sessions, a total of 7 papers was presented under the sessions of JENDL and shielding experiment for high energy neutron, nuclear data needs from non-nuclear engineering fields and beam of unstable nuclei. In the poster session, presented were 29 papers concerning cross section measurements, nuclear data evaluation, parameter systematic on nuclear model, integral experiment and data validation. All of the 43 papers, the summary record of the panel discussion and summary talk are compiled in this report.

Program

November 18 (Thr.)

9:45 Opening

9:45-9:50

1. Opening Address — T. Hiraoka (JAERI)

9:50-11:55

2. International Session (1) — Chairperson: Y. Kikuchi (JAERI)

2.1 Review of Nuclear Data Activities in U.S.A. [20+5] — F.M. Mann (HEDL)

2.2 Study of Nuclear Data in Indonesia [20+5] — R.S. Lasijo (NAEA)

2.3 Nuclear data activities at Khlopin Radium Institute, Russia [20+5] — A.A. Rimski-Korsakov (KRI)

2.4 Recent Nuclear Data Activities in China Related to CENDL-2 [20+5]
Zhao Zhixiang (IAE)

2.5 Status Report EFF/EAF Projects [20+5] J. Kopecky (ECN)

12:00-13:00 Lunch

13:00-13:55

3. International Session (2) Chairperson: H. Maekawa (JAERI)

3.1 The ITER Blanket and Shield Design Status as of September 1993 [25+5]
Y. Gohar (ANL) [presented by Y. Seki (JAERI)]

3.2 Status of the International Fusion Evaluated Nuclear Data Library (FENDL) [20+5] A.B. Pashchenko (IAEA)

14:00-16:00

4. Poster Presentation

16:00-18:00

5. JENDL and Shielding Experiment for High Energy Neutron
Chairperson: S. Ishikawa (PNC)

5.1 JENDL-3 Revision 2 [50+10] T. Nakagawa (JAERI)

5.2 Integral Test of JENDL Activation Library for Fusion Applications [25+5]
Y. Ikeda (JAERI)

5.3 Shielding Experiments with Quasi-Monoenergetic Several Tens MeV Neutron at 90 MV AVF Cyclotron Facility TIARA [25+5]
T. Nakamura (Tohoku Univ.)

18:15-20:00 Reception (Akogi-ga-ura Club)

November 19 (Fri.)

9:00-10:50

6. Nuclear Data Needs from Non-nuclear Engineering Fields
Chairperson: N. Kishida (CRC)

6.1 Atomic, Molecule's and Nuclear Data for Medical Application [50+10]
S. Iwanami (Kitazato Univ.)

6.2 Nuclear Data for Space Engineering
--- Theoretical Approach to Proton Upset --- [50+10]
Y. Shimano (NASDA)

10:50-11:00 Coffee Break

11:00–11:55

6.3 Nuclear Astrophysics and Critical Roles of Nuclear Data [50+10]

Y. Nagai (TIT)

11:55–13:00 Lunch

13:00–14:00

7. Beam of Unstable Nuclei Chairperson: S. Iwasaki (Tohoku Univ.)

7.1 Review of Study Using Unstable Nuclei [50+10] S. Kubono (INS)

14:00–14:05 Coffee Break

14:05–16:45

8. Panel Discussion for the 30th Anniversary of JNDC

--- Nuclear Data Activity being at the Crossroads ---

Chairperson: M. Nakazawa (Univ. of Tokyo)

8.1 Keynote Address: The 30 Years of JNDC [20] R. Nakasima (Hosei Univ.)

8.2 Panelist Presentation [70]

for Measurement and Evaluation of Nuclear Data S. Chiba (JAERI)

for Reactor Physics and Shielding A. Zukeran (Hitachi, Ltd.)

for Fusion Reactor Development Y. Seki (JAERI)

for Nuclear Fuel Cycle and Waste Transmutation T. Iwasaki (Tohoku Univ.)

for Medical Application S. Iwanami (Kitazato Univ.)

for Space Engineering Y. Shimada (NASDA)

for Environment of Nuclear Energy Development and International Cooperation T. Fuketa (NEDAC)

8.3 Discussion [60]

Nuclear Data Activities in Future and Cultivation of Successors

8.4 Summary [10]

16:45–17:00

9. Closing Address T. Yoshida (Toshiba Corp.)

2. Papers Presented at Oral Session

2.1 International Session

2.1.1 Nuclear Data Activities in the United States

Dr. Frederick M. Mann
Westinghouse Hanford Company
Post Office Box 1970
MSIN HO-36
Richland, WA 99352 USA

The recent United States (U.S.) activities in nuclear data measurement, evaluation, and testing will be presented. The information presented is based on the recent meeting of the Cross Section Evaluation Working Group (CSEWG) meeting held October 5 - 7, 1993 and on input from important committee chairmen.

I. Cross Section Evaluation Working Group Overview (see Appendix A)

The 42nd meeting of the Cross Section Evaluation Working Group (CSEWG) was held October 5 through 7, 1993. A review of progress was made, but the occasion was also used to assess the status of the U.S. nuclear data program and to formulate strategy to guide us into the future.

The ENDF/B-VI evaluations released during the summer included:

1. Neutron-induced reaction evaluations for ^{14}N, ^{45}Sc, ^{59}Co, $^{63,65}Cu$, ^{73}Ge, ^{98}Tc, $^{101,102}Ru$, $^{106,108,110,112,114,116}Cd$, ^{127}I, $^{143,145}Nd$, $^{150,152}Sm$, $^{174,176,177,178,179,180}Hf$, $^{235,237,238}U$, ^{238}Np, $^{239,240,243}Pu$, ^{241}Am, $^{245,246,247}Cm$, and $^{250,251,252,253}Cf$,

2. neutron-induced fission product yields for 31 materials: $^{227,229,232}Th$, ^{231}Pa, $^{232,233,234,235,236,237,238}U$, $^{237,238}Np$, $^{238,239,240,241,242}Pu$, $^{241,242m,243}Am$, $^{242,243,244,245,246,248}Cm$, $^{249,251}Cf$, ^{254}Es, and ^{255}Fm,

3. spontaneous fission product yields for 9 materials: ^{238}U, $^{244,246,248}Cm$, $^{250,252}Cf$, ^{253}Es, and $^{254,256}Fm$; and

4. high energy reaction evaluations (neutron and proton) for 4 materials: ^{12}C, ^{56}Fe, ^{208}Pb, and ^{209}Bi.

Reports on the International Conference on Nuclear Data for Fusion (May, 1993), the Nuclear Energy Agency Nuclear Science Committee (NEANSC) meeting (June, 1993), the Joint Evaluation File (JEF) meeting (June, 1993), the NEANSC Working Group on International Evaluation Cooperation (June, 1993), the International Atomic Energy Agency Consultants' Meeting on Standard Input Data Sets for Nuclear Model Computations of Nuclear Data (June, 1993) were given.

II. Evaluation Committee Report from CSEWG (see Appendix B)

The following neutron-induced reaction evaluations are tentatively expected from; Argonne National Laboratory (ANL), Knolls Atomic Power Laboratory (KAPL), Los Alamos National Laboratory (LANL), Lawrence Livermore National Laborary (LLNL), and Oak Ridge National Laboratory (ORNL), and are to be submitted to CSEWG for review before the next meeting:

^{1}H	LLNL	extension to 250 MeV
^{12}C	LLNL, LANL	extension to 150 MeV
^{14}N	LANL	small error for E_n > 14 MeV
	LLNL, LANL	extension to 250 MeV
^{16}O	LLNL, LANL	extension to 250 MeV
^{27}Al	LANL	extension to 40 MeV
Si	ORNL	new isotopic evaluations
^{31}P	LLNL, LANL	extension to 250 MeV
^{40}Ca	LLNL, LANL	extension to 250 MeV
^{56}Fe	LANL	extension to 40 Mev
^{59}Co	LANL	extension to 40 MeV

Zr	KAPL	new natural and isotopic
Cd	ANL	new isotopic evaluations
^{208}Pb	LANL	extension to 40 MeV
^{235}U	KAPL	thermal region
^{241}Pu	ORNL	resolved resonances

The Standards Subcommittee is tracking the progress of $^{10}B(n,\alpha)$, $^{237}Np(n,f)$, and $^{1}H(n,n)$ experiments and noting their possible effect on the ENDF/B-VI standards. "The ENDF/B-VI Neutron Cross Section Measurement Standards" (ENDF-351) has been published.

III. Data Testing Report from CSEWG (see Appendix C)

Thermal benchmarking continues with results available from Bettis Laboratory, KAPL, LANL, ORNL, and Australian Nuclear Science and Technology Organization (ANSTO). The ENDF/B-VI values for k_{eff} are lower than found from ENDF/B-V. Possible causes were postulated and are being investigated.

Extensive fast data testing results are also available from LANL. The agreement with experiment is slightly better with ENDF/B-Vi than with ENDF/B-V for most of the criticals.

IV. CSEWG Strategy Session

The need to more closely interact with the ultimate customer of nuclear data was recognized. Mrs. V. McLane of National Nuclear Data Center-Brookhaven National Laboratory will lead an Outreach Task Force to consider ways to strengthen ties to the user community.

There also may be a need to reorganize CSEWG to face the changing times. Because of requirements of U.S. law concerning federally sponsored committees, the U.S. Nuclear Data Committee has been disbanded with most of its functions taken over by CSEWG.

V. LANL Activities

Dr. Bob MacFarlane released a frozen version of NJOY (91.91) to the Radiation and Shielding Information Center. Using this version, LANL processed ENDF/B-VI into 30x12, 80x24, 175x46, 69x24, and 187x24 group libraries. Eighty-three materials have been processed in the ACE format of MCNP.

Dr. Phil Young et al., are developing an improved code for higher energy calculations, called FKK-GNASH, which utilizes quantum-mechanical pre-equilibrium models based on Feshbach-Kerman-Koonin theory. Figure 1 presents the results for ^{208}Pn(n,2nγ).

Dr. Dave Madland is continuing his efforts on the fission process by investigating fission cross sections for short-lived uranium isotopes and fission spectra from n + ^{239}Pu.

VI. ORNL Activities

The Oak Ridge Electron Linear Accelerator has passed the 100,000 hours of operation milestone. Recent measurements include scattering experiments on Si, transmission experiments on ^{10}B, ^{52}Cr, ^{113}Cd, ^{165}Ho, Cd, and Pb, capture to fission ratios for ^{235}U, eta for ^{235}U, fission cross sections of ^{239}Pu, ^{10}B(n,α), and radionuclide production from γ + Ta.

New level density formulations have been added to TNG. Improvements to SAMMY included the ability to analyze angular distributions of differential elastic cross sections and incorporation of multiple scattering corrections which provide the capability to analyze capture data.

The ORNL is active in four of the NEANSC subgroups as well as in IAEA activities.

Preparation for the International Conference on Nuclear Data for Science and Technology to be held in Gatlinburg, TN May 9-13, 1994 is continuing.

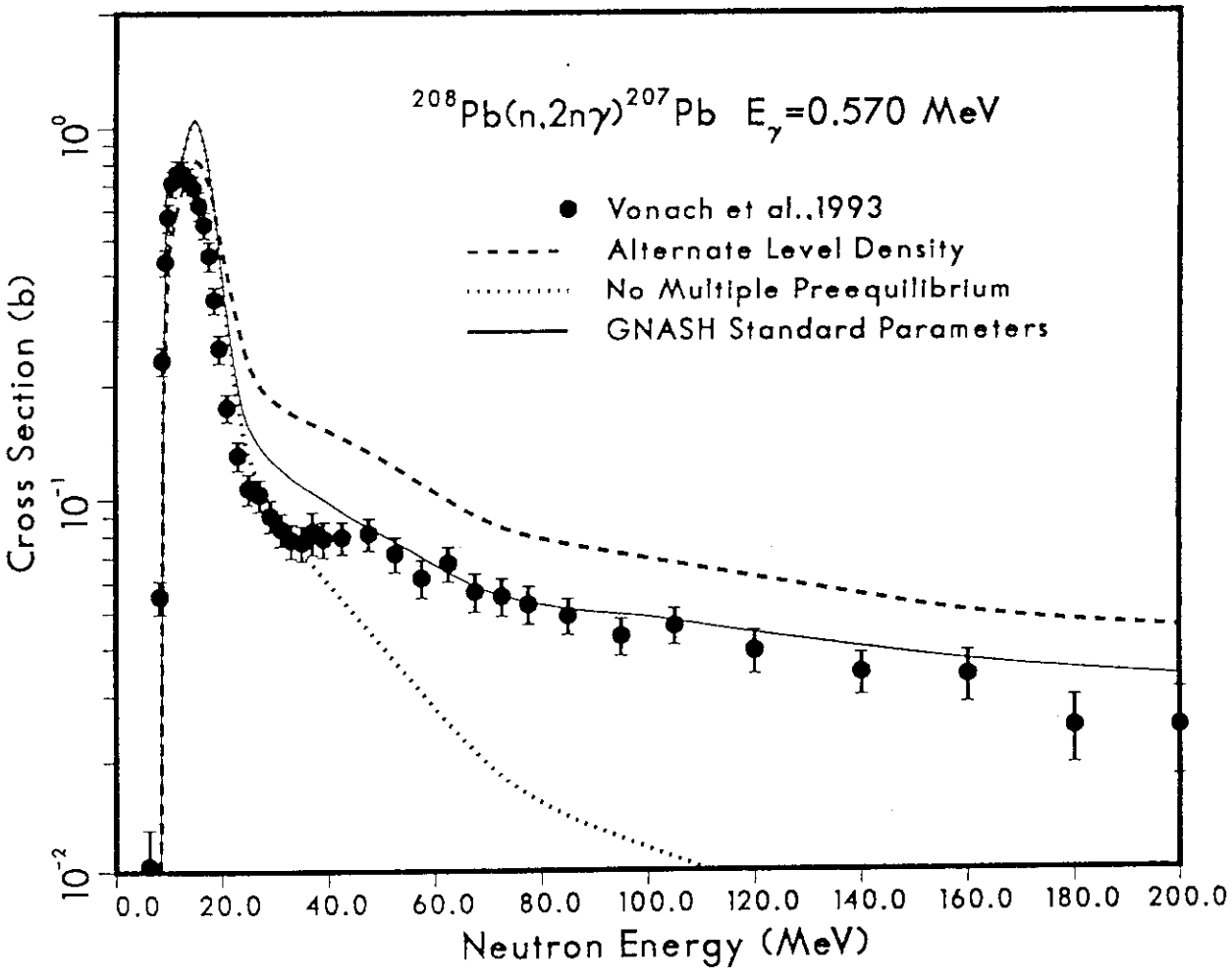

Fig. 1 Comparison of calculated and measured cross sections between E_n=5 and 200 MeV for production of the 0.570-MeV gamma ray from $^{208}Pb(n,2n\gamma)^{207}Pb$ reactions. The solid curve is obtained with our best set of parameters, the dashed curve results when an alternate (Gilbert-Cameron) level density formulation is used instead of the preferred Ignatyuk model, and the dotted curve results when the multiple preequilibrium model is turned completely off.

Appendix A

GENERAL PURPOSE DATA SUBCOMMITTEE REPORT

D. Larson and P. Young, Co-Chairmen

1. Status of silicon evaluations (D. Larson)

^{28,29,30}Si isotopic evaluations are complete and checked except for the resonance region. New ORELA total and differential elastic scattering data in the resonance region are being analyzed with SAMMY, and we plan to include resonance region inelastic scattering data from 1.78 MeV to 4.0 MeV in this analysis.

2. Status of nitrogen evaluation (P. Young)

The original ENDF/B-VI evaluation was revised to include an improved R-matrix analysis by Hale that incorporates recent ORELA transmission data from Harvey (see Attachment 2D-1 for comparisons with data and ENDF/B-VI). Additionally, the evaluation was extended to 40 MeV. This evaluation was issued in Release 2, but subsequently an error was discovered that was missed in the Phase 1 review. The error only affects data above ~ 14 MeV, but results in elastic cross sections as much as 20-30% too low. The problem has been fixed, and the corrected evaluation is available for the next release of ENDF/B-VI, after a Phase 1 review. A review package will be assembled by Young and provided to the Phase 1 reviewers (Larson and White).

3. Status of SAMMY R-matrix code (D. Larson)

SAMMY has been upgraded to include multiple scattering and attenuation corrections, thus extending it's analysis capabilities to differential scattering and capture data (including targets with arbitrary ground state spins). Current activities include upgrading documentation to reflect the new capabilities and an activity to speed up selected portions of the code. Future activities include adding additional channels (it now has 3). The code continues to serve as a "benchmark" against which processing and plotting codes are checked for correct operation in the resonance region.

4. Summary of ^{238}U, ^{239}Pu, and ^{241}Pu revisions for second release of ENDF/B-VI (P. Young).

Larry Weston has updated the resolved resonance regions of the ^{238}U, ^{239}Pu, and ^{241}Pu evaluations based on recent resonance parameter analyses. His comments are summarized below.

a. ^{238}U

Resolved resonance region revised on the basis of Moxon and Sowerby's final evaluation, which is the same as JEF. The original V6 evaluation was based on a preliminary and incomplete evaluation by Moxon and Sowerby.

b. ^{239}Pu

The resolved resonance region was revised by Herve Derrien during his stay at JAERI. The new evaluation utilized new experimental data by Weston at ORNL and by Wagemans at GEEL, in addition to older data. The same evaluation is being used in JEF.

c. ^{241}Pu

Resolved resonance region re-evaluated by Herve Derrien, using new fission cross section data by Wagemans of GEEL. Main effect is a lowering of the normalization of the fission cross section in the resonance region by about 3% [see Attachment 2A-1(1)]. The capture cross section above 300 eV was raised 9.2% [see Attachment 2A-1(2)]. In the original ENDF/B-VI evaluation, Derrien lowered the capture cross section by 14% relative to the data of Weston and Todd, but Derrien determined that this was an overcorrection. Presumably, this file will also be incorporated in JEF and JENDL.

d. Recommendation

Larry stated that there is nothing controversial about any of these revisions, and he recommended they be adopted by CSEWG for ENDF/B-VI as soon as possible. Young performed Phase 1 reviews for the ^{238}U and ^{239}Pu evaluations, and they are included in the Release 2 of ENDF/B-VI that occurred in the summer. Because Phase 1 reviews have not yet been performed for the new ^{241}Pu evaluation, it will be held over until Release 3 of ENDF/B-VI occurs.

5. Status of Zr Evaluation (C. Lubitz)

C. Lubitz described a reevaluation of Zr natural and isotopic data that is in progress at KAPL. An R-function analysis is being performed, using modern data from GEEL and ORELA. Previously the resonance integral for Zr was low, but using the newer measurements by J. Harvey, it has increased to an acceptable value. The KAPL evaluation will be merged with an analysis by A. B. Smith above 1 MeV. The evaluation is expected to be complete within a couple of months.

6. Status of ^{235}U Evaluation (C. Lubitz)

C. Lubitz described the progress in addressing the long-standing question of the ^{235}U aqueous criticals that suggests the need for a higher value of alpha in the epithermal region. Several possible approaches to resolving this problem have been investigated. The best approach appears to be to slightly increase gamma-ray widths at low energies, together with small adjustments to the thermal $^{1}H(n,\gamma)^{2}H$ cross section and to thermal nubar for ^{235}U. It appears that these adjustments can be made largely within the uncertainties in the microscopic data base. It was decided to form a task force to pursue the solution of this problem. C. Lubitz agreed to chair the task force, and A. Carlson agreed to serve on it. Other members may be recruited by Lubitz. A goal for the task force is to present their results at a special meeting of the Evaluation Committee in conjunction with the Gatlinburg Conference, assuming we can arrange for a meeting at that time.

7. Future Evaluations and Releases

It was agreed that the primary focus of CSEWG should be to complete the testing, processing, and implementation of ENDF/B-VI before we consider a complete new version. It was decided that the next issue of ENDF/B-VI, Release 3, should not occur until after the Fall CSEWG meeting in 1994. Phase 1 reviews for new evaluations or updates should be complete by the 1994 CSEWG meeting. The group decided to hold a meeting of the General Purpose Evaluation Subcommittee at the Gatlinburg conference in May, 1994 to discuss evaluation plans for Release 3 and to arrange for Phase 1 reviews. Duane Larson was requested to check with Kirk Dickens about arrangements for a short (~ 2-3 hr) meeting at Gatlinburg.

Summaries of the new evaluations discussed by the subcommittee that are possible for Release 3 are given in Tables 2A-1 (general purpose evaluations) and 2A-2 (high energy evaluations). Some of the evaluations planned for the high energy library (Table 2A-2) might in

fact wind up in the general purpose library, depending on the detail that can be included in the evaluations to higher energy.

8. Evaluation Documentation

A plan was formulated for providing summary documentation for Release 2 of ENDF/B-VI which occurred this past summer. Evaluators are asked to provide summary documentation for a new issue of ENDF-201. Contributions are to be sent to Vicki McLane by December 31, 1993, in a word processor form that will be specified by Vicki. If no contribution is received for a given evaluation, Vicki will simply adapt the MF=1 data for the summary documentation.

A discussion was held concerning the need for a concise, up-to-date summary that can be used to inform data users of the vintage and status of all evaluations in the ENDF/B system. Such a summary should give a clear but compact breakdown of information in the file. P. Young agreed to attempt a draft of such a document by the next CSEWG meeting.

Appendix B

Minutes of the Standards Subcommittee Meeting Brookhaven National Laboratory 5 October 1993

Allan D. Carlson (NIST), Chairman

1. Recent Experimental Activity and Plans for Measurements on the Standards.

Significant experimental activity on the standards has occurred since the completion of the standards evaluation for ENDF/B-VI. Most of that work and its possible impact on the standards was reported in the paper "The Data Base of The Standards and Related Cross Sections After ENDF/B-VI," by W.P. Poenitz and A.D. Carlson which was given at the Symposium on Nuclear Data Evaluation Methodology in October of 1992 at BNL. An update of the data available since that meeting was given at the present meeting. Several measurements were made which will improve the data base for the $^{10}B(n,\alpha)$ standards. Problems with this data base received considerable attention during the evaluation of the standards for ENDF/B-VI. The measurements of Schrack *et al.* of the shape of the $^{10}B(n,\alpha_1\gamma)$ cross section were recently published in Nuclear Science and Engineering. These data were obtained at the ORELA facility with a black neutron detector for the fluence measurement and covered the energy range from 0.3 to 4.0 MeV. The shape of these data are consistent with that of the ENDF/B-VI evaluation to about 1 MeV but differ by up to 40% for energies above 1 MeV. New shape measurements are now being made of this cross section by Schrack *et al.* using a hydrogen gas proportional counter for the fluence determination so that the measurements could be extended to lower neutron energies. Both the measurements with the black detector and the hydrogen proportional counter have been normalized to the ENDF/B-VI evaluation at low neutron energies. The normalization should be more accurate with the measurements using the hydrogen proportional counter than those with the black detector since these data extend to lower energies where the uncertainty in the ENDF/B-VI evaluation is less. New measurements of the ^{10}B total cross section by Wasson *et al.* at the ORELA facility have recently been completed. These data extend from 0.2 to 20 MeV. The measurements agree with the ENDF/B-VI evaluation for energies above about 1.5 MeV but deviate by more than 4% for the lower energies. Also ^{10}B total cross section measurements are now being made at the GEELINA facility by Brusegan. These data extend from 80 eV to about 100 keV neutron energy.

New measurements of the $^{237}Np(n,f)$ dosimetry standard cross section by Carlson *et al.* at the LANSCE facility at LANL have recently been completed. Preliminary analysis of this data indicates that the ENDF/B-VI evaluation is about a factor of three low in the resonance region.

Feldman *et al.* have reported new measurements of the hydrogen scattering cross section from 65-250 MeV. These data were obtained at the WNR facility at LANL. The data support the results recently obtained at Uppsala by Rönnqvist *et al.* at 96 MeV neutron energy and disagree with the older measurements made by Scanlon *et al.* (Harwell) and Stahl *et al.* (Harvard).

New measurements of the hydrogen scattering cross section at 10 MeV neutron energy are planned at the beginning of 1994 at the tandem facility at Ohio University. The NIST-OU-TUNL-LANL collaboration for this work was formed in part to resolve differences between the ENDF/B-V and ENDF/B-VI evaluations for the hydrogen scattering cross section. Measurements are planned at angles between 60 and 180 degrees in the center-of-mass system.

2. Meeting of The NEANSC Collaboration on The $^{10}B(n,\alpha)$ Standard Cross Sections.

A meeting is planned of the NEANSC Endorsed International Inter-Laboratory Collaboration on the $^{10}B(n,\alpha)$ Cross Sections at the Gatlinburg nuclear data conference. The $(n,\alpha_1\gamma)$ and total cross section measurements and the recently published branching ratio data of Weston will be the subjects of investigation at this meeting. Their impact on the determination of the standard cross sections will be pursued.

3. Preserving the Data Bases used in the Standards Evaluations.

It has been suggested that a means be established to ensure that the data bases and evaluation codes used for the ENDF/B-VI standards evaluations be available for future standards evaluations. They could possibly be archived at the NNDC at BNL. Most important are the data bases which represent a significant effort and in some cases contain corrections and information about experiments which are not generally known. W. Poenitz has agreed to make the data base which was used for the simultaneous evaluation available if he can properly document the evaluation process. Funding is not available at his laboratory for this work. Some sources for funding have been investigated but this has not been successful. Suggestions for sources of funding for this documentation were discussed and will be pursued.

4. Documentation of ENDF/B-VI Standards.

The report ENDF-351, "The ENDF/B-VI Neutron Cross Section Measurement Standards" has been finished and distributed to the entire CSEWG and ENDF/B-VI Summary Documentation (ENDF-201) distribution lists. The report contains a description of the evaluation process for the standards which involved separate

R-matrix analyses for the H(n,n), ^{3}He(n,p) and C(n,n) reactions; and a combination of R-matrix and simultaneous evaluations for the remaining standards. Measurements of the ^{238}U(n,f), ^{238}U(n,γ) and ^{239}Pu(n,f) cross sections and an evaluation of the thermal constants were also included as input data for the evaluation. Also given are plots showing comparisons of the R-matrix, simultaneous evaluation and combination results; comparisons of the smoothed with the combination results; and comparisons of the output with the ENDF/B-V evaluations. Tables are given of the cross sections and uncertainties for the standards. Expanded estimated uncertainties are also given for the standards obtained from the combination of the R-matrix and simultaneous analyses. Complete sets of references showing the quantity determined are given for the data bases for the R-matrix and simultaneous evaluations used in the combination process. A detailed description of the combination process is given in an appendix. For completeness the entire output listing from the cross section evaluation process, as it was when it first became available, is given in an appendix. This appendix contains the non-standards cross sections including the thermal constants, and data beyond the standards regions for the standards.

5. Updates or Mods to the Standards.

The uncertainty as to when ENDF/B-VII will be a reality has caused some concern. Improved evaluations are being accepted for the non-standards as new releases, revisions or mods. In the past there has been a policy that the standards should not change for a given ENDF version. There has been significant experimental activity on the standards which will lead to changes in the standards for ENDF/B-VII. Faced with the prospect that it may be a long time before ENDF/B-VII is available, how long should we wait before considering making changes to the standards? The consensus of the group was to investigate the process and see how large the changes will be. R. Peelle has noted that with the process used for the determination of the standards for ENDF/B-VII, it should be relatively easy to add a limited number of data sets to the existing evaluation and check for changes in the standards. He has proposed doing this and was given unanimous support by CSEWG. He also still plans to continue his work on the collapsing of the covariance matrix for the ENDF/B-VI standards that resulted from the combination process.

Appendix C

Thermal Reactor Data Testing and Applications Subcommittee October 5, 1993

M. L. Williams, LSU (Chairman)

The TRDTAS met from 1:00 - 2:30 PM on Tuesday, October 5, 1993 and discussed results of recent benchmark calculations performed with ENDF/B-VI.1. As the chairman, M. Williams (LSU), was unable to attend this meeting, R. Q. Wright (ORNL) served as acting chairman and conducted the meeting.

Mark Williams had prepared a summary of thermal reactor data testing results performed and submitted by Graham Robinson (Australian Nuclear Science and Technology Organization). This summary was presented by R. Q. Wright and is included in Attachment 4A-1. Results were presented based on ENDF/B-IV and ENDF/B-VI. The calculations used S_8P_3 transport approximation with 200 group cross sections obtained with a modified version of NJOY. Results were presented for a rather extensive set of thermal benchmarks, including the homogeneous ORNL $^{235}U - H_2O$ moderated criticals ORNL-1, -2, -3, -4 and -10, the homogeneous PNL $Pu- H_2O$ moderated criticals PNL-1, -2, -3, -4, -5, -6B, -7A, -8A, -9, -10, -11, -12A, the low-enriched $U- H_2O$ moderated BAPL lattices BAPL-1, -2 and -3, three ZEEP $U- D_2O$ moderated lattices and the low-enrichment $U- H_2O$ moderated TRX lattices TRX-1, -2, -3 and -4. The conclusions from the ENDF/B-VI results are: (i) Eigenvalues for all of the uranium criticals are too low; (ii) Eigenvalues for the highly enriched homogeneous ORNL criticals are 0.3-0.6 % delta-k low; (iii) Epithermal capture in ^{238}U is too high; (iv) There is a trend for eigenvalues to increase versus ^{28}C / ^{25}F ratio in heavy water lattices; and (v) Homogeneous PNL (plutonium) criticals are computed better with ENDF/B-VI.

R. Q. Wright presented results of his thermal reactor benchmark calculations using ENDF/B-VI. Calculations were performed for the L-series Uranyl-fluoride, H_2O benchmarks, the highly enriched ORNL spheres ORNL-1, -2, -3, -4 and -10, the TRX-1 and -2 and BAPL-1, -2 and -3 lattices, and the UH3 and HISS benchmarks. These results are included in Attachment 4A-2. His conclusions included: (i) Eigenvalues of the L-Series benchmarks are significantly improved with ENDF/B-VI (average k-eff is ~1.0008 and is ~0.6% delta-k lower than with ENDF/B-V due to improvements in U-235 and O-16 data), (ii) Trend with leakage for the L-Series is reduced with ENDF/B-VI, (iii) Highly enriched ORNL spheres are about 0.5% low with ENDF/B-VI (whereas results with ENDF/B-V were close to unity), (iv) Results for the TRX-1 and -2 lattices are quite low using their preliminary VITAMIN-B6 library, and (v) Trend with pitch for the BAPL lattices is eliminated using VITAMIN-B6 cross sections.

Bob MacFarlane (LANL) presented new ENDF/B-VI results which were also obtained via a discrete ordinates code using multigroup data processed with NJOY. He compared results calculated with two different group; structures obtained with ENDF/B-V.2 and -VI.1 for an extensive set of thermal benchmarks, which included the unreflected ORNL spheres ORNL-1, -2 and -10, the L-series of uranyl fluoride

assemblies L7, L8 and L9, four unreflected spheres of plutonium nitrate solution PNL-1, -2, -3 and -4, and the thermal lattices TRX-1 and -2 and BAPL-1, -2 and -3. The handouts for this talk are included in Attachment 4A-3. (Note that this Attachment also includes his results and discussion for an extensive series of fast reactor benchmarks.) Conclusions from these calculations include: (i) Eigenvalues for the ORNL spheres are lower by ~0.3% delta-k with ENDF/B-VI (relative to ~1.000 with ENDF/B-V), (ii) Trend versus leakage (as indicated by results for L7 and ORNL-10) is not improved with ENDF/B-VI, (iii) Results for the PNL series (which have always been widely scattered) are improved on the average with ENDF/B-VI, (iv) Eigenvalues for TRX-1 and -2 (which were low by ~1% with ENDF/B-V) are very slightly lower with ENDF/B-VI, (v) Integral parameters Rho-28 and Delta-25 are reduced slightly in TRX-1 and -2 with ENDF/B-VI, (vi) Similar results were obtained with ENDF/B-VI for BAPL-1, -2 and -3 (eigenvalues lower and worse by ~0.3% delta-k).

U. Decker (ABB Combustion Engineering) discussed their progress in preparation of a DIT library based on ENDF/B-VI cross sections. His handout is included as Attachment 4A-4. His conclusions included that ENDF/B-VI with drooping eta for U-235 satisfies both requirements of going more positive on the moderator temperature coefficient (MTC) and more negative in PWRs at operating conditions.

Other participants who did not prepare handouts summarized their results obtained in earlier studies. These included Cecil Lubitz (KAPL) and Skip Kahler (Bettis). These results may be included in the minutes of the Resonance Region subcommittee of the Methods and Formats Committee.

Thermal Reactor DTAS Attendees
October 5, 1993

A. Aronson	BNL
U. Decher	ABB-CE
C. Durston	S. Levy, Inc.
T. England	LANL
K. Hu	BNL
D. Ingersoll	ORNL
A. Kahler	BAPL
C. Lubitz	KAPL
R. MacFarlane	LANL
R. McKnight	ANL
M. Milgram	CRNL
C. Wemple	EG&G
J. White	ORNL
R. Wright	ORNL

2.1.2 Study of Nuclear Data in Indonesia

R.S. Lasijo, F. Aziz, B. Santoso, I.R. Subki

National Atomic Energy Agency, Jakarta, Indonesia

ABSTRACT

A team for the installation of the evaluated nuclear data libraries has been formed. The team is expected to be the embryo for the formation of the nuclear data group in Indonesia. The first task of the team was to install the evaluated nuclear data libraries ENDF through the IAEA technical assistance. Experts from the IAEA have been sent to Indonesia to help the installation of the libraries together with the preprocessing and the processing codes, and to train the local scientists on the applications of several codes. Utilization of evaluated nuclear data in nuclear reactor core calculations is the most concerned objective in the moment. Applications in other fields like radiation protection and shielding, nuclear medicine, etc., may follow. The possibilities of working on the nuclear data measurements and evaluations are also considered.

INTRODUCTION

The idea of establishing a nuclear data group in Indonesia was put forward in 1986. Activities of the group may be divided into three parts :

1. Nuclear Data Measurement.
2. Nuclear Data Evaluation.
3. Nuclear Data Utilization.

These are the three consecutive steps which have to be done if a right procedure has to be followed.

Our situation does not permit us to do the right consecutive steps as mentioned above, but we have to start from the last step, and will possibly be followed by the others.

NUCLEAR DATA UTILIZATION

Probably nuclear data utilization is the most feasible activity which can be done at the moment. One of the end users of nuclear data is the reactor people. Calculationsrelated to nuclear reactor core and fuel management analyses are very popular among senior as well as young scientists and engineers, especially since the operation of the multipurpose research reactor G.A. Siwabessy in Serpong, near Jakarta. For this reactor, a diffusion equation and burn-up code IAFUEL has been available, which was provided by Interatom GmbH, Germany. The local scientists and engineers have also been trained by the company experts in using the code. The code was originally taken from the bigger code called IAMADY. The lattice constants needed to run the code were also provided by Interatom, but the cross-section generation code to obtain the lattice constants is not available to us.

The task of nuclear data group is to study the link of the diffusion equation code to the evaluated nuclear data files which have been available through IAEA as well as other nuclear data centres. Therefore when a team was formed (which is expected to be the embryo of the nuclear data group) its first assignment was to apply technical assistance to the IAEA. The team is headed by Dr. Budi Santoso, the head of Nuclear Technology Assessment Centre. The first technical assistance was granted by the IAEA through TA No. INS/0/008 in 1988. The evaluated nuclear data libraries ENDF/B format were received from the Nuclear Data Section, including the preprocessing codes COMPLOT, CONVERT, DICTION, EVALPLOT, GROUPIE, LINEAR, MERGER, RECENT, and SIGMA. A fellowship was also awarded to Mr. Riyanto Rahardjo to study nuclear data format and retrieval system in Vienna.

Other codes were also obtained from the NEA Data Bank in France, until three groups of codes have been available as shown in the following figure.

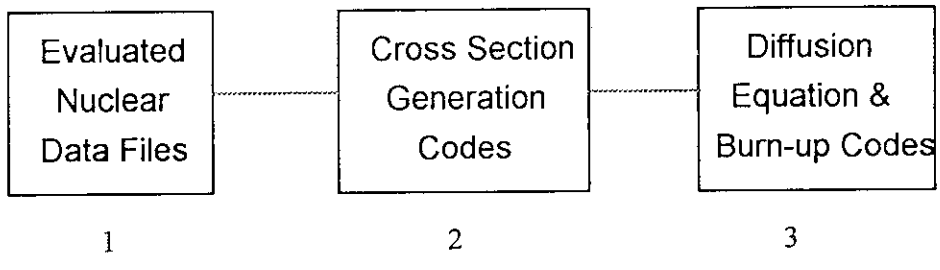

Fig. 1. Three groups of reactor codes.

Codes in group 2 available are a.o. WIMS-D/4, LEOPARD, NJOY. Both mainframe and PC version for WIMS have been available. NJOY has been used to modify library used in WIMS-D/4, but this code run only on the mainframe. Codes in group 3 available are a.o. IAFUEL, 2DB, and 3DB.

Experts sent by the IAEA were, among others, Dr. A. Trkov, Dr. S. Ganesan, Dr.M. Lee, Mr. V. Gopalakrishnan, and Dr. T. Kulikowska. Generally they came to discuss codes for each group, and did not discuss the link between the three groups in detail. Hence it is still our task to study the link of the three groups of codes in a complete and continuous manner. More technical assistances and cooperation with other research centres are still expected which can be accomplished through the IAEA or by bilateral agreement.

NUCLEAR DATA MEASUREMENT

It is our plan that for the next step we will be exercising nuclear data measurements. The neutron generator which was reinstalled in Yogyakarta Nuclear Research Centre, Central Java, is still struggling to get more beam to obtain more neutron source for nuclear experiments. The machine is expected to be used for 14 MeV neutron nuclear data collection.
A neutron time of flight spectrometer which is being installed at Research Centre for Nuclear Techniques in Bandung is expected to be used for epithermal neutrons. The neutron chopper was received from the German Government which was formerly used by the University of Kiel at GKSS Research Centre in Geesthacht.
Technical assistances for both machines are still expected through the IAEA or by bilateral channels.

NUCLEAR DATA EVALUATION

Like the case of the nuclear data measurement, the nuclear data evaluation is short of qualified or experienced manpower. Knowledge in nuclear reactions, which is one of the requirements that the activity in nuclear data evaluation may run well, experimentally as well as theoretically, is practically minim. Interested young man who is willing to devote himself to this activity is also hardly to be

found. We hope that by training and cooperation with more advanced research centre like JAERI may help us to realize the activity in the near future. Computers available for the purpose are VAX-8550, which has been used for various calculations for more than four years, and some PC's.

OTHER RELATED ACTIVITIES

Prospect of using silicide fuel elements for the multipurpose research reactor G.A. Siwabessy in the future is very promising. Irradiation test for silicide fuel element, which was assembled locally, has been accomplished. Precalculation and theoretical analysis were done using the IAFUEL code. The lattice constants used for the diffusion calculations were still provided by Interatom (Siemens), since the linked cross section generation code, MONSTRA, is not available to us. This is one of the reasons that we have to study seriously the connection between the three groups of codes as mentioned in the previous chapter, so that in the near future we will be in a position to provide ourselves the lattice constants needed for any new component or material inserted into the reactor core.

Based on the present rate of energy demand, it has been predicted that in the coming twenty-first century there will be energy shortage if we only count on the conventional energy resources. The most feasible alternative to overcome the problem is the nuclear energy. The feasibility study of the construction of the nuclear power plants has been carried out for several years. The siting study resulted in choosing the nominated locations around the northern coast of central Java. More sophisticated codes and bigger and faster computer will be needed to do the analyses and the calculations of the shielding problems when the construction of the nuclear plant is being carried out later on.

The study of high temperature reactor is another subject of interest recently, eventhough such a reactor is still behind the popularity of PWR, BWR, or PHWR. The efficiency of such reactor might be interesting in the future if most of the problems involved could be solved. The heat at high temperature not only can be used for power generation but also for other purposes. The evaluated nuclear data will certainly be very important in the study of such reactor.

FUTURE PROSPECT

The availability of the evaluated nuclear data files from various sources like ENDF/B, JENDL, BROND, etc. together with the preprocessing and the other calculational codes as the result of international cooperation, may enable the developing countries to exercise and develop their capabilities, at least in analysing the available nuclear facilities in their respective countries, in a more systematic and mature way.

In Indonesia nuclear data group may have a very important role along the nuclear development activities in the future, provided first of all that this group can achieve the capabilities of handling the evaluated nuclear data and linking the data to the end codes used for nuclear designs, analyses, shielding problems, and others. To reach such an achievement, more trainings, constant contacts and cooperation with universities and other research centres domestically as well as abroad, are necessary. Furthermore technical assistances from the IAEA and other advanced research centres are certainly still needed.

2.1.3 Nuclear Data Activities at Khlopin Radium Institute, Russia

Alexander A. Rimski-Korsakov

V.G.Khlopin Radium Institute, 194021, St.Petersburg, Russia

Khlopin Radium Institute in St.Petersburg is one of the oldest scientific establishments in Russia to deal with phenomena of radioactivity, nuclear energy and their applications. The task of releasing nuclear fission energy in the forties became an apparent field of work for physicists in Russia and that meant measurement of such crucial data as neutron fission cross-sections for uranium isotopes and emitted neutron multiplicities. The first radium-beryllium neutron sources in Russia have been prepared here, for the obvious reason that all radium available in Russia has been mined and separated by institute's geologists and chemists. Later, in 1937, the first cyclotron in Europe (second in the world) has been built at KRI by I.Kurchatov and his team, that provided a much more intense monoenergetic neutron source for the measurements, that today would be called "nuclear data research". In 1939 two Kurchatov's colleagues, G.Flerov and K.Petrzhak at KRI, while studying the newly discovered neutron-induced fission of uranium, found that some fission count rate could not be eliminated even without neutron source. They interpreted the fact correctly, and proved that spontaneous fission of U-238 was the reason. This discovery, among others, proved an important step in understanding the nuclear fission. Chain fission reaction possibility depended to a great extent on fission neutron multiplicity, and KRI physicists took active part in measuring this data using a very ingenious idea of multiple coincidence neutron counting, that permitted to extract absolute multiplicity values without actual knowledge of counters efficiency. Later, in the 60-ies, the fission neutron multiplicity values have become a specialty of KRI physicists, and for many heavy nuclei these values have been measured at KRI to the relative accuracy of 0.2% [1]. Fission physics developed fast, and measurements of many fission parameters were done at KRI using the so-called associated particle techniques (APT), when the measurement is triggered by some associated particle, marking the desired (measured) event, which reduces all background extremely effectively. This method (APT), used with time-of-flight (TOF) neutron spectrometry in the 70-ties permitted M.Blinov at KRI to build and operate several high-precision neutron spectrometers, and measure fission neutron spectra of Cf-252 to be used as neutron spectrum standard by IAEA and other Nuclear Data Centers [2]. At that time a wider Nuclear Data Program has been started at KRI in cooperation with official Nuclear Data Centers both in USSR (in FEI, Obninsk, in Kurchatov Institute, Moscow) and abroad (IAEA/NDS).

The contemporary period in ND work at KRI includes several directions, that are summarized in Table 1. All of these are aimed to applications in modern technology such as fission reactor development, fusion technology, nuclear waste handling and disposal, spacecraft shielding, radiation damage to electronic components etc. Two most typical examples of nuclear data measurements at KRI are measurements of 14 MeV neutron reaction cross-sections [2] and study of neutron spectra produced in massive targets by GeV protons [4].

First experiment is based on KRI D-T fast neutron source (300 keV deuteron beam with 1.5 mA current, pulsed with 3 nS duration). The tritium-titanium target is air-cooled and mounted in low-mass setup. The activated samples are mounted at various angles around

the target, thus providing energy selection from 13.5 MeV to 14.9 MeV and neutron flux about 50 million neutrons per square cm per second. Time−of−flight monitor could move around the target assembly thus measuring the neutron energy spectra in various directions from the target. At present more than 50 reactions (n,p), (n,alpha), and (n,2n) etc. have been studied with isotopes of Na, V, Fe, Co, Ni, Cu, Zr, Nb, Ag, In, Eu and Au with 5% statistical accuracy while measuring the activation products gamma radiation with 180 cc Ge(Li) gamma−spectrometer. Nb−93 cross−section has been used as reference value. Typical sources of error were:

Gamma spectrum line statistics	1−1.5 %
Spectrometer efficiency uncertainty	3 %
Reference cross−section uncertainty	1.5 %
Irradiation geometry	< 6 %
Decay data uncertainties	1 − 15 %

The cross−section data have been systematically compared to IRDF, ENDF/B−V, JENDL−3 and some other well established nuclear data files.

Another example is the so−called "massive" target experiment with 1 GeV proton beam stopped in 20 cm dia. and 80 cm long lead target − where neutron spectra on the surface of this "benchmark" target have been measured by foil activation technique, and some relatively new reactions (fragment production in Ti, Cu and Cd foils) specific for neutrons and protons > 200 MeV. For the region below 100 MeV the threshold activation reactions in Al, Co, Nb, Au and fission of Bi−209 and U−238 have been used. Cross−section library compiled by Greenwood [12] for these reactions proved a very helpful instrument in unfolding the neutron spectra by well−known STAYSAIL code. As a result reaction rates, neutron multiplicities and double−differential spectra have been measured to be used and compared to same data computed using high energy transport codes under development at KRI − SITHA and others. Later similar experiments have been done at KRI with Al, Cu and U targets [8].

References :

1) Blinov M. et al.: in "Properties of Neutron Sources", IAEA−TECHDOC−410, IAEA, Vienna, (1987), pp.65 and 201
2) Blinov M. et al.: International Workshop on Nuclear Data for Fusion Reactor Technology, Del Mar, CA, USA (1993)
3) Alkhazov I. et al.: in Proc. Int. Conf. on Nuclear Data for Science and Technology, Mito, Japan, p.145 (1988)
4) Bakhmutkin S. et al.: Atomnaya Energia, v.62, 59 (1987) (In Russian)
5) Daniel A.: Preprint RI−181, Khlopin Radium Inst. (1984) (In Russian)
6) Bunakov B. and Matveev G.: Izv.AN SSSR Ser. Phys. v.47, p.2115, (1983)
7) Perov V., Daniel A. and Rimski−Korsakov A.: Preprint RI−237, Moscow, Atominform (1992)
8) Ivanov R. et al.: Proceedings of Soviet V−th Seminar on Experimental Studies for a Meson Generating Facility, p.85, Zvenigorod, USSR (1987) (In Russian)
9) Yakovlev R. et al.: Radium Inst. Report No.1267−I (1989) (In Russian)
10) Rimski−Korsakov A.: in Proceedings of Sp. Meeting on Neutron Cross Section Standards for Energy Region > 20 MeV, Uppsala, Sweden (1991) p.65
11) Ivanov A. et al.: Pribory i Tekhnika Experimenta, No.3 (1992) p.229 (In Russian)

Table 1 Nuclear data activities at Khlopin Radium Institute

Activity	Results [references]	Application
Neutron generator experiments	Activation data in 2 - 15 MeV neutron energy region [1,2]	Neutron dosimetry for fission reactors
		Fusion technology development
Benchmark and activation experiments at 1-3 GeV particle accelerators in Gatchina and in Dubna	Minor actinide cross-sections [3,10]	Nuclear Waste and actinide transmutation technology development
	Reaction yields [8]	
	Hadron double-differential spectra [4,9]	
High energy particle transport computer modelling	High energy particle transport code verification and improvement [5,6,7]	Spacecrew dosimetry and shielding development for prolonged space missions
Neutron, gamma, and particle spectrometry in space [11]	Actual spacecrew exposure data	

2.1.4 Recent Nuclear Data Activities in China Related to CENDL-2

Zhao Zhixiang and Zhang Jingshang

Chinese Nuclear Data Center, China Institute of Atomic Energy
Beijing, P. O. Box 275(41), 102413, P.R.China

Abstract: Recent nuclear data activities in China related to CENDL-2 is summarized in this presentation.

I. Introduction

The CENDL-2 was released worldwide in 1992. The neutron induced data for total 54 nuclides / elements included in CENDL-2[1]. Since then, some feedback information on CENDL-2 are obtained from users and through intercomparison with other evaluated nuclear data libraries. Based on these information, a working plan on improvement and complement to CENDL-2 was worked out. In this report, the main conclusions of the intercomparison and the preliminary results of the improvement and complement to CENDL-2 will be presented. Evaluation methodology and codes of nuclear data calculation for improvement of CENDL-2 are developed and summarized in this presentation.

II. Intercomparison of CENDL-2 with Other Libraries

This activity was organized by Chinese Nuclear Data Center(CNDC) and carried out by Chinese Nuclear Data Coordination Network(CNDCN). The purpose of this activity is to provide further information for improvement and renew of CENDL-2. The intercomparisons were mainly performed for cross sections. The ENDF / B6, JENDL-3, BROND-2 and JEF-1 were involved in the intercomparison.The main conclusions obtained from the intercomparison are as follows:

a)Large discrepancies were found among the libraries for (n,p), (n,α) and (n,2n) reactions. One of reasons for this is that the existing evaluations for these reactions are usually based on model theory calculation. To improve the theory calculation, more measurement information would be needed for guiding theory calculation. Some measurements for this purpose have been arranged in CNDCN:

1) DDX measurement for ^{58}Ni(n,α), ^{40}Ca(n,α) reactions at En = 5–7, 18 MeV, 4.5 MV Van de Graaff at Beijing University;

2) Cross section and angular distribution measurement for ^{58}Ni(n,α), ^{58}Ni(n,2n), ^{60}Ni(n,α) and ^{60}Ni(n,2n) reactions at En = 5–7, 16–20 MeV, 4.5 MV Van de Graaff at Beijing University; Fig.1 shows the measured angular

distribution for $^{58}Ni(n,\alpha)$ reaction at $E_n = 5.1$ MeV.

3) DDX measurement of (n,xp) and (n,xα) for Cr, Fe and Ni at En = 14.0 MeV, Neutron Generator at China Sci. and Tech. University;

etc.

b) Compared with other libraries, only files 1－5 are included in most of evaluations of CENDL－2, so CENDL－2 should be improved by complementing gamma－production data, covariance file and DDX for some important nuclides. For this purpose, the UNF program, for fast neutron data calculation based on semi－classical theory model, is developed. This program is capable of calculating DDX and gamma－production data.[2] The methodology for evaluation of covariance files is also studies.

c) Some inconsistency problem involved in the evaluations of CENDL－2 should be resolved, for example, $^{N}Ag \neq {}^{107}Ag + {}^{109}Ag$.

III. Intercomparison among CENDL－2, ENDF / B－6, JENDL－2 and BROND－2 of Natural Cr, Fe and Ni(Liu Tingjin et al.)

The activity is performed cooperated with Center for Nuclear Data (CJD) of Obninsk, Russia. In the end of this May, Dr. Blokhin, staff member of CJD visited CNDC for one week and exchanged the progress with chinese colleagues on the intercomparisons.

The preliminary results of this activity are as follows:

a) Large discrepancies exist for cross sections of threshold reactions. Sometimes, the evaluated data from different libraries differ several times.

b) Large discrepancies have also been found for angular distribution and spectra of secondary neutrons.

In the CENDL－2, evaluations for structural materials were only carried out on natural elements. Based on the information from intercomparison, re－evaluations should be done for cross sections of all threshold reactions up to 20 MeV for all separate isotopes. And also re－calculation by means of UNF code should be carried out for spectra of secondary particles, especially around 14.5 MeV.

On the other hand, nuclear data processing and verification will be carried out to provide libraries for integral test. The calculation will be done for Iron sphere and slab.

IV. Complement of CENDL－2

So far CENDL－2 includes 54 nuclides / elements only. To meet the needs from users and for benchmark calculations, a working plan to complement the CENDL－2 by adding other 42 nuclides / elements is going on. Most of these 42 nuclides / elements are fission product(see Tab.1).

Table 1 Nuclides/elements need to be included in CENDL-2

Fission Products (28):
^{83}Kr; $^{103,105}Rh$; $^{131,135}Xe$;
$^{133,134,135}Cs$; $^{143,145}Nd$; $^{147,148,148m}Pm$;
$^{147,149,150,151,152}Sm$; $^{153,154,155}Eu$;
$^{154,155,156,157,158}Gd$; ^{164}Dy; ^{176}Lu
Actinides (10):
$^{233,234,236}U$; $^{238,241,242}Pu$; $^{242,244}Cm$;
$^{242m,243}Am$
Others (4):
$^{63,65}Cu$; Ag; ^{182}W

The working plan is divided into two stages:

In first stage, the intercomparison among several evaluated libraries will be done and better evaluations will be recommended and selected for including in CENDL－2.

In second stage, improvement will be carried out based on the information provided in first stage.

The first stage of this activity is fully completed. The review of the results of the intercomparison will be carried out on an Evaluation Working Group Meeting in the end of this year.

In addition to these 42 nuclides / elements, the evaluations for neutron induced data on Cl, Ca, Ga, Lu, Hg and Tl are also preparing. The neutron data for these elements are needed from point of view of fusion reactor application, but no or only very old evaluations are available in ENDF / B－6 and JENDL－3. These evaluations will be also included in CENDL－2 after completed.

V. Re－evaluation for Several Important Nuclides

The re－evaluations for some important nuclides including ^{238}U and ^{56}Fe are also preparing. The purpose of this activity is not only to provide high quality evaluated data but also to improve evaluation approaches such as UNF code through these evaluations.

1, Evaluation of ^{56}Fe(Zhao Zhixiang et al.):

Up to now, the evaluation for ^{56}Fe has been completed. The evaluated data includes cross sections, angular distributions, DDX, gamma production data and covariance files for resonance parameters, cross sections, angular distributions and DDX.

The main improvements of this evaluation are as follows:

a) Obvious improvements are obtained for DDX of secondary particles compared with ENDF / B－6(see Fig.2).

b) Covariance files are completely given. Among them, covariance files for DDX are obtained based on an analysis of measured DDX for total neutron, proton and alpha emissions and in file 36 format suggested by Vonach[3].

2, Evaluation of ^{238}U(Tang Guoyou et al.):

The revised version for ^{238}U is nearly completed based on a calculation by means of FMT code, which is a special version of UNF to be used for fission nuclides calculation.

The main changes of the new version for ^{238}U evaluation are as follows:

a) Files 6, 12, 13, 15 are supplemented based on FMT calculation;

b) The cross sections for total and partial inelastic scattering are re－evaluated. The contributions from direct interaction are calculated by coupled－channel optical model code CCOM for 1st and 2nd levels and by distorted－wave Born approximation code DWUCK for other levels. This evaluation compared with measured data and those of ENDF / B－VI and JENDL－3 are shown in Fig.3 and 4.

c) The cross sections for (n,2n) reaction are also re－evaluated based on FMT calculation.

VI. Methodology and Codes for Improvement of CENDL－2

Since the early stage of the establishment of CNDC, various model theories, evaluation methods and related codes have been studied and developed[4]. These methods and codes have played an important role in completion of CENDL－2. In recent two years, to further improve the CENDL－2, the researches related to evaluation methodology and codes for nuclear data calculation, plotting and processing have been carried out.

1, Evaluation Methodology

a) To improve the evaluations of averaged resonance parameters, especially the average level spacing, a method based on Bayesian approach for correcting the energy level missing has been established. This method has been used to calculate average level spacing for 240 nuclides. (Zhao Zhixiang and Huang Zhongfu)

b) The studies of model parameters and their systematics, such as optical model parameters, level density parameters, giant dipole resonance parameters and fission barrier parameters, are going on. These studies could improve model theory calculations for the nuclei without measured data. (Su Zhongdi et al.)

c) Evaluation methodology for covariance files also are studied. A simple method to evaluate covariance file for DDX has been developed and applied to ^{56}Fe evaluation. (Zhao Zhixiang et al.)

d) Impacts of negative and distant level on resonance cross sections

have been studied and analysis codes developed. (Qiu Guochun and Huang Zhongfu)

e) A method of simultaneous evaluation for correlated data are developed and used to evaluate the cross sections of ^{239}Pu(n,f), ^{238}U(n,f), ^{238}U(n,γ), $\sigma_f(^{239}Pu) / \sigma_f(^{235}U)$, $\sigma_f(^{238}U) / \sigma_f(^{235}U)$ and $\sigma_\gamma(^{238}U) / \sigma_f(^{238}U)$.(Liu Tingjin et al.)

2, Model Theory Codes for Nuclear Data Calculation

In recent two years, several model theory codes have been developed, perfected and replanted for nuclear data calculation.

UNF(Zhang Jingshang)

Developed for structural material calculation with the unified treatment of the pre－equilibrium and equilibrium reaction processes with angular momentum and parity conservations. The pick－up mechanism of composite particle emission and the discrete level effects are taken into account for improving the calculations of reaction cross section concerned. This code is capable of calculating DDX of particles, recoil nuclei and γ－ray produced in the reactions. The code has been used in the evaluations of ^{56}Fe, Cl, Ca, Ga, Lu, Hg and Tl.

FMT(Zhang Jingshang)

This code is a special version of UNF to be used for fission nuclides and has been used in the evaluation of ^{238}U.

RAC92(Chen Zhenpeng et al.)

A comprehensive R－matrix analysis code based on multi－channel and multi－level R－matrix theory. It has been used to analyse the n+^{10}B system.

MUP3(Yu Ziqiang et al.)

Revised version of MUP2. Compared with MUP2, MUP3 is capable of calculating DDX of particles produced in the reactions. The refraction effect of incident particles on the surface of the nuclei and pre－equilibrium effect for secondary process are taken into account in MUP3.

CFUP1(Cai Choghai and Shen Qingbiao)

A code for calculation of charged particle as well as neutron induced reaction of fissile nuclei at energy region up to 35 MeV, including 1－5 particles emission. It has been used to calculate p+^{241}Am and p+^{235}U systems, the incident energy from 4 to 35 MeV.

SPEC(Shen Qingbiao and Zhang Jingshang)

SPEC is a code for calculating cross sections and spectra of the neutron or charged particles(p, d, t, ^{3}He, α)induced reactions of medium－heavy nuclei in incident energy up to 60 MeV.

DDCS(Shen Qingbiao)

DDCS is a code for calculating nucleon and composite double differential cross sections of the neutron or charged particles(p, d, t, ^{3}He, α) induced reactions in energy region up to 50－100 MeV.

The codes mentioned above are developed by ourselves. To meet the needs of nuclear data evaluation, some useful codes obtained from abroad have been or are being replanted. Among them, there are coupled–channel optical model code ECIS79, R–matrix analysis code SAMMY, distorted–wave Born approximation code DWUCK, as well as nuclear data calculation codes ALICE and GNASH etc.. Some of them have been used in evaluation.

The fundamental researches related to model theory improvement are also carried out.

3, Codes for Nuclear Data Processing and Plotting

DDXB1(Zhang Jin and Liu Tong)

Used to produce n, p and α particle total emission spectra integrated over angles in c.m. system or total spectra at given angle in Lab. system from File 6 in ENDF / B format.

MAINPLT(Liu Tong and Zhao Zhixiang)

This code can be used to process and plot the evaluated cross section (File 3) and angular distribution (File 4) in ENDF / B format and EXFOR data.

Code System for Intercomparison(Liu Tingjin and Sun Zhengjun)

This code system can automatically retrieve the evaluated data and EXFOR data and plot out the figure of comparison among several evaluated data and measured one in batches. This code system can deal with the comparison of cross section, DA, DE and DDX.

EXFOR Library and Related Software(Liang Qichang et al)

To make the evaluation more convenient, the EXFOR data library has been installed in hard–disk of CNDC Vax–II computer. Related storage and retrieval system are replanted and provided to users.

VII, Chinese Evaluated Nuclear Parameters Library(CENPL)(Su Zhongdi et al.)

To provide evaluators input data for nuclear data calculation and make evaluation more convenient the CENPL has been established. Of course, the CENPL will be also valuable for fundamental research of nuclear physics and other scientifical fields.

The CENPL consists of two parts, data files and management–retrieval code system. The data files store evaluated nuclear basic constants and model parameters in certain format and the management–retrieval code system can retrieve, print out or plot the parameters user interested.

The CENPL–1 contains six sub–libraries:

MCC Sub–Library: Atomic masses and characteristic constants for nuclear ground states;

DLS Sub–Library: Discrete level schemes and branch ratios of γ decay;

LDL Sub–Library: Level density parameters;

GDP Sub–Library: Giant dipole resonance parameters for γ–ray strength function;

FBP Sub–Library: Fission barrier parameters;

OMP Sub–Library: Optical model parameters.

Up to now, the data files and management–retrieval code system for six sub–libraries have been established and some of them have been used in evaluation. The next step is to further improve and perfect some of sub–libraries and assemble all sub–libraries in CENPL–1.

A code to transform the parameters in CENPL format into input file of the model theory calculation codes such as UNF, FMT, MUP and FUP is to be developed.

VIII Generation of Multigroup Constant and Benchmark Testing

1, NSLINK Installed and PASC–1 Modified(Liu Guisheng et al.)

The code system NSLINK for multigroup constant generation, developed by Delft University and obtained from NEA Data Bank, has been installed on a working station at CIAE. And some modules of PASC–1 have been modified to enable it to calculate reaction rates. The Multigroup library by NSLINK is suitable for both fast and thermal reactor calculating.

2, 69 Group Library and Thermal Reactor Benchmark Testing(Liu Guisheng et al.)

Using NSLINK system, AMPX master library in WIMS 69 group structure are made from microscopic evaluated data selected from CENDL–2, ENDF / B6, JENDL–3 and JEF–1. Some integral quantities of 10 thermal reactor benchmark assemblies recommended by the U.S. CSEWG are calculated by using modified PASC–1 code system. 3, Fast Reactor Multigroup Constant Library CL50G(Liu Guisheng et al.)

The CL50G is an adjusted library on L50G library which is generated by NJOY–89.31 from ENDF / B6 and JEF–1. The CL50G includes 53 nuclides and will be used in fast reactor design calculation. It has same energy structure as those of LIB–IV. To make sure that the multigroup library adjustment is reasonable and acceptable, the adjustments were made within the range given by the differences among CENDL–2, ENDF / B6, JENDL–3 and JEF–1.

IX. Concluding Remarks

To further improve CENDL–2, the feedback information from benchmark testing would be very necessary. The overall benchmark calculations to CENDL–2 will be carried out after the complements finished.

References

(1) . Chinese Nuclear Data Center, "The Chinese Evaluated Nuclear Data Library for Neutron Reaction Data", IAEA / NDS–61,

Rev.1, 1992
〔2〕. Zhang Jingshang, "UNF Program of Fast Neutron Data Calculation", Communication of Nuclear Data Progress, No.7, p.14, 1992
〔3〕. H.Vonach, "Direct Covariance Data for Coupled Energy－Angle Distribution", IAEA Specialists' Meeting on Covariance Evaluation", Oak Ridge, Oct., 1992
〔4〕. Cai Dunjiu et al., "Progress of Nuclear Data Work of CNDC", Proc. Conf. on Fast Neutron Physics, Beijing, p.324, 1991

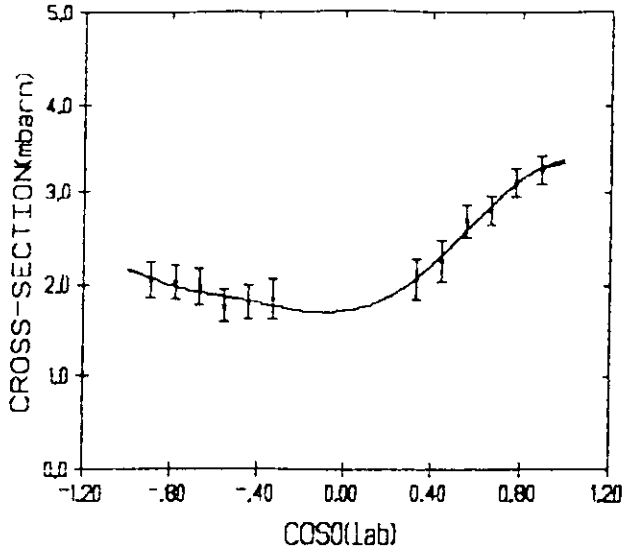

Fig. 1 Angular distribution of alpha from 58-Ni(n,a) reaction

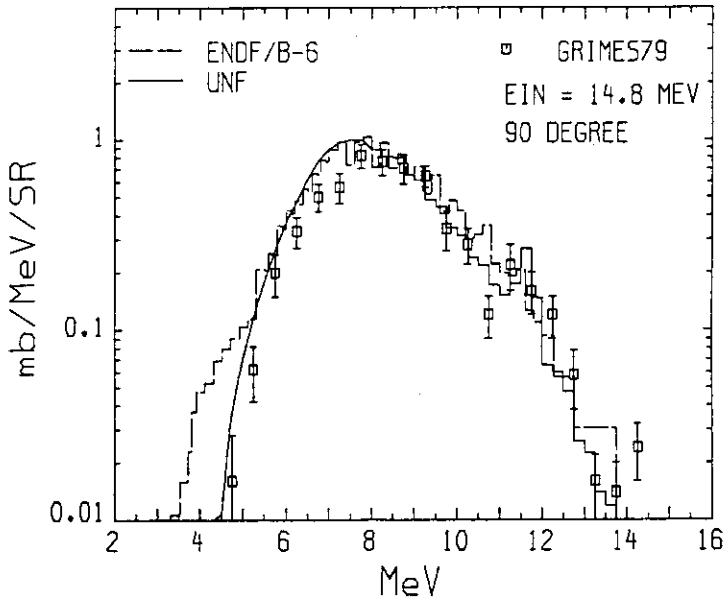

Fig. 2 FE-56 (n,x) a spectrum in LAB system

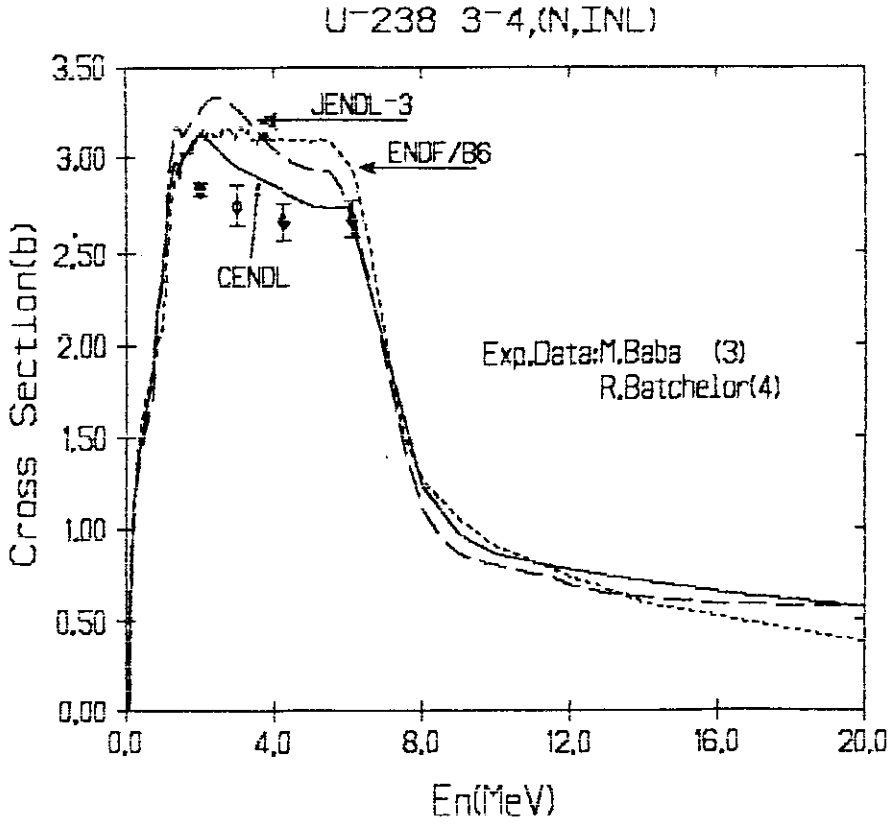

Fig. 3 Total inelastic cross section neutron induced on 238-U

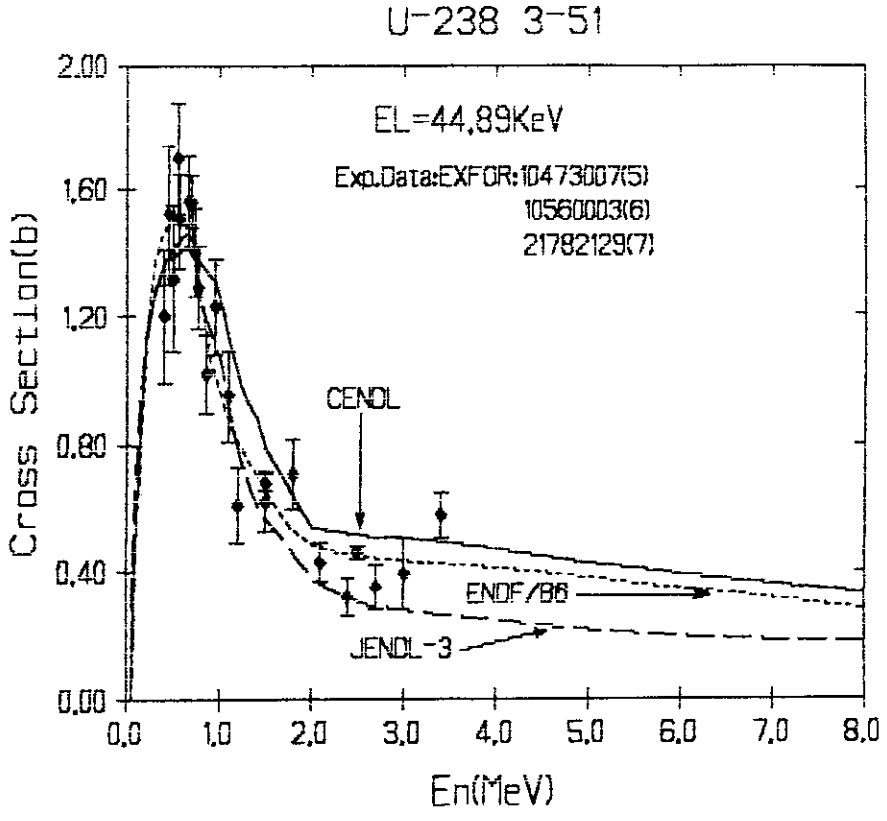

Fig. 4 Neutron inelastic cross section of first level on 238-U

2.1.5 Status Report EFF/EAF Projects

- European Fusion and Activation File Projects -

H. Gruppelaar and J. Kopecky

Netherlands Energy Research Foundation ECN-Nuclear Energy,
P.O. Box 1, 1755 ZG Petten, The Netherlands

The EFF and EAF projects are joint projects of European laboratories, partly sponsored by the Fusion Technology Programme of the European Community (EC). In addition various European laboratories contribute on a voluntary base. The structure of this collaboration is shown in Appendices 1 and 2 for the present three years period of 1992-1994.

1. EFF-1

The EFF-1 data file is used by the NET-team at Garching and by European users. It does not only consist of a basic data file, but it has been distributed as a complete user-oriented package with neutron-photon coupled multigroup cross sections in VITAMIN-J structure, a consistent MCNP library, a multigroup response function library and a multigroup covariance library. Benchmarking indicates that this package gives rather good overall results for fusion reactor design calculations. The full file package is offered to be used by the ITER design team.

2. EFF-2

The EFF-2 basic data file has essentially been completed and preliminary benchmarking has been performed on shielding and neutron multiplication problems. It consists of materials of interest for fusion neutronics design calculations with special EC evaluations for Li-7, Be-9, Al, Si, the major isotopes of Fe, Cr and Ni, the Mo isotopes and natural Pb. Other materials have been taken from various evaluations with minor updates. The same complete package of derived data files is being made for EFF-2 as for EFF-1. The coupled neutron-photon multigroup library is almost ready, but some additional work is needed on the response library and the covariance library. The entire package, with the exception of the Monte Carlo library, is expected to be available by the end of this year for a second phase of benchmarking. The MCNP library is ready for most minor materials, but waits for recent updates of NJOY and MCNP to be completed for the major materials. Benchmarking of existing shielding experiments with a high "representativity" for the NET design has been performed and results are being combined to indicate "trends" in nuclear data. This feedback will be considered in more detail next year as well as the results of two EC benchmark experiments performed at Dresden and Frascati on streaming and bulk shielding, respectively. The EFF-2 file package, probably with the exception of the Monte Carlo library, is scheduled to be available for the European Fusion Programme and the ITER project, by the end of this year. A benchmarked version with the Monte Carlo library

will be issued later in 1994.

3. EAF

The current version of the European Activation File is version EAF-3.1. It is designed for activation, transmutation and gas-production calculations and contains a huge set of reactions. It is applied for the development of low-activation materials (LAM), but can also be used for short-lived decay product calculations and decay heat evaluation. The file has been coupled to the FISPACT inventory code which contains additional libraries for decay and other required data. The combined package, called EASY, is a very valuable product for fusion-reactor design calculations. The EAF-3.1 version is also equipped with an uncertainty file for all reactions and the inventory code can actually calculate uncertainty margins in decay curves as a function of time. At present quality improvements are made to achieve a new version (EAF-4) to be completed at the beginning of 1994.

4. Future plans

The main objective of the **EFF-2** programme for 1994 is to bring the file to the user, together with results of benchmarking. Some minor corrections may be introduced as result of user feedback. Furthermore, an important new development is a further update of Fe, using the very accurate re-evaluation of IRK-Vienna, combined with recently calculated DDX data by ENEA-Bologna and results of high-resolution data in the unresolved resonance range by IRM-Geel/KfK. This and other re-evaluations will be included in the future EFF-3 data file.
For the **EAF** file further quality improvement on data and uncertainty file is planned during this year and 1994. Also the energy-dependence of the isomeric ratio will be taken into account in much more detail.

5. Cooperation with JEF, NEA-NSC

The intensive cooperation between the EFF and JEF projects may lead to merging the two files into a single "JEFF" data file. Proposals for this are being considered by the EFF and JEF parties at present. Further benefit of NEA projects is obtained by means of active participation in the Nuclear Science Committee and the Evaluation Coordination Working Party.

6. Orientation towards ITER needs

Recently the ITER team has expressed increased interest in nuclear data for design calculations and has requested additional data as compared to those resulting from the European NET programme. This naturally has lead to a further orientation towards the ITER project. Thus, the EFF basic programme will be adjusted. Apart from **Fe**, **Cr** and **Ni**, which should revive in the ITER context as constituents of the austenitic steel (reference structural material), **V** and **Ti** will be of importance for the advanced blanket (V-5Ti-5Cr alloy as structural material), **Cu** this time as First Wall material for the reference shield and as divertor material, **Mn**, **Ta** and **W** in addition to V as alloying

elements for a reduced activation ferritic/martensitic steel, which is still recommended as a possible alternative for vanadium alloy. If the so-called convertible blankets should remain of interest for ITER, **Na** and **K** are significant if a Li blanket is first operated with NaK, or **Mg** or **Bi** are important in context with the eutectic fluids Pb-Mg or Pb-Bi for a blanket which is later operated with Pb-Li. Hence further improvements for V, Ti, Cu, Mn, Ta, W, Na, K, Mg, and Bi should be considered, taking into account the specific applications for ITER. It is noted that some of these materials the present data files are insufficient.

Also the work on the EAF data file and the corresponding inventory code will be further tuned to ITER needs. In particular the application of the EASY system for decay heat evaluation will be stressed. To this end the next meeting of the EFF-project in December 6-8, 1993, will be organized at Garching to include further discussions with the ITER design team and a proposal for a long-range programme will be made. The existing infrastructure of the European EFF/EAF projects, including capabilities for differential measurements, evaluation, processing, benchmark experiments, analysis and applications will be offered to reach the ITER and European requests for nuclear data and neutronics tools.

7. Cooperation with FENDL

The ITER preference for a "reference" file for fusion design calculations may favour IAEA's FENDL-1 selection of evaluated data as an initial data file. Europe has contributed to this IAEA activity, but has meanwhile developed its own data files in the framework of the EFF and EAF projects. On the short range EC's data and neutronics infrastructure could be mobilized to contribute to processing and benchmarkig of FENDL. Furthermore, the full EFF-1 package is offered to ITER as a back-up solution as long as FENDL-1 derived data files are not ready for distribution. Likewise, the very complete EAF and FISPACT packages (EASY system) are offered as complete and immediate solutions for a reference activation file. On a longer time schedule continued participation in the FENDL-2 updating project from the side of the EFF and EAF projects is foreseen. However, an important condition for a suitable EC contribution is that from the ITER side there is a strong need for data improvements and consequently this item is kept in their long term programme. This would greatly facilitate the EC to accept suitable evaluation tasks for new materials proposed by the ITER team.

Appendix 1

EUROPEAN FUSION (NET) PROJECT

(short term)

1992 - 1994

NDB1 NEUTRONICS DATA BASE － EFF DEVELOPMENT

NDB1-1	ECN	. EFF File management
NDB1-2	ECN	. Improvements of processing with NJOY
NDB1-3	ENEA	. Generation of working libraries
NDB1-4	ECN	. Kerma Uncertainty Assessment
NDB1-5	CEA	. Analysis of shielding benchmarks
NDB1-6	KfK	. Cross-section improvement below 1 MeV
NDB1-7	ENEA	. Cross-section improvement in the high energy range

NDB2 NEUTRONICS DATA BASE － BENCHMARK ECPERIMENTS

NDB2-1	CEA	. Bulk shield experiments
NDB2-1	ENEA	. Bulk shield experiments
NDB2-2	KfK	. Shield penetration experiments

NET CONTRACTS

IRK Vienna	. Uncertainties for structural materials
	. Re-evaluation of Fe-56

CROSS SECTION MEASUREMENTS

IRMM Geel	. High resolution Fe-56 data
	. High resolution Ni-58,60 data

Appendix 2

EUROPEAN FUSION (LAM) PROJECT

(long term)

1992 - 1994

LAM2 CROSS SECTION DATA BASE - (EAF DEVELOPMENT)

LAM2-1 ECN
- Generation of EAF File
- File management

LAM1-2 KfK
- Generation of sequential reactions data files
- File management

ACTIVATION CODE SYSTEMS (EASY DEVELOPMENT)*

AEA Harwell (Culham)
- FISPACT code developments
- EASY system management

* Partially supported by LAM project

2.1.6 The ITER Blanket and Shield Design Status as of September 1993

Y. Gohar
Group Leader
Blanket and Shield Group
ITER Joint Central Team
Garching Joint Work Site

Symposium on Nuclear Data 1993
November 18-19, 1993
JAERI, Japan

ITER
First Wall, Blanket, and Shield Design

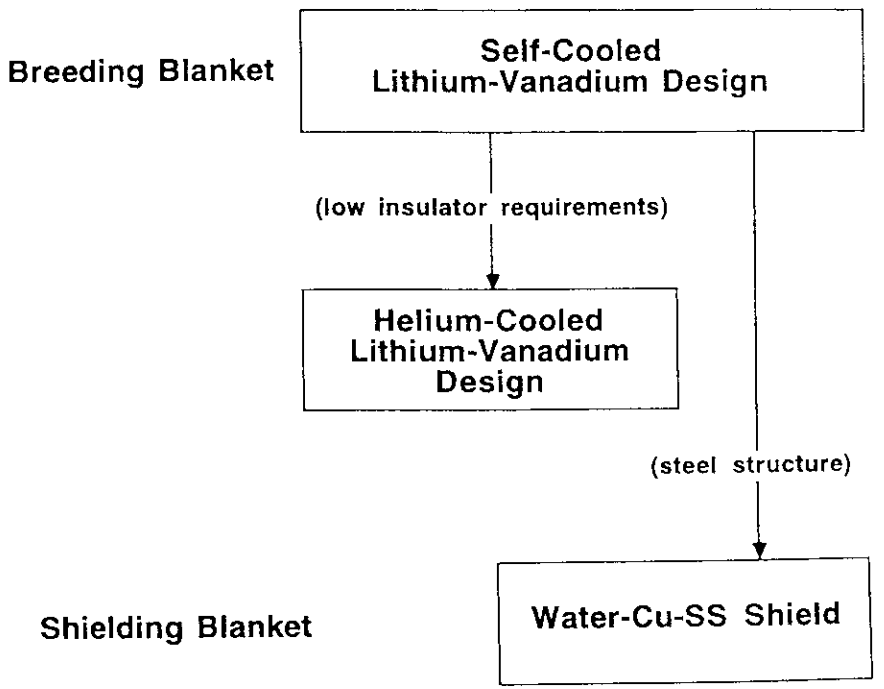

yg/Japan/09-93/01

First Wall, Blanket, and Shield
Current Design Basis

- Hot first wall during operation and between pulses, first wall temperature above 200°C between pulses.
- Low pressure system of about 1 MPa for the blanket structure.
- Electrical insulator to reduce MHD pressure drop and electromagnetic loads during plasma disruption events.
- First wall, blanket, and shield integrated into single unit.
- First wall, blanket, and shield service and maintenance from the top.
- Design for double the normal operating power of ~1 MW/m^2 average neutron wall load, if possible, and total neutron fluence of 3 $MW \cdot y/m^2$.
- Operate in both phases without hardware changes.
- Maximum radial temperature variation of <100°C in the first wall, blanket, and shield structural material.
- Reactor relevant wherever possible.
- Simple and reliable design.

yg/Japan/09-93/09

Main Features of First Wall, Blanket, and Shield

- Advanced Blanket Design

  - Self-Cooled Lithium-Vanadium Design with Electrical Insulators

    - Accommodates 3 GW "high performance" operation
    - Wide design margin for 1.5 "nominal" operation
    - Low activation materials
    - Low decay heat
    - Tritium self-sufficiency
    - Radiation resistance
    - High temperature capability
    - Low pressure system
    - Reactor relevant

    - Require intensive R&D program for development of vanadium structure and electrical insulator materials

  - Helium-Cooled Lithium-Vanadium Design

    - Lower sensitivity to the electrical insulator performance

    - High Pressure coolant tubes

- Water-Copper-Steel Shield

    - Less R&D than for blanket
    - Higher design margin for FW heat flux

    - Very little relevance for DEMO
    - Cost, availability, and transportation of tritium become issues for testing program
    - No tritium breeding
    - High activation and decay heat
    - Large volume of radioactive waste

yg/Japan/09-93/10

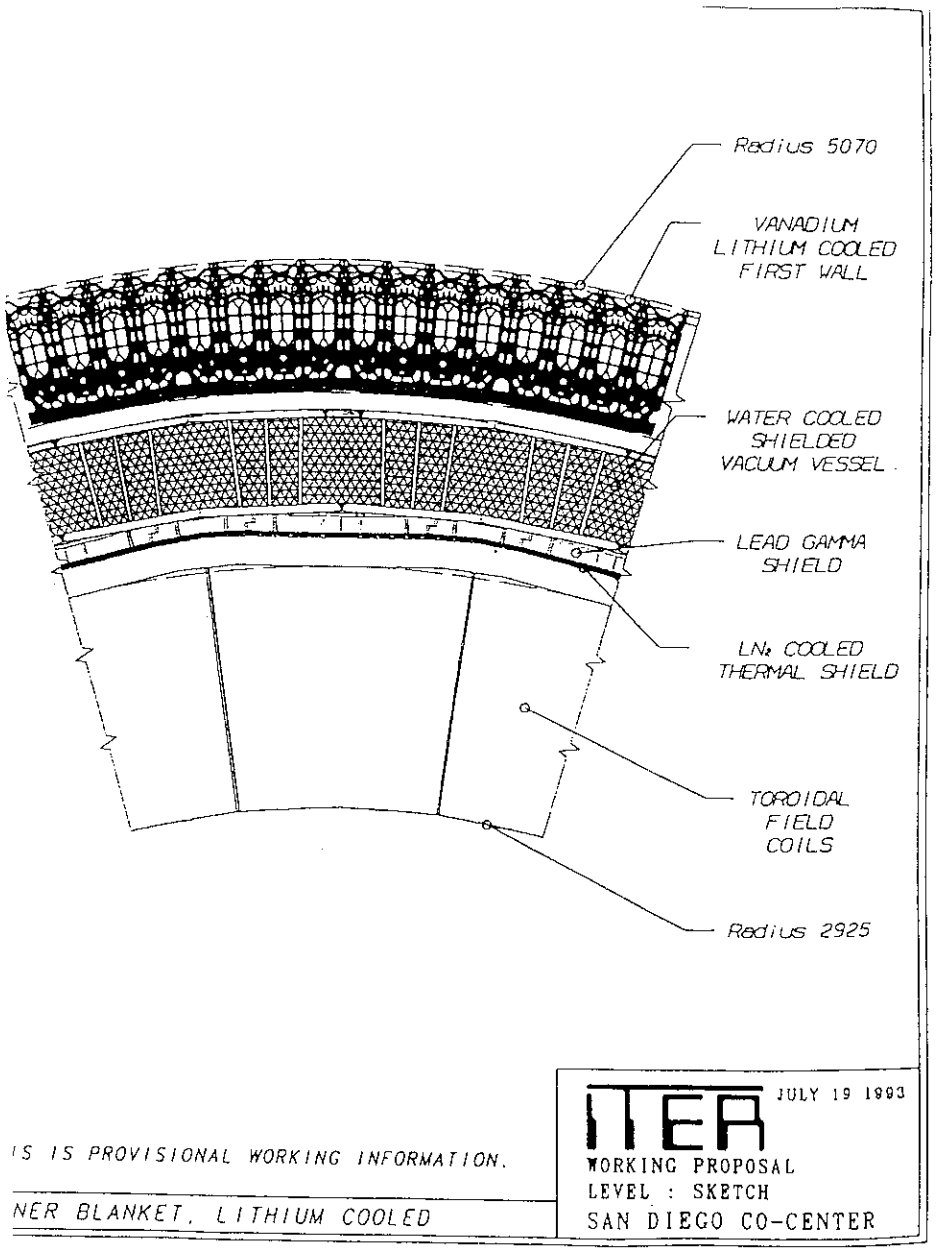

POLOIDAL FLOW CONCEPT

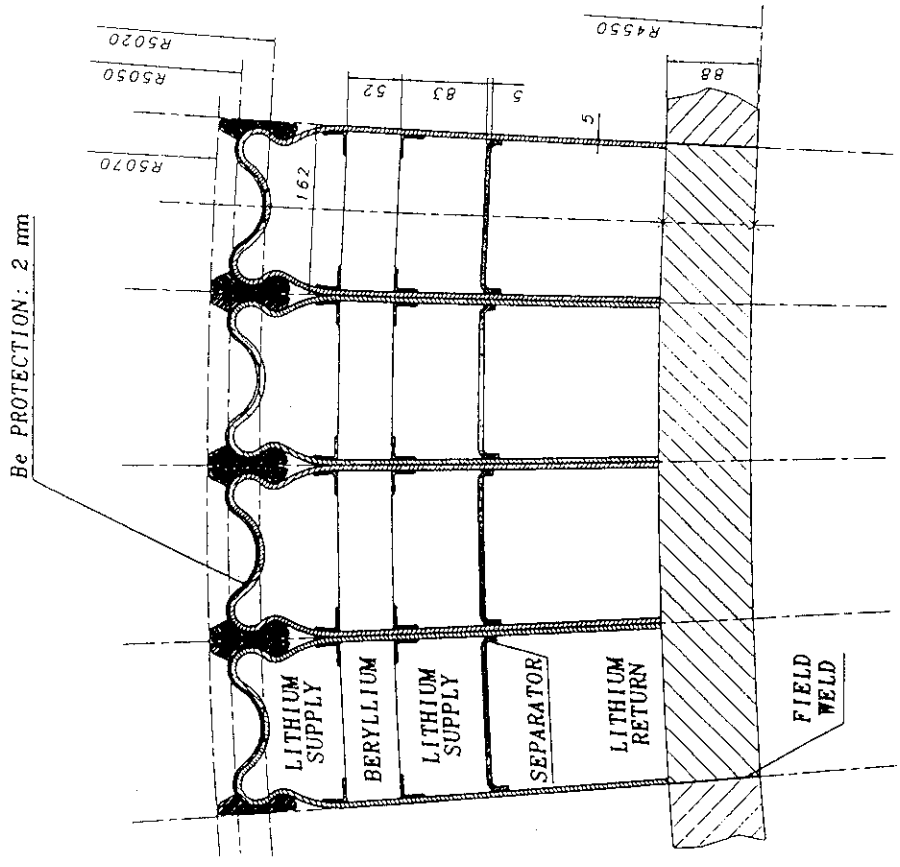

FIG: 1a

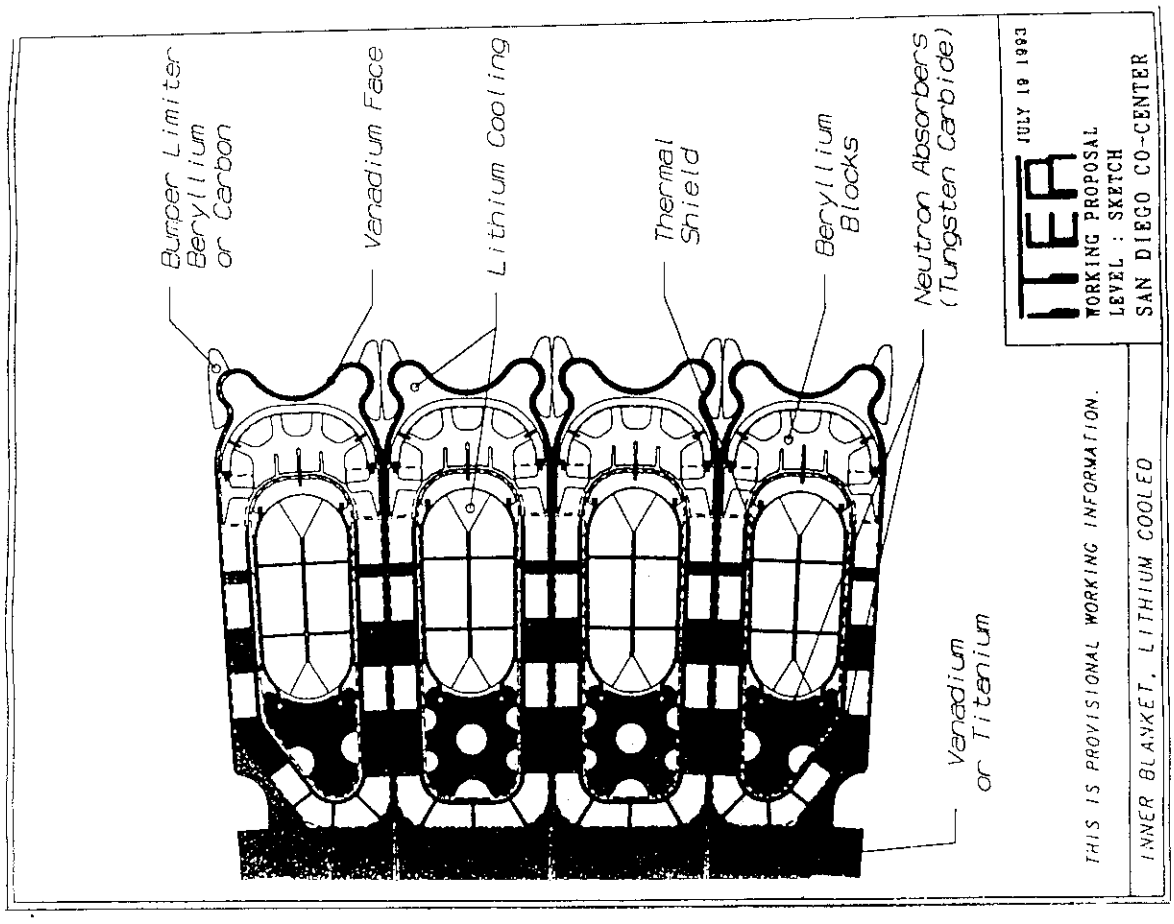

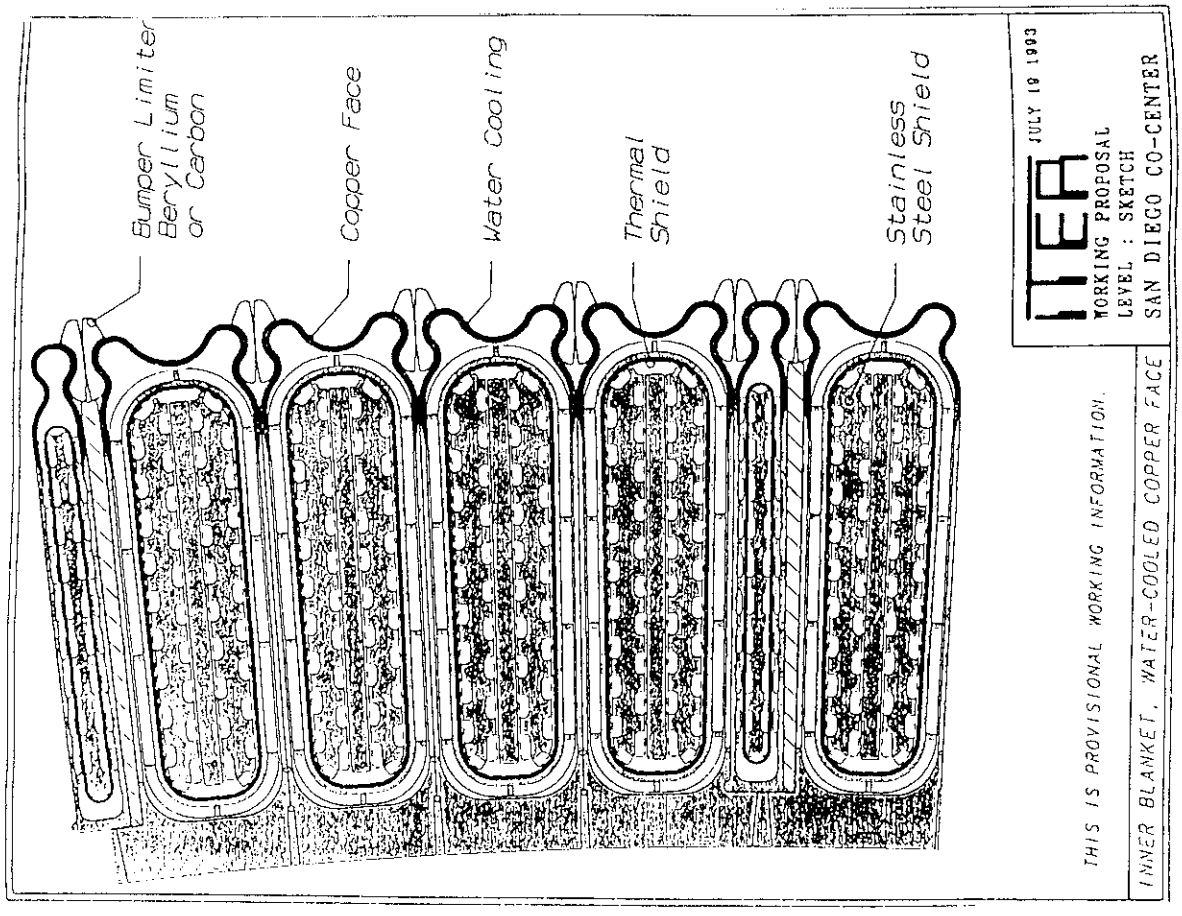
Bumper Limiter
Beryllium
or Carbon
Copper Face
Water Cooling
Thermal
Shield
Stainless
Steel Shield
ITER
JULY 19 1993
WORKING PROPOSAL
LEVEL : SKETCH
SAN DIEGO CO-CENTER
THIS IS PROVISIONAL WORKING INFORMATION.
INNER BLANKET, WATER-COOLED COPPER FACE

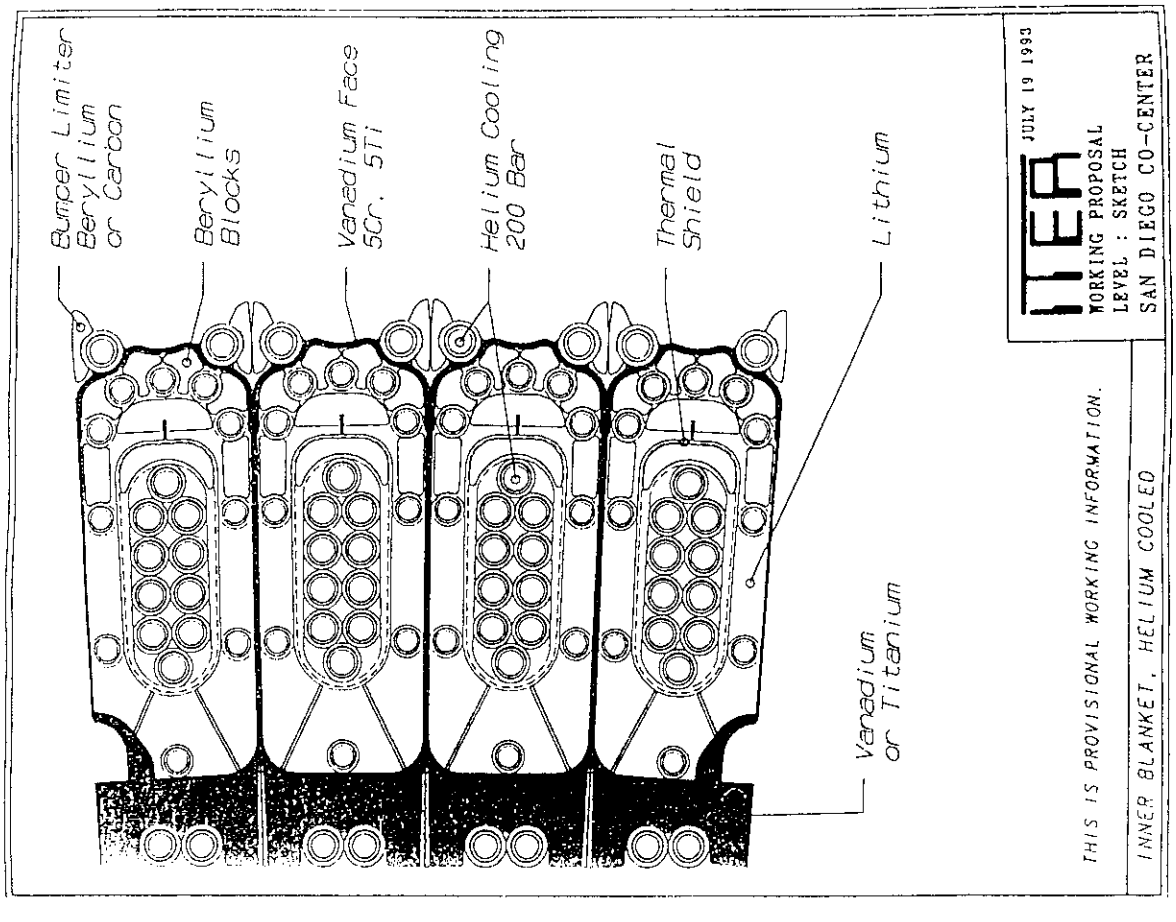
Bumper Limiter
Beryllium
or Carbon
Beryllium
Blocks
Vanadium Face
5Cr. 5Ti
Helium Cooling
200 Bar
Thermal
Shield
Lithium
Vanadium
or Titanium
ITER
JULY 19 1993
WORKING PROPOSAL
LEVEL : SKETCH
SAN DIEGO CO-CENTER
THIS IS PROVISIONAL WORKING INFORMATION.
INNER BLANKET, HELIUM COOLED

Requirements and Cost of Tritium Based on 1 GW of Fusion Power for Different Fluence Goals and Breeding Potential.

Tritium Breeding Ratio	Purchased as Required 3 MW•a/m^2 Kg	B$	Purchased as Required 1 MW•a/m^2 Kg	B$	Fixed Supply Rates with 20 Kg Initial Inventory 3 MW•a/m^2 Kg	B$	Fixed Supply Rates with 20 Kg Initial Inventory 1 MW•a/m^2 Kg	B$
0.0	180	5.74	68	2.16	202	6.44	78	2.49
0.5	96	3.05	40	1.26	109	3.48	47	1.50
0.6	79	2.52	34	1.09	90	2.89	41	1.31
0.7	62	1.98	28	0.91	72	2.29	35	1.11
0.8	45	1.44	23	0.73	53	1.70	29	0.91
0.9	28	0.91	17	0.55	35	1.11	22	0.71

- Operating scenario of 0.05 MW.a/m^2 physics phase over four years, and nuclear testing phase over ten years.
- A breeding blanket will be installed after the physics phase.
- A tritium inventory of about 5 Kg.
- The tritium cost is based on the U.S. Department of Energy unit cost of $31,900 a gram.

yg/Japan/09-93/03

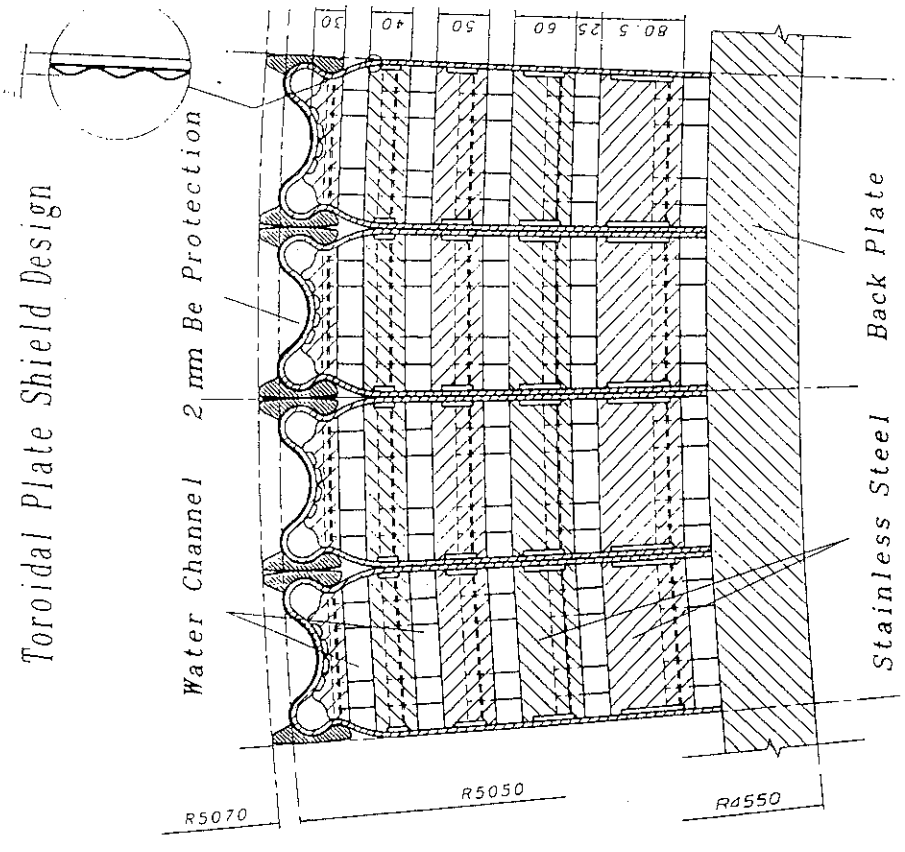

Thermal-Hydraulic Analysis of the Self-Cooled Inboard Blanket for 3 GW Fusion power

Machine Parameters

Structural material	Vanadium Alloy
Coolant	Li
Average neutron wall loading, MW/m^2	2.0
Average surface heat flux, MW/m^2	0.4
Inlet coolant temperature, °C	250
Peak wall temperature, °C	<500
Total pressure drop, MPa	<1.0
FW thickness, m	0.005
Radial depth for front (supply) ducts, m	0.16
Radial depth for back (return) ducts, m	0.16
Poloidal length, m	12.5
Toroidal field, T	12.0

Thermal Hydraulics Parameters

Inlet temperature, °C	250
Exit temperature, °C	305
Peak first wall temperature, °C	484
Average lithium temperature at bottom (U bend), °C	290
Average flow velocity, m/s	2.0
Volumetric flow rate, m^3/s	8.75
Mass flow rate, kg/s	4421
Total pressure drop, MPa	0.61
Pumping Power, MW	5.3

Thermal-Hydraulic Parameters of the Helium-Cooled Design

Fusion Power	3 GW
Total Power to Blanket/FW Coolant	3.9 GW
Peak Neutron Wall Loading at Outboard	2.78 MW/m^2
First Wall and Bumper Limiter Surface Heat Flux	0.4, 0.5 W/m^2
Helium Coolant:	
One-Way Flow Area (based on 624 segments)	2.25 m^2
Inlet Pressure	200 bar
Inlet Temperature	200 C
Temperature Rise	150, 200, 250 C
Average Volumetric Heat Generation:	
Be (limiter)	19.5 MW/m^3
Be (Blanket)	16.7 MW/m^3
Lithium	26.4 MW/m^3
Vanadium	22.1 MW/m^3
Thermal Conductivity (500 C):	
Be	109 W/m-K
Vanadium alloy	28 W/m-K
Lithium	46 W/m-K
Sodium	88 W/m-K

Thermal-Hydraulics Parameters for Different Outlet Helium Temperatures

He Temperature Rise (°C)	150	200	250
He Mass Flow Rate (kg/s)	5021	3766	3013
He Velocity (m/s) (based on average He temp.)	126	99	82
Re for d = 22 mm	1.6×10^6	1.2×10^6	9.5×10^5
h (W/m^2-K) for d = 22 mm	1.7×10^4	1.38×10^4	1.15×10^4
DP (in-reactor) (MPa)	2.8	1.6	1.1
Pumping Power (MW)	755	327	183
Estimated He Temperature at Maximum Neutron Wall Load Location (°C)	250	267	283
Maximum Limiter Be Temperature for Different Surface Heat Fluxes:			
q" = 0.4 MW/m^2	724	750	775
q" = 0.5 MW/m^2	800	827	853
Maximum Vanadium Temperature for Different Surface Heat Fluxes:			
q" = 0.4 MW/m^2	651	677	703
q" = 0.5 MW/m^2	715	742	768

Liquid Metal Coolant Assessment for ITER

Coolant Assessed:

Na, NaK, K, Ga, Pb, BiPb, Li, 17Li83Pb

Advantages:

- Low pressure system
- High temperature capability
- Simple first wall, blanket, and shield design
- Lithium provides the cooling and the tritium breeding functions
- Low tritium inventory system
- Lithium is low activation material
- Lithium reduces the structural material decay heat
- Good capability to accommodate power excursion
- Reactor relevant system
- Lithium system does not require external tritium supply with natural lithium

Disadvantages:

- Requires electrical insulator to reduce MHD pressure drop
- Activated coolant except for lithium
- Melting point above room temperature except for NaK (-12°C)
- Safety concern related to reactivity with air and water

Concerns:

- Lifetime insulator performance

yg/Japan/09-93/16

Liquid Metal Electrical Insulators

- **Thin insulator coating (1-10 μm) on the coolant channel walls.**
- **Coating technology for the candidate structural materials based on aluminized layer is well established and can be applied to large/complex shapes.**
- **AlN or Al_2O_3 formed on the surface provides adequate electrical insulation.**
- **This technology Al_2O_3 has already been successfully used as an in-reactor tritium barrier.**

yg/Japan/09-93/29

Aluminized Coatings On Structural Materials

Fabrication Procedures

- Hot-dip aluminizing process (used in the industry to coat steel with an aluminium layer (used by KFK for vanadium and vanadium alloys)
- Chemical diffusion processes (used in the chemical industry)
- In-situ formation in liquid lithium containing dissolved aluminium (developed by ANL)
- The first two procedures can be used to install the aluminized layer at the start. The last procedure can be used for self-healing or repairing the insulator coating.
- Subsequently the aluminized layer is converted to oxide or nitride using gas, chemical process, or flowing liquid metal.

Lithium vanadium Corrosion and Compatibility Issues

- Corrosion rate from the forced circulation loop is ~ 0.1 μm/y, which is negligible.
- Oxygen concentration in cold trapped lithium is ~ 100 wppm.

-Oxides of V, Ti, Cr, Nb, Al, and Zr are not thermodynamically stable at this level for the temperature range of 200 - 700 °C.

- Nitrogen solubility in cold trapped lithium is ~ 4000 wppm

-Controlling the nitrogen concentration in lithium to 100-300 wppm, the nitrogen activity will be low enough that Cr- nitrides will not be formed.

-At such level AlN and TiN will be stable.

- Carbon solubility in cold trapped lithium is ~ 200 wppm. Hot trapping can be used to control the carbon concentration to lower levels.
- Hydrogen concentration will be controlled to the level of 1 wppm to reduce the tritium inventory. This concentration level does not effect the vanadium alloy.

Water Coolant Assessment for ITER

Advantages:

- **Good data base**
- **Low activation material**
- **Good shielding material**
- **Good capability to accommodate power excursion**
- **Natural convection improve blanket performance during LOFA and LOPA accidents**

Disadvantages:

- **Require high pressure system for the current first wall temperature requirements**
- **Aqueous stress corrosion is a problem for coolant temperature above 150°C**
- **Constrain the chemistry of the structural material**
- **Safety concern related to water interaction with PFC material**

yg/Japan/09-93/23

Helium Coolant Assessment for ITER

Advantages:

- Good safety features
- Low activation
- Easy to clean
- Reactor relevant system if used with solid breeder material

Disadvantages:

- High helium pressure (>50 atm) is required to reduce the cross-sectional flow area and pumping power
- Helium requires high temperature limit for the structural material (~650°C) - thermal stress problem
- Extra shielding thickness (25 cm) is required to protect the TF coils
- No design margin to accommodate power excursion
- Poor performance during LOFA, LOCA, and LOPA accidents
- High pumping power
- An order of magnitude increase in the size of the heat exchanger

Concerns:

- Helium leakage through micro-cracks developed during operation may destroy the required vacuum boundary

yg/Japan/09-93/11

Structural Material Assessment

- Vanadium alloys (V5Cr5Ti)
- Austenitic stainless steels (316 SS)
- Ferritic stainless steels (HT9)

yg/Japan/09-93/14

JAERI—M 94—019

Austenitic Stainless Steel

Advantages

- Well established fabrication technology
- Most extensive radiation database
- Compatibility with non-water coolants and breeding materials to 500°C

Design Issues

- Limited capability to accommodate high surface heat loads
  - Compositional variations to improve strength
  - Use of cold-worked material with higher strength
- Radiation-induced embrittlement
  - Significant embrittlement observed at 7-8 dpa
  - Embrittlement is highly temperature dependent
  - Most severe from 200-350°C
  - Exacerbated by H and He
  - Preferred operating temperatures RT-150°C or 400-550°C
- Radiation-induced swelling
  - High temperature dependent
  - Sensitive to He/dpa ratio
  - Negligible below 300°C
  - Significant above 400°C at modest fluences
  - Major concern is differential swelling in 400-500°C range
- Aqueous stress corrosion
  - Concern even at low fluences
  - Sensitive to stress (cyclic) and water chemistry (radiolysis)
  - Effect of hydrogen at higher fluences
  - Effect of weldments and crevices
  - Greater resistance to SCC at <150°C

yg/Japan/09-93/15

Ferritic Stainless Steels

- **Advantages**
  - **Established fabrication base**
  - **Resistance to radiation swelling**
  - **Improved surface heat load capability compared to austenitic stainless steel**
  - **Compatibility with coolants to 500°C**
- **Design Issues**
  - **Influence on magnetic field distribution**
    - Uncertainties in effects and requirements
  - **Need for post weld heat treatment**
    - At T ~ 700°C
    - Requires T and time control
  - **Irradiation induced embrittlement**
    - Shift in DBTT with irradiation
    - Most severe at 250-350°C (Range of interest for operation)
    - Enhanced DBTT shift with high He
    - Commercial alloys exhibit larger shifts
    - Limited data on modified compositions
  - **Insulator coating development**
    - Should be able to use same methods as for SS

Vanadium Alloys (V5Cr5Ti)

Advantages

. High heat flux capability
. High temperature capability
. Good mechanical properties at high temperatures
. Radiation resistance (low swelling, high ductility, low gas production)
. Good compatibility with liquid lithium
. Low nuclear heating rate
. Good activation characteristics (low activation and low decay heat)

Design Issues

. Design data base
. Fabrication technology
. R&D and material costs

yg/Japan/09-93/14

Conclusions

- Both blanket and shield designs having design margins for nominal fusion power of 1.5 GW and up to 3.0 GW are being developed.

- For the blanket, a vanadium first-wall and structure cooled by lithium is the baseline option. A helium-cooled variant is being carried as a back up. In a non-breeding phase, the lithium would be replaced by another liquid metal such as NaK.

- For the shield, the baseline option is similar to the blanket option. However, low temperature water is used as coolant, vanadium is replaced by stainless steel for most of the structure, and copper alloy is used for the first wall.

- With an aggressive and focused R&D program, the self-cooled vanadium blanket can be qualified within the EDA time-frame.

JAERI—M 94—019

2.1.7 Status of the International Fusion Evaluated Nuclear Data Library (FENDL)

A.B. Pashchenko and S. Ganesan
Nuclear Data Section
Division of Physical and Chemical Sciences
International Atomic Energy Agency (IAEA)
P.O. Box 100, A-1400 Vienna, Austria/Europe

This paper briefly describes status, plans and international co-operation in the preparation of the Fusion Evaluated Nuclear Data Library (FENDL). The ultimate aim of this international project is to establish a comprehensive set of evaluated nuclear data libraries covering the necessary nuclear input data for all physics and engineering aspects of the material development, design, operation and safety of current and future fusion reactor projects, with a particular emphasis on fulfilling the requirements of the ITER project in its current engineering design activities (EDA) phase.

1. INTRODUCTION AND BACKGROUND

Following the recommendation of the International Nuclear Data Committee (INDC), an advisory body for the nuclear data programme of the IAEA, the Nuclear Data Section (NDS), in co-operation with several national nuclear data centres and research groups, is creating an internationally available Fusion Evaluated Nuclear Data Library (FENDL), which will serve as a comprehensive source of processed and tested nuclear data tailored to the requirements of the Engineering Development Activities (EDA) of the International Thermonuclear Experimental Reactor (ITER) Project and other fusion reactor development projects. This activity, known as the FENDL project, is supported by several IAEA Coordinated Research Programs. A series of international meetings in 1986, 1987, 1989, 1990, 1991, 1992 and 1993 and projected to continue with about the same frequency in the next few years, has been organized by the International Atomic Energy Agency with the goal of assembling, processing and testing a comprehensive, fusion-relevant nuclear data base with unrestricted international distribution [Refs. 1-8]. The fusion data experts at these meetings have addressed in detail

(a) the nuclear data requirements and status of available nuclear data for integral calculations for blanket, shielding, and activation problems in fusion reactors;

(b) status of differential data, theory and possibilities to meet data needs;

(c) the creation of an international fusion nuclear data file; and

(d) IAEA sponsored international comparison of benchmark measurements and calculations on the subject of fusion neutronics and activation.

The current version of the evaluated data file, FENDL-1, was released in 1993 and preparations are being made to process it with the latest version of the NJOY code. The file is divided into four parts: general purpose evaluations (65 isotopes and elements); activation cross sections and decay data (approximately 636 targets and 11,000 reactions); charged-particle fusion reactions; and dosimetry reactions. Following processing, the FENDL-1 data base will be tested against benchmark experiments.

Evaluation in the next version of the file, FENDL-2, will include improvements suggested from the benchmark calculations, as well as additional and improved evaluations from various research activities in several countries over the next 2-3 years.

This paper describes the international co-operation leading to the establishment of the FENDL data base, the present composition of FENDL-1 and plans for future development.

2. INTERNATIONAL COOPERATION AND SELECTION OF EVALUATED DATA

The recommendations of the INDC were implemented by IAEA/NDS with a series of meetings with the following tasks and achievements:

(1) IAEA Advisory Group Meeting on "Nuclear Data for Fusion Reactor Technology", Gaussig, (former) German Democratic Republic, December 1986 [Ref. 1]:

- achieved a review of the changes in nuclear data requirements for fusion reactor technology since the last IAEA Advisory Group Meeting on Nuclear Data for Fusion in 1978;
- identified the experimental and theoretical research required to satisfy the current and foreseeable needs; and
- developed the ground rules for the creation of an international nuclear data library for fusion reactor neutronics calculations for specific use in the design of the International Thermonuclear Experimental Reactor (ITER) project.

(2) IAEA Specialists' Meeting on the Fusion Evaluated Nuclear Data Library Related to the ITER Activity, Vienna, Austria, November 1987 [Ref. 2]:

- specified the procedures for the assembly of the global FENDL library;
- selected a preliminary list of evaluations for individual elements and isotopes to be included in this library;
- identified special purpose files of activation, dosimetry reaction, charged-particle and photon interaction data to be added to the global library; and
- developed a programme on benchmark calculations for nuclear data testing starting with the Dresden Pb sphere measurements.

(3) IAEA Specialists' Meeting on the Fusion Evaluated Nuclear Data Library (FENDL), Vienna Austria, May 1989 [Ref. 3]:

- analysed the differences in neutron reaction cross sections between some major evaluated nuclear data files for several of the main fusion reactor materials in comparison with the international experimental data file EXFOR and, based on the results of this analysis, identified definitely the evaluations to be included in the first version of FENDL, FENDL-1;
- set up a first list of more than 200 important activation reactions to be included in the activation sublibrary of FENDL-1 and initiated a first international intercomparison of activation cross sections;
- developed actions for the updating of the IRDF-85 neutron dosimetry file to be included in FENDL-1;
- developed specifications for the creation of pointwise evaluated nuclear data files (PENDF) from FENDL-1 and of neutron and gamma multigroup cross section libraries for use in discrete ordinate codes and of a special library for Monte Carlo codes, starting from PENDF files;
- compared the results of the calculations of the Dresden Pb benchmark and identified further Pb and Be benchmarks and important fusion reactor materials for future integral data testing and verification of neutron transport codes.

(4) IAEA Consultants' Meeting on First Results of FENDL-1 Testing and Start of FENDL-2, Vienna, Austria, June 1990 [Ref.: 4]:

- reviewed the status of the evaluations identified at the previous meeting for inclusion into FENDL-1 for necessary modifications to be made before input to FENDL-2. The complete results of this recommendation are reproduced in Table 1.

- identified 8 additional materials (Na, Mg, P, S, Cl, K, Ca, and Ta) to be added to the FENDL-1 library (these materials are presented in Table 2 along with the sources of new evaluations);
- finalized the selection of more than 300 activation reactions for inclusion in the FENDL-1 activation data sublibrary;
- initiated a second International Fusion Activation Calculation Comparison Study;
- recommended to include in the FENDL-2 activation data sublibrary a decay data library and a complete activation cross section library with at least all targets with half lives > 10 days and all reactions energetically possible for $E_n < 20$ MeV.

(5) IAEA Advisory Group Meeting on Nuclear Data for Neutron Multiplication in Fusion Reactor First-Wall and Blanket Materials, Chengdu, China, November 1990 [Ref.: 5]:

- resolved the previous discrepancies between predictions and measurements of Be multiplication, except for a still unexplained difference of 5 - 10% between recent US and Chinese thick sphere neutron multiplication measurements on Be;
- tentatively attributed the 3 - 5% differences still existing between the latest predictions and best measurements of neutron multiplication in Pb to deficiencies in microscopic nuclear data;
- reviewed in detail the status of nuclear data evaluations, differential data and further requirements for 7Li, Be and Pb;
- recommended that IAEA/NDS collect and distribute a series of documents describing, in a consistent format, high-quality fusion-relevant benchmark experiments;
- strongly recommended the processing and international distribution of the FENDL library to serve as a unique reference data file.

(6) IAEA Advisory Group Meeting on FENDL-2 and Associated Benchmark Calculations, Vienna, Austria, November 1991 [Ref.: 6]:

- recommended to the IAEA to issue FENDL-1 by July 1992 and to make it available to ITER and other fusion reactor projects;
- recognized the inadequacy of FENDL-1 to fulfill all demands of fusion reactor design activities and therefore strongly recommended, after completion of FENDL-1, to continue the FENDL-related activities and establish an improved version of FENDL-1, i. e. FENDL-2;
- showed that, for several materials, new evaluations will become available for consideration for the FENDL-2. These materials are presented in Table 3 along with the sources of new recommendations;
- reviewed the status of neutron and gamma-ray data processing, integral experiments and benchmark calculations for FENDL;
- recommended to adopt the ENDF/B-6 integrated charged particle cross section evaluations for the reactions 2H(d,n)3He, 2H(d,p)3H, 3H(t,2n)4He, 3H(d,n)4He and 3He(d,p)4He included in the Livermore TDF library and the reactions in the Arzamas library involving t+3He and 3He+ 3He for the charged particle sublibrary of FENDL.

The co-ordinated collection, evaluation, intercomparison and testing activities at and between the above-mentioned meetings were supplemented by several co-ordinated research programmes aiming at the improvement of existing and production of new required data.

3. PRESENT COMPOSITION OF FENDL

The FENDL project aims at the development of a set of evaluated nuclear data libraries covering input data to all physics and engineering aspects of the material development, design, operation and safety of current and future fusion reactor projects, with a particular emphasis on the requirements of the ITER

project in its current engineering design activities (EDA) phase. With the welcomed international release of ENDF/B-VI, JENDL-3 and BROND in early 1990, the FENDL project has turned from its earlier emphasis on the review and selection of candidate neutron-interaction evaluations to

(a) processing and testing of cross sections for neutron and gamma-ray transport and
(b) assembling, processing and testing of large special-application files needed to supplement the available files, especially in the field of activation and decay data.

The first version of FENDL, FENDL-1, is composed of the following sublibraries:

(i) a coupled 175 group neutron - 42 group gamma cross section library (VITAMIN-J structure) for neutron and gamma ray transport calculations for 65 elements and isotopes [Ref. 9];

(ii) a 175 group neutron-induced activation cross section library FENDL/GA-1.1 containing 636 stable and unstable target nuclides with half lives > 1/2 day and about 11,000 activation reactions for incident particle energies up to 20 MeV for the computation of radioactivities and estimation of radiation hazards [Ref. 10];

(iii) a sublibrary of charged particle nuclear fusion reaction cross sections for interaction between the D-T plasma constituents p, d, T, 3He and 4He [Ref. 7]; and

(iv) a sublibrary of fusion-relevant neutron dosimetry cross sections [Ref. 11] for the determination of neutron flux energy spectra with the multiple foil activation method.

These sublibraries and the methods for their generation as well as the many problems encountered during the file processing are described in detail in the papers [Refs. 9,10,12] reported at the International Workshop on Nuclear Data for Fusion Reactor Technology held in Del Mar, California, from 3 to 6 May 1993. Therefore, only the most important features of each of these sublibraries are briefly outlined in the following paragraphs.

3.1. Global or multiple purpose file, FENDL/E-1

The first step in the production of the multipurpose file was the intercomparison and selection of suitable microscopic evaluations from the recently released files ENDF-B-6, JENDL-3.1, BROND-2, JEF-2, and CENDL-2 at and between the aforementioned coordination meetings since 1986. In the selection of materials for inclusion in FENDL the following criteria were applied:

- presence of gamma ray production cross sections and spectra;
- correlated energy-angle emission data (MF=6);
- energy spectra for secondary charged particles;
- presence of complete covariance data;
- consistency of the cross section data with evaluations chosen for the FENDL-1 activation and dosimetry files.

As is shown in Table 1, 45 evaluations were selected from ENDF/B-6, 9 from JENDL-3.1, and 11 from BROND-2; none was so far chosen from JEF-2 or CENDL-2, since these files became only afterwards available. Photon-atomic interaction cross sections were altogether taken over from ENDF/B-6 for 34 elements, i. e. the same number of elements as contained in the neutron cross section sublibrary.

The next step consisted in the pre-processing of the microscopic cross section files into zero Kelvin pointwise data files. These pointwise data files were then transformed into two GENDF formatted multigroup data files for neutrons and photons. The GENDF files were post-processed into three libraries of multigroup data files, i.e. one photon, one neutron, and one coupled neutron-photon library in MATXS format. For this data processing the most recent available version of the NJOY

code system, NJOY 91.38 [Ref. 13], was used and the accuracy of the calculated line shapes at zero Kelvin checked by comparison with the results obtained with the IAEA/NDS processing codes [Ref. 14]. So far only multigroup libraries for use in discrete ordinate transport codes such as ANISN, DOT 3.5 and others could be developed: lack of resources prevented IAEA/NDS so far to generate point libraries for use in Monte Carlo codes such as MCNP.

The following elements and isotopes are available in FENDL/E-1: they are listed below together with the originating ENDF:

NEUTRON INTERACTION AND PHOTON PRODUCTION CROSS SECTIONS

ENDF/B-VI: 1H, 3H, 6Li, 7Li, 9Be, 10B, 11B, C, 14N, 16O, 19F, P, S, Cl, K, 55V, 50,52-54Cr, 55Mn, 54,56-58Fe, 59Co, 58,60-62,64Ni, 63,65Cu, 134-138Ba, 182- 184,186W, 206-208Pb

JENDL 3.1: 23Na, Mg, 27Al, Ca, Ti, 55Mn, Mo, 181Ta, 209Bi

BROND-2: 2H, 14N, 15N, Si, 90-92,94,96Zr, 93Nb, Sn

PHOTON-ATOMIC INTERACTION CROSS SECTIONS

ENDF/B-VI: H, Li, Be, B, C, N, O, F, Na, Mg, Al, Si, P, S, Cl, K, Ca, Ti, V, Cr, Mn, Fe, Co, Ni, Cu, Zr, Nb, Mo, Sn, Ba, Ta, W, Pb, Bi.

The basic evaluated data ENDF/B-VI, JENDL-3.1 and BROND-2 were drawn from the basic libraries available from the NDS [Ref. 15]. The main specifications for the multigroup data processing were as follows (see Ref. 9 also for further details):

- number of neutron groups: 175 (VITAMIN-J structure)
- number of gamma groups: 42 (VITAMIN-J structure)
- neutron weighting function: thermal + 1/E + fission + fusion (IWT=6 in NJOY)
- gamma weighting function: 1/E with rolloffs (IWT=3 in NJOY)
- legendre order for neutrons: P6 for transport correction to P5
- legendre order for gammas: P8 for transport correction to P7
- temperatures: 300, 900, and 1500 Kelvin
- dilution factors: 1, 10, 100, 1000, 10^4 and 10^{10} barns.

2.1. Activation data file

The following steps led to the development of the present FENDL-pointwise (FENDL/PA-1.1) and groupwise (FENDL/GA-1.1) activation cross section libraries:

(1) First, cross sections for 372 neutron-induced activation reactions for 150 isotopes and neutron energies up to 20 MeV were selected from the libraries REAC-2 [Ref. 16], REAC-ECN-5 [Ref. 17], ENDF/B-6 [Ref. 18], SINCROSACT [Ref. 19], ADL-90 [Ref. 20], plus a few reactions from JENDL-3 [Ref. 21] and BROND-2 [Ref. 22]. For all data the data format was

changed to ENDF/B-6 and, where necessary, the original data pre-processed into pointwise data with the codes LINEAR and RECENT developed by D. E. Cullen [Ref. 14]. The resulting first version of the pointwise activation cross section sublibrary, FENDL/PA-1, was issued in the fall of 1991 [Ref. 23].

(2) A revised edition of this library, FENDL/PA-1 (Revised) was established early in 1992 following the November 1991 Advisory Group Meeting on FENDL [Ref. 6], incorporating the first results of the Long-lived Activation CRP [Ref. 24] and of new evaluations by Kopecky et al [Ref. 25] and Badikov et al. [Ref. 26].

(3) In the middle of 1992 FENDL/PA-1 (Revised) and the EAF-2 library by Kopecky et al. [Ref. 25] in pointwise form were combined to the greatly expanded activation cross section sublibrary FENDL/PA-1.1; this was released in early 1993 [Ref. 10]. This library contains now all stable and unstable (altogether 636) target nuclides with half lives $>$ 1/2 days with about 11000 reactions with non-zero cross sections below 20 MeV.

(4) As a next step FENDL/PA-1.1 was processed with the GROUPIE processing code [Ref. 14] into 175 multigroup cross sections using the VITAMIN-J group structure [Ref. 27]. The resulting multigroup library FENDL/GA-1.1 was distributed to several interested groups for preliminary tests and integral checking.

(5) For use of activation cross section data in inventory codes nuclear decay data are needed. The IAEA FENDL Meeting in November 1991 [Ref. 6] recommended to IAEA/NDS to take over the decay data used by the REAC code and data system, which are based on decay data contained in ENDF/B-6 and ENSDF for about 2900 nuclides. These data were kindly supplied to IAEA/NDS by F. Mann in March 1992 and were incorporated in the sublibrary FENDL/D-1.1.

3.3. Charged particle data files

The charged particle data files can be subdivided in fusion reactions between the plasma constituents and sequential charged particle induced activation reactions. As for the first type, the IAEA Consultants' Meeting held in October 1992 at Brookhaven National Laboratory [Ref. 7] recommended that for the FENDL fusion charged particle reaction sublibrary the data from the Livermore ECPL library [Ref. 28] for the reactions D(d,n)3He, D(d p)T, T(d,n)4He, T(t,2n)4He and 3He(d,p)4He be adopted, and for all reactions involving t+3He and 3He+3He the data from the Arzamas ECPNDL library [Ref. 29]. For the sequential charged particle reactions the Brookhaven meeting recommended that IAEA/NDS take over in FENDL the Obložinský-Cierjacks library [Ref. 30] and supporting computer codes.

3.4. Neutron dosimetry file

The IRDF-90 file has been adopted as FENDL sublibrary with fusion-relevant neutron dosimetry reactions [Ref. 11].

4. FUTURE DEVELOPMENT OF FENDL

FENDL is the nuclear data base covering input data for many physics and engineering aspects of fusion reactor projects. Its quality determines the accuracy of all predictions concerning tritium breeding, nuclear heating, radiation damage to materials, shielding, and many other important properties of fusion reactor design. The first version of the library, FENDL-1, represents fairly well the present status of knowledge of neutron cross sections of the materials covered. This knowledge, however, is still not good enough to fulfill all demands of the fusion reactor designers and makes it necessary to include undesirably large safety margins in fusion reactor design which substantially increase the cost of such devices. Considering the progress which had currently been achieved in the development of FENDL-1 and in view of the urgent

need for one consistent evaluated nuclear data library such as FENDL for the Engineering Design Activity (EDA) phase of ITER and other fusion reactor projects, the fusion experts of the IAEA AGM held in Vienna in November of 1991 [Ref. 6] strongly recommended that, after the completion of FENDL-1, the FENDL-related activities be continued and an improved version of FENDL-1, i.e., FENDL-2, be established.

FENDL is based on national evaluated nuclear data libraries. The major deficiencies in evaluations of nuclear data of various materials important for ITER were identified and discussed recently at the International Workshop on Nuclear Data for Fusion Reactor Technology held at Del Mar, California, USA, in May 1993. Plans were outlined at the Workshop to correct the deficiencies which are listed in the Summary [Ref. 31] of the Workshop.

Following the NDS plans, the future work towards establishing FENDL-2 should be focussed on the following tasks:

4.1. Global data file for neutronics calculations

- The process of generation of multigroup libraries can only be considered as completed after successful testing in several fusion-related experimental and calculational benchmarks; this is already underway in several laboratories.

- Based on user feedback, FENDL will be gradually updated.

- FENDL/E-1 must be completed with neutron emission and gamma production data; also new evaluations will become available for several materials; their inclusion in FENDL/E-2 will be considered according to user needs.

- Integral benchmark testing and sensitivity studies of FENDL/E-1 will have to be co-ordinated by IAEA/NDS. This activity should include the collection and publication of complete specifications of fusion-relevant benchmark experiments. The IAEA Consultants' and Advisory Group Meetings on "Preparation of Fusion Benchmarks in Electronic Format for Nuclear Data Validation Studies" and on "Improved Evaluations and Integral Data Testing for FENDL" are foreseen for 13-16 December 1993 in Vienna and September 1994 in Garching respectively.

- On a longer time scale uncertainty/covariance files will have to be developed for FENDL. This activity will be started with the consideration of FENDL uncertainties by an IAEA Advisory Group Meeting which was held at JAERI in the previous week from 8 to 12 November 1993.

- The new CRP on "Measurement, Calculation and Evaluation of Photon Production Data" is started at the Agency now in order to fill the gaps in photon production data still existing in FENDL.

4.2. Activation data file

- FENDL/PA-1.1 is rather complete, but still primarily applicable to fusion reactor activation calculations with hard neutron spectra. Apart from improvements of its quality, the range of applicability should be extended to low energy cross sections.

- As a consequence, the creation of a second version, FENDL/PA-2 is planned which will include the addition of (n,gamma) and (n,n'gamma) cross section data by Petten, of charged particle induced activation data from the Karlsruhe library and of isomer production cross sections.

- The test of inventory codes and the validation of the activation cross section and decay data libraries will be pursued against experimental irradiations of realistic materials in high neutron flux 14 MeV neutron generators, thermal and fast reactors.

- Nuclear model predictions of large amounts of unknown and/or unmeasurable cross sections will have to be improved and a link established to the IAEA/NDS project concerned with the development of a reference nuclear input parameter library for nuclear model calculations [Ref. 32].

- The addition of uncertainties must be foreseen and carefully planned.

- The importance of sequential charged particle reactions and their improvements and of photon-induced reactions must be further investigated.

- A long-term effort will be the extension to reactions above 20 MeV incident particle energy.

4.3 Charged particle data files

- In the fusion charged particle data library integrated cross sections and angular distribution data for reactions between H and Li, Be and B should be included [Ref. 7].

- The discrepancy of about 4 % between the different charged particle libraries in the low-energy cross section data for the T(d,n)4He reaction must be solved.

- A processed file of fusion charged particle reaction cross sections should be developed.

- The future co-operation between Arzamas, LLNL and LANL for the improvement and further development of the fusion charged particle library should be strengthened.

- Concerning sequential charged particle reactions, the Brookhaven Meeting [Ref. 7] recommended that the Karlsruhe effort be continued by improving the starter library by better modelling of d, t and 3He emission cross sections as well as by considering special important cases such as the 7Li(t,gamma)10Be reaction, identifying important reaction chains via inventory calculations and validating the corresponding parts of the library, and by performing benchmark experiments.

- The Brookhaven meeting recommended finally that a library of photonuclear data be prepared for incident gamma energies up to 25 MeV for the structural and shielding materials of ITER.

4.4. Neutron dosimetry cross section library

- Testing and necessary corrections of the existing IRDF-90 library of reference neutron dosimetry cross sections are currently underway [Ref. 33].

References

1. IAEA Advisory Group Meeting on Nuclear Data for Fusion Reactor Technology, Gaussig, (former) German Democratic Republic, December 1986; Proceedings published as IAEA-TECDOC-457, 1988.

2. IAEA Specialists' Meeting on the Fusion Evaluated Nuclear Data Library Related to the ITER Activity, Vienna, Austria, November 1987; summary report prepared by V. Goulo and A. Lorenz and published as report INDC(NDS)-201/GF, 1988.

3. IAEA Specialists' Meeting on the Fusion Evaluated Nuclear Data Library (FENDL), Vienna, Austria, May 1989; summary report edited by V. Goulo and published as report INDC(NDS)-223/GF, 1989.

4. IAEA Consultants' Meeting on First Results of FENDL-l Testing and Start of FENDL-2, Vienna, Austria, June 1990; summary report prepared by A.B. Pashchenko and D.W. Muir and published as report INDC(NDS)-241/LF, 1990.

5. IAEA Advisory Group Meeting on Nuclear Data for Neutron Multiplication in Fusion Reactor First - Wall and Blanket Materials, Chengdu, China, November 1990; summary report prepared by D.W. Muir and A. B. Pashchenko and published as report INDC(NDS)-264/G, 1992.

6. IAEA Advisory Group Meeting on FENDL-2 and Associated Benchmark Calculations, Vienna, Austria, November 1991; summary report prepared by A.B. Pashchenko and D.W. Muir and published as report INDC(NDS)-260/LF, 1992.

7. IAEA Consultants' Meeting on Charged Particle and Photonuclear Data Libraries for FENDL, Brookhaven National Laboratory,USA, October 1992; summary report prepared by A.B. Pashchenko and published as report INDC(NDS)-268/G, 1993.

8. IAEA Advisory Group Meeting on Review of Uncertainty Files and Improved Multigroup Cross Section Files for FENDL, Mito, Japan, November 1993; Summary Report to be published by S. Ganesan as INDC(NDS)-document.

9. S. Ganesan, "Current Status of Production of Coupled Neutron-Photon Multigroup Cross Section Libraries of FENDL for Use in Fusion Neutronics Calculations", paper presented at International Workshop on Nuclear Data for Fusion Reactor Technology, Del Mar, California, USA, May 1993.

10. A.B. Pashchenko, "Status of FENDL Activation File and Plans for Future Development", paper presented at the International Workshop on Nuclear Data for Fusion Reactor Technology, Del Mar, California, USA, May 1993; see also A.B. Pashchenko and P.K. McLaughlin, report IAEA-NDS, to be published, 1993.

11. N. Kocherov and P. K. McLaughlin, report IAEA(NDS)-141, April 1990.

12. S. Ganesan, A.B. Pashchenko, J.J. Schmidt. Summary of present composition of FENDL and plans for future development. Paper presented at International Workshop on Nuclear Data for Fusion Reactor Technology, Del Mar, California, USA, May 1993.

13. R.E. MacFarlane, D.W. Muir et al., "NJOY 91.38, A Code System for Producing Pointwise and Multigroup Neutron and Photon Cross Sections from ENDF/B Evaluated Nuclear Data", PSR-171, Radiation Shielding Information Center, Oak Ridge National Laboratory, USA, July 1992.

14. D. E. Cullen, "The 1992 ENDF Pre-processing Codes", IAEA-NDS-39, Rev.7, February 1992.

15. H.D. Lemmel, "Index of Data Libraries available on magnetic tape from the IAEA Nuclear Data Section," IAEA-NDS-7 (Rev. 91/10), October 1991. See also H.D. Lemmel, "Index to BROND-2, CENDL-2, ENDF/B-VI, JEF-I, JENDL-3", IAEA-NDS-107 (Rev. 6), June 1992.

16. F.M. Mann, Proceedings International Conference on Nuclear Data in Science and Technology, Mito, Japan, May/June 1988, p.1013.

17. J. Kopecky and H. Gruppelaar, ref. 16, p. 245.

18. C.L. Dunford, Proc. International Conference on Nuclear Data for Science and Technology, Juelich, Germany, May 1991, p. 788; see also US National Nuclear Data Center, "ENDF/B-6, the US Evaluated Nuclear Data Library for Neutron Reaction Data", summary documentation report ENDF 201, edited by P.F. Rose, 1992; summary of contents by H.D. Lemmel, report IAEA-NDS-120, Rev. 1, April 1991.

19. N. Yamamuro, report NEANDC(J)-146 "U" (INDC(JPN)-133/L), February 1990.

20. O. T. Grudzevich, A. V. Zelenetskij and A. B. Pashchenko, Preprint FEI-2043, Obninsk, 1989.

21. Computer Database Japanese Evaluated Nuclear Data Library, JENDL-3, Japanese Nuclear Data Center, JAERI, Tokai-Mura, 1990.

22. Computer Database USSR Evaluated Neutron Data Library, BROND, (former) USSR Nuclear Data Centre, FEI Obninsk; summary documentation in report IAEA-NDS-90, Rev. 2.

23. A.B. Pashchenko, report IAEA-NDS-148, November 1991.

24. IAEA CRP on Activation Cross Sections for the Generation of Long-lived Radionuclides of Importance in Fusion Reactor Technology, 1989-95; see e. g. Proceedings of the IAEA Research Co-ordination Meeting on Activation Cross Sections for the Generation of Long-Lived Radionuclides, Vienna, November 1991, Report INDC(NDS)-263, July 1992.

25. J. Kopecky, H.A.J. Van der Kamp, H. Gruppelaar and D. Nierop, The European Activation File EAF-2 with Neutron Activation and Transmutation Cross Sections, ECN-C-91- 073, July 1991.

26. S.A. Badikov et al., Proceedings International Conference on Nuclear Data for Science and Technology, Juelich, Germany, May 1991, p. 930.

27. E. Sartori, Standard Energy Group Structures of Cross Section Libraries for Reactor Shielding, Reactor Cell and Fusion Neutronics Applications: VITAMIN-J, ECC0-33, ECC0-2000 and XMASS, OECD/NEA Data Bank Report JEF/DOC-315, December 1990.

28. R.M. White, D.A. Ressler and S.I. Warshaw, Proceedings International Conference on Nuclear Data for Science and Technology, Juelich, Germany, May 1991, p. 834.

29. S.N. Abramovich, B.Ya. Guzhovskii, V. Zherebcov and A. Zvenigorodskii, "Jaderno-fizicheskie Konstanty Termojadernogo Sinteza", Spravochnoe Posobie, Moskva, CNII Atominform, 1989; English translation by A. Lorenz published by IAEA as report INDC(CCP)-326/LF.

30. P. Oblozinsky et al., Proceedings Topical Conference on Nuclear Data for Fusion Reactor Technology, Karlsruhe, Germany, October 1991, edited by S. Cierjacks and published as report NEANDC-307 "U" (INDC(GER)-035/L; KFK 5062), April 1992, p. 77; S. Cierjacks, Fusion Engg. and Design 13, 1990, 229.

31. E.T. Cheng and F.M. Mann. Summary of the International Workshop on Nuclear Data for Fusion Reactor Technology, 3-6 May 1993, Del Mar, California, to be published.

32. IAEA Consultants' Meeting on Reference Nuclear Parameter Library for Nuclear Data Computation, Vienna, November 1991. Summary report prepared by G. Reffo, O. Bersillon, D.W. Muir and A.B. Pashchenko and published as report INDC(NDS)-266/G in November 1992; see also report INDC(NDS)-282/G, September 1993.

33. S. Ganesan, N. Kocherov, A.B. Pashchenko, J.J. Schmidt and H. Vonach, "Status of Important Nuclear Data Required for ITER", paper presented at the International Workshop on Nuclear Data for Fusion Reactor Technology, Del Mar, California, 3-6 May 1993.

Table 1 Results of review of FENDL-1 general purpose evaluations identified at previous meetings†

Nuclide or Element	Library	γ-Ray Data	MF6 Data	Chg.Part. Spectra	Covariance Data	Act,/Dos Consistency	Comments
H	V6	Y	MA	Y	Y	–	Correct AWR for nuclear rather than atomic mass. Consider use of MF=30 for covariances.
D	BROND	Y	Y	Y	N	–	Several improvements have been made to the file since last meeting.
T	V6	Y	N	N	N	–	
Li-6	V6	Y	N*	NC	NC	–	
Li-7	V6	Y	N*	NC	Y	–	(EFF2/ENDF/B-VI, Revision 1) will be considered for FENDL-2 after testing.
Be-9	V6	Y	Y	Y	N	–	Neutron emission spectra appear to be underestimated at back angles.
B-10	V6	Y	N*	NC	NC	–	
B-11	V6	Y	Y	Y	N	–	
C	V6	Y	N*	NC	Y	–	
N-14	BROND	Y	Y	Y	N	–	
N-15	BROND	Y	Y	Y	N	–	
O-16	V6	Y	N*	NC	N	–	
F-19	V6	Y	Y	Y	Y	N?	New BROND analysis using Pade approximates should be compared. (n,2n) cross sections might not be consistent with activation file. file.
Al-27	JENDL-3	Y	N	N	N	N	
Si	BROND	Y	NC	Y	N	–	Use EFF-2 if completed in time. ENDF/B-VI isotopic evaluations will be available for consideration for FENDL-2.
Ti	JENDL-3	Y	N	NC	N	N	$^{47}Ti(n,p)$ not consistent with activation file.
V-51	V6	Y	N	N	Y	Y	
Cr-50 52-54	V6	Y	Y	Y	Y	Y	Questions raised regarding resonance region for even Cr isotopes that should be checked.
Mn-55	V6/ JENDL-3	Y	Y	Y	Y	Y	Collaborative evaluation but only ENDF/B-VI contains MF=6 data.
Fe-54 56-58	V6	Y	Y	Y	Y	Y	14 MeV neutron emission spectrum at 30° higher than Takahashi data in pre equilibrium region. Should be checked.
Co-59	V6	Y	N	N	Y	Y	
Ni-58, 60-62,64	V6	Y	Y	Y	Y	Y	Check first few resonances in Ni isotopes for completeness.
Cu-63,65	V6	Y	Y	Y	Y	Y	
Zr-90-92, 94,96	BROND	Y	Y	Y	N	N	Cheng recommended that isotopic evaluations be used. $^{90}Zr(n,2n)$ not consistent with activation file.
Nb-93	BROND	Y	Y	N	N	NC	$^{93}Nb(n,n')^{93m}Nb$ and $(n,2n)^{92m}Nb$ should be added from activation/dosimetry files.
Mo	JENDL-3	Y	N	N	N	N	Isotopic evaluations do not include γ-ray data. Recommend addition of γ-ray data before FENDL-2.
Sn	BROND	Y	N	Y	N	N	MF=3 is a combination of full evaluation of major isotopes. MF=4,5 based on calculations for two isotopes.
Ba-134- -138	V6	N	N	N	N	–	Fission product evaluations of limited scope.
W-182- -186	V6	Y	N	N	N	N	Some improvement in 14-MeV-neutron emission spectra possibly needed. Use of isotopic evaluations recommended by Cheng.
Pb-206- -208	V6	Y	Y	N	Y	N	$^{206}Pb(n,alpha)$ not consistent with activation file. ^{204}Pb evaluation is encouraged.
Bi-209	JENDL-3	Y	N	N	N	N	$^{209}Bi(n,2n)$ and (n,γ) not consistent with activation file.

† Table Explanation

Table 2 Additional evaluations recommended for FENDL-I+

Nuclide or Element	Library	γ-Ray Data	MF6 Data	Chg.Part. Spectra	Covariance Data	Act./Dos Consistency	Comments
Na-23	JENDL-3	Y	N	N	N	N	
Mg	JENDL-3	Y	N	N	N	N	
P-31	V6	Y	N	N	N	Y	JENDL-3 only includes files thru MF=5 − no γ-ray data.
S	V6	Y	N	N	N	N	JENDL-3 has no γ-ray data.
Cl	V6	Y	N	N	N	−	JENDL-3 has no γ-ray data.
K	V6	Y	N	N	N	−	JENDL-3 has no γ-ray data.
Ca	JENDL-3	Y	N	N	N	−	
Ta-181	JENDL-3	Y	N	N	N	N	Should be compared with BROND update.

+ Table Explanation

Y = Yes, data present
N = No, data not present
* = Indicates excitation energy bins (pseudo levels used in lieu of MF=6)
NC = not complete but some data present
NA = not applicable
V6 = ENDF/B-VI

Table 3 Additional files proposed to be considered for inclusion in FENDL/E-2

Nuclide or Element	Library	γ-ray Data	File-6 Data	Chg.Part. Spectra	Covariance Data	Comments
^{1}H	CENDL-2	?	Y	Y	N	
^{2}H	CENDL-2	N	N	N	N	
^{3}He	CENDL-2	N	Y	N	Y	New eval. added for FENDL/E-2.
^{4}He	ENDF/B-VI	?	?	?	?	New eval. added for FENDL/E-2.
^{6}Li	JENDL-3 R2	Y	N	Y	N	
^{7}Li	JENDL-3 R1	Y	N*	Y	N	
^{7}Li	EFF-2	Y	Y	Y	N	
^{9}Be	EFF-2	Y	Y	Y	N	
^{9}Be	JENDL-3 R2	Y	N*	Y	N	Possibly completed.
^{14}N	ENDF/B-VI	Y	Y	Y	Y	
^{14}N	JENDL-3 R2	Y	N*	Y	N	
^{15}N	ENDF/B-VI	Y	Y	Y	Y	
^{27}Al	EFF-2	Y	Y	Y	N	
^{27}Al	JENDL-3 R2	Y	Y	Y	N	
^{28}Si	EFF-2	Y	Y	Y	N	
^{28}Si	ENDF/B-VI	Y	Y	Y	Y	
^{29}Si	ENDF/B-VI	Y	Y	Y	Y	
^{30}Si	ENDF/B-VI	Y	Y	Y	Y	
^{nat}Ca	JENDL-3 R2	Y	Y	Y	N	
$^{isotopes}Ti$	JENDL-3 R2	Y	Y	Y	N	
^{nat}Ti	JENDL-3 R2	Y	Y	Y	N	
^{52}Cr	EFF-2	Y	Y	Y	Y	
^{nat}Cr	JENDL-3 R2	Y	Y	Y	N	
^{56}Fe	EFF-2	Y	Y	Y	Y	
^{56}Fe	CENDL-2	Y	Y	Y	Y	
^{56}Fe	JENDL-3 R2	Y	Y	Y	N	
^{59}Co	JENDL-3 R2	Y	Y	Y	N	
^{58}Ni	EFF-2	Y	Y	Y	Y	
^{58}Ni	JENDL-3 R2	Y	Y	Y	N	
^{60}Ni	EFF-2	Y	Y	Y	Y	
^{nat}Cu	JENDL-3 R2	Y	Y	Y	N	
^{93}Nb	JENDL-3 R2	Y	Y	Y	N	
^{nat}Mo	JENDL-3 R2	Y	Y	Y	N	
^{nat}Pb	JENDL-3 R2	Y	Y	Y	N	
^{209}Bi	JENDL-3 R2	Y	Y	Y	N	

+ Table Explanation:

Y = Yes, data present
N = No, data not present
* = Indicates excitation energy bins (pseudo levels used en lieu of File-6)

2.2 JENDL and Shielding Experiment for High Energy Neutron

2.2.1 JENDL−3 Revision 2

Tsuneo Nakagawa
Japan Atomic Energy Research Institute
Tokai−mura, Naka−gun, Ibaraki−ken 319−11

The data for 340 nuclides will be stored in the second revised version of JENDL−3, JENDL−3.2, and about half of them will be modified more or less. An outline of modifications for JENDL−3.2 is described here in particular on double−differential cross sections, total cross sections and inelastic scattering cross sections of structural materials, data of fission product nuclides, resonance parameters and fission spectra of heavy nuclides, and γ−ray production data.

1. Introduction

The third version of Japanese Evaluated Nuclear Data Library, JENDL−3[1], was released in December 1989, and its first revised version, JENDL−3.1, was made in December 1990. In JENDL−3.1, data are given for 324 nuclides and the γ−ray production data for 59 nuclides. After extensive benchmark tests, drawbacks of JENDL−3.1 have been pointed out. The following are examples of the drawbacks:

(1) The double differential cross sections (DDX) of neutron emission reactions of ^{14}N, Ti, ^{59}Co, Zr, Mo, W, etc. are not in good agreement with experimental data[2].
(2) The total cross sections of ^{23}Na and Fe, and inelastic scattering cross sections of Fe should be re−evaluated[3].
(3) Cross sections in the resonance region of ^{235}U[4], inelastic scattering cross sections and fission neutron spectra of ^{233}U[5] should be re−evaluated. The upper boundary of the unresolved resonance region of ^{238}U is too low[6].
(4) The resonance parameters and the capture cross sections of about 40 fission product nuclides have to be modified on the basis of recent experimental data.
(5) All γ−ray production data in JENDL−3.1 should be re−examined because the evaluation for JENDL−3.1 might be immature.

Work for the second revision was started in 1991 by organizing Working Groups for Modification of Heavy Nuclide Data and γ−ray Production Data in Japanese Nuclear Data Committee (JNDC). The present revision work for JENDL−3.2 has been made by these two working groups[7,8] and Working Group on Fission Product Nuclear Data[9] of JNDC and JENDL Compilation Group in Nuclear Data Center of JAERI. After the modification, quick benchmark calculations for important data were carried out by members of JNDC in order to confirm improvement of the data. In the following, revision work for JENDL−3.2 is explained by showing typical examples.

2. Light−mass Nuclides and Structural Materials

2.1 Double−differential cross sections

The DDX data of neutron emission reactions are important for fusion neutronics.

However, the DDX data of several nuclides calculated from JENDL-3.1 such as ^{14}N and Mo are not in good agreement with experimental data measured at Tohoku University and/or Osaka University. For JENDL-3.2, the DDX data of ^{14}N were modified by assuming hypothetical levels in the high energy region up to 20 MeV. **Figure 1** is a comparison of JENDL-3.1 and JENDL-3.2 with experimental data measured by Baba et al.[10] For the nuclides heavier than N, JENDL Fusion File[11] is being made in order to improve the DDX data in JENDL-3.1. This is one of JENDL special purpose files and provides precise DDX data to fusion neutronics applications. In JENDL Fusion File, the data for 21 elements (F, Al, Si, Ca, Ti, Cr, Mn, Fe, Co, Ni, Cu, Ge, As, Zr, Nb, Mo, Sn, Sb, W, Pb and Bi) and their isotopes will be stored by adopting the MF6 representation of the ENDF-6 format. For JENDL-3.2, the data in JENDL Fusion File are adopted by approximately transforming the MF6 representation to usual MF4-MF5 representation, because most of users except fusion people do not need very precise DDX data. The DDX data of Mo is shown in **Fig. 2** as an example. JENDL-3.1 data shown with dashed line are largely modified with JENDL-3.2 data translated from JENDL Fusion File.

2.2 Total cross sections of Fe and ^{23}Na

The drawbacks of Fe and ^{23}Na total cross sections were revealed by the benchmark calculations[3] for Broomstick experiments[12]. They measured neutron flux transmitted through samples with a diameter of 4 inches and several kinds of length located in the neutron flux of a reactor of ORNL Tower Shielding Facility. For example, in the case of Fe, JENDL-3.1 underestimates the measured neutron flux in the neutron energy range below 3 MeV, while ENDF/B-IV is in good agreement with the experiment, as is shown in **Fig. 3**. This indicates that the total cross sections given in JENDL-3.1 might be too large at cross section minima. For JENDL-3.2, the cross-section shape was sharpened by considering energy resolutions of the experiments:

$$\sigma_{J3}(E_0) = \int_{E_0-D}^{E_0+D} \sigma_{mod}(E) R(E) dE, \qquad (1)$$

where $\sigma_{J3}(E_0)$ is the total cross section given in JENDL-3.1 which is affected by experimental resolution, $\sigma_{mod}(E)$ modified cross section to be obtained and R(E) resolution function with a Gaussian form. We assumed simply that $\sigma_{mod}(E) = C(E_0) \times \sigma_{j3}(E)$ and the factor $C(E_0)$ was obtained by solving Eq.(1). Results are shown in **Fig. 4**. The cross-section curve with almost the same sharpness as ENDF/B-IV was obtained and agreement with the Broomstick experiment was improved as is shown in Fig. 3 with a dashed line. This procedure was adopted also to Cr and Ni total cross sections.

In the case of ^{23}Na, JENDL-3.1 adopted the total cross section measured at KfK[13]. However this total cross section is systematically smaller than that measured by Larson et al.[14] at ORNL, and Broomstick benchmark calculation pointed out that JENDL-3.1 was too small. Therefore, the total cross section of ^{23}Na was re-evaluated on the basis of the ORNL data.

2.3 Inelastic scattering cross section of Fe

The number of discrete levels in the ENDF format is limited to 40. In the case of natural iron data of JENDL-3.1, therefore, the inelastic scattering cross sections with almost the same threshold energies were summed up to one level so as to reduce the number of inelastic scattering

levels. However it was found[15] that this procedure caused a serious problem for neutron spectra in the low energy part. **Figure 5** is comparison of calculated neutron spectra with those measured by KfK iron experiment[16]. The neutron spectra coming out from an iron sphere with ^{252}Cf at its center were measured at a distance of about 1 m. There are large discrepancies between spectra calculated from JENDL-3 and ENDF/B-IV below the 24-keV iron window. **Figure 6** shows the cross section of MT=55 of JENDL-3.1 natural iron data. This is a sum of the cross section of 810-keV level of ^{58}Fe and that of 847-keV level of ^{56}Fe. The Q-value of -810 keV is given to this level, while almost of all part of this cross section comes from that of ^{56}Fe. Therefore, the neutrons emitted from this level have energies about 35-keV higher than actual energies. The discrepancies shown in Fig. 5 are caused by the inadequate Q-values given to the inelastic scattering cross-section data. This problem was corrected by re-grouping the data. Then calculated spectra from revised data became almost the same as ENDF/B-IV. The inelastic scattering cross sections of Ni were also modified concerning this problem.

3. Fission Product Nuclides

JENDL-3.1 contains the data for 172 nuclides in the fission product mass range. The data of about 60 nuclides among them are modified to JENDL-3.2 by Working Group on FP Nuclear Data[9] of JNDC.

The capture cross sections of ^{90}Sr and ^{137}Cs were largely changed on the basis of recent experimental data measured at JAERI[17,18]. The capture cross section of ^{90}Sr in JENDL-3.1 is 900 mb which is the same as ENDF/B-VI and JEF-2. However the new data adopted in JENDL-3.2 is only 15.3±1.3 mb at 0.0253 eV[18]. Lone et al.[19] reported also smaller cross section of 9.7±0.7 mb.

The capture cross section in the keV region was updated by considering recent experimental data. **Figure 7** is the capture cross section of ^{148}Sm. JENDL-3.1 was normalized to the data of Kononov et al.[20], while JENDL-3.2 was determined on the basis of the data of Wisshak et al.[21] JENDL-3.1 in the energy range between about 6 and 10 keV where is in the resolved resonance region seems to be too small because of missing of weak resonances. The upper boundary of the resolved resonance region was set down to 5.5 keV to avoid underestimation of the cross section. The same considerations were made for many other nuclides in the FP region.

Resolved resonance parameters were modified for about 25 nuclides. This modification was based on recent experimental results and re-normalization of capture area data. Unresolved resonance parameters were also replaced with new fitting results if the capture cross section was modified in the unresolved resonance region.

Inelastic scattering cross sections of Zr, Mo, Nd and Sm isotopes were modified by considering the direct processes.

4. Heavy Nuclides

Modification of important heavy nuclide data was discussed by Working Group for Modification of Heavy Nuclides Data[7]. Effects of the modification to integral quantities were investigated with a sensitivity analysis system CATEX[22].

4.1 Resolved resonance parameters

The resolved resonance parameters of ^{233}U, ^{235}U, ^{238}U, ^{239}Pu and ^{241}Pu were replaced with Reich-Moore parameters analyzed with SAMMY[23] as follows:

^{233}U	up to 150 eV	new evaluation by Derrien[24]
^{235}U	up to 500 eV	taken from ENDF/B−VI[25] with slight modification of Γγ

Moxon[26] reported that the ^{235}U capture resonance integral of ENDF/B−VI was too small. This problem is remained for future work.

^{238}U	up to 10 keV	taken from JEF−2[27] and divided into 10 energy intervals
^{239}Pu	up to 2.5 keV	Evaluation made by Derrien[28]
^{241}Pu	up to 300 eV	ENDF/B−VI parameters[29] and modification was made by Derrien[30]

The Reich−Moore parameters are not convenient for the users because it takes long CPU time to reconstruct the resonance cross sections. Therefore, a point−wise file will be provided especially for the nuclides with the Reich−Moore parameters.

4.2 Unresolved resonance parameters

The unresolved resonance parameters of ^{235}U and ^{238}U were updated. The fission cross section of ^{235}U was determined on the basis of experimental data of Weston and Todd[31] The capture cross section of ^{235}U became smaller than JENDL−3.1 as a results of adoption of small α values measured by Muradjan et al.[32] The unresolved resonance region of ^{238}U was extended from 50 keV up to 150 keV because Doppler effects are important in this region.[6] The average capture cross section of ^{238}U is almost the same as JENDL−3.1.

4.3 Inelastic scattering cross sections

The ^{233}U inelastic scattering cross section was re−evaluated with ECIS[33] and CASTHY[34]. The results are given in **Fig. 8**. They are somewhat smaller than JENDL−3.1 and in good agreement with experimental data of Smith et al.[35]

The inelastic scattering cross sections of ^{238}U were also re−evaluated because the data of JENDL−3.1 cannot reproduce DDX data measured at Tohoku University[36].

4.4 Fission spectra

The ^{233}U fission spectra adopted in JENDL−3.1 are too hard because of a trivial mistake occurred at the time of compilation. They have been modified with new calculation from Madland−Nix formula[37] by adopting the level density parameters of a = A/9.

The fission spectra of ^{235}U, ^{238}U and ^{239}Pu were newly calculated with modified Madland−Nix model proposed by Ohsawa[38] which took account of effects of a non−equitemperature fission fragments and multi−chance fission. **Figure 9** shows the ^{235}U fission spectrum at the incident neutron energy of 500 keV. JENDL−3.2 is a little softer than JENDL−3.1.

5. Gamma−ray Production Data

The γ−ray production data in JENDL−3.1 have been reviewed and the following modifications were made by Working Group for Modification of γ−ray Production Data.[8]

To keep energy balance of capture γ−rays, Q−values of natural elements were replaced with weighted average of Q−values of isotopes, and multiplicities of capture γ−rays were

calculated so as to keep the energy balance. Energy spectra of capture γ-rays were calculated with CASTHY[34] in the low energy region. Primary transition probabilities were adjusted to spectrum data measured at the thermal energy. Discrete γ-rays from the inelastic scattering were given in the neutron energy range up to 2 or 3 MeV. **Figure 10** shows total γ-ray spectrum of Ni. JENDL-3.2 is in better agreement with experimental data[39] than JENDL-3.1. Additional new evaluations were made for ^{3}He, ^{19}F, ^{31}P, S, K, ^{51}V and ^{59}Co.

6. Conclusion

Re-evaluations and modifications of data for JENDL-3.2 were reviewed. JENDL-3.1 stores the data for 324 nuclides. New evaluation of additional 16 nuclides has been made. JENDL-3.2 will contain the data for 340 nuclides. The data of about 170 nuclides out of 340 will be updated more or less for JENDL-3.2.

The revised data are being compiled in the ENDF-5 format. However they will be changed to the ENDF-6 format without MF6 representation. JENDL-3.2 will be released at the end of March 1994.

References

1) Shibata K., Nakagawa T., Asami T., Fukahori T., Narita T., Chiba S., Mizumoto M., Hasegawa A., Kikuchi Y., Nakajima Y., and Igarasi S.: "Japanese Evaluated Nuclear Data Library, JENDL-3," JAERI 1321 (1990).
2) For example, (eds.) Nakajima Y., and Maekawa H.: Proc. 2nd Specialists' Meeting on Nuclear Data for Fusion Reactors, Tokai, Dec. 20-21, 1990, JAERI-M 91-062 (1991).
3) Kawai M., Hasegawa A., Ueki K., Yamano N., Sasaki K., Matsumoto Y., Takemura M., Ohtani N., and Sakurai K.: to be published as JAERI report.
4) Takano H. and LWR Integral Data Testing WG, JNDC: Proc. 1991 Symposium on Nuclear Data, Tokai, Nov. 28-29, 1991, JAERI-M 92-027, p.147 (1992).
5) Tian D., Hasegawa A., Nakagawa T., and Kikuchi Y.: J. Nucl. Sci. Technol., 30, 1087 (1993).
6) Takano H.: private communication.
7) Kikuchi Y., and Nakagawa T.: Proc. 1992 Symposium on Nuclear Data, Tokai, Nov. 26-27, 1992, JAERI-M 93-046, p.16 (1993).
8) Igarasi S.: *ibid.*, p.27 (1993).
9) Kawai M.: presented in this proceedings.
10) Baba M., Ono M., Yabuta N., Kikuchi T., and Hirakawa N.: Proc. Int. Conf. on Nuclear Data for Basic and Applied Sci., Santa Fe, May 13-17, 1985, p.223 (1986).
11) Chiba S., Yu B., and Fukahori T.: Proc. 1991 Symposium on Nuclear Data, Tokai, Nov. 28-29, 1991, JAERI-M 92-027, p. 35 (1992).
12) Straker E.A.: "Experimental Evaluation of Minima in Total Cross Sections of Several Shielding Materials," ORNL-TM-2242 (1968).
13) Cierjacks S., Forti P., Kopsch D., Kropp L., Nebe J., Unseld H.: "High Resolution Total Neutron Cross-sections between 0.5-30 MeV," KFK 1000 (1968).
14) Larson D.C. ORNL-TM-5614 (1976).
15) Yamano N.: private communication (1993).
16) Werle H., Kappler F., and Kuhn D.: "Measurements of Neutron Leakage Spectra from Iron Sphere with a ^{252}Cf Source in the Center," NEACRP-U-73 (1976).

17) Harada H., Watanabe H., Sekine T., Hatsukawa Y., Kobayashi K., and Katoh T.: J. Nucl. Sci. Technol., 27, 577 (1990).
18) Harada H., Sekine T., Hatsukawa Y., Shigeta N., Kobayashi K., Ohtsuki T., and Katoh T.: Proc. 1991 Symposium on Nuclear Data, Tokai , Nov. 28－29 1991, JAERI－M 92－027, p. 298 (1992).
19) Lone M.A., Edwards W.J., and Collins R.: Proc. GROBAL'93, Seattle, Sep. 12－17, 1993, Vol. 1, p.445 (1993).
20) Kononov et al.: YK－22, 29 (1977). Data were taken from EXFOR.
21) Wisshak K., Guber K., Voss F., Kaeppeler F., and Reffo G.: "Neutron Capture in ^{148,150}Sm: A Sensitive Probe of the s－Process Neutron Density," KfK 5067 (1992).
22) Hasegawa A.: private communication.
23) Larson N.M.: "Updated Users' Guide for SAMMY: Multilevel R－Matrix Fits to Neutron Data Using Bayes' Equations," ORNL/TM－9179, Revision 1 (1985).
24) Derrien H.: to be published in J. Nucl. Sci. Technol. (1994).
25) Leal L.C., de Saussure G., and Perez R.B.: Nucl. Sci. Eng., 109, 1 (1991).
26) Moxon M.C.: "Comments on the ENDF/B－VI Evaluation for ^{235}U in the Neutron Energy Region from 1 to 20 eV," ORNL/TM－12304 (1993).
27) Moxon M.C., Sowerby M.G., Nakajima Y., and Nordborg C.: Proc. 1988 Int. Reactor Physics Conf., Jackson Hole, Sep. 18－22, 1988, Vol.1 p.281 (1988).
28) Derrien H.: J. Nucl. Sci. Technol., 30, 845 (1993).
29) Derrien H., and de Saussure G.: Nucl. Sci. Eng., **106**, 415 (1990).
30) Derrien H.: "Revision of the ^{241}Pu Reich－Moore Resonance Parameters by Comparison with Recent Cross Section Measurements," JAERI－M 93－251 (1994).
31) Weston L.W., and Todd J.H.: Nucl. Sci. Eng., 88, 567 (1984).
32) Muradjan G.V., Shchepkin Ju.G., Adamchuk Ju.V., and Voskanjan M.A.: Proc. 5th All Union Conf. Neutron Physics, Kiev, Sep. 15－19, 1980, Vol. 2, p.119 (1980).
33) Raynal J.: IAEA SMR－9/8 (1970).
34) Igarasi S., and Fukahori T.: "Program CASTHY - Statistical Model Calculation for Neutron Cross Sections and Gamma Ray Spectrum -," JAERI 1321 (1991).
35) Smith A.B., Guenther P.T., McKnight R.D.: Proc. Int. Conf. Nuclear Data for Sci. Technol., Antwerp, Sep. 6－10, 1982, p.39 (1983).
36) Baba M., Wakabayashi H., Ito N., Maeda K., and Hirakawa N.: J. Nucl. Sci. Technol., 27, 601 (1990).
37) Madland D.G., and Nix J.R.: Nucl. Sci. Eng., 81, 213 (1982).
38) Ohsawa T., and Shibata T.: Proc. Int. Conf. Nuclear data for Science and Technology, Juelich, 13－17 May, 1991, p.965 (1992).
39) Dickens J.K., Love T.A., and Morgan G.L.: "Gamma－ray Production from Neutron Interactions with Nickel for Incident Neutron Energies between 1.0 and 10 MeV: Tabulated Differential Cross Sections," ORNL－TM－4379 (1973).
40) Takahashi A., Gotoh M, Sasaki Y., and Sugimoto H.: "Double and Single Differential Neutron Emission Cross Sections at 14.1 MeV: Vol.2," OKTAVIAN Report A－92－01 (1992).

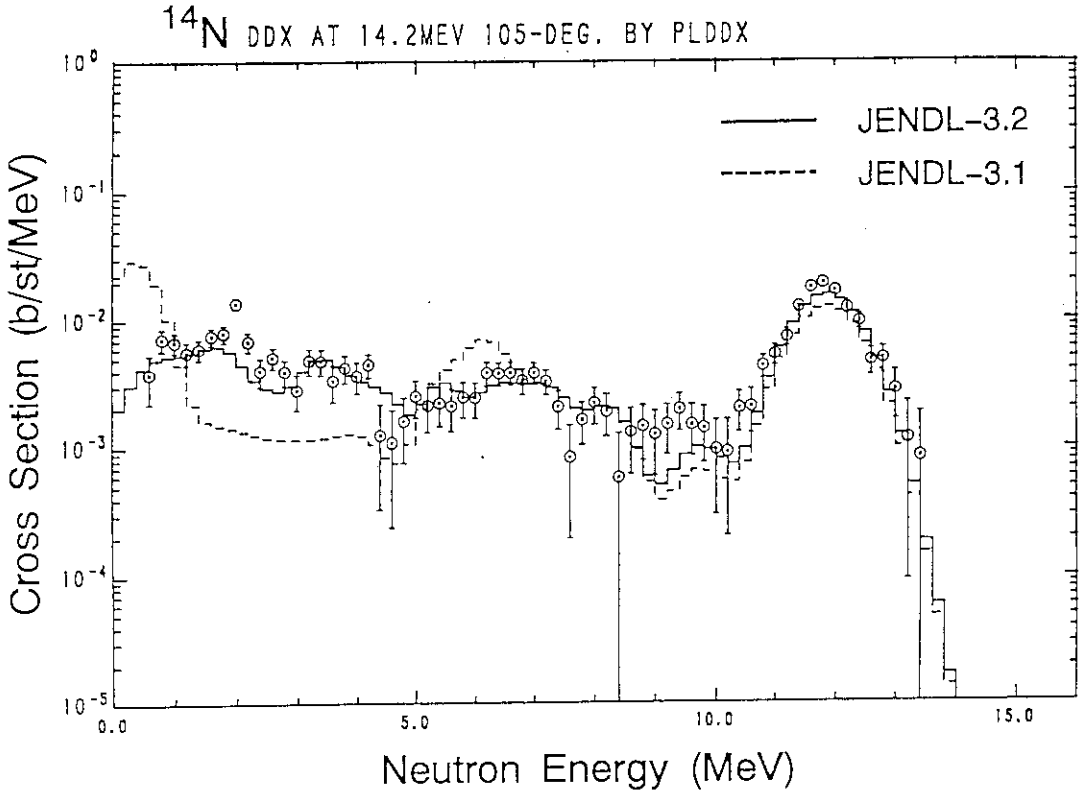

Fig. 1 ^{14}N DDX data at the incident neutron energy of 14.2 MeV and scattering angle of 60 degrees. Experimental data were measured by Baba et al.[10]

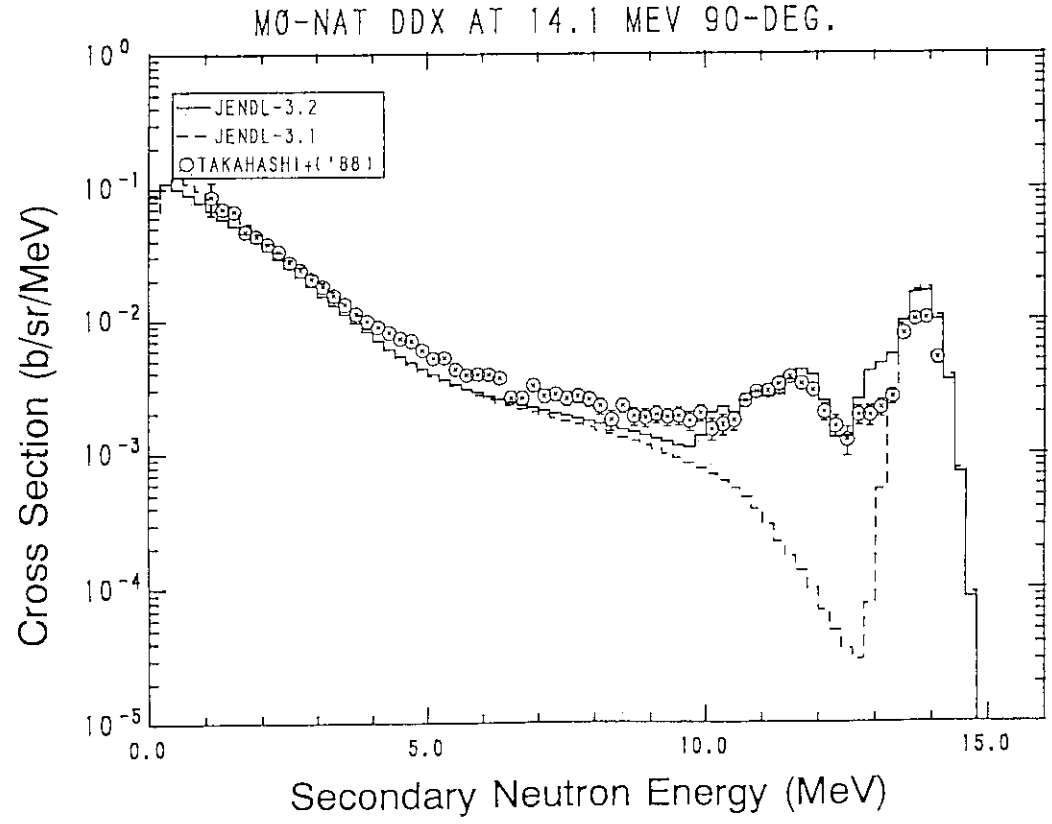

Fig. 2 Mo DDX data at the incident neutron energy of 14.1 MeV and scatterig angle of 90 degrees. Experimental data were measured by Takahashi et al.[40]

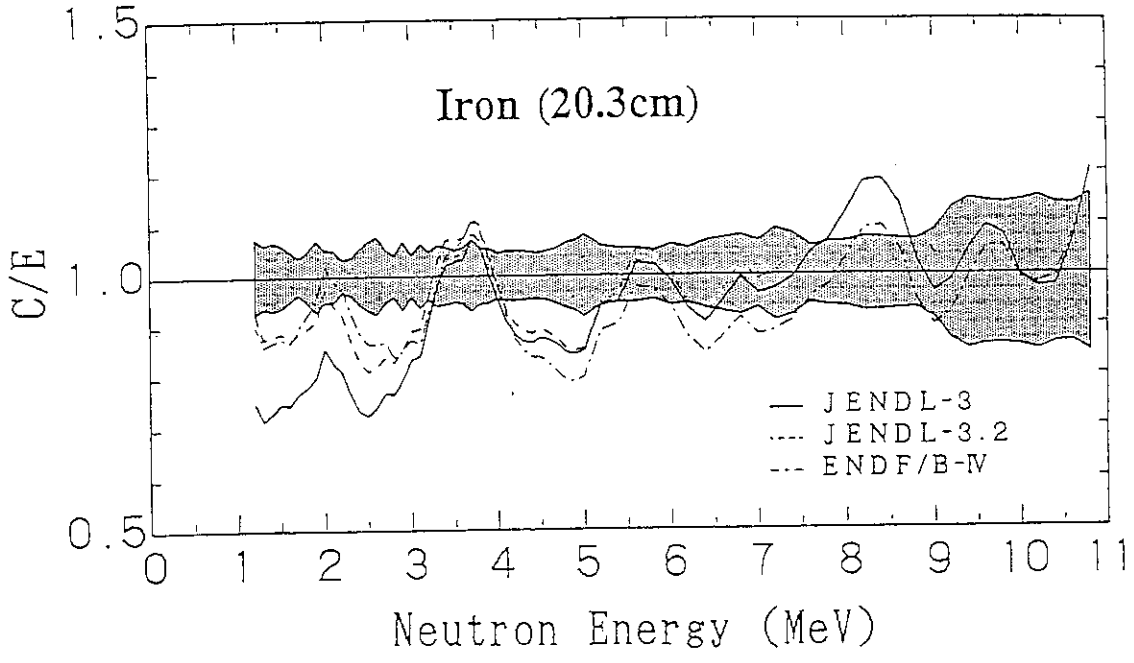

Fig. 3 Ratio of calculated flux to measured one at Broomstick experiment. A shaded area indicates experimental error.

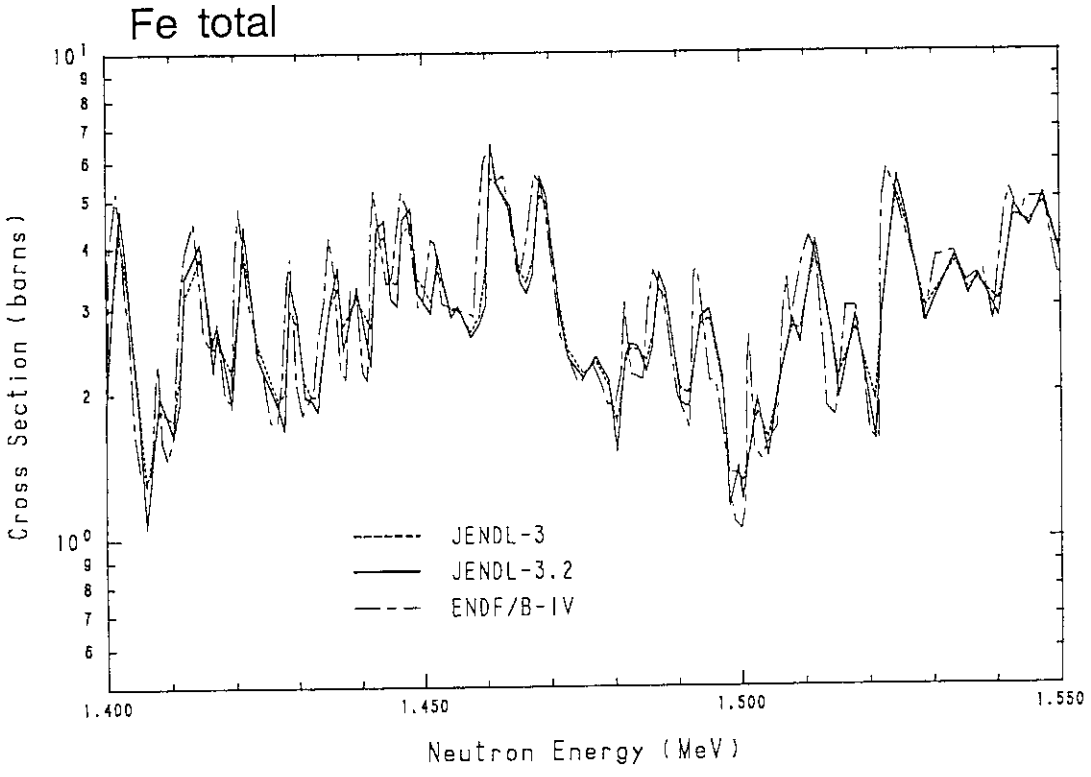

Fig. 4 Total cross section of natural Fe in the energy range from 1.5 to 1.55 MeV.

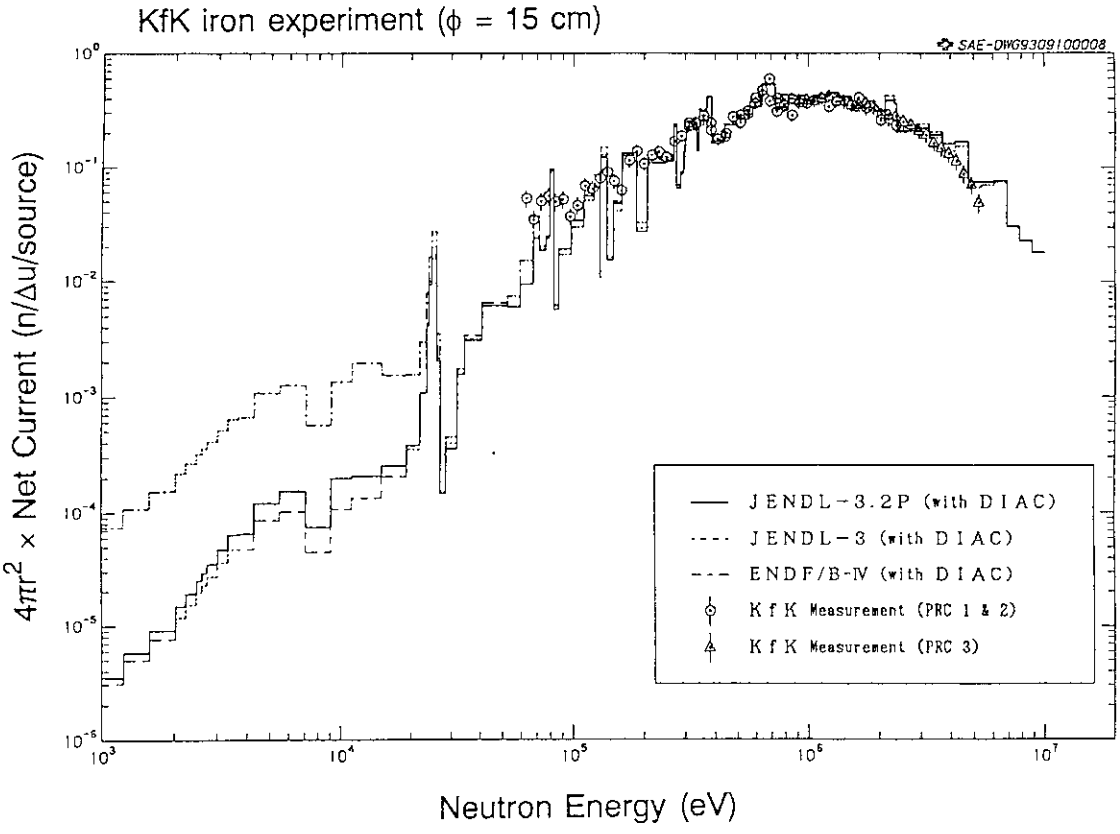

Fig. 5 Neutron spectra from KfK iron sphere with a diameter of 15 cm. A dashed line shows a spectrum calculated from JENDL-3.1 and a solid line named JENDL-3.2P from a tentative data set after modification of the total cross section. This calculation was made by Yamano[15].

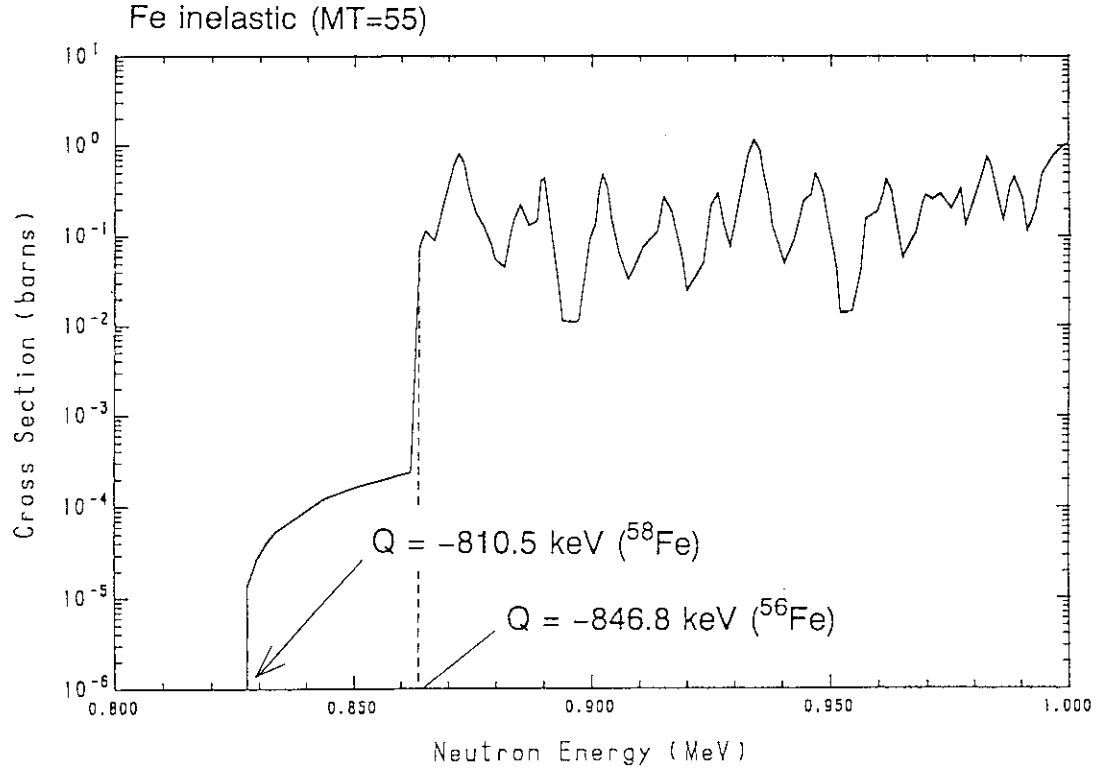

Fig. 6 Inelastic scattering cross sections of Fe (MT=55 of JENDL-3.1).

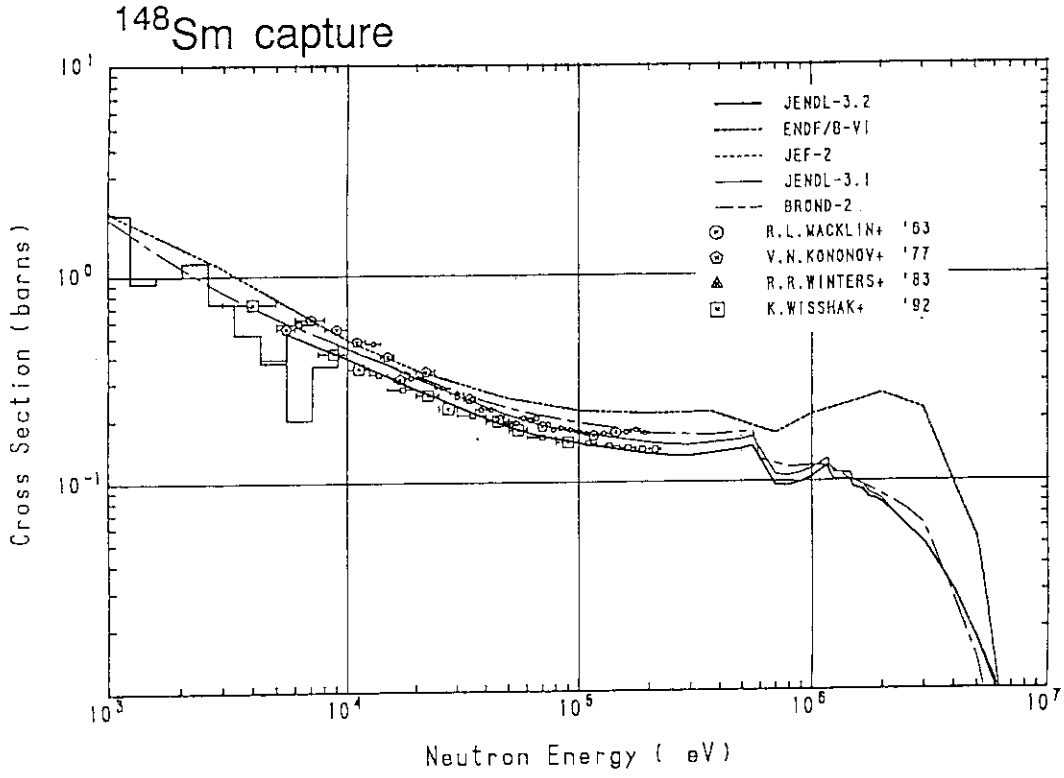

Fig. 7 Capture cross section of ^{148}Sm.

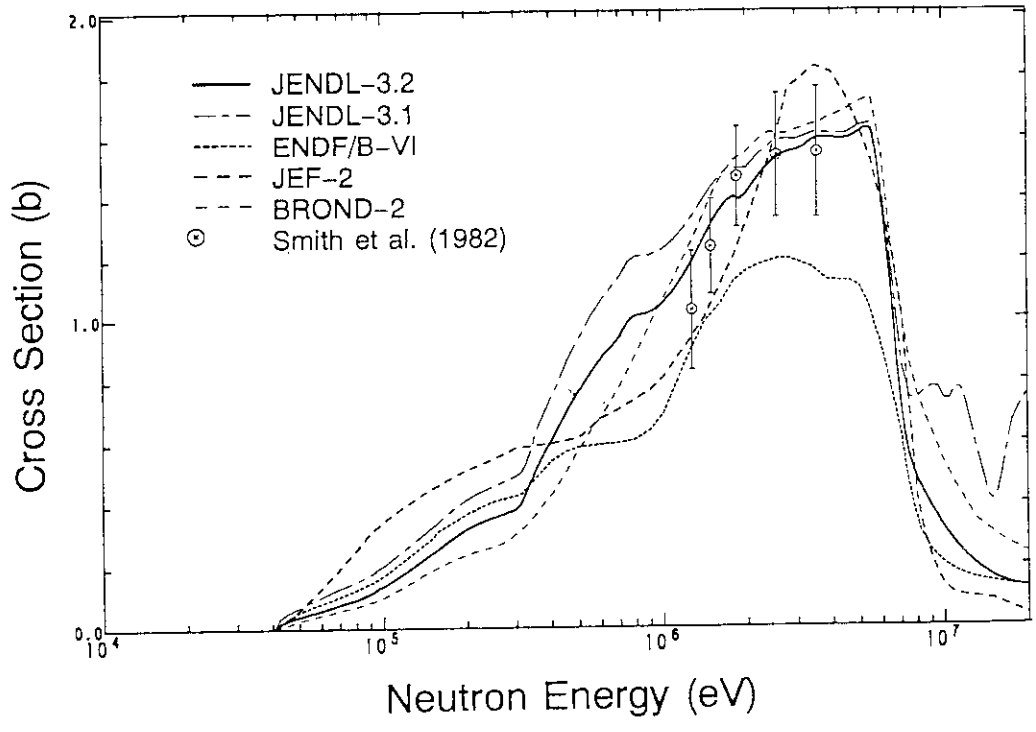

Fig. 8 Inelastic scattering cross section of ^{233}U. Experimental data are taken from Smith et al.[35]

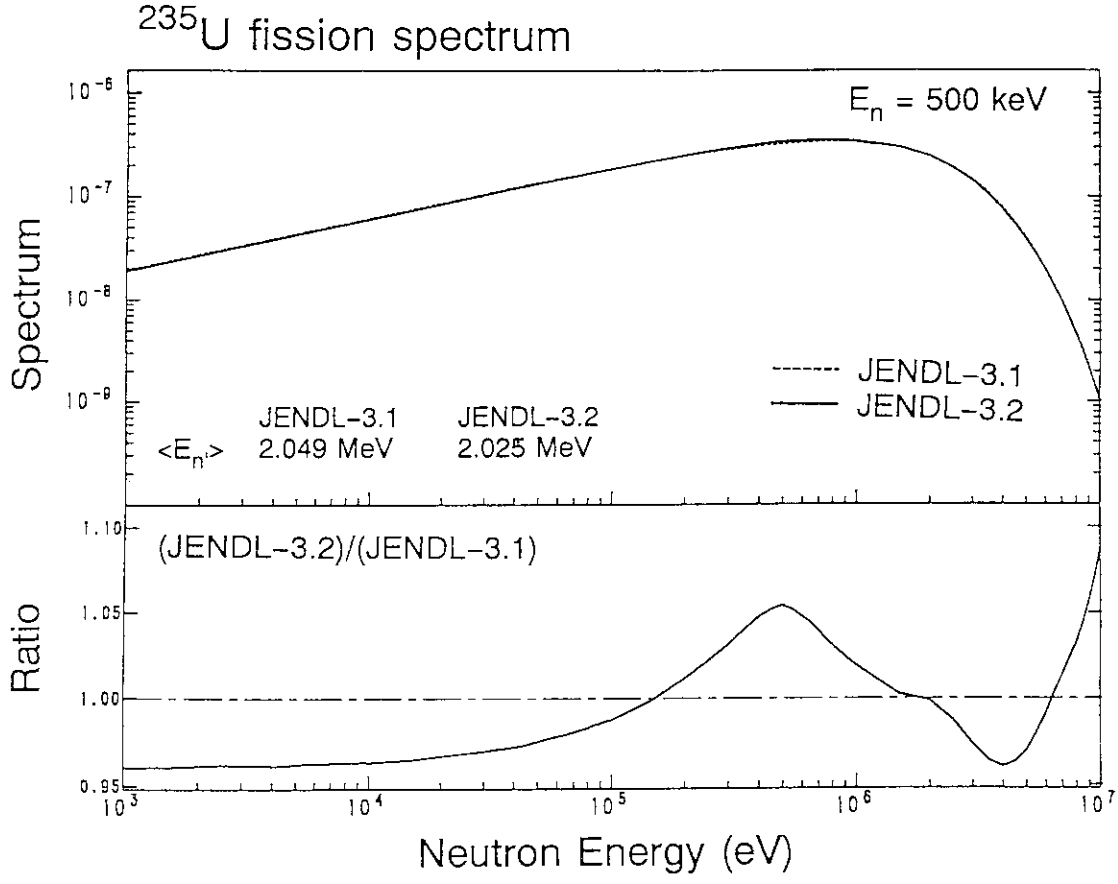

Fig. 9 Fission neutron spectrum of ^{235}U at the incident neutron energy of 500 keV. The lower part shows ratio of spectrum in JENDL-3.2 to that in JENDL-3.1. $<E_n'>$ is an average neutron energy.

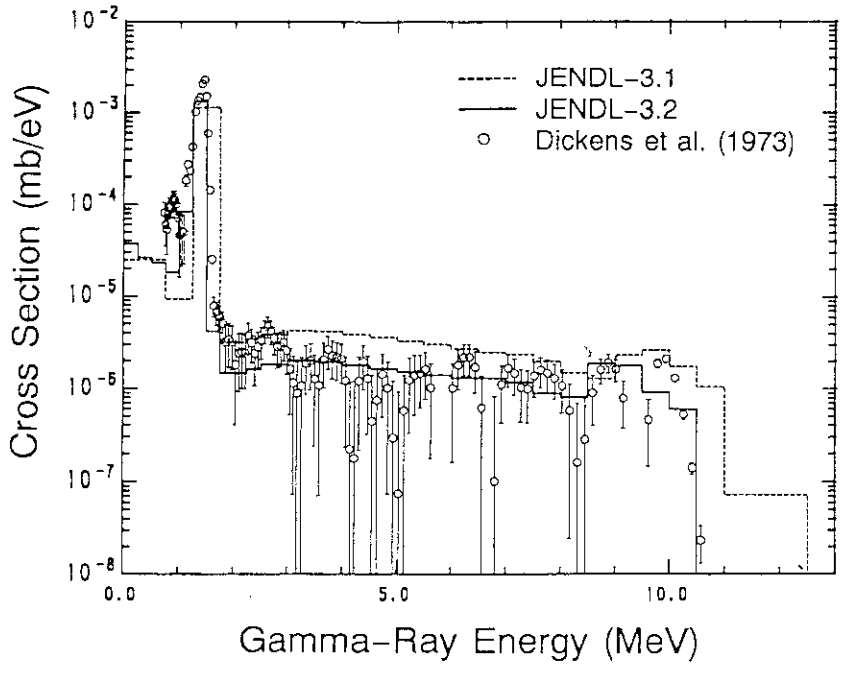

Fig. 10 Total γ-ray spectrum of natural Ni at the incident neutron energy of 1.74 MeV. Experimental data are those measured in the energy interval from 1.49 to 2.0 MeV by Dickens et al.[39]

2.2.2 Integral Test of JENDL Activation Library for Fusion Applications

Y. Ikeda

Department of Reactor Engineering, Japan Atomic Energy Research Institute,
Tokai-mura, Naka-gun, Ibaraki-ken 319-11 Japan

Abstract:

To meet urgent requirements for the data validation, an experimental analysis has been carried out for isotopic Radioactivities induced by D-T neutron irradiation in structural materials. The primary objective is to examine the adequacy of the activation cross sections implemented in the current activation calculation codes considered for use in fusion reactor nuclear design. The JENDL activation file has been evaluated and now in under integral testing with valuable experimental data. This presentation deals with the present status of results of the test concerning fusion applications. Three other activation cross section libraries along with the JENDL activation file, namely, LIB90, REAC63 and REAC175, were investigated in this present analysis. The isotopic induced radioactivity calculations using these four libraries are compared with experimental values obtained in the JAERI/USDOE collaborative program on fusion blanket neutronics. Nine materials subjected are Al, Si, Ti, V, Cr, MnCu alloy, Fe, Ni, Nb and SS316. The adequacy of cross sections is investigated through the C/E analysis,. As a result, most of discrepancies in the calculations from experiments can be explained by inadequate activation cross sections. In addition, uncertainties due to neutron energy groups, neutron transport calculation are discussed. JENDL gives the best agreements with experiments as a whole, followed by REAC175, LIB90 and REAC63 in this order. In conclusion, activation cross sections predominantly impact on the prediction accuracy in the radioactivity calculation.

1. INTRODUCTION

Induced radioactivity due to D-T fusion neutrons is an important issue in terms of the reactor safety considerations as well as the radioactive waste management of fusion reactors. Extensive efforts have been devoted to radioactivity calculations in various reactor design studies.[1-6] The neutrino design of on-going projects, e.g., ITER, should address the need for critical validations of data base relevant to the radioactivity production to meet requirement for licensing. All of design calculations, however, assume validity of the present status of knowledge of activation characteristics in the D-T neutron fields expected. Many codes and data libraries have been developed in various countries. The quality has been improved by incorporating a wealth of experimental data. An international comparison of these codes has been conducted to realize the appreciable differences in the calculations.[7] Nevertheless, it should be noted that these codes and data libraries have not been fully examined by appropriate

experiments.[8] In order to justify the reliability of data base, a more systematic endeavor is requested.

A series of experiments on the induced radioactivity have been conducted at the fusion neutronics source (FNS)[9] facility at Japan Atomic Energy Research Institute (JAERI), in the framework of JAERI/USDOE collaborative program on fusion blanket neutronics[10-14] in order to offer the data base for the validation of currently available calculational codes as well as relevant nuclear data. This paper reviews the present status of the JENDL activation cross sections[15] through C/E studies based on the above mentioned experimental data. In addition, this paper deals with several state of art other activation cross section libraries, two versions of libraries in REAC*3 code system[16], the activation file, CROSSLIB90, which is implemented in THIDA code system[17].

2. OUTLINE OF EXPERIMENT

2.1 Neutron spectrum

The sample materials were irradiated in the experimental system of the Phase-IIC[18], under the JAERI/USDOE collaborative program[10-14]. The positions of sample materials are indicated by A and B, at 100 mm from the D-T source and at 820 mm from the source corresponding to 50 mm depth into the Li_2O region. A rotating neutron target system was employed to produce high intensity D-T neutrons. The experimental system consisted of (i) Li_2O solid breeder zone in which three polyethylene layers were imbedded to simulate the water coolant, (ii) Li_2CO_3 enclosure and (iii) Polyethylene insulator zone in the outermost region. The D-T neutron source was located inside the cavity. This configuration was considered to be the best choice to realize the D-T fusion neutron environment with reflecting component. It was accepted that the position of A corresponded to the locations near the first wall. On the other hand, the position B was considered to be a representative one in the breeders blanket zone with certain amounts of Li element.

Figure 1 shows the neutron spectra of A and B, calculated by MORSE-DD[19] with FUSION-J3[20] based on the JENDL-3 nuclear data library[21]. Spectrum A represents a neutron spectrum at locations near first wall where the 14 MeV neutron flux dominates the field. The spectrum B is characterized by reduced 14 MeV neutron flux, due to larger distance from the D-T neutron target and attenuation in Li_2O region, and relatively high neutron flux in ~ MeV region. However, thermal neutron flux is lower than that in A because of the large absorption cross section of the $^6Li(n,t)^4He$ reaction in Li_2O, where the samples were irradiated. The digital data of fluxes are given in a previous report.[22]

2.2. Materials

This paper deals with candidate materials for fusion structural components. Table 1 gives the basic data for sample materials investigated. Aluminum and Silicon are the major components for the Al alloy and SiC for low activation materials Titanium, vanadium and chromium are the major constituents of the vanadium alloy (V-5Cr-5Ti) addressed in a comprehensive ITER design. Iron, nickel, again chromium, and manganese are the elements common in austenite steels, e.g. SS-316. Importance of cobalt is recognized as an impurity in almost all materials, which produces long-live ^{60}Co. Copper is also a major material used in

many parts of device. Other materials for plasma facing and functional elements are treated in an accompany paper[41].

2.3. Irradiation and counting schedule

The D-T neutrons were generated by bombarding a Ti-^{3}T target with deuteron beams, energy and intensity of which were 350 keV and 20 mA, respectively. The nominal D-T neutron yield for sample irradiation was about 1.2 x 10^{12} neutrons/s at the neutron source. Two irradiation schemes of S and L, "Short" for 30 m and "Long" for 10 h, respectively, were applied for both A and B sample positions. Induced radioactivities were measured at various cooling times after irradiation, which ranged from 10 m to several hours for "Short", and from an hour to several days for "Long".

2.4. Induced radioactivity measurement

Emission rates of γ-rays which are associated with specific radionuclides of interest are used as the experimental values to be compared with calculations. The γ-ray spectrum is also directly compared with calculations based on the same library of JENDL. Both comparisons give absolute validation of calculation which is a product of neutron flux, activation cross section and decay properties, i.e., half-life, and γ-ray emission probability. The isotopic decay rate was assigned to be the quantity for the experimental analysis.

3. EXPERIMENTAL ANALYSIS

3.1 Calculation codes and nuclear data libraries

The activation cross section libraries, presently examined, were (a) a multigroup activation cross section library with 125 energy structure based on the JENDL activation file[15] which is now under testing in the working group of one of Japanese Nuclear Data Committee, (b) CROSSLIB90 with 42 energy groups, which was implemented in the induced radioactivity calculation code system, THIDA[17], (c) cross section data file with 63 multigroup in REAC*3[16] code system and (d) updated cross section library with 175 multigroup (VITAMIN-J format) for REAC*3 code system. ACT4, the main module for activity calculation in THIDA code system, was employed for two libraries of (a) and (b). The main module of REAC was used for both calculations with two version of REAC*3 libraries. Gamma-ray decay data and chain libraries were created generally based on ENSDF. The decay and chain libraries implemented in the THIDA code system were used for the calculation with CROSSLIB90. In general, there is no serious discrepancy among decay libraries. Thus, through the comparison of radioactivity calculations with experimental measurement, straightforward discussion on the cross section validity is possible.

3.2. Spectrum condition

The neutron spectra at positions of A and B, calculated with MORSE-DD[19] were collapsed into energy groups corresponding to multigroup cross section libraries, 42 for CROSSLIB90, 63 for REAC*3 old and 175 for REAC*3 new. The original neutron spectra

with 125 energy groups were directly used for JENDL calculation. The comparison of these collapsed neutron spectra at the position A is given in **Fig. 2**. The discrepancies among the integrated flux over 10 MeV were agreed within ± 0.01 % with each other. It should be noted that there is large difference in the energy boundaries among the libraries. The coarse energy group structure was observed in the 63 energy groups structure and the 42 energy group structure show a poor resolution near the D-T neutron peak. As indicated by the 125 energy group structure, there is a distribution in neutron flux around D-T neutron peak. The neutron flux of 175 group structure almost follows the flux structure of 125 energy groups.

3.3. Comparison of calculations with experiments

The γ-ray emission rate of observed radionuclides was derived from the induced radioactivity calculations. As mentioned previously, γ-ray spectra were also compared against the measured spectra. The ACT4 module has the capability to calculate the γ-ray spectrum in which total γ-ray emissions were integrated over a given period. This capability allows γ-ray emission profiles to be directly compared with the measurements without any approximation.

4. RESULTS AND DISCUSSION

The results of experimental analysis are given material wise and isotopic radionuclides product wise. The calculations with libraries of JENDL activation file, CROSSLIB90, REAC library with 63 energy groups and that of 175 energy groups, are, hereafter, denoted as JENDL, LIB90, REAC63 and REAC175, respectively. Also, the notations of Φ(A) and Φ(B) are used for the neutron spectra at position A and position B, respectively. The indices for irradiation and cooling times are assumed the same as described in the experiments. Some demonstrative examples for validations of the isotopic radioactivities are given as follows on materials of aluminum and nickel:

Aluminum

Figure 3.1 shows C/Es for ^{27}Mg and ^{24}Na decay rates in both Al samples at position A and B.

^{27}Mg: The activity of ^{27}Mg is produced via the ^{27}Al(n,p)^{27}Mg reaction which is well known in the dosimetry application. The cross section has been extensively studied. As the four libraries give similar cross sections values at 14 MeV region, all calculations exhibited close C/Es, although there are slight underestimations ranging from 0.85 to 0.95. Though these C/Es seem adequate from consideration of the overall experimental uncertainty range of ± 10 %, cross sections should be reevaluated. Recent precise measurements for this cross section suggested that the data in a energy region from 14.5 to 15 MeV in JENDL are 5 to 10 % lower than the new experimental data for this reaction.

^{24}Na: The reaction of ^{27}Al(n,α)^{24}Na is one of most accurately studied and cross section has been evaluated precisely. The JENDL gives most preferable results with C/Es around 1.0. REAC*63 shows comparable good results. LIB90 is slightly lager than 1.0 by 10 %. The cross

section of REAC*175 is very close to those of JENDL and REAC*63, as shown in **Fig. 4.1**. However, C/E with REAC*175 is systematically high being 1.3 to 1.4 for all cases. This overestimations are due to contribution of $^{27}Al(n,\alpha)^{24m}Na$, the cross section curve of which is shown in **Fig. 4.1**. The ^{24m}Na is the isomeric state of ^{24}Na and deexcites to the ground state of ^{24}Na with 2 ms half-life. In the REAC*175, both the reactions are treated separately. However, in general, the cross section of $^{27}Al(n,\alpha)^{24}Na$ is given as a sum of both the meta-stable and ground state productions. In this view, the cross section of $^{27}Al(n,\alpha)^{24m}Na$ is doubly counted in the REAC*175 library. For completeness, different reaction paths should be treated independently as in the REAC*175. However, the cross section for the meta-stable state production should be subtracted from the ground stated production cross section.

The good results of ^{24}Na except for the case of REAC*175, demonstrate that the neutron spectra used in the present analysis are adequately validated as far as the high energy fluxes are concerned. This assures the validity of the present test for many threshold reactions.

Nickel

^{57}Ni: As shown on **Fig. 3.2**, JENDL gives C/Es close to 1.0 while the other libraries tend to exhibit lower C/E than 1.0. The cross section of $^{58}Ni(n,2n)^{57}Ni$ reaction strongly dependent on the neutron energy in the 14 MeV region because of the high threshold energy at 12.5 and steep excitation function of this reaction. When the D-T neutrons dominate the spectrum, the evaluated average cross section tends to be small. As long as D-T fusion neutron fields are present, the cross sections for the high threshold reaction such as $^{58}Ni(n,2n)^{57}Ni$ should be prepared with a sufficiently fine energy group structure. Otherwise, unreasonable underestimation or overestimation could easily occur. The validity of JENDL calculation is also assured by the fact that the cross section of this reaction in JENDL is consistent with the recent measurement at FNS[44].

^{57}Co: The ^{57}Co is yielded from the direct reaction of $^{58}Ni[(n,np)+(n,d)]^{57}Co$ and the decay of the parent nuclide of ^{57}Ni, which is produced via the $^{58}Ni(n,p)^{57}Ni$ reaction. Considering the decay half-life of 36 h for ^{57}Ni and the large cross section of $^{58}Ni[(n,np)+(n,d)]^{57}Co$, the decay rate of ^{57}Co at the rather short cooling time corresponds to ^{57}Co due to the direct reaction. Except REAC*63, calculations agree with the experiments within overall experimental uncertainty. JENDL treated the cross section as sum of both (n,np) and (n,d), while other libraries separately give the cross sections for the two different channels. The overestimations in REAC*63 are caused by the one order of magnitude higher cross section for (n,d) reaction.

^{58}Co: As shown in **Fig. 3.2**, JENDL and REAC*175 are in good agreement with measurement. LIB90 and REAC*63, however, largely overestimate the experiments. It is found from **Fig. 4.2** that there are unreasonable large overestimations in this cross section in libraries of LIB90 and REAC*63. This obviously give unreasonably large C/Es. The difference in C/Es for cases with long irradiation and cooling time between JENDL and REAC*175, however, should be noted. This is due to the difference in the isomer production cross section. At the short irradiation and cooling time, ^{58m}Co doesn't contribute to the ^{58}Co because of delay by the decay half-life of 9 h as discussed in ^{58}Co production in cobalt. However, $^{58}Ni(n,p)^{58m+g}Co$

should be considered in the case with long irradiation and long cooling time. The overestimation in REAC*175 for the case of B indicates that the cross section of ^{58m}Co production is too large in the energy region below 14 MeV.

^{60}Co: The ^{60}Co is one of the most important long-lived radionuclides. JENDL and REAC*175 underestimate measurement by 25 and 20 %, respectively. This is reflected by the evaluation of JENDL-3 cross section lower by 20 % than the recent experimental value at FNS[44]. The cross section of REAC*175 seems lower than the current experimental value by 20 %. When the cross sections are revised by using the new experimental value, better agreement could be achieved. The overestimation of LIB90 by 20 % is explained by the large cross sections at 14 MeV being 180 mb, which is 20 % larger than the experimental value of 150 mb. The best agreement is observed in REAC*63, even though the cross section in the library seems too coarse.

^{65}Ni and ^{62m}Co: Concerning ^{65}Ni production, only ratios to JENDL are shown in Table III. REAC*63 show a factor of two larger value than those of other libraries. For ^{62m}Co production, JENDL has a problem giving a C/E of 5. This can not be explained by the difference in the cross sections at 14 MeV. Other possible sources in the decay chain and γ-ray yield libraries should be investigated. An overestimation by a factor of 2.7 in REAC*63 is attributable not only to large cross section of ^{62}Ni(n,p)^{62m}Co at 14 MeV, but to the unreasonably high cross section of ^{64}Ni(n,t)^{62m}Co reaction in the library. The ratio of C/E in REAC*175 to that in LIB90 corresponds to the ratio of cross section of ^{62}Ni(n,p)^{62m}Co at 14 MeV in REAC*175 library to that in LIB90.

5. DISCUSSION

5.1 C/E distribution

The validity of the currently available cross section libraries has been examined through the C/E in fusion neutron environment. The total number of cases is 95 on 44 reaction products for 12 elements were considered according to the data examined. **Figures. 5.1** to **5.4** show more specific C/E distributions given as (C-E)/E for JENDL, LIB90, REAC*63 and REAC*175, respectively. The C/E distribution for JENDL exhibits a very sharp peak in the number of cases. Except one case showing deviation of a factor of 4, all calculations show deviations from measurements less than a factor of 2. There is also a peak around the center [(C-E)/E=0] in LIB90's distribution. It, however, gives a distribution broadened profile. Contrary to rather symmetric distributions in JENDL and LIB90, deviations in REAC*63 show a distorted distribution. A tail in the positive region indicates that REAC*63 tends to give overestimations. The distribution of REAC*175 seems similar to that of LIB90. As long as the present study is concerned, it is concluded that JENDL with 125 energy bin structure is the best in quality among libraries test. Although, REAC*175 is assumed to based on updated cross section data base, it is pointed out that there is still a need to improve its quality. LIB90 showed a modest result, however, the data is insufficient, and should be replaced with the more

realistic data of JENDL. REAC*63 now should be substitute with the new version of REAC*175.

5.2 Uncertainty in experimental data

Experimental error assessment is the starting point to evaluate C/E. Here, the experimental error is outlined to give a fundamental idea of the uncertainty range in C/E consideration. For the quantity of radioactivity intensity per gram, per normalized source intensity, the major sources of experimental error consists of (i) statistical error for γ-ray peak counts of interest, (ii) error of γ-ray detector efficiency, and (iii) neutron yield at the source. In the present study, some of γ-ray results with poor statistics were discriminated in order to provide data with reasonable accuracy, even though activities of these γ-rays were identified. In general, errors due to counting statistics were less than ± 10 %, in many cases, less than ± 5 %. The error associated with the γ-ray detector efficiency normally was assigned to ± 3 %. In the measurement, multiple relative γ-ray detectors were employed to make consecutive counting of plural samples. Thus, additional errors due to efficiency calibrations should be taken into. The error of neutron yield was less than ± 2 %. As a result, overall experimental error ranged from ± 5 to 15 % in most cases.

5.3 Uncertainty in the calculation

In general, the coarse energy group structure tend to offer results less sensitive to neutron energy spectrum; averaging the cross section in a broad energy interval. For example, reaction rate calculations for reactions with steep excitation functions around 14 MeV energy requires careful treatment for the cross section averaging. **Figure 6** illustrates changes of reaction rate with change of mean D-T peak energy for three representative (n,2n) reactions; $^{46}Ti(n,2n)^{45}Sc$, $^{58}Ni(n,2n)^{57}Ni$ and $^{63}Cu(n,2n)^{62}Cu$, and the $^{27}Al(n,\alpha)^{24}Na$ reaction. The calculations are based on the JENDL library with 125 energy group structure. The neutron energy spectra at different emission angles, calculated with the MORSE-DD for the rotating neutron target system, were used in the present analysis. In **Fig. 6,** boundaries of the other energy group structures are shown. The finest energy structure in the energy region around 14 MeV is found in JENDL, even the total number of groups, 125, is less than the 175 groups in REAC175. This figure demonstrates that the calculation with coarse group structures can be insensitive to changes of the neutron spectrum. For D-T fusion reactor, we can assume that the mean D-T neutron peak energy is close to 14.1 MeV. Most of multigroup libraries have been prepared based on this assumption. In general, the peak energy of accelerator based D-T neutron source is strongly dependent on the angle of sample position with respect to the incident d^+ beam energy, as in the case of the present experiment at FNS. In this case, we have to use the fine neutron spectrum as the weighting function to prepare the cross sections with coarse energy structure. This seems impractical. Thus, it is recommended to use an energy group structure as fine as possible in the activation calculation. Recent development of computer with high speed, large disk space and less expensiveness mitigates the difficulty to run a code system with fine energy bin structure such as 125 and 175 groups.

Another uncertainty, we must consider, is associated with the transport calculation of neutron flux. Throughout the present examination, we assumed that spectra A and B are well

defined with certain accuracy. For the high energy part, in fact, validity of these spectra was assured from the excellent agreement between calculations and experiments for radioactivities of ^{24}Na and ^{92m}Nb production cross sections of which are considered to be the most reliable. The reasonably good agreement of the MORSE-DD calculation with the measurement for $^{115}In(n,n')^{115m}In$ reaction rate[23] also demonstrated the validity of calculation in the MeV region of the neutron flux. Thus, the uncertainty range of ± 10 % could be assured for the neutron fluxes in the energy range higher than 1 MeV from the considerations of C/E values as well as the cross section uncertainties for the dosimetry reactions.

However, it is extremely difficult to quantify the uncertainty range of neutron flux below 0.1 MeV because there were no effective verification with appropriate dosimetry reactions. **Figures 7** shows the differential sensitivities of reaction rates derived by multiplying reaction cross sections in JENDL and the spectrum A, for representative (n,γ) reactions, $^{63}Cu(n,\gamma)^{64}Cu$, $^{55}Mn(n,\gamma)^{56}Mn$ and $^{59}Co(n,\gamma)^{60}Co$. It is found that in the both spectra, the neutron flux in the resonance energy region contributes predominantly to the total reaction rate. In particular, more than 70 % of the total is contributed from that flux. Large differences among the calculations of four libraries were observed not only in the total reaction rate, but in the fractional contributions. These discrepancies are partly attributable to the difference in the energy group structures and partly due to the difference in the cross section values themselves. Therefore, in the present test, there should be a limitation for further discussion on the dominant radionuclides produced by the (n,γ) reactions.

6. CONCLUSION

Precise analysis of induced radioactivities in the structural materials for D-T fusion reactor components were conducted in order to examine the adequacy of activation cross section libraries which are commonly used or are to be utilized in neutronic calculations for comprehensive reactor designs analysis. JENDL activation library, and REAC*3 library were thoroughly tested by using broad experimental data obtained under the framework of JAERI/USDOE collaboration.

We found that almost all deviations of calculation from experiments can be attributed directly to inadequacy in the activation cross sections or improper treatment of decay chains. Requirement from the "Completeness" for activation cross section library has to be satisfied by theoretical calculation or systematic estimation for rare reactions for which there is no experimental data. The outcome of this work clearly provides direct information on the deficiency of the cross sections and inadequacy of these values. We are encountering the crucial decision on which library should be taken as the foremost data library which is well validated for the critical design of ITER, or DEMO. If the validation is the foremost issue in adopting the library, JENDL activation library would be the best choice as far as the libraries tested in the present study. The weakness of JENDL is characterized by the incompleteness for covering all physically possible reactions. However, the effort is still vigorously in progress. The final version of JENDL, no doubt, will satisfy both requirements. REAC175 seems the most preferable library among the libraries tested here, at present, from the "completeness" requirement point of view with sufficient energy group structure. However, as pointed out in

the present study, there are a lot of unreasonable implementations of cross sections, even though they are well known and frequently appear in the radioactivity calculations. When the cross sections are to be revised based on the suggestions made in the present work, the REAC175 will be the best library from the completeness point of view.

References

[1] S. Blow, "Some Features of the Behavior of Structural Materials in a Possible Fusion Reactor Blanket," AERE-R 6845 (1971).

[2] W. F. Vogelsang, et al., Nucl. Technol., 22, 379 (1974).

[3] D. J. Dudziak and R. A. Krakowski, Nucl. Technol., 25, 32 (1975).

[4] R. W. Conn, T. Y. Sung and M. A. Abdou, Nucl. Technol., 26, 391 (1975).

[5] M. L. WIlliams, R. T. Santoro and T. A. Gabliel, Nucl. Technol., 29, 384 (1976).

[6] W. F. Vogelsang, "Radioactivity and Associated Problems in Thermo-nuclear Reactors," UWFDM-178 (1976).

[7] E. T. Cheng, et al., "International Fusion Activation Calculation Comparison Study," TSIR-12 (1991).

[8] Y. Ikeda et al., Fusion Technology, 8, 1466 (1985).

[9] T. Nakamura, et al., Proc. 4th Symp. on Accelerator Sci. and Technol., RIKEN, Saitama, November 24th - 26th, 1982, pp155-156.

[10] T. Nakamura and M. A. Abdou, Fusion Technology,10, 541 - 548 (1986).

[11] H. Maekawa and M. A. Abdou, Fusion Design and Engineering, 18, 275-280 (1991).

[12] T. Nakamura, et al., Fusion Technology, 19, 1873 (1991).

[13] Y. Oyama, et al., Fusion Technology, 19, 1879 (1991).

[14] Y. Oyama, et al., Fusion Engineering and Design, 18, 203 (1991).

[15] Y. Nakajima, "JENDL Activation Cross Section File," JAERI-M 91-032 (1991) pp43-57.

[16] F. M. Mann, "REAC*3 Nuclear Data Libraries," Proc. Intl. Conf. on Nucl. Data for Sci. and Technol., Jülich, Germany, 12-17 May 1991, pp936-938.

[17] Y. Seki et al., "THIDA-2: An Advanced Code System for Calculation of Transmutation, Activation, Decay Heat and Dose Rate, " RSIC computer code collection, CCC-410 (April 1987).

[18] Y. Oyama, et al., "Phase-IIC Experiments of the USDOE/JAERI Collaborative Program on Fusion Blanket Neutronics -- Experiments and Analysis of Heterogeneous Fusion Blanket--Vol-I: Experimental Results," JAERI-M 92-183 (1992), UCLA-FTN-64, UCLA-ENG-93-19.

[19] M. Nakagawa and T. Mori, "MORSE-DD; A Monte Carlo Code Using Multi-Group Double Differential Form Cross Section," JAERI-M 84-126 (1984).

[20] K. Maki, et al.: "Nuclear Group Constant Set FUSION-J3 for Fusion Reactor Nuclear Calculations Based on JENDL-3," JAERI-M 91-072 (1991).

[21] K. Shibata, et al., "Japanese Evaluated Nuclear Data Library, Version-3," JAERI-1319 (1990).

[22] Y. Ikeda, et al., "Joint Report of JAERI/USDOE Collaborative Program on Fusion Neutronics --Induced Radioactivity Measurements in Fusion Neutron Environment --," JAERI-M 93-018 (1993), UCLA-ENG-91-32, UCLA-FTN-53

[23] M. Nakagawa, et al., "JAERI/U.S.Collaborative Program on Fusion Blanket Neutronics -- Analysis of PhaseIIA and IIB Experiments --," JAERI-M 89-154 (1989).

Table 1 Atomic weight, density and chemical composition of primary impurities in the samples used in induced activity irraditions

Sample Material	Atomic Weight (g)	Density (g/cm^3)	Chemical composition by weight %
Aluminum (Al)	26.98154	2.70	Al (99.97), Mg (0.006)
Silicon (Si)	28.0855	2.42	Si (99.99)
Titanium (Ti)	47.88	4.5	Ti (99.6), O (0.13), Al (0.03), Cr (0.03), Mn (0.03), Ni (0.03), V (0.03), Fe (0.02)
Vanadium (V)	50.9415	5.87	V (99.82), Si (0.044), Ta (0.03), O (0.03), Mo (0.013), Zr (0.01), Fe (0.01), Al (0.01), Hf (0.01)
Chromium (Cr)	51.996	7.14	Cr (99.0), Fe (0.43), Al (0.10), Si (0.05)
Iron (Fe)			Fe (99.92), Mn (0.059), C (0.02)
Mn-Cu alloy (MnCu)	-------	7.58	Mn (79.78), Cu (19.66), Ni (0.46), Fe (0.07)
Iron (Fe)	55.847	7.86	Fe (99.92), Mn (0.059), C (0.02)
Cobalt (Co)	58.9332	8.71	Co (99.95), Ni (0.04)
Nickel (Ni)	58.69	8.80	Ni (99.97), C (0.016)
SS316	-------	7.90	Fe (66.22), Cr (17.75), Ni (11.60), Mo (2.08), Mn (1.33), Si (0.42), Co (0.19), Cu (0.34), V (0.06)
Niobium (Nb)	92.9064	8.57	Nb (99.91), Ta (0.018), Zr (0.01)

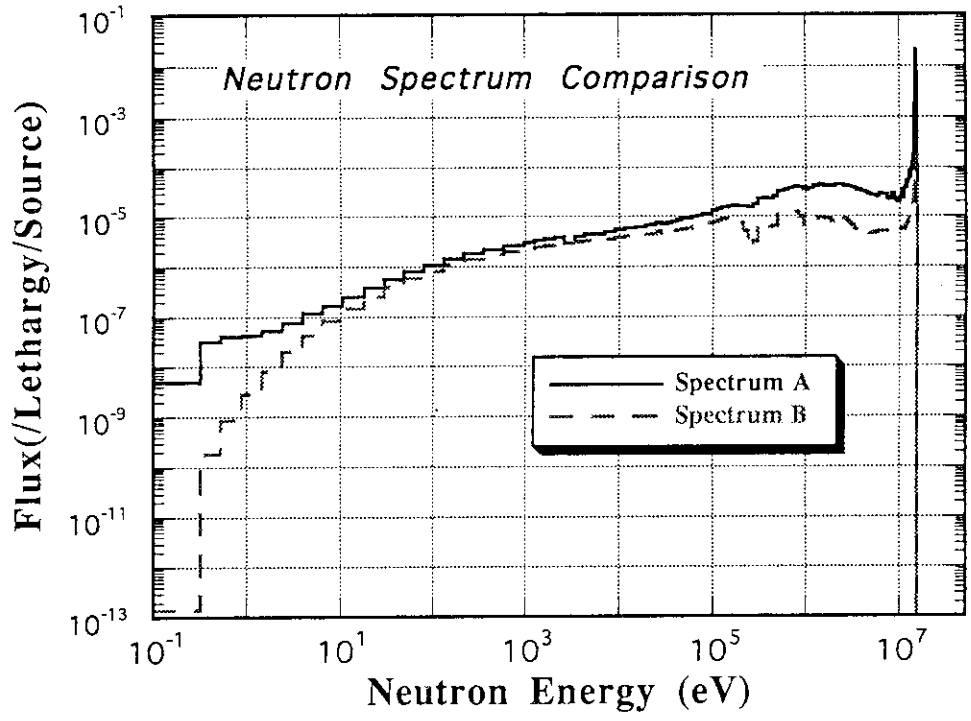

Fig. 1 Neutron spectra at positions of A and B, calculated with MORSE-DD incorporated with JENDL-3.

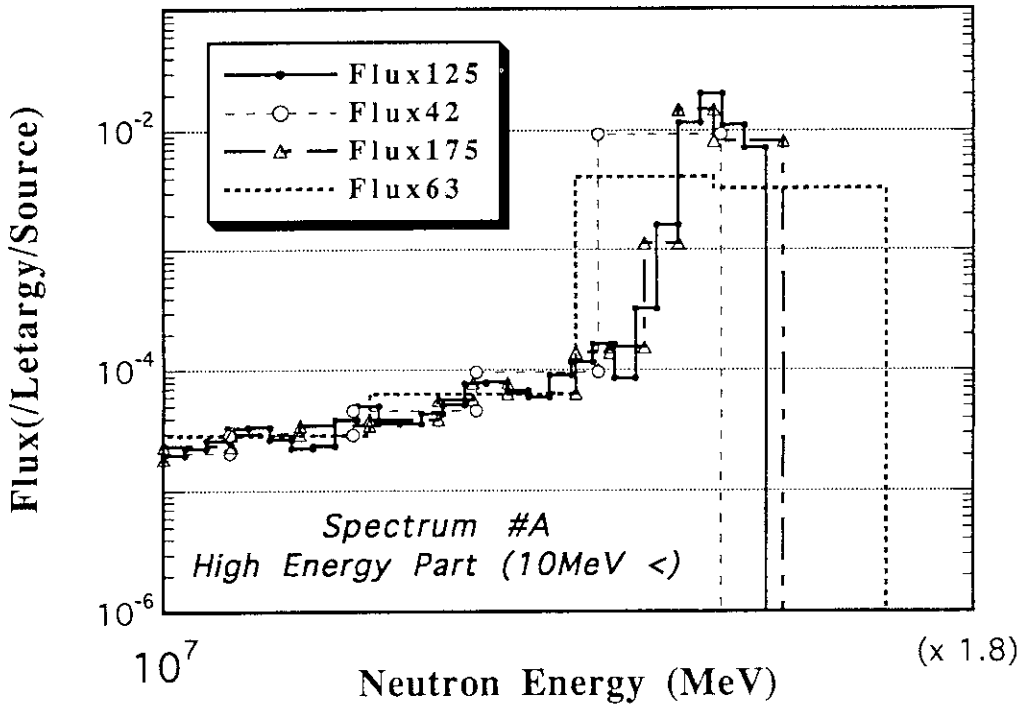

Fig. 2 Comparison of neutron energy spectra with different energy groups around D-T neutron peak region.

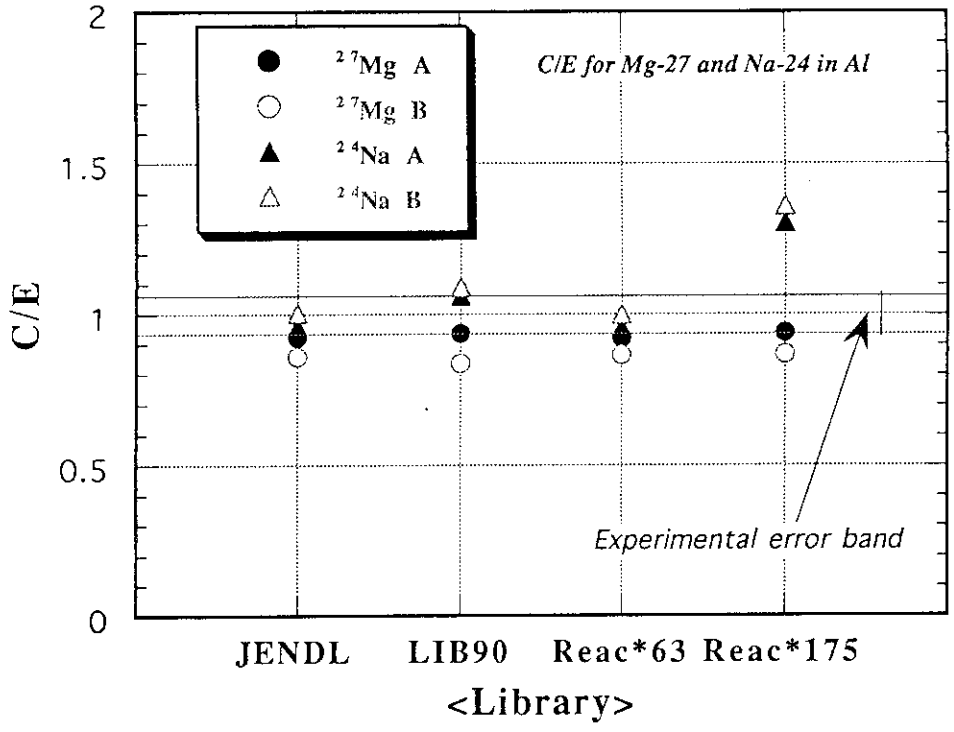

Fig. 3.1 C/E values of isotopic radioactivities in Al.

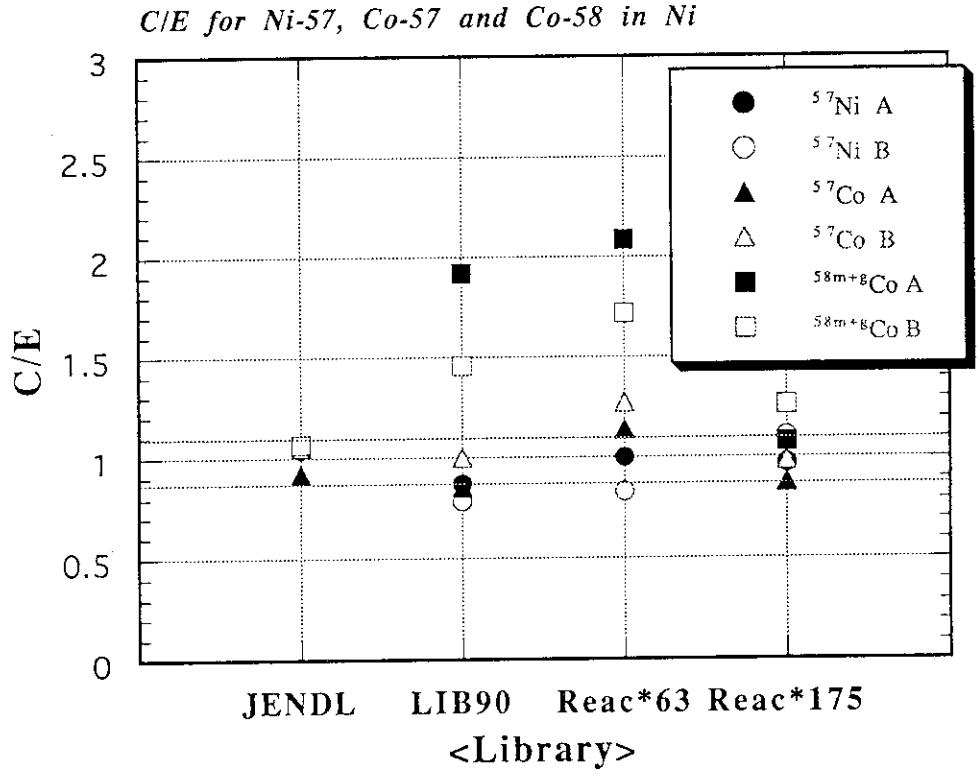

Fig. 3.2 C/E values of isotopic radioactivities in Ni.

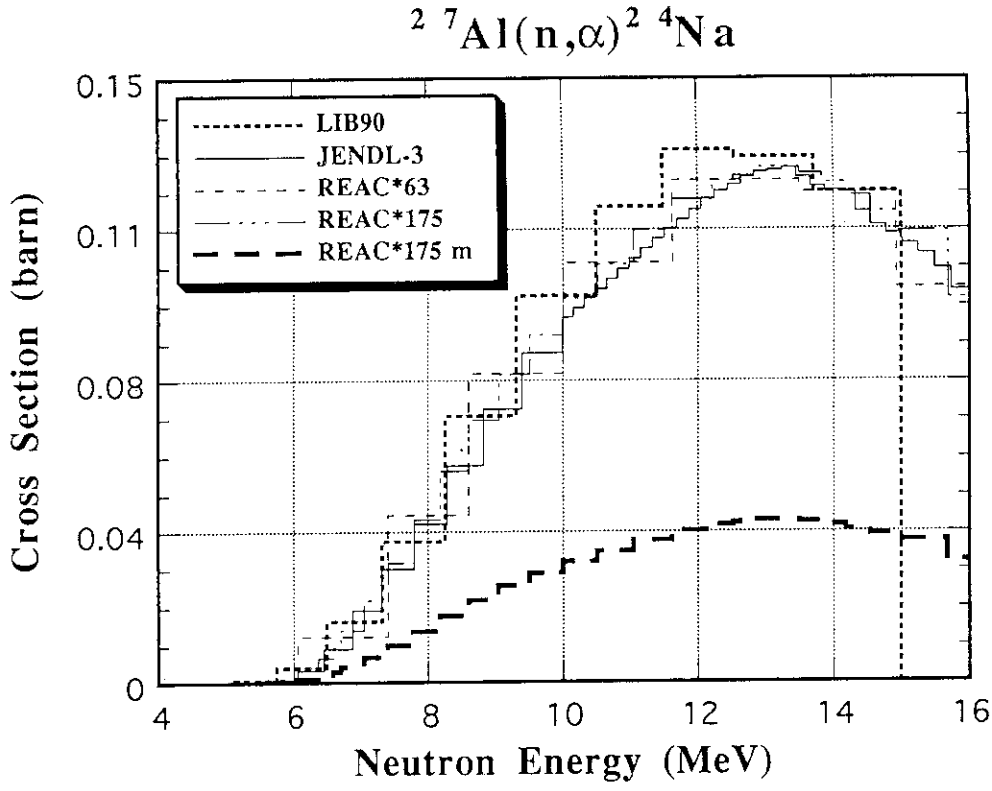

Fig. 4.1 Cross sections for the $^{27}Al(n,\alpha)^{24}Na$ in the four different libraries.

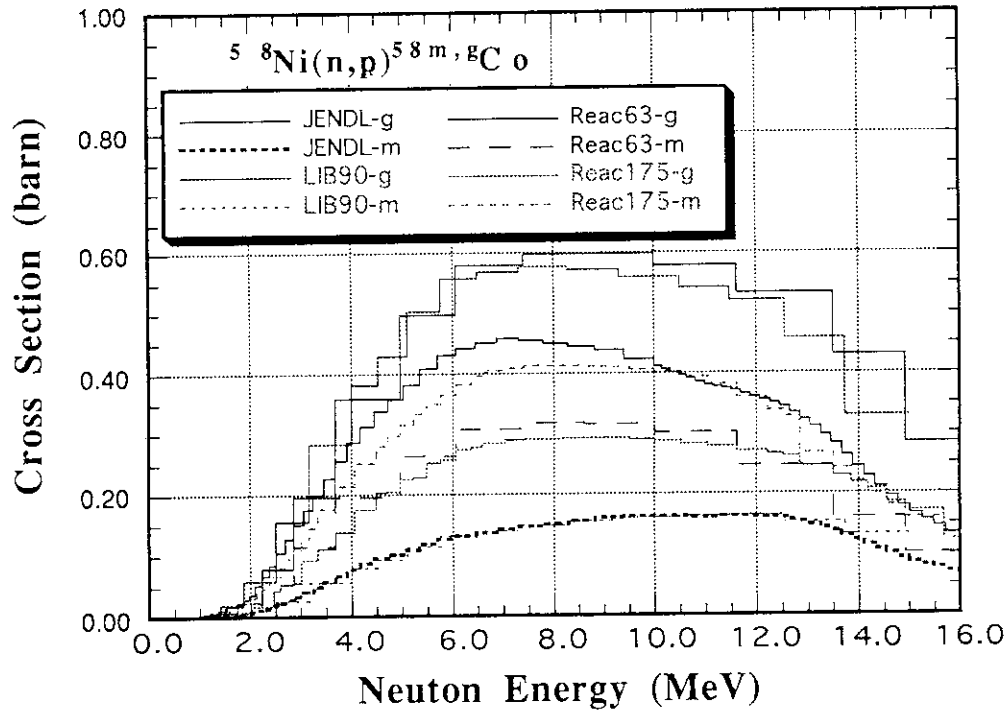

Fig. 4.2 Cross sections for the $^{58}Ni(n,p)^{58m,g}Co$ in the four different libraries.

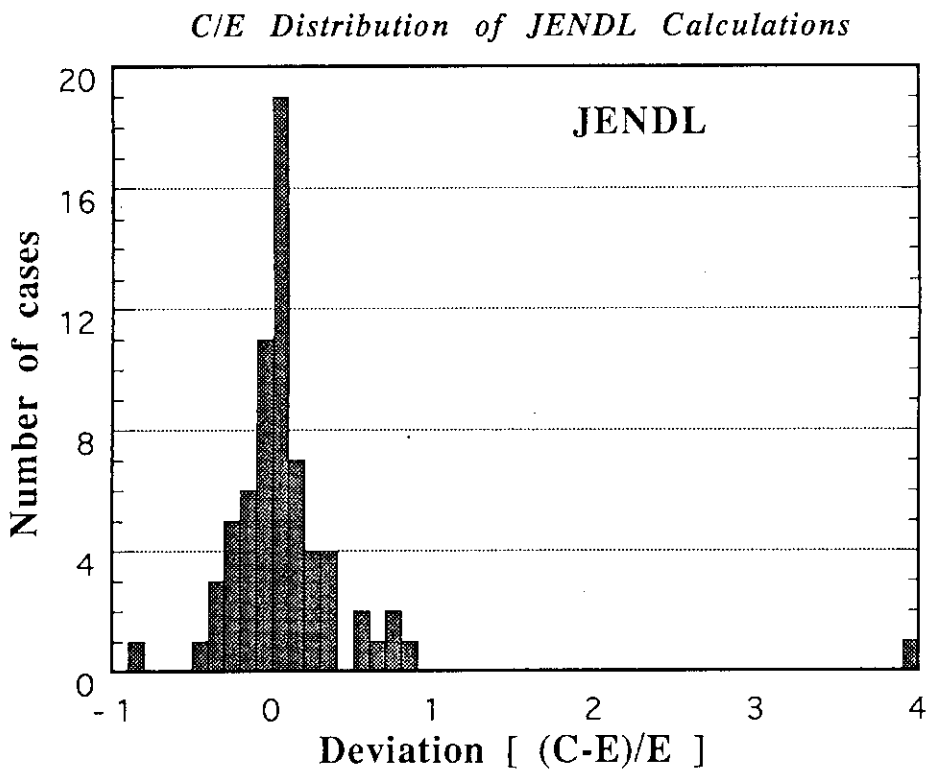

Fig. 5.1 C/E distribution for JENDL.

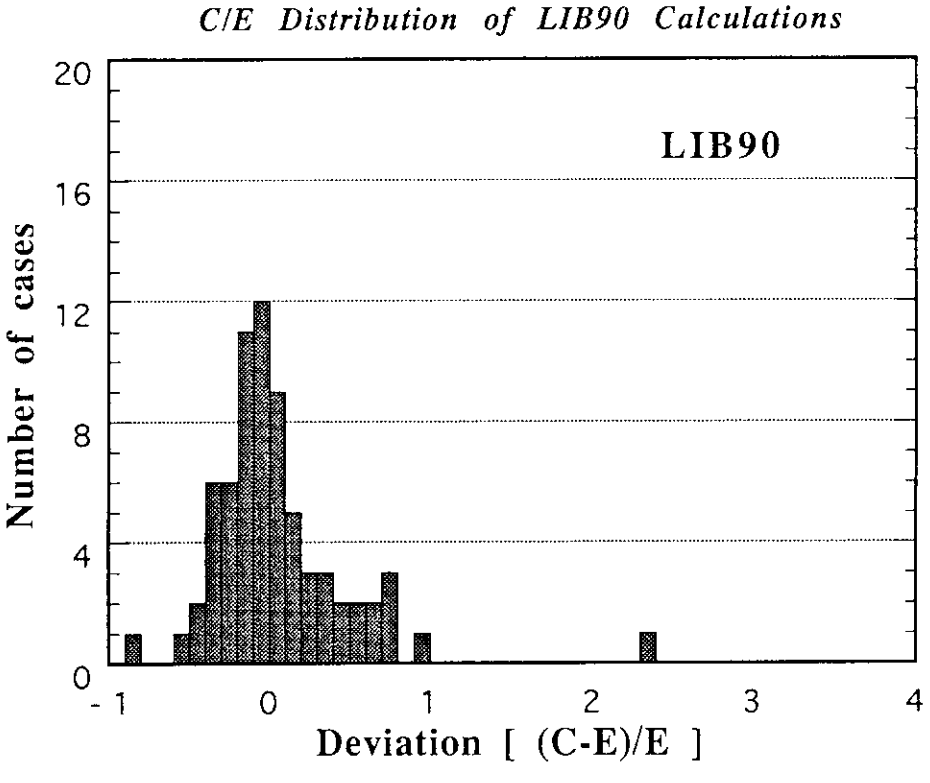

Fig. 5.2 C/E distribution for LIB90.

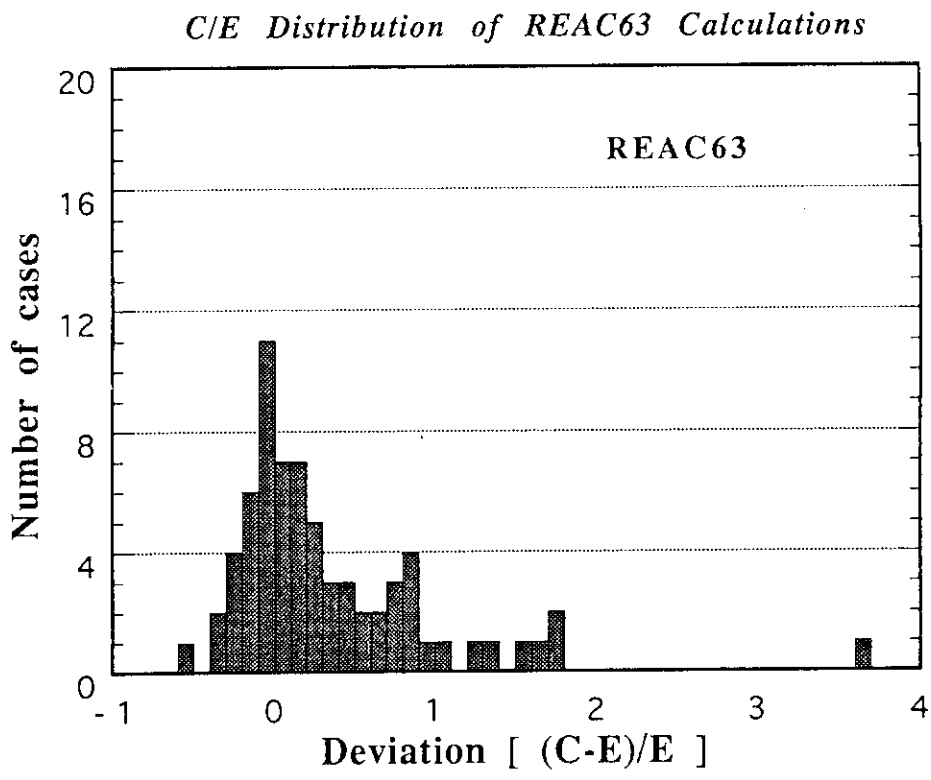

Fig. 5.3 C/E distribution for REAC*63.

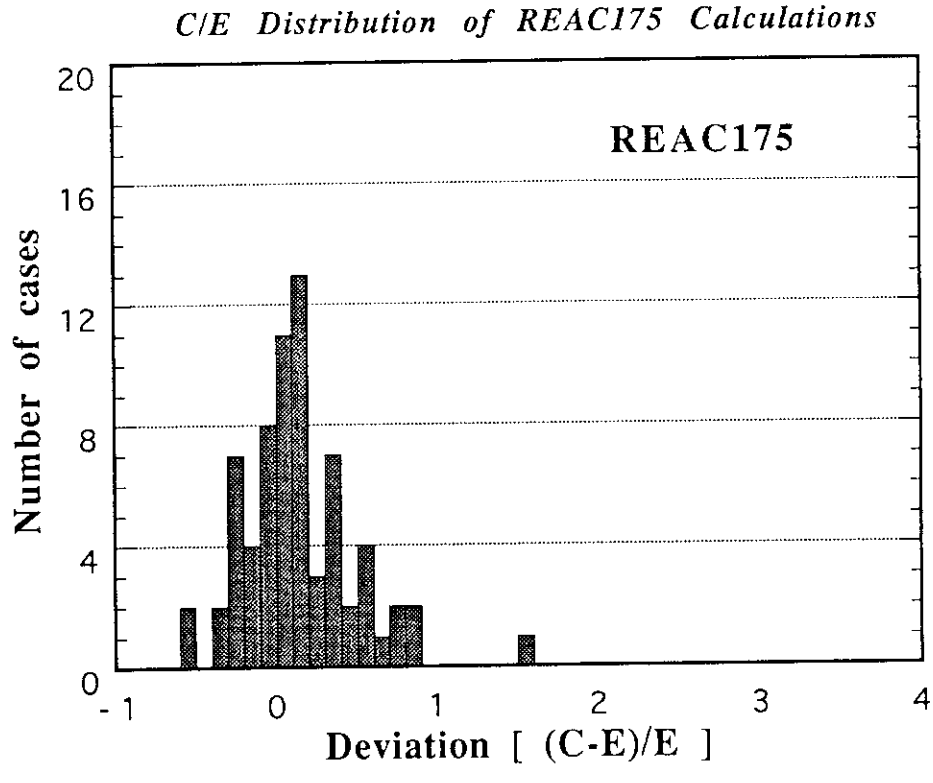

Fig. 5.4 C/E distribution for REAC*175.

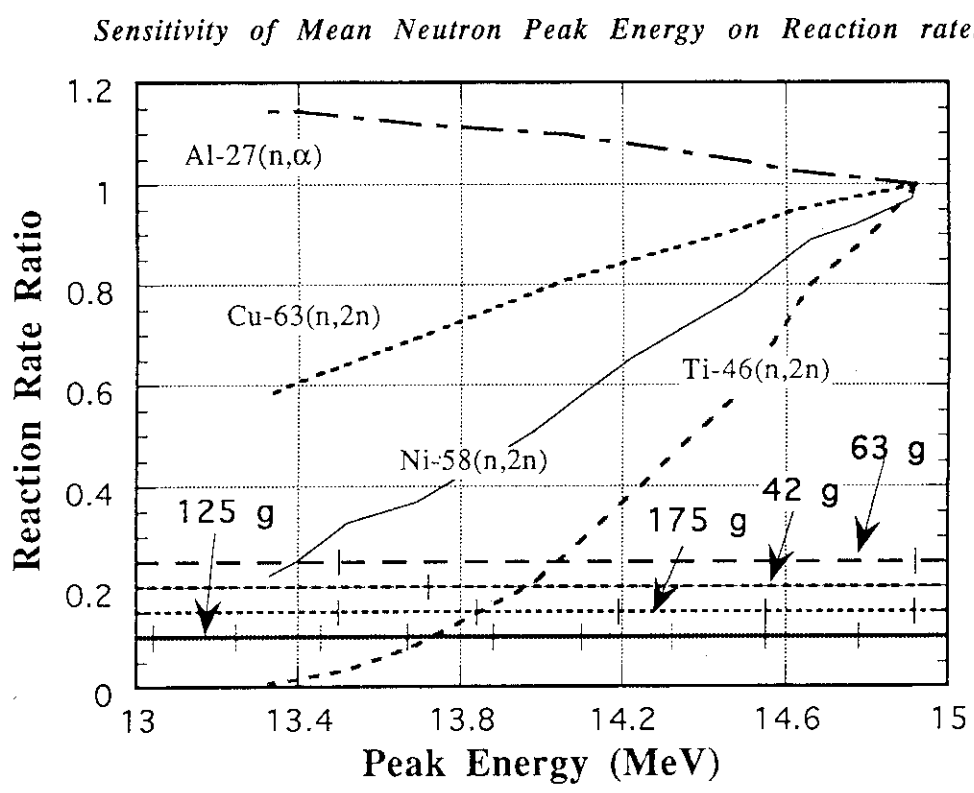

Fig. 6 Changes in reaction rates for high energy threshold reactions with respect to neutron energy changes.

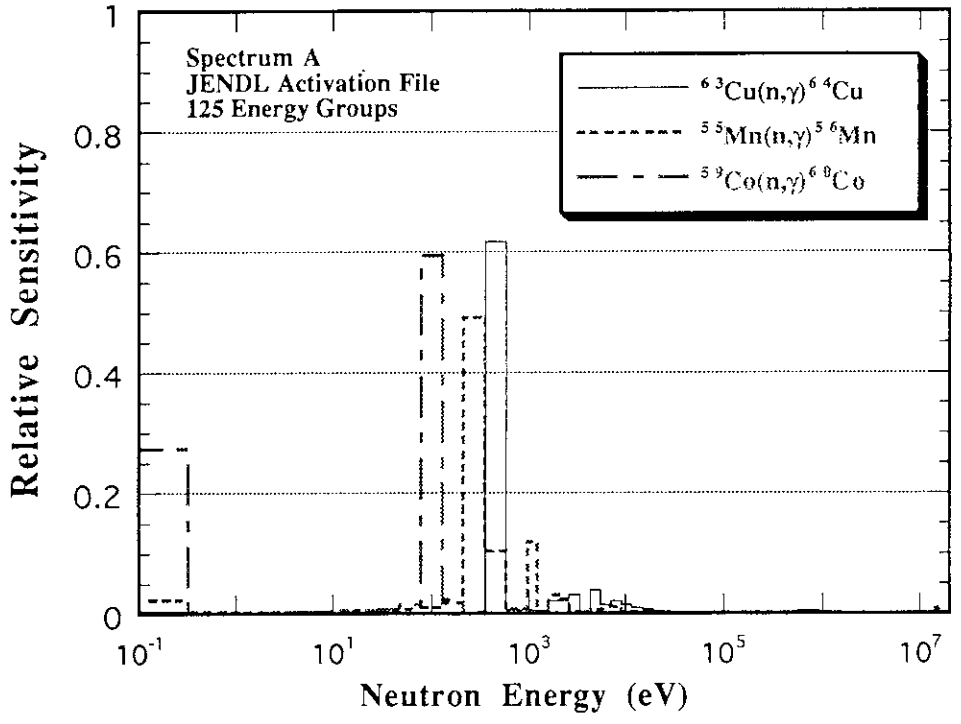

Fig. 7 Differential sensitivities of the (n,γ) reactions for the spectrum A.

2.2.3 Shielding Experiments with Quasi-monoenergetic Several Tens MeV Neutrons at 90 MV AVF Cyclotron Facility TIARA

Takashi Nakamura* and Accelerator Shielding Experiment Group

*Cyclotron and Radioisotope Center, Tohoku University

Aoba, Aramaki, Aoba-ku, Sendai 980, Japan

Abstract

The research programme has started as a cooperative project between Japan Atomic Energy Research Institute (JAERI) and several universities to acquire the cross section and shielding data for 15 to 90 MeV neutrons by using a p-Li quasi-monoenergetic neutron field established at 90 MV AVF cyclotron facility, TIARA in JAERI. In the present stage, we obtained some preliminary experimental results on neutron penetration and charged particle production and activation cross sections.

Introduction

The research programme has started as a cooperative project between Japan Atomic Energy Research Institute (JAERI) and several universities to acquire the cross section and shielding data for 15 to 90 MeV neutrons by using a p-Li quasi-monoenergetic neutron field established at 90 MV AVF cyclotron facility, TIARA (Takasaki Ion Accelerator for Advanced Radiation Application), in JAERI. This project will continue at least five years. Experiments planned in this programme are as follows,

1. Penetration through shielding materials of concrete, iron and polyethylene,
2. Streaming through duct and maze,
3. Double differential neutron scattering cross section measurements,
4. Activation and spallation cross section measurements,
5. Charged particle and photon production cross section measurements,
6. Thick-target neutron and photon yields produced by charged particles,

7. Detection efficiency and response function measurements of neutron detectors.

In the present stage, we have been proceeding the themes 1, 4, 5, 7, and have just started the themes 2 and 6.

Source neutron spectral measurement and shielding experiment

As for the theme 1, we made an experiment on the penetration of 40.5 and 64.5 MeV quasi-monoenergetic neutrons through iron and concrete. These neutrons were produced from 3.6 mm and 5.2 mm thick Li targets bombarded by 43 and 67 MeV protons which were extracted from the cyclotron, respectively. Protons passed through the Li target were bent down to the beam dump by a clearing magnet and neutrons ejected in the forward direction were extracted toward the experimental hall through the 220 cm thick concrete wall with a 10 cm diam collimator. The neutron beam was injected into 120 cm by 120 cm iron slab of 20 to 130 cm thickness and 120 cm by 120 cm concrete slab of 25 to 200 cm thickness, which were fixed in contact with the collimator exit located at 4 m from the target. Figure 1 shows the cross-sectional view of the experimental arrangement.

The source neutron intensity was monitored with two micro-fission counters of ^{232}Th and ^{238}U placed near the target. The absolute spectra of p-Li source neutrons above 15 MeV were measured with a proton recoil counter telescope consisting of an annular polyethylene radiator (0.2 to 1 mm thick) and the ΔE-E telescope. The ΔE detector is a 900 mm^2 Si-SSD and the E detector is a 2-in. diam by 2-in. long NaI(Tl) scintillator. They are shielded from the direct neutron beam by a brass shadow bar, in order to detect only charged particles emitted from the radiator. Source neutron spectra were also measured with a 5-in. diam by 5-in. long organic liquid scintillator, BC-501, by using the TOF and unfolding methods. Figures 2 and 3 show the obtained source neutron spectra. The FWHMs and yields of monoenergetic peak of source neutrons were the respective values of 2.0 MeV and 1.1 x 10^4 n cm^{-2} μC^{-1} for 43 MeV p-Li neutrons, and 2.1 MeV and 1.7 x 10^4 n cm^{-2} μC^{-1} for 67 MeV p-Li neutrons, both at 5.5 m away from the Li target.

Behind the shield, neutron spectra were measured with the BC-501 and the multi-sphere spectrometer loading a 2-in. diam ^{3}He counter, so-called Bonner spheres. Fission reaction rates and neutron dose equivalents were measured with ^{232}Th and ^{238}U fission counters and a rem counter. Three kinds of dosimeters were also used, solid state truck detector of CR-39, thermoluminescent dosimeters of ^{6}LiF and ^{7}LiF, and PIN diode. We have hitherto analyzed the data obtained with BC-501, CR-39 and fission counters. In advance to this, we have measured the response functions of BC-501 with the TOF method.

The neutron spectra measured with BC-501 were compared with the MORSE Monte Carlo calculation(1) using the DLC-119/HILO86 group cross section library(2). The comparison for concrete-penetrated neutron spectra is shown in Fig. 4 and revealed in general the good agreement between experiment and calculation. In Figs. 5 and 6, the measured ^{238}U fission reaction rates behind concrete and iron for 64.5 MeV p-Li neutrons are compared with those calculated by the DOT 3.5 code(3) and the ^{238}U fission cross section data(4). The attenuation profiles except at several points in concrete and iron give good agreement between experiment and calculation.

Charged particle and activation cross section measurements

Replacing the polyethylene radiator of the proton recoil telescope with a 0.5 mm thick carbon plate, we first measured the double differential C(n,p), (n,d), (n,t) cross sections for 67 MeV p-Li neutrons at 7 laboratory angles between 7 deg and 120 deg. The proton and deuteron spectra exhibit very strong forward peaking due to direct reaction. We are going to measure these charged particle production cross sections for other targets.

In order to get activation cross sections, we irradiated samples of carbon, aluminum, cobalt, iron, copper, nickel and bismuth. Figure 7 exemplifies our experimental data of ^{209}Bi(n,Xn) reactions obtained at TIARA and at INS (Institute for Nuclear Study), University of Tokyo, together with other experimental

results(5) and the calculated ones(6). For estimating these cross section curves, it is needed to do the activation experiment for proton energies other than 43 and 67 MeV.

Conclusion

We could establish the quasi-monoenergetic neutron source field of 40.5 and 64.5 MeV energies for 43 and 67 MeV p-Li reactions, respectively, at TIARA, and obtained some experimental results on neutron penetration and charged particle production and activation cross sections in good accuracy as the first stage. In order to proceed our systematic experimental programs, we are urgently waiting for proton acceleration of energies other than 43 and 67 MeV at TIARA.

We wish to thank the cyclotron staff members at TIARA for their cyclotron operation during our experiment. This work is partly supported by a Grant-in-Aid for Cooperative Research of the Japanese Ministry of Education. Our experimental group members are as follows;

T. Nakamura, N. Nakao, M. Takada, Y. Uno,
Cyclotron and Radioisotope Center, Tohoku University,
M. Baba, T. Iwasaki, S. Matsuyama, T. Kiyosumi, M. Yoshioka,
Department of Nuclear Engineering, Tohoku University,
M. Imamura, Y. Uwamino, T. Shibata, S. Shibata,
Institute for Nuclear Study, University of Tokyo,
K. Shin, E. Tanabe,
Department of Nuclear Engineering, Kyoto University,
Shun. Tanaka, H. Nakashima, Y. Sakamoto, Y. Nakane, S. Meigo,
Tokai Establishment, Japan Atomic Energy Research Institute,
Su. Tanaka,
Takasaki Establishment, Japan Atomic Energy Research Institute.

References

(1) Straker, E.A., et al.: ORNL-4585 (1970).

(2) Alsmiller, R.G. Jr., Barnes, J.M., Drischler, J.D.: ORNL/TM-9801 (1986).

(3) Rhodes, W.A., Mynatt, F.R.: ORNL/TM-4280 (1979).

(4) Lisowski, P.W., et al.: Proc. Specialists Meeting on Neutron Cross Section Standards for the Energy Region above 20 MeV, Uppsala, Sweden, 21-23 May, 1991, p.177-186 (1991).

(5) McLane, V., Dunford, C.L., Rose, P.F.: "Neutron Cross Sections", Vol. 2, Academic Press Inc., New York (1988).

(6) Fukahori, T.: Private Communication.

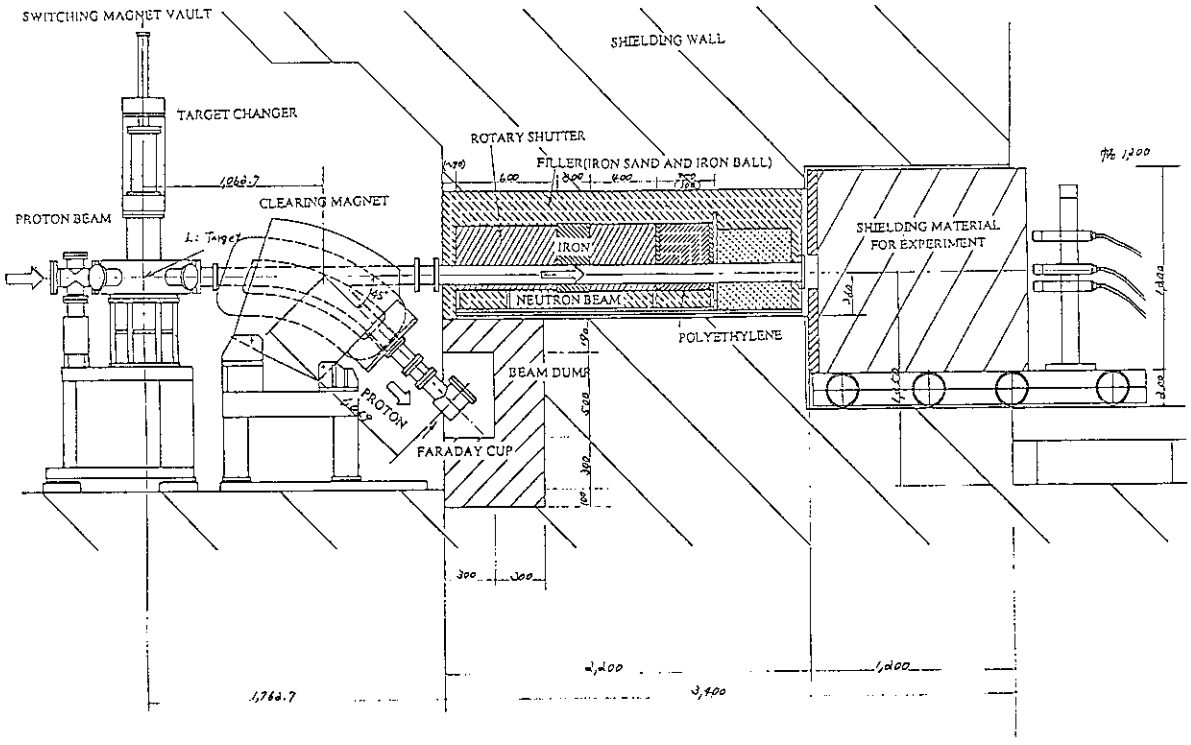

Fig. 1 Cross-sectional view of experimental arrangement.

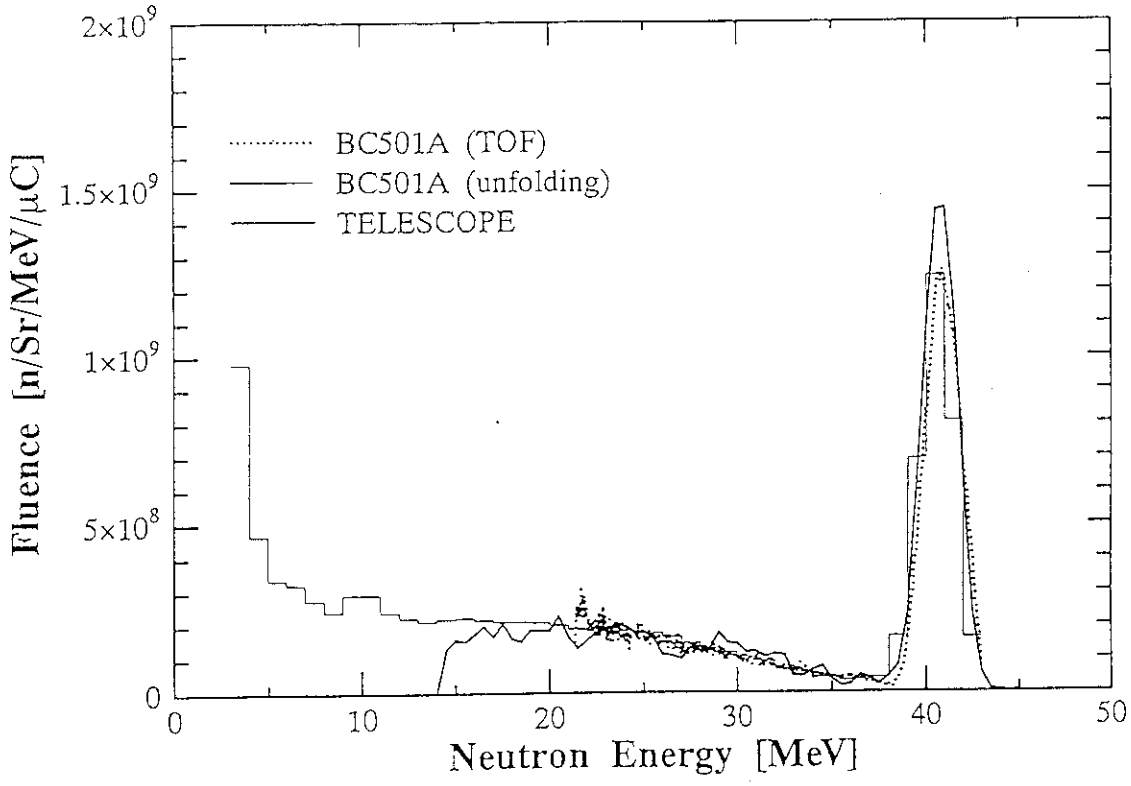

Fig. 2 Source neutron spectrum of 43 MeV p-Li reaction measured with BC-501 and counter telescope.

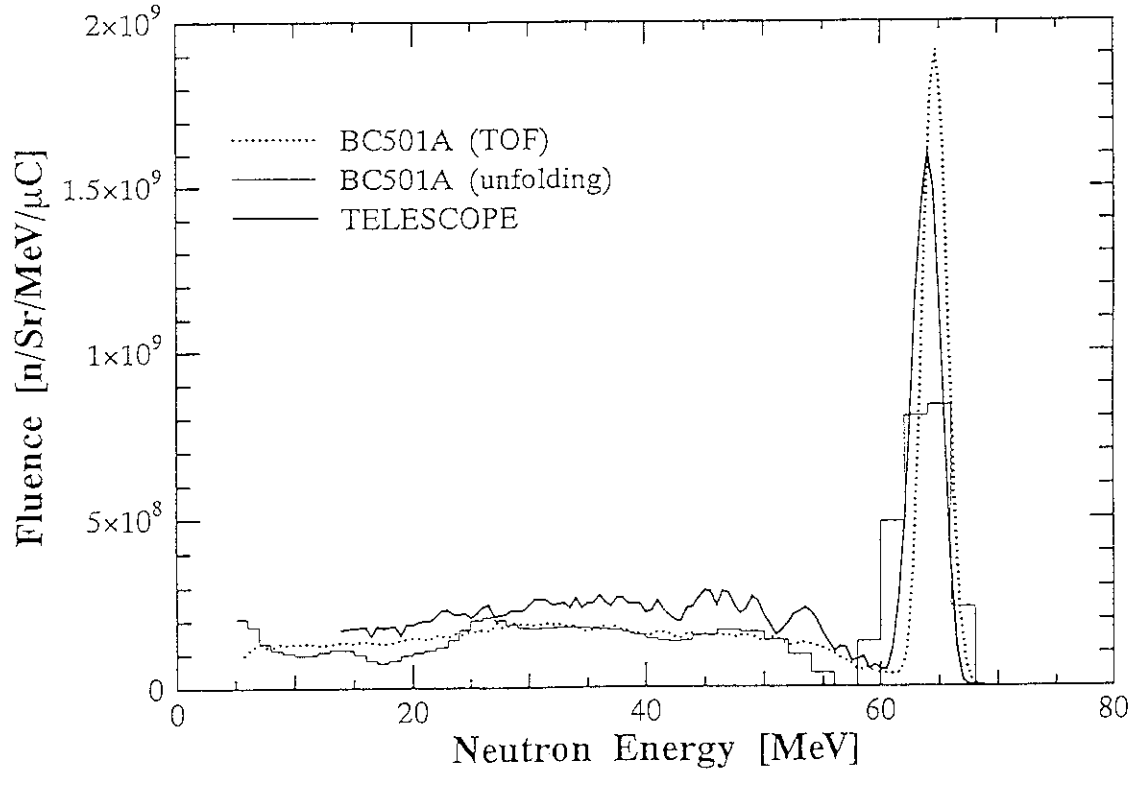

Fig. 3 Source neutron spectrum of 67 MeV p-Li reaction measured with BC-501 and counter telescope.

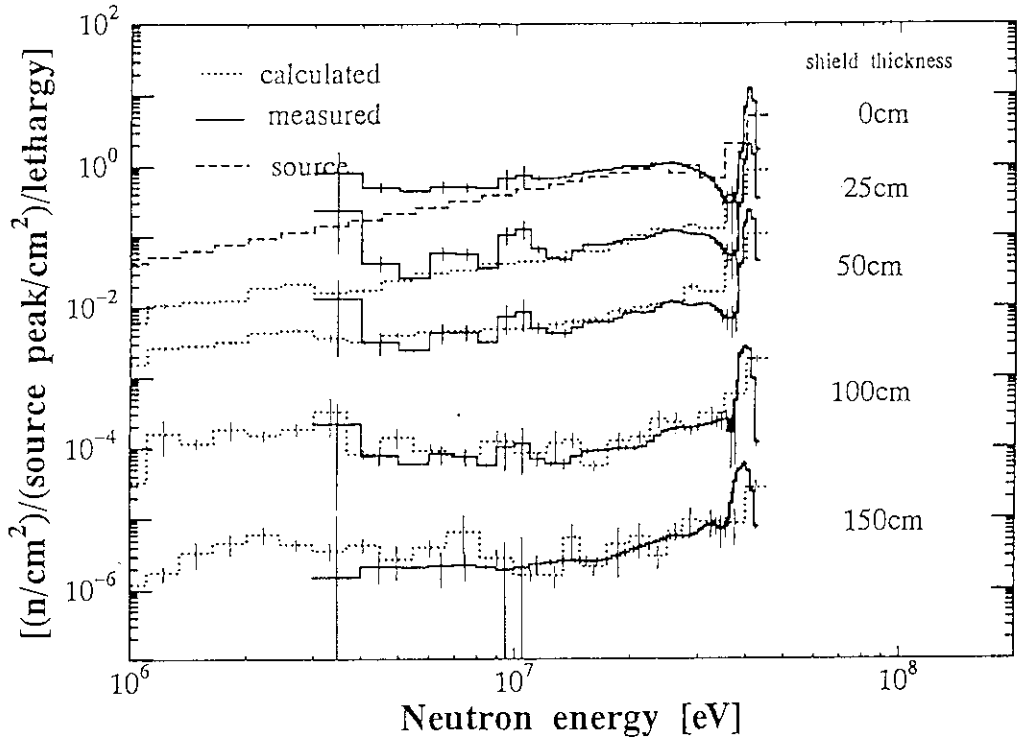

(a) 43 MeV p-Li neutron source

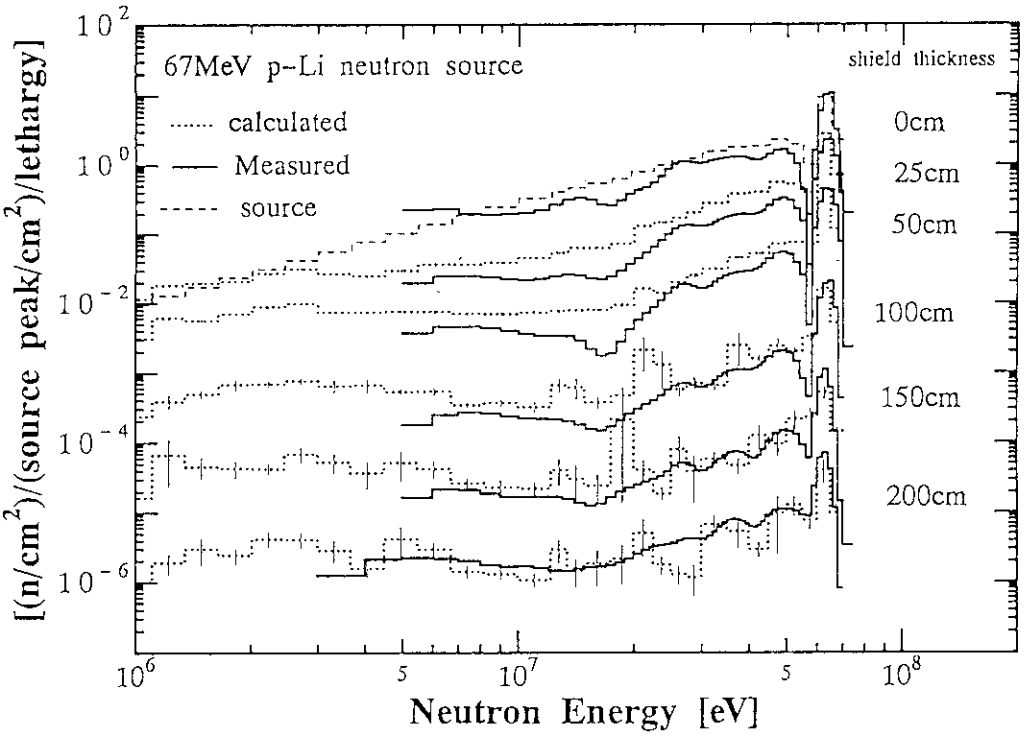

(b) 67 MeV p-Li neutron source

Fig. 4 Neutron spectra on the beam axis penetrated through concrete.

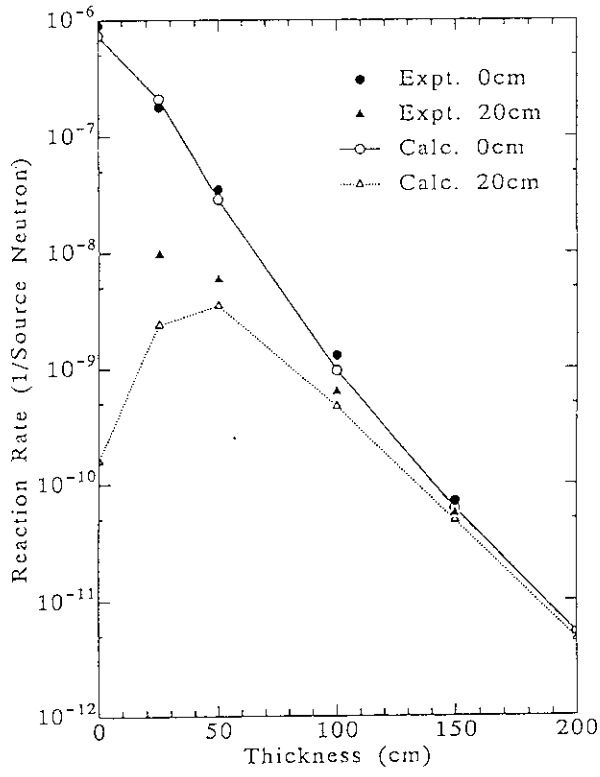

Fig. 5 ^{238}U fission reaction rates on the beam axis and 20 cm off axis penetrated through concrete.

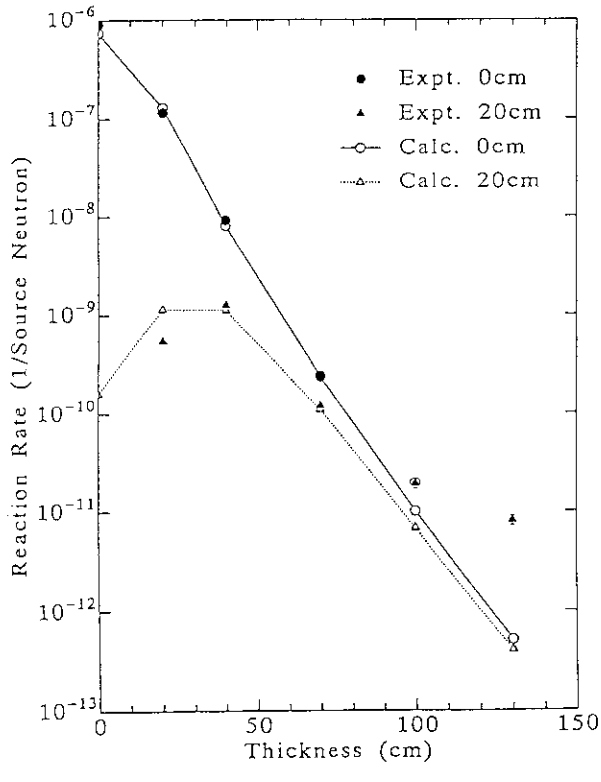

Fig. 6 ^{238}U fission reaction rates on the beam axis and 20 cm off axis penetrated through iron.

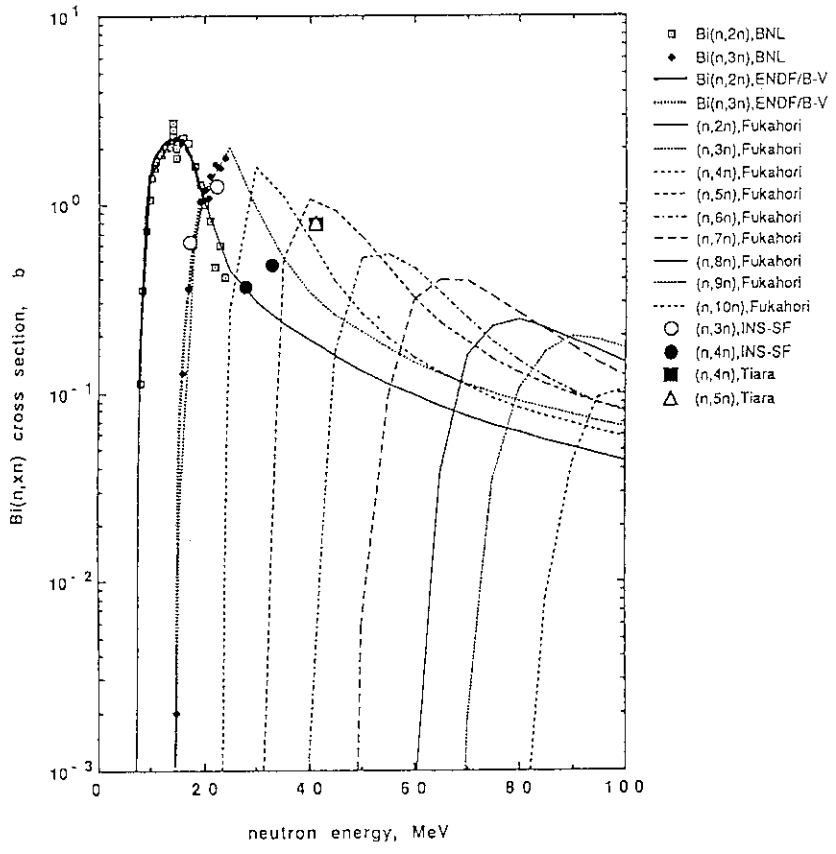

Fig. 7 Excitation functions of ^{209}Bi(n,Xn) reactions.

2.3 Nuclear Data Needs from Non-nuclear Engineering Fields

2.3.1 Atomic, Molecule's and Nuclear Data for Medical Application

Shigeru IWANAMI

Department of Radiology, School of Medicine
Kitasato University
1-15-1, Kitasato, Sagamihara, Kanagawa-ken 228

Medical physicists need atomic and nuclear data. What kinds of data do they need? One answer is "JARP Medical Physics Data Book". So we introduce this DATA BOOK as a typical example of atomic, molecule's and nuclear data for medical applications.

1. Who Want to Have Atomic and Nuclear Data for Medical Applications?

The answer is "Medical physicists". But they are professions known hardly in Japan[1]. They have two associations; Japanese Association of Radiological Physicists (JARP) and Japanese Association of Medical Physics (JAMP). Their foundations and members are shown in Table 1.

Table 1 Medical physics organizations in Japan

	Foundation	Members(1991)
JARP	1961	695
JAMP	1980	157

JAMP was established by the members of JARP for making possible the affiliation to the "International Organization for Medical Physics" (IOMP). So both members are overlapped each other.

2. JARP Medical Physics Data Book

What kinds of data medical physicists need? Table 2 shows research fields of presentations of JARP Annual Meetings for 30 years. Physics in radiation dosimetry and X-ray diagnosis constitute 60% of all presentations.

Table 2 Research fields of presentations of JARP Annual Meetings[1]

Dosimetry	35.2%
X-ray diagnosis	24.9%
Radiation therapy	9.5%
Radiation protection	7.8%
Nuclear medicine	6.0%
Radiation biology	3.2%
Information processing	2.6%

For the past 3 years the ad-hoc committee of JARP has worked for publications of Medical Physics Data Book, which give a source of reliable and readily accessible data for the practicing medical physicists. The book is during editing. Taking into considerations of Table 2 and NBS Medical Physics Data Book[2], the contents are divided into six main chapters: General Physics, Radiation Measurement, Physics in Radiation Therapy, Physics in Diagnostic Radiology, Information Processing for Radiology, and Radiation Protection. The editors try to assemble selectively the most useful information for each chapter while maintaining a text of manageable size. Each entry is referenced so the user can refer the original sources of data.

3. General Physics

Atomic, molecule's and nuclear data are assembled mainly in the chapter of General Physics of the DATA BOOK. So we report here this chapter. The contents of General Physics are given as follows:

1. General Physics
  1.1 Atom and Nucleus
    1.1.1 Atomic Structure
    1.1.2 Nuclear Structure
    1.1.3 Radioisotope
    1.1.4 Nuclear Magnetic Resonance
  1.2 Ionizing Radiation
    1.2.1 Type of Radiations
    1.2.2 Interaction of Radiation with Matter
    1.2.3 Production of Radiation
  1.3 Non-Ionizing Radiation
    1.3.1 Ultrasound
    1.3.2 Visible Radiation
    1.3.3 Infrared Radiation
    1.3.4 Ultraviolet Radiation
    1.3.5 Laser
    1.3.6 Radiofrequency and Microwave
  1.4 Others
    1.4.1 Characteristics of Reference Man
      1.4.1.1 Soft Body Tissues in Reference Adult Male and Female
      1.4.1.2 Elemental Composition, Density, Electron Density of Human Tissue
    1.4.2 Atomic Weight and density of Element

Since many instruments using non-ionizing radiations have been introduced to hospitals, they are esteemed much as same as ionizing radiations.

4. Atom and Nucleus

The contents of the section 1.1 of General Physics are given as follows:

1.1 Atom and Nucleus
  1.1.1 Atomic Structure
    1.1.1.1 Bohr Model of the Atom
    1.1.1.2 Electron Binding Energy
    1.1.1.3 Moseley's Low
    1.1.1.4 Characteristic X-ray

1.1.1.5 Emission Yields of Characteristic X-ray and Auger electron
1.1.2 Nuclear Structure
1.1.3 Radioisotope
1.1.4 Nuclear Magnetic Resonance
1.1.4.1 Principle of Nuclear Magnetic Resonance
1.1.4.2 Magnetic Property of Nucleus
1.1.4.3 Chemical Shift
1.1.4.4 Spin-Spin Coupling

An example of data referred in 1.1.1 is shown as follows:

Core-electron binding energy:
J.A.Bearden and A.B.Burr, 1967[3].

Wavelength of X-ray fluorescence:
J.A.Bearden, 1967[4].

X-ray fluorescence yields, Auger, and Coster-Kronig transition probability:
J.H.Scofield, Atomic Data and Nuclear Data Tables, 1974[5].

In 1.1.3, kinds of radioisotopes are limited to ones used in hospitals and clinics. In 1.1.4, those of nuclei are also limited to measurable ones in human tissues with MRI.

5. Ionizing Radiation

The contents of the section 1.2 of General Physics are given as follows:

1.2 Ionizing Radiation
1.2.1 Type of Radiation
1.2.2 Interaction of Radiation with Matter
1.2.2.1 Photon
1.2.2.2 Electron and Positron
1.2.2.2.1 Mass Stopping Power
1.2.2.2.2 Range and Radiation Yield
1.2.2.2.3 Mass Scattering Power
1.2.2.2.4 Straggling

1.2.2.2.5 Data on Mass Stopping Power, Range, Radiation Yield and Mass Scattering Power
Appendix I Moliere's Theory
Appendix II Production of Secondary Particles
1.2.2.3 Heavy Charged Particle
1.2.2.4 Neutron
1.2.3 Production of Radiation
1.2.3.1 X-ray
1.2.3.2 Electron
1.2.3.2.1 Linear Accelerator
1.2.3.2.2 Microtron
1.2.3.2.3 Betatron
1.2.3.3 Proton and Heavy Charged Particle
1.2.3.4 Neutron
1.2.3.5 SOR

Table 3 shows type of radiations for medical use.

Table 3 Type of ionizing radiations for medical applications

Radiation		Medical application
Indirectly ionizing radiation		
Photon	X	X-ray diagnosis, Radiation therapy
	γ	Nuclear medicine, Radiation therapy
Neutron	n	Radiation therapy
Directly ionizing radiation		
Electron	e^-	Nuclear medicine, Radiation therapy
Positron	e^+	Nuclear medicine
Proton	p	Radiation therapy
Heavy charged particle		Radiation Therapy
Pion	π^+, π^-	Radiation Therapy

Since photons and electrons are used generally in hospitals, data on them are assembled mainly in this Data Book. Furthermore, data necessary for their dosimetry are esteemed. 5% error of the patient dose affects clinical results of radiation therapy. There are many steps in the

process of determining dose in a patient. Since each step may introduce errors, the precision within 3% is necessary for physical quantities used in the dosimetry[6].

For photons, the following data are dealt with the section 1.2.2.1.

(1) The mass attenuation coefficient
(2) The mass energy transfer coefficient
(3) The mass energy absorption coefficient
(4) Photonuclear reaction

Since an energy of a linear accelerator for radiation therapy becomes higher, data on photonuclear reactions are necessary for radiation protection in the treatment room[7].

For electron's data, it is necessary that data will be reevaluated for electrons of energy smaller than 10keV in future. For heavy charged particles, the following data are necessary for their dosimetry; mass stopping power, range, total cross section of nuclear reaction, and cross section of nuclear fragmentation. An example of data is presented in 1.2.2.

Recently, applications of the Monte Carlo technique make progress in medical physics[8]. For example, we reported absorbed doses in a patient irradiated with photon narrow beams which use for radiosurgery[9]. They were calculated by the Monte Carlo method. Sets of cross section data on various process of radiation interactions are necessary for the Monte Carlo Method, but they are not dealt with this DATA BOOK.

6. Non-Ionizing Radiation

The contents of the section 1.3 of General Physics are given as follows:

1.3 Non-Ionizing radiation
  1.3.1 Ultrasound
    1.3.1.1.Medical Application
    1.3.1.2 Acoustic Properties of Non-Biological Materials
      1.3.1.2.1 Density, Acoustic Velocity, and Acoustic Attenuation for Non-Biological Materials

1.3.1.2.2 Acoustic Velocity vs Temperature for Water, Ethanol, and Sodium Chloride Solutions
1.3.1.2.3 Acoustic Velocity vs Concentration for of Sodium Chloride Solutions
1.3.1.3 Acoustic Properties of Biological Materials
1.3.1.3.1 Acoustic Velocity and Attenuation for Human Tissues
1.3.1.3.2 Dispersion of Velocity of Sound in Solutions of Human Hemoglobin
1.3.1.3.3 Volumetric Scattering Coefficient vs Hematocrit for Human Blood at 5 MHz
1.3.1.3.4 Scattering Intensity vs Angle for Human Blood
1.3.1.3.5 Magnitude of Ultrasonic Pulse-Echo Reflection from Biological Interfaces
1.3.1.4 Cavitation
1.3.1.5 Acoustic Field Data
1.3.1.5.1 Field Parameters for a Typical Ultrasonic Wave in Biological Tissue
1.3.1.5.2 Acoustic Power and Intensity for Diagnostic Ultrasound Instruments
1.3.1.5.3 Spatial Distribution of Acoustic Intensity for a Narrow-Band Focused Transducer
1.3.1.5.4 Acoustic Field Focal Zone Widths for 5 MHz Focused Transducers as a Function of Focal Length and Diameter
1.3.1.5.5 Acoustic Field Focal Zone Width after Penetration through Human Tissue
1.3.2 Visible Radiation
1.3.2.1 Biophysical Data on Vision
1.3.2.1.1 Structure of Eyeball
1.3.2.1.2 Structure of Retina
1.3.2.1.3 Visual Pathway and Vision
1.3.2.2 Light Perception and Color Vision
1.3.2.2.1 Light Perception and Adaptation
1.3.2.2.2 Photopic Vision and Scotopic Vision
1.3.2.2.3 Color Vision
1.3.2.3 Visual Acuity and Spatial Resolution
1.3.2.3.1 Visual Acuity
1.3.2.3.2 Spatial Resolution

1.3.3 Infrared Radiation
1.3.3.1 Radiation
1.3.3.1.1 Thermal Radiation
1.3.3.1.2 Infrared Spectrum
1.3.3.1.3 Radiation Law
1.3.3.1.4 Radiator
1.3.3.1.5 Emissivity
1.3.3.1.6 Temperature Reference Source
1.3.3.2 Transmission in Air
1.3.3.2.1 Absorption and Scattering of Infrared Radiation
1.3.3.2.2 Atomospheric Window
1.3.4 Ultraviolet Radiation
1.3.4.1 Light Source and Emission Spectrum
1.3.4.2 Absorption Spectra of Biomaterials
1.3.5 Laser
1.3.5.1 Wavelength of Laser
1.3.5.2 Medical Application
1.3.6 Radiofrequency and Microwave
1.3.6.1 Properties of Electromagnetic Waves in Muscle and Tissues with High Water Content
1.3.6.2 Properties of Electromagnetic Waves in Bone and Tissues with Low Water Content
1.3.6.3 Electromagnetic Properties of Phantom Materials

Now basic physical data on non-ionizing radiations are insufficient for biomaterilas.

References

1) Takaku, Y.: The Medical Physicists, Today and Tomorrow - The status, responsibilities and educational program in Japan, Jpn. Radiol. Phys., 11, 59 (1991).
2) Nat. Bur. Stand. (U.S.): Medical Physics Data Book, NBS Handbook 138 (1981).
3) Bearden, J.A. and Burr, A.B.: Rev. Mod. Phys., 39, 125 (1967).
4) Bearden, J.A.: Rev. Mod. Phys., 39, 78 (1967).

5) Scofield, J.H.: Atomic Data and Nuclear Data Tables, 14, 121 (1974).
6) Svensson, G.K.: Int. J. Radiation Oncology Biol. Phys., 10, Suppl.1, 23 (1984).
7) Iwanami, S., Tatokoro, K., Nakazawa, K., Matsubayashi, T., Takahara, H. and Uemae, M.: Jpn. Radiol. Phys., 11, 45 (1991).
8) Andreo, P.: Phys. Med. Biol., 36, 861 (1991).
9) Iwanami, S., Uehara, S. and Onizuka, Y.: J. Jpn. Soc. Ther. Radiol. Oncolo., 5, Suppl.1, 209 (1993).

2.3.2 Theoretical Approach to Proton Upset

Yosuke Shimano

National Space Development Agency of Japan

2-1-1 Sengen, Tsukuba-shi, Ibaraki-ken 305, Japan

1.Abstract

A three-part simulation program for calculating the cross section of proton upset was developed. The first part, NUREAC, is for the calculation of the cross section of proton-silicon inelastic diffusion. The second, ELASTIC, is for that of elastic diffusion. The last one, SEU, calculates the global proton-upset cross section, using the results of NUREAC and ELASTIC. The calculated values of this program for DRAM (Dynamic Random Access Memory) devices were compared with the real experimental values.[1]

2.Introduction

Single event upset of the electronic parts is caused by heavy ions coming from the interior or exterior of the galaxy, solar heavy ions and protons emitted by the sum during the flare period and the energy protons trapped in the radiation belt. Upset means the change of information held in the memory devices in the space environment. The upset caused by the high energy protons, namely proton upset, is different from that caused by the heavy ions in its mechanism. The cause of heavy-ion upset is the direct ionization of silicon by the entering ions. The cause of proton upset is, on the other hand, elastic or inelastic diffusion of silicon nucleus by the incident high-energy protons. Proton upset is a significant problem especially for the electronic devices installed in low-orbit satellites and launchers which pass through the radiation belt.[2]

3.Calculation of inelastic diffusion (NUREAC)

In the model that we used the nucleons inside the silicon nucleus are Fermi gas; namely there is no mutual interaction nor external force. In this model, however, the potential is not uniform, because the density of nucleons inside the nucleus is not uniform. For simplification, we divided a nucleus into ten concentric layers. If the nucleus is in a state of equilibrium, the fermi level is flat. We assume that the fermi level is identical with the average binding energy of the nucleus. Note that the potential is always negative inside the nucleus. Outside of the nucleus it becomes positive because of the coulomb potential (Fig.1).

Model of interaction The interaction of the proton-silicon inelastic diffusion can be divided into two process. The first process is a pre-equilibrium process and this can be simulated by cascade model. The second process is an equilibrium process and this can be expressed by the evaporation model.

Cascade model In this model we assume that the nucleus does not move for all the period of this process. The orbit of impinging proton will be bent by the coulomb force (Fig.2). This effect causes a decrease of inelastic cross section at low incident energy. The particles inside of the nucleus are refracted at the boundary of each two layers. If a particle collides with another nucleon, the energy of this nucleon is boosted up beyond the fermi level and it collides with another nucleon again. This is the reason this model is called "cascade model". After the cascade, the energy of excitation is left in the nucleus and this compound nucleus restores the equilibrium.

Evaporation model It is indicated that the usual approach to the evaporation can be adapted to the equilibrium compound nucleus. In this model the probability of evaporation of the nucleons is expressed as a function of the energy of excitation. It is assumed that the evaporation of each nucleon is isotropic.

Calculation of cross section　Using the models mentioned above the total cross section for the inelastic diffusion was calculated as a function of the kinetic energy of the incident proton in the laboratory system (Fig.3). The experimental data for aluminum nucleus is indicated in Fig.3 for comparison. The average recoil energy is also calculated (Fig.4).

4.Calculation of elastic diffusion (ELASTIC)

The cause of elastic diffusion can be classified into two categories. One is the coulomb force and the other is the nuclear force. It is not difficult to obtain the cross section of elastic diffusion caused by the pure coulomb force. For the nuclear force, however, knowledge is so far inadequate. Some kind of assumption based on the experiments is necessary to calculate the cross section. Optical model is often used for that purpose. In this model the potential of nuclear force can be expressed by U+iV. U is a real number and means the real diffusion. iV is, on the other hand, an imaginary number and it signifies the absorption of the incident proton by the nucleus. In this case, the inelastic diffusion is supposed to occur. U and V can be obtained by the fitting with the experimental values.[3] First we calculate the cross section of elastic diffusion by solving the Klein-Gordon equation assuming that the cause of the diffusion is only the pure coulomb force. After that we added the effect of nuclear force using the optical model. The calculated total cross section and the average recoil energy for a case in which the recoil energy exceeds 100 MeV is indicated in Fig.5 and Fig.6 respectively.

5.Calculation of proton upset cross section (SEU)

Mechanism of proton upset　If there is a collision between an incident proton and a silicon nucleus inside or near the collection volume, the recoil nucleus which acquired kinetic energy from the incident proton moves inside the collection volume. The recoil nucleus is silicon if the diffusion is elastic and is some nucleus lighter than phosphorus, which is a compound nucleus of silicon and proton, if the diffusion is inelastic. The recoil nucleus ionizes the silicon atoms. A silicon atom is taken apart into an electron and

a hole. The hole has a positive electric charge and the electron has a negative electric charge. The holes and electrons are collected to the cathode and anode of the electric memory device respectively. The collected charge change the voltage of the node. If the quantity of the charge is greater than a certain amount, the information held in a memory cell will be changed. This phenomenon is called upset and this amount of charge, that determines whether the upset will occur or not, is called critical charge. Even if the collision occurs outside the collection volume, there is a possibility that upset might occur, because the recoil nucleus can enter the collection volume after the collision. When the collision inside a certain domain possibly causes the upset, this domain is called the sensitive volume. The critical charge and the size of collection volume is inferred from the data of the heavy ion (direct ionization) test.

Model of sensitive volume Using the results of the calculation for inelastic and elastic diffusion, we can calculated the upset cross section caused by proton particles. In this calculation we adopted the Monte-Carlo method. We assume that the collection volume is a parallelepiped or a box. We limited the sensitive volume to the domain with a distance less than the average range of recoil nucleus in silicon. Therefore also the sensitive volume becomes a box. In Fig.7 a schematic of this model is shown.

6.Results and comparison with experimental value

The calculations were made for the DRAM devices; INTEL 2164A and FUJITSU MB814100. The results are compared with the experimental values (Fig.8,9). The results of the calculation have, on the whole, good agreement with the experimental values. In this model, the evaporation of the substructure (α, d, t, He^3) is not taken into account in NUREAC subprogram. There is a possibility that we can improve the results by considering this effect.

7.Conclusion

A simulation program for the calculation of proton upset cross section was developed. In this program, both the inelastic diffusion and the elastic diffusion between the incident proton and the silicon nucleus are taken into account. The results of the calculation are in good agreement with the experimental values.

8.References

[1] Y.Shimano, "Prediction of the Cross Section of Proton Upset Using a Monte-Carlo Simulation", ETUDE CERT-ONERA 43706, 1992

[2] Y.Shimano et al., IEEE Trans. NS-36, pp2344, 1989

[3] Y.Gervais de Lafond, "Interactions Proton-Silicium et Proton-Germanium entre 1 et 3000 MeV", Thèse de doctora, l'Université de Toulouse, N° 347, 1969

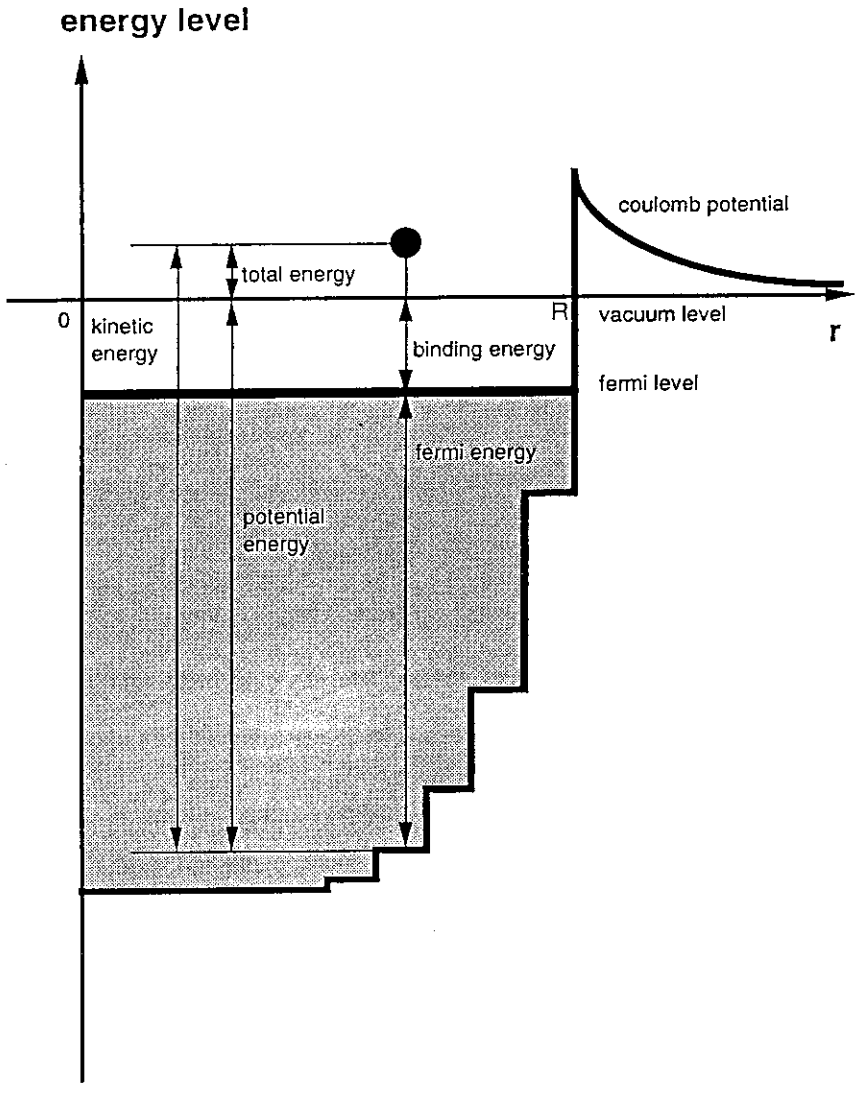

Fig. 1 Model of the nucleus.

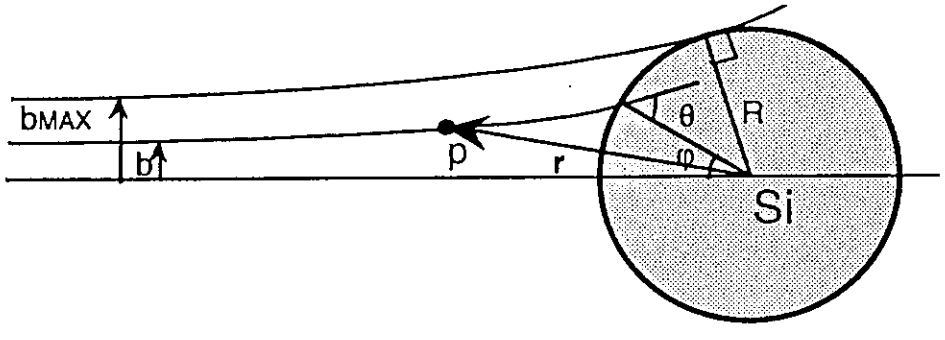

Fig. 2 Coulomb effect to the incident proton.

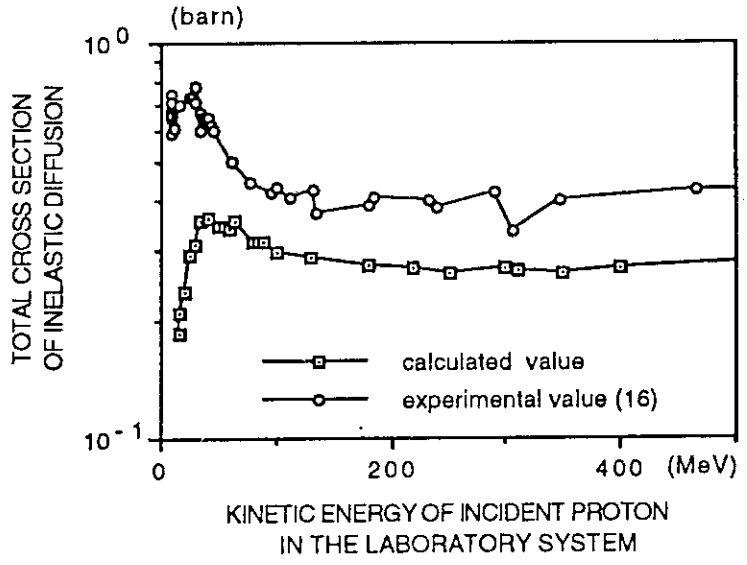

Fig. 3 Total cross section of inelastic diffusion.

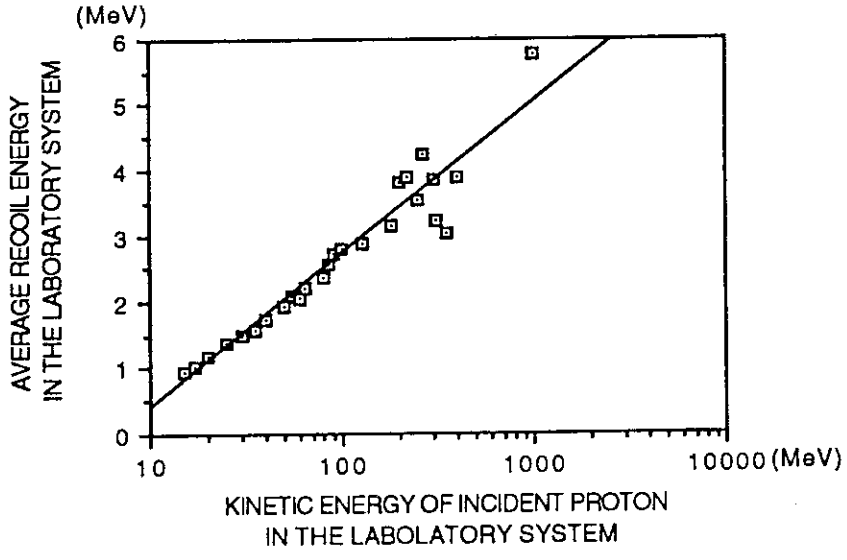

Fig. 4 Average recoil energy of inelastic diffusion.

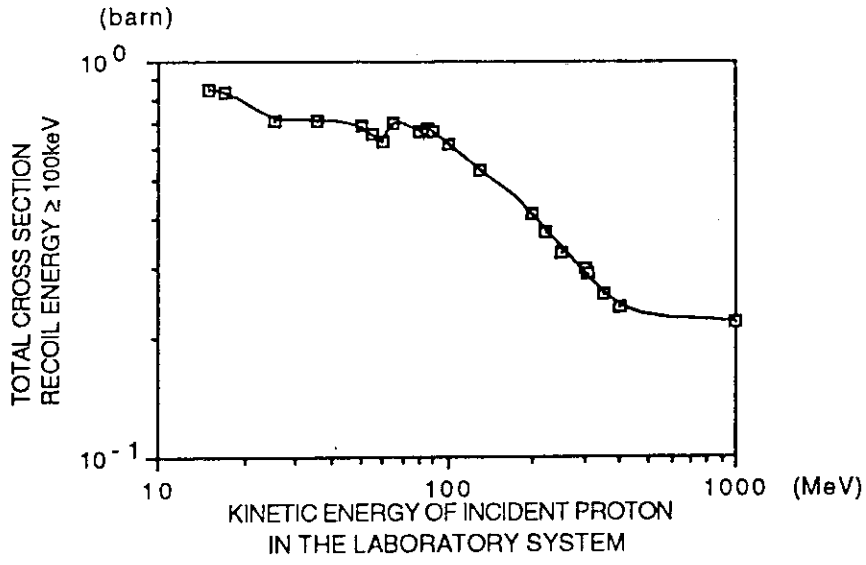

Fig. 5 Total cross section of elastic diffusion.

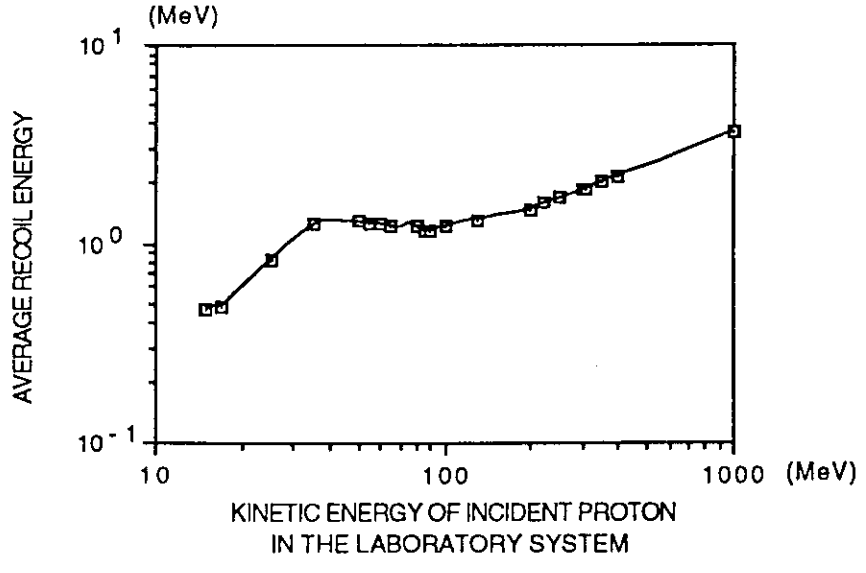

Fig. 6 Average recoil energy of elastic diffusion.

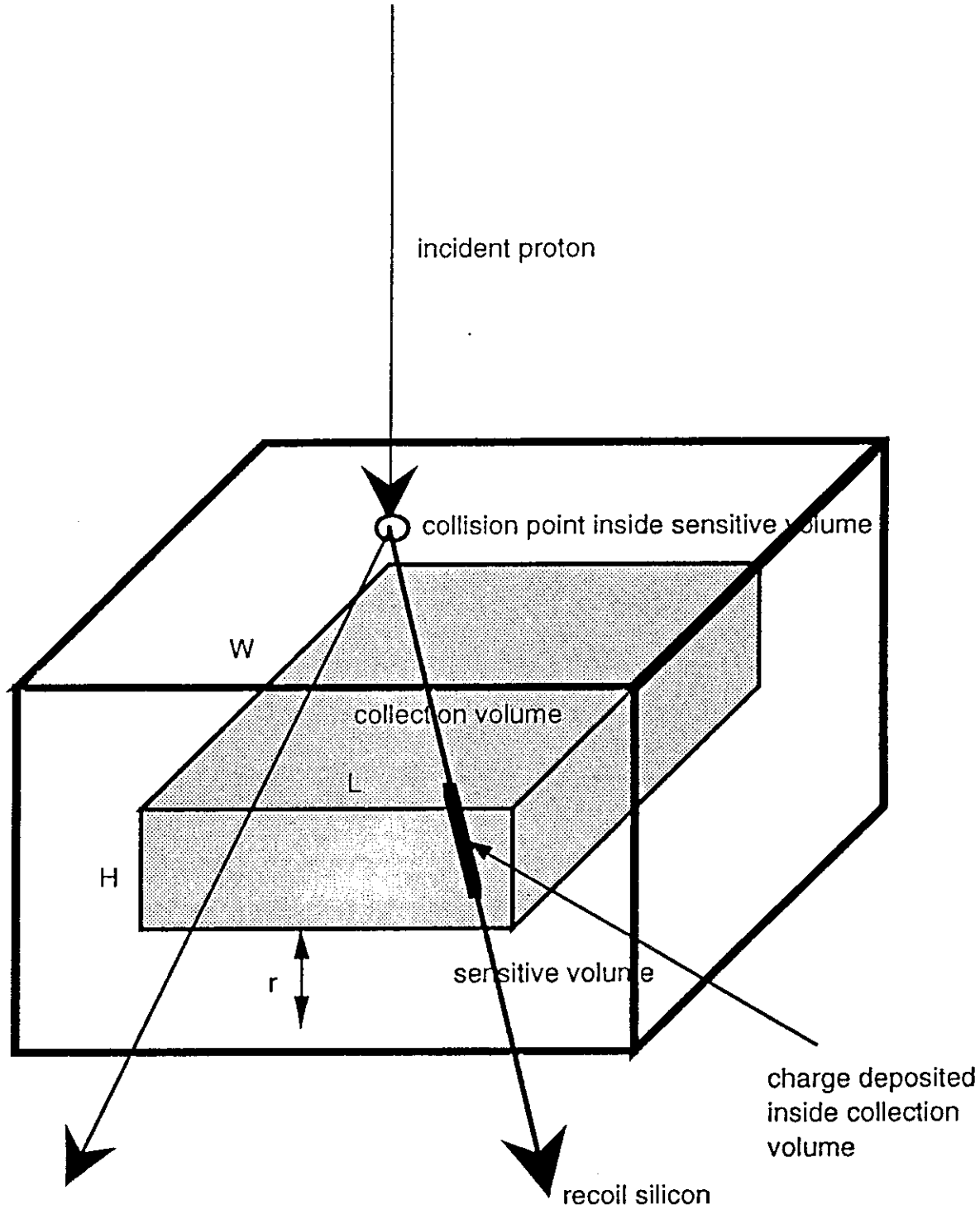

Fig. 7 Box model.

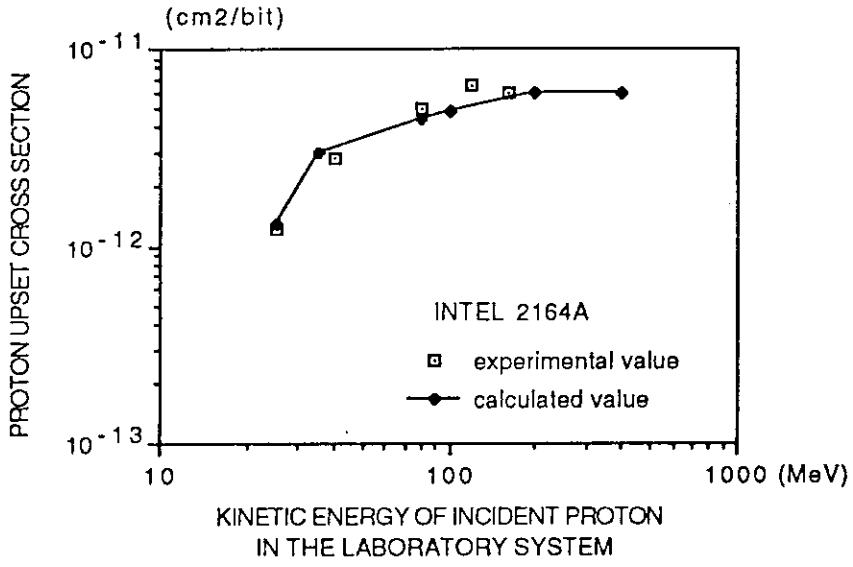

Fig. 8 Proton upset cross section (INTEL 2164A).

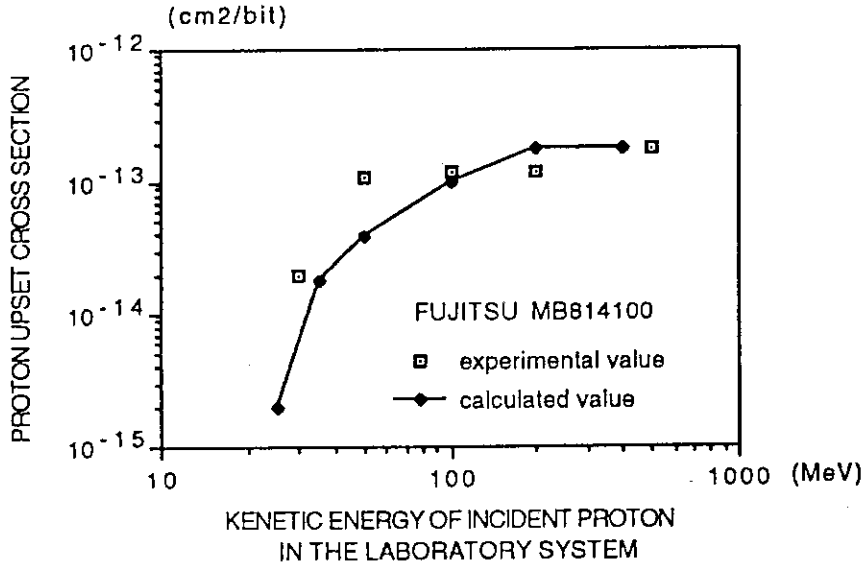

Fig. 9 Proton upset cross section (FUJITSU MB814100).

2.3.3 Nuclear Astrophysics and Critical Roles of Nuclear Data

Y.Nagai, M.Igashira,* T.Shima, T.Ohsaki, T.Irie, S.Seino,
K.Senoo, K.Watanabe, H.Satoh, T.S.Suzuki and H.Kitazawa**

Department of Applied Physics,Tokyo Institute of Technology, O-okayama,Meguro-ku,Tokyo 152,Japan

* Research Laboratory for Nuclear Reactors,Tokyo Institute of Technology,O-okayama,Meguro-ku,Tokyo 152,Japan

** Department of Electrical and Electronical Engineering,Tokyo Institute of Technology,O-okayama,Meguro-ku,Tokyo 152,Japan

Neutron capture reactions are considered to play important roles in the primordial nucleosynthesis and stellar nucleosynthesis. In this paper we discuss the experimental study of the neutron capture reaction of light nuclei in connection with the nucleosynthesis of intermediate-mass nuclei in inhomogeneous big-bang models and during stellar evolution. In the experiment we used pulsed neutrons and detected prompt γ-rays from radiative neutron capture into the low-lying states of residual nuclei.

1.Introduction

It has been claimed that standard big-bang models can explain nicely the observed abundances of light nuclei from D to Li with a baryonic density of a few % of a critical density, which closes a universe [1]. Therefore the bulk of the baryons in the universe are considered to be dark and one needs non-baryonic dark matter [2]. Recently,however, an inhomogeneous

big-bang model has been proposed as an alternative model of standard models[3]. When the early universe cooled below 200 MeV, the quark-hadron transition occurred. If the transition is a first-order, it could produce baryon-density fluctuations which would lead to high-density proton-rich regions and low-density neutron-rich regions[3]. According to these inhomogeneous big-bang models, a sufficient production of primordial heavy nuclei could have been achieved in the latter regions, which is quite different from the predictions of the standard big-bang models. Since the inhomogeneous models have been claimed to reconcile the observed primordial light elements with a critical baryonic density, extensive studies are being carried out[4]. The heavy elements could be produced mainly through the following reaction sequence[5].

$$\mathrm{H(n,\gamma)^2H(n,\gamma)^3H(d,n)^4He(t,\gamma)\ ^7Li(n,\gamma)^8Li(\alpha,n)^{11}B(n,\gamma)\ ^{12}B(\beta^-)^{12}C(n,\gamma)^{13}C,\ etc.}$$

Since these reaction cross sections have not been well known, it is necessary to measure them in order to quantitatively estimate the production rates of heavy elements.

In the stellar nucleosynthesis theory, neutron-capture reactions are necessary for the production of isotopes heavier than iron through both slow(s) and rapid(r) processes[6]. The s-process is assumed to occur during the He-burning phases of stellar evolution. Two reactions of $^{13}C(\alpha,n)^{16}O$ and $^{22}Ne(\alpha,n)^{25}Mg$ are considered to be the neutron sources for producing the s-process isotopes[7]. However, if the neutron capture cross sections of ^{12}C and ^{22}Ne were very large, they

would become neutron poisons[8]. Therefore, measurements of the capture cross section of these isotopes are quite important concerning s-process nucleosynthesis. Since the s-isotopes are considered to be synthesized at a low temperature of 10×10^7 K in low- and/or intermediate-mass asymptotic giant branch stars, it is necessary to measure the cross section for neutron energies of astrophysical importance between 10 and 250 keV.

2. Experimental procedure

The experiment was done by using pulsed neutrons provided from the 3.2 MV Pelletron Accelerator of the Research Laboratory for Nuclear Reactors at the Tokyo Institute of Technology, and by detecting prompt γ-rays from the neutron capture reaction. A typical experiment of $^{12}C(n,\gamma)^{13}C$ reaction is briefly discussed and the experimental detail is found in ref.9). A ^{6}Li-glass scintillation detector was used to measure the neutron energy spectrum by a time-of-flight(TOF) method. A typical energy spectrum is shown in Figure 1.

A natural carbon sample and a gold (Au) sample were used. The Au was used to obtain the absolute cross section by normalizing the γ-ray yields of the carbon sample with those of Au, since the cross section of Au has been well known[10]. Prompt γ-rays from a capturing state were measured using an anti-Compton NaI(Tl) spectrometer[11]. The TOF spectrum measured by the NaI(Tl) spectrometer using is shown in Figure 2. Several gates were set on the broad peak region and on the flat region in order to obtain the prompt γ-ray spectrum as well as the background spectrum.

3.Experimental results

The typical backgroud-subtracted γ-ray pulse-height spectrum is shown in Figure 3. In order to obtain the partial capture cross sections corresponding to the γ-transitions from a captured state to low-lying states, these γ-ray intensities were obtained. Consequently, the partial capture cross sections at various neutron energies were obtained as shown in fig.4. The figure shows that the partial capture cross sections from a captured state to the ground ($1/2^-$) and the second excited states($3/2^-$) follow the extrapolated values of the measured thermal-neutron capture cross section, by assuming a 1/v law. On the other hand, the partial capture cross section from a captured state to the first excited state($1/2^+$) does not agree with the extrapolated value, and increases with the laboratory neutron energy E(lab). From this energy dependence of the partial capture cross section, the neutron must be captured dominantly by a p-wave when the neutron energy increases. The total capture cross section obtained from these partial capture cross sections was fitted by the formula as

$$\sigma(E)=(17.0\pm0.3)E^{-1/2}+(1.50\pm0.11)E^{1/2} . \quad (1)$$

In equation (1) E is the center-of-mass energy. The Maxwellian-averaged capture cross section $\langle\sigma\rangle$(μbarn) at a temperature of T is given

$$\langle\sigma\rangle = \{17.0\pm0.3 + (2.25\pm0.16)kT\}/(kT)^{1/2} . \quad (2)$$

The Maxwellian-averaged capture cross section at 30 keV is about five-times larger than the extrapolated value of the measured thermal capture cross section, assuming a 1/v law.

4.Discussion and conclusion

The cross section of the $^{12}C(n,\gamma)^{13}C$ reaction was measured for neutron energies of between 10 and 250 keV. The present results have implications concerning nucleosynthesis from low-metallicity asymptotic giant-branch stars, for neutrino-induced nucleosynthesis as well as for the heavy-element nucleosynthesis yields in models of inhomogeneous big-bang models.

The present result concerning the $^{12}C(n,\gamma)^{13}C$ reaction shows that the capture cross section increases as the neutron energy increases. This can be explained qualitatively by p-wave neutron capture. Namely, the capture cross section given by the formation cross section of a compound nucleus times the probability of the radiative transition is proportional to v^{2L-1} Here v is the neutron velocity and L is an orbital angular momentum of the incident neutron. Since the present result indicates that the partial capture cross section from a captured state to the first excited $(1/2^+)$ state is proportional to the square root of the neutron energy, the neutron is captured dominantly by a p-wave (L=1) at higher neutron energies.

REFERENCES:

1) Boesgaard,A.M.,Steigman,G.,Ann.Rev.Astron.Astrophys.,23, 319 (1985).

2) Silk,J.,ApJ.297, 1 (1985).

3) Applegate,J.H.,and Hogan,C.J.,Phys.Rev.D31,3037 (1985)

4) Kurki-Suonio,H.,and Matzner,R.A.,Phys.Rev.D39,1046 (1989). Mathews,G.J.,Meyer,B.S.,Alcock,C.R., and Fuller,G.M.,ApJ,358,36 (1986). Terasawa,N.,and Sato,K., Progr.Theor.Phys.,81,254 (1989).

5) Malaney,R.A.,and Fowler,W.A.,ApJ,333,14 (1988).

6) Burbidge,E.M.,Burbidge,G.R.,Fowler,W.A., & Hoyle,F.,Rev.Mod.Phys.,29,547 (1957).

7) Urlich,R.K.1973, in Explosive Nucleosynthesis, ed. D.N.Schramm and W.D.Arnett(Austin:University of Texas Press),p.139

8) Gallino,R.,Busso,M.,Picchio,G.,and Renzini,A.,ApJ,334,L45 (1988).

9) Nagai,Y.,Igashira,M.,Takeda,K.,Mukai,N.,Motoyama,S., Uesawa,F.,Kitazawa,H.,and Fukuda,T.,ApJ,372,683 (1991).

10) ENDF/B-V data file for ^{197}Au (MAT=1379). 1979, evaluated by S.F.Mughabghab

11) Igashira,M.,Kitazawa,H.,and Yamamuro,N.,Nucl.Instr.Meth. A245,432 (1986).

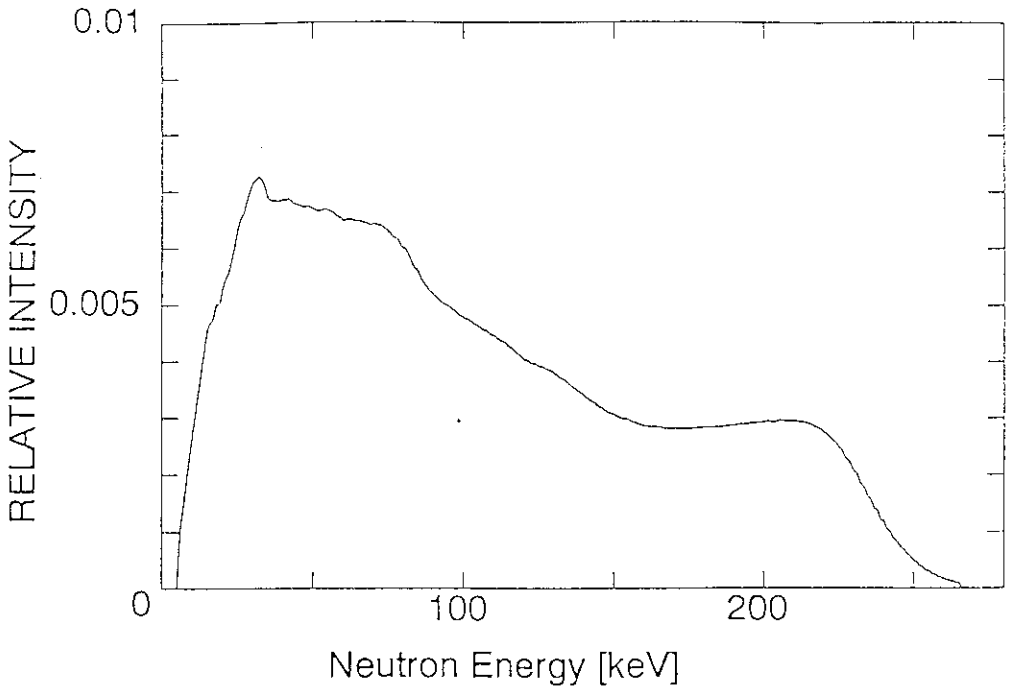

Fig. 1 Neutron energy spectrum measured by a time-of-flight method with a ^{6}Li-glass scintillation detector. The neutron was produced by the $^{7}Li(p,n)^{7}Be$ reaction.

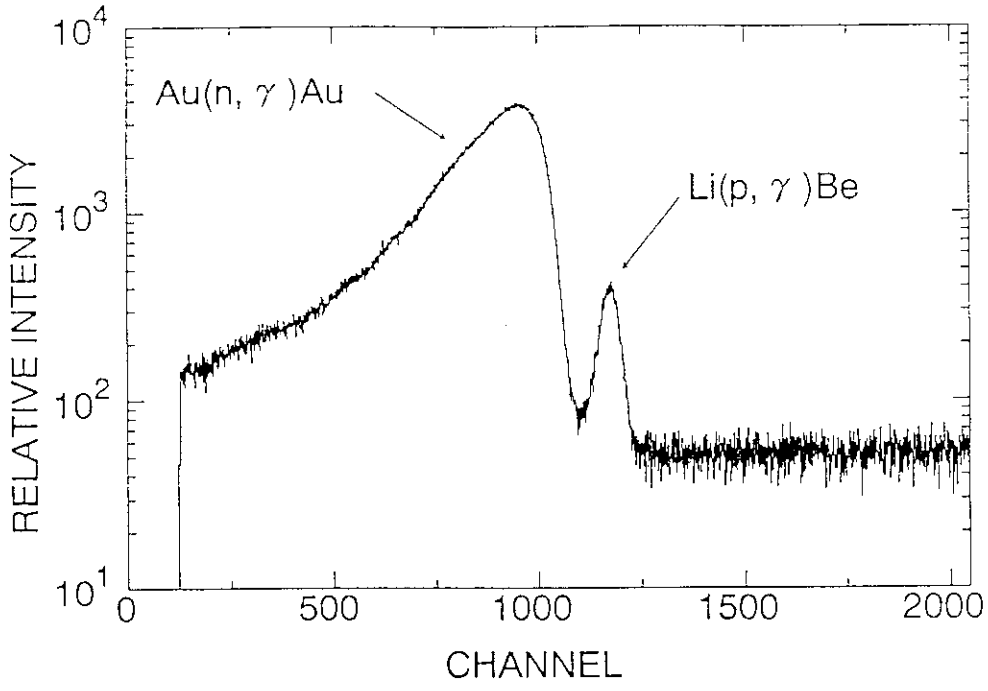

Fig. 2 Time-of-flight spectrum measured by a NaI(Tl) detector with a ^{197}Au sample.

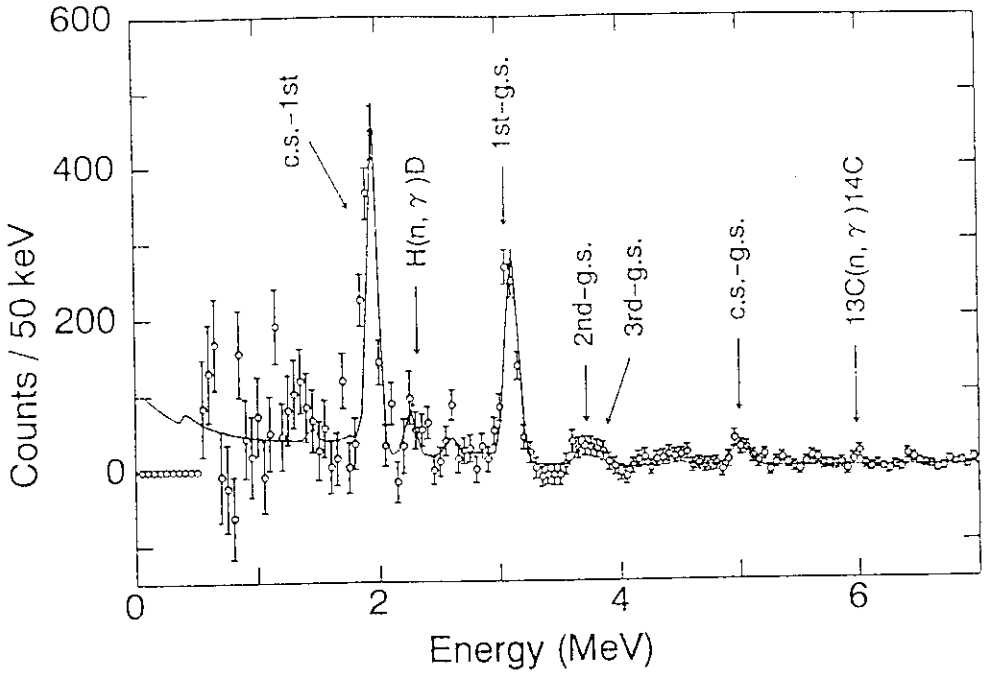

Fig. 3 Background subtracted γ-ray energy spectrum from the $^{12}C(n,\gamma)^{13}C$ reaction.

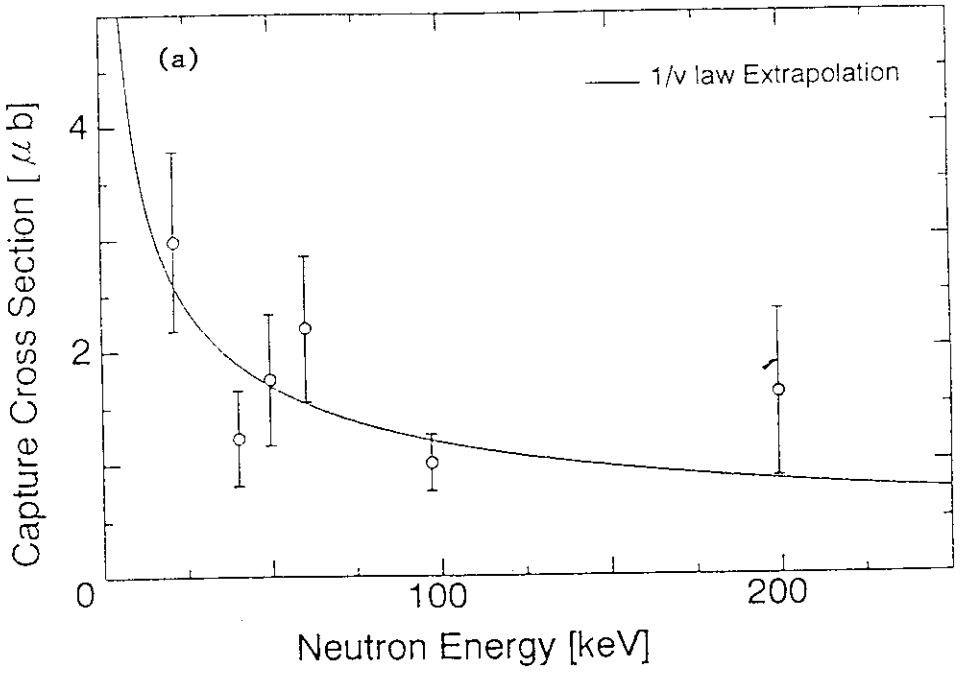

Fig. 4 Excitation functions of the partial capture cross sections of ^{12}C corresponding to the γ-rays from a captured state to (a) the ground ($1/2^-$)

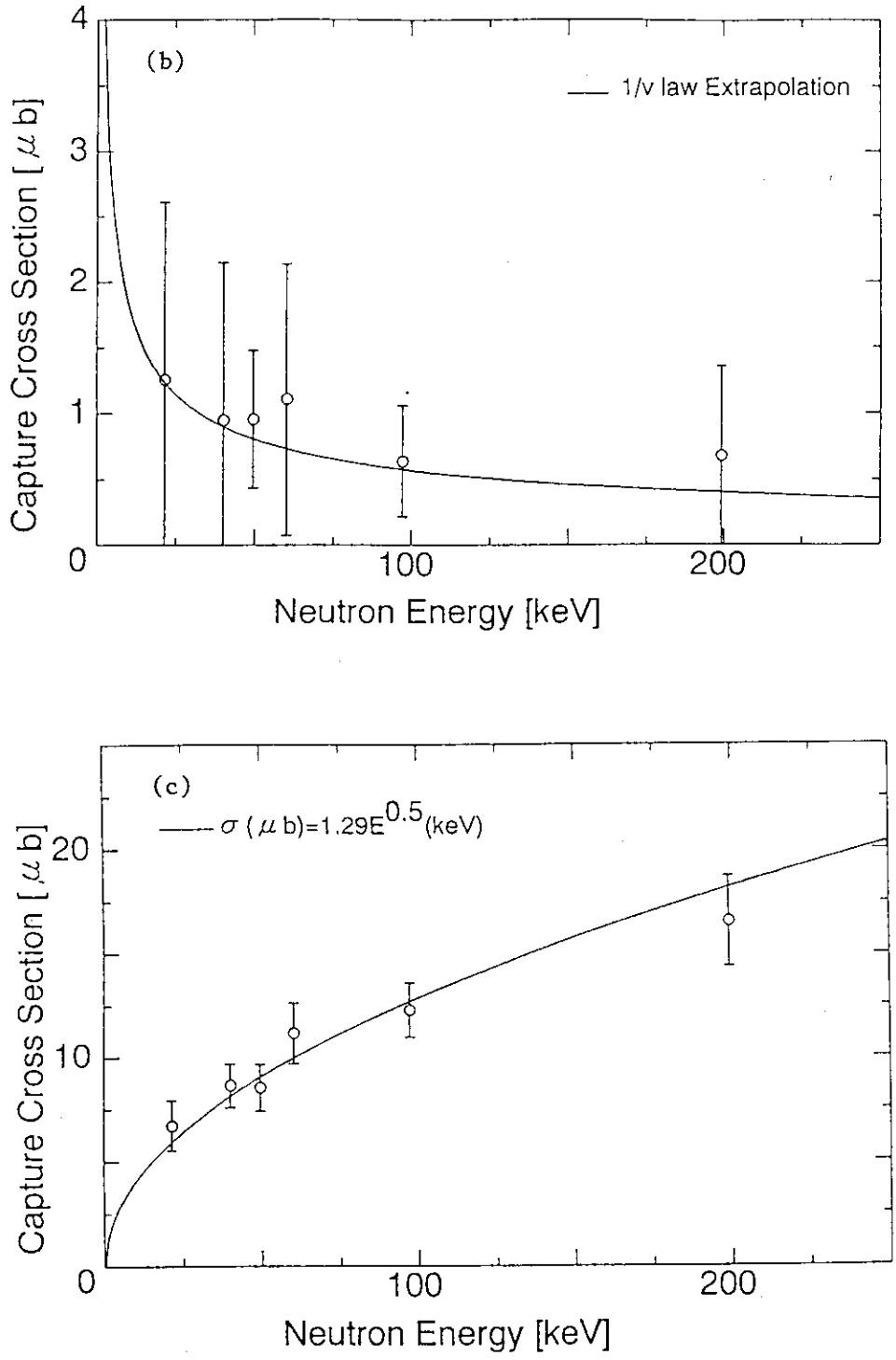

Fig. 4 Excitation functions of the partial capture cross sections of ^{12}C corresponding to the γ-rays from a captured state to (b) the second excited ($3/2^-$) and to (c) the first excited ($1/2^+$) states, respectively.

2.4 Beam of Unstable Nuclei

2.4.1 Frontiers in Nuclear Physics and Nuclear Astrophysics with Radioactive Nuclear Beams

Shigeru KUBONO

Institute for Nuclear Study, University of Tokyo
3-2-1 Midori-cho, Tanashi, Tokyo, 188 Japan

Abstract

New research fields developed recently with radioactive nuclear beams, especially in nuclear physics and nuclear astrophysics are discussed briefly. The present status of the radioactive beam factory projects in the world also are reviewed, including the one at Institute for Nuclear Study, University of Tokyo.

1. RADIOACTIVE NUCLEAR BEAMS OPEN NEW RESEARCH FILEDS

Nuclear physics has been expanding toward the extreme limit of proton and neutron excesses and also to the heaviest mass[1-5]. Short-lived nuclei have been produced efficiently by the use of heavy-ion induced projectile-fragmentation process at intermediate and high energies. The knowledge of nuclear physics was restricted to about 2000 nuclei near the stability line, out of 6000 nuclei predicted. Figure 1 displays possible unstable nuclei and the nuclear reaction processes in nuclear astrophysics on a schematic nuclear chart. In many respects, nuclear physics would not be the same if one extends the research toward the drip lines. For instance, the shell closure would not hold with the same number as for the nuclei near the stability line.

Unstable nuclear beams also have opened up a new field in nuclear astrophysics[1,2,6-10]. Explosive nucleosynthesis in high-temperature high-density environments in the universe inevitably involves short-lived nuclei. Nuclear reaction studies of unstable nuclei have just started very recently, and enable one to simulate exactly in the laboratories the nuclear reactions in such phenomena.

There also are many interesting fields which can be conducted exclusively using radioactive nuclear beams[1,2]. Since radioactivity is a labeled nucleus, it can be a unique probe of an extreme sensitivity for investigating material science, i.e., structures of the lattice and the surrounding fields, the mobility of ions in material, etc. It should be in the order of one atom out of 10^{23} atoms (order of 1 gram). These radioactive nuclei can be also implanted in a controlled depth. It should be also quite useful for medical use as has been used for many years. A

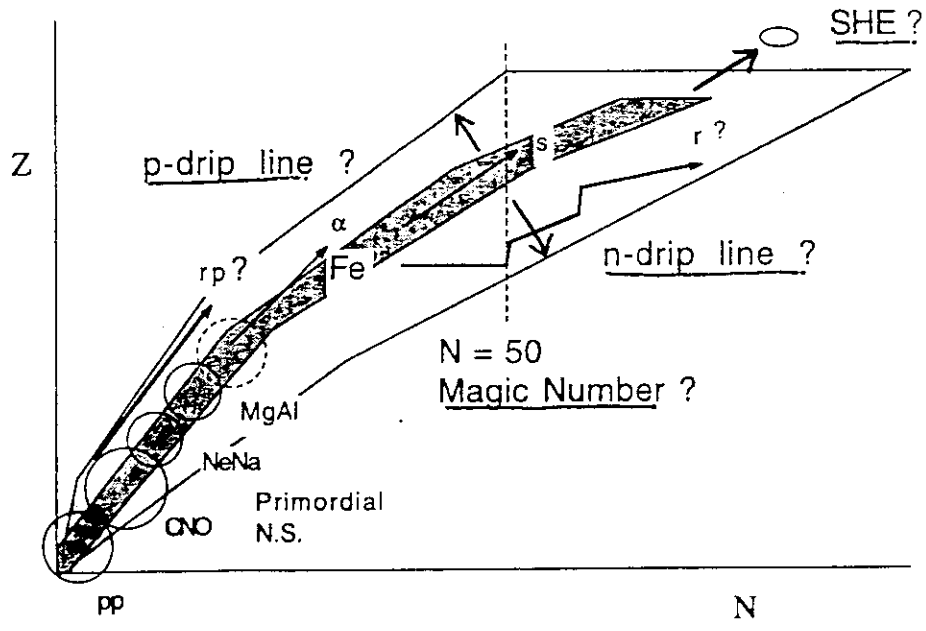

Fig. 1 A schematic plot of nuclei and nuclear reaction processes on the nuclear chart. The light colored area indicates the region of unstable nuclei.

variety of applications of radioactive nuclear beams are discussed in the proceedings of the series of the workshops on the sciences with radioactive nuclear beams. See refs. 1 and 2).

2. FRONTIERS IN NUCLEAR PHYSICS

Nuclear physics of unstable nuclei has made a great advance in the last decade after finding a new method for production of unstable nuclei; i.e. projectile fragmentation process at intermediate and high energies. This process produces efficiently a variety of nuclides with a beam-like velocity, and they are separated with a fragment separator.

One of the most striking findings is a new behavior of the nuclear matter in the extreme neutron-rich nuclei in the light mass region. Neutron halo is found in some nuclei such as ^{11}Li[11], which has a quite large neutron-tail distribution of very low density. This is mainly due to the very small binding energy for the last neutrons together with a large neutron excess. Neutron-skin phenomena are also suggested[11] recently in the neutron-rich unstable nuclei. Because of the large energy gap of the Fermi surfaces of protons and neutrons in unstable nuclei far from the stability line, the protons and neutrons are restricted in different binding potentials, giving different radii for proton and neutron

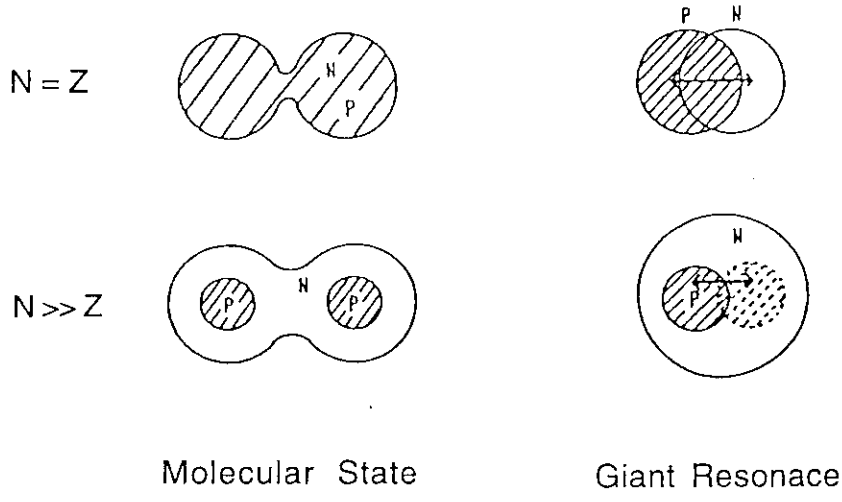

Fig. 2 Possible new modes of nuclear excitation in neutron-rich nuclei. Molecular states with neutron skin and soft giant resonance we predicted in JHP proposal in June, 1987[12].

distributions. The neutron radius is larger than the proton radius considerably for neutron-rich unstable nuclei.

New type collective modes are also predicted. Figure 2 depicts two possible modes for neutron-rich nuclear matter, which we predicted in the proposal of the Exotic Nuclei Arena in Japanese Hadron Project in June, 1987[12]. The first one is a kind of molecular shape or neck-formation in the fission process. Similar cluster states are predicted very recently by the AMD calculation by Horiuchi[13], which is to be investigated experimentally. This clusterization seems to be due to the recovery force of charge symmetry, i.e., the large excess of neutron matter pulls out some protons to produce di-nuclear system. This structure also suggests that a very neutron-rich nuclear beam gives a chance for producing super heavy elements through such di-nuclear states[1]. The second one is a new type giant resonance. The inner core includes a matter of proton and neutron, and this moved back and forth with a very small recovery force. This new mode was later formulated theoretically[14]. This gives a dipole-mode giant resonance but with very low excitation energy. A possible excitation of this mode was reported in ^{11}Li[15].

As was found at first for the anomalous interaction radius in ^{11}Li, the nuclear interaction should be an interesting subject. Specifically, the effective nucleon-nucleon interaction would be changed as one goes to the drip-line regions, where neutron-proton density ratio would change drastically as in the skin region. Variational shell model proposed by Otsuka and his collaborators[16] are taking care of the weakly bound

nuclear systems. This could be, in other word, also a problem of the effective interaction.

There are many other interesting developments reported recently for unstable nuclei. One interesting and beautiful experimental result is an observation[17] of a bound-state beta decay of $^{163}Dy^{66+}$ to $^{163}Ho^{66+}$. The nucleus of the neutral atom of ^{163}Dy is stable, but the fully ionized, or bare $^{163}Dy^{66+}$ nucleus is unstable against beta decay to $^{163}Ho^{66+}$. This was observed for the first time in the experiment with the storage ring, ESR at GSI. The life times of the nuclei of highly ionized atoms generally changes from the neutral atoms, but they are not known well experimentally. They have a quite important significance for nuclear astrophysics. For instance, some heavy nuclides, which are used for cosmochronology, can decay by the present mode.

Another interesting subject to be investigated with radioactive nuclear beams is high spin states in nuclei. High-spin isomer beams could be able to bring more spin quanta into the nuclear system than the ordinary low spin beams do in fusion reactions. These reactions might populate nuclear states of an extreme deformation, much larger than the axis ratio of a : b = 3 : 1.

Recent development in nuclear physics of unstable nuclei can be seen in refs. 1 - 5).

3. NEW FIELD IN NUCLEAR ASTROPHYSICS WITH RADIOACTIVE NUCLEAR BEAMS

Nucleosynthesis plays a crucial role in the stellar evolutions and also in the early universe just after the big bang. Study of the mechanism of nucleosynthesis is one of the stringent tests of the stellar and primordial models for the moment. If we know well the nuclear physics information for nuclear astrophysical requirement, we should be able to deduce the conditions of the astrophysical sites. As was mentioned already in sec. 1, short-lived radioactive nuclei are inevitably involved in explosive nucleosynthesis in the universe.

A typical evidence would be the light curve of the super nova 1987A. The light curve observed for the SN1987A is well explained by the nuclear irradiation of ^{56}Co[18]. This is a clear evidence that abundant short-lived nuclei ^{56}Co were synthesized in the supernova explosion. Here, ^{56}Co is believed to have been produced from the beta decay of ^{56}Ni.

Explosive phenomena take place in high-density high-temperature sites, where successive nuclear reactions go on before beta decays, and thus the nucleosynthesis flow goes away very easily from the stability line on the nuclear chart. Figure 3 depicts leakout from the Hot-CNO cycle to the Ne-Na cycle, and so on, which leads to the onset of the

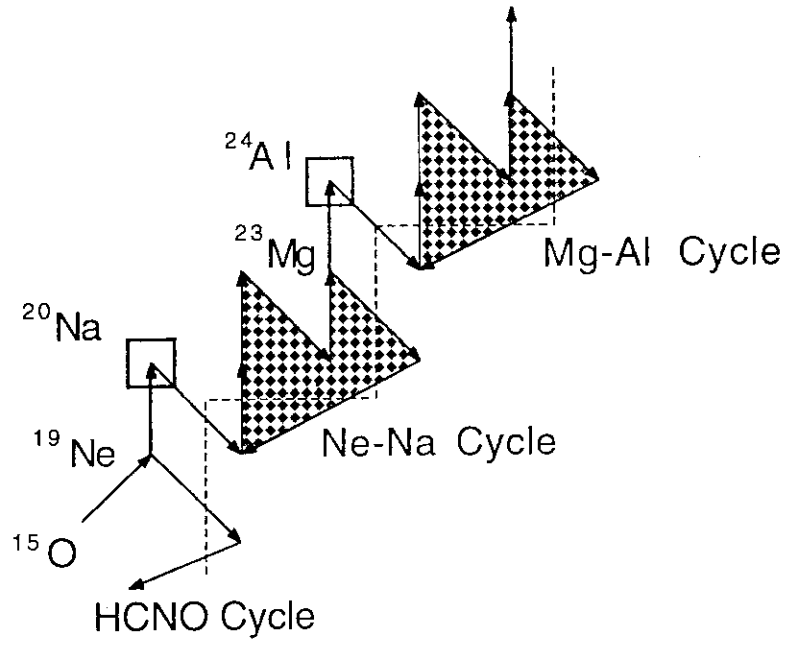

Fig. 3 A schematic nucleosynthesis diagram of the Hot-CNO cycle, Ne-Na cycle, etc., and the leakout on the N-Z plane. These breakouts lead to the onset of the rapid-proton process[19-21]. The right-hand side of the dashed line are stable nuclei.

rapid-proton process which is an explosive hydrogen burning process[19-21]. These situation requires nuclear physics informations on the proton-rich unstable nuclei such as ^{15}O, ^{19}Ne, ^{20}Na, etc., and their reactions.

Although the facilities and the quality of unstable nuclear beams are still limited for nuclear astrophysics experiments, some important reactions already have been investigated. They include the ^{13}N(p,γ)^{14}O reaction[22] for the onset of the Hot-CNO cycle, and the ^{8}Li(α,n)^{11}B reaction[23] for the primordial nucleosynthesis[24-27]. So many important nuclear reactions involve unstable nuclei and await to be studied. The present status of nuclear astrophysics can be seen in refs. 1, 2, 6-10).

4. PROSPECTS OF RADIOACTIVE NUCLEAR BEAM PROJECTS

As we sketched in the preceding sections, there are many new fields to have been opened up with the radioactive nuclear beams. Radioactive nuclear beams become available from very low to high energies. Although the quality of the secondary beams from the projectile fragmentation processes of heavy ion beams is limited, there

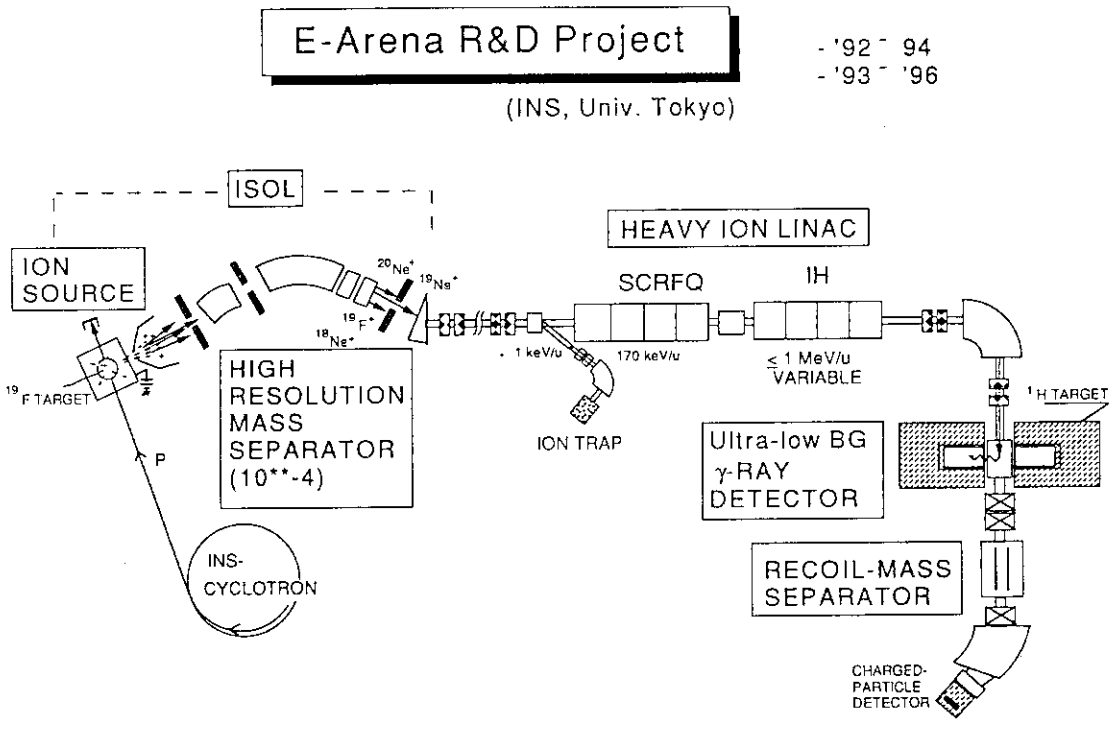

Fig. 4 A typical setup of ISOL-based unstable nuclear beam factory: the layout of Research and Development project under construction for the Japanese Hadron Project at Institute for Nuclear Study, University of Tokyo.

are many interesting experiments to be made. A new method for improving the beam quality of the secondary beams is being developed at GSI, Germany by using a storage ring.

More promising method could be ISOL + post-accelerator scheme[1-3,12]. This includes an ISOL system to produce intense unstable nuclei and an accelerator to boost the kinetic energy up to the region of interest. An example is displayed schematically in Fig. 4. The beam quality to be provided is as good as ordinary stable nuclear beams. A pioneer work was the $^{13}N(p,\gamma)^{14}O$ experiment for nuclear astrophysical interest, as discussed in sec. 3. This method should provide more intense beam than the projectile fragment method as discussed above, because one can use much thicker target with high-energy proton beams for unstable-nuclei production. The major concern here may be the absolute efficiency of ionization and acceleration of the radioactive products, which is under development. This type factory of unstable nuclear beams are under construction at Institute for Nuclear Study, University of Tokyo, Oak Ridge National Laboratory in U.S.A, and GANIL

in France. There are similar, several plans under discussion in Europe and Russia.

In summary, radioactive nuclear beams have opened up new fields not only in nuclear physics but also in nuclear astrophysics and material sciences. Specifically, exploiting the structure of nuclei far from the stability line and the nuclear reactions is the new research domain to be investigated in collaboration of the two fields, nuclear physics and nuclear astrophysics.

REFERENCES

1) Proc. Exotic Nuclei Arena Workshop/ Sciences with Radioactive Nuclear Beams, JHP-Suppl. 2, 3, 5, 7, 8, 12, and 13 (Institute for Nuclear Study, Univ. Tokyo).
2) Proc. First Int. Conf. Radioactive Nuclear Beams (Berkeley, 1989), World Scientific, 1990, ed. W.D. Myers et al.
Proc. Second Int. Conf. Radioactive Nuclear Beams (Belgium, 1991), Adam Hilger, 1991, ed. Th. Delbar.
3) Proc. Nucleus-Nucleus Collisions IV (Kanazawa, 1991), Nucl. Phys. A538c (1992).
4) Proc. Int. Symposium Structure and Reactions of Unstable Nuclei (Niigata, 1991), World Scientific, 1991, ed. K. Ikeda and Y. Suzuki.
5) Proc. Nuclei Far from Stability/ Atomic Masses and Fundamental Constants 1992(1992, Bernkastel-Kues), IOP Conf. Series 132 (1993).
6) S. Kubono, Proc. Fourth Int. Conf. Nucleus-Nucleus Collisions (Kanazawa, 1991), Nucl. Phys. A538 (1992) 505c.
7) S. Kubono, Comments Astrophys. 16 (1993) 287.
8) Proc. Int. Symposium on Heavy Ion Physics and Nuclear Astrophysical Problems (Tokyo, 1988), World Scientific, 1989, ed. S. Kubono, M. Ishihara, and T. Nomura.
9) Proc. Int. Workshop on Unstable Nuclei in Astrophysics (Tokyo, 1991), World Scientific, 1992, ed. S. Kubono and T. Kajino.
10) Proc. Int. Symposium Origin and Evolution of the Elements (Tokyo, 1992), World Scientific, 1993, ed. S. Kubono and T. Kajino.
11) I. Tanihata, Proc. Int. Conf. Nuclear Physics (Wiesbaden, 1992), ed. R. Bock et al., Nucl. Phys. A553 (1993) 361c.
12) Proposal of Japanese Hadron Project, Institute for Nuclear Study, University of Tokyo, June 1987.
13) H. Horiuchi, private communication.
14) K. Ikeda, INS Rep. JHP-7 (1988).

15) T. Kobayashi, Proc. Int. Conf. Nuclear Physics (Wiesbaden, 1992), ed. R. Bock et al., Nucl. Phys. A553 (1993) 465c.
16) T. Otsuka, N. Fukunishi, and H. Sagawa, Proc. Nuclei Far from Stability/ Atomic Masses and Fundamental Constants 1992 (1992, Bernkastel-Kues), IOP Conf. Series 132 (1993) 361.
17) M. Jung, et al., Proc. Int. Conf. Nuclear Physics (Wiesbaden, 1992), ed. R. Bock et al., Nucl. Phys. A553 (1993) 309c.
18) S. Kumagai, T. Shigeyama, and K. Nomoto, Astron. Astrophys. 243 (1991) L13.
19) R. K. Wallace and S. E. Woosley, Astrophys. J. Suppl. 45 (1981) 389.
20) S. Kubono, et al., Astrophys. J. 344 (1989) 460.
21) S. Kubono, Proc. Int. Conf. Nuclear Physics (Wiesbaden, 1992), ed. R. Bock et al., Nucl. Phys. A553 (1993) 481c.
22) P. Decrock, et al., Phys. Rev. Lett. 67 (1991) 808.
23) R. N. Boyd, I. Tanihata, N. Inabe, T. Kubo, T. Nakagawa, T. Suzuki, M. Yanokura, X. X. Bai, K. Kimura, S. Kubono, S. Shimoura, H. S. Xu, and D. Hirata, Phys. Rev. Lett. 68 (1992) 1283
24) J. H. Applegate and C. J. Hogan, Phys. Rev. D31 (1985) 3037.
25) T. Kajino, G. J. Mathews, and G. M. Fuller, Int. Symp. Heavy Ion Physics and Nuclear Astrophysical Problems (Tokyo, 1988), ed. S. Kubono, et al., World Scientific, 1989, p. 51.
26) T. Paradellis, et al., Z. Phys. A337 (1990) 211.
27) S. Kubono, et al., Z. Phys. A341 (1991) 121.

3. Panel Discussion for the 30th Anniversary of JNDC
—Nuclear Data Activity being at the Crossroads—

3.1 Keynote Address

3.1.1 Recollections of JNDC in the Early Stage

R. Nakasima (Hosei University)

When the Japanese Nuclear Data Committee (JNDC) has been established 30 years ago, in February 1963, some of the European and American advanced countries were already at the mature age of their activities in the nuclear data field. These western countries have been discussing about mutual cooperation within the European American Nuclear Data Committee (EANDC). Therefor the members of the JNDC at that time aimed at the same level of activity as in these advanced countries, and intended to have a "Sigma Center" like that of Brookhaven National Laboratory (BNL). In the meantime, the JNDC was invited by International Atomic Energy Agency (IAEA) as a member country of International Nuclear Data Scientific Working Group (INDSWG) in May 1963. This was quite lucky to the JNDC, since some members of the INDSWG were also the participants of EANDC and thus many valuable information on nuclear data from the advanced countries could be obtained easily. Thus the participation in INDSWG can be said as one of the most remarkable facts in the past 30 years of JNDC.

During its busy infancy (1963 to around 1968), the members of JNDC discussed eagerly the policy on the primary activities and confirmed the following main objects.

(1) Organization of compilation activities on nuclear data.
(2) Promotion of evaluation works of nuclear data.
(3) International cooperation in the field of nuclear data.
(4) Encouragement of experimental groups in Japan working on nuclear data.

Needless to say, both of the compilation and the evaluation of nuclear data are fundamental affairs in the function of "Sigma Center". In the early stage of JNDC, however, it was hard to continue the compilation work because of the strong objection based on the view−point of the man−power. In fact, the subjects of nuclear data planned had been covering not only data of neutron induced reactions but those of charged particle and photon induced reactions. This was probably too premature for JNDC about 30 years ago.

As to the evaluation activity, the works generally have been continued favorably. The effort in this activity was successful and achieved in making nuclear data libraries like well known JENDL (Japanese Evaluated Nuclear Data Library).

In 1966, JNDC joined EANDC in addition to INDSWG. This made the members of JNDC too busy, but the effect was much favorable for the research of nuclear data in Japan. Since then the international cooperation in the field of nuclear data has gone on rather smoothly and the excellent results thus obtained by the members of JNDC are quite remarkable.

Based on the mutual agreement within the member countries of EANDC or INDSWG, JNDC has prepared the List of Requested Neutron Data (RENDA) and (Annual) Progress Report of Japan. Through these works JNDC kept close contact with mainly the experimental groups in Japan, and this served necessarily as stimulation of the experimenters working on the neutron physics. It was, however, regrettable that the contact with theoretical nuclear physicists in early days not so close. This is probably due to the indifference of theoreticians in universities toward the nuclear data field. In this connection, the following is quite impressive. On looking back upon the 30 years history of JNDC, the fact that the activities of the members from industries which were mainly theoretical one are very outstanding seems to be a characteristic of the field of nuclear data.

At the 30−th anniversary of its establishment, the JNDC is hoped to work actively as until now while the world−wide trend in the nuclear data field seems to be inactive.

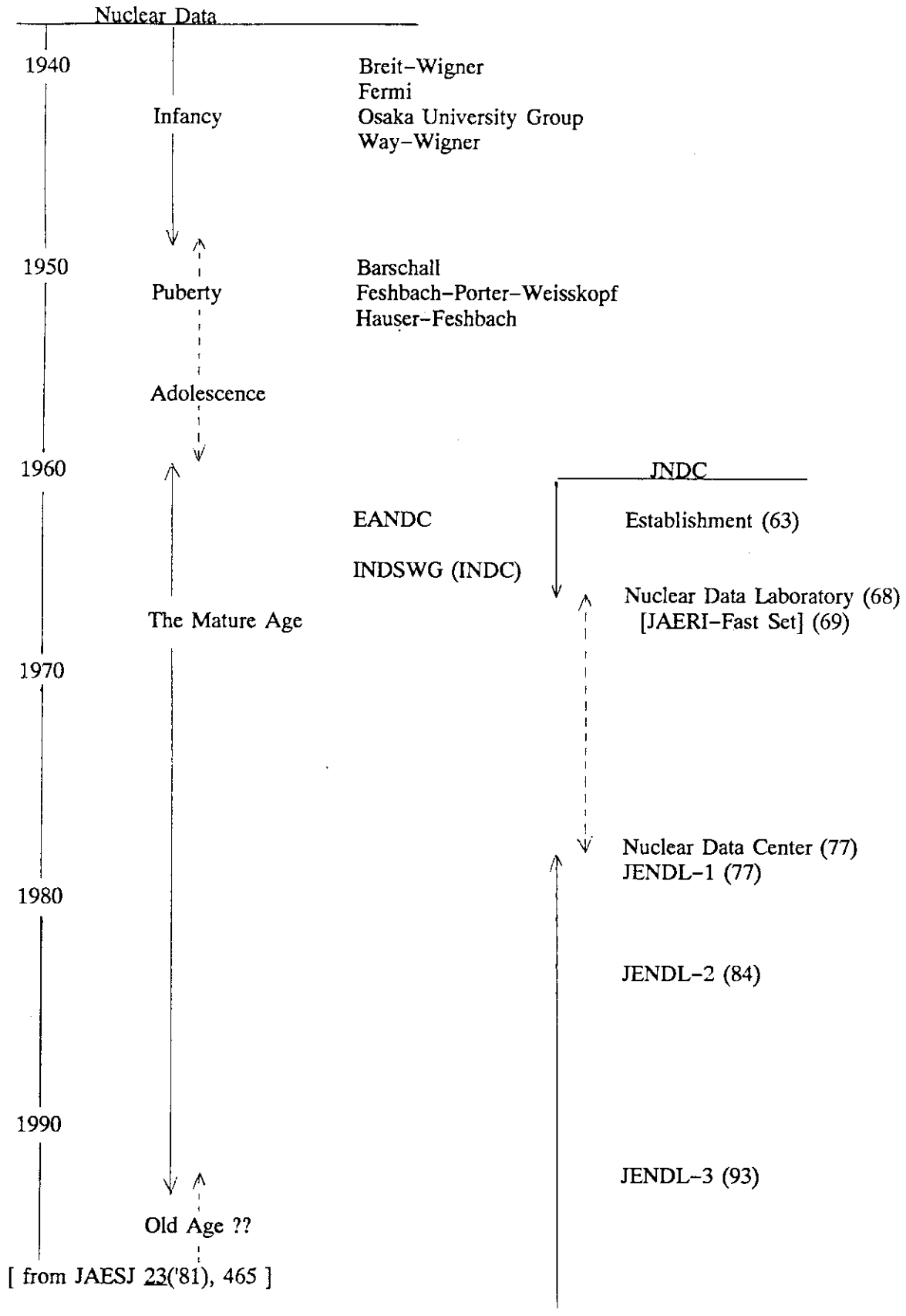
Nuclear Data
1940
Infancy
Breit-Wigner
Fermi
Osaka University Group
Way-Wigner
1950
Puberty
Barschall
Feshbach-Porter-Weisskopf
Hauser-Feshbach
Adolescence
1960
JNDC
EANDC
Establishment (63)
INDSWG (INDC)
Nuclear Data Laboratory (68)
[JAERI-Fast Set] (69)
The Mature Age
1970
Nuclear Data Center (77)
JENDL-1 (77)
1980
JENDL-2 (84)
1990
JENDL-3 (93)
Old Age ??
[from JAESJ 23('81), 465]

3.2 Panelist Presentation

3.2.1 Some Personal Comments on Evaluation and Measurements of Nuclear Data

Satoshi Chiba

Japan Atomic Energy Research Institute

Japanese Nuclear Data Committee (JNDC) has been functioning quite successfully over the last three decades. I, as a new comer, wish to acknowledge all those who have been working in this field and have constructed such an efficient cooperation framework among universities, private companies and governmental organizations. Recently, however, there is a strong decline of such activities in the U.S. and Europe. The same tendency unfortunately is more or less true also in Japan.

It seems to me that the nuclear data activity is not particularly an attractive field for young people to join although it is of vital importance in nuclear and many other field of science and technology. There may be several reasons for such pessimism. First of all, the community seems to be isolated from other world, where much high-tech stuffs are going on. Secondly, the format of the evaluated data, i.e., the ENDF-based format, is becoming more and more complicated and at first glance it is almost impossible for a beginner to understand the contents of its manual[1]. This kind of stuff may discourage people from outside to penetrate into this community unless some strong motivations do not exist. Furthermore, this format seems to be a little bit old-fashioned in the sense of the up-to-date information science. There must be many other reasons to be resolved.

It seems to be our responsibility to achieve a mild but drastic change in the way how JNDC should function after 30-years of smooth voyage.

3.2.2 Problems in Reactor Physics and Shielding Design

Atsushi Zukeran
Energy Research Laboratory, Hitachi Ltd.
2-1, Omika-cho, 7-chome, Hitachi-shi, Ibaraki-ken, 319-12 Japan

1. INTRODUCTION

The contents and qualities of the evaluated nuclear data files for conventional reactor, BWRs, PWRs and FBRs, are significantly improved in past 30 years. Typical examples of their improvements are shown in Fig. 1 where capture cross sections of ^{238}U of Bondarenko cross section set, denoted by ABAGYAN, published at 1962, evaluated data for JENDL-2, -3T and -3 libraries, and experimental data are compared. The consistency of the last three evaluated data with experimental data are clear and they are within the error boundaries of the experimental data.

According to the previous presentations by the invited authors from another countries in this conference, the emphases have been placed on the charged particle relating to the accelerator or fusion reactors. The refinements or evaluation activities for the nuclear data for the conventional reactors could not be found. It's seemed that the fields of nuclear data activities have been shifted to the charged particle or higher energy regions.

2. PROBLEMS IN REACTOR AND SHIELDING DESIGNS

In this presentation, some status or situations are discussed in the stead of the problems of the individual isotope and reaction in the evaluated nuclear data files, since the future trends of the evaluation works are of interest. Status of the nuclear data for fission reactors or advanced reactor including TRU burners can be outlined as follows.

(A) No essential problems for conventional reactors but minors are in
1) Reich-Moore presentations : Computing time,
2) DDX in File 6: not processed by conventional codes,
3) γ-ray production cross sections, and
4) Charged particle induced reaction cross sections.

In order to avoid confusion and los of labor preparing the multigroup cross section sets for reactor physics and core design, JENDLE-3.2's intensive Benchmark tests have to be made before released.

(B) For advanced reactor/TRU Burners

The advanced reactors of uranium and/or Plutonium fuels can be designed by using current evaluated nuclear data files although the higher reliabilities of data are continuously requested.

The TRU burners cooperating with accelerators, however, require more new data especially relating to higher actinides and charged particle induced reactions. The TRU burning is a key issue to be carried over for future sources of nuclear energy, which has an avoidable background as

Background

Power Reactor → Rad Waste → FPs and/or Actinides Burning

in which process

Accelerator ····· Secondary activation data, and

Burner ····· Actinide nuclear data, e.g., β_{eff}

are still provided and their evaluations should be continued.

(C) Nuclear Data and Methodology

Methodological uncertainties in reactor design and reactor physics can not be ignored. In some cases, these uncertainties are greater than those of nuclear data themselves. The continuous Monte Carlo method can reduce in general the methodological uncertainties for some properties such as effective multiplication factor Keff, but due to statistical limitations the overall accuracy is limited. Therefore, in order to predict the rector core parameter with high accuracy, the data and methods have to be improved simultaneously. Reactor physicists should be encouraged.

3. DISPOSITION of NUCLEAR DATA ACTIVITY

(1) The activity of nuclear data evaluation is passive work depending on user's needs, and active works suggesting new fields of nuclear data have never been reported. If possible, the more active approaches from nuclear data are welcome. "Nuclear data Application Working Group" is an idea to create new fields and new data, i.e.,

Evaluation Works → Passive: Need oriented

↓

Active : Seed oriented

"Applied Nuclear Data Sub. WG." to develop new fields.

(2) Goals of Nuclear Data Evaluation and Measurement

The goals can be considered at two categories; the first one is for the satisfactory accuracy of existing evaluated nuclear data and the second one for unknown nuclei, for instance, unstable isotopes. The goal for the first case may be set by the target accuracy given by user's needs where the evaluations of the target accuracy based on the sensitivity analyses are of interest. The theoretical approaches from nuclear physics to improve current data, however, can not be necessarily promised since the situations of evaluated data are in the range of experimental uncertainties as shown in Fig. 1. For the second case, there exist a lot of nuclei whose nuclear data are not given and which are seemed to be useful for medical use and for new application of nuclear data. Therefore,

Goal of Nuclear Data ?: no goal from user and evaluator,
e.g., evaluated data are straggling in the
uncertainty band of experimental data !
↓
then
Cross Section Adjustment is a effective approach
like KARNAVAL-V
↑
As an advanced and future approach,
"Superfine Group Adjustment" including Resonance Parameters may be possible
but the revision of nuclear data files are still needed as the reference.

(3) For Future Activities: Evaluation Software Development
- Man-power Saving
- Efficient Evaluation
- Technical Transfer

SUMMARY

1) More active researches developing new field, 2) Maintain evaluation and measurement activity, 3) Establish efficient evaluation methods.

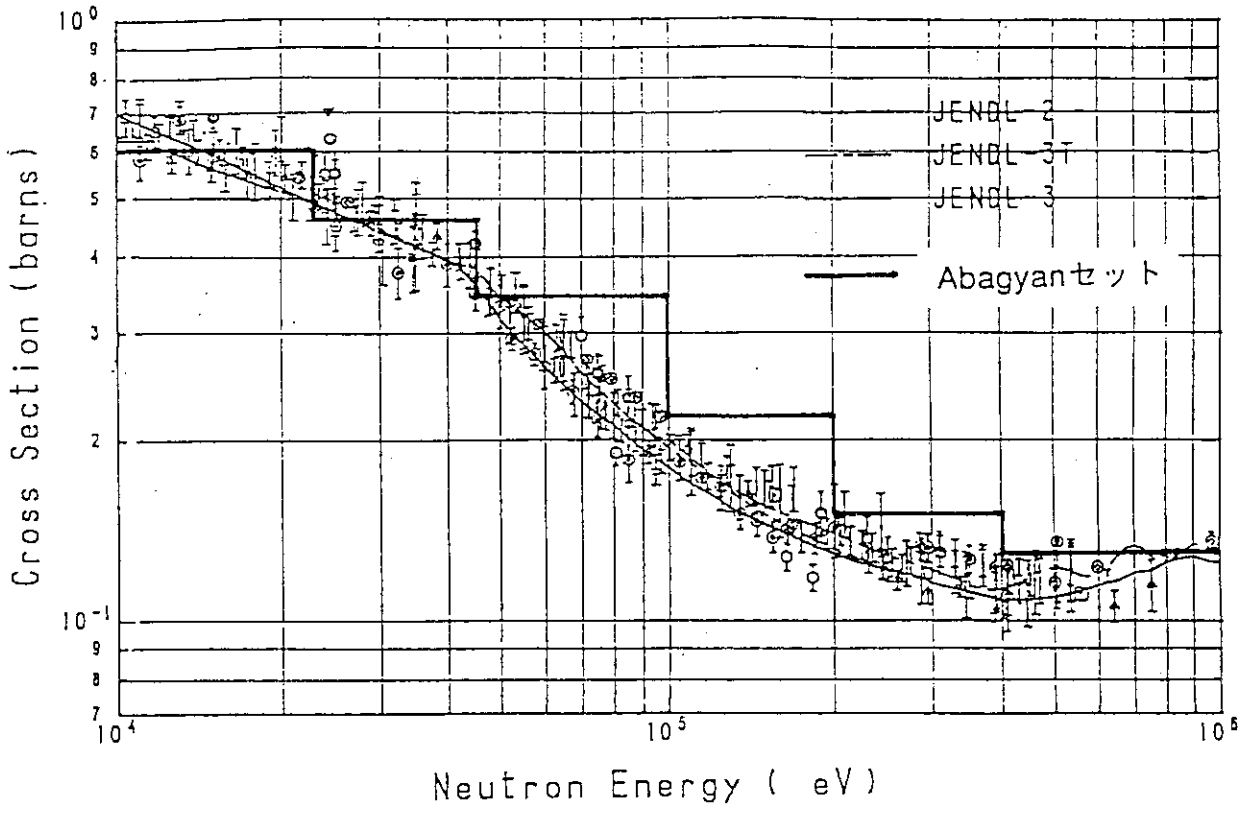

Fig. 1 Comparison of ^{238}U capture cross sections

3.2.3 Nuclear Data Needs for Fusion Reactor Development

Yasushi Seki

Naka Fusion Research Establishment
Japan Atomic Energy Research Institute
Naka-machi, Naka-gun, Ibaraki-ken, JAPAN

A personal view on the status and strategy of fusion reactor development from the International Thermonuclear Experimental Reactor ITER to DEMO and future commercial reactors is introduced based on the experience of nuclear design and safety analyses of fusion reactors. Some comments on nuclear data needs for fusion reactor development are discussed.

1. Fusion Reactor Development

What is most important for world fusion program is to achieve a self-ignition plasma by ITER. As it may be seen from the Fig. 1, ITER could be the largest fusion device needed in the pathway to commercial fusion plant because the next DEMO plant, the Steady State Tokamak Reactor (SSTR), could be smaller if higher magnetic field coil is developed [1]. Construction of ITER through a world wide collaboration is one of the biggest challenge for mankind after the end of the cold war. The author believes that once the self-ignition plasma is achieved in ITER, people will recognize fusion as a candidate for the energy source of future and many breakthrough will follow. The future prospects of fusion power reactors are shown in Table 1. By the extrapolation from ITER and SSTR, the reduction of tritium and activation products inventory could be expected if the components development and materials development are achieved as expected. Safety characteristics are improved by the use of helium coolant in place of water. Furthermore the improved thermal efficiency will result in reduced thermal pollution.

Table 1. Comparison of safety and environmental parameters for ITER, SSTR and Future Power Reactors

Item	ITER	SSTR	Future Prospects of Power Reactors
Fusion power	1 GWt	3 GWt	4.5 GWt
Tritium inventory	6 kg	5 kg	3 kg
Activation product inventory	~10^9 Ci, SS-316	<10^9 Ci, Reduced activation steel	<<10^9 Ci, Ti-Al, SiC
Primary coolant	Water	Water	Helium
Coolant inlet/outlet temperature	60°C~100°C	285°C/325°C	400°C/700°C
Thermal efficiency	-	~30%	~40%

2. Comments on Nuclear Data Needs for Fusion Reactors

There are many excellent reviews on the nuclear data needs for fusion reactors [2]-[7]. With the development of Fusion Evaluated Nuclear Data File (FENDL) [8] in the frame work of IAEA, the nuclear data file need for ITER will be satisfied and a standard file for ITER design will be developed. For an international project like ITER, a standard file is necessary for comparison along with the national data files.

Little can be added in the presence of many reviews by nuclear data experts. My feeling is that development of nuclear data should be carried out with proper balance between the existing uncertainties in the design area such as uncertainty in the plasma design, thermal mechanical design, and materials data base. At the same time proper balance is also required between the development of nuclear data, nuclear data file, group constants, radiation transport calculation codes, activation analysis calculation codes. For this purpose, a sensitivity analysis is suggested to show what is most sensitive to improve the accuracy of nuclear design and the proper allocation of development efforts.

References

[1] Y. Seki et al., The Steady State Tokamak Reactor (SSTR), ibid. IAEA-CN/G-1-2

[2] Nuclear data for Fusion Reactor Technology, IAEA-TECDOC-223, IAEA (1979)

[3] E. T. Cheng et al., Magnetic Fusion Energy Program Nuclear Data Needs, GA-A18152, UC-20 (1985)

[4] V. Goulo, edited., Fusion Evaluated Nuclear Data Library (FENDL), INDC(NDS)-223/GF (1989)

[5] K. Maki, Requirements for Nuclear Data for ITER/FER Nuclear Design, Proc. Second Specialists' Meeting on Nuclear Data for Fusion Reactors, JAERI-M 91-062 (1991) 183

[6] Y. Seki, Nuclear Data Needs from Fusion Reactor Safety Analysis, Proc. Second Specialists' Meeting on Nuclear Data for Fusion Reactors, JAERI-M 91-062 (1991) 173

[7] E. T. Cheng, Nuclear Data Needs and Status for Fusion Reactor Technology, Nuclear data for Science and Technology, S. M. Qaim (Ed.) Springer Verlag (1992) 273

[8] A. B. Pashchenko, Status of International Fusion Evaluated Nuclear Data Library (FENDL), presented at this Symposium.

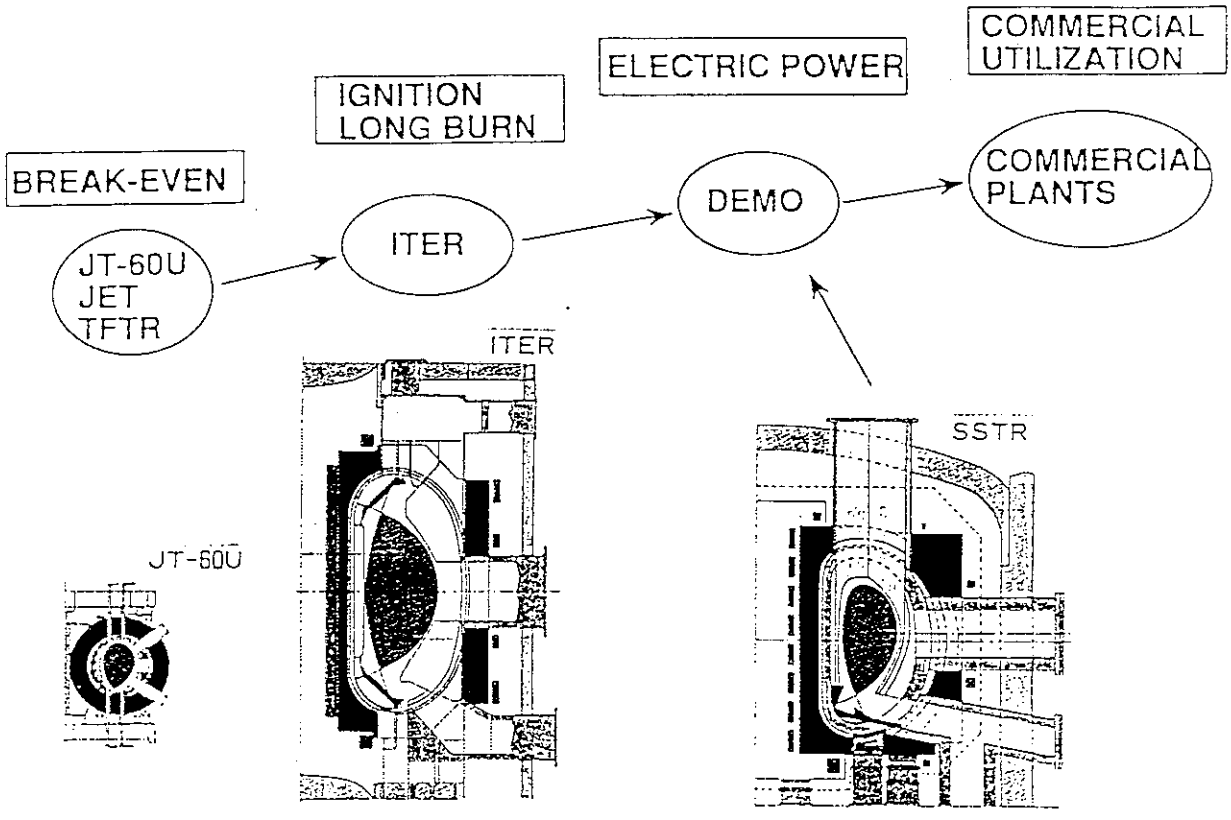

Fig. 1 Development strategy to commercial fusion

3.2.4 Request of Nuclear Data File for Study of New Application of Transmutation

Tomohiko IWASAKI

Department of Nuclear Engineering, Tohoku University

Abstract: Following two topics concerning on transmutation of hazardous materials are described. (1) Transmutation of TRU wastes in higher flux field. (2) Transmutation of chemical hazardous materials. The most important base-data for the transmutation of hazardous materials is nuclear data. However, the nuclear data for the nuclides of hazardous materials are not contained in JENDL-3. The nuclear data containing minor or rare isotopes are required.

(1) Transmutation of TRU wastes in higher flux field:

The aim of transmutation of TRU waste is to eliminate the long-term management. Burn-up with less residuals is needed to achieve this role. The transmutation in higher flux field of order of 10^{16} n/cm^2/s by Advanced Neutron Source and Spallation Source is desirable considering the limited time period of burn-up. The burn-up chain in that field is largely different from that in conventional reactor fields. Shorter-life nuclides such as ^{238}Np and higher isotopes such as Es and Fm are largely produced. Although the nuclear data of actinide are greatly improved by JENDL-3, it is not sufficient by lack of the nuclear data of those nuclides.

(2) Transmutation of chemical hazardous materials:

Three materials with chemical toxity are presented in the following table. Dioxin ($C_{12}H_4O_2Cl_4$) is the most hazardous materials and causes cancer risk only by intake of ~200 pg (6 x 10^{-13} mol) in one year. The transmutation of those materials may become

an effective method to reduce toxity even in current reactors or accelerators. Although the nuclear data of principal nuclide itself and the neighbor nuclides are required to examine burn-up of those materials, JENDL-3 is not sufficient as shown in the table.

The current nuclear data files are not enough to study of transmutation in new fields or for new materials as it is found from these two topics. In future, other objects or applications of transmutation will be found. The most important base-data is nuclear data for these investigation. The nuclear data for conventional reactors are almost complete by JENDL-3. However, nuclides which are not contained in JENDL are more important to investigate and develop new applications of transmutation. More general purpose file of nuclear data containing minor or rare isotopes are required.

Material	Dioxin (PCB)			As compound		
Weight causing cancer with prob. of 10^{-6} (*1)	219 pg (61 ng)			1.7 μg		
Nuclide necessary for study of transmutation	S	Cl	Ar	Ge	As	Se
JENDL-3 ("o" included, "x" not included.)	o	x	x	x	o	o

(*1) Yuko Makino, private communication.

3.2.5 Needs of Atomic, Molecule's and Nuclear Data for Medical Application in Japan

Shigeru IWANAMI

Department of Radiology, School of Medicine
Kitasato University
1-15-1, Kitasato, Sagamihara, Kanagawa-ken 228

Abstract

There are large potential needs of atomic and nuclear data for medical applications in Japan. But number of medical physicists who need their data is very small. The status of medical physicist does not formally exist in Japanese hospitals. Then practical needs for atomic and nuclear data are small in Japan.

Technical innovations in medical physics have been intensively introduced to hospitals in recent year. Table 1 shows available data of the total number of sophisticated machines currently used in Japan. Medical physicists want to have atomic, and molecule's and nuclear data. What kind of data do they need? Table 2 shows roles and responsibilities of them. The most important role is to engage in research work. Table 3 shows research fields of presentations at annual meetings of Japanese Association of Radiological Physicists (JARP) for 30 years. Medical physicists are expected to contribute creative work to a Department of Radiology, but the subject is limited to radiation physics.

In 1991, Symposium entitled "Medical Physicists, Today and Tomorrow" was held at the World Congress on Medical Physics and Biomedical Engineering in Kyoto[1]. Takaku who was the chairperson of the symposium reported that a number of medical physicists is very small in Japan. Table 4 shows composition of JARP members. Table 5 shows number of departments of medical physics in Japan. A few departments of medical physics have been working in some cancer research institutions, but no department of medical physics has ever been established in any university hospital. The status of medical physicist does not formally exist in Japanese hospitals. They are not recognized profession in our country. Therefore, although there are large potential needs for atomic and nuclear data, their practical needs are small in Japan.

Some universities have plans to found schools of health care sciences and technology, which have departments of medical physics. So number of medical physicists will increase and practical needs of atomic and nuclear data for medical application will increase in future.

The author would like to thank Dr. Takaku for providing data on status of medical physicists in Japan.

References

1)Takaku Y.: The Medical Physicist, Today and Tomorrow - The status, responsibilities and educational program in Japan, Jpn. Radiol. Phys., 11, 59

Table 1 Medical machines installed in hospitals in Japan (Takaku, 1991)

Linac	472
Co-60 Teletherapy unit	400
Treatment planning system	289
X-ray CT	6096
MRI	500
CR	140
DSA, DFA	638
Gamma Camera	1194
SPECT	881
PET	17
Data processing unit	1230

Table 2 Roles and responsibilities of medical physicists

1) Research work
2) Supporting a high standard of medical services
3) Safety analysis of newly developing method
4) Health physics
5) Education

Table 3 Research fields of presentations at annual meetings of Japanese Association of Radiological Physicists (JARP) for 30 years(Takaku, 1991)

Radiation dosimetry	35.2%
X-ray diagnosis	24.9%
Radiation therapy	9.5%
Health physics	7.8%
Nuclear medicine	6.0%
Radiation biology	3.2%
Information processing	2.6%

Table 4 Composition of JARP members(Takaku, 1991)

Certified physicists	90
Physicists	188
Medical doctors	139
Technologists	222
Others	56
Total numbers	695

Table 5 Number of departments of medical physics in Japan

Institution	NIRS, etc.
School of Medicine	0
Hospital	0

3.2.6 Experiments Using Accelerators for Space Application

Yosuke Shimano

National Space Development Agency of Japan

2-1-1 Sengen, Tsukuba-shi, Ibaraki-ken 305, Japan

1. Abstract

It is necessary for space application to conduct experiments using accelerators. We would like to discuss the situation and the problems of using the accelerators for engineering purpose.

2. Purpose of Experiments

Our experiments using accelerators are mainly engineering purpose. There are lots of routine work and the methodology is almost always the same. It is very difficult in this point to get understanding to our experiments from the scientists. We should not, however, underestimate the importance and the contribution of the engineering test to the science.

3. System of Cooperation

Generally speaking it is not easy for outsiders to use the accelerators effectively and freely. This is because the system of the cooperation of the organizations which have an accelerator facility is not so open. We really hope the user-friendly system of cooperation. There will be more users who are not familiar with the accelerator of the nuclear physics in the near future. The system of the cooperation between the owners of the accelerator and the users should be reconsidered.

3.2.7 Environment of Nuclear Energy Development and International Cooperation of Nuclear Data Activity

Toyojiro FUKETA

Nuclear Energy Data Center
2-4, Shirane, Shirakata, Tokai-mura
Naka-gun, Ibaraki-ken, 319-11 Japan

[Abstract] The world nuclear data activity achieved a reasonable level in the 1980's, and the power reactor development should have been given a stimulus. But, unfortunately the Chernobyl accident happened on 26th April 1986, since then the world nuclear energy development has been suffering from a very serious adverse wind, and governmental supports to the nuclear data activities in most countries have been declining also. It is clear for us that nuclear fission is the best major energy source for the preservation of the global environment in the foreseeable long future. More accurate nuclear data and hitherto unavailable kind of nuclear data are requisite for an advanced nuclear research and development. Under the existing circumstances of the nuclear data activity, an increased effort for the international cooperation in the nuclear data field is indeed required.

The activity which comprises measurements, collections, evaluations, compilations, disseminations, etc. of nuclear data is called the nuclear data activity. The worldwide motivation of promoting nuclear data activity extensively from about the end of 1950's was primarily for the development of advanced power reactors particularly fast breeder reactors.

It may be said that the world nuclear data activity achieved a reasonable level in the 1980's, and the power reactor development should have been given a stimulus. But, unfortunately the Chernobyl accident happened on 26th April 1986, since then the world nuclear energy development has been suffering from a very serious adverse wind, and governmental supports to the nuclear data activities in most countries have been declining also.

It is clear for us that nuclear fission is the best major energy source

for the preservation of the global environment in the foreseeable long future. Although the safety level of nuclear power plants in Japan is considered to be reasonable, in order to meet the energy demand with the world population increase and to keep the world integrated safety level of nuclear facilities better or at least same as the present best notwithstanding an increase of the number of nuclear facilities and the operation years, it comes naturally to the conclusion that efforts to improve the safety level of individual nuclear facilities and to develop new types of nuclear facilities of higher efficiency must be continued forever.

More accurate nuclear data and hitherto unavailable kind of nuclear data are requisite for an advanced nuclear research and development. The activity on massive nuclear data is required to be consistently continuous extending over a long period of time. If once a degradation of the nuclear data activity exceeded a certain level, an enormous effort in the long term would be necessary to recover the level. Under the existing circumstances of the nuclear data activity, an increased effort for the international cooperation in the nuclear data field is indeed required.

Recently, "A Strategic View on Nuclear Data Needs", Report by the NEA Secretariat, September 1993, was appeared. This report of 33 pages is a fruition of the effort of the Nuclear Energy Agency of OECD over the recent few years under a direct leadership of Dr. Kunihiko Uematsu, Director General of NEA, through the discussions of the NEA Nuclear Science Committee and the NEA Think Tank Meetings in January 1991 and May 1993.

An exact reproduction of "Executive Summary" of the above NEA Report is given as follows in 『 and 』:

『

This report examines the present and future needs for scientific nuclear data and discusses ways of meeting any such needs.

Different applications areas have been covered and well founded requests for scientific data have been expressed both within the "traditional" fission reactor area and new areas, such as radioactive waste transmutation, medicine and fusion. Specific examples of cost savings to be made using improved data, or of potential penalties for current or future applications which may be incurred by relying on inadequate data are given.

The resources of qualified manpower are falling below a minimal level and the situation appears particularly alarming when the age structure of the staff presently working in the field is considered. If the present staff policy is not changed very soon, there is a clear danger that indispensable know-how in nuclear data will be lost.

Support from industrial users are needed, but the ultimate responsibility for financing nuclear data work must, in the long term, rest with governments. A better cooperation between data producers and users should be established.

Data centres play an important role in coordinating national efforts and in helping to avoid unnecessary duplication of work. A minimum of two international data centres are needed.

NEA proposes to undertake the following actions in the nuclear data field:

- Continued strong support for the NEA International Evaluation Cooperation, and within the Data Bank Member countries, for the Joint Evaluated File project.
- Setting up a forum to facilitate the dialogue between users and producers of nuclear data.
- Promoting a framework for international collaboration in the field of nuclear data measurements.

It should be emphasised that any international cooperative effort undertaken by NEA would never replace national efforts, but would improve productivity from existing and future resources.

The nuclear data needs are clearly explained in the above report, and we can extend the discussion on the needs further in wider fields of specialties. Some of the discussions in this context are also found in this Panel and the other Sessions of this Symposium.

When the support from the nuclear fission energy R & D to the nuclear data activity is declining, it may be natural that an appeal on nuclear data needs tends to put emphasis upon needs in the fields of non-fission-energy. I do not think little of the nuclear data needs in the fields of non-fission-energy, but the nuclear fission energy R & D leaves a vast room for various R & D efforts; a maturity in technology is found in the field of light-water power reactors, though even this maturity does not mean to make light of the R & D needs for the light-water power reactors. An essential issue is in the world declining tendency of nuclear energy development at large rather than in an apparent decline of resources support for the nuclear data activities.

3.3 Summary

3.3.1 A Review Talk and Panel Discussion on Nuclear Data Activities at a Turning Point

Reviewer : Ryuzo Nakasima (Hosei-Univ.)
Panelists : Satoshi Chiba (JAERI)
Atsushi Zukeran (Hitachi Corp.)
Yasushi Seki (JAERI)
Satoru Iwasaki (Tohoku Univ.)
Shigeru Iwanami (Kitazato Univ.)
Yosuke Shimano (NASDA)
Toyojiro Fuketa (NEDAC)
Chairman : Masaharu Nakazawa (Univ. of Tokyo)

Abstract ; On the occasion of 30 years anniversary meeting of Japanese Nuclear data committee, a memorial review talk has been made by Professor R. Nakasima, and the panelists have made discussions on to which direction shall we go under the present difficult situations.

I. Summary of Review Talk of Prof. R. Nakasima

At the starting of JNDC(Japanese Nuclear Data Committee), the following three policies were agreed just 30 years ago.

(1) to work for Nuclear Data Collections and Evaluations.
(2) to encourage and support for Nuclear Data Measurement Groups, and
(3) to promote International Collaborative Activities.

Almost, these principles have been worked well, especially it should be remembered that the participation to the IAEA, INDC Working Group has stimulated us. And through 30 years, many discussions have been made in JNDC, on the technical subjects such as

(1) Data collections should be made also in Japan independently on CINDA activity?
(2) On the application of data adjustment procedures for data evaluation.
(3) On the termination of each working group,
(4) Collaboration with JEF group.
(5) On a plan of the Asian Nuclear Data Centre, and
(6) On the man-power problem.

On the present scope, prof. Nakasima has summarized, at first the increasing JNDC efforts are expected through the International collaborations, although the situations

became worse. And secondly invitations on new young scientists in this field are required from industries, JAERI, universities including nuclear theoretical physicists.

II. Panel discussion

At first, seven panelists have talked their opinions on this subject what is the present situations and to which way shall we make our steps.

As new fields which need nuclear data besides the present nuclear fission reactor field, it was pointed out the nuclear fusion , the nuclear incineration of poison such as dioxin, medical and space fields. Their demands is, however, not so strong as so from the nuclear fission reactor, but their demands is essentially very diverse. Additionally the demands are not only the nuclear data but also relating nuclear technology including experimental and analytical procedures.

If the aim of JNDC activities is expanded towards to these new fields, several present policies of JNDC should be changed. At first, practical advertisements of nuclear data & technology to those fields should be made using many possible means, such as publication of booklets, lectures in those society meetings. Practical demonstration of availability of nuclear data in each fields, and so on. Then, meaningful cooperative works between JNDC and other fields should be planned. This is one important result of this panel discussions.

As the second issue of JNDC, it is discussed how to increase or bring up the younger researchers in this field, including the theoretical nuclear physicists. The importance of attractive research subjects and/or the expectations on the new nuclear technology such as Hadron Engineering, Ultra strong neutron source as the Synchrotron radiation in optics have been emphasized. In addition, it is also discussed how to raise the researchers position of nuclear technology especially nuclear data, for example using the licensing or the qualification system of nuclear evaluators.

In addition to those domestic efforts, the importance of international collaborative works has been recognized in every participants. The chairman of the panel has made a summary of discussions, that we have obtained the common understanding on the present situation surrounding the JNDC, and also we have obtained here the practical action plan to improve it.

4. Closing Session

4.1 Evolution of Data Requirement Since the Early 1980's

Tadashi Yoshida
Nuclear Engineering Laboratory, Toshiba Corporation
4-1 Ukishima-cho, Kawasaki-ku, Kawasaki

Thirteen years ago, at the turning point of the decade, the objective of the nuclear data activities in Japan seemed to be rather obvious. High priority was placed on providing the fast breeder project with the best cross section data at that time. In this sense, the mountain to climb was clearly in the center of our sight (Fig.1). We also started talking about the fusion neutronics, but it still belonged to the future. The reactor physicists and designers were well learned in nuclear data and were in full cooperation with the nuclear data people. They used to discuss all together about the topics of vital importance such as the reactor-contant generation and the cross-section adjustment based on integral experiments.

Since then the situation has changed considerably. The most conspicuous feature of the nulear data scene in 1993 seems to be dispersion and broadening of its coverage (Fig.2). We still talk about the adjustment, but the fast breeder cannot be a motivation for the revision in the near future of the Japanese Evaluated Nuclear Data Library Version 3.2, which is going to be frozen, at least for five years, in order to guarantee a stable use of the present version. Data requirement from the fusion community is quite active but it does not dominate others. Requirement from the fuel cycle thechnology, reprocessing and spent fuel management, for instance, is steadily growing.

Today we had a very good chance to listen to many experienced lecturers from a wide variety of disciplines; medical physics, space technology, astrophysics and ion-beam science. We hope the nuclear data community in Japan, which was fostered by the nuclear energy program in its infancy, could also supply excellent data to these growing fields. I believe, however, there is still much to do for the nuclear energy. I raise only one example among others. That is a possible effort to generate an inclusive set of one-group constants from JENDL-3.2 for several versatile burn-up codes, which are widely used in our country from the utilities to the reactor venders. It would be an excellent gift to the nuclear energy technology from her son, and would certainly be used long for the future along with the development of the Japanese nuclear fuel cycle.

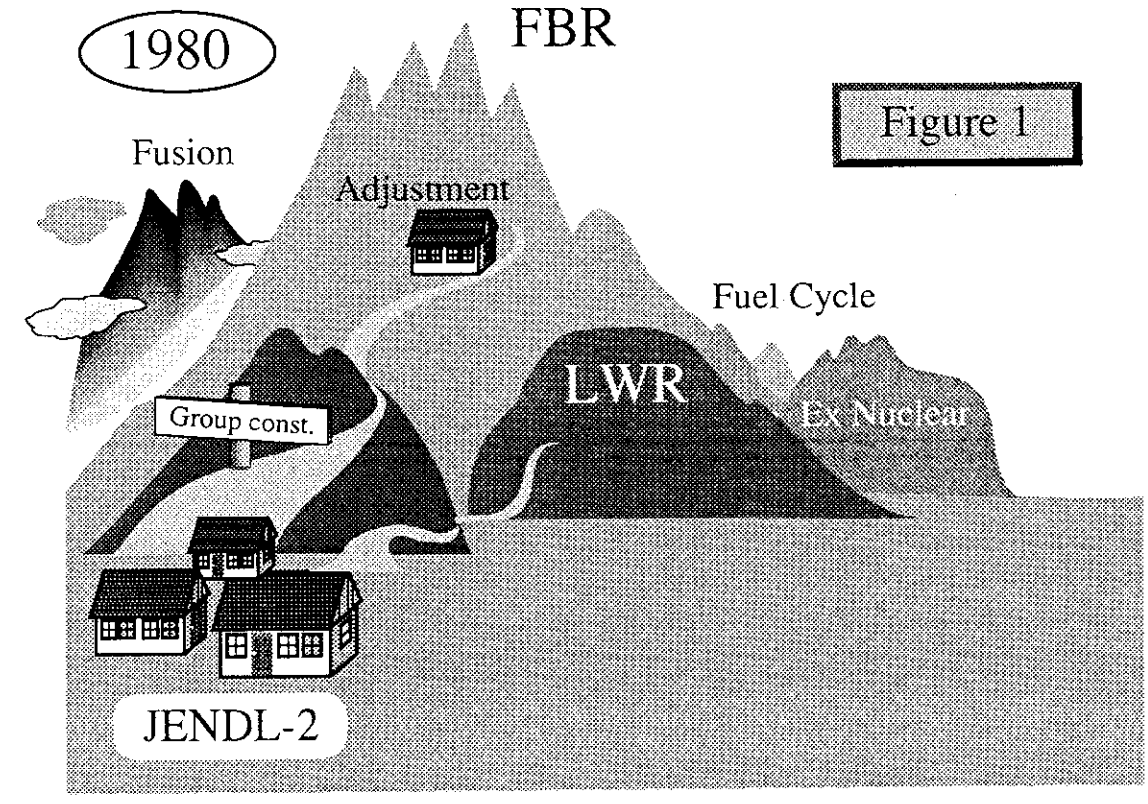

Figure 1

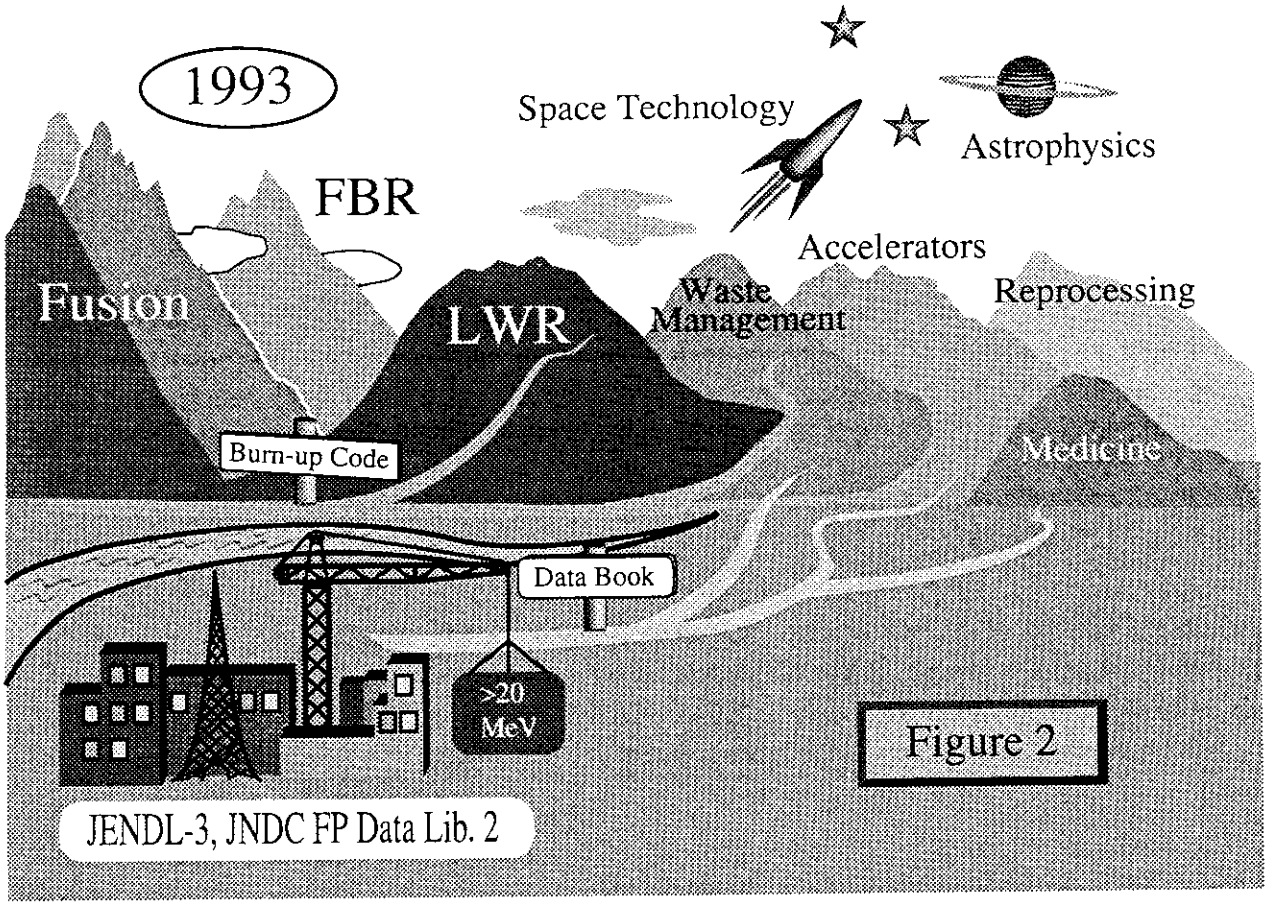

Figure 2

5. Papers Presented at Poster Session

5.1 Measurements of Thermal Neutron Cross Section and Resonance Integral for the ^{237}Np(n, γ)^{238}Np Reaction

Katsuhei Kobayashi[1], Akihiro Yamanaka[2,3], and Itsuro Kimura[2]

1. Research Reactor Institute, Kyoto University
   Kumatori-cho, Sennan-gun, Osaka 590-04, Japan
2. Department of Nuclear Engineering, Kyoto University
   Yoshida-honmachi, Sakyo-ku, Kyoto 606-01, Japan
3. Present address: Hitachi Works, Hitachi, Ltd.
   Saiwai-cho, Hitachi-shi, Ibaraki 317, Japan

Making use of a standard neutron spectrum field with a pure Maxwellian distribution at the heavy water thermal neutron facility of the Kyoto University Reactor (KUR), thermal neutron cross section for the ^{237}Np(n,γ)^{238}Np reaction was measured by the activation method, using a high purity Ge detector. The result is 158±3 b, which is obtained relative to the reference value of 98.65±0.09 b for the ^{197}Au(n,γ)^{198}Au reaction. The present value is lower by about 7 % than that with the ENDF/B-V data. The data given by Mughabghab and obtained from JENDL-3 are larger by 11 to 15 % than the present measurement.

The resonance integral for the ^{237}Np(n,γ)^{238}Np reaction was measured with a 1/E standard neutron spectrum in the cavity of the central graphite reflector region between the two-divided cores of the Kinki University Reactor (UTR-KINKI), relative to the reference value of 1550±28 b for the ^{197}Au(n,γ)^{198}Au reaction. By defining the Cd cut-off energy as 0.5 eV, present resonance integral is 652±24 b, which is in good agreement with the JENDL-3, ENDF/B-V and Mughabghab data. However, most of the old experimental data are, in general, larger by 24 to 38 % than the present measurement.

1. Introduction

Neptunium-237 is one of the minor actinides with a long half-life, which are abundantly produced in light water reactors. In order to make the nuclear power more acceptable and practical, much interest has been paid to the nuclear waste management in these days[1-3]. One of the waste managements for ^{237}Np is to adopt the nuclear transmutation using reactor neutrons. Quite a number of experimental data for the ^{237}Np(n,f) cross section are obtained in the MeV energy region and these data are rather well evaluated. However, large discrepancies exist in the lower energy region for this cross section. Very recently, the present authors have measured the ^{237}Np(n,f) cross section by using a lead slowing-down spectrometer coupled to an electron linear accelerator[4]. The cross section values averaged from eV to keV energies are 10 to 500 mb. The ^{237}Np(n,γ)^{238}Np reaction cross section, which is combination of the 1/v and resonance cross sections in lower energy region, is much higher than the fission cross section, and hence this reaction would be more effective in lower energy region for the nuclear transmutation of ^{237}Np than the ^{237}Np(n,f) reaction, considering the reaction rates averaged over the energy spectrum of reactor neutrons.

Calculations for fuel burn-up and for the reactor design aiming at the transmutation of high level radioactive materials have been carried out. In these cases, it is said that the evaluated

nuclear data, which would be mainly based on the experimental results, are not always enough, especially for the $^{237}Np(n,\gamma)^{238}Np$ reaction used for the transmutation. There exist scarcely the energy dependent cross section data for the $^{237}Np(n,\gamma)^{238}Np$ reaction, and most of the thermal neutron cross sections and the resonance integrals for this reaction are rather old. It may not be said that the information of neutron spectrum fields used for the previous measurements is good enough as a standard.

In the present study, thermal neutron cross section and resonance integral for the $^{237}Np(n,\gamma)$ ^{238}Np reaction have been measured by the activation method, making use of standard neutron fields with a pure Maxwellian distribution and with a 1/E neutron spectrum, respectively.

2. Neutron Spectrum Fields

Thermal Neutron Spectrum Field

The Kyoto University Reactor (KUR) of the Research Reactor Institute, Kyoto University (KURRI) is a highly enriched uranium-fueled light water-moderated research reactor, whose nominal power is 5 MW. Besides the core, there is a heavy water thermal neutron facility with a heavy water tank of 1.4 m in length. Outside the heavy water tank, a removable graphite layer of 48 cm in thickness and a removable bismuth layer of 60 cm in diameter and 15 cm in thickness are placed, as illustrated in Fig.1. The irradiation room is about 2.4 x 2.4 x 2.4 m^3 and surrounded by 90 cm thick heavy concrete shields. The leakage neutrons from the heavy water tank and/or graphite layer can be used as a thermal neutron source of beam or plane-type in a large space.

Kanda et al. measured the neutron spectra from the heavy water tank and from the graphite layer by the time-of-flight technique using a fast chopper[5]. The former showed good agreement with a Maxwellian distribution having neutron temperature of 60 °C, while the latter had small structures below 0.015 eV due to the fine crystal properties of graphite. The measured results are displayed in Fig.2. The Cd-ratio measured with a Au foil in a Cd cover of 0.7 mm in thickness was more than 5000 at the bismuth layer, and epithermal neutrons could be almost negligible[5,6].

1/E Neutron Spectrum Field

The UTR-KINKI is a highly enriched uranium-fueled light water-moderated and graphite-reflected research reactor[7], which has the separate cores at an interval of 46 cm. The nominal output power is 1 W. At the center of the internal graphite reflector between the two divided cores as shown in Fig.3, a graphite stringer of 9.6 x 9.6 cm square and 122 cm long can be withdrawn to make a void region or a central cavity for sample irradiation[7]. The neutron energy spectrum at the central graphite cavity has been calculated[8] using the SRAC code system[9]. In this calculation, geometrical conditions were assumed to be that the separate cores with MTR-type enriched uranium fuels closely resembled a cylindrical ring. The two-dimensional transport Sn code TWOTRAN[10] was employed to calculate the neutron spectrum in the central void region. One hundred and twenty-two group constants were produced from ENDF/B-IV data. The results of the neutron spectra are shown in Fig.4. The calculated spectrum satisfactorily agrees with a standard 1/E neutron spectrum field from about 1 eV to a few hundreds keV.

The neutron spectrum was also obtained[7] by the adjustment of the above calculated spectrum with multi-foil activation data for 5 kinds of (n,γ) reactions and 4 kinds of threshold reac-

tions using the NEUPAC code[11]. This code contains energy dependent group cross section libraries for main important neutron dosimetry reactions in ENDF/B－V. We adopted 144 energy groups from 0.01 eV to 16.4 MeV. The results of the adjusted spectrum are shown in Fig.4, comparing with the above transport calculations. It can be seen that the neutron spectrum at the core center gives a good 1/E shape in the relevant energy range and that the neutron flux distribution is almost flat in the central cavity of the UTR－KINKI.

The sandwiched foil method has been also employed[7] to measure epithermal neutrons at the main resonances for 4 kinds of (n,γ) reactions. Neutron fluxes at 1.46, 4.94, 18.8 and 337 eV resonances for ^{115}In, ^{197}Au, ^{186}W and ^{55}Mn are shown in Fig.4, respectively. These results are in good agreement with the calculated and the adjusted spectra in the 1/E spectrum region.

3. Measurement of Thermal Neutron Cross Section

The thermal neutron cross section σ_x averaged over the Maxwellian distribution spectrum is defined as

$$\sigma_x = \frac{\sigma_x(v_o)}{1.128}\, g_x(T_n)\, \frac{T_o}{T_n}$$

where v_o=2200 m/s, T_o=293.6 K, T_n is neutron temperature and $g_x(T_n)$ is a g－factor for the relevant reaction.

In the present measurement, thermal neutron cross section for the ^{237}Np(n,γ)^{238}Np reaction has been measured relative to that for the ^{197}Au(n,γ)^{198}Au reaction as a standard, by rewriting the above relation as follow;

$$\sigma_x(v_o) = \frac{\sigma_x}{\sigma_{Au}}\, \frac{g_{Au}(T_n)}{g_x(T_n)}\, \sigma_{Au}(v_o) = \frac{R_x}{R_{AU}}\, \frac{g_{Au}(T_n)}{g_x(T_n)}\, \sigma_{Au}(v_o)$$

where R_x and R_{Au} are relative reaction rates for the ^{237}Np and ^{197}Au reactions.

The ^{237}Np samples, which were chemically purified as aqueous solution[4], were prepared in the form of dried filter－paper with a drop of the solution. The sample was sealed with vinyl sheet and the amount of the ^{237}Np atoms was to be 10^{16} to 10^{17} for each sample, which was experimentally determined by the gamma－ray measurement of ^{237}Np using a high purity Ge (HPGe) detector. Induced activities of ^{238}Np from the irradiated ^{237}Np sample are simultaneously measured with the ^{233}Pa activities which were in radioactive equilibrium to ^{237}Np. The detection efficiency was experimentally determined by the mixed gamma－ray standard sources.

Thermal neutron flux was monitored with a Au foil of 3 mm in diameter and 50 μm thick and/or with a Au－Al alloy wire, 0.0314 % in weight of Au, 0.5 mm in diameter. The ^{237}Np and the Au samples were set at about 10 cm away from the Bi surface in the irradiation room of the heavy water thermal neutron facility of the KUR. Irradiation time was about 10 hours during the 5 MW operation of the KUR. Nine irradiations were made, and neutron fluxes for six of them were monitored with Au－Al wires and the remains were made by Au foils. The thermal neutron flux at the irradiation position in front of the Bi plate attained to about 1.5x10^9 n/cm^2/s at the nominal KUR power level of 5 MW.

Nuclear data for the produced radioactive isotopes of ^{238}Np and ^{198}Au are shown in Table 1, where the data used for the determination of number of ^{237}Np atoms are included[12]. The g－factors[13] for both of ^{237}Np and ^{197}Au are also given in the table.

4. Measurement of Resonance Integral

The resonance integral is defined by the relation;

$$I_x = \int_{E_{Cd}}^{\infty} \sigma_x(E)\, dE / E$$

where $\sigma_x(E)$ is cross section as a function of energy E, and E_{Cd} is a Cd cut−off energy, which is assumed to be 0.5 eV. The resonance integral for the $^{237}Np(n,\gamma)^{238}Np$ reaction has been measured relative to that for the $^{197}Au(n,\gamma)^{198}Au$ reaction, as seen in the following relation;

$$I_x = I_{Au} \frac{\varepsilon_{Au}}{\varepsilon_x} \frac{R_x}{R_{Au}} \frac{S_x}{S_{Au}} .$$

where I_{Au} is a standard value of the Au resonance integral, ε, R and S are detection efficiency, reaction rate and self−shielding correction, and the subscripts Au and x mean the data for Au and ^{237}Np samples, respectively. The neutron self−shielding correction in the Au foil was obtained by the continuous energy Monte Carlo code VIM[14].

The ^{237}Np samples were also in the form of dried filter−paper, which was prepared as same as those used for the thermal neutron cross section measurements. For the Au sample, metallic foil of 12.7 mm in diameter and 50 μm in thickness was used. The ^{237}Np sample and the Au foil each were covered with Cd−cover of 0.5 mm in thickness and stuck on an aluminum holder, which was set at the central graphite cavity of the UTR−KINKI. The ^{237}Np sample with Cd−cover was set between the Au foils with Cd−cover for the neutron flux monitor. Moreover, two Au foils without Cd−cover were also inserted in the central cavity region for the data normalization between the irradiation runs. Five hours irradiation runs with the sample/foil were repeated 9 times during the 1 W operation. Induced activities from the samples were measured with a HPGe detector, whose detection efficiency had been calibrated with standard gamma−ray sources. The nuclear data used for the present measurement are also taken from Table 1, as done in the thermal neutron cross section measurement.

In the present measurement, thickness of the Cd−cover is 0.5 mm, whose thickness usually corresponds to a cut−off energy of about 0.5 eV. However, ^{237}Np has a big resonance at 0.49 eV, and the cut−off energy with Cd−cover of 0.5 mm in thickness is about 0.3 eV for the neutron spectrum at the central graphite region of the UTR−KINKI. We have corrected the resonance integral for the $^{237}Np(n,\gamma)^{238}Np$ reaction to define the cut−off energy to be 0.5 eV by using the VIM code.

5. Results and Discussion

Thermal Neutron Cross Section

Thermal neutron cross section for the $^{237}Np(n,\gamma)^{238}Np$ reaction was obtained, relative to the well known 2200 m/s reference cross section value of 98.65±0.09 b for the $^{197}Au(n,\gamma)^{198}Au$ reaction. The present value is shown in Table 2, comparing with the existing data. The experimental uncertainties were carefully analyzed by considering the correlations between the measured data[15]. The correlation coefficient between the data for the $^{237}Np(n,\gamma)^{238}Np$ and $^{197}Au(n,\gamma)^{198}Au$ reactions is 0.05 in the present measurement. Main sources of the uncertainties are due to the statistical errors and from the detection efficiencies for the induced gamma−ray measurements. The experimental uncertainties for 9 irradiations are summarized, and the resultant value

is about 1.9 %. The measured data which were derived from two kinds of neutron monitors by the Au foil and the Au−Al alloy wire showed a good agreement within the experimental error, each other. We have also made neutron irradiations of ^{237}Np with the 0.5 mm thick Cd−cover at the heavy water thermal neutron facility of the KUR. From the result, the induced activities of ^{238}Np could not be observed.

As seen in Table 2, previous experimental thermal neutron cross sections exist between 172 and 187 b and larger by 9 to 18 % than the present measurement. The evaluated data, which are rather based on these experimental data, are also higher, and the data from ENDF/B−V are larger by about 7 % than the measurement. The Mughabghab's and JENDL−3 data are larger by 11 to 15 %. These discrepancies may be due to the fact that the previous measurements cannot be always good enough to measure the cross section correctly, from the points of experimental techniques, the neutron spectrum field used as a standard and of the prepared sample completion.

Resonance Integral

Resonance integral for the ^{237}Np(n,γ) ^{238}Np reaction was obtained from 9 irradiation runs by normalizing to the reference value of 1550±28 b for the ^{197}Au(n,γ)^{198}Au reaction. The present value is summarized in Table 3 with the experimental uncertainties of 3.7 %, taking account of the correlations between the measured data. Most of the experimental errors were from the statistical counts, the detection efficiencies and from the reference value as those in the case of thermal neutron cross section measurement. The correlation coefficient between the ^{237}Np(n,γ) ^{238}Np and the ^{197}Au(n,γ)^{198}Au reactions was 0.48. Self−shielding correction for the Au foil 50 μm thick was made by the VIM code. For the ^{237}Np samples, the self−shielding effect was not considered because the sample was diluted in the form of dried filter−paper.

We have investigated the effect which is observed in the resonance integral by changing the Cd cut−off energy, and found that a 10 % change in energy results in only a 0.2 % shift in the integral data, if the cross section is assumed to be 1/v shape. Moreover, the correction was made for the fact that the neutron energy spectrum in the UTR−KINKI was deviated from the ideal 1/E spectrum, especially at energies below 1 eV.

Since ^{237}Np has a big resonance at 0.49 eV, the effective Cd cut−off energy becomes much lower than 0.5 eV whose value is used for the definition of the resonance integral. For the experimental determination of the resonance integral for the ^{237}Np(n,γ)^{238}Np reaction, therefore, the measured data must be corrected. In the present measurement, correction factor due to the difference of the effective cut−off energy was estimated to be 30 % by the Monte Carlo calculations using the VIM code. We have obtained 931±35 b as a resonance integral for the ^{237}Np(n,γ) ^{238}Np reaction before the Cd cut−off energy correction. The reason why the old experimental data are much larger than the present value may be due to the fact that the correction of E_{Cd} was not considered properly.

Recent evaluations of JENDL−3 and ENDF/B−V and by Mughabghab are in good agreement with the present measurement, as shown in Table 3. However, most of the experimental values which are rather old are larger by 24 to 38 %, except for that by Hellstand.

6. Conclusion

Thermal neutron cross section for the ^{237}Np(n,γ)^{238}Np reaction was measured with the pure Maxwellian distribution field at the heavy water thermal neutron facility of the KUR, and the resonance integral for the same reaction was measured with the 1/E neutron spectrum field at the central graphite cavity of the UTR−KINKI, relative to the ^{197}Au(n,γ)^{198}Au reaction cross section

for both ^{237}Np cross section measurements. For the thermal neutron cross section measurement, most of the previous experimental data are larger by 9 to 18 % than the present data(158±3 b), and the evaluated values are also larger by 7 to 15 % than the present. On the other hand, the evaluated resonance integrals are in good agreement with the present result(652±24 b). However, the old measurements are larger by 24 to 38 % than the present value.

REFERENCES

[1] Mukaiyama, T., et al., "Conceptual Study of Actinide Burner Reactors", Proc. of the 1988 Int. Reactor Phys. Conf., Jackson Hale. Vol.IV, 369 (1988).
[2] Berwald, D. H. and Duderstadt, J. J., Nucl. Technol., Vol.42, 34 (1979).
[3] Takano, H., et al., "Concept of Actinide Transmutation with Intense Proton Accelerator", 6th Int. Conf. on Emerging Nuclear Energy Systems", Monterey, USA 1991.
[4] Yamanaka, A., Kimura, I., Kanazawa, S., Kobayashi, K., et al., J. Nucl. Sci. Technol., Vol.30, No.9, 863 (1993).
[5] Kanda, K., et al., Nucl. Instr. Meth., Vol.148, 535 (1978).
[6] Kobayashi, T., et al., Private communication (1983).
[7] Kobayashi, K., Yamamoto, S., Kimura, I., Annu. Rep. Kinki Univ. Atomic Energy Res. Inst., Vol.25, 21 (1988).
[8] Miki, R., et al., ibid., Vol.23, 33 (1986).
[9] Tsuchihashi, K., et al., JAERI 1285 (1983).
[10] Lathrop, K. D., et al., LA−4848−MS (1973).
[11] Nakazawa, M. and Sekiguchi, A., Proc. 2nd ASTM−Euratom Symp. on Reactor Dosimetry, NUREG/CP−0004, Vol.3, 1423 (1977).
[12] Browne, E. and Firestone, R., "Table of Radioactive Isotopes", John Wiley & Sons, New York 1986.
[13] Mughabghab, S. F., "Neutron Cross Sections", Vol.1, Neutron Resonance Parameters and Thermal Cross Sections, Part B, 1984.
[14] Blomquist, R. N., et al., ORNL/RSIC−44, pp 31−46 (1980).
[15] Kobayashi, K., Kimura, I. and Mannhart, W., J. Nucl. Sci. Technol., Vol.19, No.5, 341 (1982).

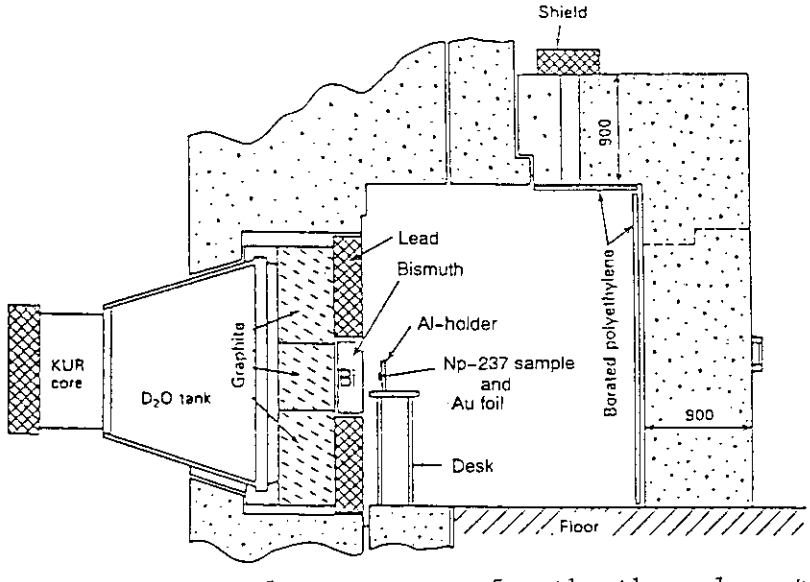

Fig. 1 Experimental arrangement for the thermal neutron cross section measurement at the heavy water thermal neutron facility of the KUR.

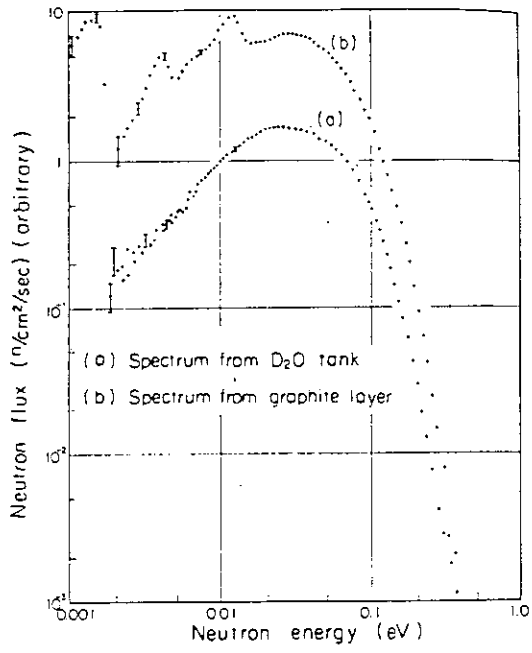

Fig. 2 The measured thermal neutron spectra from the heavy water tank and from the graphite layer[5].

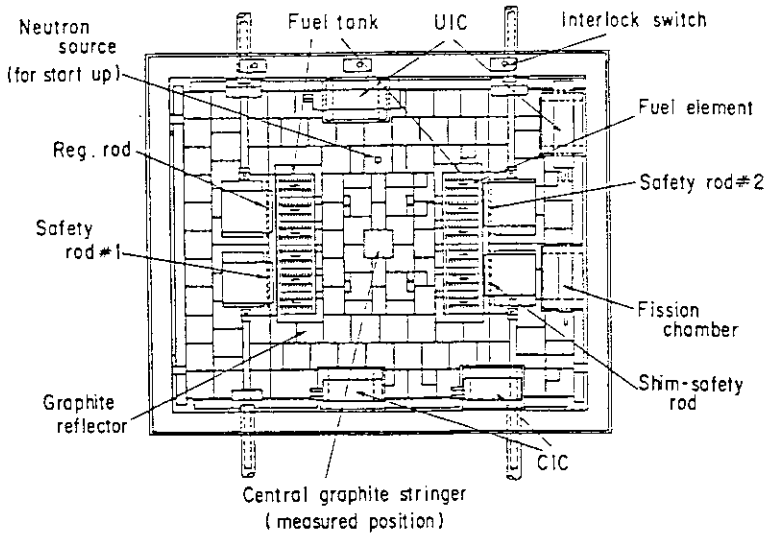

Fig. 3 Experimental arrangement at the core of the UTR-KINKI.

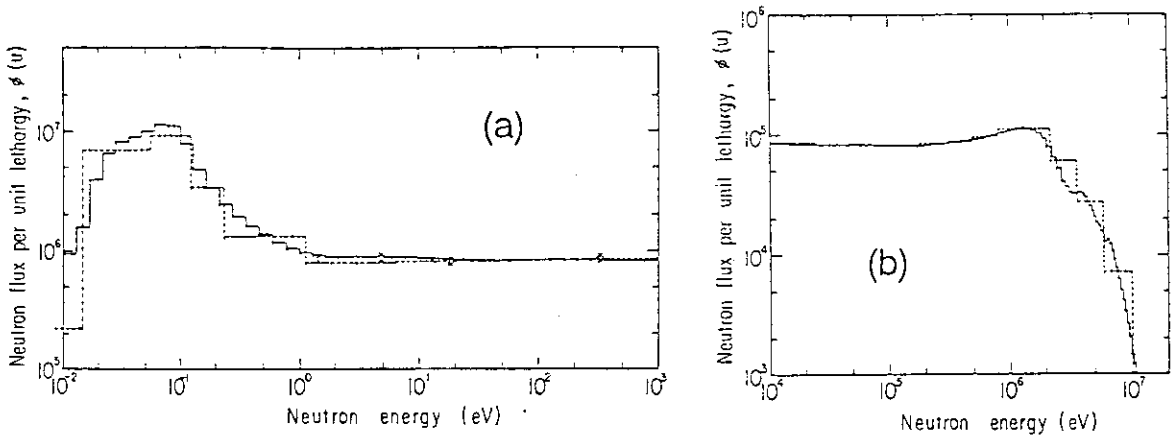

Fig. 4 Neutron energy spectra obtained at the central graphite cavity of the UTR-KINKI[7].
(a) in the lower energy region, and (b) in the higher energy region.
o□Δ▽ were measured by sandwiched foils,
---- calculation,
—— adjusted spectrum.

Table 1 Nuclear data of ^{237}Np, ^{233}Pa, ^{238}Np, ^{197}Au and ^{198}Au used for the present measurements.

Isotope	Half-life	Gamma-ray energy	Gamma-ray intensity	g-factor
^{237}Np	2.14×10^6 y			0.982
^{233}Pa	27.0 d	0.312 MeV	37.0 %	
^{238}Np	2.12 d	0.984 MeV	27.8 %	
		1.029 MeV	20.3 %	
^{197}Au				1.0051
^{198}Au	2.694 d	0.412 MeV	95.5 %	

Table 2 Thermal neutron cross section (2200 m/s value) for the $^{237}Np(n,\gamma)^{238}Np$ reaction.

Present	158 ± 3 b
JENDL-3('90)	181.0
ENDF/B-V('79)	169.1
Mughabghab('84)	175.9 ± 2.9
IAEA handbook('87)	169 ± 3
Weston('81)	185 ± 12
Eberle('71)	187 ± 6
Hellstrand('70)	172 ± 3
Schuman('69)	185 ± 12

Table 3 Resonance integral for the $^{237}Np(n,\gamma)^{238}Np$ reaction.

Present	652 ± 24 b
JENDL-3('90)	663.0
ENDF/B-V('79)	662.6
Mughabghab('84)	640 ± 50
IAEA handbook('87)	821.5 ± 58.0
Hellstand('79)	640 ± 50
Schuman('69)	807 ± 40
Scoville('68)	900 ± 300

5.2 Measurement of Cross Section for ^{241}Am(n, f) Reaction between 0.5 eV and 10 keV with Lead Slowing-down Spectrometer

K.Kobayashi[1], M.Miyoshi[2], S.Yamamoto[1], Y.Fujita[1],
I.Kimura[2], I.Kanno[2] and S.Kanazawa[2]

[1] Research Reactor Institute, Kyoto University, Kumatori-cho, Sennan-gun, Osaka, 590-04 Japan
[2] Department of Nuclear Engineering, Kyoto University, Yoshidahonmachi, Sakyo-ku, Kyoto, 606-01 Japan

By making use of a lead slowing-down spectrometer coupled to an electron linear accelerator and back-to-back type double fission chambers, the fission cross section of ^{241}Am was measured relative to that of ^{235}U in the energy region from 0.5 eV to 10 keV. The measured result has been compared with (1) the evaluated nuclear data files, JENDL-3 and ENDF/B-VI, and with (2) the existing experimental data. Although the shape of the present energy dependent fission cross section is close to that of the evaluated data files, the absolute values of the present data are about 3 time larger than those of the evaluated data and of the measurements by Dabbs, and are rather closer to those measured by Gayther and Bowman above about a few tens of eV.

A lead neutron slowing-down spectrometer was installed beside the 46 MeV electron linear accelerator (linac) at the Research Reactor Institute, Kyoto University (KURRI). This spectrometer was named KULS. At the center of KULS, we set an air-cooled Ta photoneutron target to generate pulsed neutrons. We obtained its performance, namely the relation between the slowing-down time t and the neutron energy E, and the energy resolution E/E, using a BF_3 counter or an Ar-gas counter with several kinds of resonance filters. Good linearity was observed between 1/ E and t, and the energy resolution was determined to be about 40 % in the relevant neutron energy region. The detailed characteristics of KULS were reported in the previous works[1,2].

By making us of KULS, we have measured the fission cross section of ^{241}Am relative to that of ^{235}U from about 0.5 eV to about 10 keV. Back-to-back type double fission chambers which appears in Fig. 1 were employed for the fission cross section measurement[3]. As the electrodes of the chambers, we electrodeposited $^{241}AmO_2$ and $^{235}UO_2$

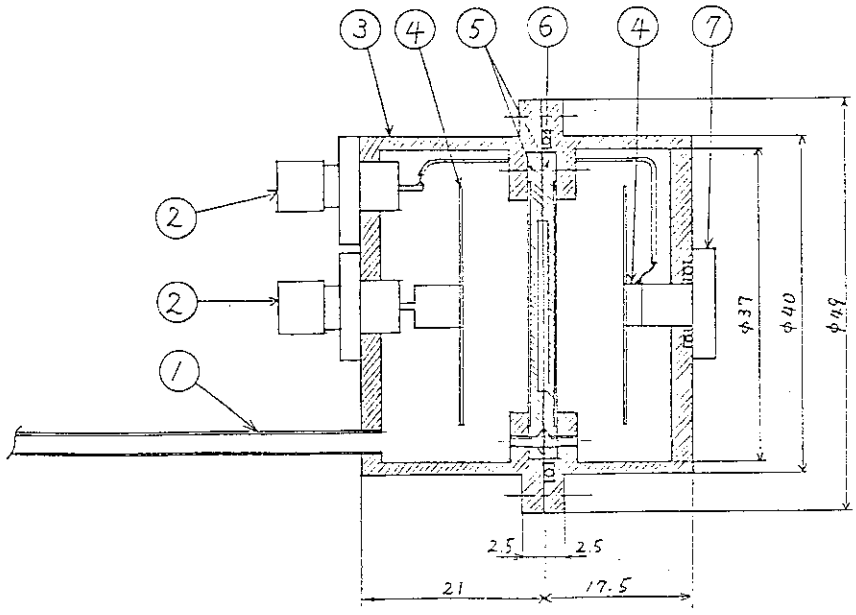

Fig. 1 Cross sectional view of back－to－back type double fission chambers. (1)Tube for vacuum, (2) Connector, (3) Chamber, (4) Electrode, (5) Support of electrodeposits, (6) O－ring, (7) Teflon support of electrode. (unit: mm)

layers on stainless steel plates of 28 mm in diameter and 0.2 mm thick. The diameter of the deposits was 2 cm. After the electrodeposition, each plate was set into the chambers. The number of atoms in the deposits was determined by the alpha－ray spectrometry with a Si surface barrier detector. The chambers were filled with a mixed gas of 97 % Ar and 3 % N_2 at 1 atm, and then put into an experimental hole covered by Bi layers in KULS.

By an operation of the electron linac for about 200 hours, the cross section for the ^{241}Am(n,f) reaction was obtained relative to the ^{235}U(n,f) cross section in ENDF/B－VI as a standard. In Fig. 2, the present result, in which only the statistical error is taken into account, is compared with the values in two newly evaluated nuclear data files, JENDL－3[4] and ENDF/B－VI[5]. Since the energy resolution of the original files is much higher than that of the present experiment, we processed those data by multiplying a resolution function of a Gaussian with 40 % of its full width at half maximum. The present result is also compared with the existing experimental data in Fig. 3.

From these figures, it is seen that (1) the gross shape of the present measurement is close to that of the ENDF/B－VI cross section and the JENDL－3 data which are a little lower than the ENDF/B－VI in the energy region between 10 and 200 eV, (2) the absolute

value of the present result is about 3 times larger than the values in both JENDL-3 and ENDF/B-VI which was evaluated by making much of the experimental data by Dabbs[6]. Our data are roughly in the average level of the Knitter's and the Seeger's results[7,8] and are rather close to those by Gayther[9] and Bowman[10] above a few tens of eV. It has to be continued in future to investigate the discrepancies between the existing data and ours.

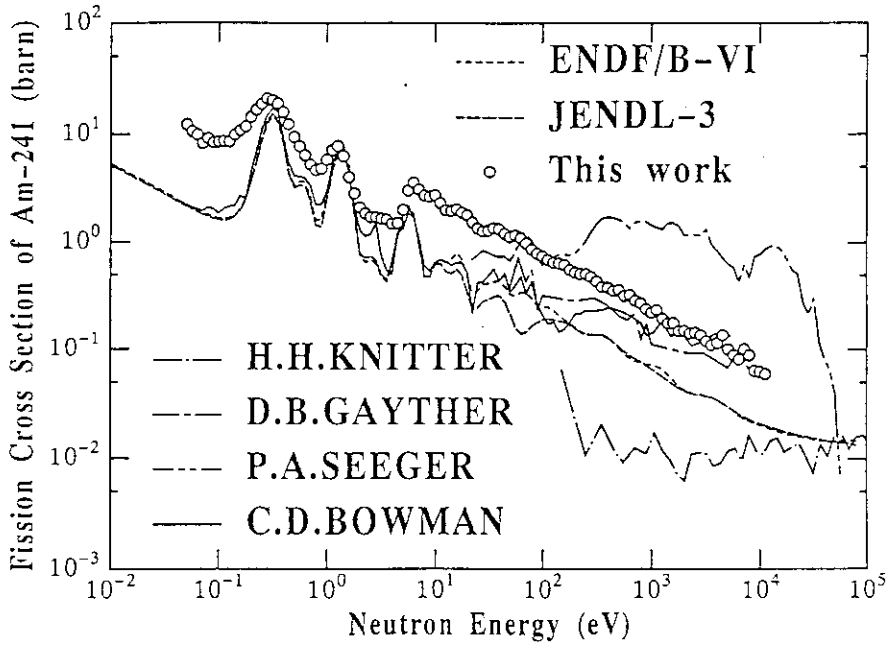

Fig. 2 Comparison of the present measurement and the evaluated data (JENDL-3: solid line, ENDF/B-VI: dotted line) which were broadened with a resolution function of 40 %.

References:

1) K.Kobayashi, et al.: JAERI-M 93-046, p.360 (1993).
2) A.Yamanaka, et al.: J. Nucl. Sci. Technol., 30[9], 863 (1993).
3) M.Obu: JAERI-M 9757 (1981).
4) K.Shibata, et al.: JAERI 1319 (1990).
5) R.F.Rose(ed.): BNL-NCS-17541 (4th ed.) (1991).
6) J.W.T.Dabbs, et al.: Nucl. Sci. Eng., 83, 22 (1983).
7) H.H.Knitter, et al.: Atomkernenergie, 33, 205 (1979).
8) P.A.Seeger, et al.: Nucl. Phys., A96, 605 (1967).

9) D.B.Gayther, et al.: 4-th All Union Conf. on Neutron Pysics, at Kiev, on 18-22 April 1977.
10) C.D.Bowman, et al.: Phys. Rev. B, 137, 326 (1965).

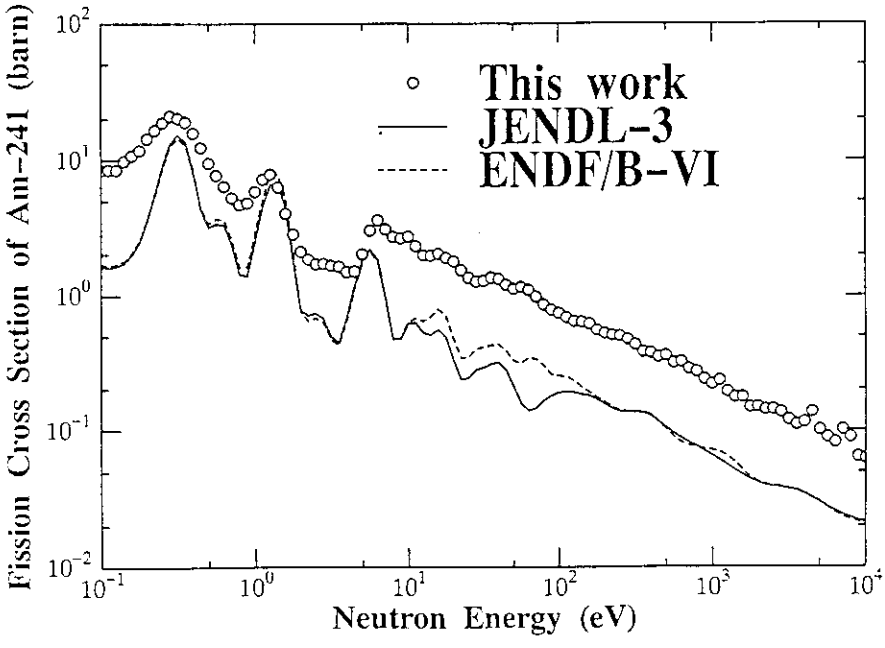

Fig. 3 Comparison of the present measurement and the existing evaluated and measured data.

5.3 Spectrometry of Several Tens MeV Neutrons Penetrating through Shields Using Organic Liquid Scintillator at 90 MeV AVF Cyclotron Facility, TIARA

Noriaki NAKAO, Takashi NAKAMURA, Masashi TAKADA
Cyclotron and Radioisotope Center, Tohoku University, Sendai, Japan

Mamoru BABA
Department of Nuclear Engineering, Tohoku University, Sendai, Japan

Shun-ichi TANAKA, Hiroshi Nakashima, Yukio SAKAMOTO, Yoshihiro NAKANE
Tokai Establishment, Japan Atomic Energy Research Institute, Tokai, Japan

Susumu TANAKA
Takasaki Establishment, Japan Atomic Energy Research Institute, Takasaki, Japan

Kazuo SHIN, Eiji TANABE
Department of Nuclear Engineering, Kyoto University, Kyoto, Japan

Abstract

We measured the neutron spectra penetrating through concrete shields which were up to 2 m thick using BC501A organic liquid scintillator with 40.5 and 64.5 MeV quasi-monoenergetic neutrons in the AVF cyclotron of the TIARA (Takasaki Ion Accelerator for Advanced Radiation Application) facility, JAERI. The source neutrons were produced from 3.6 mm and 5.2 mm thick ^{7}Li targets bombarded by 43.5 and 67.0 MeV protons, respectively, and were measured with the TOF method. For analysis of penetrating neutron spectra, we used the unfolding method with the FERDOU code[1]. In advance to the spectrum analysis, the response function of this scintillator was measured with the TOF method in TIARA, CYRIC and RIKEN, and was compared with that calculated using the Monte Carlo code, SCINFUL[2]. The comparison showed good agreement below 20 MeV, but some discrepancy above 20 MeV, owing to the inaccurate cross sections of carbon reactions and light yields of produced charged particles. The measured neutron spectra were compared with the MORSE Monte Carlo[3] calculation using the DLC-119/HILO86[4] multi-group cross section library. The comparison revealed that the calculated spectra are in good agreement with the measured spectra. From the measured results, the attenuation profile in concrete and neutron flux distribution on shield surface could be clarified for various neutron energies.

(1) Introduction

Accelerators have recently been used not only for nuclear physics and material science but also for engineering and medicine. The number of more intense and higher energy accelerators is therefore increasing, which increases the importance of shielding design study and shielding experiment of high energy neutrons. However, experimental neutron cross section and shielding data are very scarce. At present, only two neutron cross section data sets of DLC87[4] and DLC119/HILO86[5] are available beyond 20 MeV energy. These multi-group cross section libraries

are made from fusion cross section library, VITAMIN-C[6] based on ENDF/B-IV, VITAMIN-E[7] based on ENDF/B-V, respectively, in the energy range from thermal to 19.6 MeV, and in the energy range from 19.6 MeV to 400 MeV, elastic scattering cross sections are given from the calculation of optical model and nonelastic scattering ones are given from the calculation of the intranuclear cascade -evaporation model. The accuracy of these libraries has, however, not been well tested, because of very few shielding benchmark experiments.[8][9]

This study is a part of the research programme which is running as a cooperative project between Japan Atomic Energy Research Institute (JAERI) and several universities to acquire the cross section and shielding data for several tens MeV neutrons using a p-^{7}Li quasi-monoenergetic neutron field at the 90MeV AVF cyclotron facility, TIARA in JAERI. In this work, we provide the experimental benchmark data for neutrons penetrating through concrete shield.

The souce neutron spectra from the ^{7}Li target were measured with a recoiled proton counter telescope[12] and a BC501A organic liquid scintillator using the TOF method, and spectra of neutrons penetrating through shield were obtained with the BC501A using the unfolding method, which required the response functions. The response function data are usually calculated with the Monte Carlo code.[2][10][11] But there exists big disagreement in the differential light output spectrum for neutron energy higher than about 20MeV between measurement and calculation. We therefore measured the response functions of BC501A to neutrons by using the TOF method, and obtained the neutron spectra penetrating through shield by using the FERDOU[1] unfolding code and the response functions obtained in a matrix form.

(2) Measurements of response functions of organic liquid scintillator

The response functions of a 12.7-cm-diameter by 12.7-cm-long BC501A organic liquid scintillator (BICRON Co. Ltd.) coupled to a R4143 photomultiplier (Hamamatsu Photonics. Co. Ltd.) were measured in three cyclotron facilities, Cyclotron and Radioisotope Center (CYRIC) in Tohoku University, TIARA in JAERI Takasaki, and Institute of Physical and Chemical Research (RIKEN), under the following five projectile-target combinations,

(1) 35 MeV p on ^{9}Be (10mm) at CYRIC ,
(2) 50 MeV ^{3}He on ^{9}Be (10mm) at CYRIC ,
(3) 65 MeV ^{3}He on ^{9}Be (10mm) at CYRIC ,
(4) 67 MeV p on Cu (7.6mm) at TIARA ,
(5) 135 MeV p on ^{9}Be (70mm) + C (20mm) at RIKEN.

These measurements were done under the geometry that the detector was placed at about 12m away from the target which was thick enough to stop accelerated particles. White-spectral neutrons were then generated from these targets and the light output distributions of the scintillator to neutrons were

measured by using the TOF method. The neutron flight time, the pulse height and rise time of light outputs were recorded in the list mode. Figure 1 illustrates the block diagram of the measuring circuits.

The TOF spectrum was converted to the energy spectrum. Time resolutions were determined to be about 1.22-1.78 nsec from the FWHM of γ-ray-peak flushed from the target. After eliminating γ-ray pulses by two dimensional n-γ discrimination technique, we sampled neutron event data into neutron energy interval whose width was wider than that of the energy resolution determined from the time resolution. These interval widths were fixed to be 1, 2, 4, 5 MeV for energy range from 0 to 44, 44 to 70, 70 to 90, 90 to 130 MeV, respectively. We then obtained the response functions of the scintillator in the neutron energy range up to 130 MeV.

Calculations of response functions were carried out with the Monte Carlo code, SCINFUL[2]. Upper limit of the neutron energy which can be calculated in this code is 80 MeV. Since the absolute values of our measured data were not obtained, the measured values for neutron energy range up to 80 MeV were normalized to the corresponding calculated values around the upper plateau edge of the response function, where the neutron reaction in the detector is dominantly the H(n,n) reaction. This normalization can be justified, since the calculated response functions in this light range are considered to have good accuracy due to well evaluated H(n,n) cross section values. The comparisons between calculated and measured response functions are shown in Figures 2 to 5. They showed good agreement below 20 MeV, but some discrepancy above 20 MeV, because the cross sections of the carbon reactions, (n,p), (n,d), (n,pn), (n,n'3α) and so on, and light yields of produced charged particles are not so accurately estimated in the Monte Carlo code. Light attenuation correction in the scintillator should also be considered especially for a large volume scintillator.

We made the response matrix of 59 x 61 from thus obtained response functions for neutron energy range up to 80 MeV. By using this matrix, we can obtain the neutron energy spectrum from the light output distributions with the unfolding method.

(3) Measurement of neutrons penetrating through shield

We measured the neutron spectra penetrating through concrete shield using the BC501A organic liquid scintillator with 40.5 and 64.5 MeV quasi-monoenergetic neutrons in the AVF cyclotron of the TIARA. The neutron beam was injected into 120cm by 120cm concrete slab of 25 to 200cm thickness, which were fixed in contact with the 10cm diam collimator exit located at 4m from the target. The experimental arrangement at TIARA is shown in Figure 6.

Source neutron spectra

The source neutrons were produced from 3.6 mm and 5.2 mm thick ^{7}Li targets bombarded by

43.5 and 67.0 MeV protons, respectively. The absolute fluences of source neutrons in the monoenergetic peak per proton beam current were obtained from the counter telescope[12]. The counts of fluence monitors (^{238}U and ^{232}Th fission chambers) which were placed near the target were normalized to this absolute fluence values, then the source neutron fluence during each experiment was given from the fluence monitor counts.

The source neutron spectra were measured with both the BC501A using the TOF method and the recoiled proton counter telescope[12]. Figures 7 and 8 show the neutron spectra obtained by both detectors. We can find overall good agreement in the spectral shape, however, slight difference in peak fluences, around 10% lower and 15% higher values by the BC501A measurement than those by the telescope measurement in 43.5 MeV and 67.0 MeV, respectively. These disagreement probably come from the errors of the fluence monitors and the scintillator efficiency which was obtained from our measured response functions.

Measurement of neutrons penetrating through shield

The neutrons penetrating through concrete shield were measured with the BC501A which was located in contact with the shield surface on the beam axis, and also on the surface at 20cm and 40cm distance off the beam axis to investigate the surface distribution of neutrons scattered at large angle.

After elimnating γ-ray pulses, we converted the light output distributions induced by neutrons into the neutron energy spectrum using the FERDOU[1] unfolding code and the response matrix.

Calculation of transmitted spectra

The calculations of the neutron spectra transmitted through concrete shield were made with the MORSE Monte Carlo code[3] using the DLC-119/HILO86[4] multi-group cross section library. The source neutron spectra measured with the counter telescope were used in the calculations. In the calculations, source neutrons were assumed to be emitted only in a very sharp cone of 5.94×10^{-4} sr, considering the geometry of the neutron beam collimator. The point estimators were placed at the effective center of the detector for flux estimation.

Results and discussion

The neutron energy spectra measured on the beam axis are shown in Figures 9 and 10 for 43.5 MeV and 67.0 MeV p-^{7}Li experiments, respectively. The measured results for 0cm thick shield are the neutron spectra at the exit of the collimator which were obtained via the distance correction from the source neutron spectra, while 'source's in the figures are the source spectra for calculation. The comparison of penetrating neutrons in the figures revealed that the calculated spectra are in good agreement with the measured spectra especially in the 43.5 MeV p-^{7}Li experiment, excluding around

the monoenergetic peak, since the DLC119 cross sections have a group structure of 5 MeV interval above 30 MeV, while on the other hand, the measured spectra are given each 1 MeV interval in the same energy range. Figure 11 shows the peak fluence attenuation profiles in concrete shield and the attenuation lengths of concrete. The calculated and measured peak fluences obtained by summing up monoenergetic peak fluxes showed good agreement as seen in the figure.

The neutron flux distributions on the concrete surface for various shield thickness are examplified in Figures 12 and 13 for 25cm thick concrete in 43.5 MeV and 67.0 MeV p-^{7}Li experiments, respectively. A big disagreement around the neutron peak and relatively small discrepancies in lower energy region are found. The one reason for these disagreement may be due to the point-detector flux estimator in our calculations, since the detector used in the experiment had large volume. The other reason is the possibility of neutrons leaked from outside the collimator. We are now performing the flux estimation using the surface cossing estimator and the track length estimator.

(4) Conclusion

Neutrons penetrating through shields were measured for concrete shields from 25 to 200cm thickness using quasi-monoenergetic neutrons of energy 40.5 and 64.5 MeV.

The data provided a good prediction for the absolute value of neutron spectra behind the concrete shield and will be useful as the integral benchmark experimental data. The attenuation of peak fluence was also well reproduced by the calculation using MORSE Monte Carlo code and DLC119/HILO86 cross section library.

References

1) Shin K., Uwamino Y., Hyodo T., Nucl. Tecnol., 53, 78 (1981).
2) Dickens J.K., Computer in physics,Nov/Dec 62 (1989)
3) Straker G. R., Stevens P. N., Irving D. C., and Cain V. R.,ORNL-4585 (1970)
4) Alsmiller Jr. R. G. and Barish J., ORNL/TM-7818 (1981)
5) Alsmiller Jr. R. G., Barnes J. M. and Drischler J. D., ORNL/TM-9801 (1986)
6) Radiation Shielding Information Center, DLC-41 (1977)
7) Weisbin C. R., Roussin R. W. and et al. ORNL-5505 (1979)
8) Ishikawa T., Miyama Y., Nakamura T., Nucl. Sci. Eng., to be published
9) Shin K., Ishii Y., Uwamino Y., Sakai H., Numata S., Radi. Pro. Dosi. Vol.33 No.3 175 (1991)
10) Uwamino Y. et al, Nucl. Instr. and Meth. 204 179 (1982)
11) Shin K. et al, Nucl. Instr. and Meth. A308 609 (1991)
12) Baba M. et al., Private Comminucation , to be printed in this proceeding

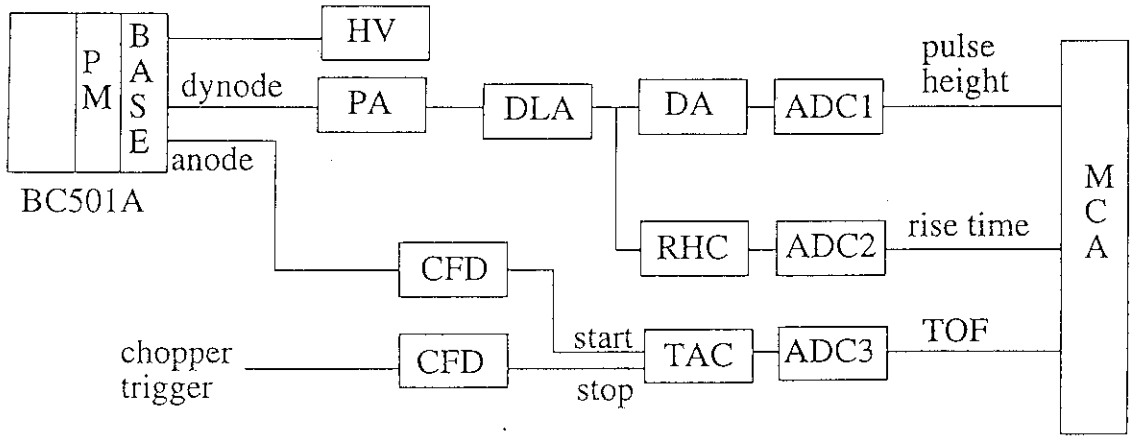

Fig. 1 Block diagram of measuring circuits

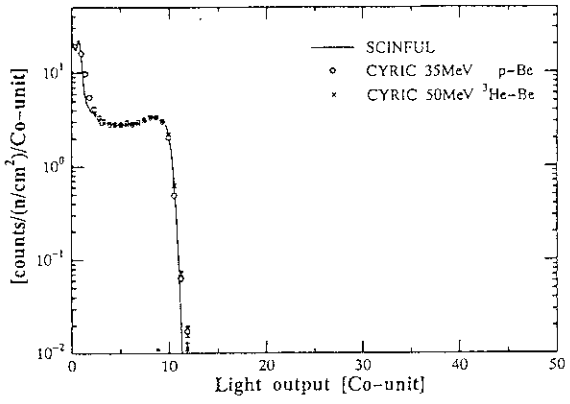

Fig. 2 Response function for 19-20 MeV neutron

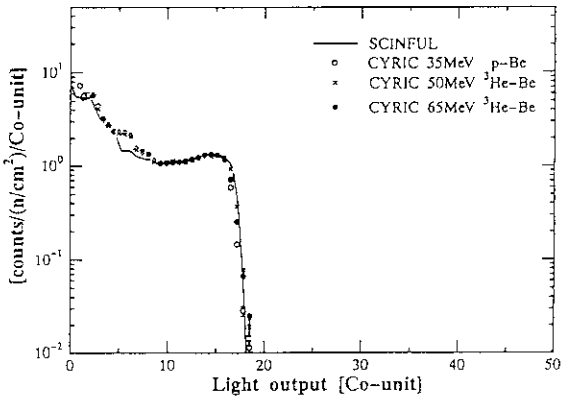

Fig. 3 Response function for 29-30 MeV neutron

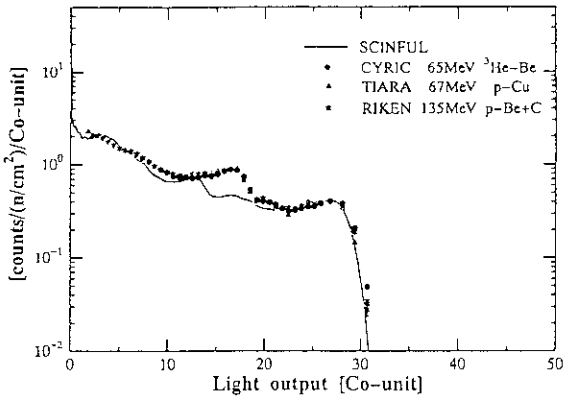

Fig. 4 Response function for 48-50 MeV neutron

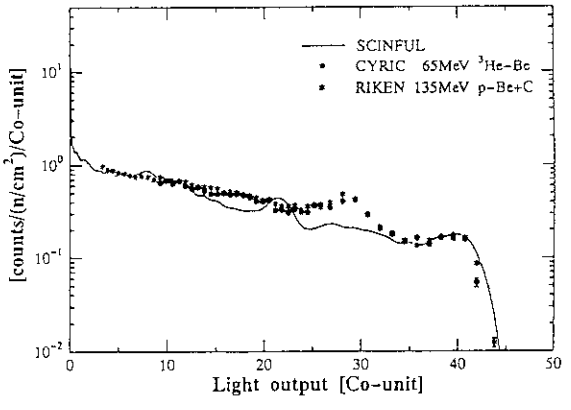

Fig. 5 Response function for 68-70 MeV neutron

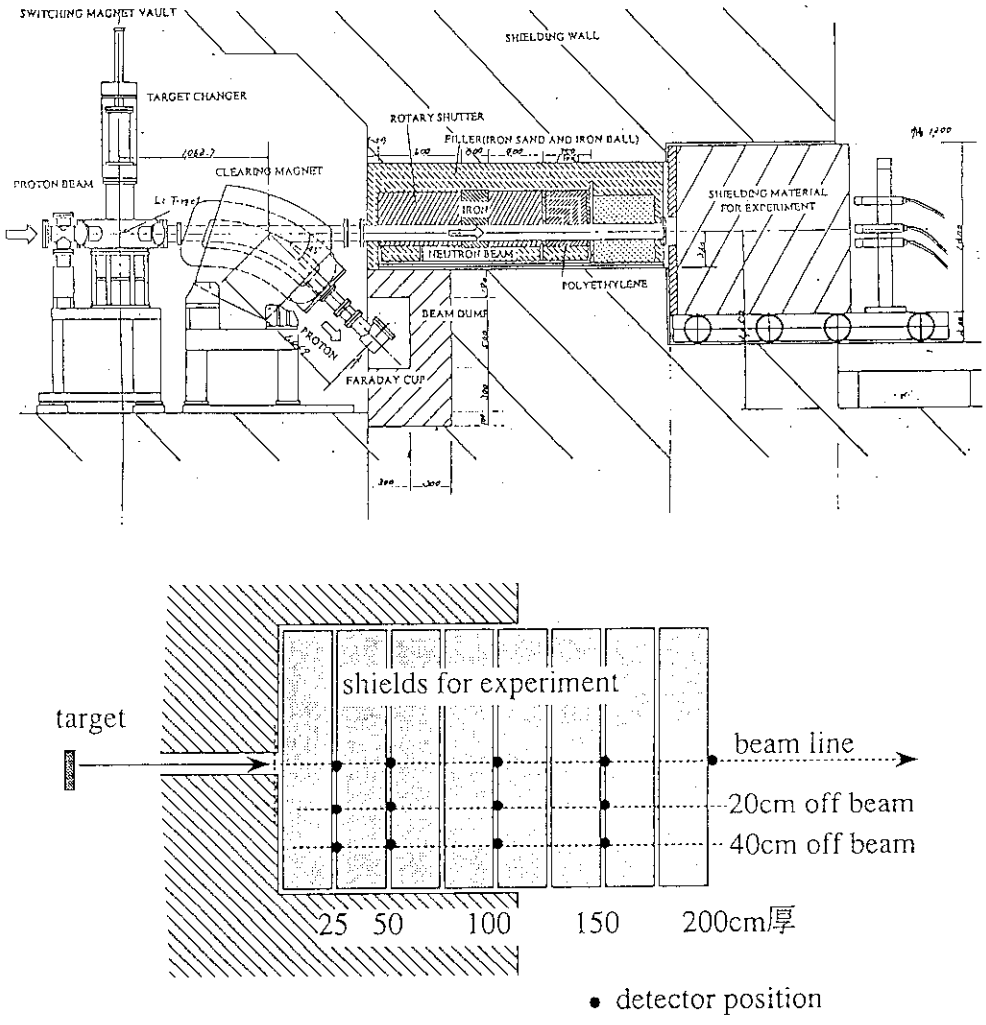

Fig. 6 Experimental arrangement at TIARA

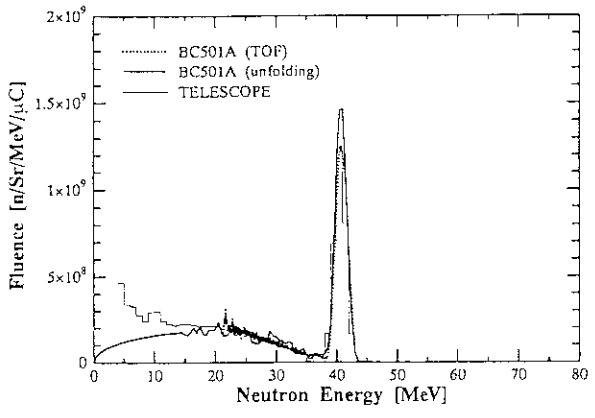

Fig. 7 Neutron spectrum of 43.5 MeV p-^{7}Li

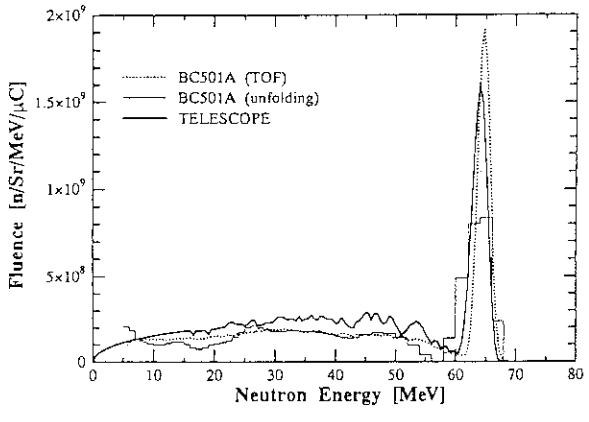

Fig. 8 Neutron spectrum of 67.0 MeV p-^{7}Li

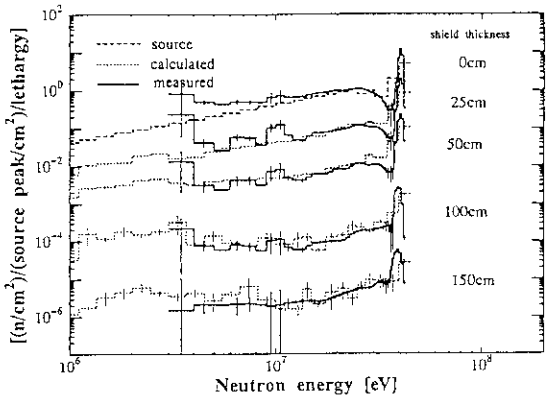

Fig. 9 Energy spectra of neutrons penetrating through concrete using 43.5 MeV p-^{7}Li

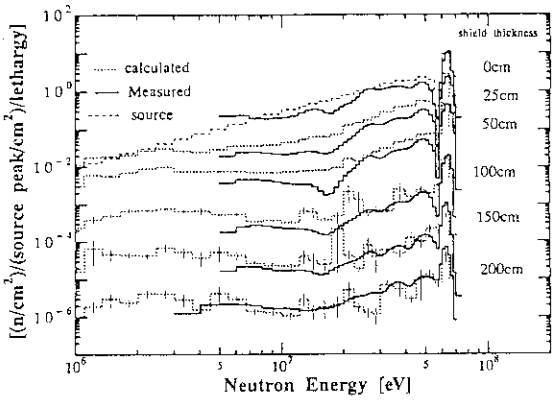

Fig. 10 Energy spectra of neutrons penetrating through concrete using 67.0 MeV p-^{7}Li

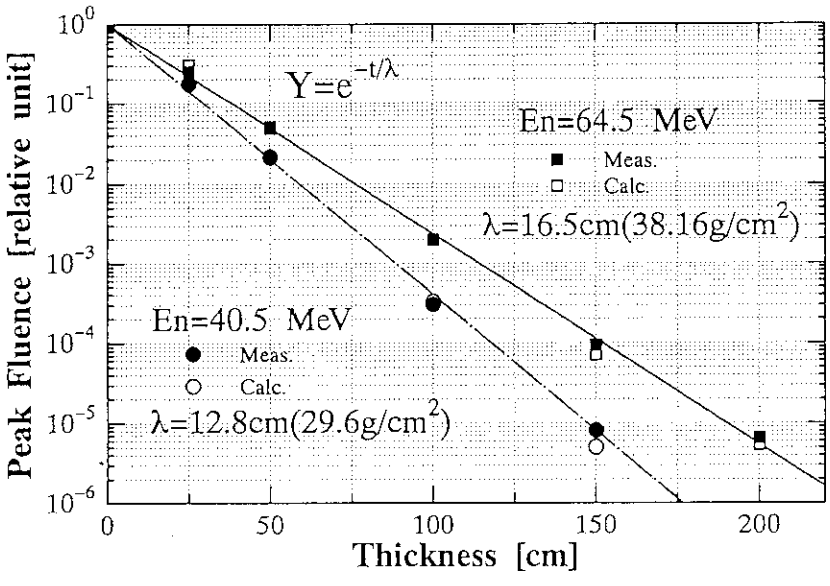

Fig. 11 Attenuation of peak fluence through concrete shield

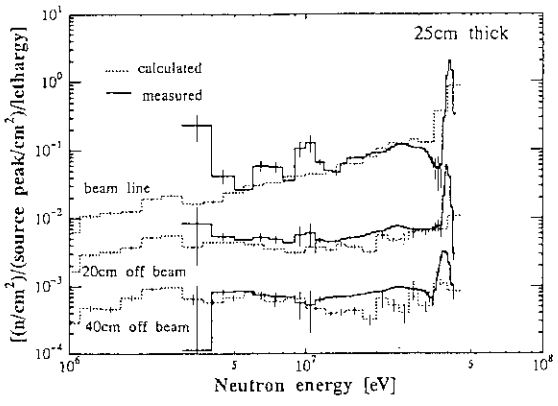

Fig. 12 Neutron flux distribution on 25 cm thick concrete surface using 43.5 MeV p-^{7}Li neutron source

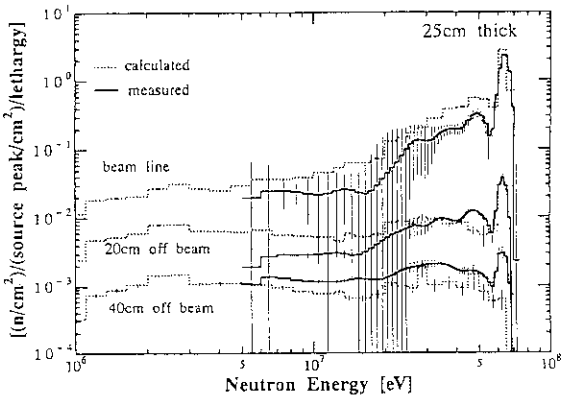

Fig. 13 Neutron flux distribution on 25 cm thick concrete surface using 67.0 MeV p-^{7}Li neutron source

5.4 Measurements of Double-differential α-Particle Production Cross Sections Using a Gridded Ionization Chamber —Application of $^{14}N(d, n)^{15}O$ and $^{15}N(d, n)^{16}O$ Neutron Sources—

Isamu MATSUYAMA Mamoru BABA Shigeo MATSUYAMA
Takehide KIYOSUMI Toshiya SANAMI and Naohiro HIRAKAWA
Department of Nuclear Engineering, Tohoku University,
Aoba, Aramaki, Aoba-ku, Sendai 980, Japan

Nobuo ITO Satoshi CHIBA Tokio FUKAHORI Motoharu MIZUMOTO
Kazuo HASEGAWA and Shin-ichiro MEIGO
Japan Atomic Energy Research Institute,
Tokai-mura, Naka-gun, Ibaraki-ken 319-11, Japan

Double-differential α-particle production cross sections of natural Ni, Fe, Cu and enriched ^{50}Cr were measured using a specially designed gridded ionization chamber for 7.6 and 11.5 MeV neutrons produced by the $^{14}N(d,n)^{15}O$ (Q=5.12 MeV) and $^{15}N(d,n)^{16}O$ (Q=9.88 MeV) reactions. The $^{14}N(d,n)^{15}O$ and $^{15}N(d,n)^{16}O$ reactions proved to be useful to obtain 7 to 13 MeV neutrons for α-production studies with a 4.5 MV Dynamitron accelerator at Tohoku University.

1. Introduction

Double-differential α-particle production cross sections are important for estimating radiation damage and nuclear heating in fusion reactor structural materials. However, the (n,xα) cross section data are scarce and there are large discrepancies among evaluations [1]. Therefore experimental data are required for wide neutron energy range.

For the study of α-particle production reaction, we have developed a gridded ionization chamber (GIC) [2,3] which has large geometrical efficiency and capability of energy-angle determination. Using the GIC, α-particle production cross sections of Ni, Fe and Cu have been measured at the neutron energy region from 4.3 to 6.5 MeV and 14.1 MeV using the D(d,n) and T(d,n) neutron sources, respectively, provided by Tohoku University 4.5 MV Dynamitron accelerator. However, mono-energetic neutrons are not available in the energy range from 7 to 13 MeV with the 4.5 MV Dynamitron accelerator.

In this work, we applied the $^{14}N(d,n)^{15}O$ [4] and $^{15}N(d,n)^{16}O$ [5] reactions as the neutron sources corresponding to these energy region. These reactions are not mono-energetic sources essentially; nevertheless, the first excited-states in ^{15}O and ^{16}O are well separated from the ground-states (6.0 MeV for ^{16}O and 5.1 MeV for ^{15}O). This is advantageous for studies of α-production reactions, since the excitation function of (n,xα)

reactions rises up around 3-5 MeV because of high coulomb barriers.

2. Neutron sources

Recently, we have tested applicability of the $^{14}N(d,n)^{15}O$ and $^{15}N(d,n)^{16}O$ reactions as 7-13 MeV neutron sources [6]. A gas target of 1 mm-wall copper tubing with a platinum beam stop was used. The gas pressure was set to about 80 kPa (600 Torr) for both ^{14}N and ^{15}N to make the deuteron energy loss to be around 500 kev. We observed that, for nitrogen gas, the entrance window of 5 μm-thick molybdenum is much stronger than 2.2 μm-thick Havar which has been used for the D(d,n) source. The present gas cell withstands beam currents up to ~4 μA. Figure 1 shows the neutron emission spectra from these reactions, which were measured by the time-of-flight method using a NE213 scintillator, 2"-diam and 2"-thick, placed in the water tank at about 6 m flight path. In both reactions, clear neutron peaks are observed at 7.6 and 11.5 MeV for deuteron energies of 3.4 and 2.5 MeV, respectively, while contaminant neutrons from the excited-states (n_1-n_5) have comparable intensities. Between n_0 and n_1, there are no appreciable background neutrons except for small bump due to the D(d,n) reaction at the platinum beam stop in the spectrum of the $^{14}N(d,n)^{15}O$ source.

3. Experiments

We measured (n,xα) reaction cross sections of Ni, Fe, Cu and ^{50}Cr for 7.6 and 11.5 MeV neutrons from the $^{14}N(d,n)^{15}O$ and $^{15}N(d,n)^{16}O$ sources, respectively. The GIC shown schematically in Fig. 2 was operated with the Kr+3%CH_4 gas mixture with the pressure optimally adjusted to the emitted α-particle energy. The details of the GIC has been described previously in Refs. [2,3]. The anode and cathode output signals, Pa and Pc respectively, are represented by the following equations [7] if charged particles emitted from the sample on the cathode stop between cathode and Frish grid;

$$Pa = E\left(1 - \sigma\frac{\bar{x}}{d}\cos\theta\right) \simeq E, \tag{1}$$

$$Pc = E\left(1 - \frac{\bar{x}}{d}\cos\theta\right), \tag{2}$$

where

E, θ = energy and angle of emitted particle, respectively,

σ = grid inefficiency of the GIC (~5.9%),

$\bar{x}$ = distance from the beginning of the ionization to the center of the gravity of the charge distribution of the trace,

d = spacing between the cathode and the Frish grid.

Therefore, we can obtain the double-differential α-particle production cross sections by processing the two-dimensional data for Pa versus Pc according to the Eqs. (1) and (2).

The experimental setup was almost same as that reported in Refs. [2,3]. The samples were natural 3 μm-thick self-supporting foils of Ni, Fe and Cu and an enriched 3 μm (2.14 mg/cm^2) -thick layer of ^{50}Cr (99.9%) evaporated on a gold backing. Neutron fluence was determined using a proton-recoil telescope whose radiator was same size as the sample foils (23 mm-diam) and positioned at the sample foils in the GIC. Two NE213 neutron monitors were employed: one was placed on the neutron beam axis and the other was at the unshielded position for flux normalization between the GIC and telescope measurements. A block diagram of the electronics for GIC is illustrated in Fig. 3. Three signals from the common cathode and two anodes of the GIC were accumulated by a 3-parameter data acquisition system. The events generated in forward- and backward-hemisphere were accumulated simultaneously.

For a few 10 hours, (n,α) measurements were carried out for each sample and the foils of Au(3 μm-thick) or W(50 μm-thick) for background measurements.

4. Data Analysis

The double-differential α-production cross sections were deduced according to the Eqs. (1) and (2). In the present experiment, backgrounds due to contaminants neutrons from the excited-states should be corrected for.

In the case of the ^{14}N(d,n)^{15}O source, neutron energies from the excited-states of ^{15}O are lower than effective threshold energies of (n,xα) reactions of structural material elements. Therefore, this neutron source can be treated as 7.6 MeV mono-energetic neutrons for α-production reaction. On the other hand, for the ^{15}N(d,n)^{16}O source, there is small perturbation caused by the neutrons of around 4.5 and 5.5 MeV, from the excited-states of ^{16}O. Then the total α-particle events C from this source are written as following:

$$C = N \cdot [\phi(E_0)\sigma_{n,\alpha}(E_0) + \sum_{i=1}^{4} \phi(E_i)\sigma_{n,\alpha}(E_i)] , \qquad (3)$$

where suffixes 0 and i denote neutrons from the ground-state and i-th exited-states, respectively. Consequently, total α-particles are the independent sum of the products of neutron fluence and cross sections for each neutron energy. The neutrons n_1 and n_2, n_3 and n_4, are treated as two mono-peaks at 4.5 and 5.5 MeV, respectively, because their energies are so close. Neutrons from states higher than the fifth level are ignored owing to lower energy. Then the second term in the Eq. (3) can be calculated by using the neutron fluence measured by the time-of-flight measurement and the (n,α) cross sections for 4.5 and 5.5 MeV neutrons measured by the D(d,n) source. Therefore, the perturbation due to background neutrons can be removed accurately by subtracting the calculated

value from the experimental values. This procedure can be applied for the angle-integrated α spectrum and also double-differential cross section. Figure 4 shows the correction for angle-integrated α spectrum of Ni(n,xα). The error associated with this subtraction is evaluated to be less than 12% from the error sources for neutron fluence determination (6%) and the (n,α) measurements for background neutrons by D(d,n) source (8%).

5. Results and Discussion

Figure 5 shows double-differential Ni(n,xα) cross section at 7.6 MeV incident neutron energy in comparison with those by ENDF/B-VI. The present results show spectra close to ENDF/B-VI, but substantially lower absolute values.

Figure 6 shows the energy-differential cross sections of Cu(n,xα) and ^{50}Cr(n,xα) in the center-of-mass system for 11.5 MeV neutrons in comparison with ENDF/B-VI and calculations by EXIFON code [8] which is based on statistical multistep model. The present results of Cu(n,xα) agree fairly well with EXIFON, but these of ^{50}Cr(n,xα) are close to ENDF/B-VI rather than EXIFON.

Lastly, the (n,xα) excitation function of Ni, Fe, Cu and ^{50}Cr are shown in Fig. 7 together with our previous results by the D(d,n) and T(d,n) sources, in comparison with other experiments [9,10,11,12,13,14,15], evaluations and calculation by EXIFON. For Ni(n,xα), the present results at 7.6 and 11.5 MeV are reasonable compared with our previous results at nearby energies measured using JAERI tandem accelerator for neutron production [16]. The excitation function by our experiments is in good agreement with those by JENDL-3 up to around 8 MeV, but smaller above 8 MeV.

6. Conclusion

At the neutron energy region from 7 to 13 MeV, we have measured double-differential α-particle production cross sections using new ^{14}N(d,n)^{15}O and ^{15}N(d,n)^{16}O sources by Tohoku University 4.5 MV Dynamitron accelerator. In this work, the measurements for Ni, Fe, Cu and ^{50}Cr(n,xα) were carried out at 7.6 and 11.5 MeV incident neutron energies, where only few data had been reported.

Acknowledgment

The authors express their thanks to Prof. H.Vonach of IRK, Vienna for his supply of ^{50}Cr sample. They wish to thank Messrs. T.Iwasaki, R.Sakamoto and M.Fujisawa for their help in the experiments using Tohoku University Dynamitron accelerator.

References

[1] C.Y.Fu, D.C.Larson, D.M.Hetrick, H.Vonach, J.Kopecky, S.Iijima, N.Yamamuro and G.Maino, Proc. Int. Conf. on Nucl. Data for Sci. and Tech.,

Jülich, Germany (1991) pp.857.

[2] M.Baba, N.Ito, S.Matsuyama and N.Hirakawa, *ibid.*, pp.477.

[3] N.Ito, M.Baba, F.Huang, S.Matsuyama and N.Hirakawa., JAERI-M, **92-027**, 257 (1992).

[4] T.Retz-Schmidt and J.L.Weil, Phys. Rev., **119**, 1079 (1960)

[5] J.L.Weil and K.W.Jones, Phys. Rev., **112**, 1775 (1958)

[6] I.Matsuyama, N.Ito, M.Baba, S.Matsuyama, M.Ito and N.Hirakawa, NETU-60, (Dept. Nucl. Eng., Tohoku Univ., 1993) pp.7.

[7] C.Budtz-Jørgensen, H.-H.Knitter, Ch.Straede, F.J.Hanbsch and R.Vogt, Nucl. Instr. and Meth., **A258**, 209 (1987).

[8] H.Kalka, Z.Phys., **A231**, 298 (1992) and private communication.

[9] A.Paulsen, H,Liskin, F.Arnotte and R.Widera, Nucl. Sci. Eng., **78**, 377 (1981).

[10] S.M.Grimes and R.C.Height, Phys. Rev. **C19**, 2127 (1979).

[11] E.Wattecamps, Proc. Int. Conf. on Nucl. Data for Sci. and Tech., Jülich, Germany (1991) pp.310.

[12] S.L.Graham, M.Ahmad, S.M.Grimes, H.Satyanarayana and S.K.Saraf, Nucl. Sci. Eng., **95**, 60 (1987).

[13] S.K.Saraf, C.E.Brient, P.M.Egun, S.M.Grimes, V.Mishra and R.S.Pedroni, *ibid.*, **107**, 365 (1991).

[14] E.Wattecamps, H.Liskin and F.Arnotte, Proc. Int. Conf. on Nucl. Data for Sci. and Tech., Antwerp, Belgium (1982) pp.156.

[15] M.Ahmad, C.E.Brient, P.M.Egun, S.M.Grimes, S.Saraf and H.Satyanarayana, Nucl. Sci. Eng., **95**, 296 (1987).

[16] N.Ito, M.Baba, S.Matsuyama, I.Matsuyama and N.Hirakawa., JAERI-M, **93-046**, 334 (1993).

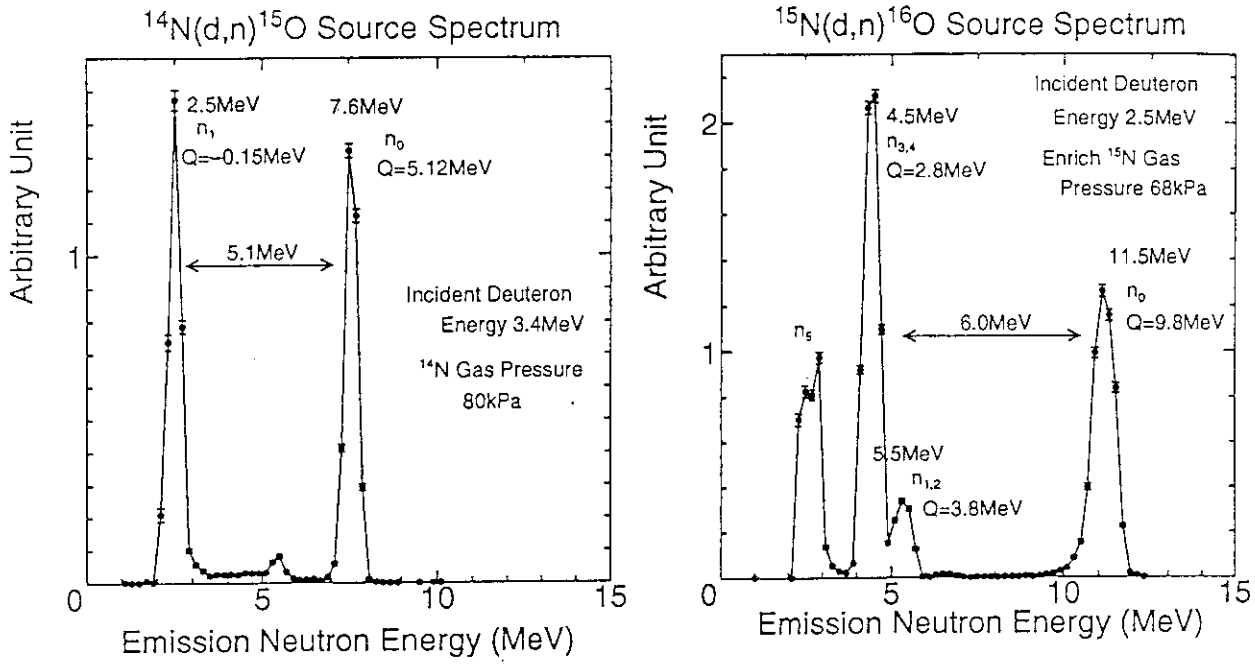

Fig. 1 Neutron emission spectra from the $^{14}N(d,n)^{15}O$ and $^{15}N(d,n)^{16}O$ reactions.

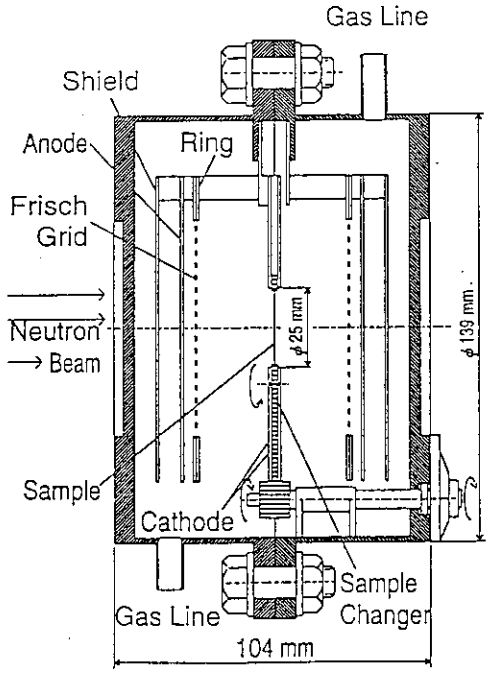

Fig. 2 Schematic view of the gridded ionization chamber (GIC).

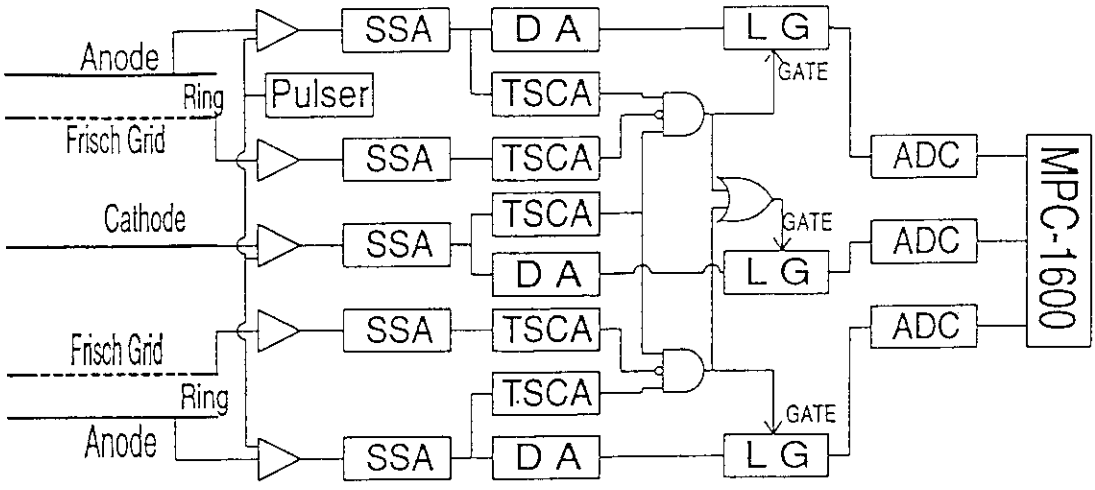

SSA : Spectroscopy Amplifire
TSCA : Timing Single Channel Analyzer
D A : Delay Amplifire
L G : Linear Gate
ADC : Analog to Degital Convertor
MPC-1600 : Multi-Parameter Controller

Fig. 3 Block diagram of the counting electronics.

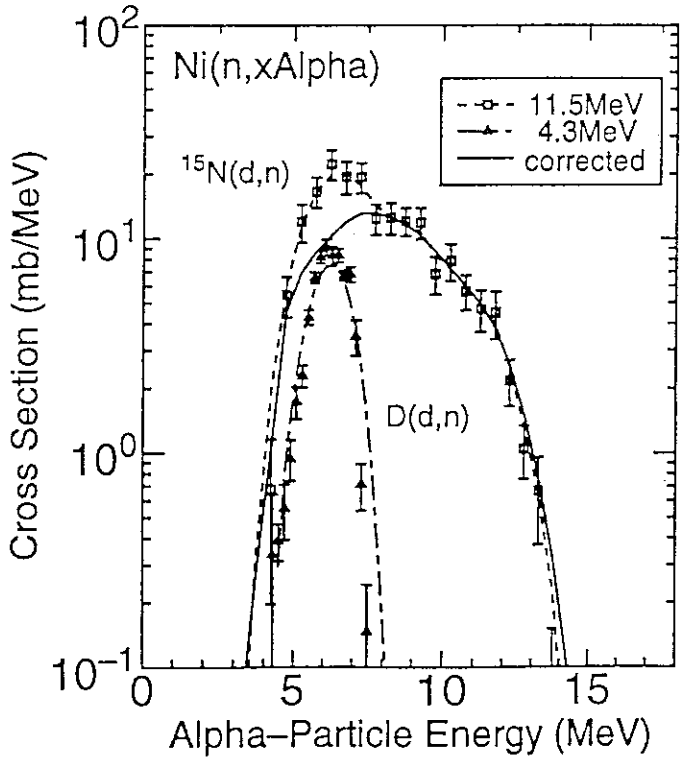

Fig. 4 Correction of angle-integrated cross section of Ni(n,xα).

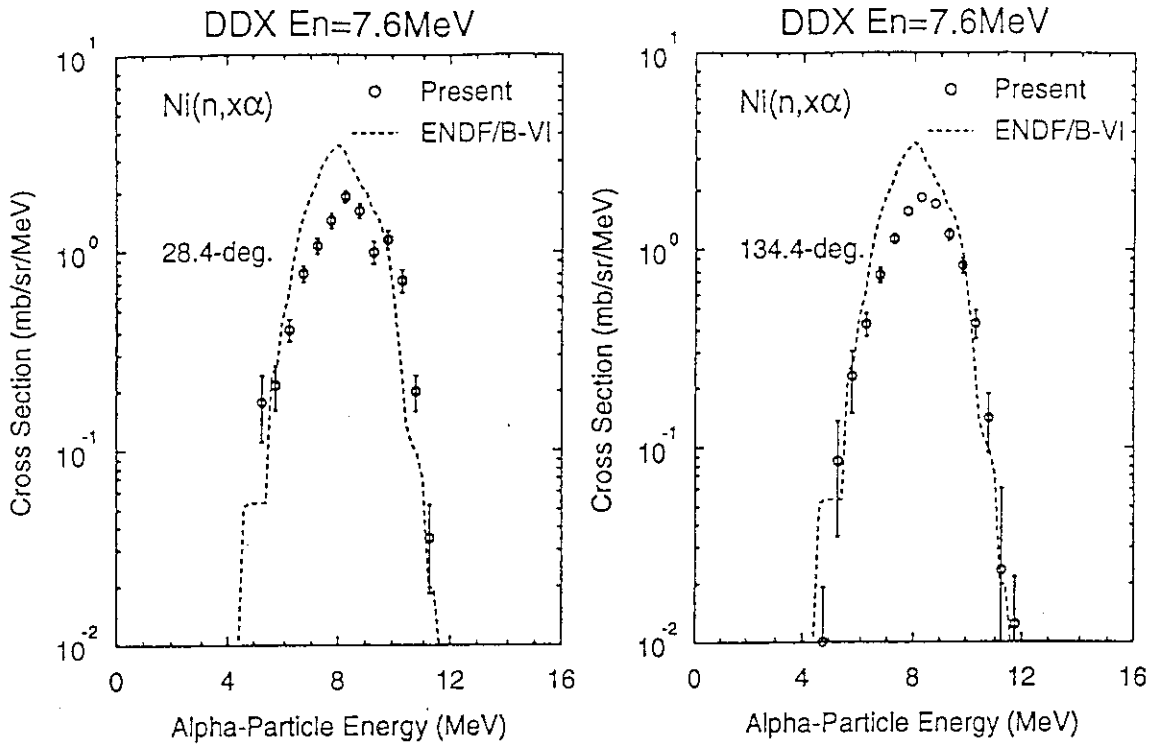

Fig. 5 The double-differential cross sections of Ni(n,xα) at 7.6 MeV incident neutron energy.

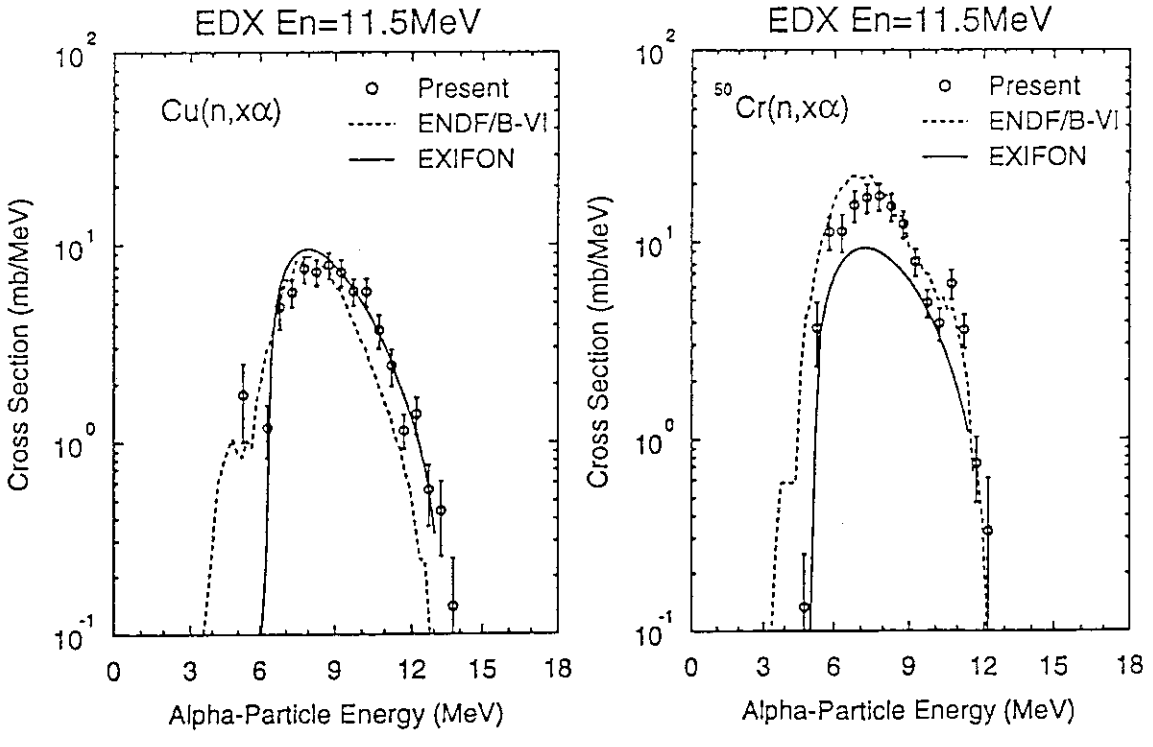

Fig. 6 The angle-integrated cross sections of Cu(n,xα) and ^{50}Cr(n,xα) at 11.5 MeV incident neutron energy compared with those by ENDF/B-VI and EXIFON.

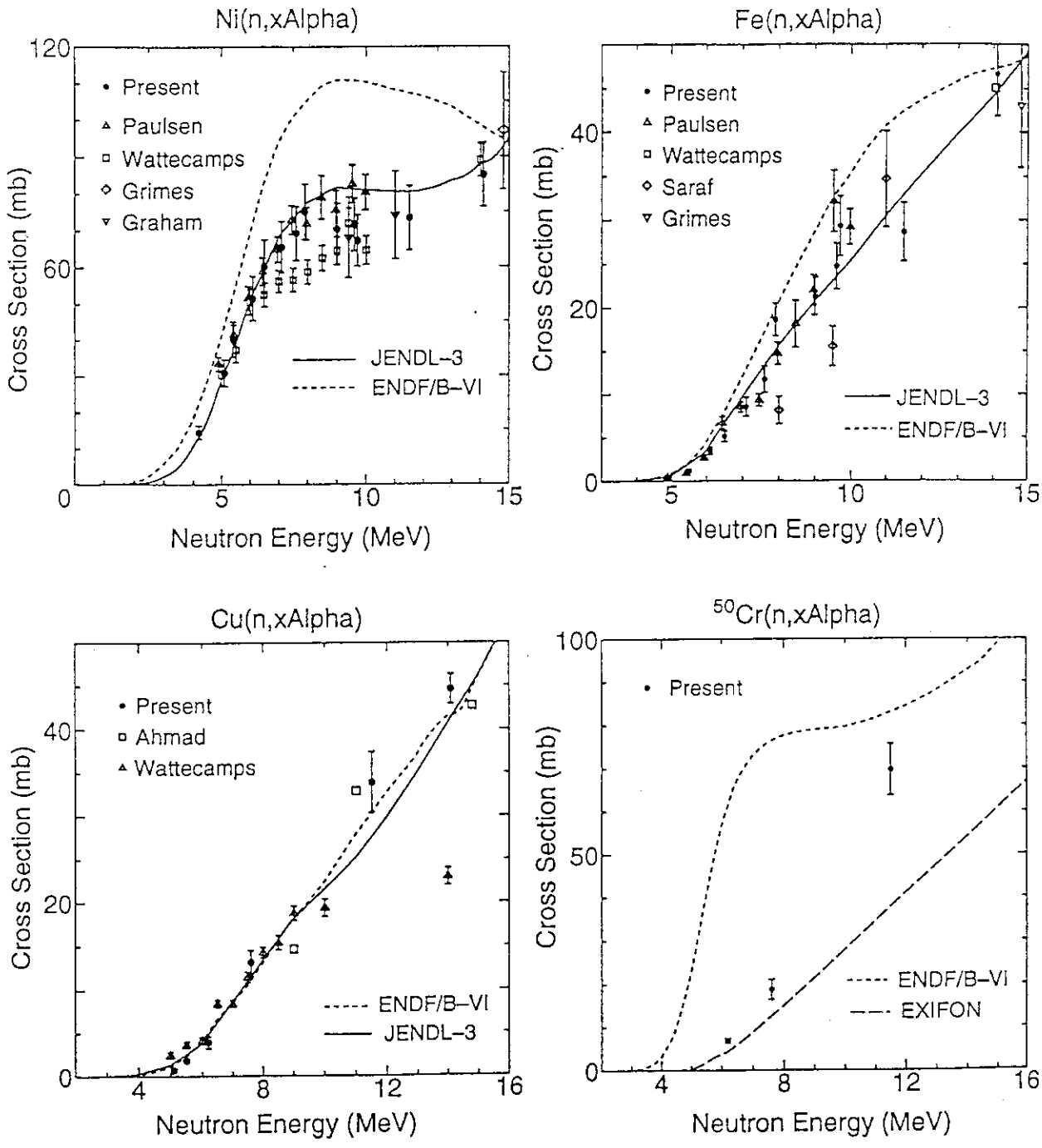

Fig. 7 The (n,xα) excitation functions of Ne, Fe, Cu and ^{50}Cr compared with those by Paulsen et al.[9], Wattecamps et al.[11,14], Graham et al.[12], Grimes et al.[10], Saraf et al.[13], Ahmad et al.[15], ENDF/B-VI, JENDL-3 and EXIFON[8].

5.5 Characterization and Application of 20–90 MeV ^{7}Li(p, n) Neutron Source at TIARA

Mamoru BABA, Takehide KIYOSUMI, Tomohiko IWASAKI,
Masahiro YOSHIOKA, Shigeo MATSUYAMA, Naohiro HIRAKAWA
Department of Nuclear Engineering, Tohoku University, Aoba-ku, Sendai 980

Takashi NAKAMURA
Cyclotron Radioisotope Center, Tohoku University, Aoba-ku, Sendai 980

Susumu TANAKA, Ryuichi TANAKA
Takasaki Establishment, Japan Atomic Energy Research Institute, Takasaki 370-12

Shun-ichi TANAKA, Hiroshi NAKASHIMA, Shin-ichiro MEIGO
Tokai Establishment, Japan Atomic Energy Research Institute, Tokai-mura 319-11

The neutron flux spectrum of the ^{7}Li(p,n) neutron source has been measured for 43 and 67 MeV protons at the mono-energetic neutron source facility of TIARA in Takasaki Establishment, Japan Atomic Energy Research Institute using a newly developed proton-recoil telescope. By use of the telescope, double-differential proton, deuteron and triton emission cross sections of carbon were measured for 64 MeV neutrons at 7 laboratory angles from 7.2° to 120°.

1. Introduction

Neutron cross section data for En>20 MeV are of increasing interest owing to growing accelerator utilization in diverse applied fields, i.e., energy, materials, medicine/biology, space and so on. However, experimental data are very scanty in the energy region partly because of lacking of appropriate neutron source.

Recently, a mono-energetic neutron source facility for 20-90 MeV range using the ^{7}Li(p,n) reaction has been established at TIARA (Takasaki Accelerator for Advanced Radiation Application) of Takasaki Establishment, Japan Atomic Energy Research Institute, aiming at shielding benchmark experiments and nuclear data measurements required for accelerator shielding designs[1]. This energy range is of great interest since reaction mechanism is greatly changing and nucleon cascade model is not applicable straightforwardly. In the facility, neutron shielding experiments and neutron cross section measurements are going on.

To provide the data on absolute flux and spectrum of the neutron source which are indispensable for the analyses of experimental data, we have developed a proton-recoil telescope (PRT) and applied to the 43 and 67 MeV protons. The PRT consists of a polyethylene proton radiator and a ΔE-E telescope proton detector, and its detection efficiency can be calculated precisely relying only on the well known n-p scattering cross section and the geometry. This technique would provide most reliable flux measurement since the detection efficiency of

conventional proton-recoil scintillators is rather uncertain because of the errors in cross sections and the light output data for charged-particles emitted from neutron-carbon interaction in it.

Using the ΔE-E charged-particle detector, we measured the double-differential charged-particle emission cross sections of carbon for Ep=67 MeV source (En=64 MeV) which are important in various applied area.

2. Experimental

2.1 Experimental arrangement

Figure 1 shows the lay-out of the mono-energetic source facility at TIARA and PRT setup. The proton beams transported from a K-110 AVF cyclotron fit a metal target of ^{7}Li(99.9% ^{7}Li) mounted on a water-cooled and remotely-controlled target holder. Transmitted protons are bent by a clearing magnet into a shielded Faraday cup. Neutrons to 0° direction are guided to the experimental room through a ~3 m thick collimator wall consisting of iron and concrete. This arrangement provides a clean source of neutrons in the experimental area. In some cases, particles attributed to neutralized protons were observed in the neutron beam; these were eliminated by use of a few mm thick brass plate in the exit of the collimator. The ^{7}Li target of 2 MeV thick is employed usually as a compromise between intensity and energy spread.

The neutron source intensity is monitored relatively by use of two fission chamber of ^{238}U and ^{232}Th located in the vicinity of the target, and of integrated beam charge in the faraday cup. These showed agreement within a few % usually, and used for normalization between runs.

2.2 Proton-recoil Telescope

The schematic view of the PRT[2] is shown in Fig.2. Protons emitted from the radiator by n-p scattering are detected by the ΔE-E counter telescope in a well defined geometry. The ΔE detector is used for particle identification. Further, background protons from carbon within polyethylene can be eliminated by a measurement for carbon. Consequently, the detection efficiency of the PRT can be calculated accurately from the well known differential n-p scattering cross section and the geometrical parameters.

The ΔE-detector is a large area (900 mm^2) transmission-type Si detector with a depletion layer of 150 or 300 μm. The E-detector is a NaI(Tl) crystal (5-cm diam by 3-cm thick) coupled to a 2"-diam photomultiplier (Hamamatsu R1826): NaI(Tl) was chosen owing to its better linearity in light response versus energy deposition, and to better energy resolution than other scintillators.[3] The signals from the ΔE and E detectors are gated by the coincidence signal between the detectors, and then accumulated by MPC-1600 multi-parameter data acquisition system (Laboratory Equipment Inc.) event by event.

The present PRT was designed so as to achieve a high signal-to-background ratio (S/N) and good energy resolution with minimal loss of detection efficiency. a) The telescope is shielded from the neutron beam by a shadow bar (50-cm long brass) to avoid backgrounds from the detector themselves. Further, the polyethylene radiator is placed in the air without using a chamber which may be a background source, and supported by thin nylon strings. b) To obtain

energy resolution comparable with the source spread, we reduced the angular spread of recoil-protons entering the telescope by separating the telescope from the radiator by around 40 cm. The reduction of the detection efficiency due to this arrangement was compensated by use of a large area proton radiator detectors. As a proton radiator, polyethylene plates, 1 mm thick were employed mainly. They were shaped to be rectangular, 8 cm x 9 cm, and the central area of 6-cm diam was cut out to avoid the uncertainty in the radiator area exposed to the neuron beam.

Programs were developed for calculation of the PRT response and efficiency. They were employed also for parametric survey of optimal geometry. The calculated efficiency was validated by comparing experimental results relative to another PRT calibrated by the associated-particle technique[4] for 14 MeV neurons.

Another geometry shown in Fig.3 (inclined geometry) was also tested. The above annular geometry proved to be much superior than the inclined geometry owing to smaller angular spread of recoil protons and to smaller volume of the neutron beam viewed by the detector. Consequently, the annular geometry was mainly adopted in the source characterization.

For the source characterization, measurements were done for polyethylene, carbon and sample-out. A carbon plate was 0.5 mm thick whose energy loss is close to the 1-mm thick polyethylene plate. The average beam intensity was 1 to 3 μA in the present experiments. In this condition, neutron spectrum could be measured within a few hours counting time owing to high efficiency of the PRT.

2.3 Telescope for C(n,z) experiment

The ΔE and E telescope described above was applied to the measurement of charged-particles emission spectra from carbon. The measurements were performed at seven laboratory angles from 7° to 120°; the annular geometry was adopted in the forward angles, and the inclined geometry at backward angles. The distance between the sample and telescope was reduced to compensate lower counting rate. The annular geometry enabled measurements at extremely forward angles like 7° which was impractical in the inclined geometry. In this geometry, the emission angle was varied by changing the distance between the sample and the telescope. A 0.5-mm thick carbon plate was employed for the measurements.

In these measurements, the signals of ΔE and E detectors were gated by the TOF signal to select events induced by the peak neutrons.

3. Data Reduction

The examples of two dimensional spectrum for ΔE versus E signals are shown in Fig.4 for the cases of polyethylene and carbon samples: The events by protons, deuterons and tritons are clearly separated according to energy loss. By selecting the particles of interest, we obtained the energy spectrum for each particle.

The resulting proton spectrum for the ^{7}Li(p,n) source at Ep=67 MeV is shown in Fig.5. In the spectrum, continuum neutrons attributed to the breakup reaction are observed as well as peak component of concern. The S/N is sufficiently good even in the continuum region, and the

protons from carbon have only very small contributions. The energy scale of the proton spectrum was determined from the peak neutron energy and the linear response of the NaI(Tl) scintillator versus energy; the neutron energy was determined by a time-of-flight measurement using a NE213 scintillator. The background subtracted spectra were corrected for the energy loss in the sample, air, ΔE detector and window materials using averaged values for possible proton paths. Then, the neutron spectrum was deduced using detection efficiency of the PRT calculated adopting recent differential n-p scattering cross section data. Employing the present PRT, we could deduce the absolute neutron flux spectrum down to ~15 MeV. The low energy limit was imposed mainly by energy loss.

In the case of C(n,z) reactions, the data by the annular geometry were corrected further for the change of solid-angle versus the emission angle.

4. Result and Discussion

4.1 Neutron Source Characterization

Figure 6(a) and 6(b) show the neutron fluence spectra of the ^{7}Li(p,n) reaction for 67 MeV and 43 MeV protons, respectively, measured around 5.5 m from the target. The target thickness was ~2 MeV, i.e., 5.2 mm for 67 MeV and 3.6 mm for 43 MeV. The spectra consist of peak due to the (p,n) reaction to the ground state and the first excited state (Ex=0.43 MeV) of ^{7}Be, and of a continuum part attributed to the breakup of residual ^{7}Be*.

The fluence of the peak neutrons is 1.6×10^{4} (n/cm^{2}/μC) at 5.81 m from the target for 67 MeV, and 9.9×10^{3} at 5.48 m for 43 MeV: These are in agreement with those expected from the cross section values reported by other authors[5),6)]. Further, peak responses agreed with the simulation calculations. Therefore, the neutron source proved to realize expected property both in intensity and spectrum.

The continuum part is also important in the analyses of shielding experiments. To estimate the energy spectra lower than the cutoff energy, the experimental spectra were parametrized with a simple model assuming the ^{7}Li(p,n^{3}He)α reaction for the continuum neutrons. The lines in the figures show the three-body phase-space distributions. For both neutron energies, this simple model reproduces fairly well the energy distribution. For lower proton energy, however, neutron spectra look softer than expected while only limited data are available. Further studies are needed to clarify the spectrum of the continuum neutrons.

4.2 C(n,z) Data

Figure 7(a),(b),and (c) illustrate the double-differential cross sections for proton, deuteron and triton emission reactions of carbon for 64 MeV neutrons. The spectra for each particles exhibit characteristic energy and angular distributions. The structures observed in high energy end and their strong angular dependencies indicates preferential excitation of discrete levels through direct processes like knock-on and/or pick-up reactions. The lower energy parts, on the other hand, show continuum like spectra and much milder angular dependencies which will be partly interpreted by the kinematic effect due to light mass of carbon. Similar spectrum and angular

dependence are observed in the data by UC Davis group[7),8)]. Such rapid change in shape and magnitude will have influence on the calculation of the response function of scintillators and KERMA factors. Then, more data will be required as well as model development.

The present spectrometer dose not permit α-particle measurement, and is limited in counting efficiency. Therefore, the spectrometer should be extended to heavier particles and to higher efficiency.

5. Summary

1)A counter telescope detector suitable for neutron flux measurement for En>20 MeV was developed and applied to the characterization of JAERI Takasaki mono-energetic neuron source using the ^{7}Li(p,n) reaction. The experiments using the telescope provided the source spectrum data including continuum part useful for the analyses of experimental data. The spectrum of continuum neutrons from the ^{7}Li(p,n) reaction is reproduced satisfactorily by a simple phase-space model while comparison for other proton energies should be done further.

2)The telescope was applied successfully to the measurement of double-differential proton, deuteron and triton emission cross sections. The spectrum showed characteristic shape of each particle and very strong angular dependence.

ACKNOWLEDGEMENT

The present work was undertaken as part of special project research between universities and JAERI. The authors wish to thank operating crew of JAERI Takasaki cyclotron for their collaboration.

References:

1)Tanaka, S., et al.; Proc. 2-nd Int. Symp. "Advanced Nuclear Energy Research -Evolution by Accelerators-" (JAERI 1992) p.342

2)Yoshioka, M., et al.; NETU-60 (Dep. Nucl. Eng., Tohoku University 1993) p.31

3)Romero, J.L., et al.: Nucl. Instr. Methods, **A301** 241(1991)

4)Iwasaki, T., et al.; Proc. Int. Conf."Nuclear Data for Sci. and Technol." (1988 Mito) p.87

5)Schery, S.D., et al.: Nucl. Instr. Methods, **147** 399(1977)

6)Taddeuchi, T.N., et al.: Nucl. Phys., **A469** 125(1987)

7)Subramanian, T.S., et al.: Phys. Rev., **C28(2)** 521(1983)

8)Brady, F.P., et al.: Phys. Rev., **C43(5)** 2284(1991)

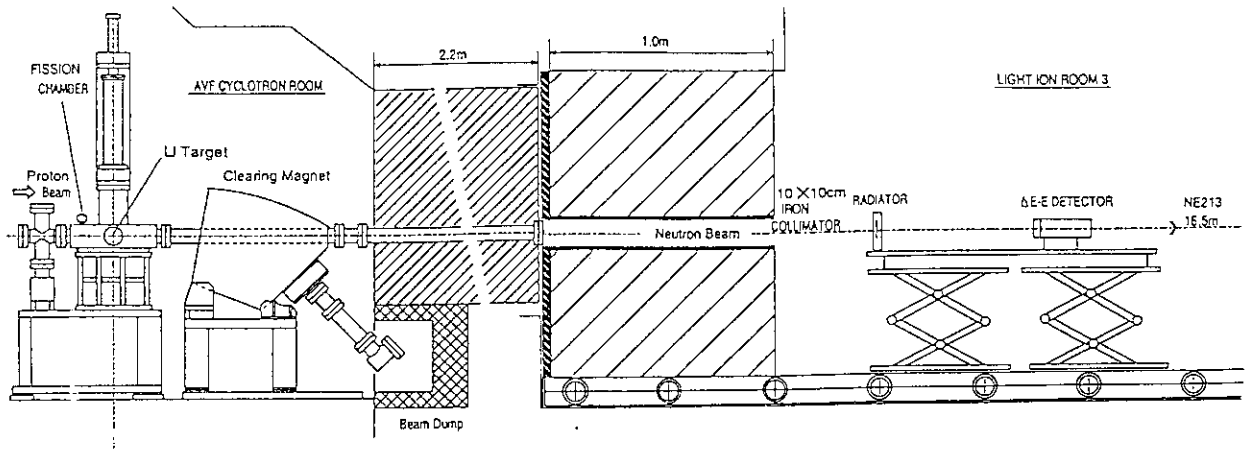

Fig. 1 Layout of TIARA mono-energetic neutron source facility and setup of proton-recoil telescope.

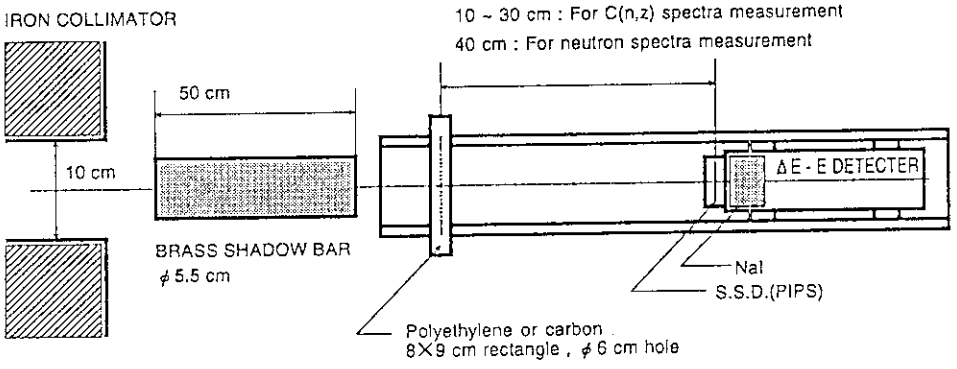

Fig. 2 Geometry of the proton-recoil telescope.

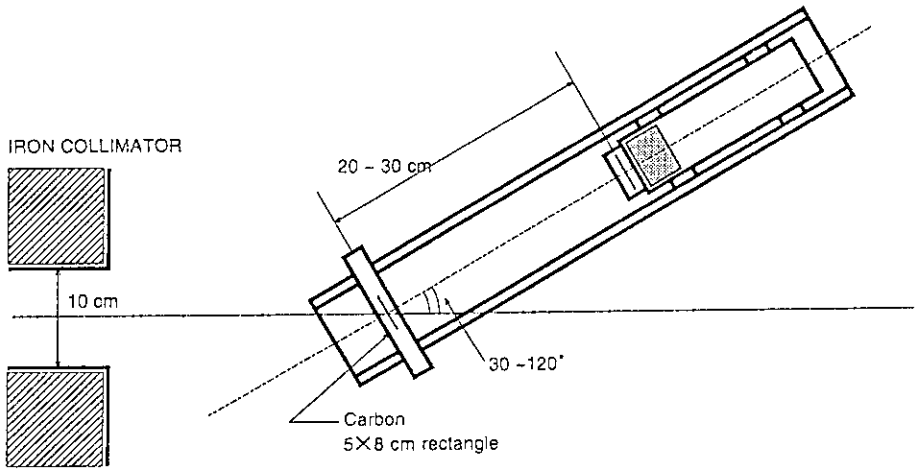

Fig. 3 Geometry of the telescope for C(n,z) measurements.

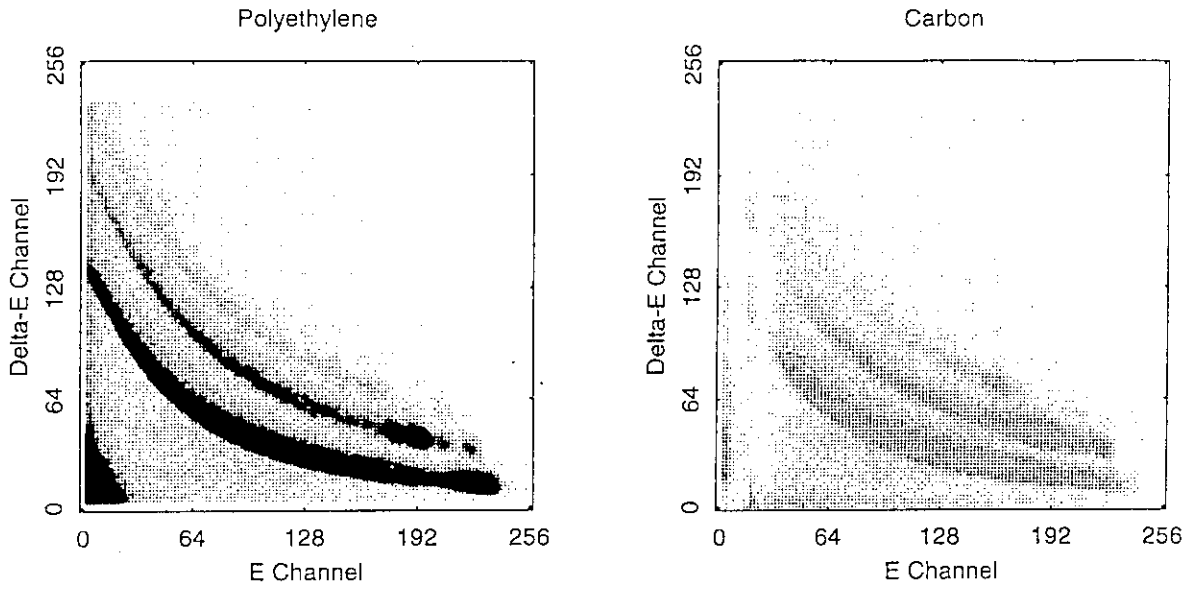

Fig. 4 Two dimensional spectra of ΔE versus E for polyethylene sample (left) and for carbon sample (right).

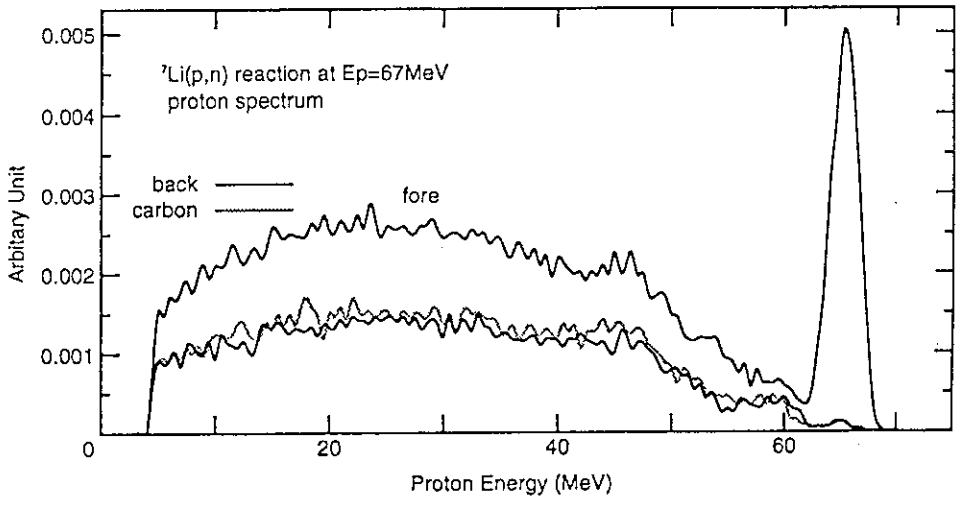

Fig. 5 Proton spectra of PRT for polyethylene (fore), background and for carbon.

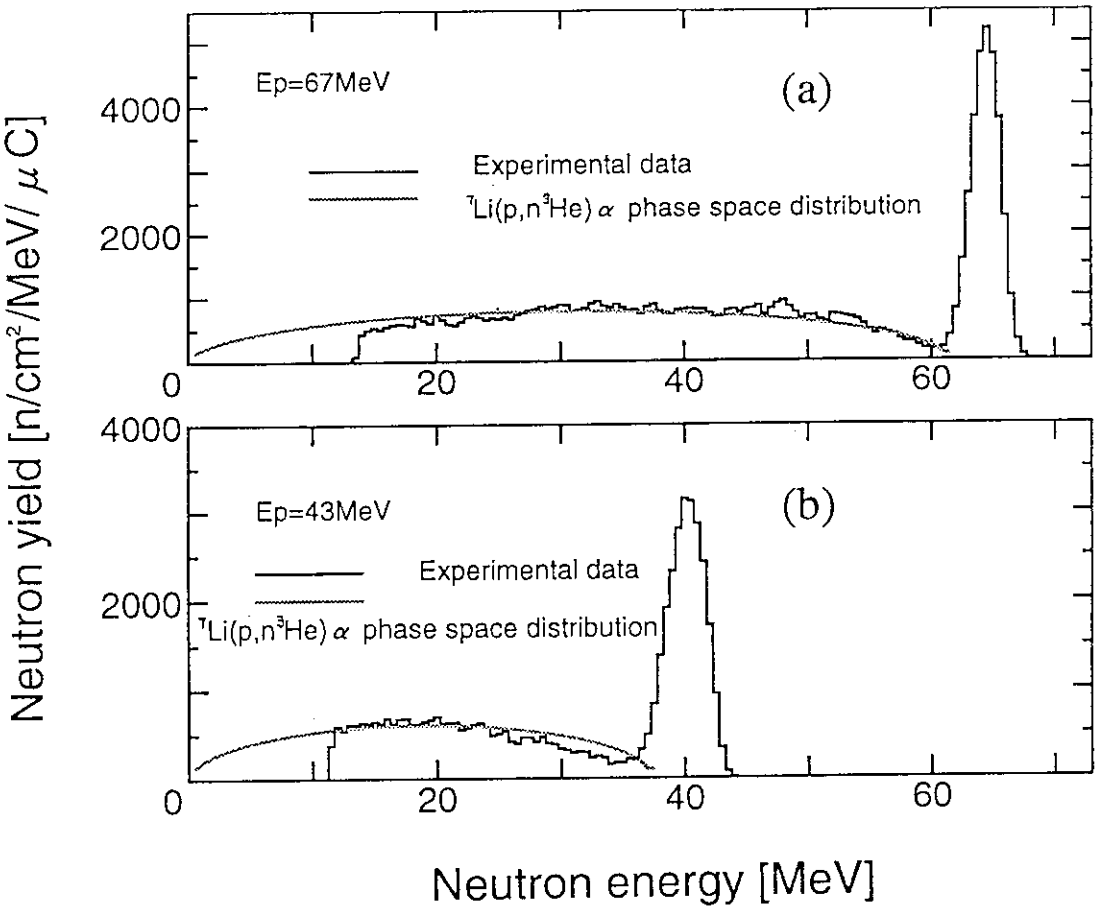

Fig. 6 Neutron spectra of the $^{7}Li(p,n)$ source reaction for 67 MeV (a) and 43 MeV (b) protons; the lines show phase-space distributions described in the text.

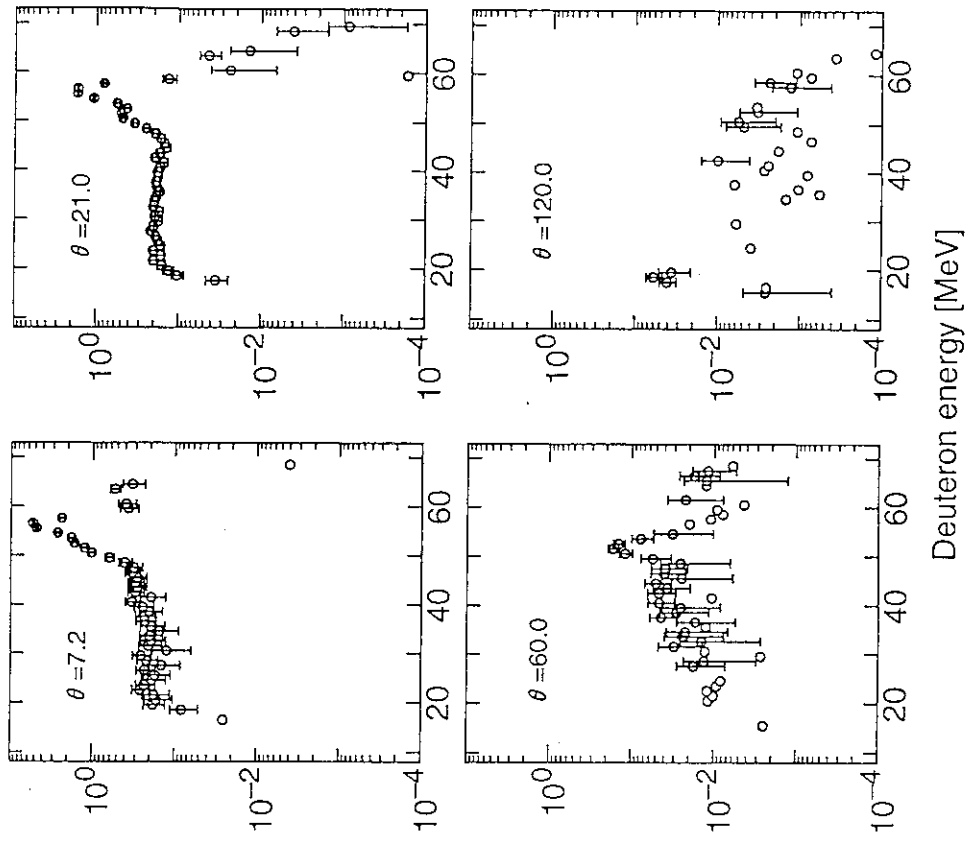

Fig. 7(a) Energy spectra of protons emitted from carbon by 64 MeV neutrons.

Fig. 7(b) Energy spectra of deuterons emitted from carbon by 64 MeV neutrons.

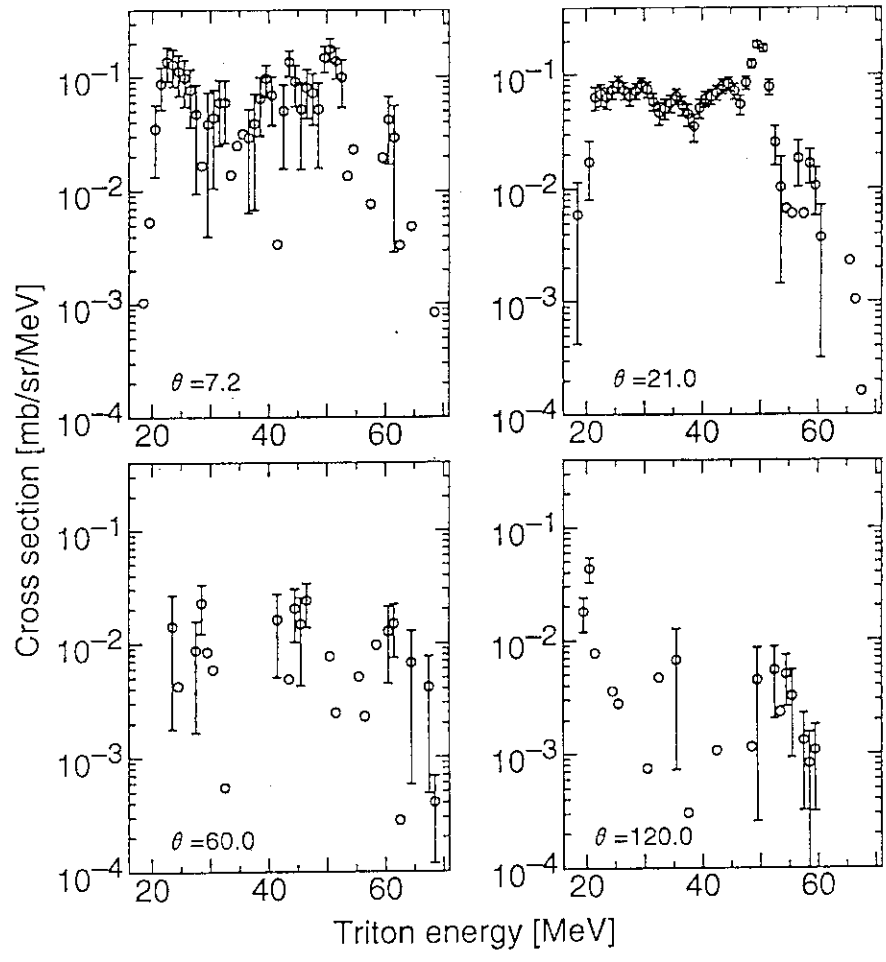

Fig. 7(c) Energy spectra of tritons emitted from carbon by 64 MeV neutrons.

5.6 Application of Large Volume Liquid Scintillator for Scattering Cross Section Measurements

Shigeo MATSUYAMA, Takeshi OHKUBO, Mamoru BABA, Shin IWASAKI,
Daisuke SODA and Naohiro HIRAKAWA

Department of Nuclear Engineering, Tohoku University,
Aramaki-Aza-Aoba, Aoba-ku, Sendai 980, Japan

We have developed a large volume NE213 liquid scintillator (LLS)/1/ and applied for scattering cross section measurements using time-of-flight (TOF) method. The scintillator cell of the LLS is a long rectangular glass tube, 80 cm long, 10 cm width and 6.5 cm thick, and is viewed by two fast photomultipliers from both end of the cell. Position information can be obtained from the time differences between two photomultipliers with resolution better than 7 cm. Time compensated signals needed for TOF experiments are provided by a mean timer. Data are acquired for main TOF, position TOF and pulse height signals, which are gated by n-γ discriminator signals, by a 3-parameter data acquisition system to get uniform bias levels independently of the event position. A data acquisition and processing method is developed for effective use of the LLS. The detector efficiency is three times larger and the timing properties is better than that of the 14 cm $\phi \times$ 10 cm thick NE213 detector used in our scattering cross section measurements.

The performance of the LLS as a position sensitive detector was examined by measuring the secondary neutron TOF spectra at 14.1 MeV. The LLS was also applied successfully to scattering cross section measurements as a single large TOF detector for 11.5 MeV neutrons by low intensity $^{15}N(d,n)^{16}O$ neutron source.

1. Introduction

Double-differential neutron emission cross sections (DDXs) for various incident neutron energies are needed for neutronics design and for estimation of radiation damage and nuclear heating in fusion and fission reactors and high-energy accelerator. Many experimental data for fusion structural materials have been accumulated for 14.1 MeV neutrons. However the data for the region between 7 and 11 MeV and higher than 20 MeV are still lacking because of the lack of mono-energetic neutron source and facility. To apply to the those energy region, we have developed a large volume NE213 liquid scintillator (LLS).

2. Detector system

2.1 Detector Design

The schematic view of the LLS is shown in Fig. 1. The scintillator cell is a long rectangular glass tube, 80 cm long, 10 cm wide and 6.5 cm thick in inner dimensions. The LLS is designed to

detect neutrons coming in perpendicular to its longer axis. The cell is made with 5 mm thick Pyrex glass and has a long reservoir cell (about 1 *l*) on the side of the cell. The surface of the cell is not coated with reflector to give best time resolution, while it introduces large light attenuation /1/. Two fast photomultipliers, HAMAMATSU R-1250, are attached on both ends of the cell by spring from the frame. The cell, photomultipliers and pre-amplifiers are encased in an aluminum box whose inside is painted in black to absorb the light from the cell. The size of the box is 198 × 198 × 1800 mm. The box has two thin entrance windows, 800 long × 100 mm wide and 0.5 mm thick, in front and back side of the cell.

The light output has a position dependence, since the light is attenuated in the scintillator. Figure 2 shows the light attenuation curve as a function of the distance between neutron incident position and the photomultiplier observed by the proton edges of 14.1 MeV neutrons. The pulse height variation is more than 70 %. This large light attenuation causes a position dependence of detection efficiency if detection threshold level is set independently of the event position.

The difference of light arrival time to both end of the photomultipliers can be used for determination of neutron incident position. To get time compensated signals for time-of-flight measurements, a mean timer is used.

2.2 Data acquisition

Figure 3 shows the block diagram of the circuit. Each anode signal from two photomultiplier is fed into a constant-fraction timing discriminator and converted into a fast logic signal. The fast logic signals are distributed to three circuits for energy TOF (E-TOF), position TOF (P-TOF) and for n-γ discrimination. P-TOF is derived from the time difference between two photomultiplier. Time compensated signals are derived using a mean timer, LeCloy model 624. The time differences between the time compensated signals from the mean timer and delayed beam pick-off signals are measured by a time-to-amplitude converter to give E-TOF. In order to distinguish neutron- and γ–events, the pulse shape discrimination technique is used. The performance of n-γ pulse shape discrimination is limited by light absorption in the scintillator. Two separate n-γ discriminators are employed for each photomultipliers and the n-γ discrimination signals are taken from the discriminator closer to the event position which is selected by a P-TOF signal. It proves to be effective to get a clear n-γ discrimination. Figure 4 shows n-γ pulse shape spectra derived from each photomultiplier as a function of neutron incident positions. The narrow peaks correspond to neutron events. It shows that n-γ discrimination of far end of the photomultiplier is worse than that of near end.

Three set of data for E-TOF, P-TOF and pulse height signals, which are gated by n-γ discrimination signals are acquired event by event on a magnetic optical disk by a 3-parameter data acquisition system.

2.3 Data reduction

The three parameter data were analyzed event by event to derive information on neutron energy and incident position after correction for bias, efficiency and backgrounds. The neutron energy was derived from flight time and flight path length for each position. The time difference at incident position were already corrected by mean timer, thus no correction was made.

We set position dependent bias levels by software to get position independent efficiency using the data of light attenuation. Figure 5 shows the bias curve as a function of event position for the proton edges for 14.1 MeV neutrons. By using this technique, we could get position independent detection efficiency. The measured relative detection efficiency as a function of detector positions are shown in Fig.6 for 14.1 MeV neutrons. It indicates that the position dependance can be eliminated almost completely by the technique and there is no position dependance.

Position resolution of the LLS was measured by using neutron beams collimated to around 4 cm by polyethylene collimators of 40 cm long. Figure 7 shows the position resolution and position linearity for 14.1 MeV neutrons. The measured resolution was around 7 cm FWHM, which correspond to 5 ～ 6 cm inherent detector resolution if the neutron beam width is taken into account.

3. Application to the double-differential neutron emission cross section measurements

The performance of the LLS as a position sensitive detector was examined by measuring the secondary neutron TOF spectra from polyethylene, natural carbon and tungsten samples at 14.1 MeV incident neutron energy. Measurements were carried out using Tohoku University 4.5 MV Dynamitron time-of-flight spectrometer. The experimental setup is shown in Fig.8. The scattering sample was suspended parallel to the beam axis at 90 degree. The flight path length was around 4 m, which was the shortest distance available in the Dynamitron TOF spectrometer. In this arrangement, the scattering angle range covered by the LLS was around 8 degree and the scattering cross section data for 7 angles could be obtained. Bias level was set to 2 MeV proton.

Figure 9 shows E-TOF vs. P-TOF matrix for polyethylene sample. The decrease in neutron energy of elastic peak from the H(n,n)H reaction with the increase of scattering angle are observed clearly between elastic and the first-level state inelastic peaks of carbon. The neutron emission spectra of tungsten and carbon are shown in Fig. 10 and 11, respectively, as a function of the scattering angles. Figure 12 shows the double-differential neutron emission cross section of carbon at a emission angle of 30 degree in comparison with our previous data measured using the 14 cm-diam and 10 cm thick NE213 detector at a flight path length of 6 m. The energy resolution of the present data are almost same with our previous data even at shorter flight path length owing to smaller thickness of the LLS.

The LLS was also applied for DDX measurements as a large single detector. The efficiency of the LLS is three times as large as that of the 14 cm-diam and 10 cm thick detector used previously for the study of scattering cross section. Therefore, the LLS will be applicable to measurements even for

the cases of low intensity neutron source and small cross sections. We applied the LLS to the scattering cross section measurements using 11.5 MeV neutrons via the $^{15}N(d,n)^{16}O$ reaction. The $^{15}N(d,n)^{16}O$ neutron source is a promising source for production of ～11 MeV neutrons with our 4.5 MV Dynamitron accelerator owing to its large positive Q value (Q = 9.885 MeV). The neutrons from the $^{15}N(d,n)^{16}O$ reaction are not mono-energetic because of the contaminant neutrons from the several excited states of ^{16}O. Nevertheless, the first excited state is separated by 6.06 MeV from the ground state, which allows us to study neutron scattering from low lying levels. Figure 13 shows the spectrum of the $^{15}N(d,n)^{16}O$ neutron source. There were no appreciable background neutrons between 11.5 and 5.5 MeV. Therefore secondary neutrons down to around 5 MeV could be measured without interference by the background neutrons. The intensity of this reaction, however, is only about one tenth of that of the D(d,n) reaction. Therefore the LLS provides a useful means for scattering cross section measurements for this neutron source.

The experimental setup was almost same as that of previous studies /2/ except for the neutron detector. Bias level was 3 MeV. The neutron target was an enriched $^{15}N_2$ gas (99.9 %) filled in a gas cell, 3 cm long and 1 cm-diam, at a pressure of around 400 mmHg. To withstand higher beam current, a 5 μm molybdenum foil is used for the entrance window. The scattering samples were metallic cylinders of elemental silicon and bismuth. Those were suspended with its vertical axis at a distance of 12 cm from the center of the gas cell. The flight path length was 6 m. Figure 14 shows the TOF spectrum for bismuth at 45 degree comparing with sample-out background. Signal to noise ratio is sufficiently good for scattering cross section measurements. Figure 15 and 16 show the typical results of silicon and bismuth in comparison of the data derived from JENDL-3 and ENDF/B-VI. In the case of silicon, both nuclear data reproduce the experimental data well. However, there exist large discrepancies for bismuth. Then the combination of the LLS and the $^{15}N(d,n)$ neutron source will be a powerful method for scattering cross section measurements around 11 MeV.

4. Summary

We have developed a large volume liquid scintillator (LLS) and applied for scattering cross section measurements as a position sensitive detector and as a single large detector. The high efficiency of the LLS enabled us to measure scattering cross sections by using a low-intensity neutron source. Presently, we tested the LLS as a position sensitive detector for 14.1 MeV neutrons in the Dynamitron TOF spectrometer. To make an efficient use of the LLS, the flight path length has to be shorten. Therefore, we are now planning to make another spectrometer which enable the measurements for large angle range at once and we are also considering to apply 'double TOF method' to reject the effect of contaminant neutrons.

References:
1. S.Iwasaki et al. : NETU-49 (Dep. Nucl. Eng. Tohoku University, 1987), p.8
2. S.Matsuyama et al. : JAERI-M 93-046 (1993), p.345

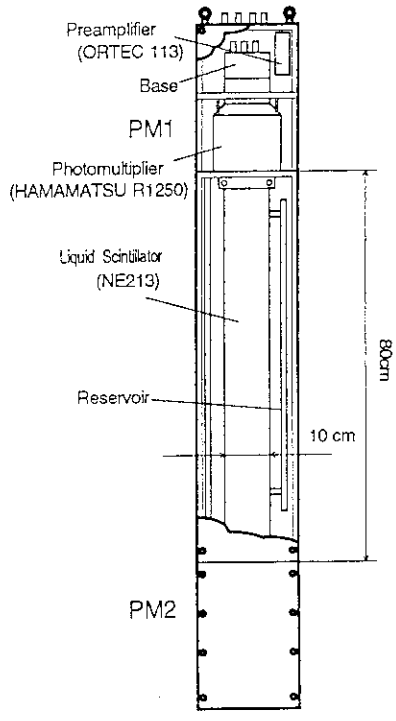

Fig. 1 Schematic view of LLS.

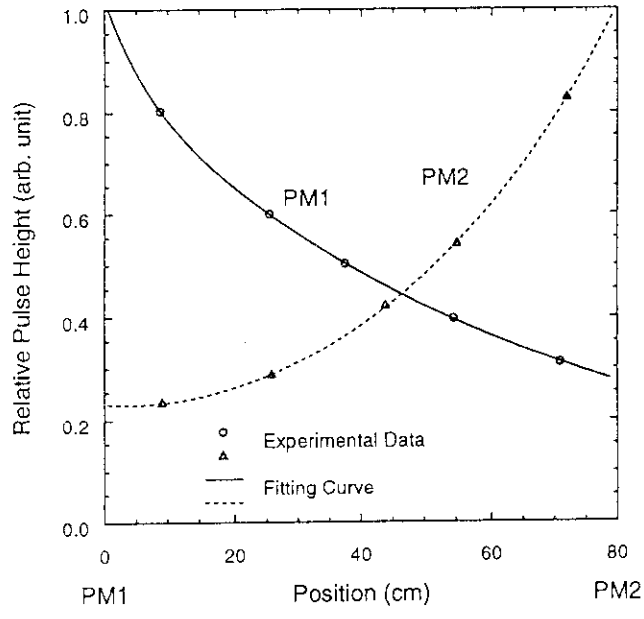

Fig. 2 Light attenuation curve.

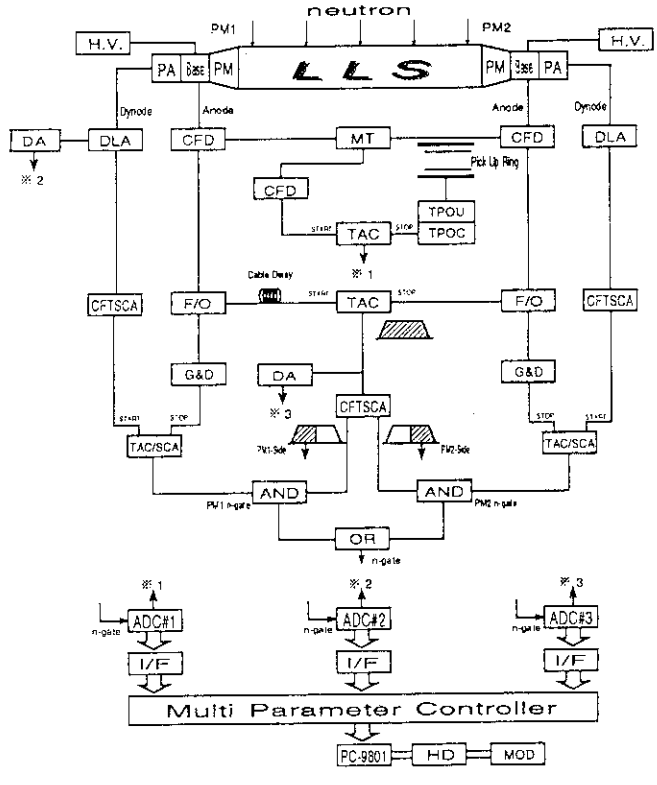

Fig. 3 Block diagram of the electron circuit.

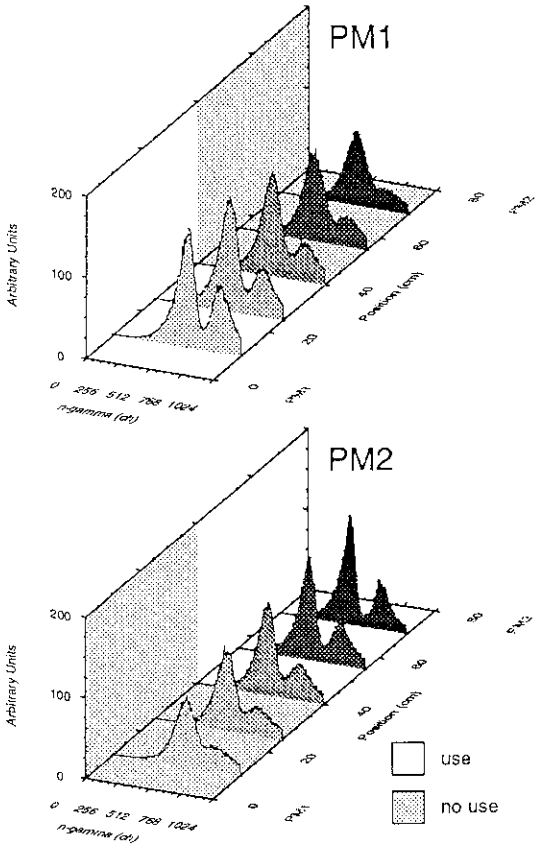

Fig. 4 Performance of n-γ discrimination.

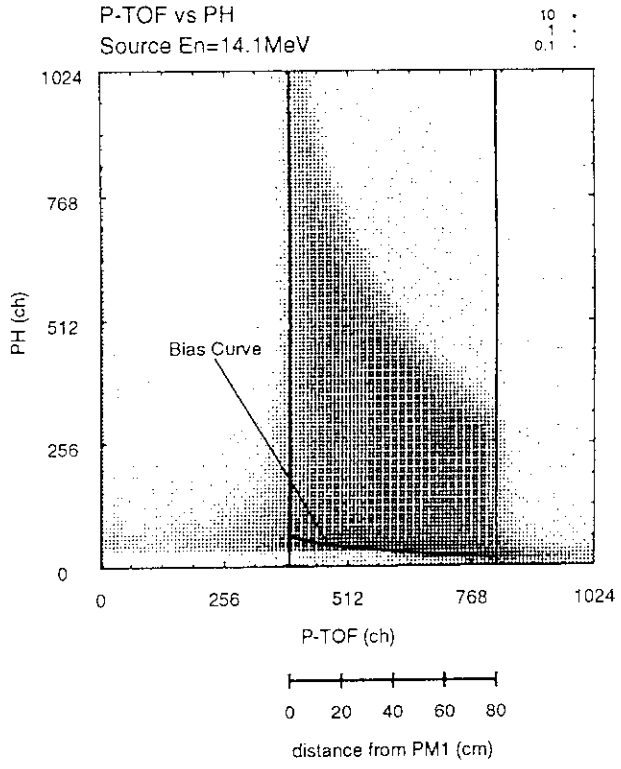

Fig. 5 Position dependent bias curve.

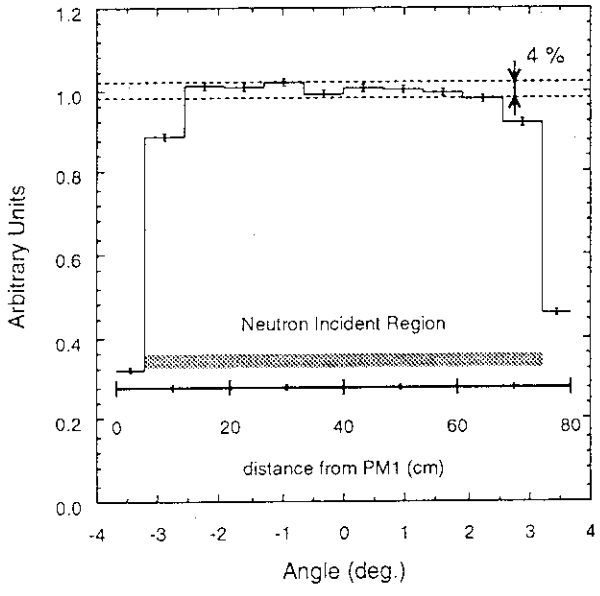

Fig. 6 Relative detection efficiency for 14.1 MeV neutrons.

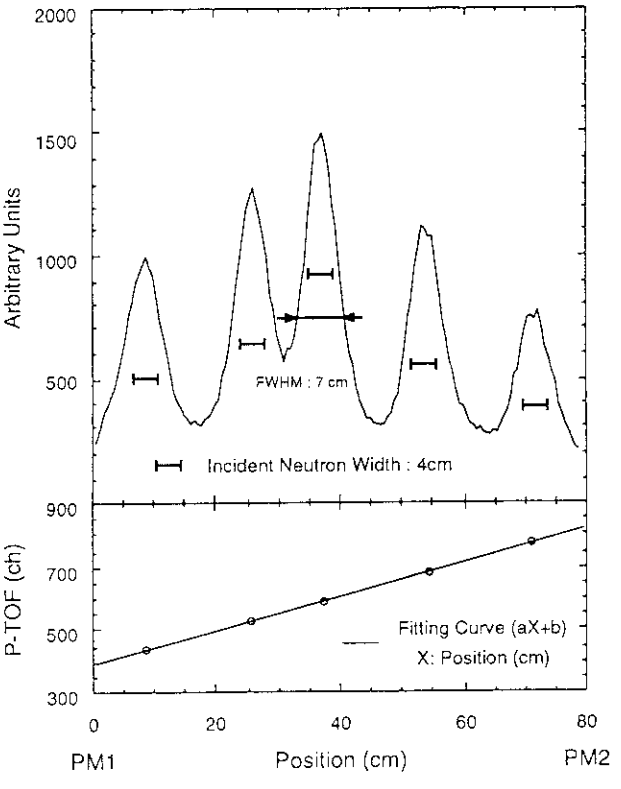

Fig. 7 Position resolution and linearity.

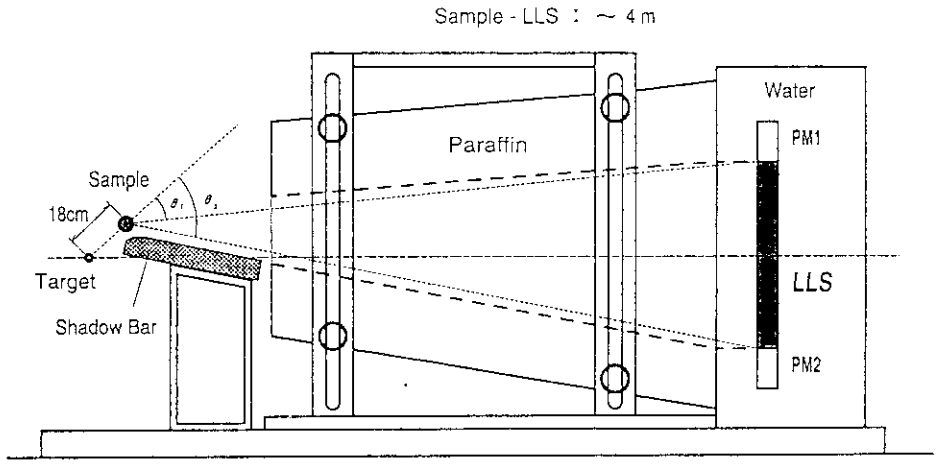

Fig. 8 Experimental scattering geometry.

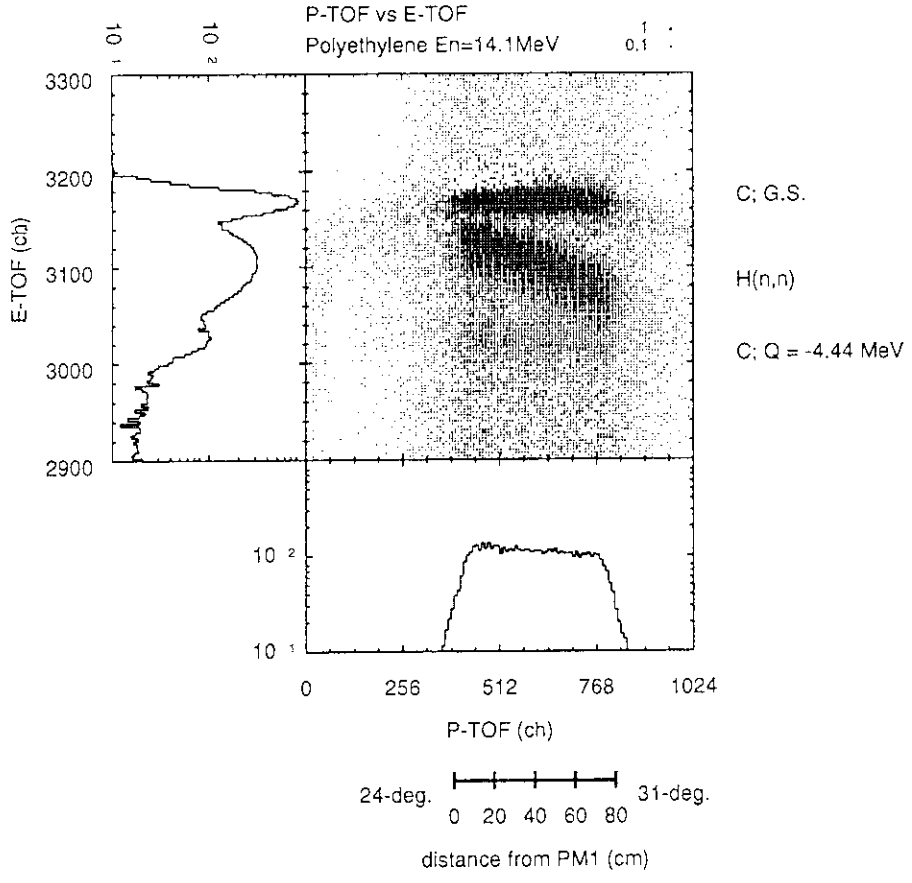

Fig. 9 Position vs. energy TOF matrix for polyethylene.

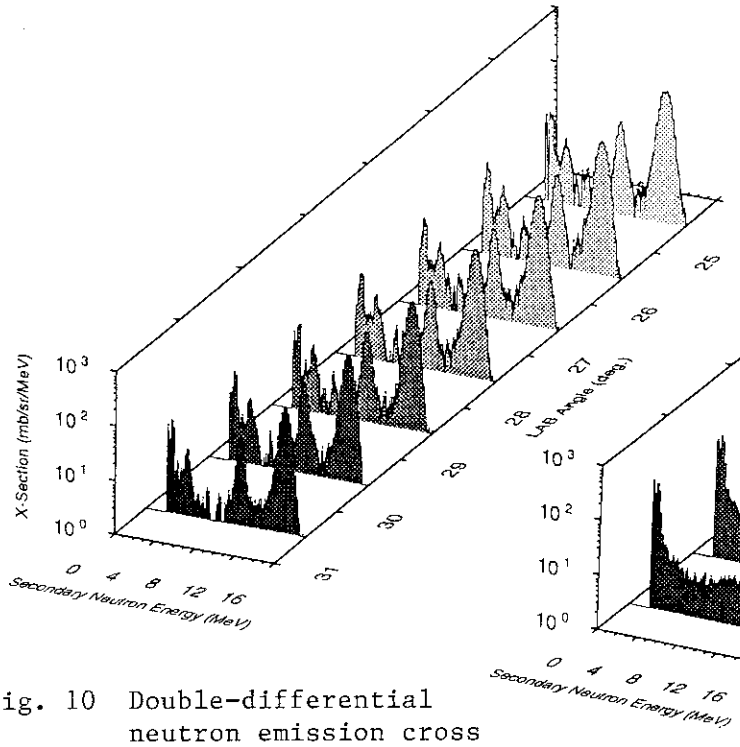

Fig. 10 Double-differential neutron emission cross sections of carbon for 14 MeV neutrons.

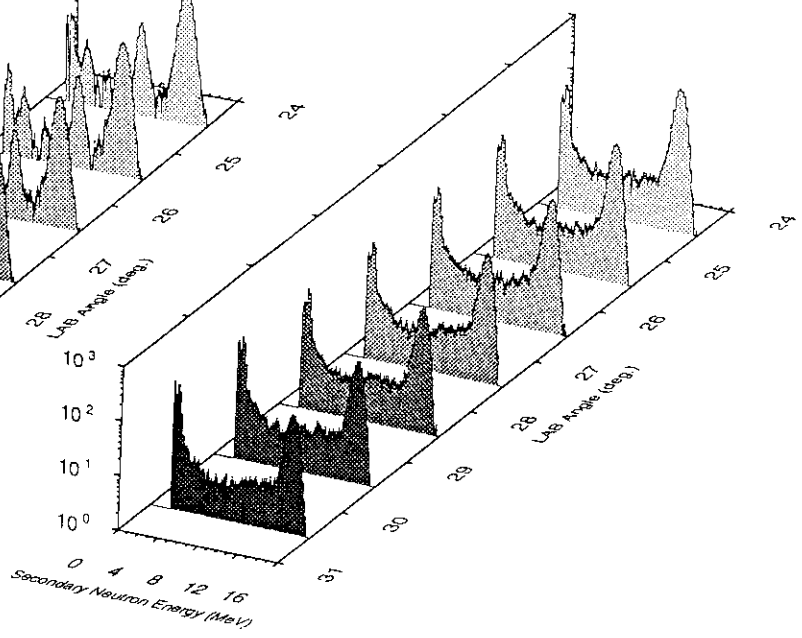

Fig. 11 Double-differential neutron emission cross sections of tungsten for 14 MeV neutrons.

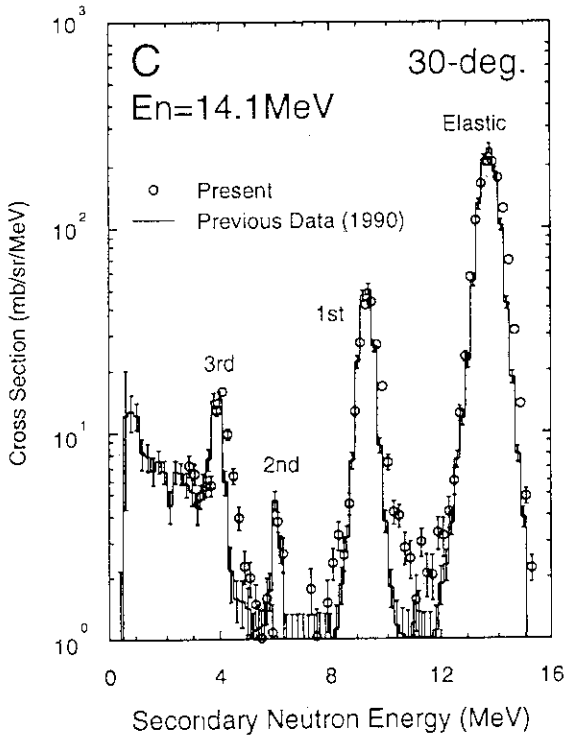

Fig. 12 Double-differential neutron emission cross section of carbon at 30 degree compared with our previous data.

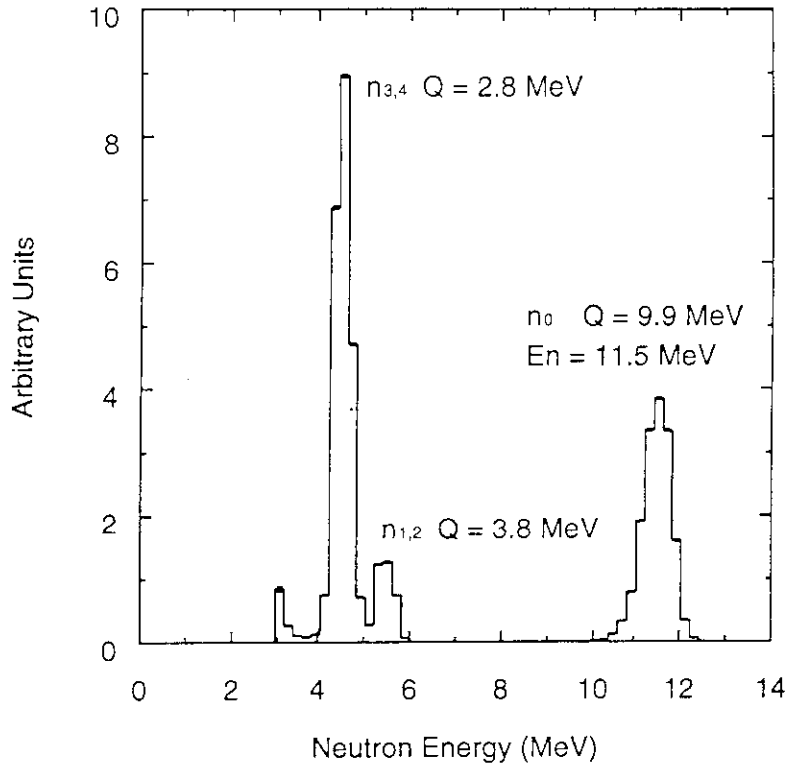

Fig. 13 Neutron spectrum for $^{15}N(d,n)$ neutron source.

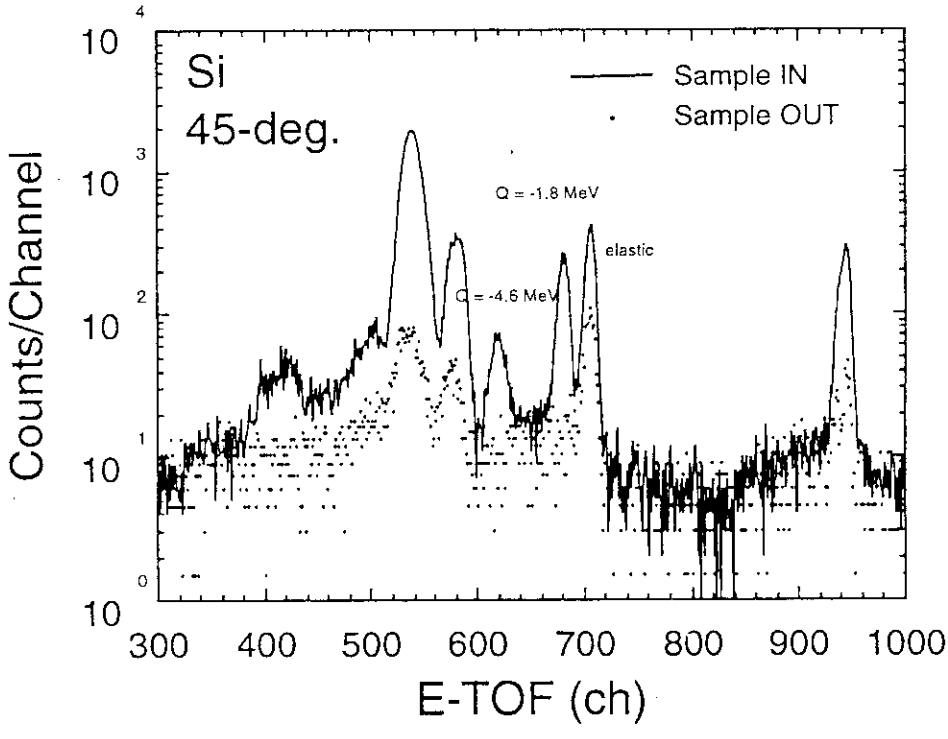

Fig. 14 Neutron TOF spectrum for silicon at 45 degree.

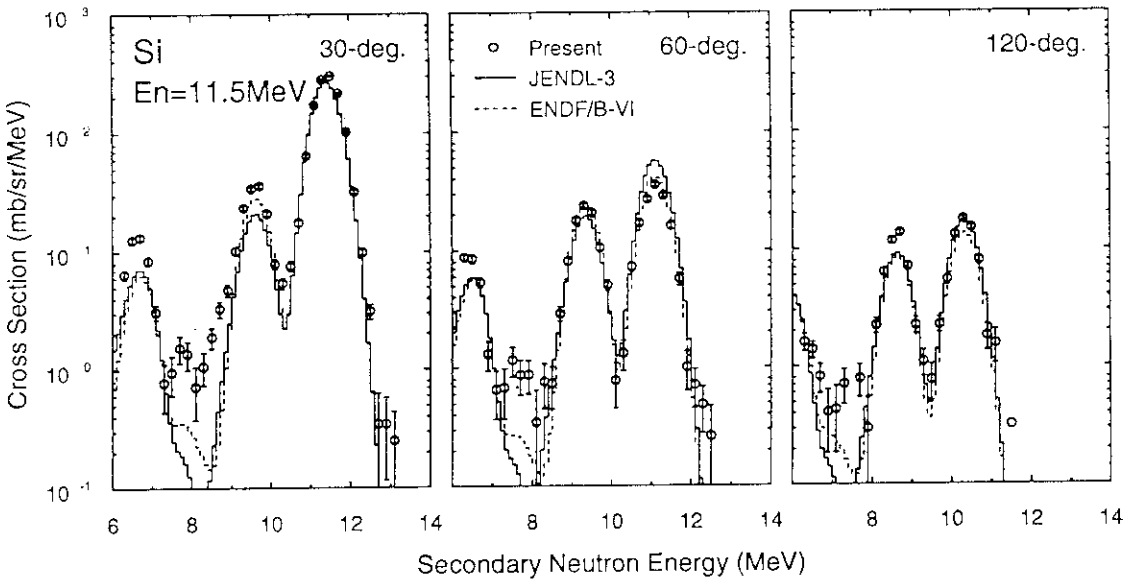

Fig. 15 Double-differential neutron emission spectra of silicon for 11.5 MeV neutrons.

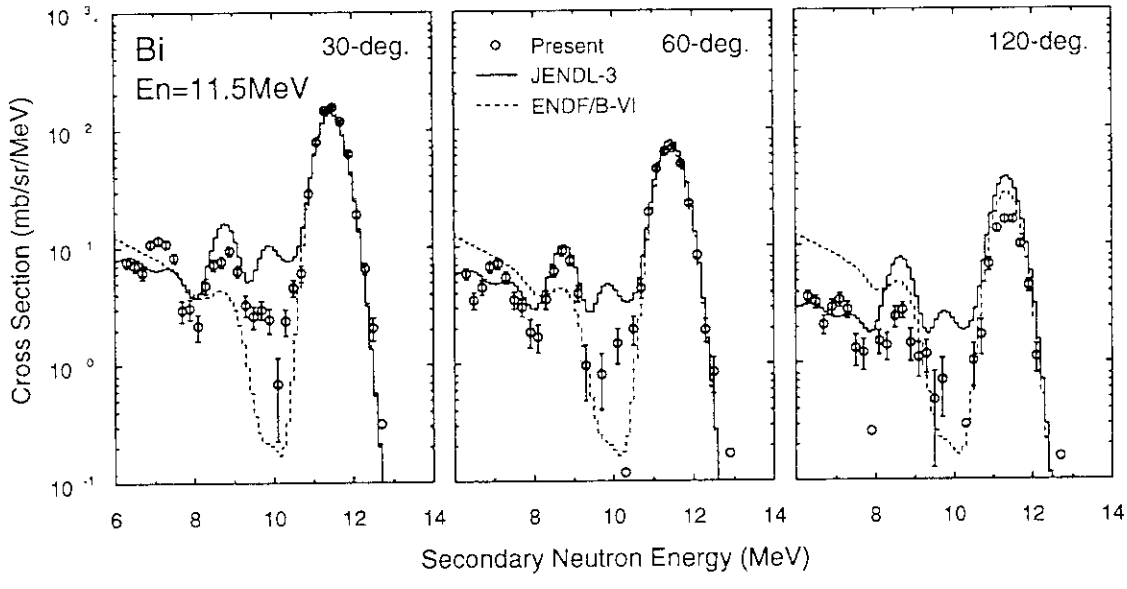

Fig. 16 Double-differential neutron emission spectra of bismuth for 11.5 MeV neutrons.

5.7 Measurements of Double Differential α-particle Emission Cross Sections of ^{12}C with 14 MeV Incident Neutrons

Hiroshi Nishizawa, Akito Takahashi, Yoshinobu Murakami*

Department of Nuclear Engineering, Faculty of Engineering, Osaka University
Yamadaoka 2-1, Suita, Osaka, 565, Japan
** Sumitomo Heavy Industry Co., Niihama, Ehime, Japan*

Double differential α-particle emission cross sections of ^{12}C with 14.1MeV incident neutrons were measured at 5 angle points between 30 and 90 degrees based on the E-TOF two dimensional analysis. Experimental method and measured data compared with Haight's data are shown. In this experiment the angular dependence of a component of the $^{12}C(n,\alpha)^{9}Be_{g.s.}$ reaction was observed; while for the continuum component of the $^{12}C(n,n')3\alpha$ reaction, angular-dependence was not clearly observed.

1. Introduction

Nuclear data of ^{12}C are required for several applications such as the dosimetry for nuclear medicine, the radiation damage estimation and the nuclear heating in fission and fusion reactors, and so on. After the interaction of incident fast neutrons such as 14MeV with carbon, the most important emitted charged-particles are α-particles from the competing reactions of $^{12}C(n,n')3\alpha$ and $^{12}C(n,\alpha)^{9}Be$, and it is presumed that the contribution of 3α-breakup from the bombardment of ^{12}C becomes dominant. Because of the complex reaction process, angular-energy distributions of emitted particles, i.e. neutron and α-particle, are important information. Although there are many experimental data of double differential neutron emission cross section (DDXn) available, double differential α-particle emission cross sections (DDXα) have seldom been measured directly up to now because of the difficulty of the measurement. Recently we have developed the measuring system of charged-particle spectra based on the E-TOF two dimensional analysis at our laboratory, and DDXα of ^{12}C at 14.1MeV incident neutrons were measured at 5 angle points between 30 and 90 degrees in laboratory system. Measured spectra were compared with Haight's experimental data.

2. Experimental procedure

The present experiment is based on the E(energy) - TOF(time-of-flight) two dimensional analysis method (Ref.1). The relation between E and TOF of emitted particles is presented by the following equation,

$$E = M_0 c^2 \left(\frac{1}{\sqrt{1-(L/cT)^2}} - 1 \right) \quad (1)$$

where c, M_0, L, and T are the velocity of light, the mass, the flight-path length, and the time-of-flight of emitted particle, respectively. Fig.1 shows the relation between energy and time-of-flight calculated by equation(1). If energy and time-of-flight of emitted particles are measured in coincidence and are analyzed in the E-TOF two-dimensional domain, emitted particles of different masses can be separated into different contours and backgrounds caused by the charged-particles from other materials in the system than the sample distribute out of the contours, and can be removed easily as shown in Fig.1. A schematic view of the present experiment is shown in Fig.2. The flight-path length for the emitted particle is about 50cm. The sample, the collimator, and the detector were located inside a 1mϕ x 1m long vacuum chamber as shown in Fig.2. Emission angle was determined by changing the position of the sample. The air pressure of the chamber was about 10^{-2} torr and the energy loss of charged-particles at this pressure was negligible. The 2ns FWHM pulsed D-T neutron source of OKTAVIAN was operated with 2MHz repetition frequency. The sample was a polyethylene film which had 60mm diameter and 18μm thickness. A CsI(Tl) scintillator which had 50mm diameter and 2mm thickness was used because of its excellent pulse shape discrimination capability. The two dimensional distributions of energy and rise-time of signals of charged-particle and γ-ray are shown in Fig.3. The rise-time is, as shown in Fig.3, dependent on energy. Contours indicated with A, B and C are corresponding to α-particles, protons and γ-rays, respectively. By the pulse shape discrimination technique, recoil protons from the sample and all the γ-rays could be removed to measure only α-particles. The net α-particle data were obtained by subtracting the data of background run for which we took out the sample. The block diagram of measuring system is shown in Fig.4. With an NE213 neutron monitor, only 14MeV neutrons were counted by the TOF-gated method in coincidence with neutron signal by the n-γ pulse shape discrimination. The E-TOF two dimensional distribution of α-particles from the neutron-bombarded ^{12}C at 30 degree is shown in Fig.5, where we can see a separated peak at high energy region. The spectra were obtained by integrating proper counts within the α-particle contour. The energy calibration was done by using an ^{241}Am α-source. Energy resolution of the experiment was 0.7MeV FWHM at 5.5MeV. For calibrating absolute values of DDXα, we adopted differential recoil proton cross section of H(n,p) in ENDF/B-VI, to measure proton contours by the polyethylene sample.

The locations of neutron source, sample and detector are shown in Fig.6a. We estimated broadening functions of angular resolution at all the angles as shown in Fig.6b. In addition, the energy loss of α-particle in the sample was not negligible so that we had to correct the raw

data for the attenuation effect. The raw data obtained from the above procedure were corrected as follows: We had done a Monte-Carlo simulation calculation, which took account the energy loss and stopping positions of α-particles in the sample considering the geometry of neutron source, sample and detector by Bethe formula of stopping power. Although for input data of this kind of calculation we usually adopt DDXα from evaluated nuclear data, we produced by ourselves the input data, since DDXα data of ^{12}C are not evaluated in the existing evaluated nuclear data libraries. Produced DDXα are listed in Table.1, which is the sums of following two reactions; the $^{12}C(n,n')3\alpha$ cross section was assumed as 750mbarn considering energy-angular distribution of ^{12}C(n,continuum) from JENDL-3. Its energy distribution was given as evaporation spectrum and its angular distribution was given as numerical table. The $^{12}C(n,\alpha)^{9}Be_{g.s.}$ cross section was assumed as 70mbarn considering angular distribution by a Legendre polynomial fit to raw data of the $^{12}C(n,\alpha)^{9}Be_{g.s.}$ component which had angular dependence, because the angular dependence of this reaction could be predicted.

The spectrum produced by the authors, i.e. input data, and the result of Monte-Carlo simulation calculation, i.e. output data, at 30 degree in laboratory system are shown in Fig.7, comparing with raw data. In order to minimize distortions by the correction, the correction factor was derived by comparing the spectra; namely, the result of calculation was shifted backward to high energy region by Bethe formula. The raw data were also shifted backward to high energy region by Bethe formula and the corrected data were deduced by multiplying the correction factor to the shifted raw data.

3. Results

Measured DDXα of ^{12}C at 30, 45, 60, 75, and 90 degree in laboratory system with 14.1MeV incident neutrons after corrections are shown in Figs.8a through 8e, comparing with other experimental data (Ref.2). The present data were bunched with 0.4MeV energy bin to improve counting statistics. The energy resolution of the present data was worse than that of Haight's data because of the difference in detector capability and neutron source strength between the present and Haight's experiments; namely we used a CsI(Tl) scintillator with pulsed D-T source and Haight used a magnetic quadruple spectrometer with the intense DC source of RTNS-II.

The separated peaks labeled α_0 indicate α-particles that leave ^{9}Be in the ground state. Angular differential cross section of this component is shown in Fig.9a and is compared with Haight's data and the value derived from the inversed reaction $^{9}Be(\alpha,n)^{12}C_{g.s.}$, the equivalent neutron energy range of which was 13.5 to 14.5MeV (Ref.2). We found discrepancies in two data; the present data was larger than the Haight's data at around 90 degree in the center-of-mass system.

The continuum spectra at low energy region indicate α-particles due to the $^{12}C(n,n')3\alpha$

reaction which is thought to be a competing process of sequential decay and multi-body simultaneous breakup. Angular differential cross section of this component in the α-energy region of more than 2.0MeV, excluding the α0 peak, is shown in Fig.9b. The cross section was much larger in forward angles than that of Haight experiment. However, we could not clearly identify the trend by the present experiment: One of the reason may be due to the fact that there was the broadening of angular resolution at each angle in our experiment as shown in Fig.6b, and therefore further investigation has to be done.

4.Conclusion

Double differential α-particle emission cross sections of ^{12}C at 14.1MeV incident neutrons were obtained at 5 angles based on the E-TOF two dimensional analysis with a pulsed D-T neutron source. Background could be reduced by analyzing E-TOF domain for seeking proper particle contour and also by applying the pulse shape discrimination technique.

We observed separated peaks due to the $^{12}C(n,\alpha)^{9}Be_{g.s.}$ reaction which showed angular dependence. The continuum spectra due to the $^{12}C(n,n')3\alpha$ reaction were also observed. Angular distribution was not in very good agreement with the Haight's data for both the $^{12}C(n,\alpha)^{9}Be_{g.s.}$ and $^{12}C(n,n')3\alpha$ reactions.

Measurements at more backward angles are needed to understand the angular distributions of these reactions with reaction mechanisms.

References

[1] S.Ogino et al., *OKTAVIAN Rep.*, 91-01 (1991)

[2] R.C.Haight et al., *Nucl. Sci. Eng.*, 87, 41 (1984)

Table 1 Input DDXα for correction, which is the sum of 1) and 2), produced by the authors.

Reaction	1) $^{12}C(n,n')3\alpha$	2) $^{12}C(n,\alpha)^{9}Be_{g.s.}$
Energy distribution	Evaporation spectrum T=1.1MeV	kinematics, folding with 0.7MeV FWHM
Angular distribution	Table (larger in forward angles)	Legendre polynomial fit to raw data
Cross section	750mb	70mb

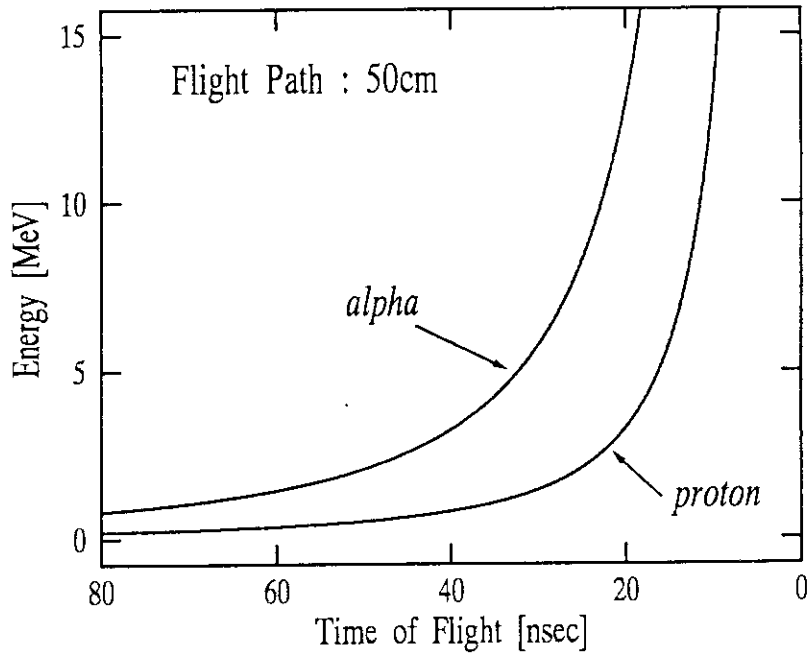

Fig. 1 The relation between E and TOF of emitted charged-particle.

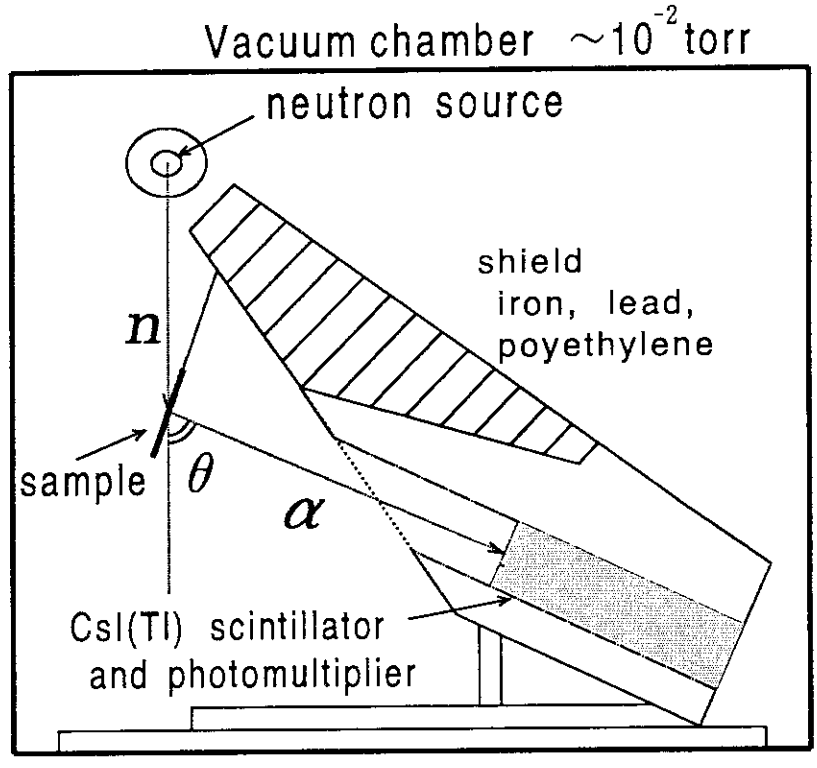

Fig. 2 Schematic view of the present experiment.

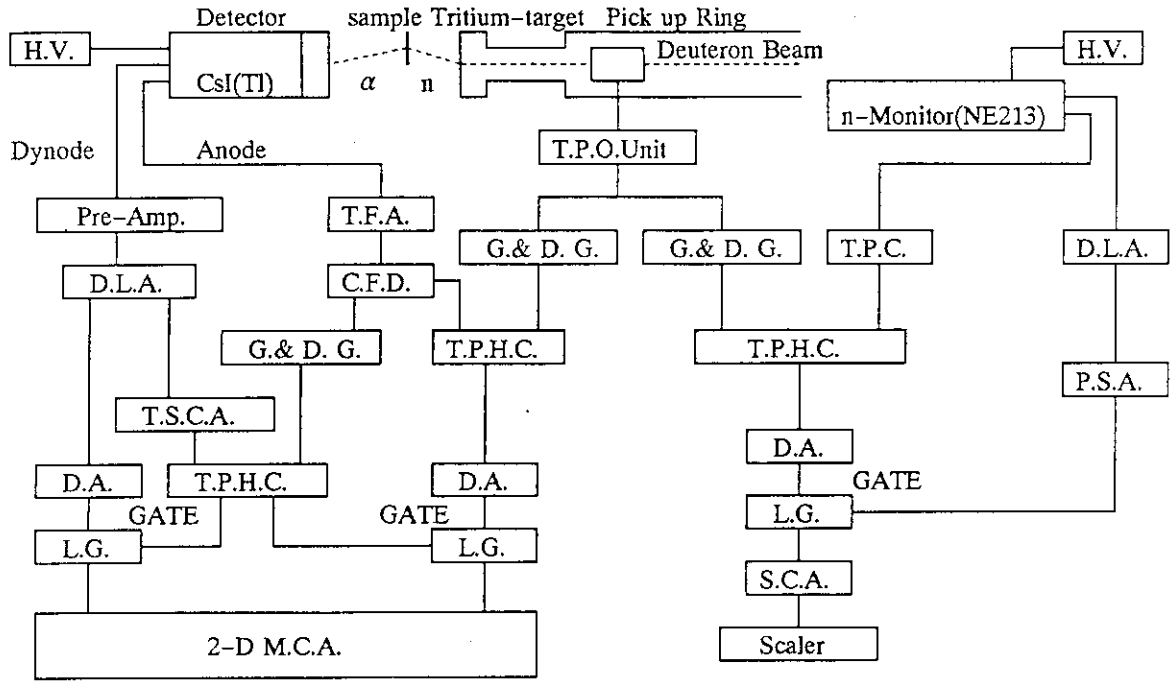

Fig. 4 The block diagram of the measuring system.

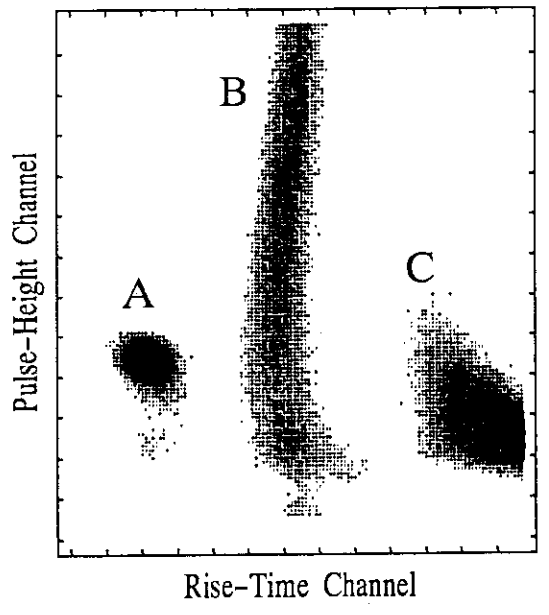

Fig. 3 Two dimensional distribution of rise-time of signal and pulse-height. A, B and C are the contours of α-particle, proton and γ-ray, respectively.

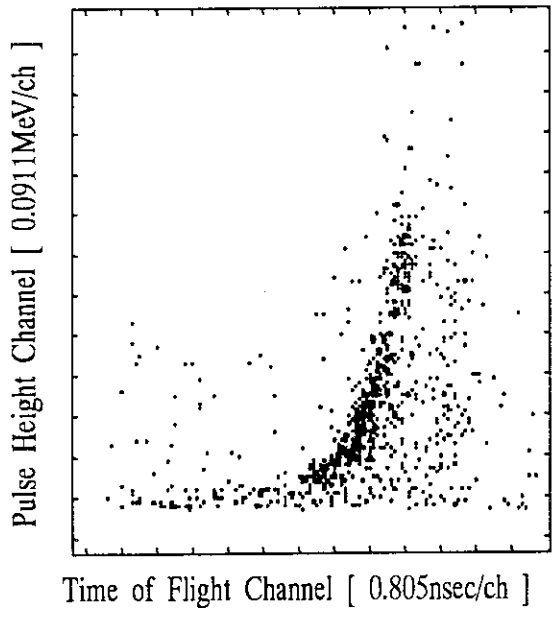

Fig. 5 The E-TOF two dimensional distribution of α-particle from the neutron-bombarded ^{12}C at 30 degree in LAB system.

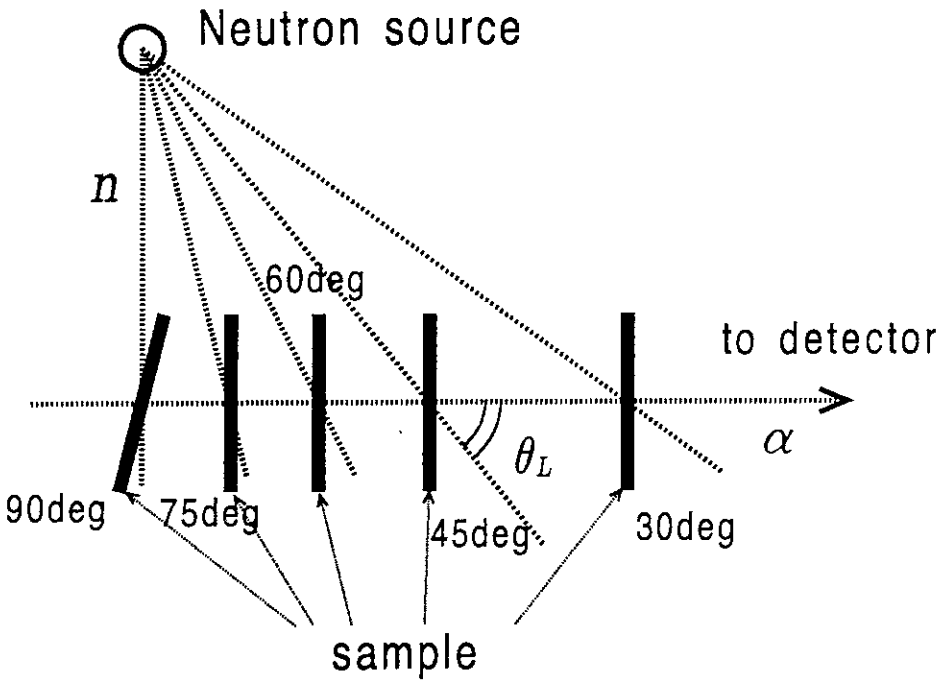

Fig. 6a The location of neutron source, sample and detector; θ_L is emission angle.

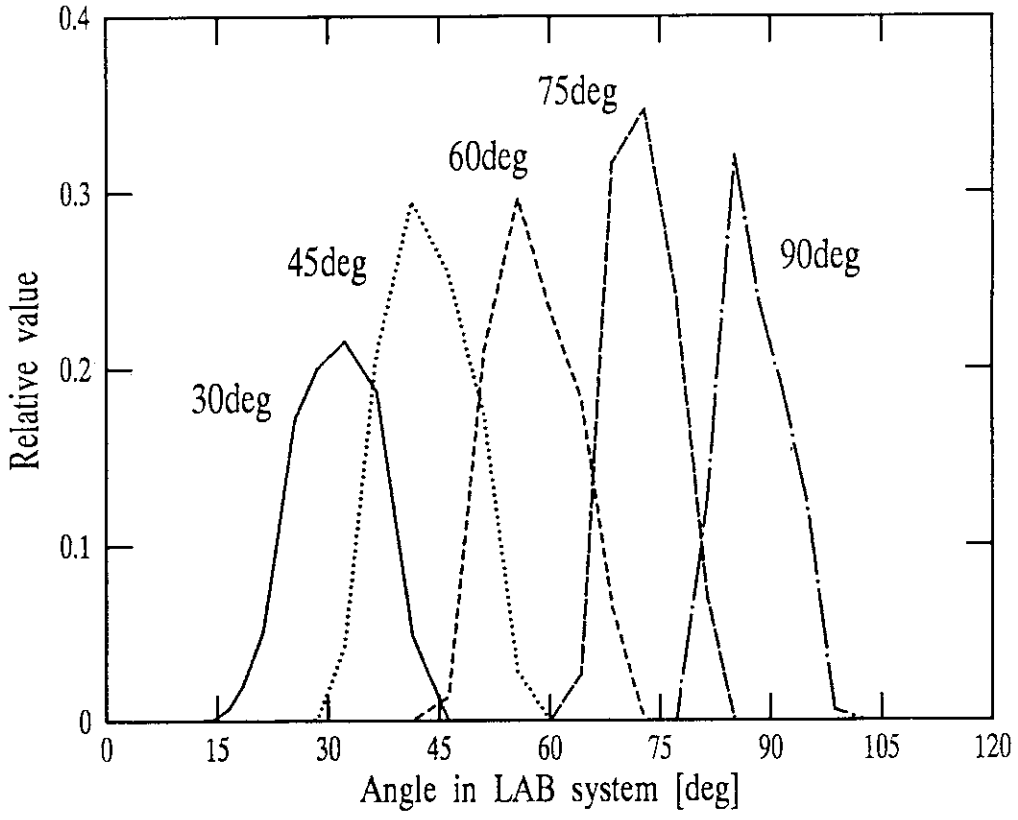

Fig. 6b Broadening function of angular resolution at each angle.

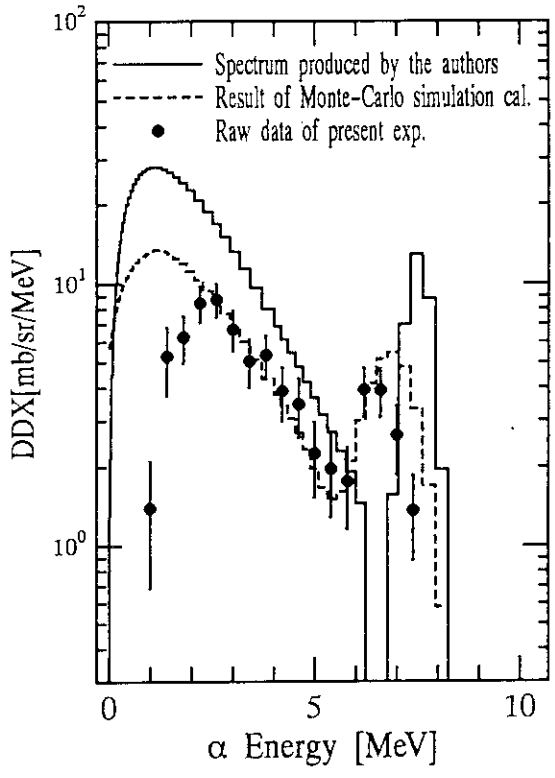

Fig. 7 Monte-Carlo simulation calculation and raw data of ^{12}C at 30 deg.

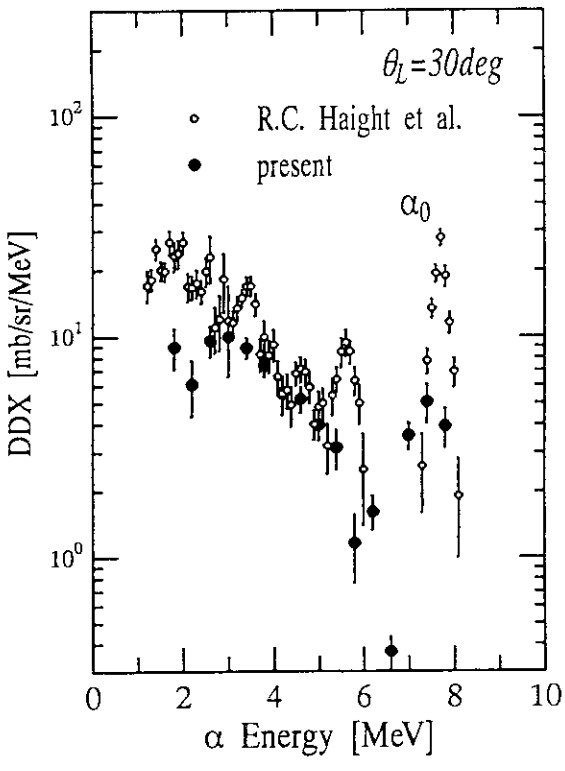

Fig. 8a DDXα of $^{12}C(n,x\alpha)$ at 30deg.

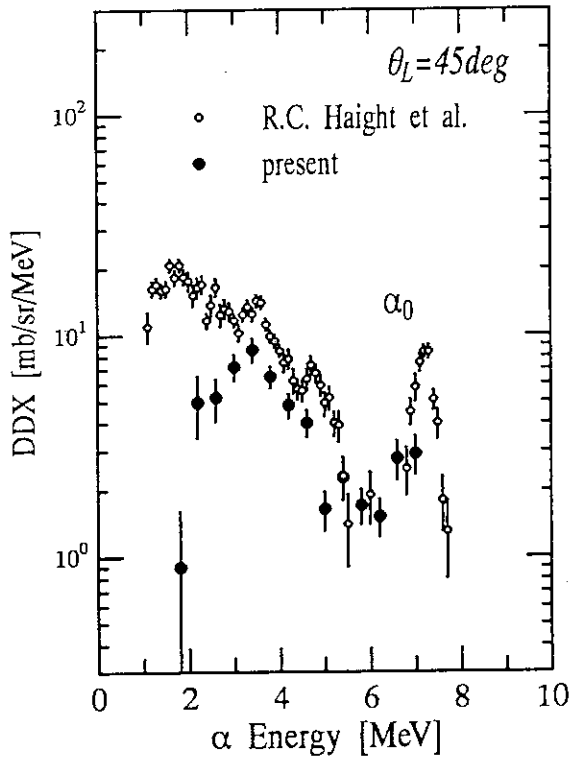

Fig. 8b DDXα of $^{12}C(n,x\alpha)$ at 45deg.

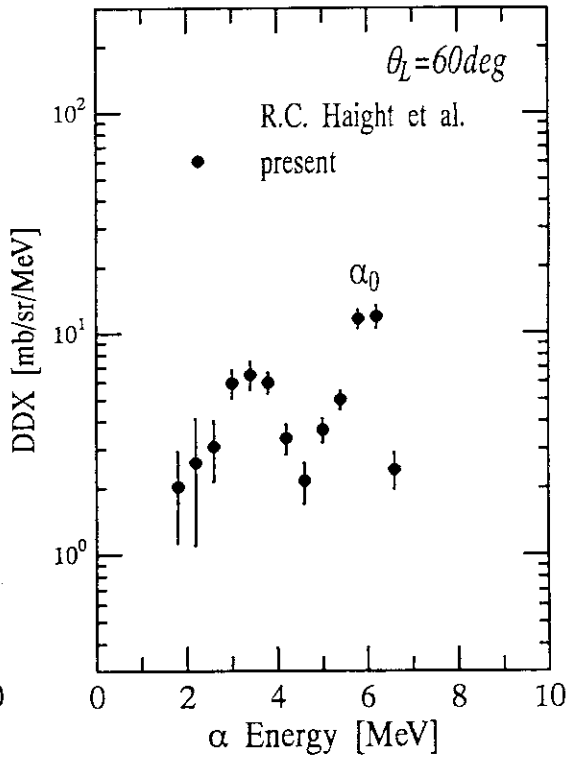

Fig. 8c DDXα of $^{12}C(n,x\alpha)$ at 60deg.

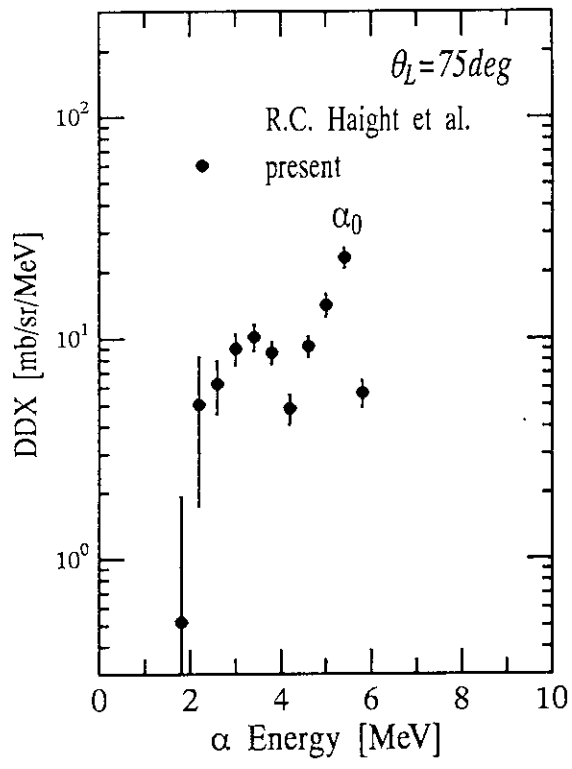

Fig. 8d DDXα of $^{12}C(n,x\alpha)$ at 75deg.

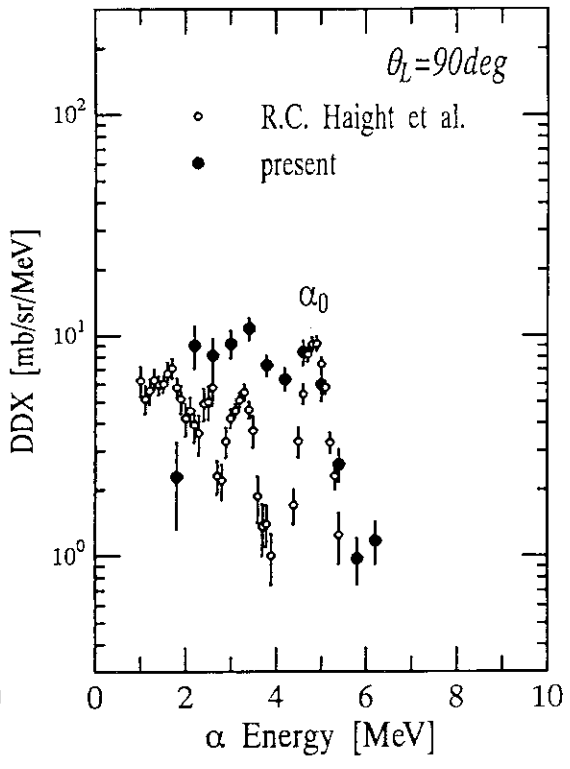

Fig. 8e DDXα of $^{12}C(n,x\alpha)$ at 90deg.

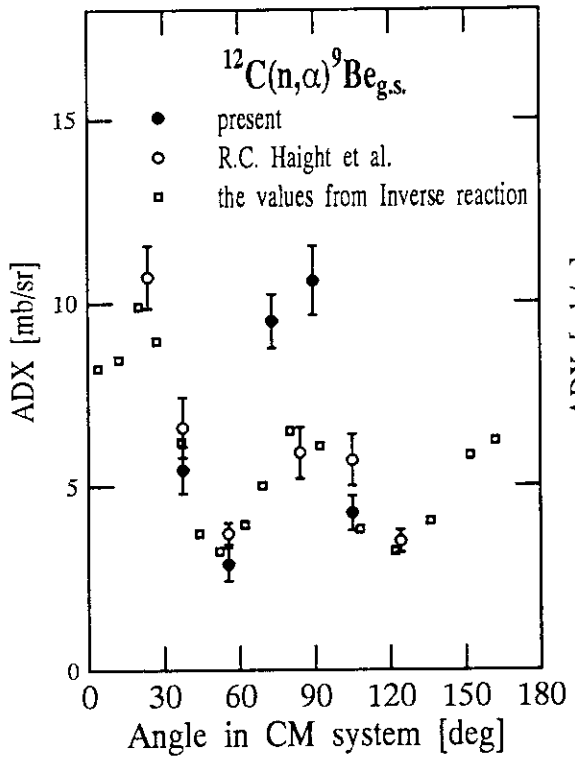

Fig. 9a Differential cross section for $^{12}C(n,\alpha)^{9}Be_{g.s.}$

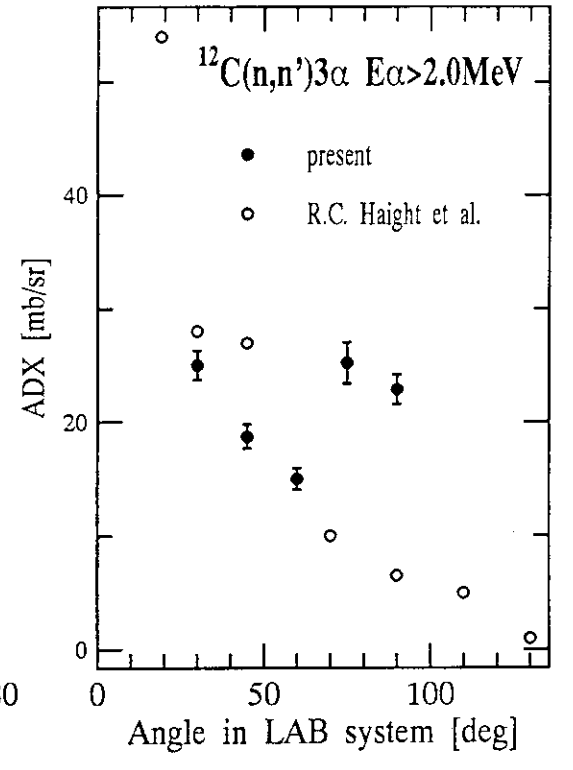

Fig. 9b Differential cross section for $^{12}C(n,n')3\alpha$.

5.8 Measurements of the Neutron Scattering Cross Sections for ^{12}C, ^{16}O, ^{40}Ca and ^{56}Fe at 14.2 MeV

Teiji NISHIO, Shoji SHIRATO and Yoshiaki ANDO

Department of Physics, Rikkyo University

Nishi-Ikebukuro 3, Toshima-ku, Tokyo 171

Abstract: Double different cross sections and energy-integrated differential ones for elastic and inelastic scattering from ^{12}C, ^{16}O, ^{40}Ca, and ^{56}Fe at 14.2 MeV have been measured at forward angles from 10^{o} to 70^{o} in 10^{o} steps.

The experimental data have been compared with the predictions of JENDL-3 as well as those of optical model and DWBA calculations.

Double differential cross sections (DDX) for elastic and inelastic neutron scattering from ^{12}C, ^{16}O, ^{40}Ca and ^{56}Fe at 14.2 MeV have been measured at forward angles from 10^{o} to 70^{o} in 10^{o} increments using the neutron time-of-flight (TOF) facility of the 300 kV Cockcroft-Walton accelerator of Rikkyo University and preliminarily analyzed.

Neutron TOF spectra were obtained from the signals of scattered neutrons and the associated α-particles produced in the ^{3}H-d reaction at 165 keV, using an NE213 liquid scintillator of 10 cm φ x 30 cm for neutrons and a thin (50 μm) NE102A plastic scintillator for α-particles[1]. The signals of the neutron detection position and of the n-γ discrimination have been also simultaneously measured by a CAMAC data taking system, as seen in Fig. 1. The characteristics of scatterers and geometry in this experiment are given in Tables 1 and 2, respectively. Cross sections were

determined absolutely using the neutron detection efficiency calculated by the Kurz code[2] and also relatively using the absolute ones measured with a 2 in ϕ x 2 in neutron detector[3,4]. The details of the experiment are described elsewhere[5].

Some of measured energy spectra (DDX) of scattered neutrons are shown in Figs. 2 - 5 together with calculations based on JENDL-3 using the code PLDDX[6]. The calculations are performed with the energy resolution of 0.7 MeV in FWHM. The experimental spectra have been corrected for the neutron attenuation in the target and the detector assembly. Measured angular distributions for elastic and inelastic scattering are compared with optical model and DWBA calculations respectively and the JENDL-3 predictions, as shown in Figs. 6 - 9. The inelastic scattering data for ^{56}Fe in Fig. 9-2 are ones measured with the 2 in ϕ x 2 in detector of the better energy resolution (FWHA = 0.4 MeV). The optical potentials and the deformation parameters $\beta_L(0^+ \rightarrow J^\pi)$ obtained are given in Table 3.

References:

1) S. Shirato, S. Shibuya, Y. Ando, T. Kokubu and K. Hata: Nucl. Instr. Methods A278, 477 (1989).

2) R. J. Kurz: UCRL-11339 (1964) unpublished.

3) K. Hata, S. Shirato and Y. Ando: JAERI-memo 02-308 (1990).

4) K. Hata, S. Shirato and Y. Ando: JAERI-M 91-032, 328 (1991).

5) S. Shirato, T. Nishio and Y. Ando: Report (in Japanese) written by summarizing the effort implemented under the Research-in-Trust in 1991 - 1992 fiscal years from the Japan Atomic Energy Research Institute (JAERI); Progress report (1993, JAERI), INDC(JPN)-166/U, p.73.

6) T. Fukahori and I. Tazaki, JAERI-memo 62-453 (1988).

7) K. Gul, M. Anwar, M. Ahmad, S. M. Saleem and N. A. Khan:
Phys. Rev. C24, 2458 (1981).

8) J. S. Petler, M. S. Islam, R. W. Finlay and F. S. Dietrich:
Phys. Rev. C32, 673 (1985).

9) G. M. Honore et al.: Phys. Rev. C3, 1129 (1986).

10) M. Hyakutake et al.: J. Phys. Soc. Japan 38, 606 (1975).

11) N. Olsson, B. Trostell and E. Ramstrom: Nucl. Phys. A496, 505 (1989).

Table 1 Specifications of the scatterer samples used in this experiment.

SCATTERER	WEIGHT* (g)	SIZE (cm)	PURITY (%)	FORM	VESSEL
^{nat}C	34.840	3.0φ x 3.0	99.9	SOLID	NON
CH_2	19.597	3.0φ x 3.0	99.9	SOLID	NON
^{nat}Fe	166.020	3.0φ x 3.0	99.9	SOLID	NON
^{nat}Ca	92.440	4.8φ x 6.0	99.5	GRAIN	CH_2**
^{nat}CaO	74.618	4.8φ x 6.0	99.9	POWDER	CH_2**

* Weight error of ± 0.005 g.

** 13.891 g (the outer size of 5.0 cm φ x 6.6 cm).

Table 2 Geometrical parameters in the TOF experiment using 14.23 MeV incident neutrons.

D : Distance between the neutron source and the detector rear surface.

= 388.15 cm.

L_{st}: Distance between the neutron source and the target center.

H : Vertical distance of the target center from the source-detector plane.

FP : Neutron flight distance from the target center to the detector rear.

θ : Scattered neutron angle at the target center.

$\Delta\theta_1$: Maximum deviation of θ for C, Fe and CH_2 targets.

$\Delta\theta_2$: Maximum deviation of θ for Ca and CaO targets.

T_{st}: Flight time of incident neutrons at the target center.

T_a : Flight time of associated α-particles.

$OFFSET_1 = DELAY_2$(= 360 ns) + $T_a - T_{st}$.

$OFFSET_2 = OFFSET_1$ - PEDESTRAL (b = -53.500 ns).

SETTING ANGLE	L_{st}	H	FP	θ	$\Delta\theta_1$*	$\Delta\theta_2$*	T_{st}	$OFFSET_1$
(deg)	(cm)	(cm)	(cm)	(deg)	(deg)	(deg)	(ns)	(ns)
10	75.78	7.6	314.26	14.28	1.14	1.82	14.53	354.60
20	50.86	5.2	341.08	23.85	1.70	2.72	9.75	359.37
30	25.38	2.6	366.51	32.53	3.41	5.45	4.87	364.26
40	25.38	2.6	369.17	42.91	3.41	5.45	4.87	364.26
50	25.38	2.6	372.43	53.26	3.41	5.45	4.87	364.26
60	25.38	2.6	376.17	63.53	3.41	5.45	4.87	364.26
70	25.38	2.6	380.26	73.71	3.41	5.45	4.87	364.26

* $\Delta\theta_{HWHM} = [(2 \ln 2)^{1/2} / 2]\Delta\theta = 0.6\Delta\theta$.

Table 3 Optical potential [U(r)] and deformation [$\beta_L(0^+ \to J^\pi)$] parameters at 14.2 MeV. [$U_c(r) = 0$]

	V (MeV)	W_s* (MeV)	V_{so}** (MeV)	r_0 (fm)	r_0' (fm)	a (fm)	b (fm)	c_{so} (fm)	$\beta_L(0^+ \to J^\pi)$	Ref.
^{12}C	Entrance channel (g.s., 0^+):									
	46.5	8.88	4.39	1.28	0.86	0.39	0.39	0.39		7)
	Exit channel (1st e.s., 2^+):									
	55.0	2.60	4.39	1.20	0.86	0.39	0.39	0.39	$0.65(2^+)$	
^{16}O	Entrance channel (g.s., 0^+):									
	49.32	4.35	4.31	1.15	1.38	0.646	0.473	0.45		8)
	Exit channel (2nd e.s., 3^-):									
	51.13	2.46	4.31	1.15	1.38	0.646	0.473	0.45	$0.33(3^-)$	
^{40}Ca	Entrance channel (g.s., 0^+):									
	46.52	6.26	5.08	1.25	1.25	0.65	0.58	0.50		9)
	Exit channel (2nd e.s., 3^-):									
	47.5	5.52	5.22	1.25	1.25	0.65	0.58	0.50	$0.33(3^-)$	
^{56}Fe	Entrance channel (g.s., 0^+):									
	43.55	10.24	6.00	1.25	1.242	0.673	0.47	0.673		10)
	Exit channel (1st e.s., 2^+):									
	43.55	10.24	6.00	1.25	1.242	0.673	0.47	0.673	$0.23(2^+)$	

The potential form is given by the following expression:

$$U(r) = U_C(r) - V/(1+f_V(r)) - i[W_V/(1+f_W(r)) + W_G/f_G(r) + 4W_S f_W(r)/(1+f_W(r))^2] - (h/m_\pi c)^2 V_{so}(1/rc_{so}) f_{so}(r)(1+f_{so}(r))^{-2} \underline{L}*\underline{S},$$

where $f_V(r) = \exp[(r - r_0 A^{1/3})/a]$, $f_W(r) = \exp[(r - r_0' A^{1/3})/b]$,

$f_{so}(r) = \exp[(r - r_0 A^{1/3})/c_{so}]$, $f_G(r) = \exp[(r - r_0' A^{1/3})^2/b^2]$.

* Note $W_s = V_I/4$ using the DWUCK4 notation.

** Note $V_{so} = V_{LS}/4$ in the $\underline{l}$-$\underline{\sigma}$ form using the DWUCK4 notation.

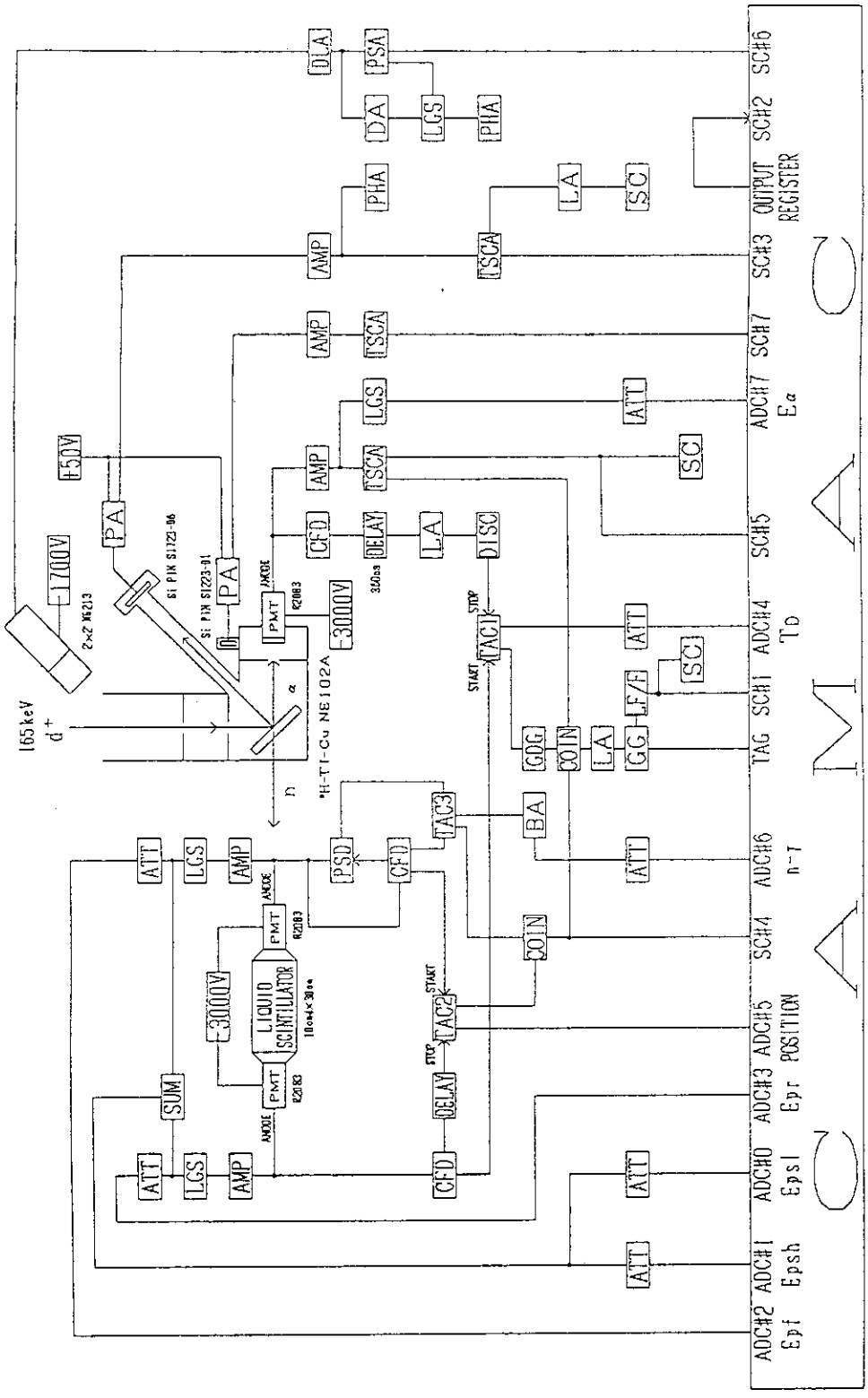

Fig. 1 Block diagram of electronics.

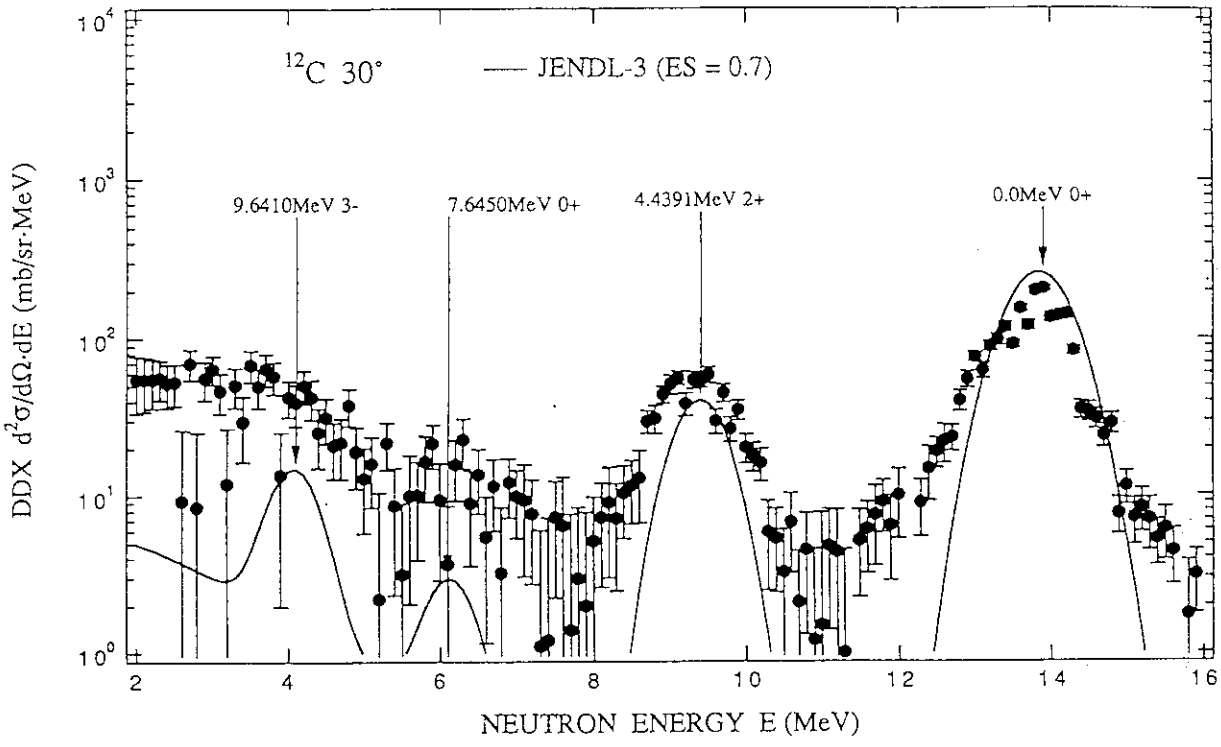

Fig. 2-1 Measured and calculated DDXs for 14.2 MeV neutron scattering from ^{nat}C at 30°.

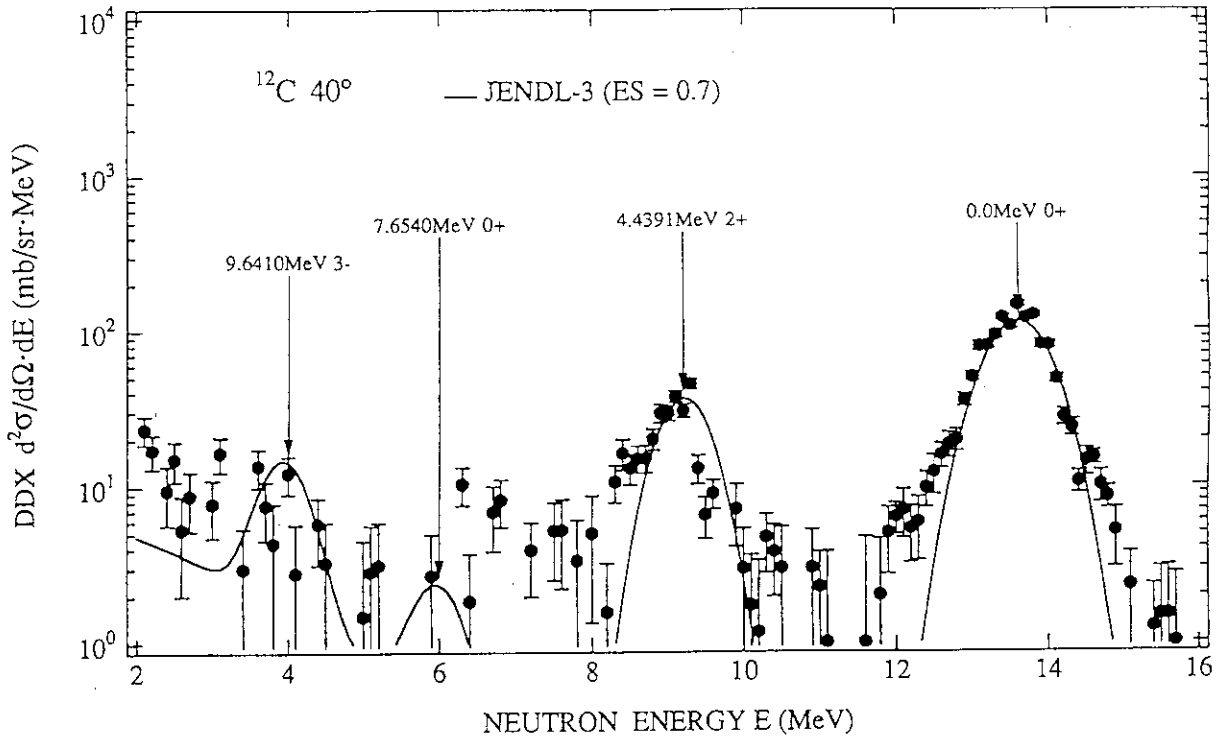

Fig. 2-2 Measured and calculated DDXs for 14.2 MeV neutron scattering from ^{nat}C at 40°.

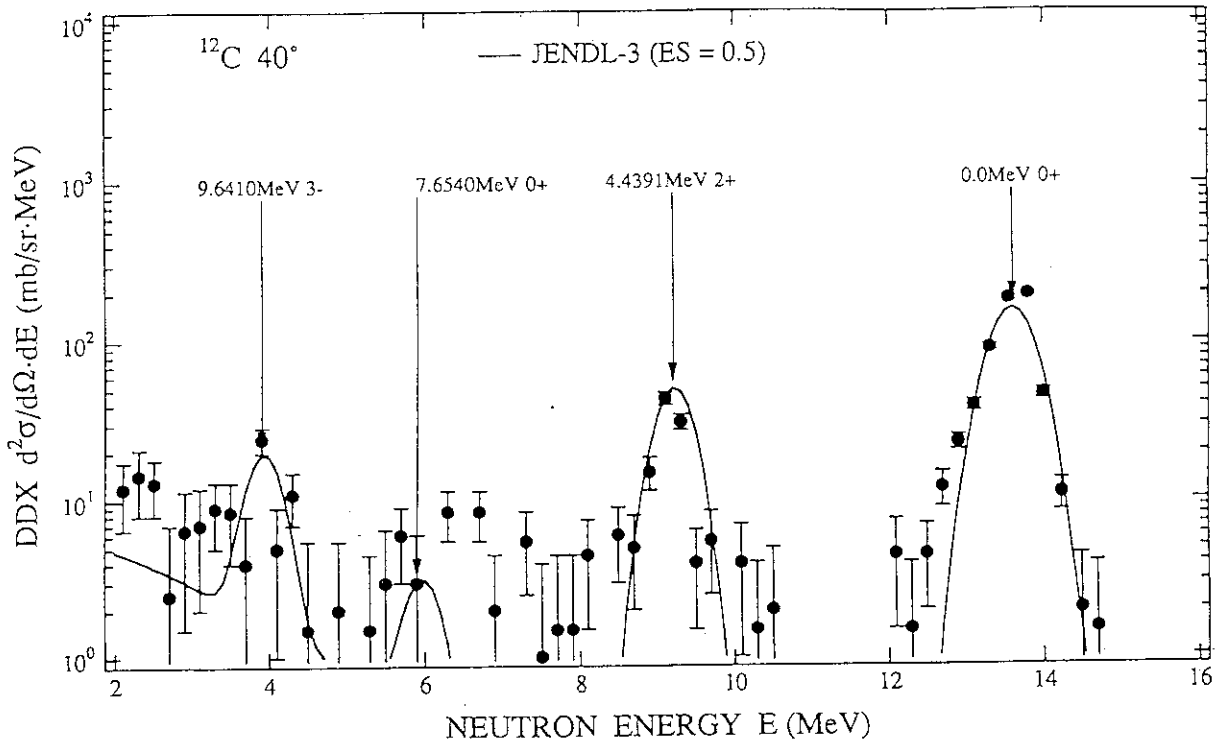

Fig. 2-3 Measured and calculated DDXs for 14.2 MeV neutron scattering from ^{nat}C at 40° (2 in ϕ × 2 in data).

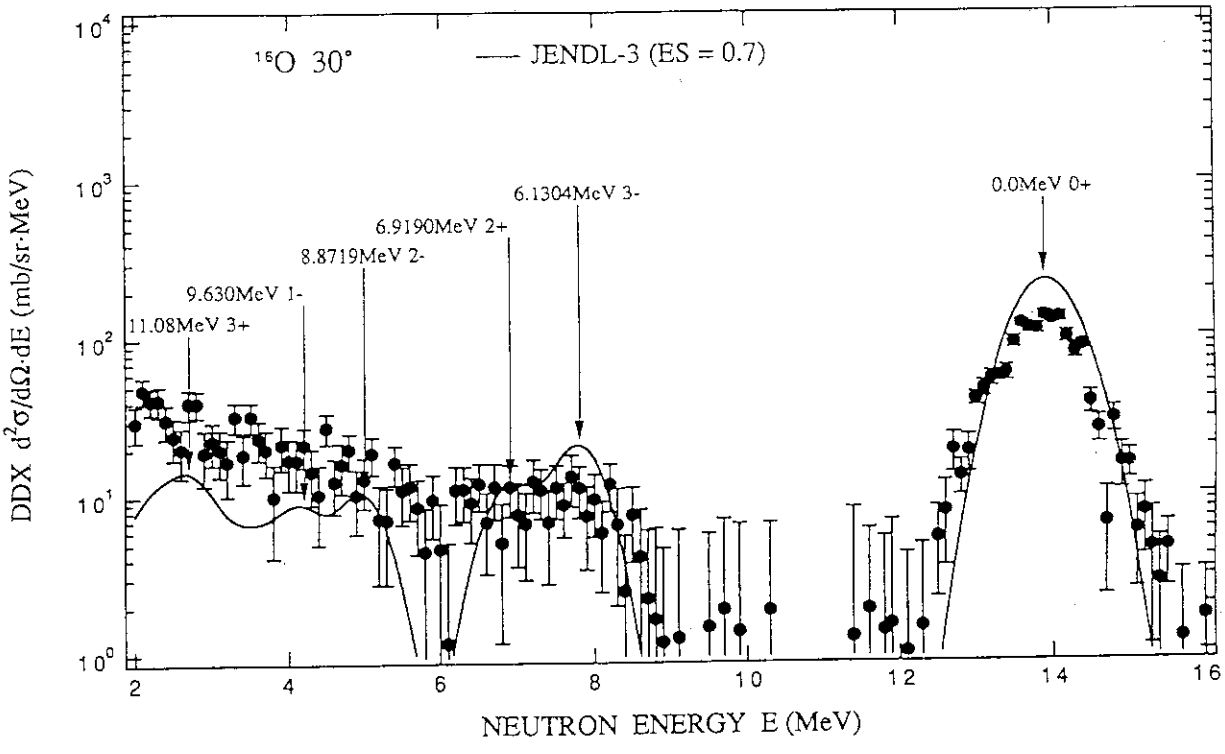

Fig. 3-1 Measured and calculated DDXs for 14.2 MeV neutron scattering from ^{nat}O at 30°

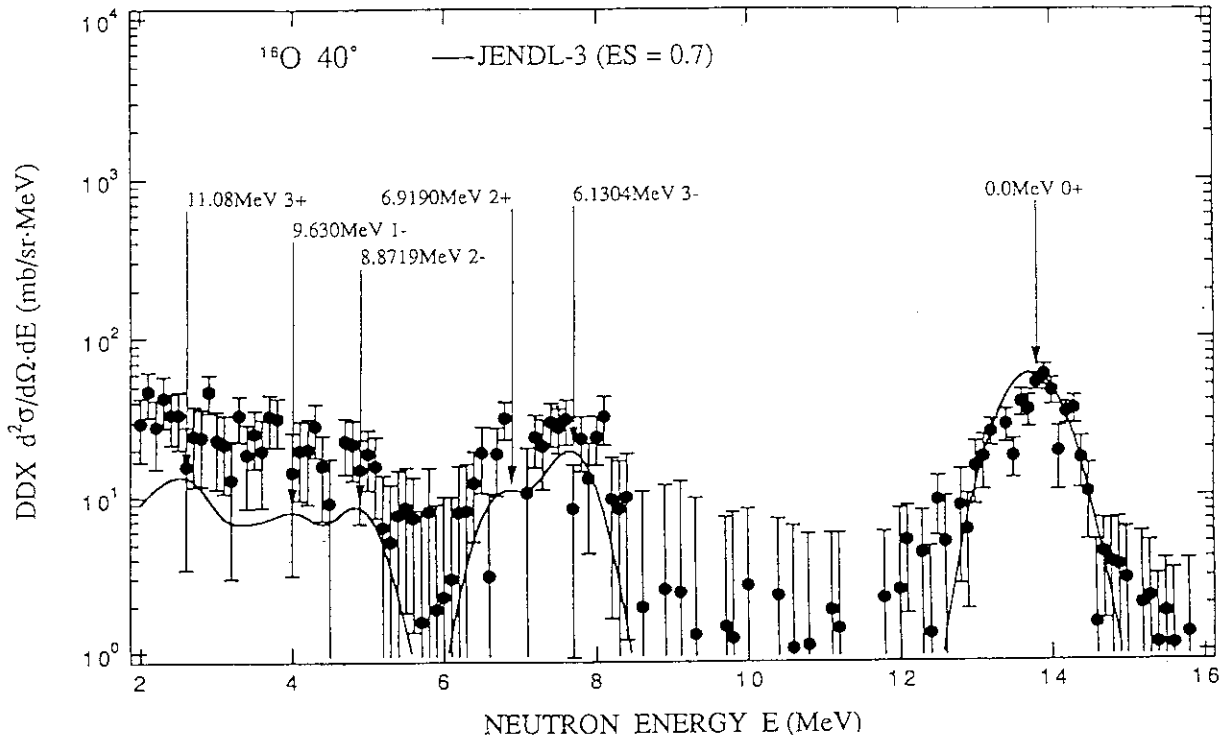

Fig. 3-2 Measured and calculated DDXs for 14.2 MeV neutron scattering from ^{nat}O at 40°.

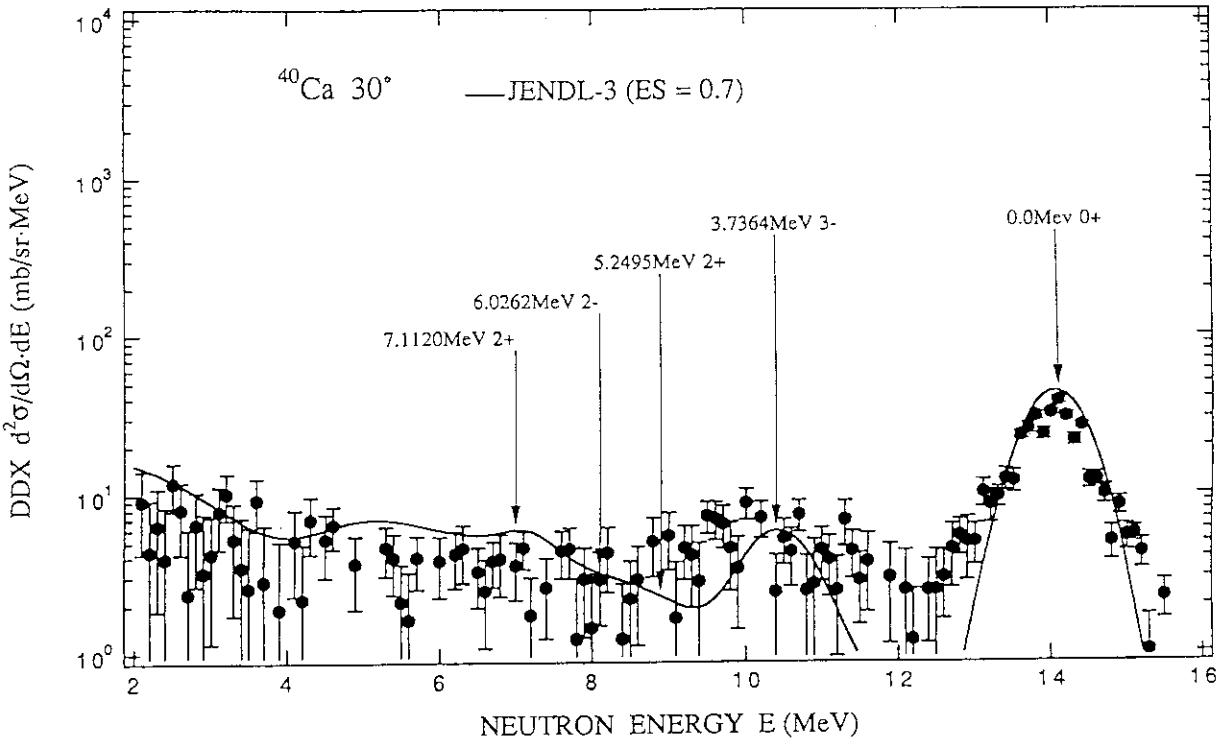

Fig. 4-1 Measured and calculated DDXs for 14.2 MeV neutron scattering from ^{nat}Ca at 30°.

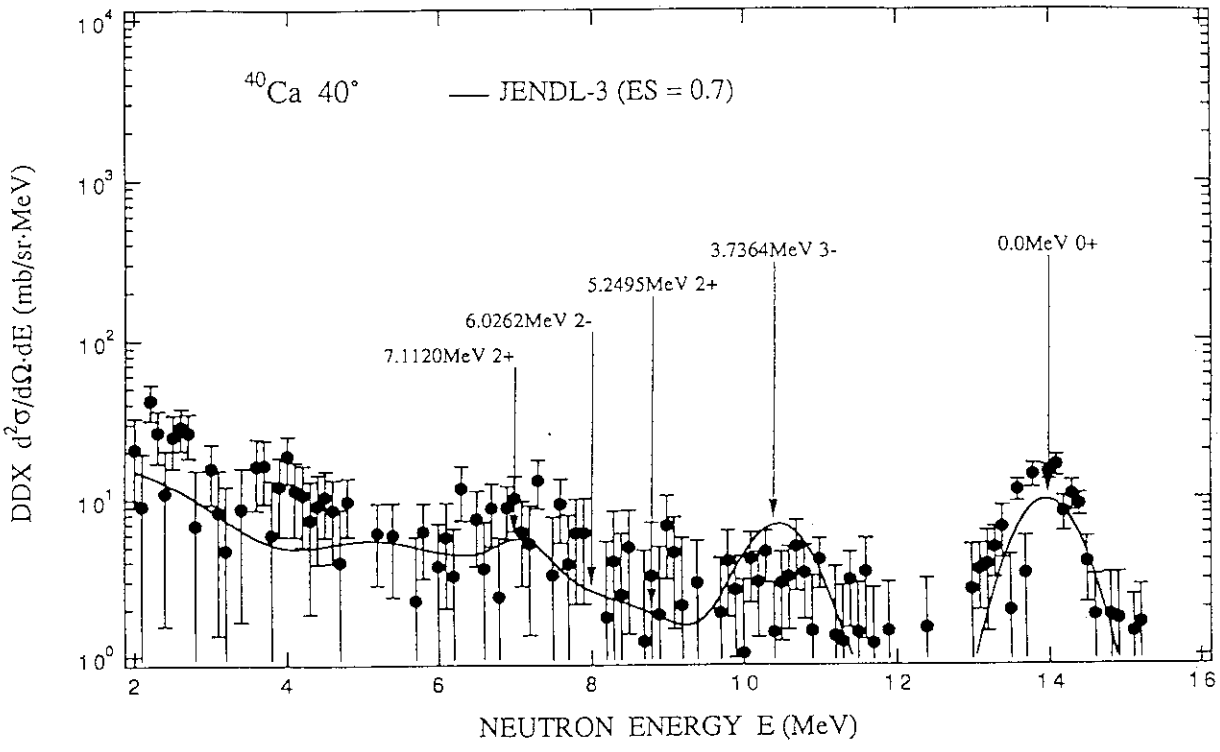

Fig. 4-2 Measured and calculated DDXs for 14.2 MeV neutron scattering from ^{nat}Ca at 40°.

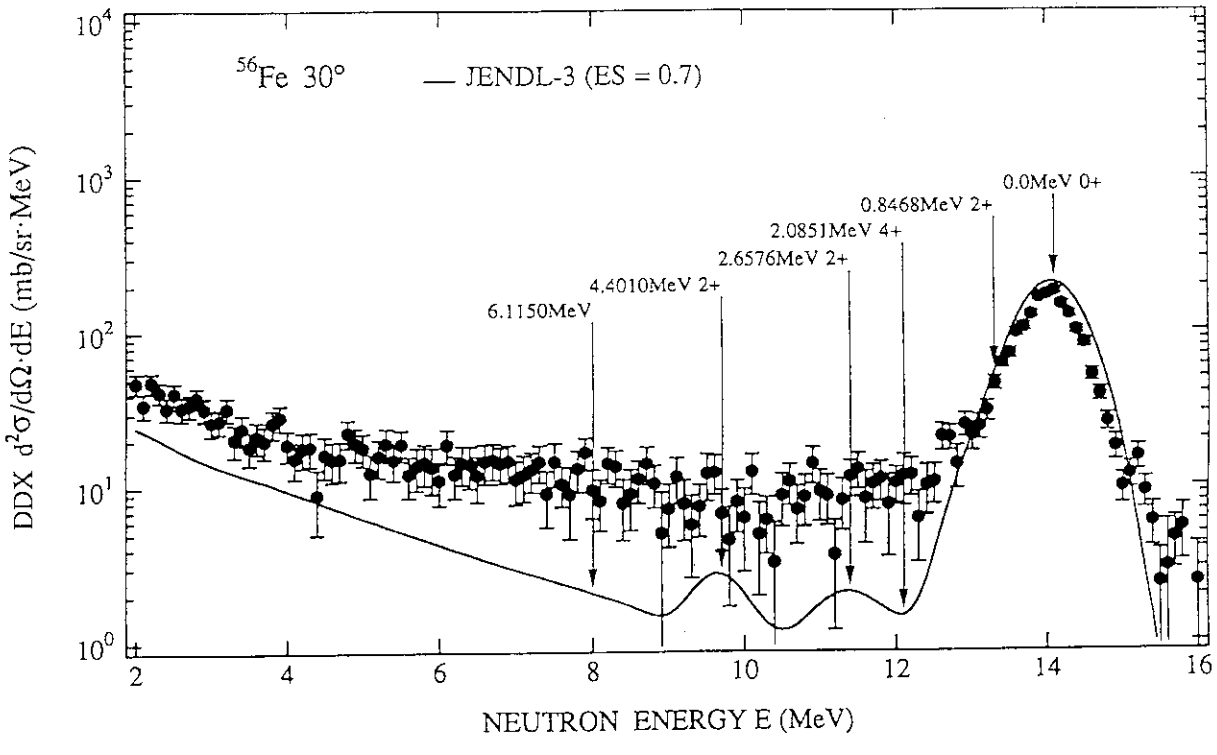

Fig. 5-1 Measured and calculated DDXs for 14.2 MeV neutron scattering from ^{nat}Fe at 30°

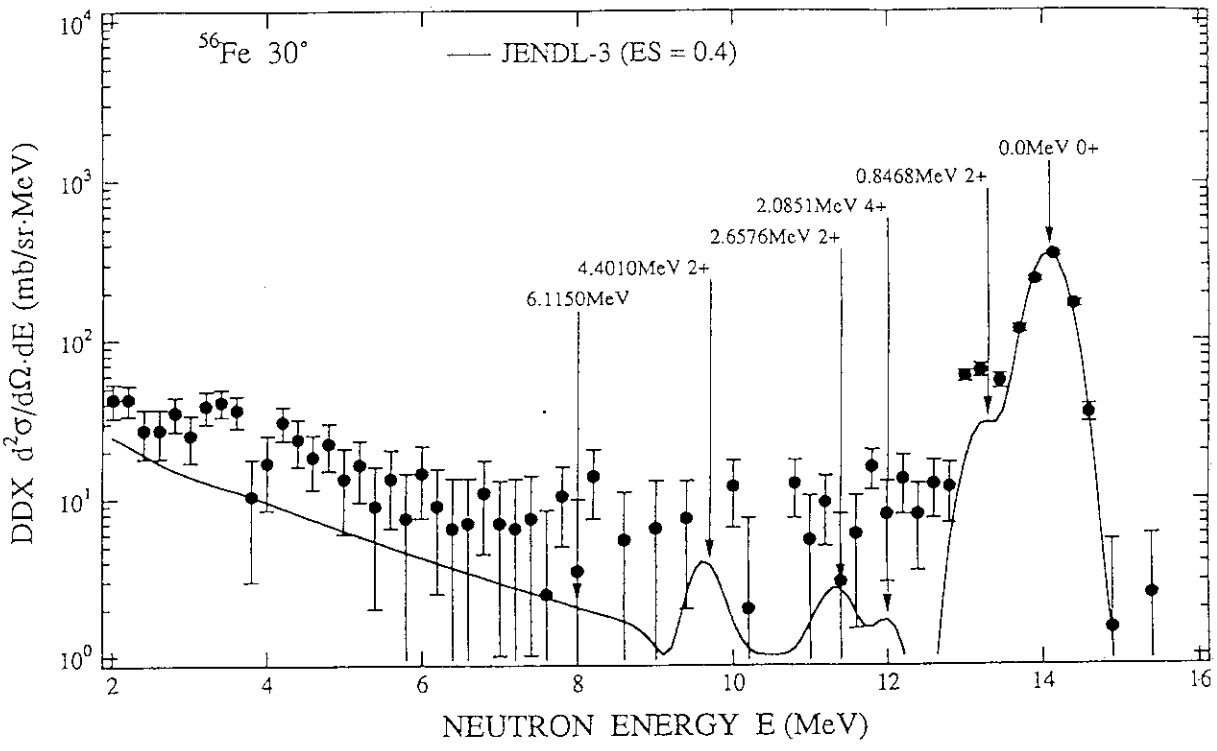

Fig. 5-2 Measured and calculated DDXs for 14.2 MeV neutron scattering from ^{nat}Fe at 30° (2 in ϕ × 2 in data).

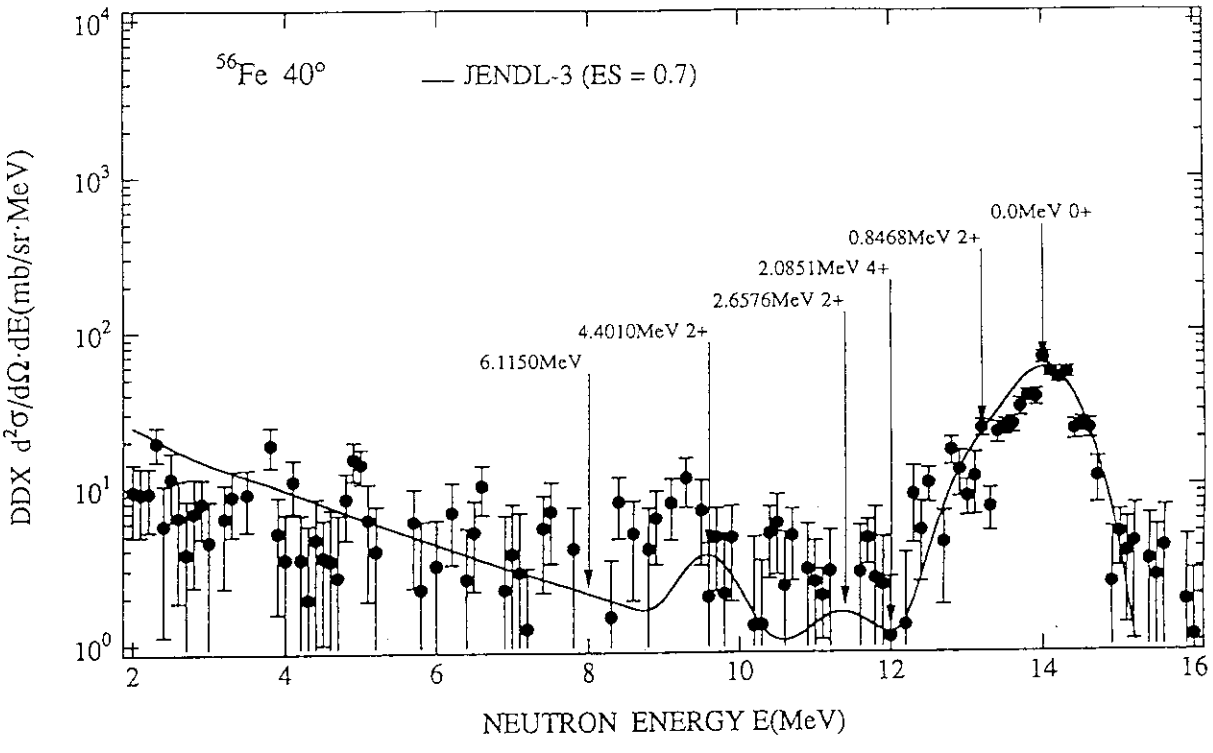

Fig. 5-3 Measured and calculated DDXs for 14.2 MeV neutron scattering from ^{nat}Fe at 40°.

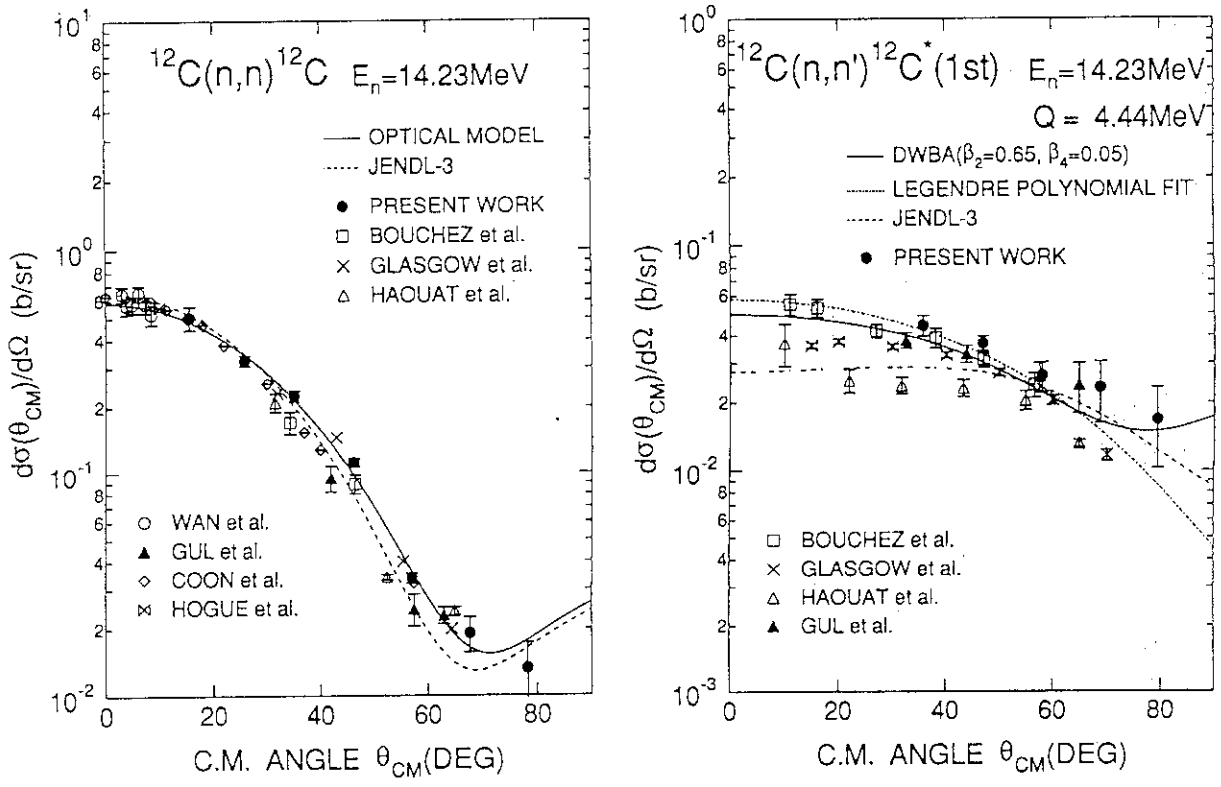

Fig. 6 Measured and calculated angular distributions for elastic and inelastic neutron scattering from ^{12}C.

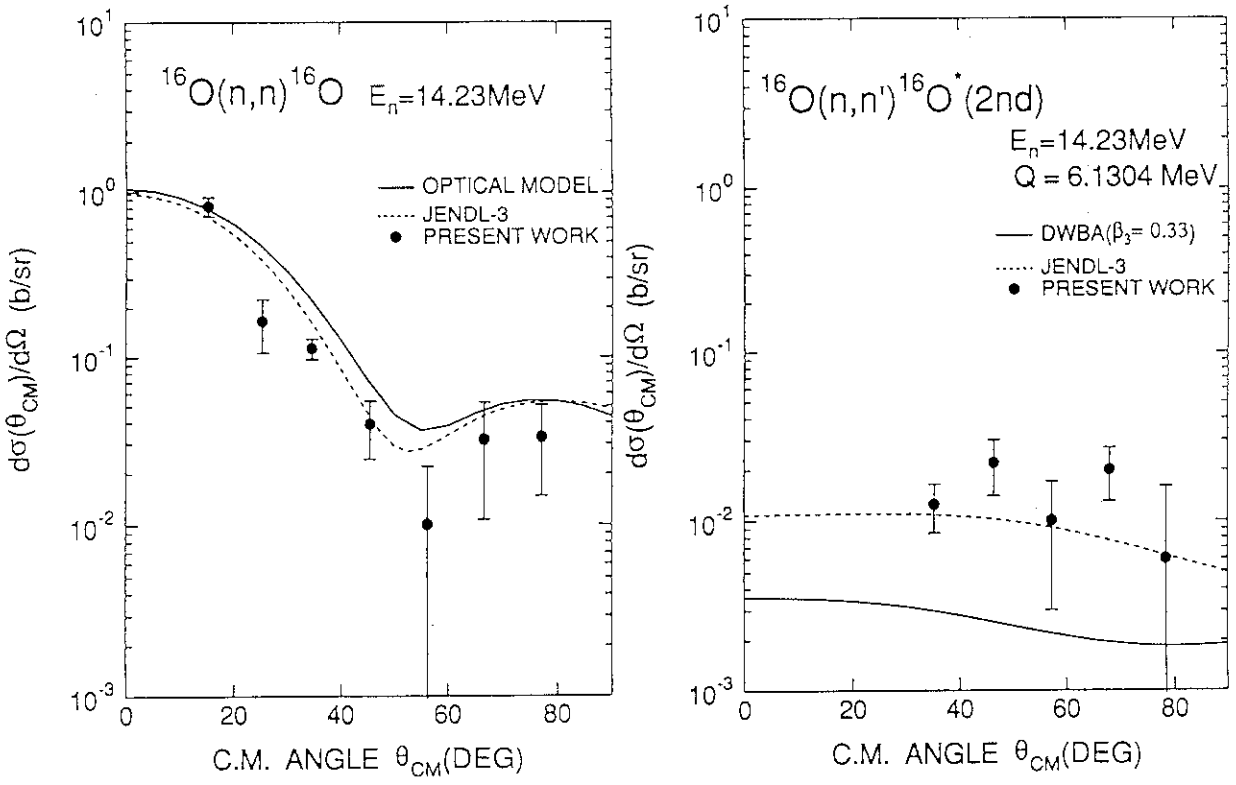

Fig. 7 Measured and calculated angular distributions for elastic and inelastic neutron scattering from ^{16}O.

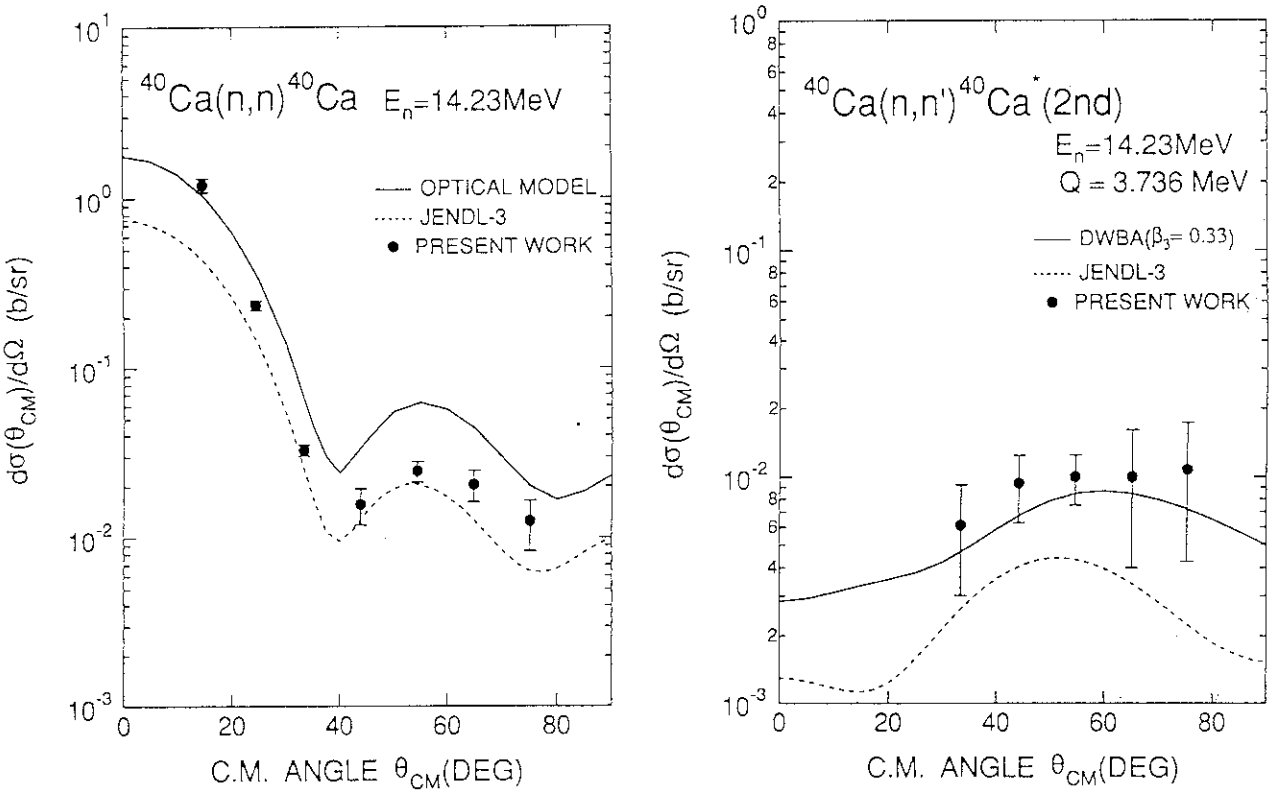

Fig. 8 Measured and calculated angular distributions for elastic and inelastic neutron scattering from ^{40}Ca.

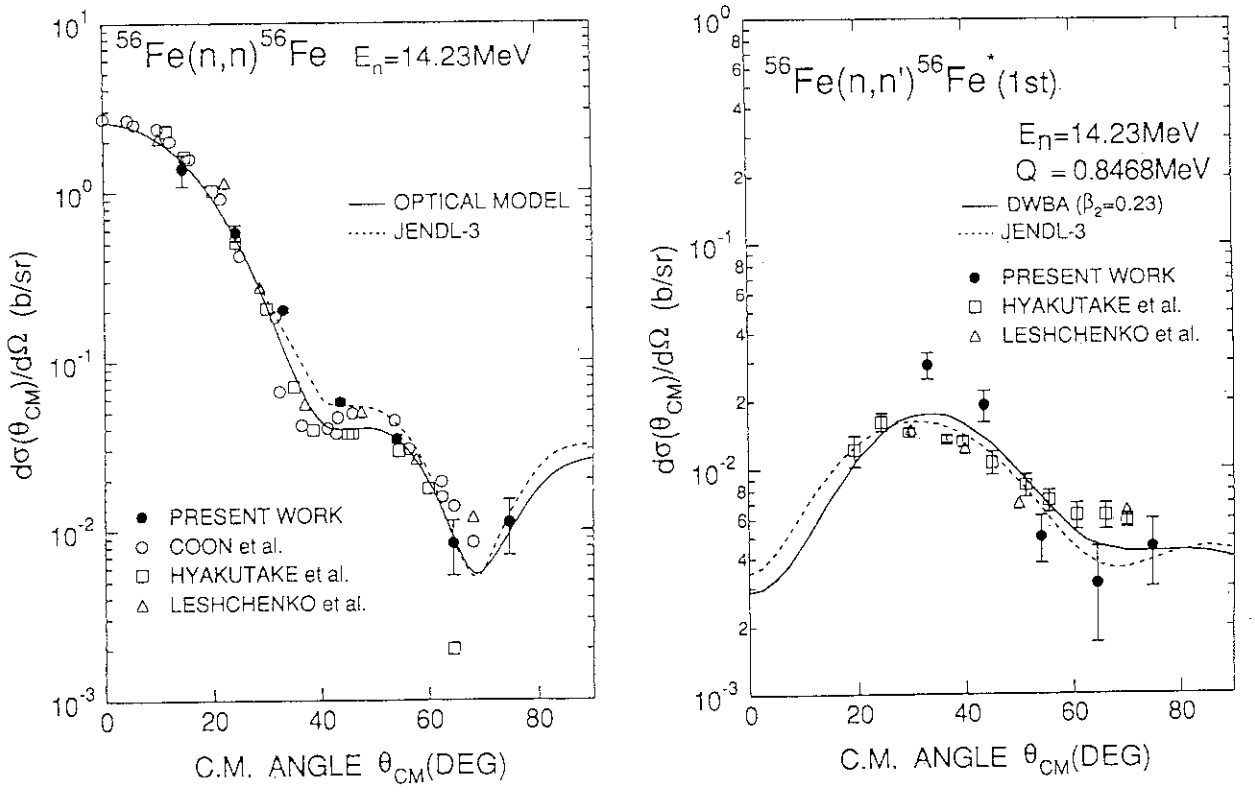

Fig. 9 Measured and calculated angular distributions for elastic and inelastic neutron scattering from ^{56}Fe.

5.9 Characterization of Neutrons Produced from the $^{1}H(^{11}B, n)^{11}C$ Reaction

Shin-ichiro Meigo, Satoshi Chiba and Tokio Fukahori
Japan Atomic Energy Research Institute
Tokai-mura, Naka-gun, Ibaraki-ken 319-11

Abstract

Properties of the neutrons produced from the $^{1}H(^{11}B,n)^{11}C$ reaction, which was proved to be suitable for producing mono-energetic neutrons in the region of 7 to 13 MeV, were measured for precise measurements of neutron cross-section using the $^{1}H(^{11}B,n)^{11}C$ neutron source. Due to poor time resolution, the energy spectra of mono-energetic area could not be measured accurately. The experimental TOF spectra are compared with calculated one that simulated the neutron production inside the H_2 gas target by the Monte-Carlo method. These results will be employed in corrections of previous data and designing future experiments.

1. Introduction

In the fast neutron cross section measurements, monoenergetic neutrons are usually produced by $D(d,n)^{3}He$, $T(d,n)^{4}He$ and $^{7}Li(p,n)^{7}Be$ reactions. However, these reactions cannot produce really monoenergetic neutrons in the energy region between about 8 and 14 MeV because of break up reactions. Consequently, only few neutron data exist in this "gap" region although data in this energy region are important for the development of D-T fusion reactor and TRU incineration reactor driven by proton accelerator.

Recently progress of heavy ion accelerator technology makes new types of monoenergetic neutron generator feasible. At JAERI tandem accelerator, the monoenergetic neutron source produced by the $^{1}H(^{11}B,n)^{11}C$ reaction has been developed[1]. The neutrons produced through the $H(^{11}B,n)^{11}C$ reactions are suitable for producing mono-energetic neutrons about 7 to 13 MeV. This monoenergetic source has been used in activation cross section measurements[2].

In these cross section measurements, the energy spectrum of the neutron was determined by the time-of-flight(TOF) method. Due to a poor time resolution of incident ^{11}B beam, the observed spectra did not represent the "true" neutron spectra needed for the correction of measured cross sections, especially for around the threshold energy of measured cross section.

In this study, the neutron spectra were measured at several incident energies and emission angles with flight paths longer than previous experiments[1]. Then, a Monte-Carlo code was developed in order to calculate the various properties of produced neutrons. The measured spectra are compared with calculated spectra to check reliability of the code. Finally, the characteristics of the neutron spectra produced from the $H(^{11}B,n)^{11}C$ reactions are discussed.

2. Experimental procedure

The measurements of the produced neutrons through the $H(^{11}B,n)^{11}C$ reactions were carried out at JAERI tandem accelerator. The beam condition used in the measurements is 4 MHz cycle repetition burst and 1-10 nA current. The energy of the incident beam was 57.3, 60.0 and 62.7 MeV.

The schematic view of the H_2 gas target assembly is shown by Fig. 1. The pressure of H_2 gas was typically 0.21 MPa. It was monitored by semiconductor vacuum gauge and dc amplifier system. The incident beam current was measured by current integrator with the electrically isolated gas cell. The electron suppression was made with a bias -300 V to repel secondary electrons.

The detector had 5"φx2" size and was located 6~8 m from the target(see Fig. 2). The detector was set in the goniometer to make easy measurement for several emission angles (0,10,20,30 and 35 deg.). Short flight path case with 4 m measurements was also carried out to avoid overlap of neutron, because repetition cycle was 4 MHz. A conventional TOF technique with a pulse-shape n-γ discriminator was used(see Fig. 3). The bias of the discriminator was set at 1 light unit of ^{22}Na corresponding to 3.0 MeV recoiled proton energy. The efficiency of the detector was calculated by O5S code.

Figure 4 shows the typical TOF spectrum of the gas-in case, the gas-out case and the net value that the gas-in spectrum is subtracted gas-out. Both gas in and gas out cases appear the neutron produced from the $^{197}Au(^{11}B,n)$ reaction in the beam stopper. The net value had no lower energy component than monoenergetic peak. The FWHM of the gamma-ray peak had about 4 nsec. Since the detector time resolution is thought to be about 1 nsec, the poor time resolution is though to mainly come from the time deviation of the incident ^{11}B. Figure 5 represents the typical net value of the neutron energy spectrum. The FWHM of the monoenergetic peak was about 2 MeV.

3. Calculation method

A Monte-Carlo code was developed to calculate the true neutron spectra. The broadening of the true spectrum was caused by the incident energy spread at reaction point due to energy loss and with kinematics spread due to solid angle between target and detector. This code simulates the energy broadening caused by these effects as well as energy straggling.

The mean energy loss of incident ^{11}B is calculated by the integral of the stopping power[3]:

$$\overline{\Delta E} = \sum_{\delta_{fo}=0}^{\Delta T_{fo}} \frac{dE}{dX}\Bigg]_{fo} \delta_{fo} + \sum_{\delta_H=0}^{\Delta T_H} \frac{dE}{dX}\Bigg]_{H} \delta_{H}$$

where ΔT_{fo} and ΔT_H are thickness (g/cm^3) of entrance foil and H_2 gas at the reaction point, respectively. ΔT_H is selected by a uniform random number in the range of 0 to the gas cell

length. In the case where the energy loss is small enough ($\chi \leq 10$), the energy spectrum of ^{11}B beam is calculated by Landau-Vavilov distribution[4]:

$$f(\chi, \overline{\Delta E}) = \frac{\chi}{\pi \xi} e^{(1+\beta^2)\chi} \int_0^\infty e^{\chi f_1} \cos(y\lambda_1 + \chi f_2) dy,$$

$$f_1 = \beta^2 (\ln y - Ci(y)) - \cos y - ySi(y), \quad f_2 = y(\ln y - Ci(y)) + \sin y + \beta^2 Si(y)$$

$$\xi = 0.3 \frac{m_e c^2}{\beta^2} \cdot \frac{Z}{A} \cdot z^2 \Delta T, \quad \varepsilon_{max} = \frac{2 m_e c^2 \beta^2}{1-\beta^2}$$

$$\chi = \frac{\xi}{\varepsilon_{max}}, \quad \lambda_1 = \frac{(\Delta E - \overline{\Delta E})}{\varepsilon_{max}} - \chi(1 + \beta^2 - C_{Euler})$$

where Z and A are the atomic number and the atomic mass of the media respectively, z is the atomic number of the incident particle, m_e is electron mass, βc is a particle velocity, C_{Euler} is Euler's constant, and Si and Ci are the integral function of sine and cosine respectively. The energy loss (ΔE) of individual particles is calculated by:

$$R = \int_{\Delta E}^{\infty} f(\chi, \overline{\Delta E}) \Big/ \int_0^{\infty} f(\chi, \overline{\Delta E})$$

where R is the uniform random number from 0 up to 1. If χ is larger than 10, the energy struggling is calculated by Bohr theory in which the energy loss distribution is represented by the Gaussian with standard deviation (σ):

$$\sigma = 2\pi^2 e^2 z \sqrt{\frac{ZN\Delta T}{A}}$$

where N is the Avogadoro number.

The neutron spectrum at the detector point is calculated by taking the energy dependence and kinematics of the $H(^{11}B,n)^{11}C$ reaction into account. The cross sections of the inverse reaction $^{11}B(p,n)^{11}C$[5] were used instead of the $H(^{11}B,n)^{11}C$ reaction.

The TOF spectrum was calculated by folding the neutron spectrum with the resolution function that was determined from the prompt γ-ray peak of the measurements. The time deviation due to spread of detection point was typically 0.2 nsec. This deviation was negligibly smaller than time uncertainty of the detection system (4.0 nsec).

4. Result and Discussion

4.1 Observed Spectra

At various incident energies(57.3,60.0 and 62.7 MeV) and emission angles(0,20,30 and 35-deg.), the measured and the calculated TOF spectra are shown in Figs 6 and 7 respectably. The folding calculated results reproduced the observed spectra quite favorably at various incident energies and emission angles.

The neutron energy spectra are shown by Fig 8 at various emission angles. The neutron

spectrum observed at 0-deg has stronger intensity than calculated spectrum. This difference comes from the error of the cross section for neutron emitted at 0-deg. Since the neutron emitted at 0-deg corresponds to emitted at 180-deg through the $^{11}B(p,n)$ reaction, this emitted cross section is thought to have many errors. Figure 9 shows normalized distributions at various energies. The calculated results reproduced the measure spectra well except for the absolute intensity differences. The results show a characteristic fluctuation that reflects the energy dependence of this reaction.

4.2 True Spectra

Figure 10 and 11 represent the true spectra at various incident energies and various emission angles, respectably. The standard deviation of the energy spectrum of the incident boron caused by straggling is 100 keV and caused by reaction point duration is 800 keV. Because the energy straggling is much smaller than the energy spread caused by reaction point duration, the neutron spectra have nearly rectangular shapes. Since the reaction cross section has several resonaces, the shapes of the neutron spectra have corresponding peaks. The full width at half maxim of the true spectra is about two times narrower than observed.

4.3 Statistical properties

To correct for the cross sections measured with the neutrons produced from the $H(^{11}B,n)^{11}C$ reaction, various characteristics on the true energy spectrum of this reaction, i.e., the mean energy, standard deviation, FWHM, skewness and kurtosis, have been calculated. At several gas pressures of the target, these properties are shown in fig 12. This shows that the mean energy of the neutron is linearly increasing as incident energy and the FWHM of the neutron is narrower than observed one. The structure in skewness and kurtosis have correspondence in the energy dependence of reaction cross section of $H(^{11}B,n)^{11}C$ (see fig 13). These results will be employed in further correction of the neutron cross section measurements.

5. Conclusion

A Monte-Carlo code was developed to calculate the true spectrum of neutron produced from the $H(^{11}B,n)^{11}C$ reaction. This calculation code simulated neutron spectra from incident boron to the neutron at detection point. The calculated spectrum with folding time resolution was in good agreement with the observed one. The true spectra and statistical properties of neutrons produced from the $H(^{11}B,n)^{11}C$ reaction were calculated and will be used in the correction of the measured data.

References

1. S. Chiba, M. Mizumoto, K. Hasegawa, Y. Yamanouti, M. Sugimoto, Y. Watanabe and M. Drosg, Nucl. Instr. Method A281,581(1989).
2. Y. Ikeda, C.Konno, M. Mizumoto, K.Hasegawa, S.Chiba, Y. Yamanouti and M. Sugimoto, "Activation Cross Section Measurement at Neutron Energies of 9.5,11.0,12.0 and 13.2 MeV Using $^{1}H(^{11}B,n)^{11}C$ Neutron Source at JAERI", Proc. of Int. Conf. of Nuclear Data for Science and Technology, 13th－17th May, 1991, Springer－Verlag, p.294(1992).
3. F. Hubert, R. Bimbot and H. Gauvin, "Range and Stopping－Power Tables for 2.5－500 MeV/Nucleon Heavy Ion In Solids", Atomic and Nuclear Data Tables 46, 1－213(1990).
4. P. Vavilov, Soviet Phys. JETP 5 , p.749(1957)
5. M. Drosg, program NEUYIE, obtainable from the Nuclear Data Section of IAEA, Vienna, computer code DROSG－87: Neutron Source Reactions, ed O. Schwere (1987).

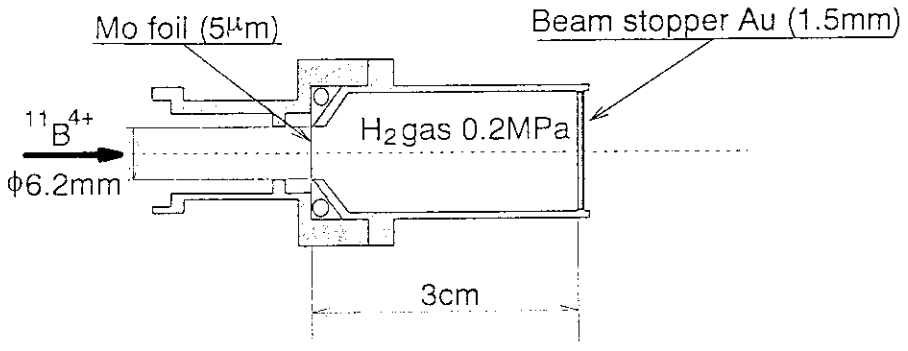

Fig. 1 Schematic view around the H_2 gas target.

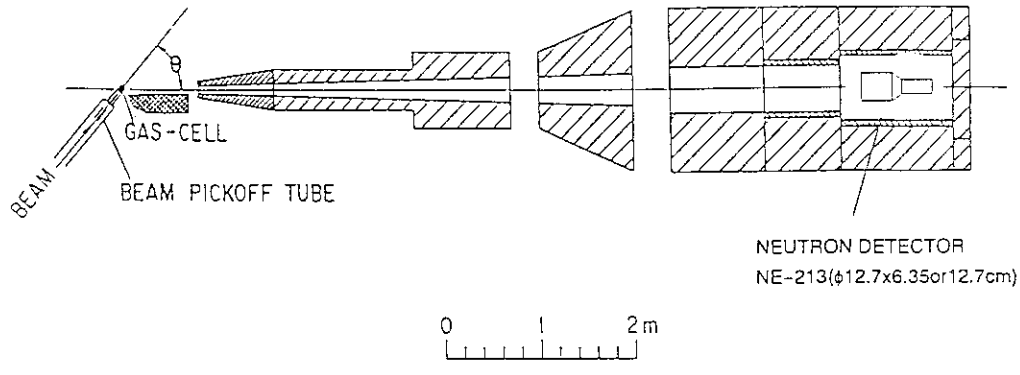

Fig. 2 Schematic view of the gas target and around the detector.

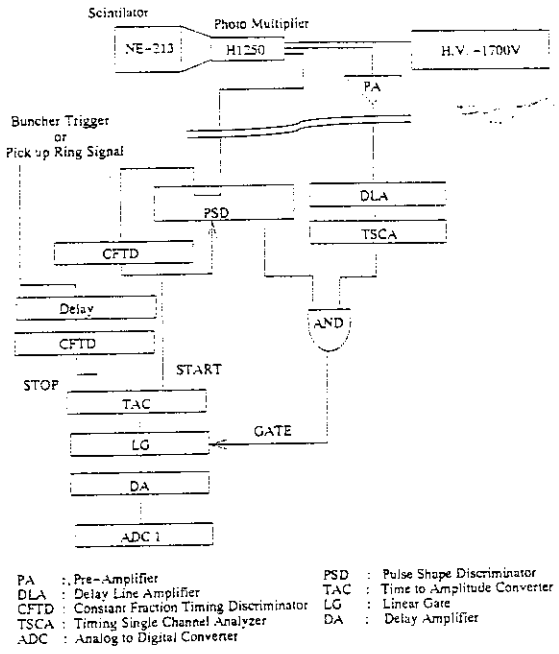

Fig. 3 Block diagram of the electronic circuit used in the measurement of neutron spectrum.

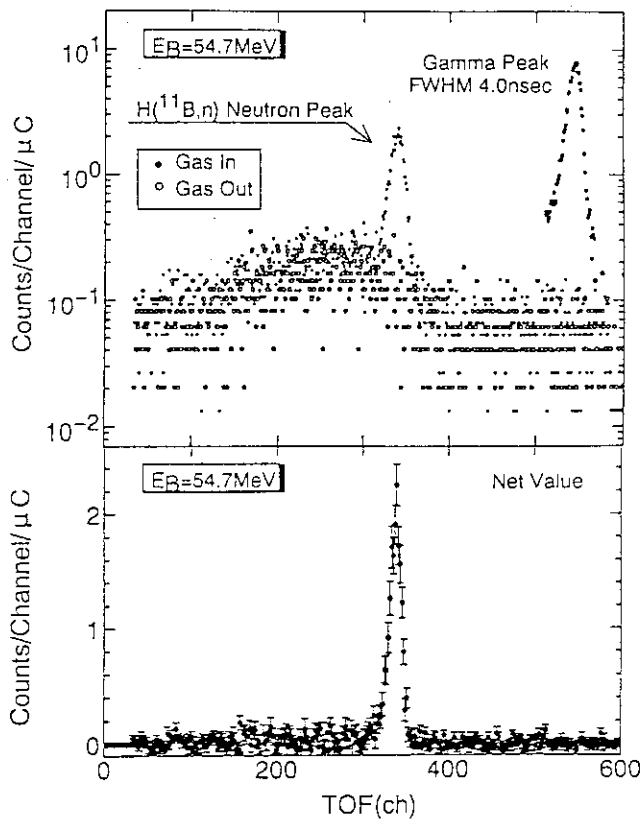

Fig. 4 Typical TOF spectrum of the gas-in case and the gas-out case and net value.

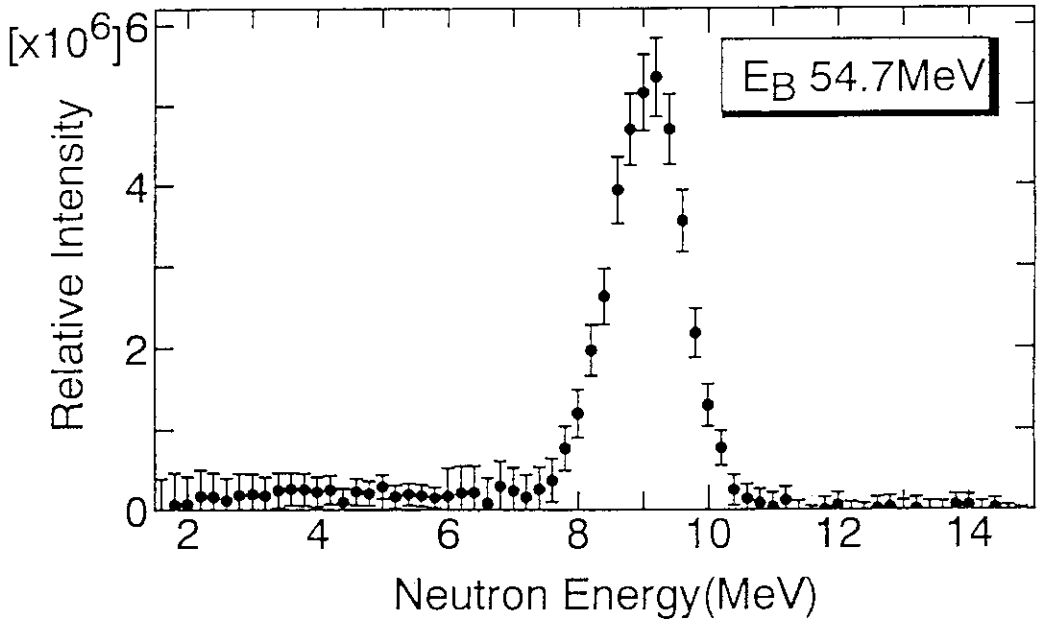

Fig. 5 Typical net neutron spectrum.

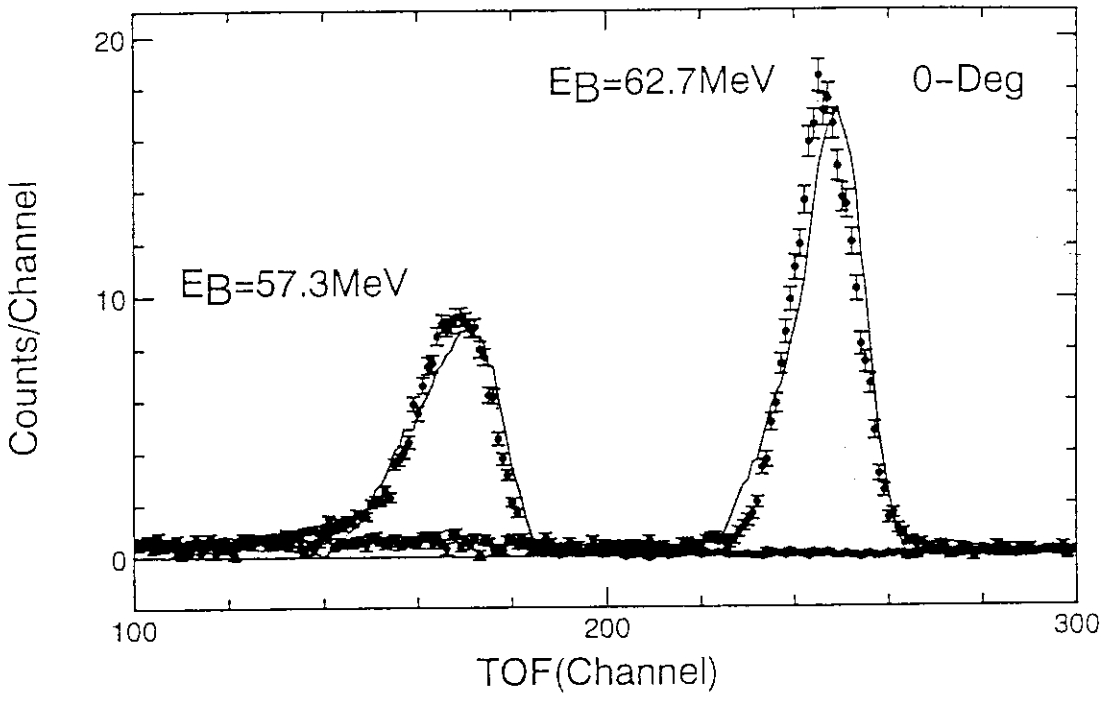

Fig. 6 Observed and calculated TOF spectra at various ^{11}B incident energies (one channel equals 0.4 nsec).

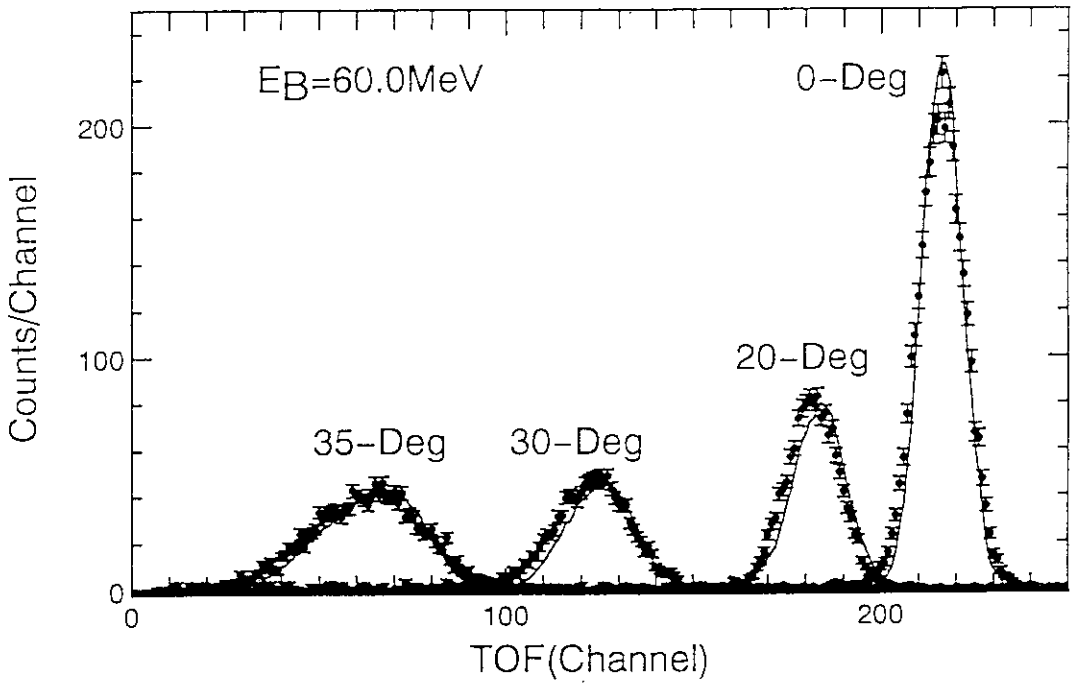

Fig. 7 Observed and calculated TOF spectra at several emission angles (one channel equals 0.4 nsec).

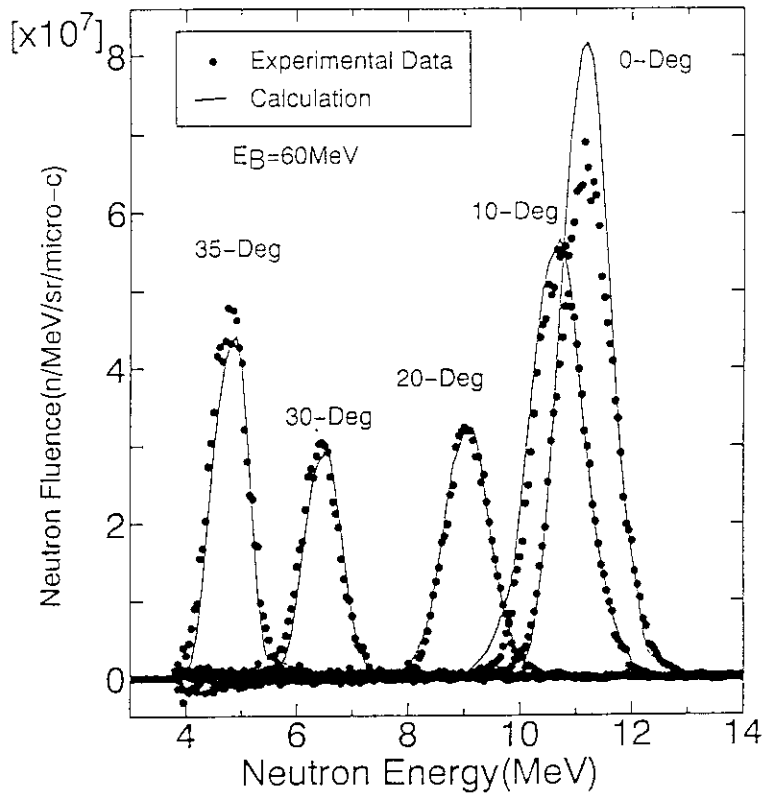

Fig. 8 Observed and calculated energy spectra at several emission angles.

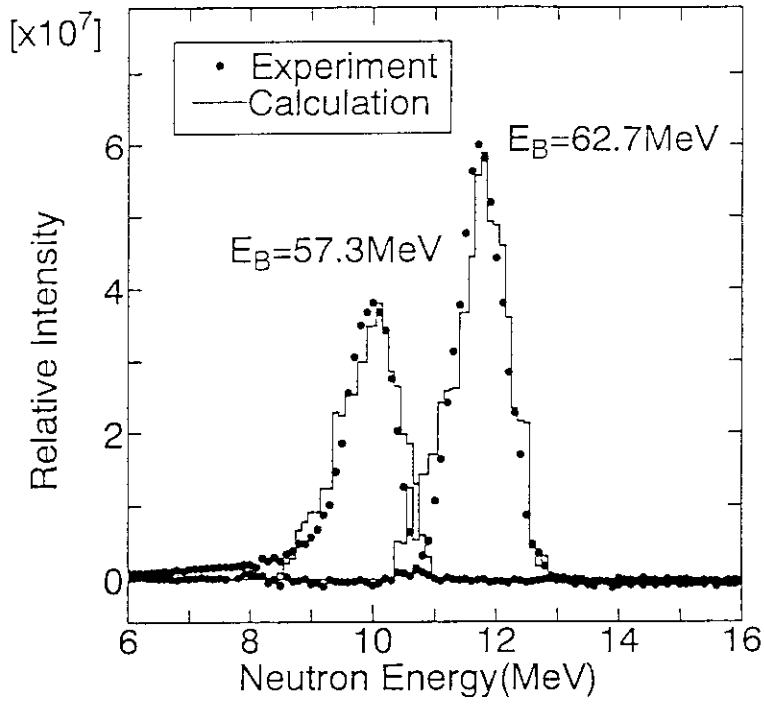

Fig. 9 Observed and calculated energy spectra at several ^{11}B incident energies. The calculated value is normalized to fit the observed peak.

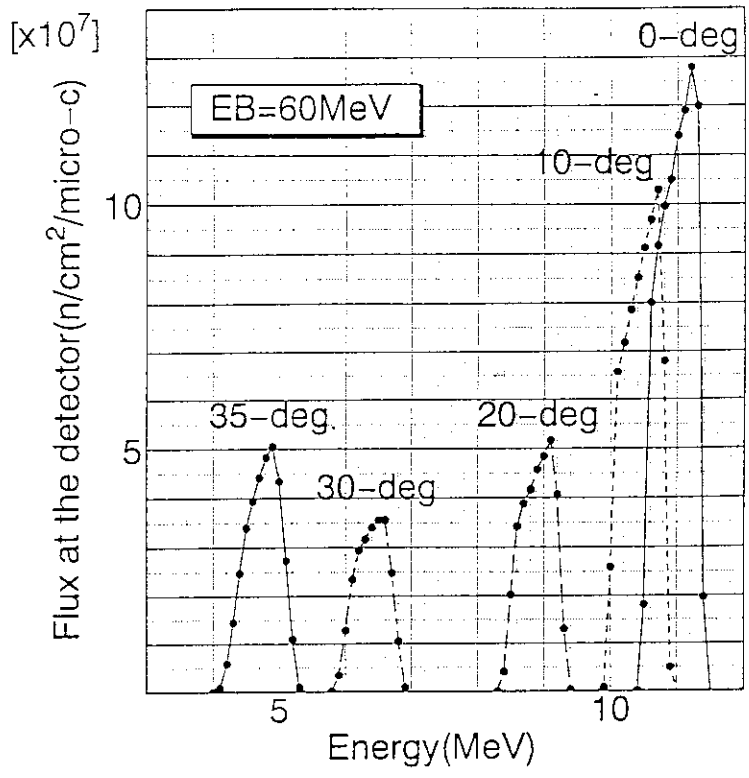

Fig. 10 True neutron spectra at several emission angles.

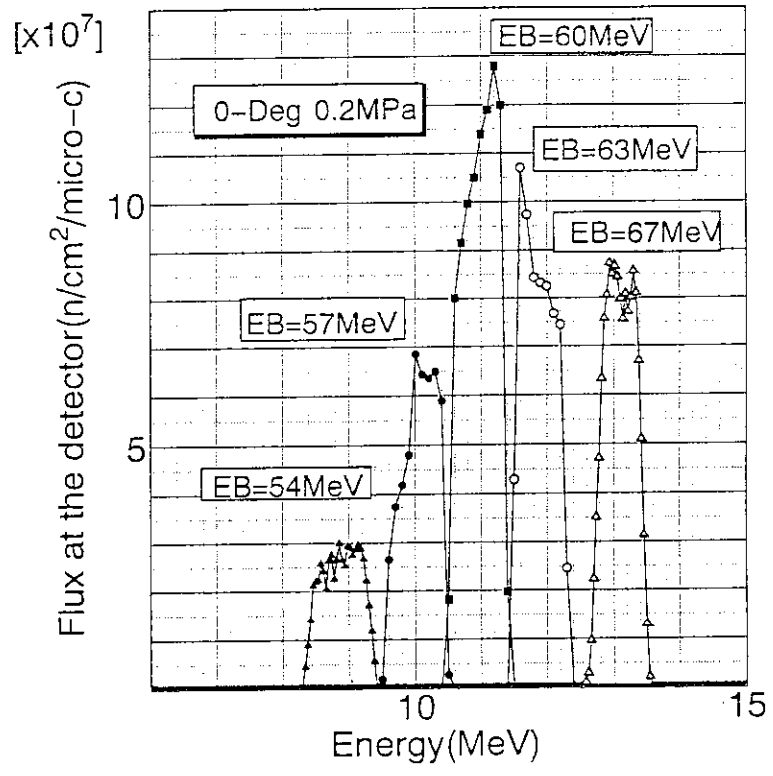

Fig. 11 True neutron spectra at various ^{11}B incident energies.

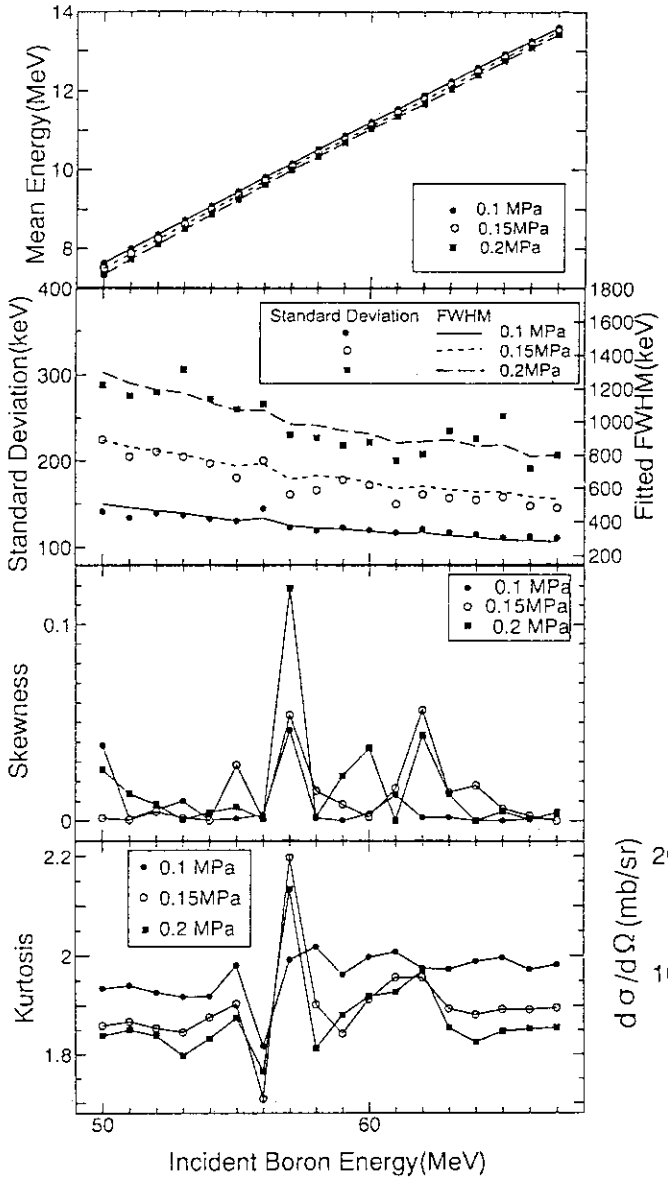

Fig. 12 Statistical properties of the neutron produced from the $H(^{11}B,n)^{11}C$ reaction at several pressure of the gas target. The FWHM is obtained by fitting Gaussian distribution.

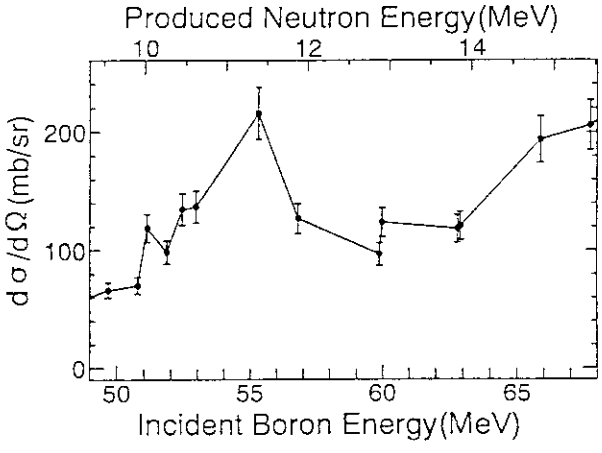

Fig. 13 Excitation function of the neutron production by the $H(^{11}B,n)$ reaction at 0° in the laboratory system. This function is obtained from $^{11}B(p,n)$ cross section.

5.10 Measurement of Formation Cross Sections Producing Short-lived Nuclei —Mg, S, Ga, Y, Mo, Pd, Sn—

K. Yamauchi, Y. Kasugai, H. Yamamoto, *A. Takahashi, *T. Iida
and K. Kawade
Department of Nuclear Engineering, Nagoya University
*Department of Nuclear Engineering, Osaka University

Abstract

Neutron activation cross sections of short-lived nuclei with half-lives between 40 s and 18 min. have been systematically measured at neutron energy of 13.4 to 14.9 MeV by activation method. Cross sections for ^{26}Mg(n,np)^{25}Na, ^{32}S(n,t)^{30}P, ^{71}Ga(n,α)^{68m}Cu, ^{98}Mo(n,np)^{97m}Nb, ^{100}Mo(n,np)^{99m}Nb, ^{106}Pd(n,np)^{105m}Rh and ^{119}Sn(n,p)^{119m}In were measured.

1 Introduction

We have carried out a measuring program for activation cross sections of short-lived nuclei around 14MeV neutrons at the Intense 14MeV Neutron Source Facility (OKTAVIAN) at Osaka University since 1988. Up to now 65 cross sections for (n,2n), (n,p), (n,np), (n,t) and (n,α) reactions leading to short-lived nuclei were measured in qualified experimental condition[1] − [4].

In this work 7 reactions were measured again in energy range from 13.4MeV to 14.9MeV for Mg, S, Ga, Y, Mo, Pd and Sn. The ^{100}Mo(n,np)^{99m}Nb reaction was newly measured at 14.9MeV

2 Experiment and Results

Experiments were performed at OKTAVIAN. For the activation of sample, pneumatic tubes were set at 6 directions (between 0°, 50°, 75°, 105°, 125° and 155°) for incident beam direction. The distance between the T-target and irradiation points were between 5.5 and 8.5 cm(see Fig.1).The induced activities were measured with two Ge detectors(12%, 16%) at an equivalent distance of 5cm. The effective neutron energies were determined by the Zr/Nb method[5](see Fig.2). The errors are estimated to be about 90 keV. The neutron flux at the irradiation points was monitored by using two aluminium foils (purity:99.2%, 1cm×1cm×0.2mm^t). The reference reaction for the flux measurement was the ^{27}Al(n,p)^{27}Mg (9.46 min.), which was determined by referring to the standard ^{27}Al(n,α)^{24}Na reaction (ENDF/B-V). Separated isotopes or natural samples were used for irradiation. The samples were between 38 and 100 mg in weight (size: 1cm×1cm).

In Table 1, measured reactions and associated data[6] of the half-life ($T_{1/2}$), the γ-ray energy (E_γ), the absolute intensity in photons per disintegration (I_γ) are listed together with Q-value.

Corrections were made for time fluctuation of neutron flux, thickness of samples, self absorption of γ-ray, sum-peak effect of γ-ray, interfering reactions and contribution of low energy neutrons below 10MeV. The details of the correction are described in Ref.[1].

The total errors (δ_t) were described by combining the experimental error (δ_e) and the error of nuclear data (δ_r) in quadratic:

$$\delta_t^2 = \delta_e^2 + \delta_r^2$$

Estimated major sources of the errors are listed in Table 2. The results are listed in Table 3. and shown in Fig.3. Evaluated data include both meta stable and ground state cross section.

3 Summary

Accuracy of the obtained cross sections were around 10% in case of good statistics. For the ^{100}Mo(n,np)^{99m}Nb reaction the cross section was measured for the first time.

References

[1] T. Katoh, K. Kawade and H. Yamamoto: JAERI-M 89-083, (1989)(in Japanese)

[2] K. Kawade, H. Yamamoto, T. Yamada, T. Katoh, T. Iida and A. Takahashi: JAERI-M 90-171,(1990)

[3] K. Kawade, H. Yamamoto, T. Kobayashi, T. Katoh, T. Iida and A. Takahashi: JAERI-M 92-020, (1992)

[4] Y. Kasugai, A. Tanaka, M. Asai, H. Yamamoto, T. Katoh, T. Iida, A. Takahashi and K. Kawade: JAERI-M 93-124,(1993)

[5] V. E. Lewis and K. J. Zieba: Nucl. Instr. Meth. 140,337,(1980)

[6] E. Browne et al.: Table of Radioactive Isotopes, (1986) John Wiley & Sons, New York

Table 1 Measured reactions and decay parameters (taken from Ref.6).

Reaction[a)]	$T_{1/2}$	E_γ(keV)	I_γ(%)	Q(MeV)[b)]
^{26}Mg(n,np)^{25}Na	59.6(7)s	389.7	12.65(71)	−14.14
^{32}S(n,t)^{30}P	2.498(4)min.	511	200	−12.69
^{71}Ga(n,α)^{68m}Cu	3.75(5)min.	525.7	75(15)	0.34
^{89}Y(n,α)^{86m}Rb	1.017(3)min.	556.1	98.19(10)	0.13
^{98}Mo(n,np)^{97m}Nb	1.00(13)min.	743.3	97.95(10)	−10.54
^{100}Mo(n,np)^{99m}Nb	2.6(2)min.	253.5	3.70(42)	−11.52
^{106}Pd(n,np)^{105m}Rh	42.4(5)s	129.6	20.0(4)	−9.35
^{119}Sn(n,p)^{119m}In	18.0(3)min.	311.4	0.99(20)	−1.86
^{27}Al(n,α)^{24}Na[c)]	14.959h	1368.6	99.994(3)	−3.13
^{27}Al(n,p)^{27}Mg[d)]	9.46min.	843.8	72.0(4)	−1.83

a) (n,np) means [(n,d) + (n,n'p) + (n,pn)]

b) Q(n,n'p) is given here. Q(n,d) = Q(n,n'p) + 2.225 MeV.

c) Standard reaction (ENDF/B-V) used in this work.

d) Secondary conventional reaction used for short-lived nuclei

Table 2 Principal sources of uncertainty in the measured cross sections.

Experimental error (δ_e)	
Source of error	Uncertainty(%)
Counting statistics	4 – 77
Sample mass and purity	0.1
Neutron flux fluctuation	< 0.6 (20% of correction)
γ-peak area evaluation	0.5
Detector efficiency	1.5 (E_γ > 300keV)
	3 (300 – 80keV)
	5 (E_γ < 80keV)
Efficiency calibration at 0.5 and 5 cm	2.0
Correction for	
true coincidence sum	< 0.5
random coincidence sum	0.2 – 4 (20% of correction)
sample thickness	0 – 0.5 (20% of correction)
self-absorption of γ-rays	0 – 0.7 (20% of correction)
low energy neutrons	0 – 0.7 (30% of correction)
Secondary reference cross section	
for ^{27}Al(n,p)^{27}Mg	0.5 (Only statistics)
Error of nuclear data (δ_r)	
Source of error	Uncertainty(%)
Reference cross section	
^{27}Al(n,α)^{24}Na (ENDF/B-V)	3.0
Absolute γ-ray intensity	0 – 20
Half-life	0 – 10

The total errors(δ_t) were derived by combining the experimental error(δ_e) and the error of nuclear data(δ_r) in quadratic: $\delta_t^2 = \delta_e^2 + \delta_r^2$

Table 3 Results of cross section measurement.

$^{26}Mg(n,np)^{25}Na$ (59.6s)					$^{32}S(n,t)^{30}P$ (2.498min.)			
E_n (MeV)	σ(mb)	δ_e(%)	δ_r(%)	δ_t(%)	σ(μb)	δ_e(%)	δ_r(%)	δ_t(%)
14.87	3.64	7.0	6.5	9.6	21.2	12	3.0	12
14.58	2.83	8.4	6.5	11	17.4	19	3.0	19
14.28					11.2	33	3.0	33
13.88	1.05	23	6.5	24	7.4	42	3.0	42
13.65	0.21	77	6.5	77	6.0	33	3.0	33
13.40								
$^{71}Ga(n,\alpha)^{68m}Cu$ (3.75min.)					$^{89}Y(n,\alpha)^{86m}Rb$ (1.017min.)			
E_n (MeV)	σ(mb)	δ_e(%)	δ_r(%)	δ_t(%)	σ(mb)	δ_e(%)	δ_r(%)	δ_t(%)
14.87	1.77	4.2	20	20	2.63	8.0	3.0	8.5
14.58	1.90	4.3	20	20	2.09	7.8	3.0	8.4
14.28	1.69	5.7	20	21	1.88	11	3.0	11
13.88	1.14	6.4	20	21	1.29	17	3.0	17
13.65	1.26	4.8	20	21	1.54	11	3.0	11
13.40	1.22	6.2	20	21	1.24	16	3.0	16
$^{98}Mo(n,np)^{97m}Nb$ (1.00min.)					$^{100}Mo(n,np)^{99m}Nb$ (2.6min.)			
E_n (MeV)	σ(mb)	δ_e(%)	δ_r(%)	δ_t(%)	σ(mb)	δ_e(%)	δ_r(%)	δ_t(%)
14.87	1.09	7.7	13	15	0.41	24	14	28
14.58	0.79	11	13	17				
14.28	0.39	23	13	26				
13.88	0.24	27	13	30				
13.65	0.14	27	13	30				
13.40								
$^{106}Pd(n,np)^{105m}Rh$ (42.4s)					$^{119}Sn(n,p)^{119m}In$ (18.0min.)			
E_n (MeV)	σ(mb)	δ_e(%)	δ_r(%)	δ_t(%)	σ(mb)	δ_e(%)	δ_r(%)	δ_t(%)
14.87	1.42	15	3.8	15	3.51	20	20	28
14.58	1.72	12	3.8	13	2.88	27	20	34
14.28	1.05	17	3.8	17				
13.88	0.64	32	3.8	32				
13.65	0.58	30	3.8	30	2.62	34	20	39
13.40	0.59	45	3.8	45	2.35	16	20	25

Error of neutron energy is estimated as about 90keV.

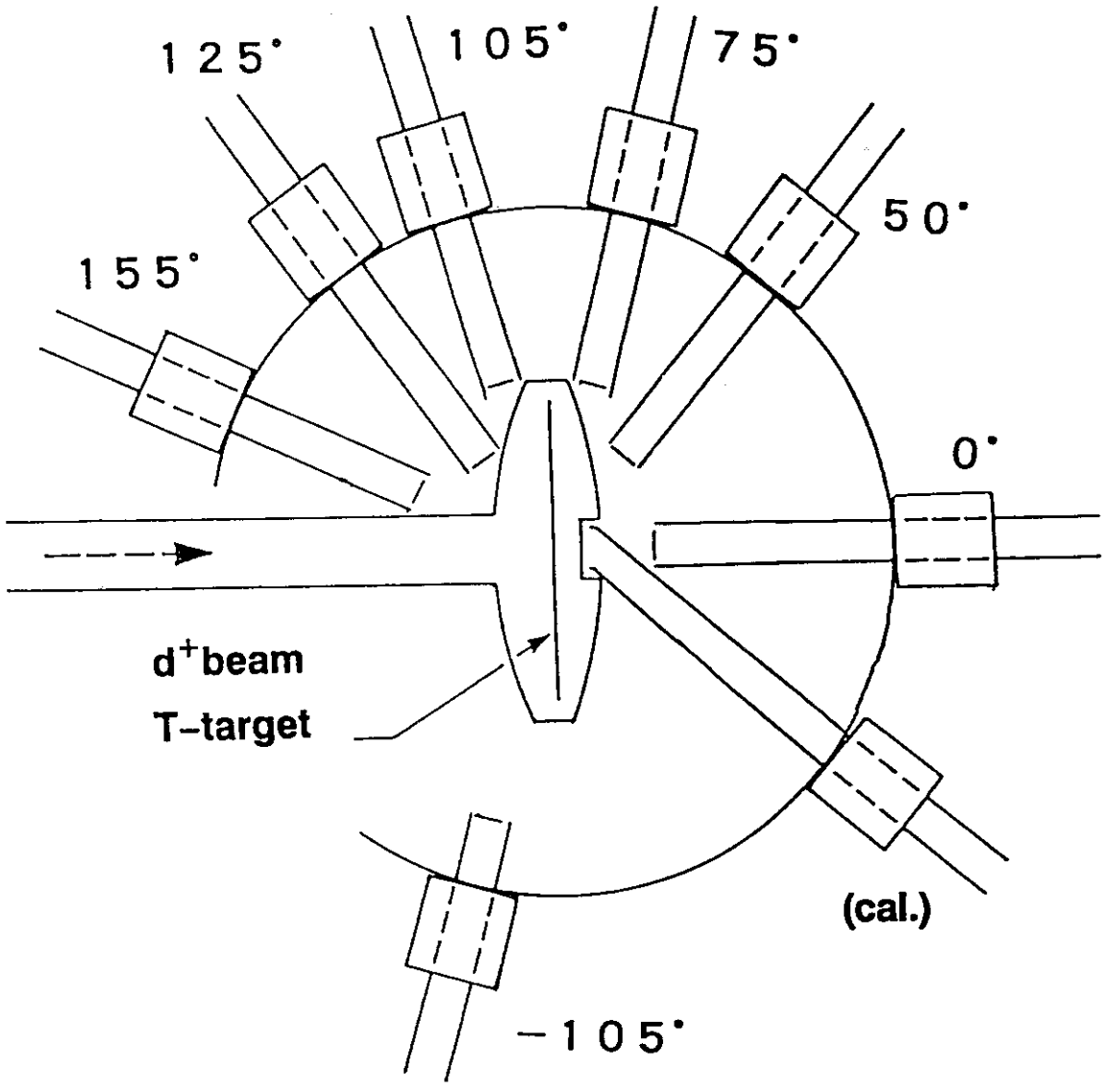

Fig. 1 Pneumatic sample transport system at OKTAVIAN. The distance between T-target and the irradiation points were 5.5cm(0°), 5.5cm(50°), 8.0cm(75°), 8.5cm(105°), 6.5cm(125°), 7.5cm(155°), 14.5cm(-105°), and 1.5cm(cal.).

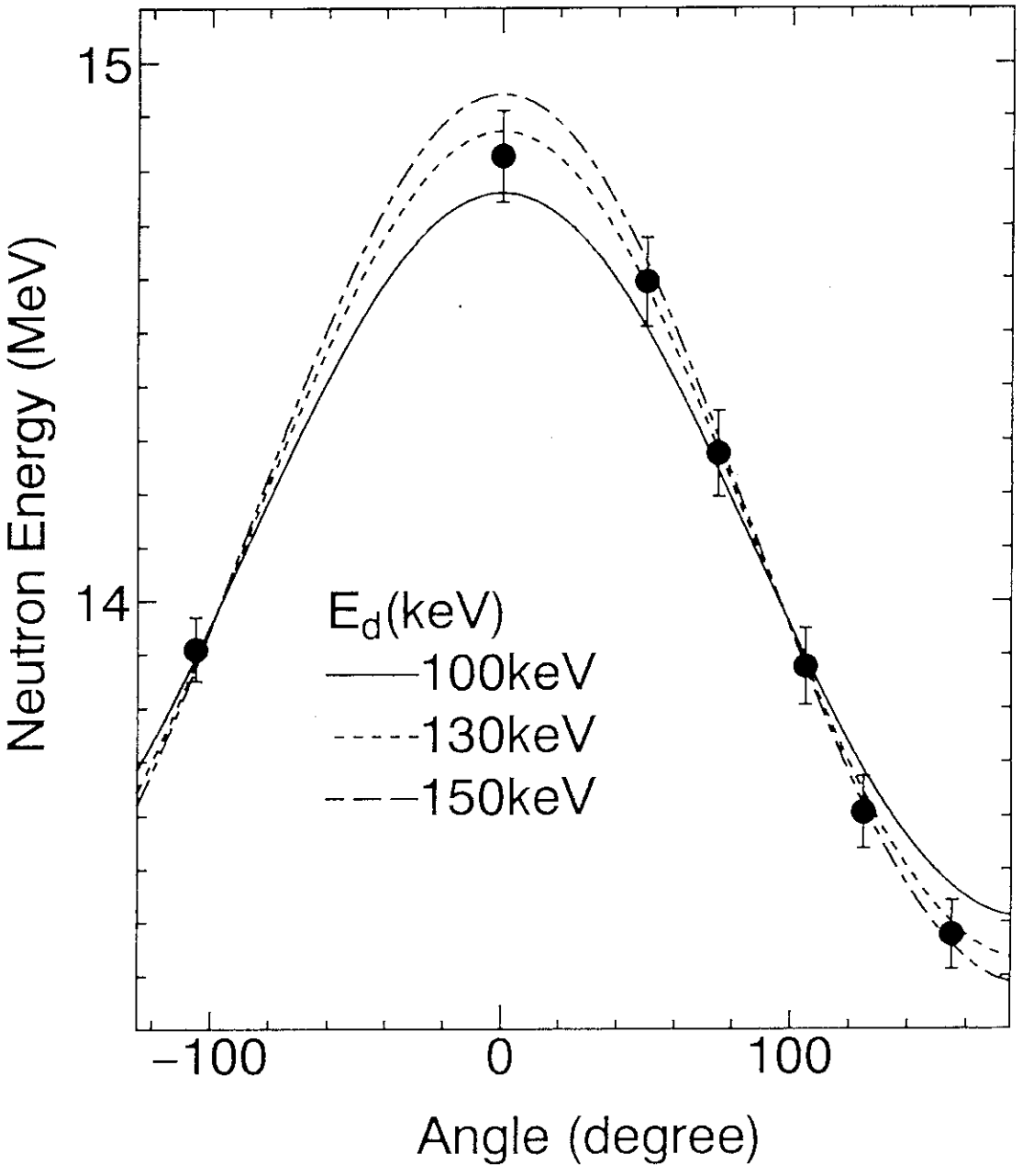

Fig. 2 Angular dependence of d-T neutron energy. The best fitting value of E_d (effective d^+ energy) is 130keV.

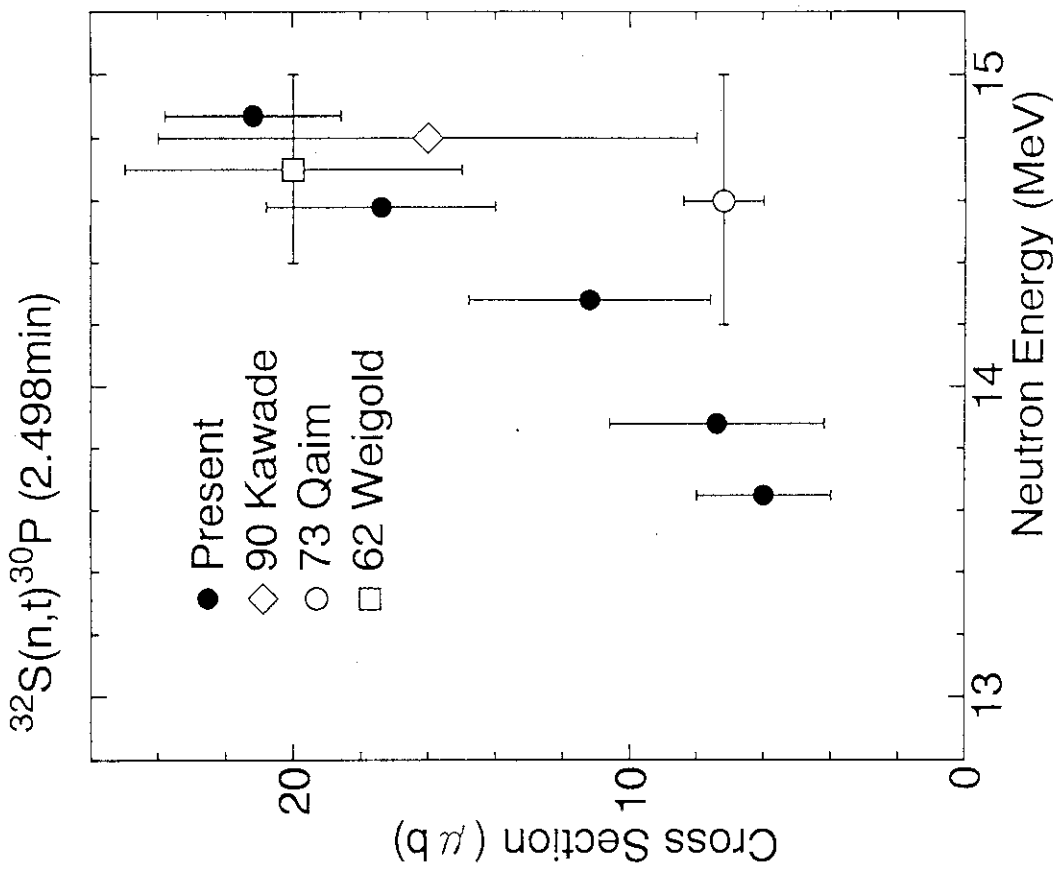

Fig. 3-2 Cross section of $^{32}S(n,t)^{30}P$.

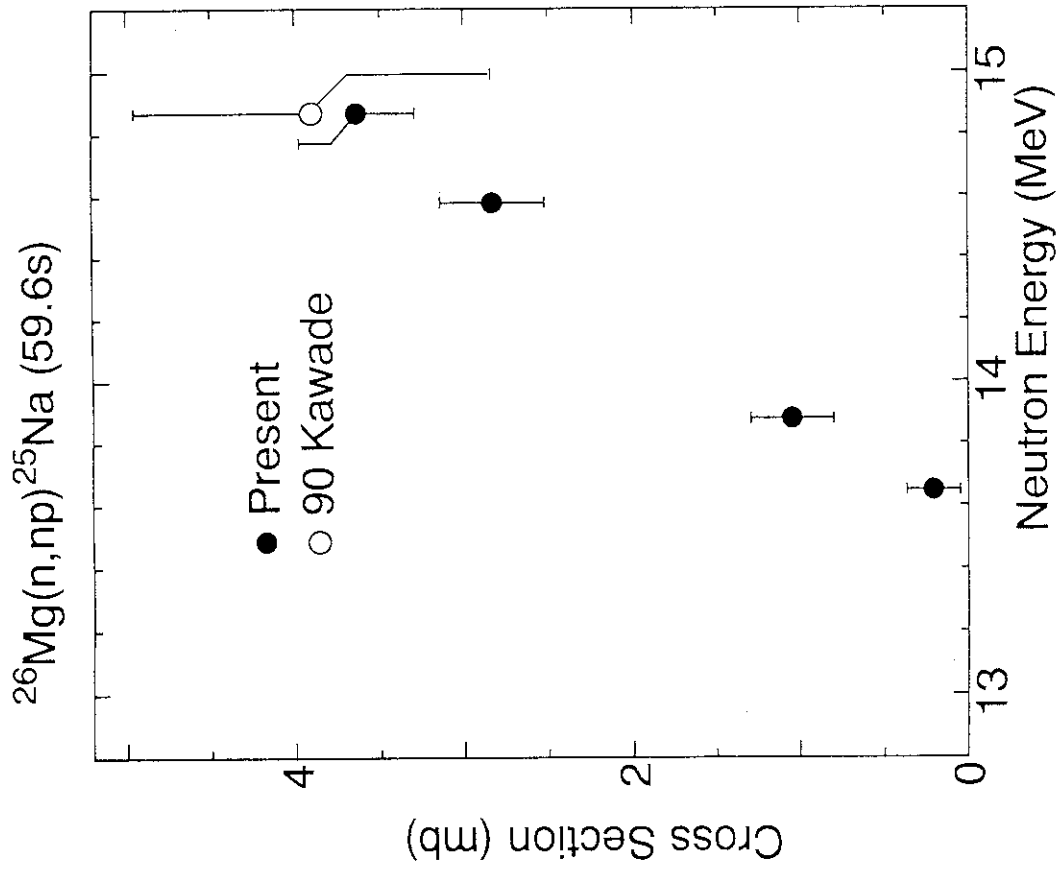

Fig. 3-1 Cross section of $^{26}Mg(n,np)^{25}Na$.

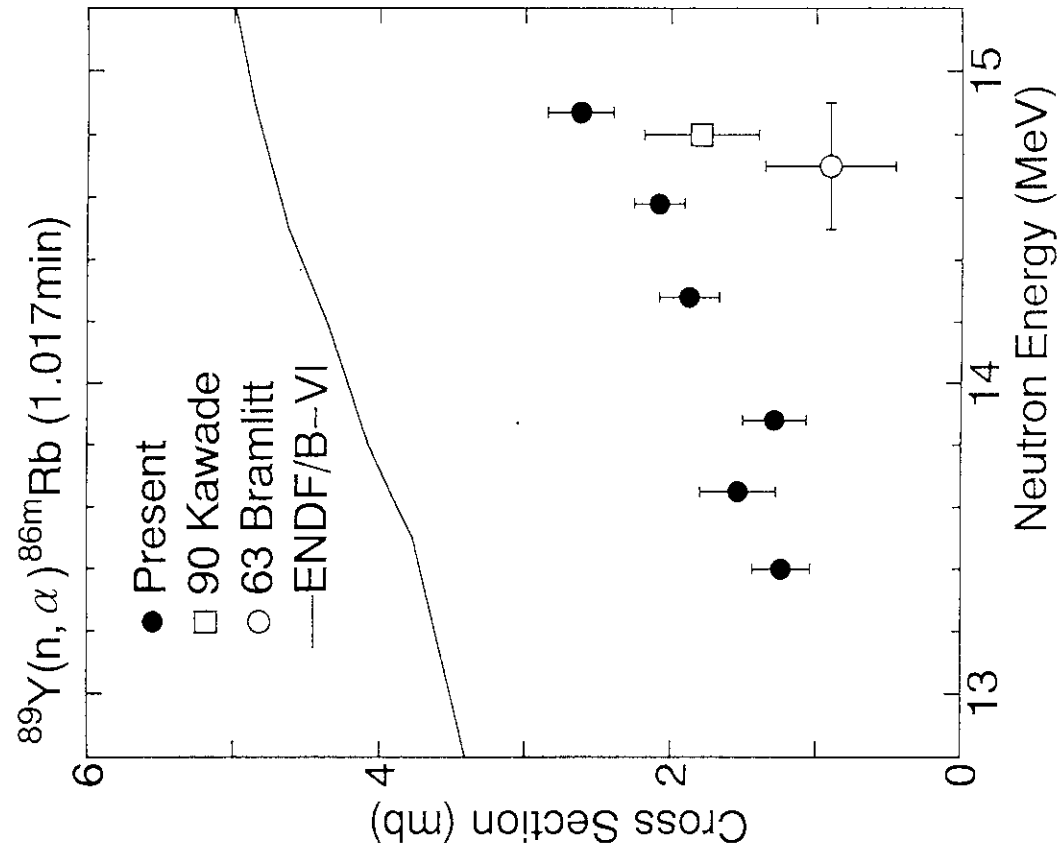

Fig. 3－4 Cross section of ^{89}Y(n,α)^{86m}Rb.

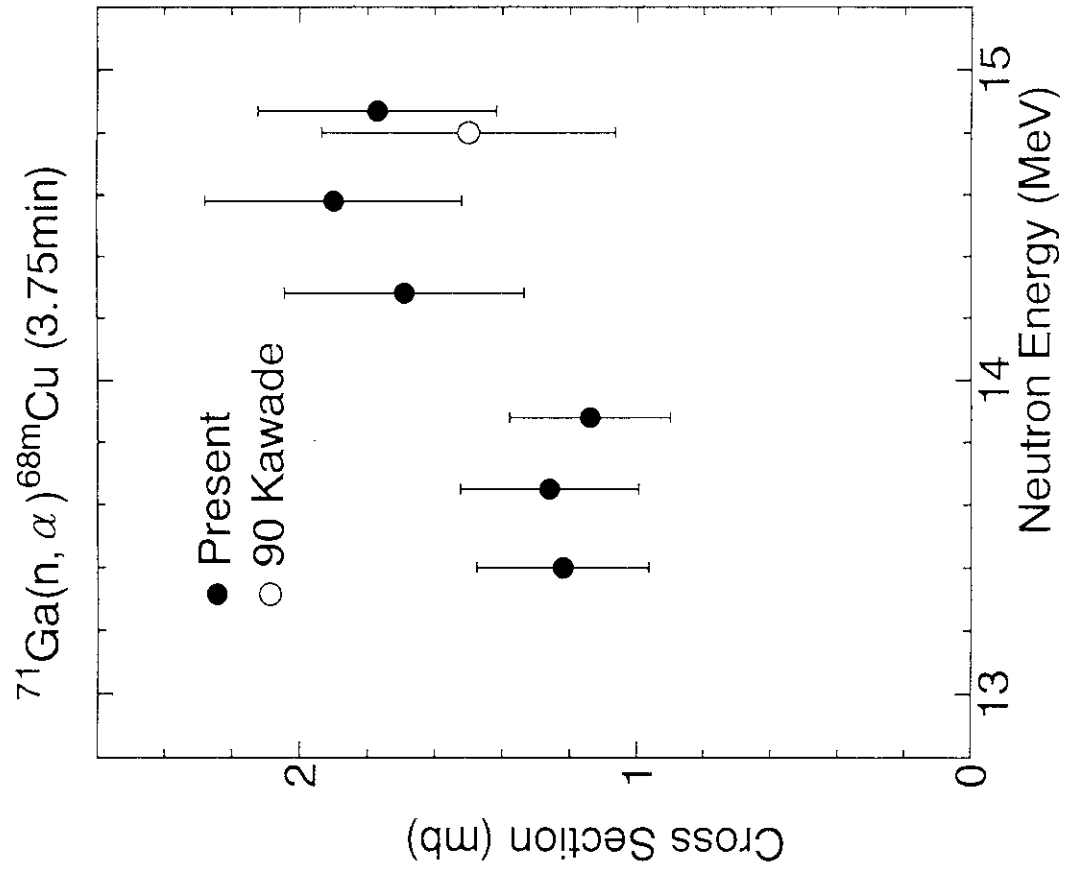

Fig. 3－3 Cross section of ^{71}Ga(n,α)^{68m}Cu.

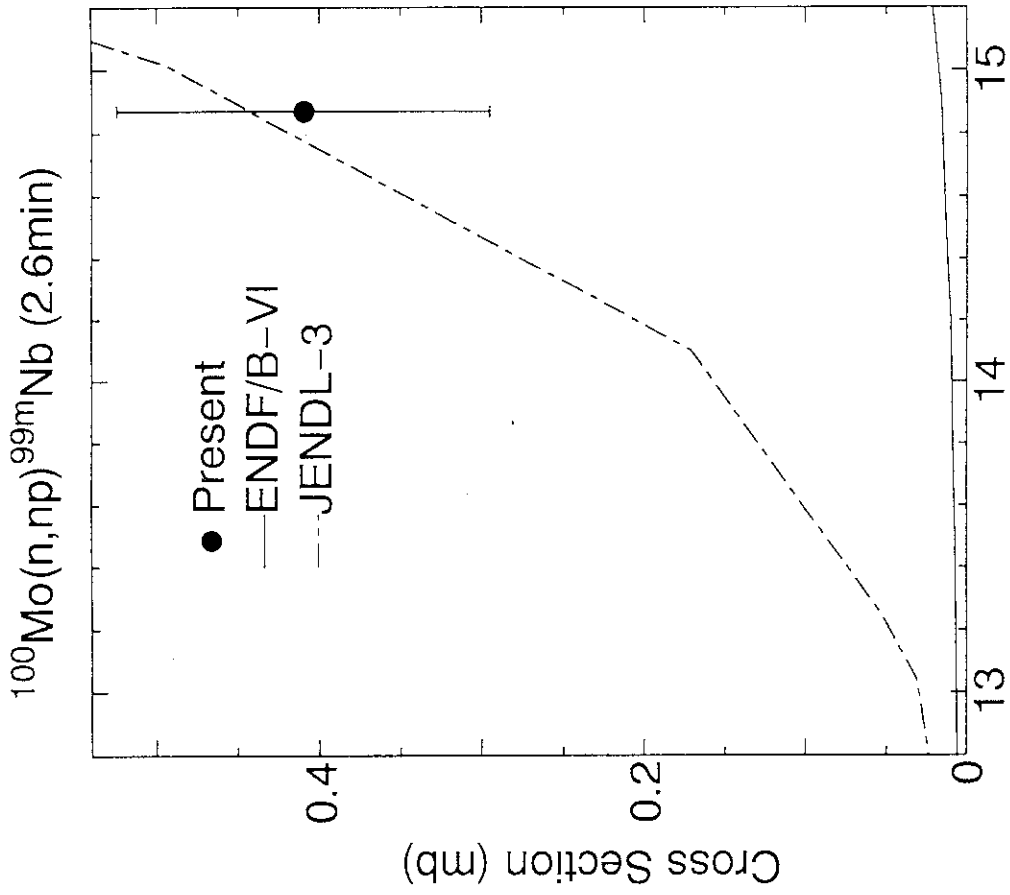

Fig. 3-6 Cross section of ^{100}Mo(n,np)^{99m}Nb.

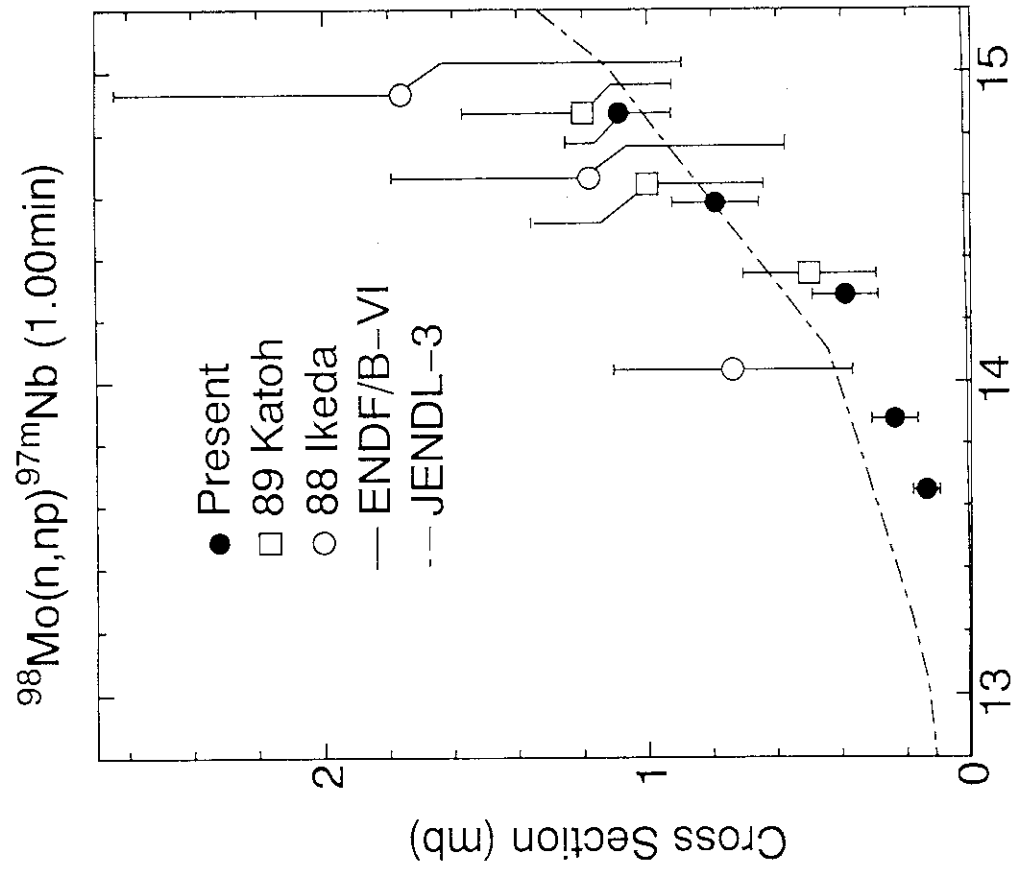

Fig. 3-5 Cross section of ^{98}Mo(n,np)^{97m}Nb.

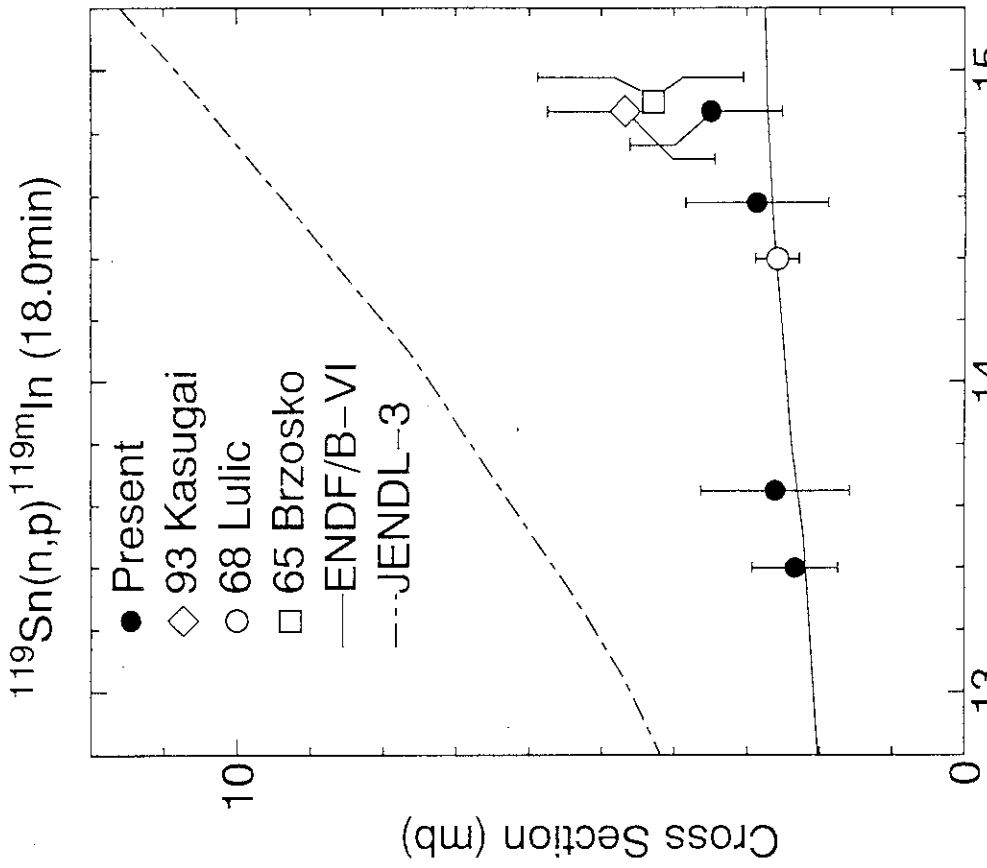

Fig. 3-8 Cross section of ^{119}Sn(n,p)^{119m}In.

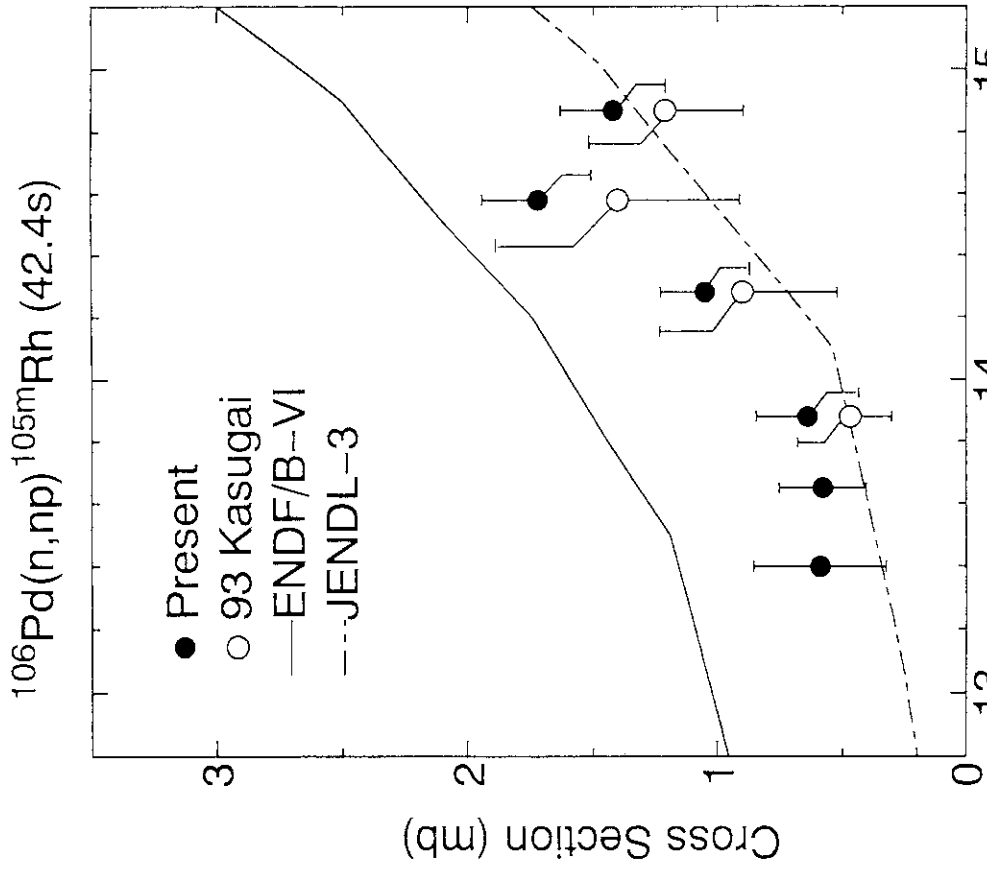

Fig. 3-7 Cross section of ^{106}Pd(n,np)^{105m}Rh.

5.11 Measurement of Beta-decay Half-lives of Short-lived Nuclei

S. Itoh, A. Tanaka, H. Yamamoto, *T. Iida
*A. Takahashi and K. Kawade
Department of Nuclear Engineering, Nagoya University
Furo-cho, Chikusa-ku, Nagoya, 464-01, Japan
*Department of Nuclear Engineering, Osaka University
Yamadaoka, Suita-shi, Osaka, 565, Japan

Abstract

The half-lives of short-lived nuclei produced by 14MeV or thermal neutron bombardments were measured with Ge detectors in the multi-scaling mode. The corrections for pile-up and dead-time losses were performed by applying source and pulser methods. The half-lives of ^{29}Al, ^{79m}Se, ^{86m}Rb, ^{107m}Pd, ^{107m}Ag and ^{122m}Sb were determined with accuracies of 0.3 $\sim$ 0.7 %.

1 Introduction

The half-life of β-decay is one of the most fundamental constants on radioactive isotopes. In the activation cross section measurements, the uncertainty brings a strong effect to the results. Most of the values previously published were obtained with GM counters, ionization chambers, proportional counters and scintillation counters. In order to improve the precision and reliability of the half-lives of short-lived nuclei ($T_{1/2}$ = 20 s $\sim$ 7 m), Ge detectors were used for the present work.

2 Experiment

The γ-rays were measured with ORTEC 20% Ge detector and PGT LEPS(Low Energy Photon Spectrometer, crystal size of 50 mm$^{\phi}$ $\times$ 10mm^{t}) in the spectrum multi-scaling mode. Decay was followed for about 10 times the half-life at equal intervals of 1/3 to 1/4 of half-life. A long-lived γ source and a constant-pulser were simultaneously measured together with the short-lived activity for the correction of the pile-up and the dead time losses (source method, pulser method). The initial counting rates were always kept to be less then 9×10^{3} cps. The detailed procedures are described elsewhere [1].

Sources of ^{29}Al, ^{86m}Rb, ^{107m}Pd and ^{107m}Ag were produced by OKTAVIAN. Sources of ^{79m}Se, ^{86m}Rb and ^{122m}Sb were produced by thermal neutron irradiation at TRIGA-II reactor of Rikkyo University(100kW).

3 Results

In Fig.1 a decay curve of ^{29}Al is shown. The results are summarized in Table 1 together with production reactions, γ-rays measured and previous values [2]. In Fig.2 the results

are compared with previous works. In Fig.3 relative deviations of previous values from the present ones are shown. It is clearly seen that previous values [3] shorter than about 10 min. systematically deviate and those become larger as the half-lives become shorter. The cause might result from insufficient correction for pile-up and dead time losses. It is likely to start measurements at too high counting rates in order to get good statistics. If the corrections at high counting rates are not enough, the decay curve will show a longer half-life compared with the true value.

4 Summary

The half-lives of short-lived nuclei were determined with a ccuracies of 0.3 $\sim$ 0.7 % and the accuracies have been much improved. Previous values shorter than about 10 min. systematically deviate and those deviations become larger as the half-lives become shorter.

References

[1] M. Miyachi et al., *Nucl. Data for Sci. and Tech.*, 897(1988,Mito)

[2] E. Browne et al., *Table of Radioactive Isotopes*, (1986) John Wiley & Sons, New York

[3] C. M. Lederer and V. S. Shirley, *Table of Isotopes 7th Ed.*, (1978) John Wiley & Sons, New York

Table 1 Results of half-life measurement.

Nuclide	*Production reaction*	E_γ (keV)	*Reference*[a] (E_γ in keV)	*Number of measurement*	*Number of point*	*Duration* (*in* $T_{1/2}$)	*Half-life* *Present*	*Reference*[b]
^{29}Al	^{29}Si(n,p)	1273.4	^{137}Cs [c] (661.7)	4	40	12	6.524(22) m	6.56(6) m
^{79m}Se	^{78}Se(n,γ)^{m}	95.7	^{241}Am (59.5)	3	35	9.1	3.843(8) m	3.91(5) m
^{86m}Rb	^{85}Rb(n,γ)^{m}	556.0	^{133}Ba(356.0)	10	30	9.8	1.0218(18) m	1.020(2) m
	^{87}Rb(n,2n)^{m}		[c]	5	30			
^{107m}Pd	^{108}Pd(n,2n)^{m}	214.9	^{170}Tm[c] (84.3)	4	30	12	20.78(9) s	21.3(5) s
^{107m}Ag	^{107}Ag(n,n')^{m}	93.1	^{170}Tm (84.3)	8	30	10	43.03(28) s	44.3(2) s
^{122m}Sb	^{121}Sb(n,γ)^{m}	61.5	Pulser only	3	22	7.9	4.196(8) m	4.21(2) m

a) These source were used for corrections of dead-time and pile-up losses.

b) Taken from ref. 2.

c) No pulser was used. Source was only used.

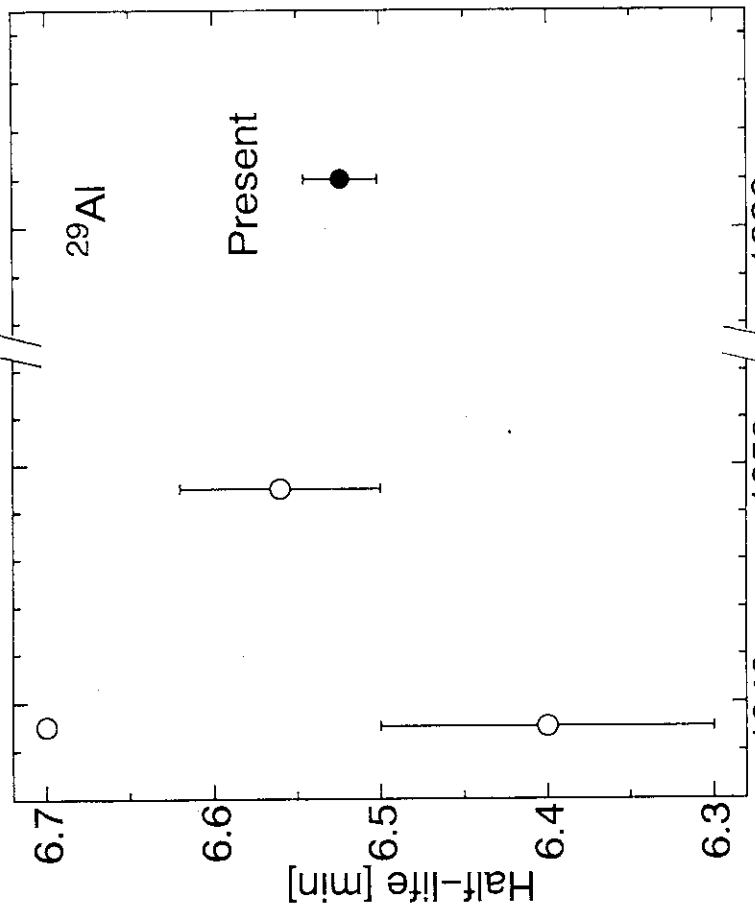

Fig. 2 Comparison with previous works taken from ref.3.

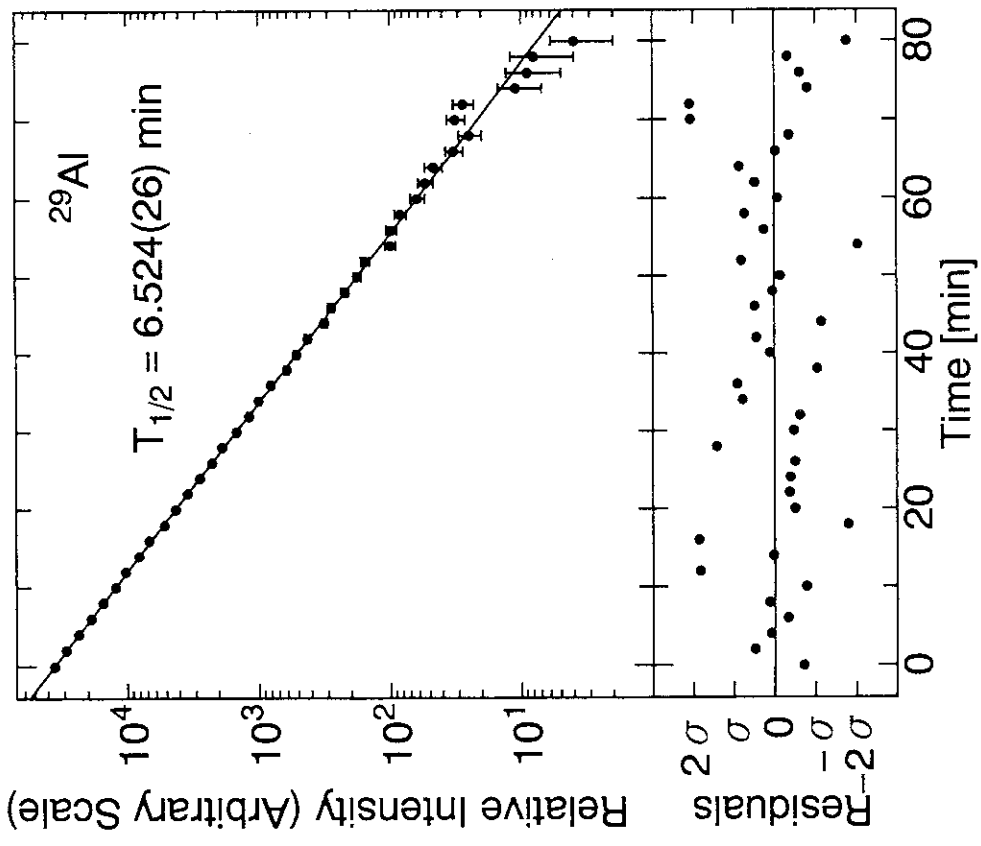

Fig. 1 Decay curve of ^{29}Al and residuals from a least squares fitting analysis.

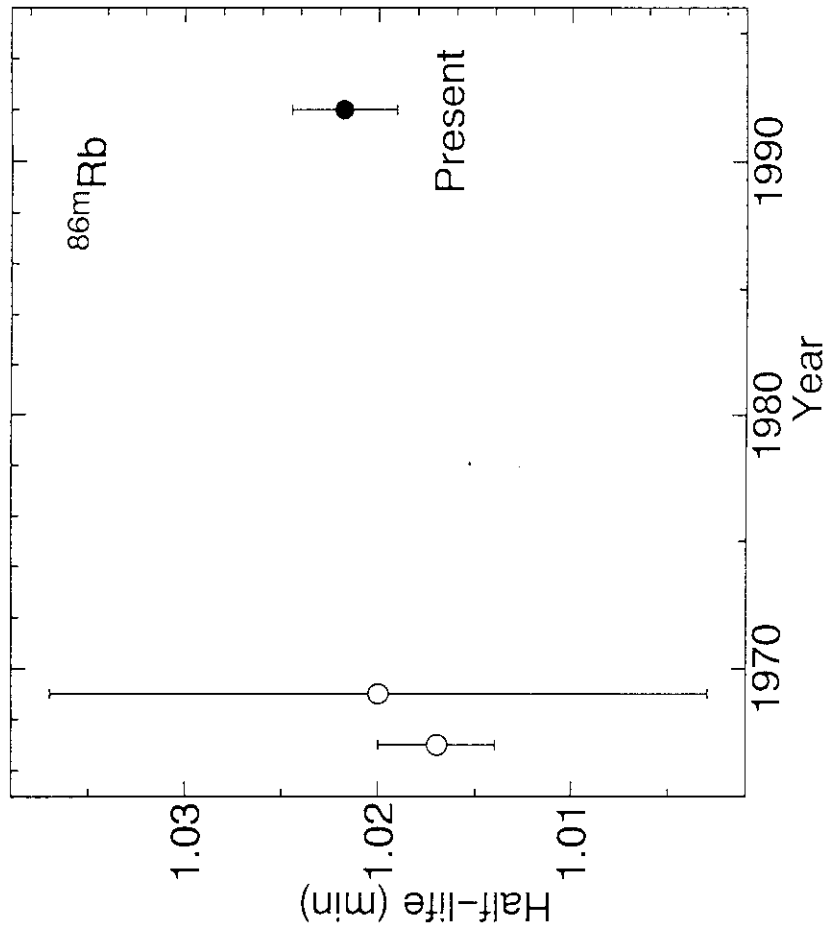

Fig. 2 (Cont.)

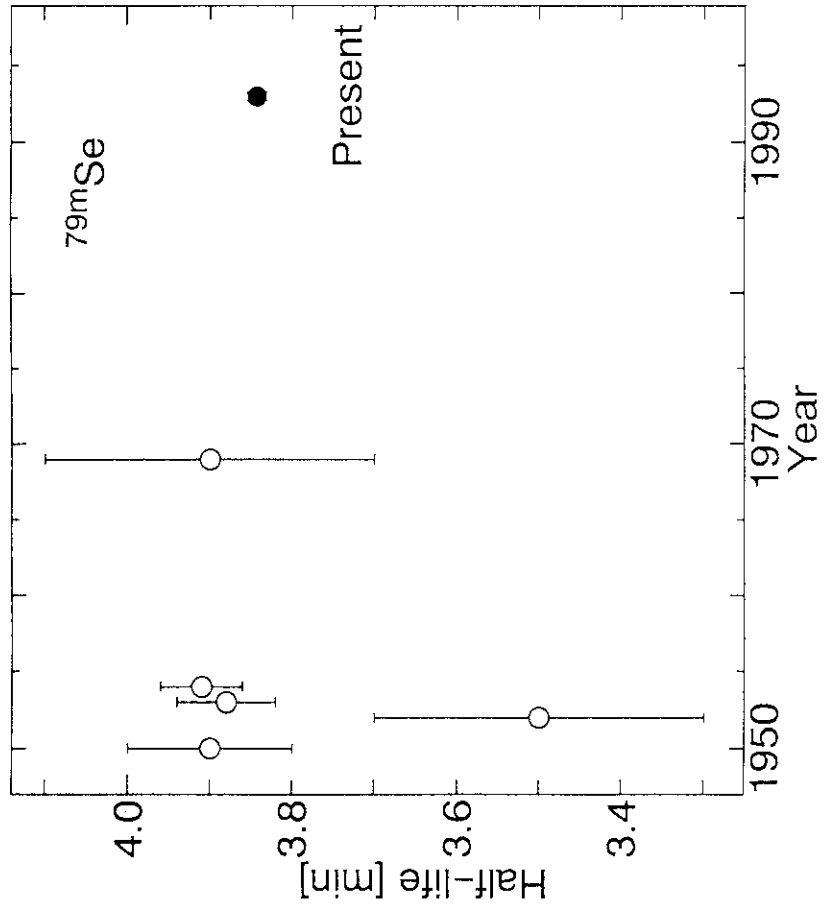

Fig. 2 (Cont.)

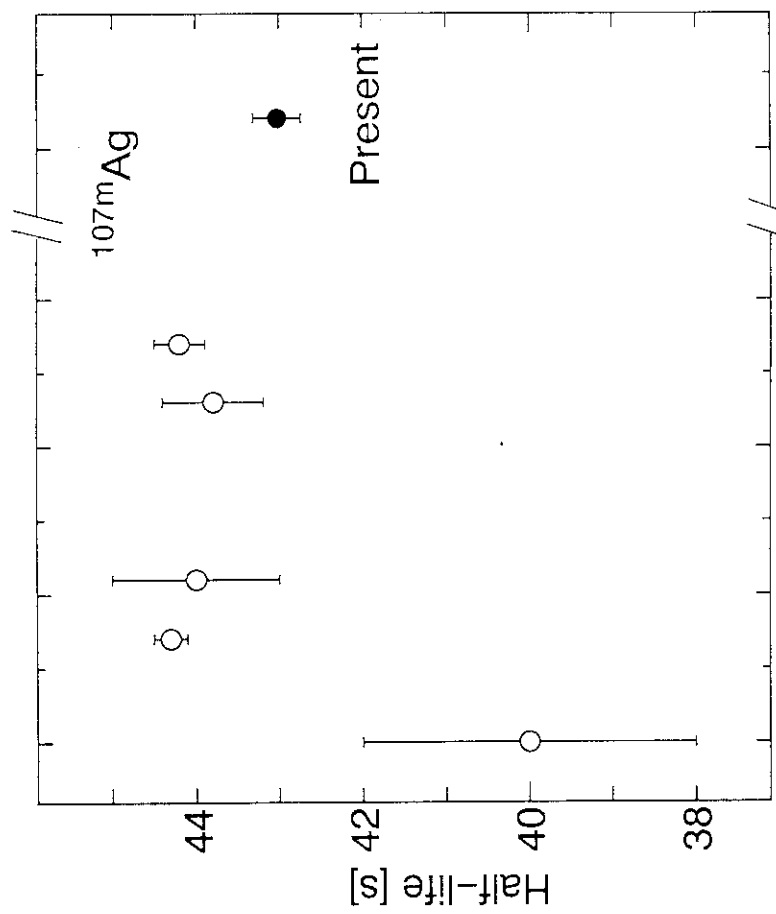

Fig. 2 (Cont.)

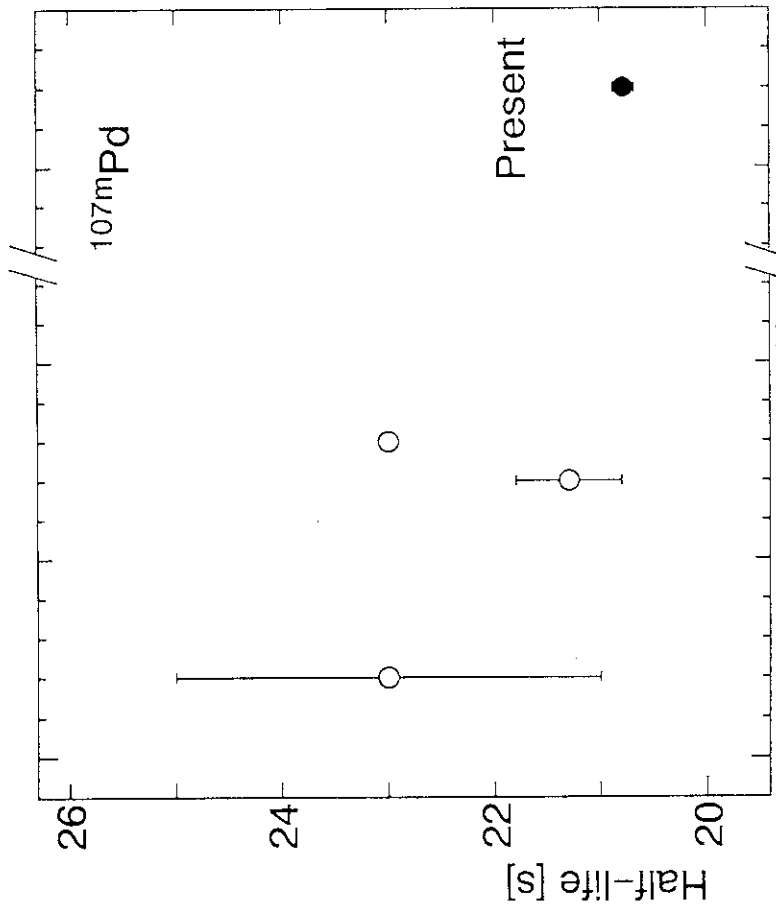

Fig. 2 (Cont.)

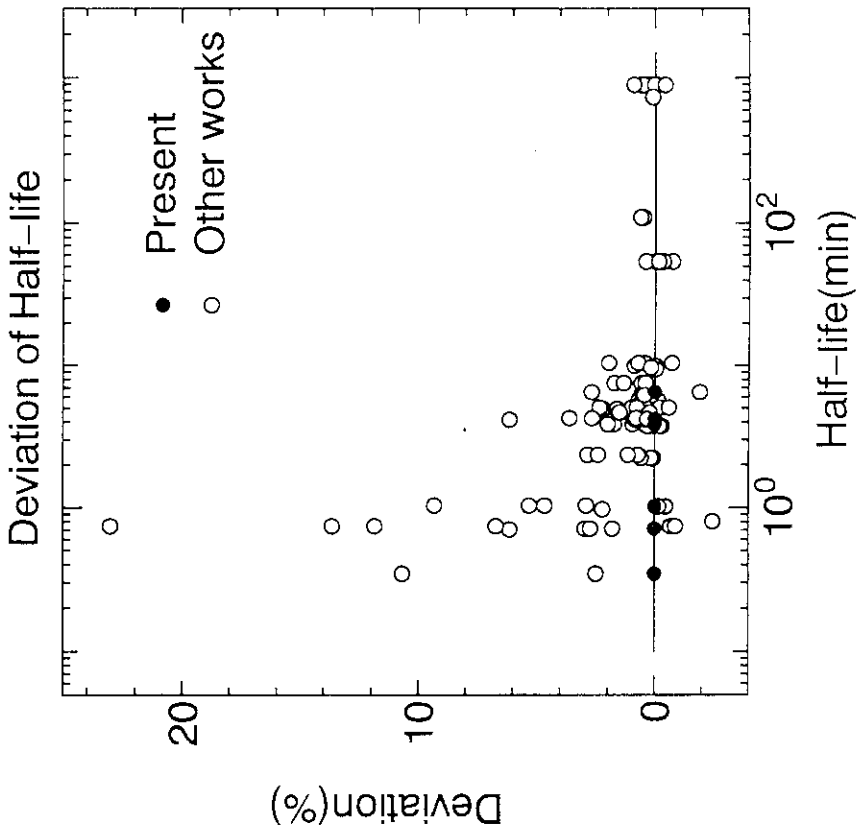

Fig. 3 Deviation of previous half-life values from the present.

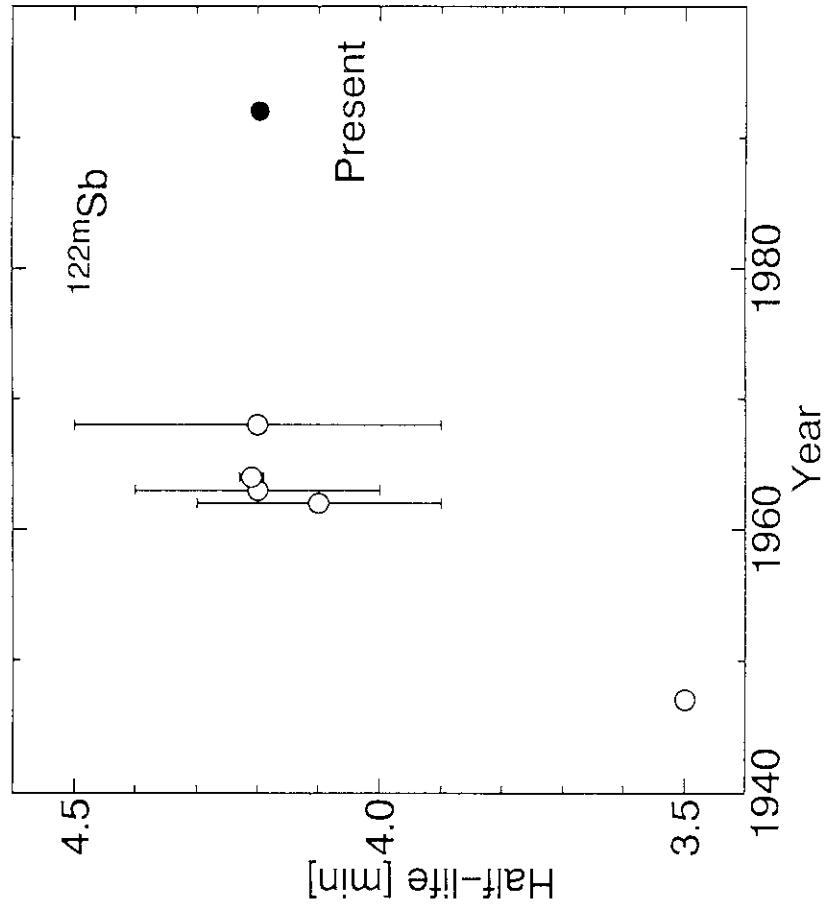

Fig. 2 (Cont.)

5.12 Measurement of Hyperfine Structure in ^{143}Pr ($T_{1/2}$=13.6d) by Collinear Laser-ion-beam Spectroscopy

Hideki IIMURA, Masashi KUBOTA*, Yoshinori NAKAHARA,
Shin-ichi ICHIKAWA and Takayoshi HORIGUCHI**

Japan Atomic Energy Research Institute, Tokai, Ibaraki 319-11
*Department of Physics, Faculty of Science,
Toho University, Funabashi, Chiba 274
**Department of Physics, Faculty of Science,
Hiroshima University, Hiroshima 730

The hyperfine structure in the radioactive isotope ^{143}Pr have been measured by collinear laser-ion-beam spectroscopy. The purpose of this work and the experimental details are given.

1. Introduction

Collinear laser-ion-beam spectroscopy can provide sub-Doppler resolution and has been used to study hyperfine structure (hfs) in ions of some stable and long-lived isotopes. Recent developments of on-line mass separation technique have made this spectroscopy applicable to short-lived isotopes. There are a few groups in the world working on this subject and they determined the hyperfine constants in long isotopic chains of several elements. However, the hyperfine constants of many isotopes remain unknown. Because nuclear moments can be determined from the hyperfine constants and are important information for nuclear structure research, more experiments on hfs are needed. At JAERI-On-Line-Isotope-Separator (JAERI-ISOL),[1] we have studied nuclear structure of rare-earth elements by β-γ spectroscopy. In order to strengthen this research we set up a beam line of collinear laser-ion-beam spectroscopy a few years ago.

The Z=59 Pr isotopes exhibit a transition from spherical to deformed shapes as the neutron number increases from N=82 to 90, providing a good chance of testing various nuclear models. In these isotopes, level scheme of ^{143}Pr ($T_{1/2}$ = 13.6d) was studied through the ^{143}Ce ($T_{1/2}$ = 1.4d) β-

decay.[2] However, the nuclear moments of the ground state of ^{143}Pr are unknown and it is an obstacle to make detailed theoretical investigations of this nucleus. In this work we performed measurements of hfs in ^{143}Pr by collinear laser-ion-beam spectroscopy to determine the nuclear moments of this nucleus.

2. Experiment and results

Samples of ^{143}Pr were prepared through the β-decay of ^{143}Ce produced by ^{142}Ce(n,γ) reaction. Each target of 10 mg CeO_2 (enriched to 92.8 % in ^{142}Ce) was irradiated for 3 days in a flux density of 9 X 10^{13} neutrons/cm^{2}s in an irradiation facility of the JRR-3 reactor in JAERI. After the irradiation, the activity was cooled for about a week until most of ^{143}Ce decayed to ^{143}Pr. Then ^{143}Pr was chemically separated with carrier of natural ^{141}Pr, from ^{142}Ce and ^{143}Ce by a solvent extraction technique. Each sample was then transferred into a surface ionization ion source of JAERI-ISOL.

The experimental setup is shown in Fig. 1. A cw dye laser with a wavemeter (Coherent 699-29) was controlled by a personal computer. The Rhodamine 6G dye in this laser was pumped by the 514 nm line of an Ar-ion laser (Coherent INNOVA-100-20). The wavemeter was used to determine the absolute frequency which was calibrated by an absorption spectrum of an I_2 cell. The relative frequency of the hyperfine lines was calibrated by a confocal etalon with a free spectral range of 150 MHz (Burleigh CFT-500).

A partial energy-level diagram of PrII involved in this investigation is shown in Fig. 2 where the laser-excited optical transition from the metastable $^5G_2^O$ level is indicated by an upward arrow and the fluorescence to the ground level is indicated by a downward arrow. A beam of 40-keV Pr^+ ions, part of which are in the metastable level, was produced by the isotope separator. The flux of mass-separated ^{143}Pr ion beam was about 3 X 10^7 ions/s, which lasted a few hours with each sample. The metastable ions were excited to the $^5H_3$ level by a counter-propagating laser beam. The interaction region was defined by a stainless-steel cage of 10 cm in length and 1 cm in diameter, which was kept at the potential of -3 kV. This potential ensures that the velocity of the ions is Dopplertuned into resonance in the cage and that depopulation pumping of the $^5G_2^O$ level does not occur far upstream from the cage.

Resonance was observed by detecting the fluorescence light from the $^5H_3$ level to the ground level. The fluorescence light was collected by an

ellipsoidal mirror onto a cooled photomultiplier (Hamamatsu Photonics R2256). A detection rate of one event per 2 X 10^5 ions in the beam was observed when the laser frequency coincided with the strongest spectral line. Stray light from the laser beam was suppressed by an appropriate combination of broad-band filters. The ion current was monitored by a Faraday cup (FC) after the interaction region. Hyperfine spectra were measured by scanning the laser frequency and recorded in multichannel scaling (MCS) mode by using a personal-computer-based data acquisition system. We measured the hyperfine spectra of ^{143}Pr and the stable isotope ^{141}Pr. For each isotope, data were acquired from several scans, typically 10 GHz in width and lasting 15 min each. One of the scans for ^{143}Pr is shown in Fig. 3. The observed linewidth was typically about 100 MHz (FWHM).

Peak identification is aided by a property that the ratio of magnetic dipole constants $A(^5H_3)/A(^5G_2{}^O)$ is relatively unchanging between ^{143}Pr and ^{141}Pr. The result of the peak assignments for ^{143}Pr is shown in Fig. 3. Fourteen out of fifteen ^{143}Pr hyperfine components were observed. These assignments were confirmed by agreement of the observed peak intensities and profiles to those predicted by a mathematical model of the system. The 9/2-11/2 component, having an intensity 56 times lower than the most intense peak, was not observed and should be at a frequency below the range of Fig. 3.

Further analysis of the data is in progress now. The results will be published elsewhere soon, which include the value of the nuclear moments of ^{143}Pr determined from the hyperfine constants A and B.

References

1) Ichikawa S., Sekine T., Oshima M., Iimura H. and Nakahara Y.: Nucl. Instrum. Methods Phys. Res. B70, 93(1992).
2) Kusnezov D. F., Nethaway D. R. and Meyer R. A.: Phys. Rev. C40, 924(1989).

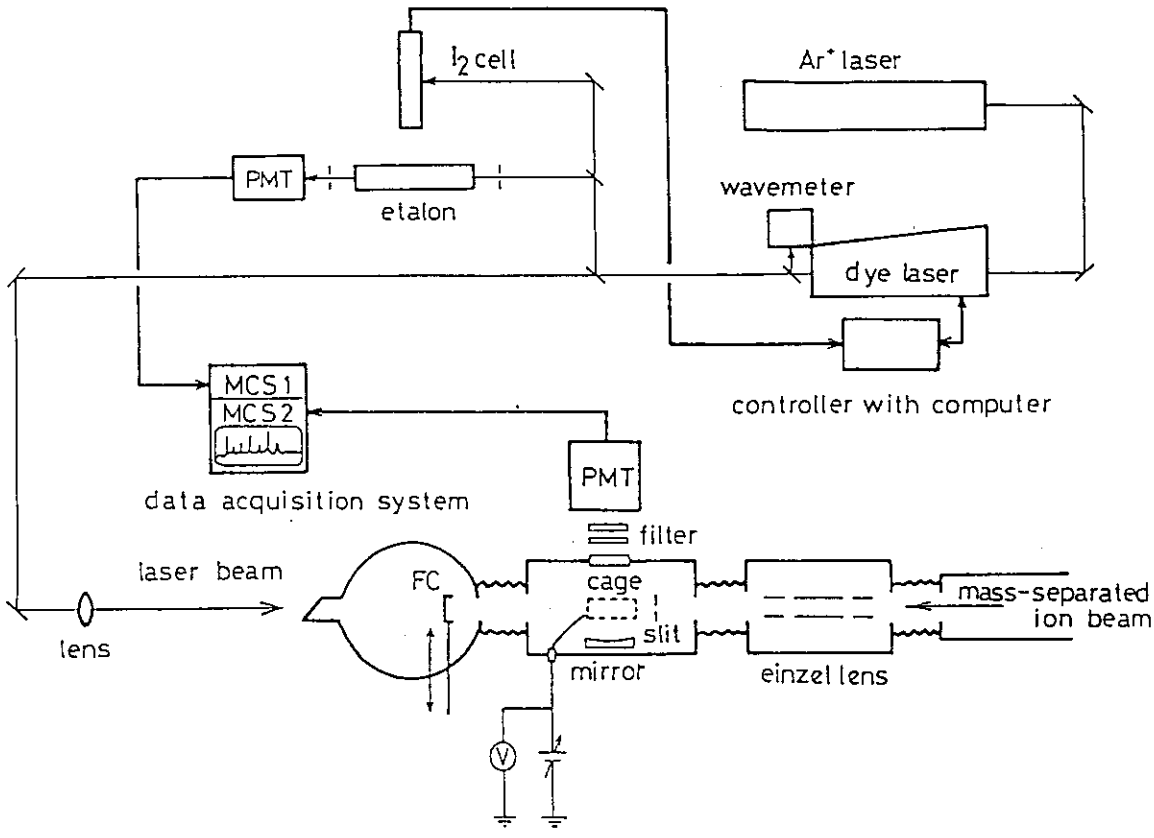

Fig. 1 Block diagram of the experimental setup.

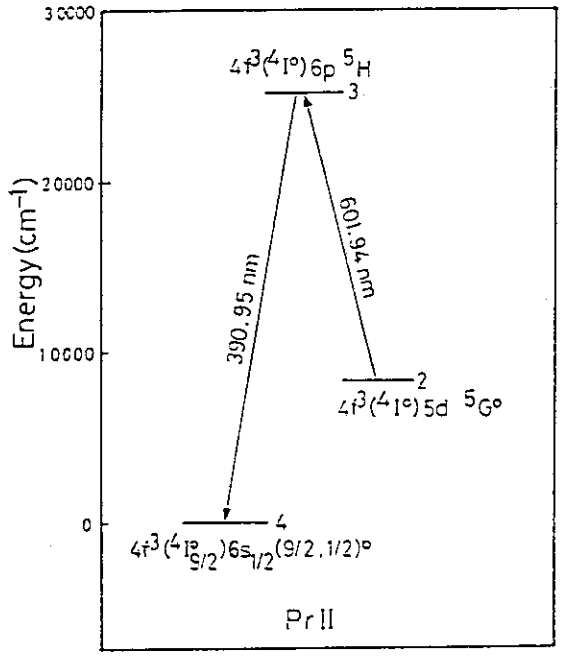

Fig. 2 Partial energy level diagram of PrII.

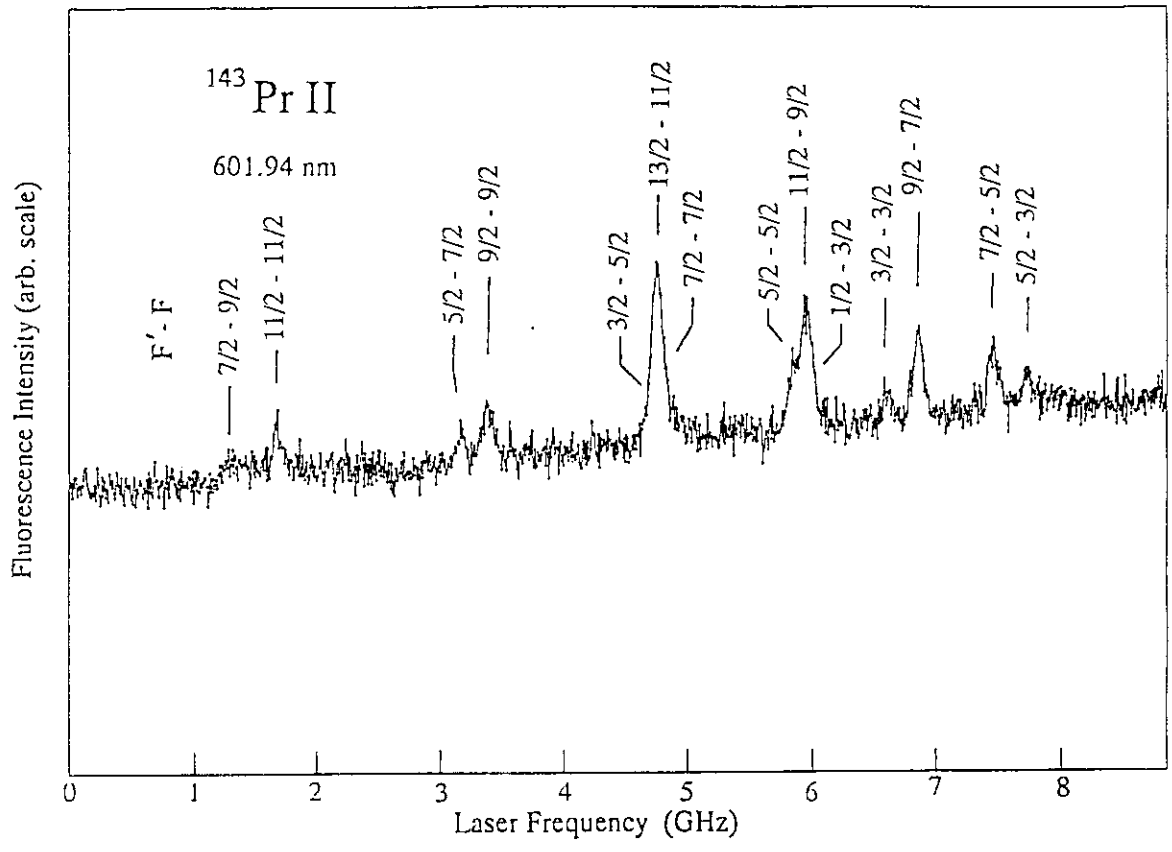

Fig. 3 Typical measured hyperfine spectrum of the transition $^5G_2{}^0$-$^5H_3$ (λ = 601.94 nm) in ^{143}PrII. F quantum numbers are indicated in order of upper state(F')-lower state(F).

5.13 Reevaluation of FP Nuclear Data for JENDL-3.2

M. Kawai and JNDC Fission Product Nuclear Data Working Group*
Toshiba Corporation
Ukishima-cho, Kawasaki-ku, Kawasaki, Japan

Reevaluation of the nuclear data for about 60 fission product nuclides has been made for JENDL-3.2, taking accounts of the new experimental data and the results of integral tests for JENDL-3. As for thermal cross sections of long lived nuclides, JRR-4 measurements at JAERI were adopted. Major part of the revision of the resonance parameters were made according to the renormalization of the experimental capture-area data of ORNL. Capture cross sections were renormalized so as to reduce the contradiction between the differential and the integral data. For some nuclides, the optical model parameters were revised to improve the energy dependence of total and capture cross sections. Direct components were added to the inelastic scattering cross sections of Zr and Mo isotopes. As for deformed nuclides such as Sm and Nd isotopes, the coupled channel calculation was made for estimation of excitation functions of rotational levels.

1. Introduction

JENDL-3 Fission Product Nuclear Data Library[1] was released in December of 1990. Its integral test for the STEK sample reactivities and the capture rates measured at EBR-II and CFRMF has clarified that the JENDL-3 data reproduce well the integral data for important nuclides within 10% accuracy, and that it has a tendency underestimating sample worths of nuclides in the mass region heavier than 130[2]. Additionally, after the evaluation for JENDL-3, new experimental data were measured at ORNL, KFK, FEI of Russia and JAERI. Accordingly, we have made for JENDL-3.2 reevaluation of the resonance parameters and cross sections for about 60 fission product nuclides given in Table 1. In this paper, a brief description of the evaluation is given.

2. Thermal Cross Section and Resonance Integral

Harada et al.[3]-[6] have recently measured thermal cross sections and resonance integral for neutron capture reaction of long lived fission product nuclides, ^{90}Sr, ^{137}Cs, ^{154}Eu and ^{155}Eu at JRR-4 of JAERI. The measured results are very different from the evaluated data of JENDL-3 which were mainly based on the compilation of Mughabghab et al.[7],[8] In the present evaluation, the JRR-4 measurements were adopted. As for ^{90}Sr and ^{137}Cs to which no resonance parameter is given, 1/v-energy dependence of capture cross section renormalized to the experimental data was assumed in the sub-resonance (i.e., thermal) energy region, and its upper energy boundary was determined to reproduce the experimental resonance integral. As for ^{154}Eu and ^{155}Eu, one negative energy resonance was given so as to reproduce both thermal cross section and resonance integral. The evaluated results are compared with the experimental data and JENDL-3 in Table 2. Figure 1 compares the presently evaluated capture cross section for ^{137}Cs with the other evaluated data. In the present evaluation (denoted with 'revised'), there is no special resonance structure.

N.B. Members of the working group:
S. Chiba, T. Nakagawa, Y. Nakajima, T. Sugi (Tokai-mura, Ibaraki-ken, JAERI),
H. Matsunobu (Chiyoda-ku, Tokyo, Sumitomo Atomic Industries, Ltd.)
T. Watanabe (Koutou-ku, Tokyo, Kawasaki Heavy Industry Co., Ltd.),
A. Zukeran (Hitachi-shi, Hitachi Ltd.) and M. Kawai (Kawasaki, Toshiba Corporation)

3. Resonance Parameters

Resonance parameters for 65 nuclides in JENDL-3 were essentially taken[9] from JENDL-2[10], which were mainly based on the BNL-325 third edition[11] and partially the experimental data reported before 1981. Those for 57 nuclides were determined on the basis of the recent experimental data and Mughabghab's compilation. In the evaluation, a higher priority was given[1),(10),(12)] to the capture measurements, particularly those at ORELA (Oak Ridge Electron Linear Accelerator), than to transmission data so as to reproduce the capture cross sections with high accuracy. After the evaluation for JENDL-2, the corrigenda concerning capture measurements at ORELA appeared[13),(14)] because an error was discovered in the computer codes that transform measured neutron capture yields taken on the ORELA Flight Path 7 to effective capture cross sections. Although the corrigenda were taken into account of in the JENDL-3 evaluation for capture cross sections, they were not all for resonance parameters. Unfortunately, such wrong data of resonance parameter are contained for some nuclides in Mughabghab's compilation and adopted to the JENDL-3 evaluation. Accordingly, we reevaluated resonance parameters for 10 nuclides for which the corrigenda indicated a correction to capture area data more than 2%. Table 3 shows the correction factors which were used for the reevaluation. The capture cross sections calculated from resonance parameters for ^{90}Zr are shown in Fig. 2. JENDL-3.2 gives 10 mb at 0.0253 eV which coincides with the exprimetal value of Lone et al.[15] As for ^{107}Ag and ^{109}Ag, the effect of level missing is observed in neutron capture cross section in the energy range between 1 keV and 2.6 keV where only transmission measurements were made. So that, we gave artificial p-wave resonance parameters in this energy region.

For tellurium isotopes (Te-122 to Te-126) and ^{144}Sm, Macklin et al.[16),(17)] have reported new data of capture measurements at ORELA. Except for Te-123 for which energy gap is found between ORELA data above 2.6 keV and the older resolved resonance parameters, the ORELA measurements were adopted to evaluation. Table 4 shows a example of the measured and evaluated resonance parameters of Te-122 which were output by the REPSTOR system[18]. Experimental data are those of transmission measurements by Tellier et al.[19] and capture measurement by Macklin et al. In the evaluation, radiation width was determined from the neutron width by Tellier and the capture area by Macklin et al. For some resonances whose neutron width was not given, the value of neutron width was estimated from the capture area and the averaged gamma-ray width derived by Macklin et al. Figure 3 shows the capture cross section of ^{122}Te. The value calculated from resonance parameters of JENDL-3.2 is in good agreement with the experimental value of Macklin et al. However, it is observed in Fig. 4 that the calculated total cross section seems to be too large above 10 keV, compared with the statistical model calculations. This overestimation probably comes from the uncertain neutron width of unresolved (maybe doublet or triplet) resonances. In addition, the neutron width reported by Macklin et al. shows a trend of being larger than the transmission data of Tellier et al. Accordingly, upper limit of resolved resonance region was determined to be 12 keV. On the other hand, level missing gives an underestimation of capture cross section, as shown in Fig. 5 for ^{144}Sm. Similar underestimation effect was found for 8 nuclides of JENDL-3.1 given in Table 1 and the upper limits of resolved resonance region was reduced. This reduction should increase the integral value of capture rates in the reactor core or some standard fields to some degree.

4. Smooth Cross Sections

Capture cross sections were reevaluated so as to reduce the contradiction between the evaluated data and the recent experimental data or the integral data. Fig's 6 and 7

show the typical result for ^{111}Cd and ^{148}Sm. For ^{111}Cd, the cross section was renormalized to the data of Musgrove et al.[20] which were corrected according to the corrigenda[14] mentioned above. This modification increasing cross section by 20.8% will affect to diminish the contradiction of integral data concerning the STEK experiments[21),(22)], because the ratio of the calculated to experimental value (C/E) is 0.92±0.13.[2] The cross section of ^{148}Sm was renormalized to the new experiments of Wisshak et al.[23]. Since the JENDL−3.2 is smaller than JENDL−3, the C/E value of 0.89±0.06 for STEK experiments must not approach to unity. Thus, we have to judge that there are some factors than cross section uncertainty to give the discrepancy of the integral data between the calculation and experiment. As for ^{137}Cs, we tried to adjust the cross section so as to reproduce the thermal value, resonance integral and integral data (capture rate measured in CFRMF standard neutron field[24]). The result became very strange as shown in Fig. 8. Then, we reevaluated by neglecting the CFRMF data. In Fig. 1, the integral data and thermal value are compared between the calculations and experiments. Revised value, i.e., JENDL−3.2 give 9.7 for CFRMF data which is by one decade smaller than the experiment.

For some nuclides around the mass number of 100 in JENDL−3, unsuitable nuclear model parameter gave the poor calculated results. Fig. 9 shows the capture cross section for ^{101}Ru. Only JENDL−3 shows a fairly huge peak at 3 MeV. In JENDL−3 evaluation, the level scheme data were those adopted to the JENDL−1 evaluation[25] and lacks many levels, compared the recent data in ENSDF. The level missing caused an underestimation of the cross sections for inelastic scattering which is a process competing with capture. In the present evaluation, the recent evaluated level scheme data were used for the calculation. The optical model parameters were revised to improve the energy dependence of total and capture cross sections for ^{98}Mo, ^{100}Mo and ^{103}Rh. Fig. 10 shows the total cross section for ^{100}Mo: JENDL−3.2 is in agreement with the experimental data[26)−(29)] in the whole energy range from 100 keV to 6 MeV. Capture cross section for ^{103}Rh was calculated with the revised optical model parameter. It is seen in Fig. 11 that JENDL−3.2 run through in the intermediate of the experimental data by Macklin et al.[30),(13)] and Wisshak et al.[31], while JENDL−3, which was evaluated with the statistical model calculation and an eye−guide technique near 10 keV, is in agreement with the experiments of Macklin et al.

Direct components calculated with the DWBA model code[32] were added to the inelastic scattering cross sections of Zr and Mo even mass isotopes, ^{144}Sm, ^{148}Sm and ^{150}Sm. Fig. 12 shows the typical result for ^{92}Zr. The effect of direct components is obvious for 0^+, 2^+ and 3^- levels. As for deformed nuclides such as ^{150}Nd, ^{152}Sm and ^{154}Sm, the coupled channel calculation was made with the ECIS−88 code[33] for estimation of excitation functions of rotational levels. Figs. 13 shows the results for ^{150}Nd. The calculation was carried out taking accounts of the 0^+−2^+−4^+−6^+−8^+−10^+ (the ground state rotational band) and -1^-−3^-−5^- (the octupole vibrational band) coupled. The optical model parameters were those used for the JENDL−3 evaluation, except that the potential strength of surface absorption was adjusted to fit to the experimental data of Haouat et al.[34] for the 2^+ level.

The threshold reaction cross sections for (n,2n), (n,np) and (n,αn) reactions of Nb, Zr and Mo isotopes were taken from the data of JENDL Fusion Library.[35] Fig. 14 compares the evaluated (n,2n) cross section of ^{100}Mo which was calculated with the GNASH code.[36]

The evaluation work has mostly completed and data compilation is now in progress. After the compilation, the integral test will be made.

References:

1) M. Kawai, et al., J. Nucl. Sci. Technol., 29, 195 (1992).
2) T. Watanabe, et al., Proc. of Specialists' Meet. on Fission Product Nuclear Data, Tokai, 25th-27th May 1992, NEA/NSC/DOC(92)9, p.411 (1992).
3) H. Harada, et al., JAERI-M 91-032, p.199 (1991).
4) H. Harada, et al., JAERI-M 92-027, p.298 (1992).
5) T. Sekine, et al., Int. J. Rad. App. and Instrum., A138, 513 (1987).
6) T. Sekine, et al., NEA/NSC/DOC(92)9, p.189 (1992).
7) S.F. Mughabghab, et al., "Neutron Cross Sections," Vol. 1, Part A (1981) Academic Press.
8) S.F. Mughabghab, "Neutron Cross Sections," Vol. 1, Part B (1984) Academic Press.
9) M. Kawai, et al., Proc. of Specialists' Meet. on Fission Product Nuclear Data, Tokai, 25th-27th May 1992, NEA/NSC/DOC(92)9, p.39 and p.495 (1992).
10) T. Aoki, et al., Proc. Int. Conf. on Nuclear Data for Basic and Applied Science, Santa Fe, May 1985, Vol. 2, p.1627 (1986).
11) S.F. Mughabghab and D.I. Garber, BNL-325, 3rd edition, Vol. 1 (1973).
12) Y. Kikuchi, et al, JAERI-M 86-030 (1986).
13) R.L. Macklin and R.R. Winters, Nucl. Sci. and Eng., 78, 110 (1981)
14) B.J. Allen, et al., Nucl. Sci. Eng., 82, 230 (1982).
15) M.A. Lone and G.A. Bartholomew, Proc. 4th Int. Conf. on Neutron-Capture Gamma-Ray Spectroscopy and Related Topics, Grenoble, Sept. 1981, p.383 (1981).
16) R.L. Macklin and R.R. Winters, ORNL-6561 (1989).
17) R.L. Macklin, et al., Phys. Rev., C48, 1120 (1993).
18) T. Nakagawa, JAERI-M 8163 (1979) [in Japanese].
19) H. Tellier and C.M. Newstead, Proc. Third Int. Conf. on Neutron Cross Section and Technology, Knoxville, March 1971, p.680 (1971).
20) A.R. der Musgrove, et al., Proc, Int. Conf. on Neutron Physics and Nuclear Data for Reactors and Other Applied Purposes, AWRE Harwell, Sept. 1978, p.449 (1978).
21) J.J. Veenema and A.J. Janssen, ECN-10 (1976).
22) R.J. Heiboer, et al., ECN-11 (1976).
23) K. Wisshak et al., KfK 5067 (1992)
24) Y. Harker, et al., NEANDC(E)-209"L", p.5 (1980).
25) Y. Kikuchi, et al., JAERI 1268 (1981).
26) M. Diradeenam, et al., Dissertation Abstract section B, 25, 3834 (1968).
27) P. Lambropoulos, et al., Nucl. Phys., A201, 1 (1971).
28) A.B. Smith et al., Nucl. Phys., A244, 2213 (1975).
29) M.V. Pasechnik, et al., Proc. 5th All Union Conf. on Nutron Physics, Kiev, September 1980, Vol. 1, 304 (1980).
30) R.L. Macklin, et al., Nucl. Sci. Eng., 73, 174 (1980).
31) K. Wisshak, et al., Phys. Rev., C42, 731 (1990).
32) P.D. Kunz, "Program DWUCK-4," unpublished memorandum, Colorado University.
33) J. Raynal, "Program ECIS-88," unpulished.
34) G. Haouat, et al., Phys. Rev., C20, 78 (1979).
35) S. Chiba, et al., JAERI-M 92-027, p.35 (1992).
36) P.G. Young and E.D. Arthur, LA-6947 (1977).

Table 1 Modification of JENDL-3 FP nuclear data library

Thermal Cross Sections and Resonance Integral

^{90}Sr, ^{90}Zr*, ^{137}Cs**, ^{154}Eu* and ^{155}Eu*.

Resolved Resonance Parameters

^{88}Sr, ^{89}Y, ^{90}Zr, ^{93}Nb, ^{99}Tc, ^{99}Ru, ^{103}Rh, ^{107}Ag, ^{109}Ag, ^{110}Cd, ^{111}Cd, ^{122}Te, ^{124}Te, ^{125}Te, ^{126}Te, ^{137}Cs**, ^{135}Ba, ^{137}Ba, ^{138}Ba, ^{139}La, ^{140}Ce, ^{141}Pr, ^{142}Nd, ^{143}Nd, ^{144}Nd, ^{145}Nd, ^{144}Sm, ^{154}Eu and ^{155}Eu.

Reducing the Upper Limits of Resolved Resonance Region

^{80}Se, ^{107}Pd, ^{113}Cd, ^{127}I, ^{139}La, ^{144}Nd, ^{147}Sm and ^{154}Sm.

Renormalization of Capture Cross Sections

^{79}Br, ^{81}Br, ^{111}Cd, ^{115}In, ^{117}Sn, ^{124}Sn, ^{121}Sb, ^{123}Sb, ^{122}Te, ^{123}Te, ^{124}Te, ^{138}Ba, ^{142}Ce, ^{148}Sm and ^{150}Sm.

Energy Dependence of Total and Capture Cross Sections

^{98}Mo, ^{100}Mo, ^{101}Ru and ^{103}Rh.

Inelastic Scattering Cross Sections

^{90}Zr, ^{92}Zr, ^{94}Zr, ^{96}Zr, ^{92}Mo, ^{94}Mo, ^{96}Mo, ^{98}Mo, ^{100}Mo, ^{150}Nd, ^{144}Sm, ^{148}Sm, ^{150}Sm, ^{152}Sm and ^{154}Sm.

N.B. *) Modification was made through evaluation of resonance parameters.
**) Uncertain resonance parameters of Cs-137 in JENDL-3.1 were removed so as to reproduce the experimental thermal and resonance integral of capture.

Table 2 Thermal value and resonance integral for capture

	Sr-90	Cs-137	Eu-154	Eu-155
(Thermal Value)				
JENDL-3.1	0.900	0.110	1,348	4,046
JENDL-3.2	0.015	0.250	1,842	3,758
JRR-4 exp.	0.0153±0.0013	0.250±0.013	1,840.±90	3,760.±170
(Resonance Integral)				
JENDL-3.1	0.485	680	1,310	18,600
JENDL-3.2	0.090	356	1,180	15,500
JRR-4 exp.	−	360.±70	2,100.±2,100	15,300.±2,700

Table 3 Contents of modification of resolved resonance parameters

A. Modification due to renormalization of capture area data (ORELA Data)[13),(14)]

Nuclide	Correction Factor	References
Sr-88	1.0737	Nucl. Phys., A269, 397 (1976)
Y-89	1.0360	Nucl. Sci. Eng., 64, 744 (1977)
Zr-90	0.967	Nucl. Phys., A246, 1 (1975)
Cd-111	1.208	Phys. Rev., C7, 780 (1973)
La-139	1.0737	Australian J. Phys., 30, 599 (1977)
Pr-141	1.0737	ibid., 32, 551 (1979)
Nd-142	0.967	AAEC/E401 (1977)
Nd-143	0.9507	ditt.
Nd-144	0.967	ditt.
Nd-145	0.9507	ditt.

N.B. 1) No correction because of small modification for Zr-92, Zr-94, Mo-92, Mo-94, Mo-96, Mo-100, Cd-110, Cd-114, Cd-116, Ba-134, Ba-135, Ba-136, Ba-137, Ba-138, Nd-146 and Nd-148.
2) No correction of ORELA data outside of energy region of the other experimental data.

B. New Experimental Data

Te-122, 124, 125, 126 :	R.L. Macklin and R.R. Winters, ORNL-6561 (1989)
Sm-144 :	R.L. Macklin, et al., Phys. Rev., C48, 1120 (1993).
Ba-135, 137, 138, Ce-141:	JAERI transmission data by M. Mizumoto, M. Ohkubo, et al.
Eu-154, 155 :	To reproduce thermal value and R.I measured at JRR-4.

Table 4 Example of RESTOR output listing the evaluated and experimental resonance parameters for ^{122}Te

TE-122 2

ENERGY (EV)	L	J	NEUTRON WIDTH (MILLI-EV)	GAMMA WIDTH (MILLI-EV)	WWS (MILLI-EV)	MISCELLANEOUS	REFERENCE
2762.0 2762.0	1	0.5	31.64	73.3	22.1 22.1 ± 0.3	GT = 104.94	JENDL-3.2 89MACKLIN+
2793.0 2793.0	1	1.5	2.48	73.3	4.7977 4.8 ± 0.2	GT = 75.78	JENDL-3.2 89MACKLIN+
2868.0 2868.0 2868 ± 3 2865.0 ± 3.0 2868.0	0 0	0.5 0.5	785.0 780.0 A 780 ±80 B 1570.0 ±180.0	69.68 154.0 -45.0 ±636.4	63.999 128.6 64.0 ± 1.1	GT = 854.68 GT = 934.0 WGH= 15 ± 1 GT = 740.0 ±630.0 GT = 1060 ±20	JENDL-3.2 JENDL-3.1 BNL325-4TH 7ITELLIER 89MACKLIN+
2920.0 2920.0	1	1.5	9.87	73.3	17.397 17.4 ± 0.4	GT = 83.17	JENDL-3.2 89MACKLIN+
2927.0 2927.0	1	1.5	6.42	73.3	11.806 11.8 ± 0.4	GT = 79.72	JENDL-3.2 89MACKLIN+
2942.0 2942.0	0	0.5	90.51	73.3	40.5 40.5 ± 0.5	GT = 163.81	JENDL-3.2 89MACKLIN+
2968.0 2966.2 2966.2 ± 3.0 2968.0 ± 3.0 2968.0	0 0	0.5 0.5	595.0 595.0 A 595 ±400 B 1190.0 ±800.0	58.42 154.0	53.197 122.3 53.2 ± 1.0	GT = 653.42 GT = 749.0 WGH= 10.9 ± 7.3 GT = 750 ±10	JENDL-3.2 JENDL-3.1 BNL325-4TH 7ITELLIER 89MACKLIN+
2987.0 2987.0	1	1.5	2.11	73.3	4.1019 4.1 ± 0.2	GT = 75.41	JENDL-3.2 89MACKLIN+
3009.0 3009.0	1	0.5	2.91	73.3	2.7989 2.8 ± 0.2	GT = 76.21	JENDL-3.2 89MACKLIN+
3086.0 3086.0	1	0.5	2.7	73.3	2.6041 2.6 ± 0.2	GT = 76.0	JENDL-3.2 89MACKLIN+
3095.0 3095.0	1	1.5	10.39	73.3	18.2 18.2 ± 0.4	GT = 83.69	JENDL-3.2 89MACKLIN+
3114.0 3114.0	1	0.5	46.6	73.3	28.489 28.5 ± 0.4	GT = 119.9	JENDL-3.2 89MACKLIN+
3122.0 3122.0	1	1.5	1.22	73.3	2.4001 2.4 ± 0.2	GT = 74.52	JENDL-3.2 89MACKLIN+
3183.0 3183.0	1	1.5	6.36	73.3	11.704 11.7 ± 0.5	GT = 79.66	JENDL-3.2 89MACKLIN+

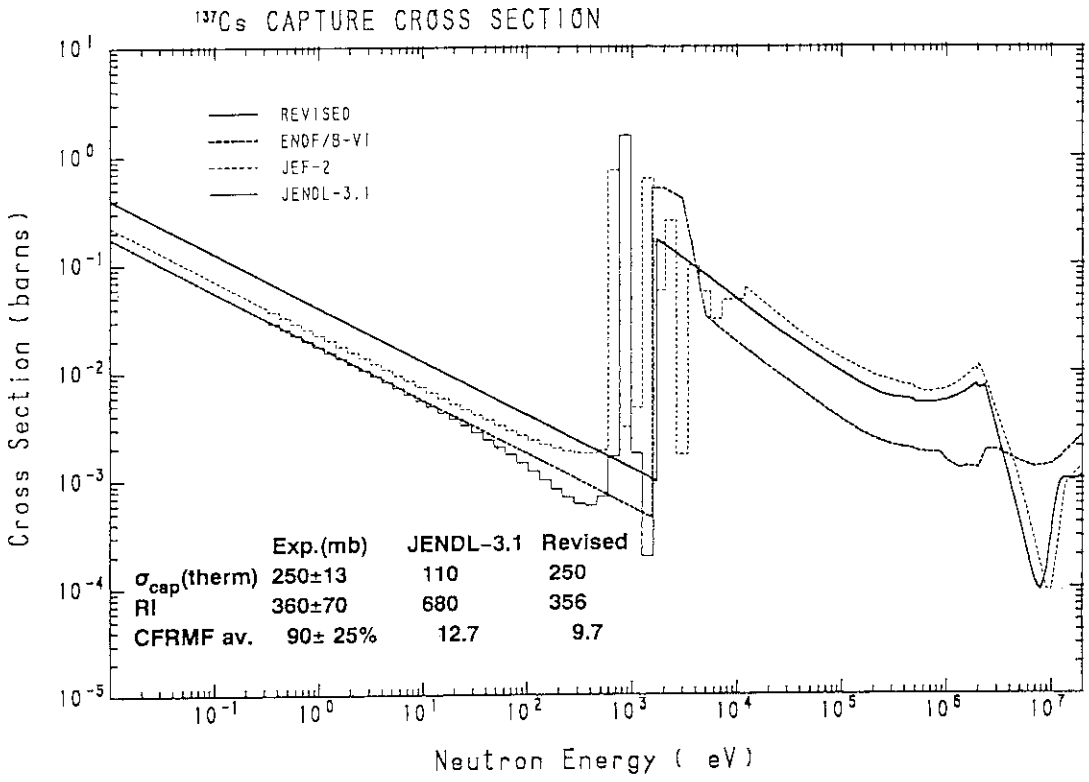

Fig. 1 Comparison of evaluated capture cross section for ^{137}Cs.

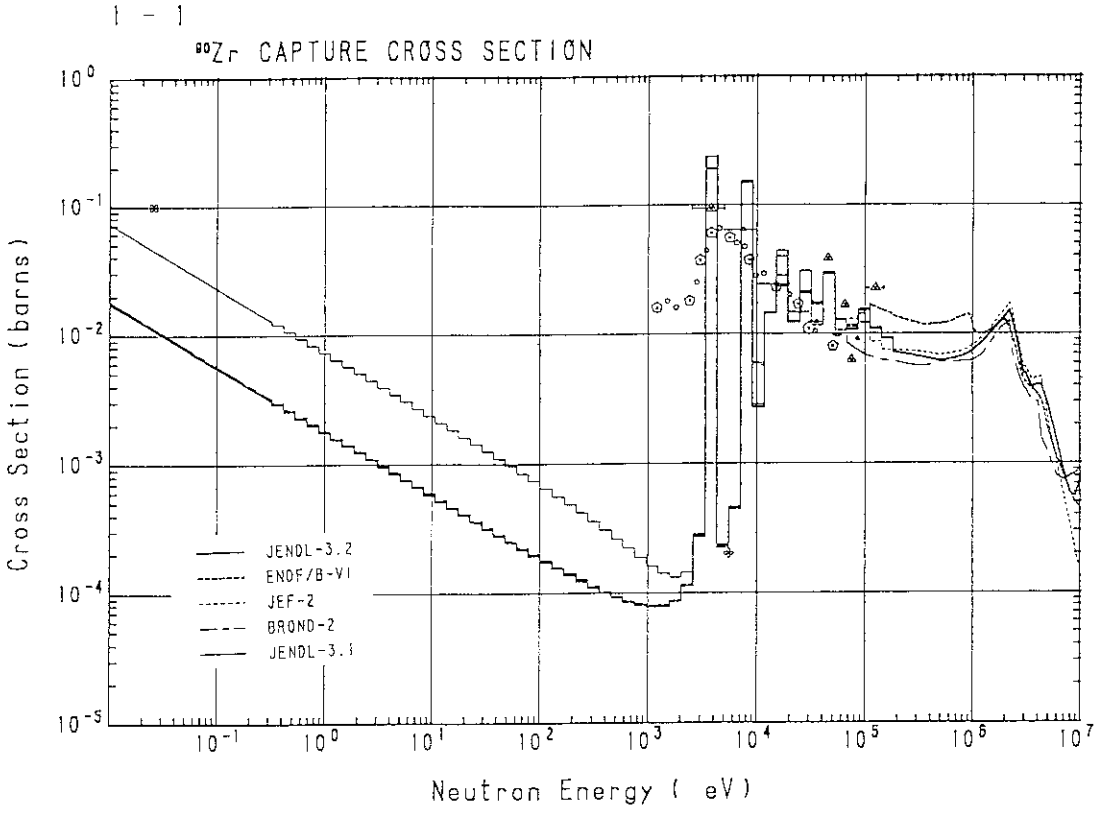

Fig. 2 Comparison of evaluated capture cross section for ^{90}Zr with the experimental data.

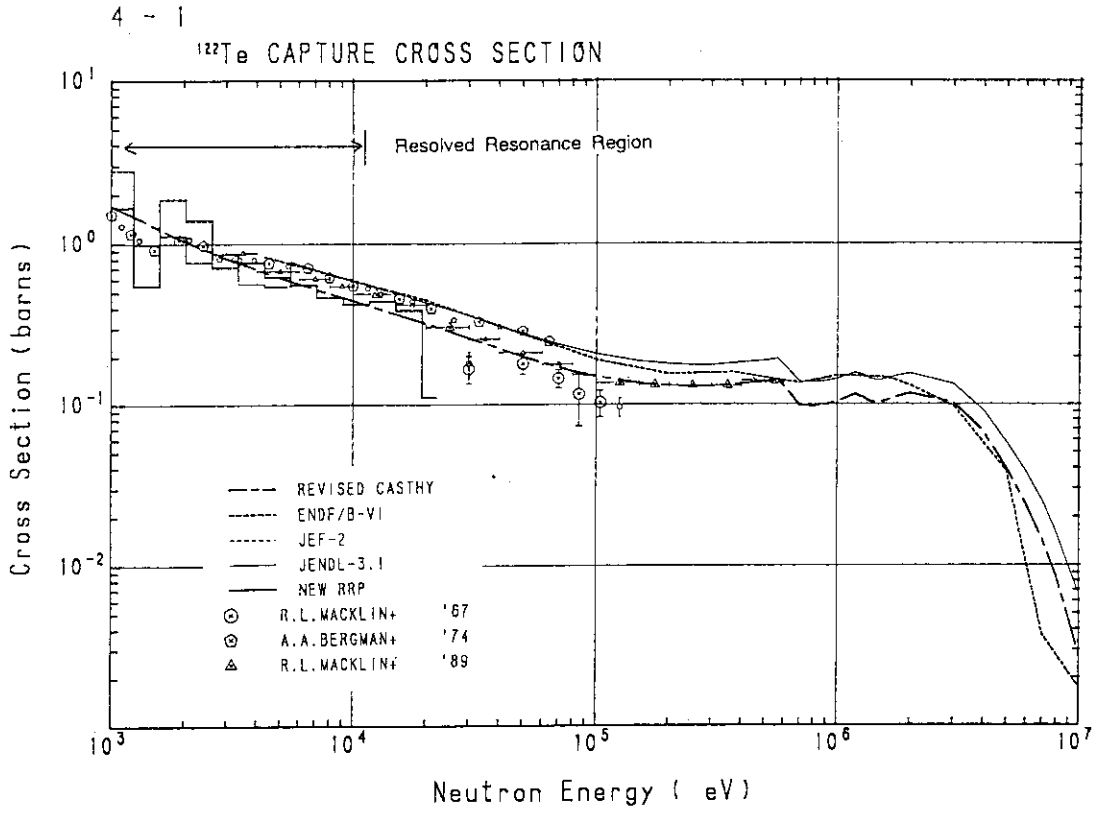

Fig. 3 Comparison of capture cross section calculated from resonance parameters for ^{122}Te with the evaluated and experimental data.

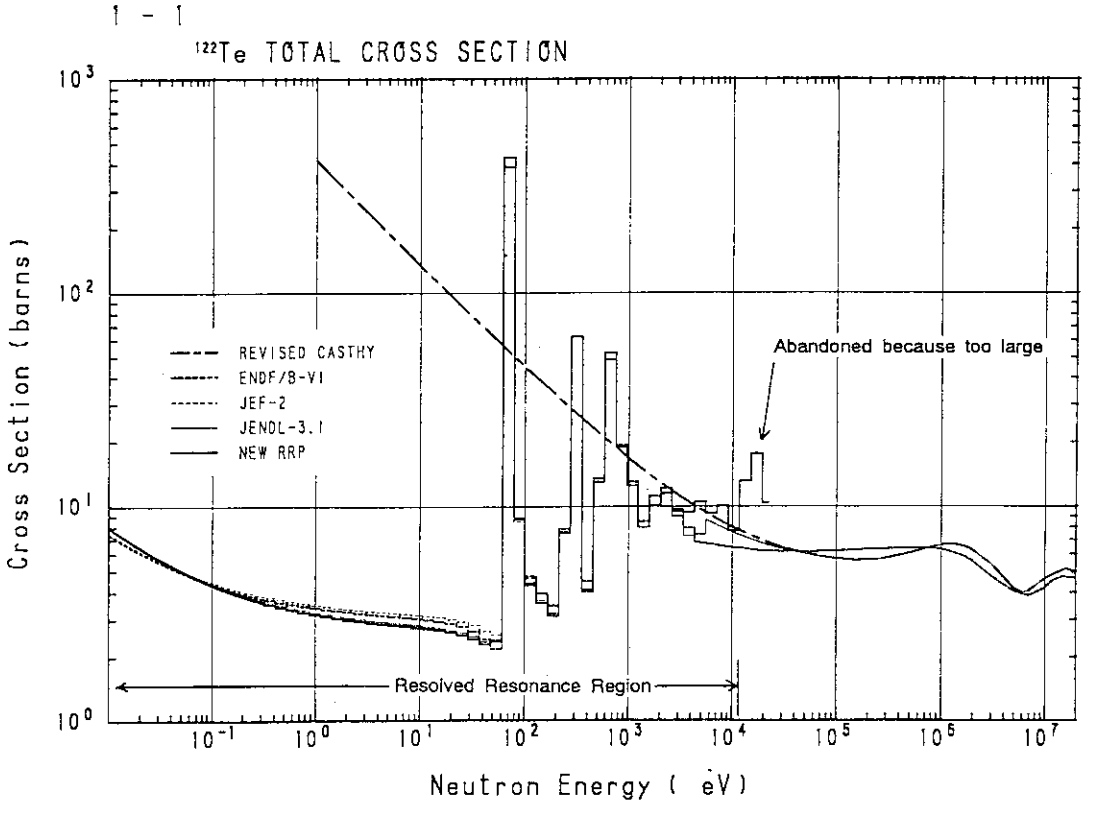

Fig. 4 Comparison of total cross section calculated from resonance parameters for ^{122}Te with the evaluated data.

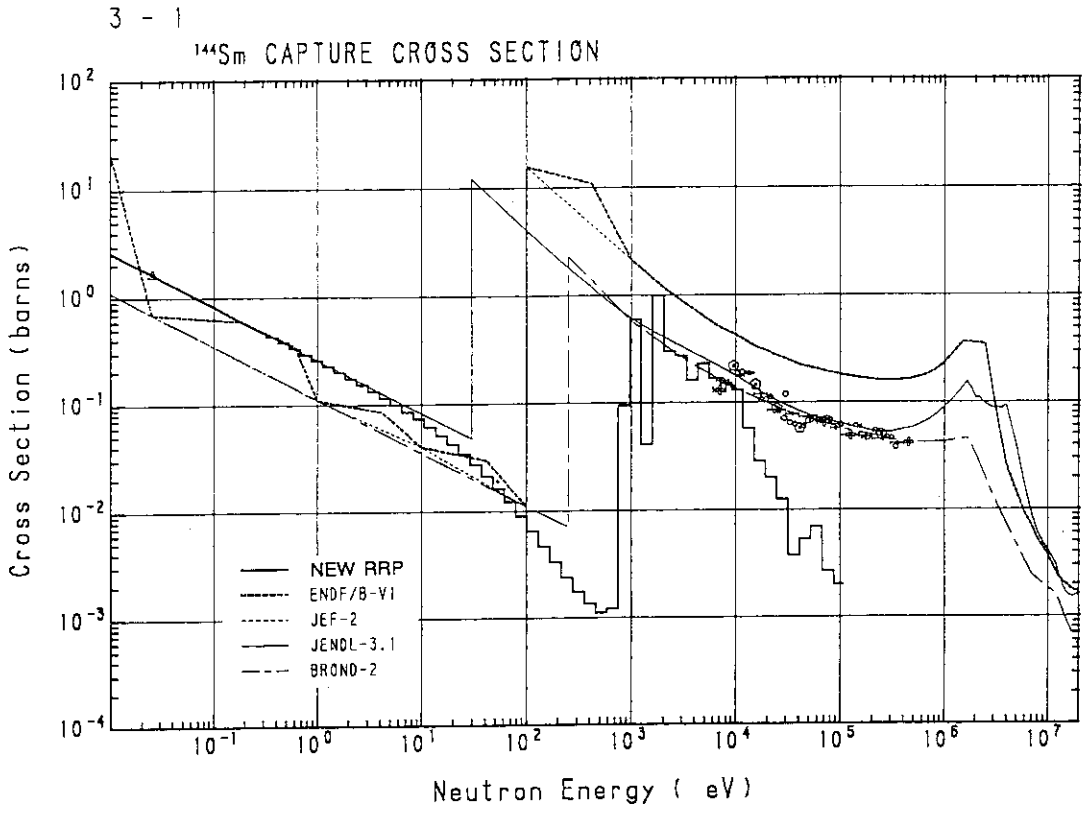

Fig. 5 Comparison of capture cross section calculated from resonance parameters for ^{144}Sm with the evaluated data.

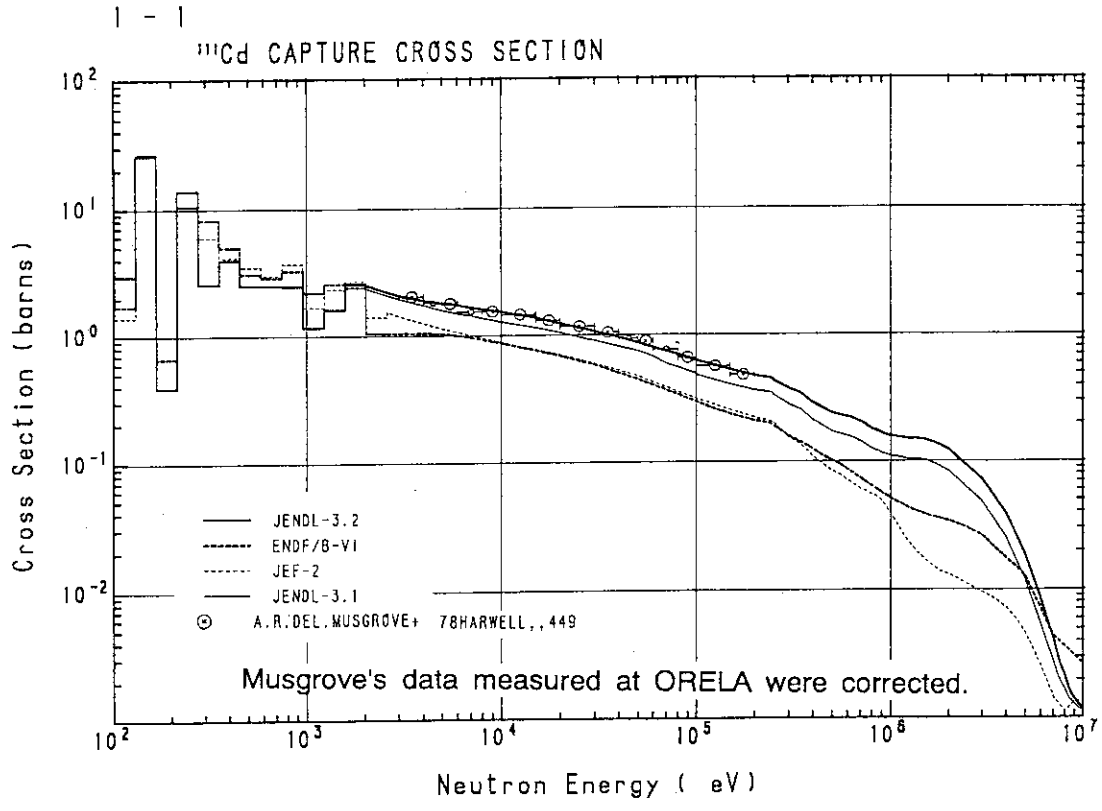

Fig. 6 Comparison of evaluated capture cross section for ^{111}Cd with the experimental data.

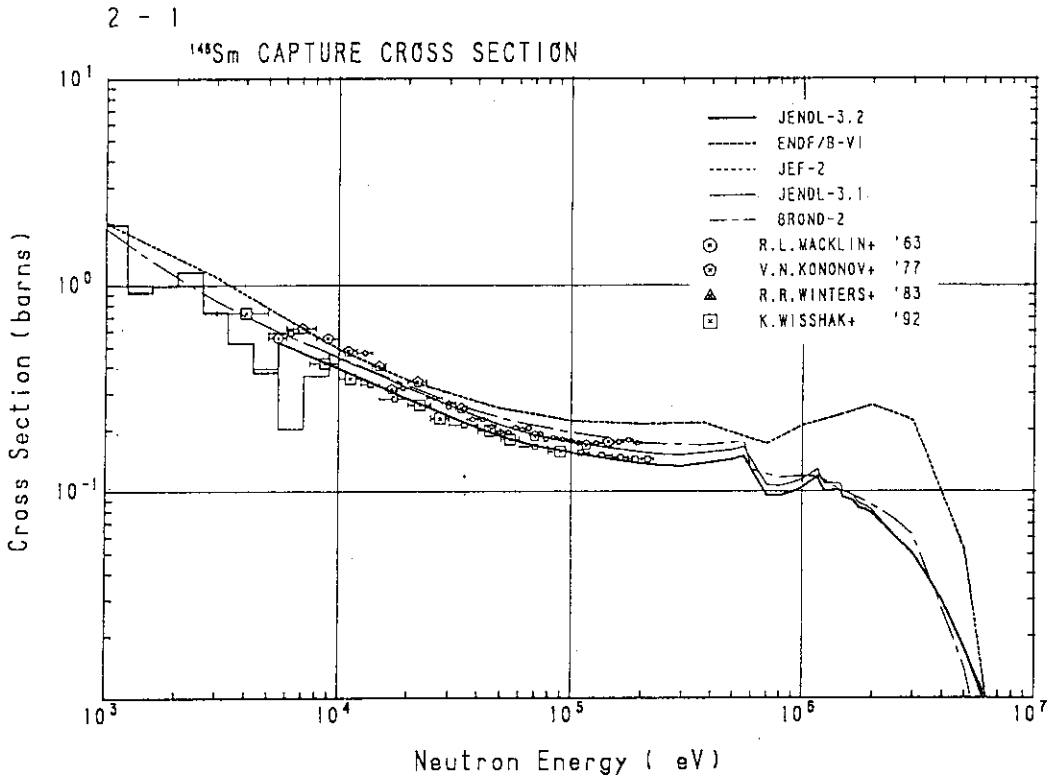

Fig. 7 Comparison of evaluated capture cross section for ^{148}Sm with the experimental data.

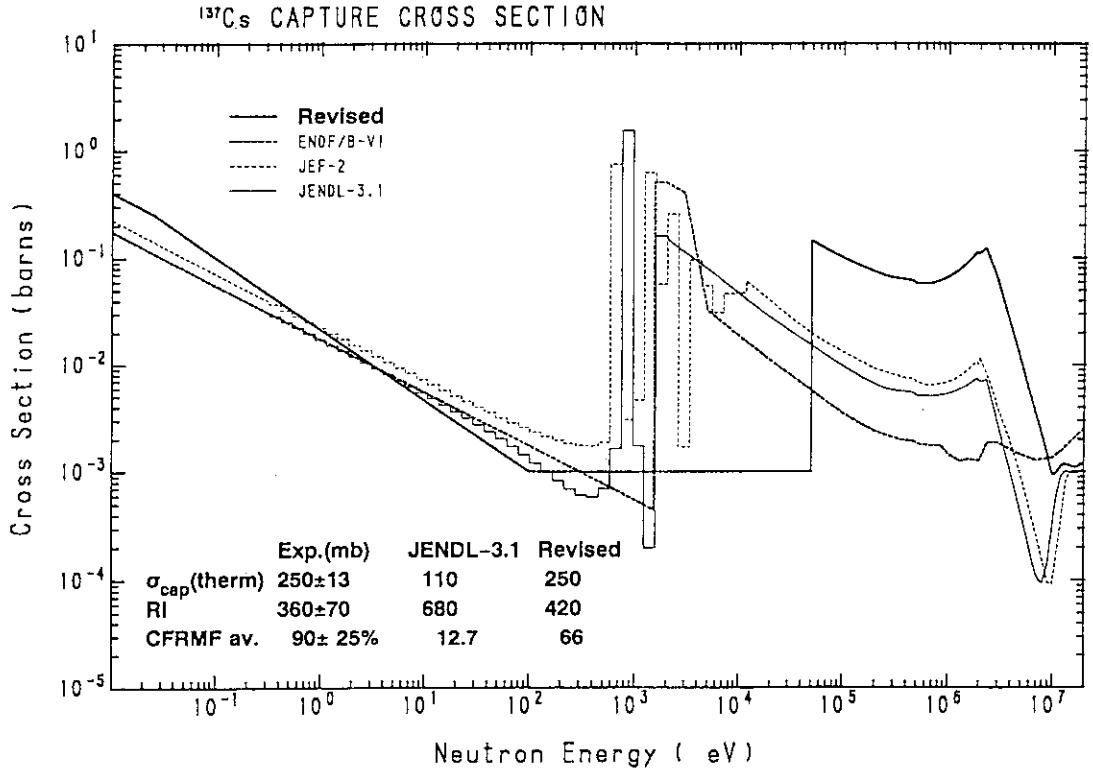

Fig. 8 Comparison of capture cross section adjusted to the integral data for ^{137}Cs with the other evaluated data.

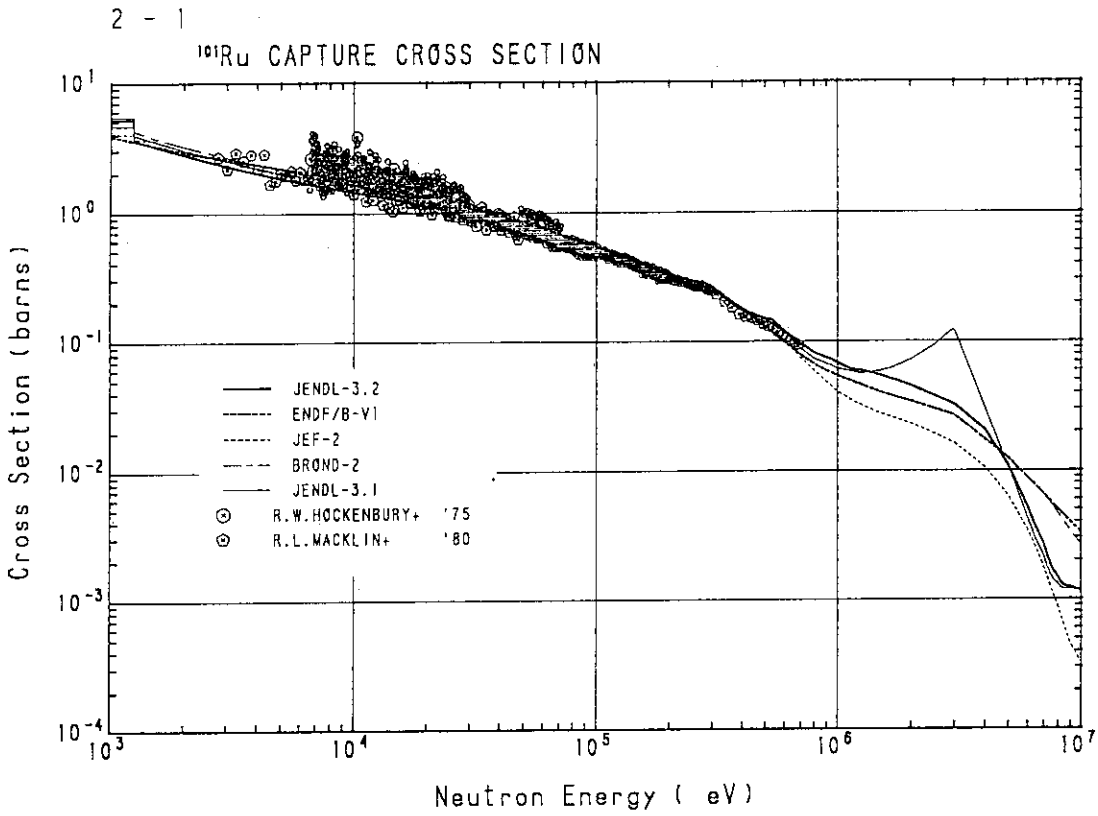

Fig. 9 Comparison of evaluated capture cross section for ^{101}Ru with the experimental data.

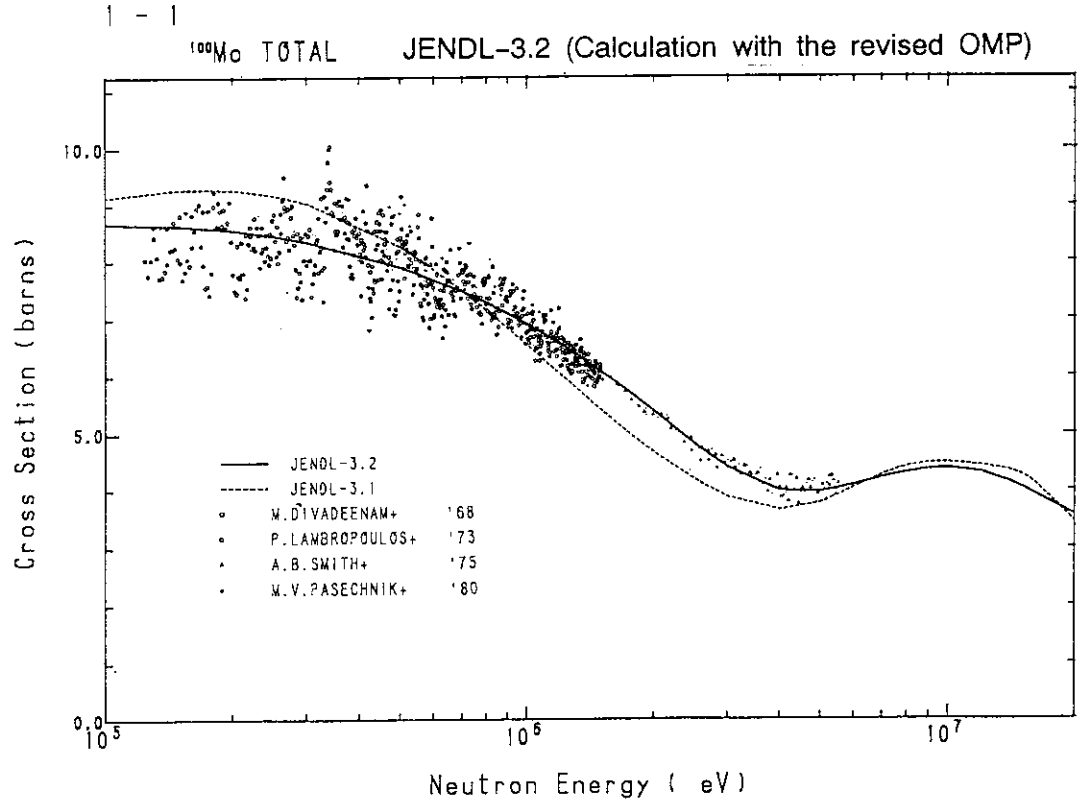

Fig. 10 Comparison of evaluated capture cross section for ^{103}Rh with the experimental data.

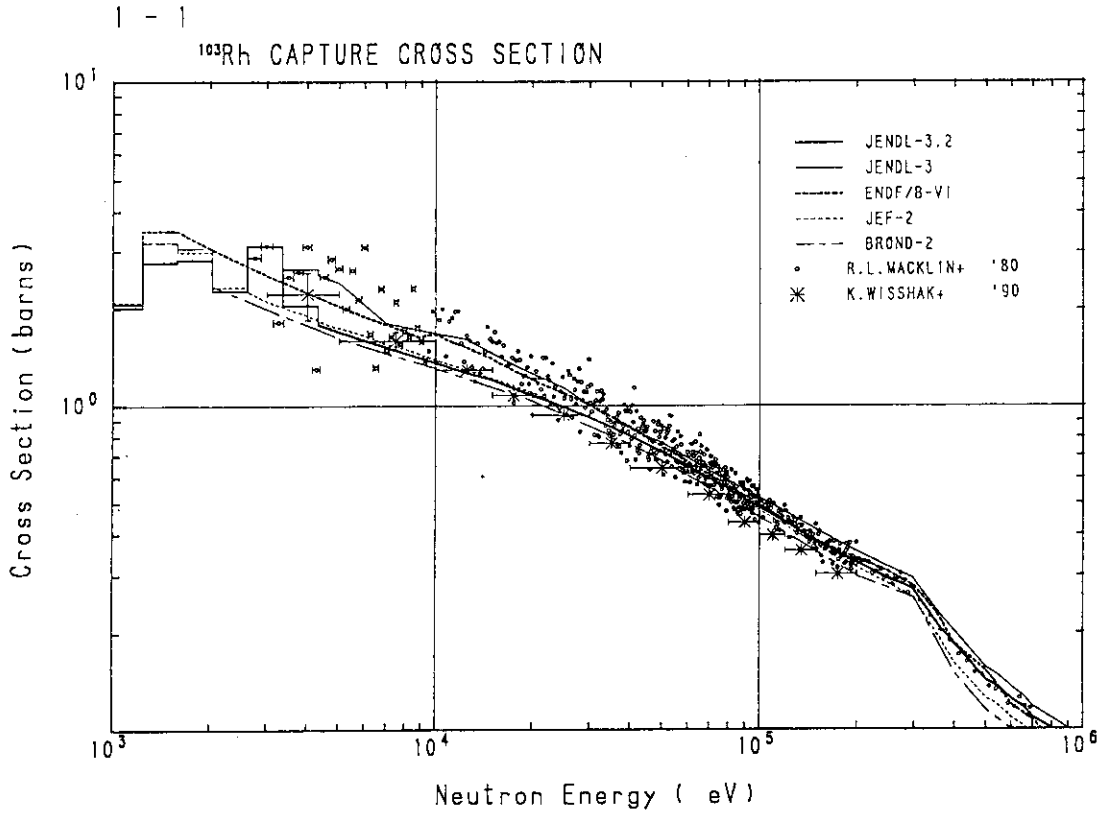

Fig. 11 Comparison of evaluated total cross section for ^{100}Mo with the experimental data.

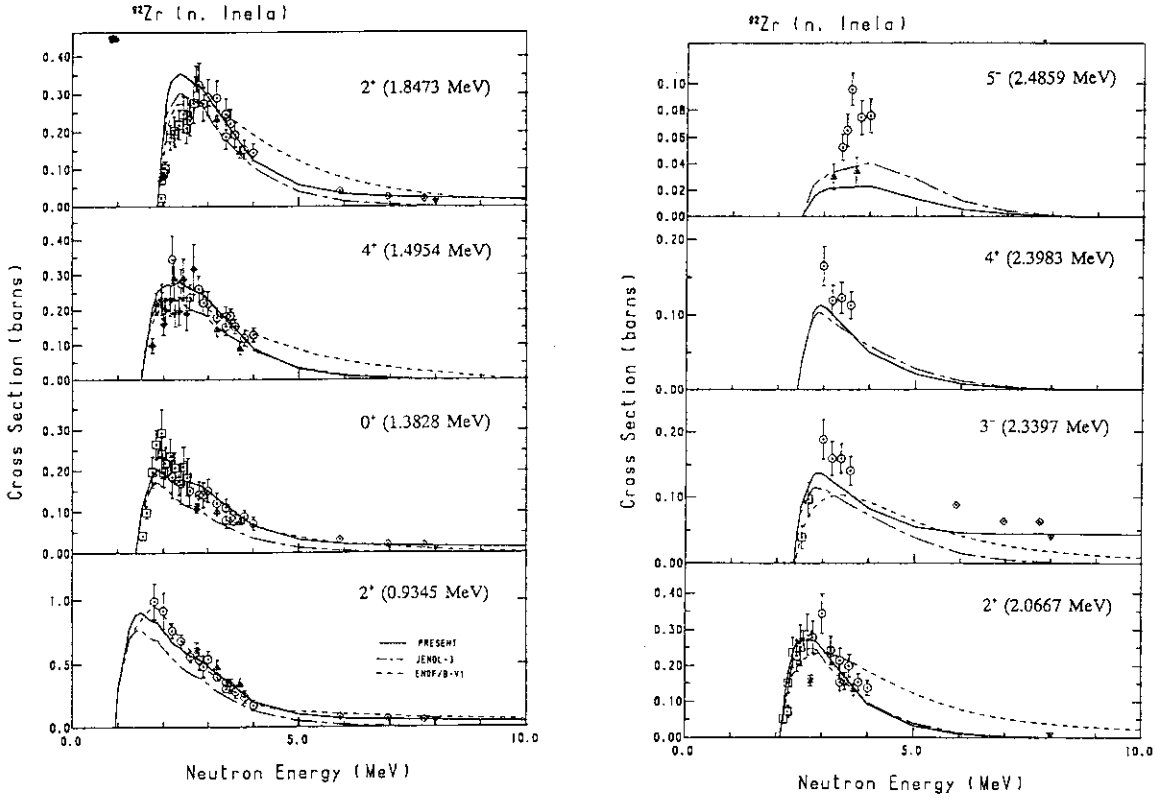

Fig. 12 Comparison of evaluated level excitation function of inelastic scattering for ^{92}Zr with the experimental data.

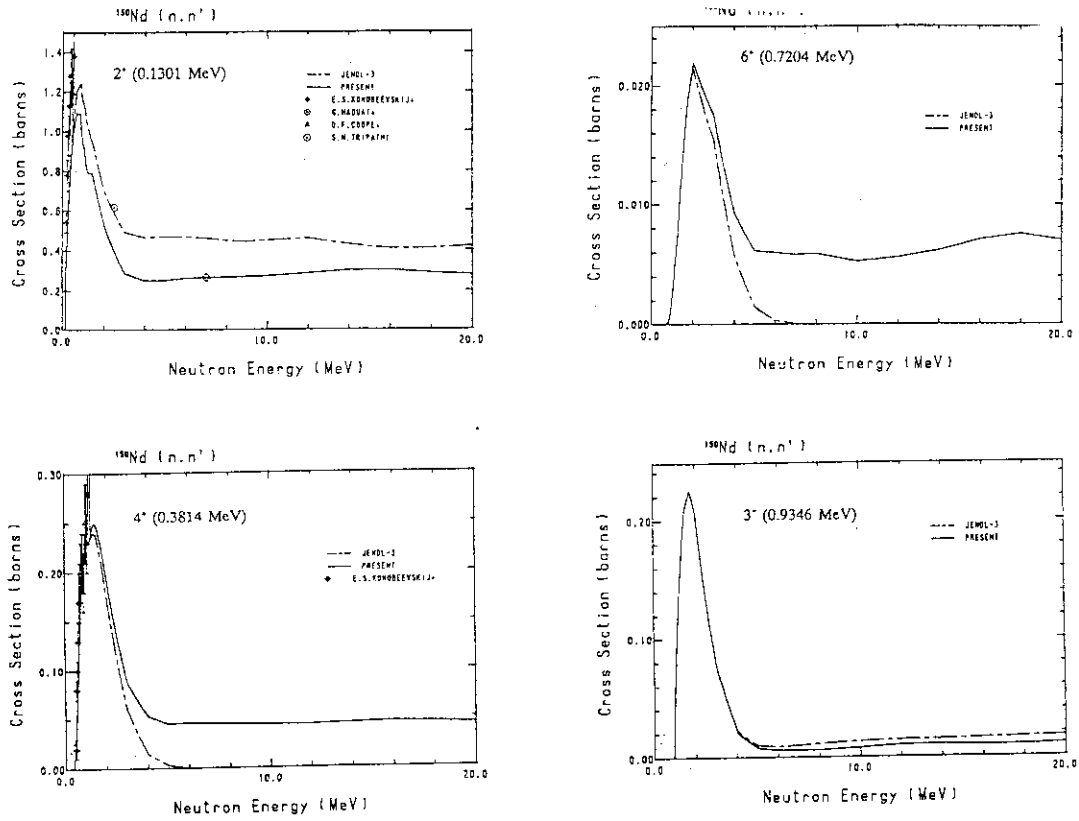

Fig. 13 Comparison of evaluated level excitation function of inelastic scattering for ^{150}Nd with the experimental data.

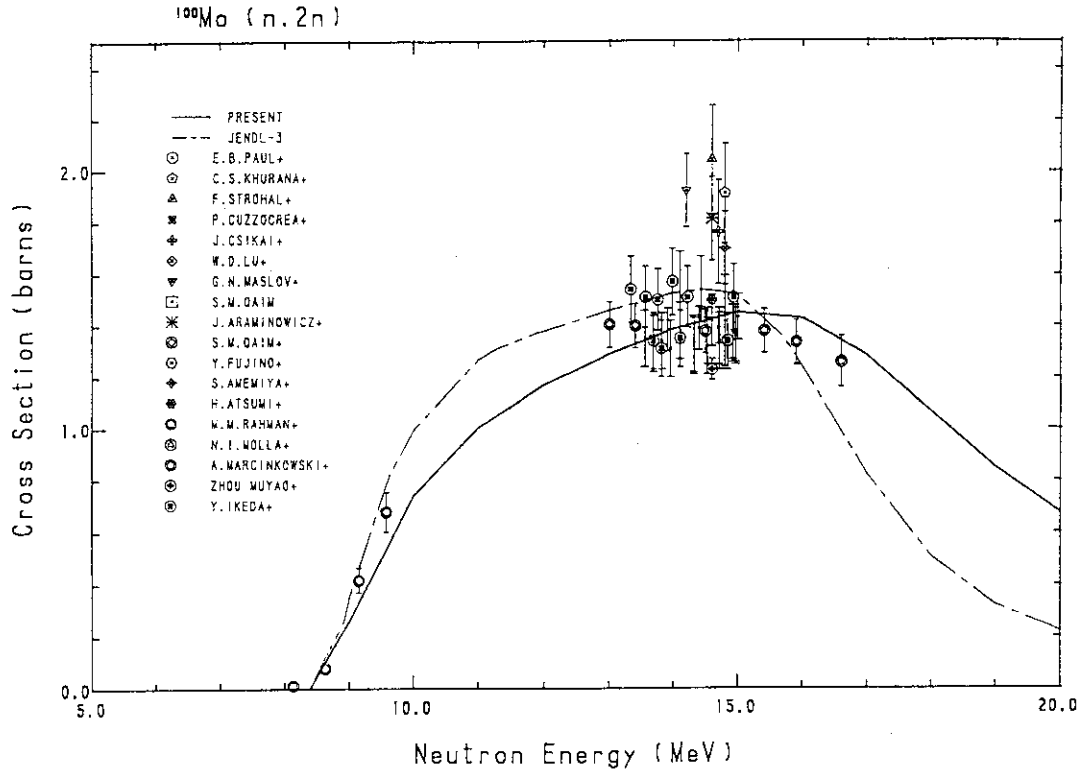

Fig. 14 Comparison of evaluated (n,2n) cross section for ^{101}Ru with the experimental data.

5.14 Evaluation of ^{238}U Inelastic Scattering Cross Section

Toshihiko Kawano, Noboru Fujikawa, and Yukinori Kanda

Department of Energy Conversion Engineering,
Kyushu University

6-1, Kasuga-kouen, Kasuga-shi, Fukuoka 816, Japan

ABSTRACT : A new evaluation of ^{238}U inelastic scattering cross sections has been made. A coupled-channels model is adopted for calculation of direct inelastic scattering cross sections to the excited levels which belong to the vibrational bands of ^{238}U, as well as the ground state rotational band. The members of a certain vibrational band are coupled to the 0^+-2^+-4^+ triad of the ground state rotational band levels. A band coupling strength β is determined from the experimental inelastic scattering data below 3 MeV. Experimental double differential cross sections (DDX) are also taken into account in the β determination. The calculated level excitation cross sections and the calculated DDX reproduce consistently the experimental data.

1. INTRODUCTION

Reliable neutron inelastic scattering cross sections for ^{238}U are demanded for reactor design. However, determination of the ^{238}U(n,n') cross sections is difficult because of scattered experimental data, and too complicated nuclear structure to calculate with nuclear models, and there are considerable discrepancies among the evaluated nuclear data libraries.

Discrete levels of ^{238}U at low excitation energies are classified into a ground state rotational band and a quadrupole, an octupole vibrational bands. A coupled channels (CC) model calculation of the direct inelastic scattering cross sections to the ground state rotational band levels $(0^+, 2^+, 4^+, \ldots)$ has been successfully applied to analyze the experimental data[1]. While the excitation cross sections of the vibrational band members are usually evaluated with a DWBA (Ref.2, for example). This method, however, may bring some uncertainties into the evaluation, because the DWBA calculations are normalized to the experimental data, and there is a discrepancy between the γ-ray and neutron detected measurements for these levels. Recently the CC model was also adopted for the vibrational states by University of Lowell group[3,4,5], and the excitation cross sections of the levels were calculated up to 3 MeV. We adopt the CC calculation for the evaluation of the vibrational states, and determine a band coupling strength β independent of the Lowell group. The β is determined from the experimental inelastic scattering data below 3 MeV. Experimental double differential cross sections (DDX) at

1.2, 2.03, 4.25, 6.1, and 14 MeV are also included in the β determination.

The evaluated nuclear data library JENDL-3.2 contains the result of the present evaluation.

2. Discrete Level Assignment

In order to evaluate the inelastic scattering cross sections for ^{238}U, a level scheme of this nucleus has to be decomposed into collective band families. Figure 1 is the decomposed band level scheme which was given according to assignment in Ref.3, and the excitation energies and J^{π} of the levels were corrected according to Ref.6. The excited levels with small J value are taken into account, since the inelastic scattering cross sections to these levels are expected to be large. There are some levels that cannot be classified into the collective band families. We take 1059.3(3^+), 1112.6(1^-), 1224.2(2^+), 1278.5(1^-), and 1285.8(5^-) levels into competition in the calculation of the compound process. Above 1290 keV, the excited levels are assumed to be overlapped.

3. Ground State Rotational Band

The evaluation of the inelastic scattering cross sections for 2^+ and 4^+ levels is conducted by the CC calculation with a deformed optical potential parameter set for ^{238}U employing the 0^+-2^+-4^+ level coupling scheme proposed by Bruyères-le-Châtel group[1]. Contribution of the compound process for these levels is significant in the energy range $E_{thresh.} \leq E_n \leq 3$ MeV. The cross sections are given by Engelbrecht-Weidenmüler transformation[7] which is an extension of the Hauser-Feshbach theory when strong absorption channels exist. The competition of a radiative capture channel is taken into account since the influence cannot be ignored near threshold energy of 44.91 keV(2^+) level. The calculation of the cross section of direct and compound process is carried out with ECIS88[8].

The calculated radiative capture cross section is somewhat different from the evaluation of JENDL-3. In addition, a fission channel must be taken into account. The compound inelastic scattering cross sections are normalized so as to conserve a compound formation cross section $\sigma_{CN}(= \sigma_R^{\text{Opt.}} - \sum \sigma_{DI}^{i-\text{th level}})$, when the capture and the fission cross sections in JENDL-3 are considered.

Comparisons of the calculated inelastic scattering cross sections for the 2^+, 4^+, and 6^+ levels with the experimental data[1,9,10,11,12,13] are shown in Fig. 2. The evaluated nuclear data libraries — JENDL-3, ENDF/B-VI, BROND-2, and CENDL-2 — are also depicted in this figure. The differences among the evaluated data seem to be small for the 2^+, 4^+ levels, and they are consistent with the experimental data. There is obvious difference among the evaluations of 6^+ level. However, only one measurement[11] with

relatively large uncertainty is available and thus the discrepancy cannot be solved from the data.

4. Vibrational Bands

The direct inelastic scattering cross sections for the vibrational bands are also evaluated with the CC calculation. The members of a certain vibrational band are coupled to the 0^+-2^+-4^+ triad of the ground state rotational band levels. The coupling between the different vibrational bands is ignored since the strength of the coupling is expected to be weak.

The compound process contribution for the vibrational levels is calculated using the Hauser-Feshbach theory with width fluctuation correction by Moldauer[14]. The optical-statistical model code CoH[15] is used for the calculation of compound inelastic scattering cross sections with a spherical optical potential parameter by Madland and Young[16]. The compound inelastic scattering cross sections are also adjusted as described in the previous section.

The band coupling strength β for each vibrational bands is estimated on the basis of the experimental level excitation cross sections. The available data are, Smith[10], Vorotnikov, *et al.*[13], Olsen, *et al.*[17], Shao, *et al.*[18], and Kazjula, *et al.*[19]. Once the band coupling strength β is obtained, the direct inelastic scattering cross sections for all levels in the band can be calculated simultaneously. Then the β has to be determined so as to be consistent with the experimental data for the considering band. Because the compound inelastic scattering cross section is dominant below $E_n = 2$ MeV, it is difficult to determine the β in this energy region. Then the β is estimated in the energy range $2 \leq E_n \leq 3$.

The calculated cross sections for the octupole $K^\pi = 0^-$ band levels — 680.1 keV(1^-), 731.9 keV(3^-), and 826.7 keV(5^-) — are shown in Fig. 3. As seen in Fig. 3, the CC calculation results in lower values in the energy range $2 \leq E_n \leq 5$ MeV than the experimental data which was obtained with the γ-ray measurements[15]. It is difficult to reproduce consistently these γ-ray detected data for these levels with the CC calculation. Then the neutron detected measurements are adopted to determine the β.

Comparisons of the calculated inelastic scattering cross sections to 950.2 keV(2^-, Octupole $K^\pi = 1^-$ band), 967.3 keV(2^+, 2γ band), and 1037.3 keV(2^+, β band) levels with the experimental data and the other evaluations are shown in Fig. 4. The present evaluations well represent the neutron detected experimental data denoted with the symbol $\diamond$.

Figure 5 displays the total inelastic scattering cross sections (heavy solid curve), the partial excitation cross sections for all levels (light curves), and continuum inelastic scattering cross sections (heavy dotted curve). The same picture for JENDL-3 and

JEF-2 is also shown in Fig. 5. The total inelastic scattering cross section in the present evaluation and that in JENDL-3 are almost the same except for the energy range 45 keV $\leq E_n \leq$ 400 keV. The present evaluation gives lower values than that in JENDL-3. The other obvious differences are the level excitation cross sections of above 680 keV levels. The cross sections in JENDL-3 (light solid curves in Fig. 5) are larger than the present evaluations in the energy range 3 $\sim$ 20 MeV. The magnitude of the continuum inelastic cross section is defined as the difference between the non-elastic cross section and the other partial cross sections that are inelastic scattering to the discrete levels, fission, capture, $(n, 2n)$, and $(n, 3n)$.

5. Double Differential Cross Section

The CC calculations are extrapolated up to 20 MeV, and a double differential cross section (DDX) is calculated and the comparison with the experimental data are made, in order to confirm an amount of the inelastic scattering cross sections. The DDX is calculated using PLDDX[20]. The fission cross sections, ν, and the energy spectra are taken from JENDL-3. The experimental DDX data were measured by Baba, *et al.*[21], at E_n = 1.2, 2.03, 4.25, 6.1, and 14 MeV. 4.25 and 6.1 MeV data are important since contribution of the vibrational band levels at the excitation energies $\sim$1 MeV is separated from the elastic group (0^+-2^+-4^+) and the experimental level excitation cross sections at these energies are not accessible.

The comparisons of calculated DDX and the experimental data at 6.1 MeV and $\theta = 30°$ are shown in Fig. 6. Note that the elastic scattering cross section was not included in the DDX calculation. As seen in this figure the present evaluation which is based on the CC calculation gives reasonable agreement with the DDX data around $Q = -1$ MeV where the inelastic scattering cross sections to the vibrational levels are dominant.

6. Conclusion

The new evaluation of the ^{238}U inelastic scattering cross sections were done. The direct process for the vibrational states were evaluated with the coupled-channels model. The calculated double differential cross sections with the present evaluation agree with the experimental data.

REFERENCES

[1] G.Haouat, J.Lachkar, Ch.Lagrange, J.Jary, J.Sigaud, and Y.Patin, *Nucl. Sci. Eng.*, **81**, 491(1982).

[2] P.E.Hodgson and A.M.Kobos, *Nucl. Sci. Eng.*, **89**, 111(1985).

[3] D.W.Chan, J.J.Egan, A.Mittler, and E.Sheldon, *Phys. Rev.*, **C26**, 841(1982).

[4] E.Sheldon, L.E.Beghian, D.W.S.Chan, A.Chang, G.P.Couchell, J.J.Egan, G.Goswami, G.H.R.Kegel, S.Q.Li, A.Mittler, D.J.Pullen, W.A.Schier, J.Q.Shao, and A.Wang, *J.Phys. G : Nucl. Phys.*, **12**, 443(1986).

[5] E.Sheldon, A.Aliyar, L.E.Beghian, J.J.Egan, G.H.R.Kegel, A.Mittler, and E.D.Athur, *Proc. Int. Conf. on Nuclear Data for Science and Technology,* Jülich, Germany, p.989(1991).

[6] E.N.Shurskikov, *Nuclear Data Sheets,* **53**, 601(1988).

[7] P.A.Moldauer, *Phys. Rev.*, **12**, 744(1976).

[8] J.Raynal, program ECIS88, unpublished.

[9] L.E.Beghian, G.H.R.Kegel, T.V.Marcella, B.K.Barnes, G.P.Couchell, J.J.Egan, A.Mittler, D.J.Pullen, and W.A.Schier, *Nucl. Sci. Eng.*, **69**, 191(1979).

[10] A.B.Smith, *Nucl. Phys.*, **47**, 633(1963).

[11] P.Guenther, D.Havel, and A.Smith, ANL/NDM-16(1975).

[12] F.Y.Tsang and R.M.Brugger, *Nucl. Sci. Eng.*, **65**, 70(1978).

[13] P.E.Vorotnikov, V.A.Vukolov, E.A.Koltypin, Ju.D.Molchanov, G.A.Otroshchenko, and G.B.Jan'kov, *Proc. 4th All Union Conf. on Neutron Physics,* Kiev, CIS, vol.2, p.119(1977).

[14] P.A.Moldauer, *Nucl. Phys.*, **A344**, 185(1980).

[15] T.Kawano, program CoH, unpublished.

[16] D.G.Madland and P.G.Young, *Proc. Int. Conf. Neutron Physics and Nuclear Data for Reactors and Other Applied Purposes,* Harwell, UK, p.349(1978).

[17] D.K.Olsen, G.L.Morgan, and J.W.McConnell, *Proc. Int. Conf. on Nuclear Cross Sections for Technology,* Knoxville, USA, p.677(1979).

[18] J.Q.Shao, G.P.Couchell, J.J.Egan, G.H.R.Kegel, S.Q.Li, A.Mittler, D.J.Pullen, and W.A.Schier, *Nucl. Sci. Eng.*, **92**, 350(1986).

[19] B.G.Kazjula, E.M.Kozulin, L.A.Pobedonostsev, G.A.Tutin, Ju.A.Nemilov, L.N.Sysoeva, and A.A.Filatenkov, *Jadernye Konstanty, Obninsk reports,* **4/39**, 14(1980).

[20] S.Chiba, PLDDX, unpublished.

[21] M.Baba, H.Wakabayashi, N.Ito, K.Maeda, and N.Hirakawa, *Nucl. Sci. Technol.*, **27**, 601(1990).

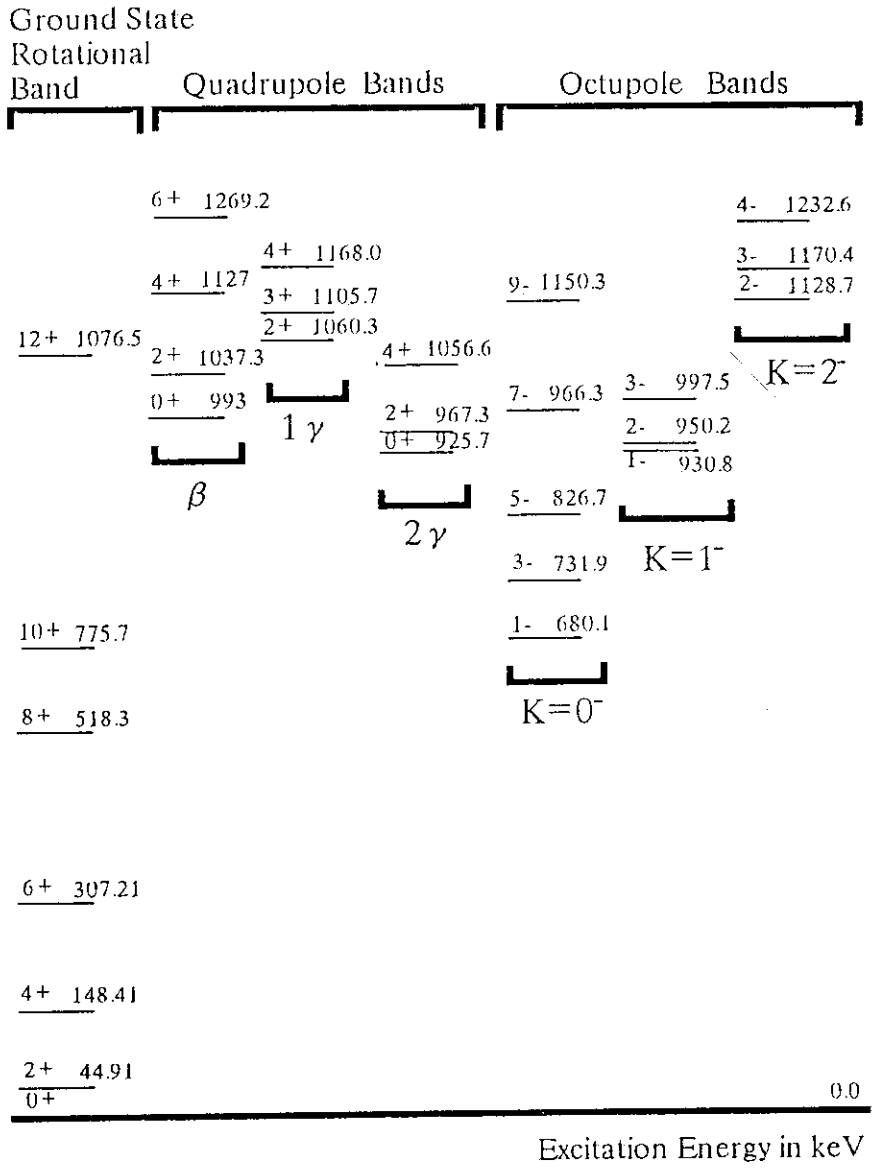

Fig. 1 Decomposition of the collective band level scheme of ^{238}U.

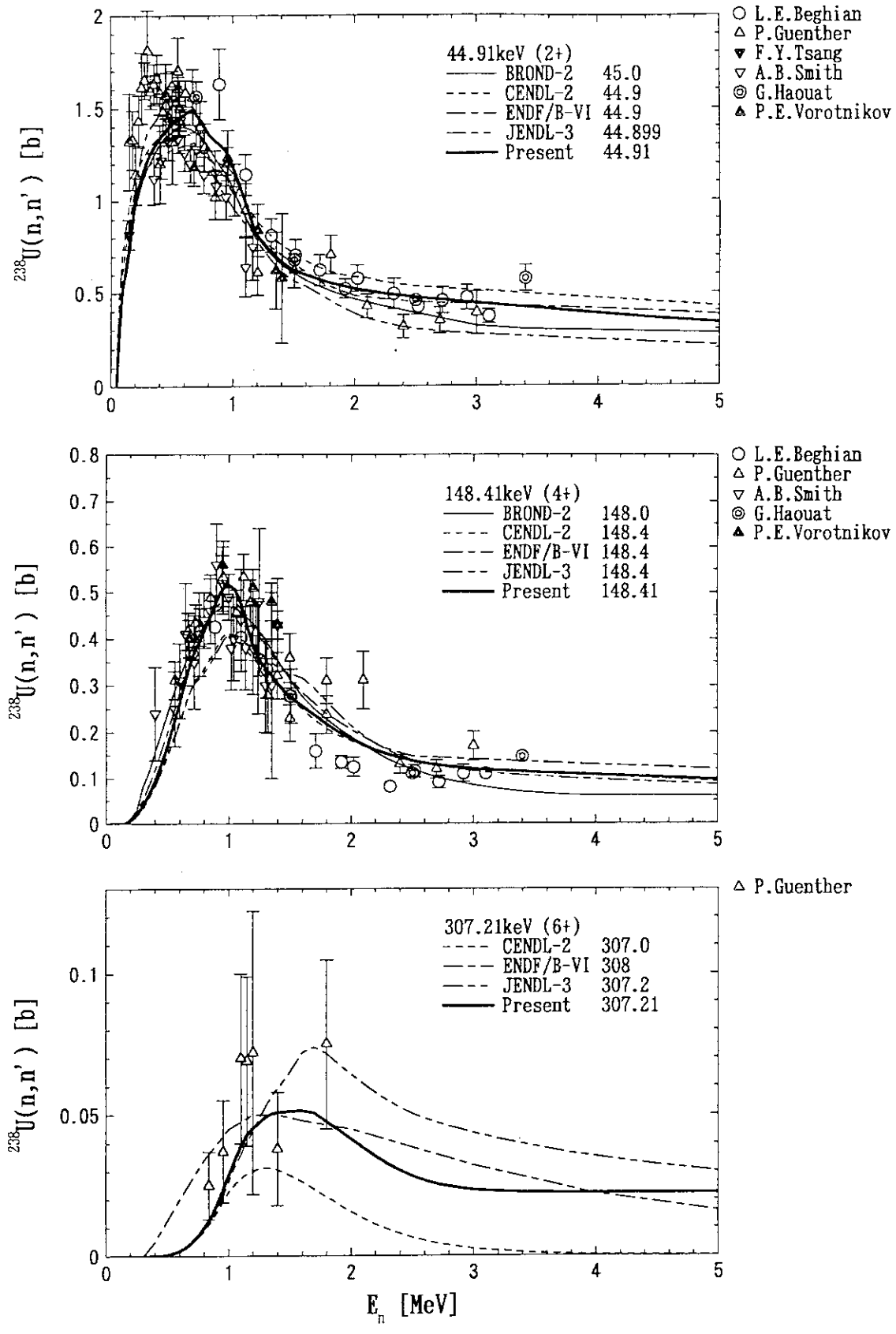

Fig. 2 Comparisons of the calculated and the experimental inelastic scattering cross sections to the ground state rotational band levels.

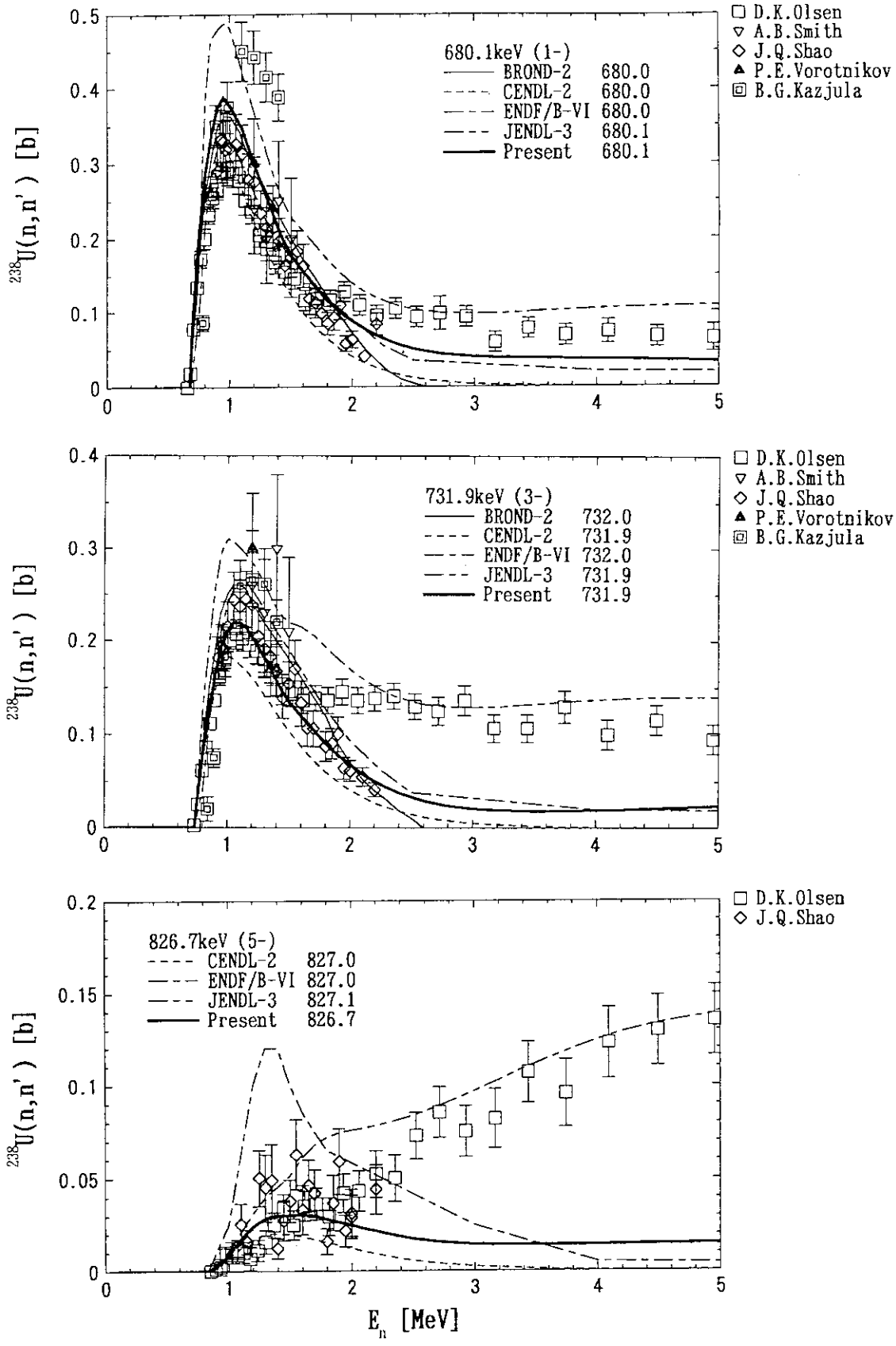

Fig. 3 Comparisons of the calculated and the experimental inelastic scattering cross sections to the octupole K = 0^- band levels.

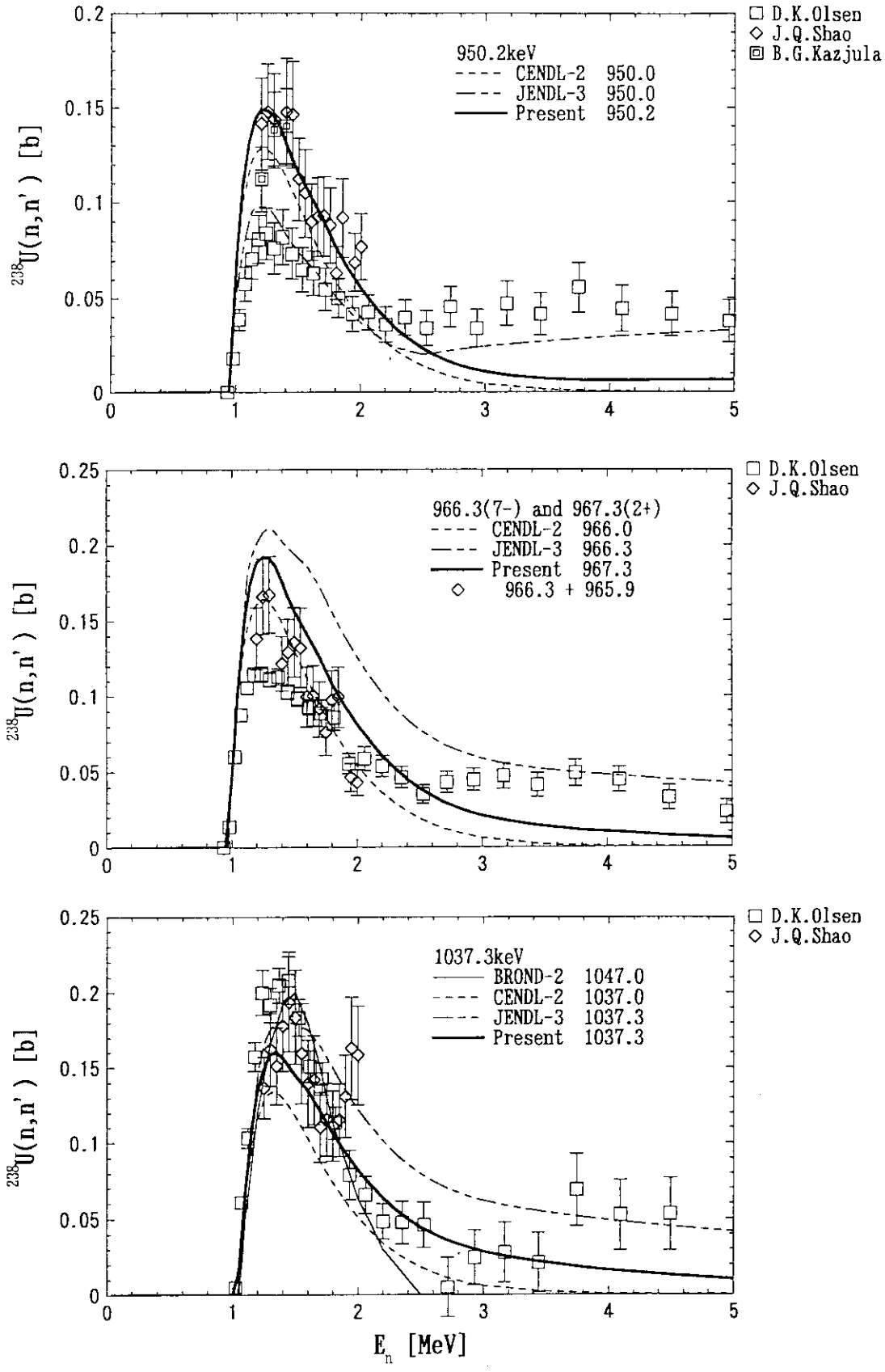

Fig. 4 Comparison of the calculated and the experimental inelastic scattering cross sections to 950.2keV(2^-) (the octupole K = 1^- band), 967.3keV(2^+) (the quadrupole 2γ band), and 1037.3keV(2^+) (the quadrupole β band) levels.

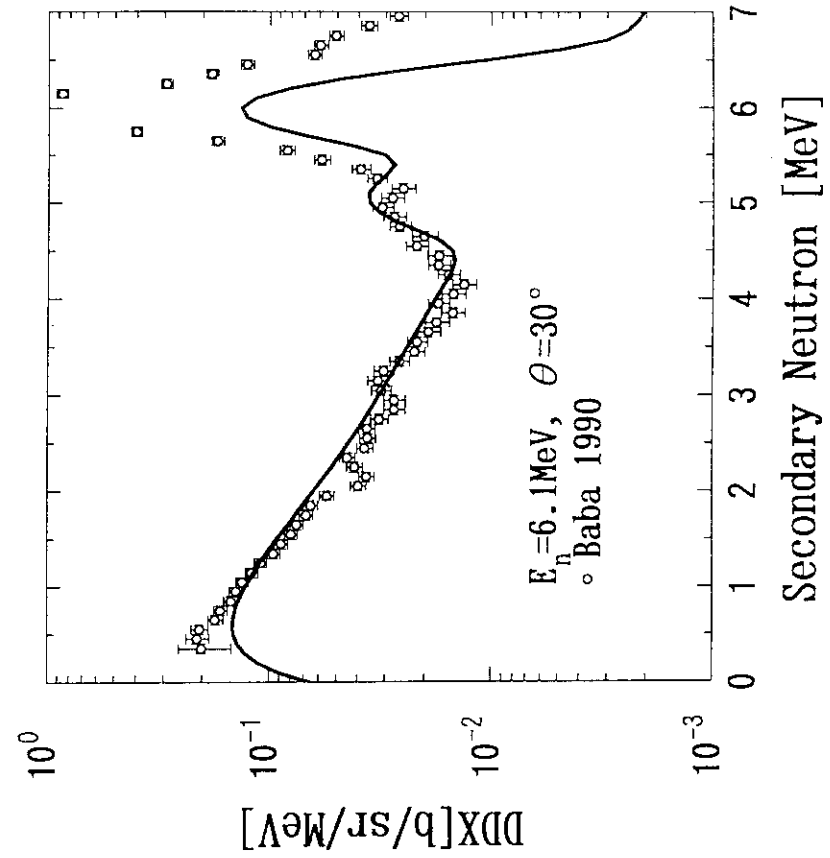

Fig. 6 Comparison of the calculated and the experimental DDX at E_n = 6.1MeV and θ = 30°.

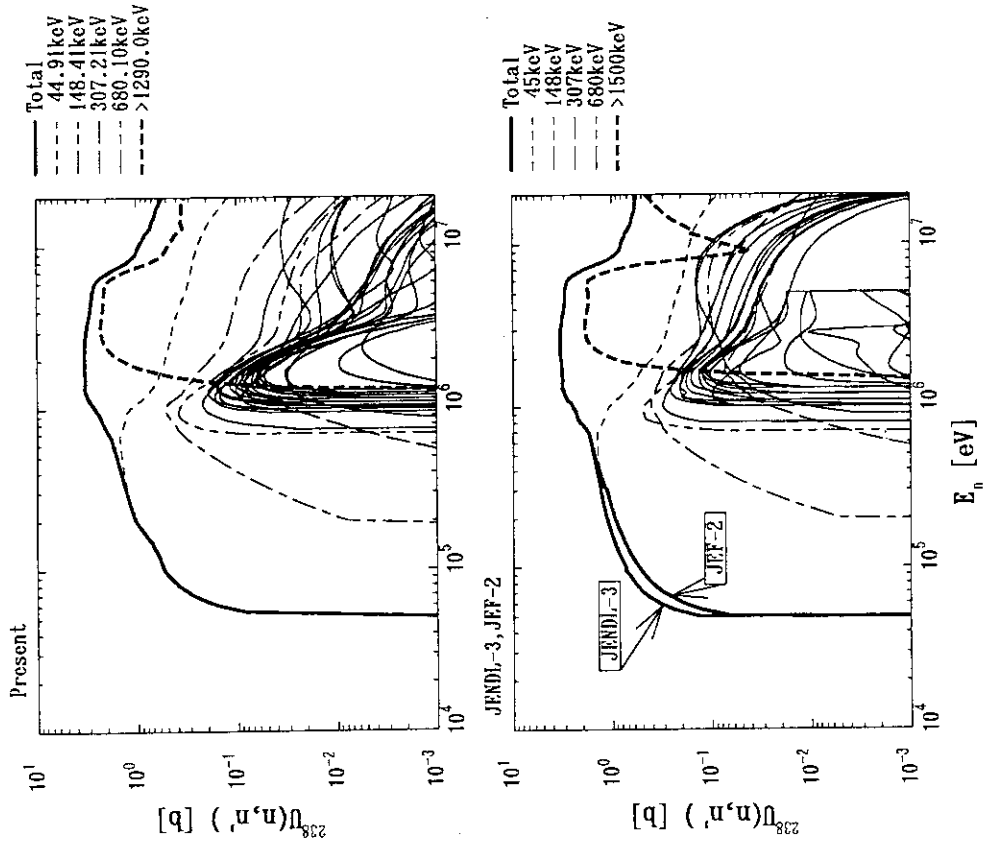

Fig. 5 Total, partial, and continuum inelastic scattering cross sections.

5.15 Evaluation of Neutron Cross Sections of ^{12}C up to 50 MeV

Satoshi Chiba, Tokio Fukahori, Yukinobu Watanabe* and Yoshihide Koyama*

Japan Atomic Energy Research Institute
* Kyushu University

Abstract

The neutron cross sections of ^{12}C have been evaluated in the energy range of 20 to 50 MeV. The total cross section was determined by the generalized least-squares method taking account of the available experimental information. Other quantities are evaluated with the aid of theoretical calculations. The spherical optical model was employed to evaluate the reaction and elastic scattering cross sections. The inelastic scattering to the first excited 2^+ state was calculated based on the DWBA. The optical potentials used in these calculations were obtained in a microscopic way. The double-differential data for neutron, proton, deuteron, triton, ^3He and α-particle emissions and recoil spectra are evaluated based on the Monte-Carlo method.

1. Introduction

The interaction cross sections of ^{12}C with energetic neutrons are of special importance in many fields of science and technology, e.g., development of radiation-tolerable materials for D-T fusion reactors, analysis of radiation dose in cancer therapy with high-energy neutrons, shielding of accelerator facilities, etc. The available evaluated data for n-^{12}C interaction is restricted mainly below 20 MeV (e.g., JENDL-3[1]). Recently, an evaluation was completed up to GeV region by Pearlstein[2]. This evaluation, however, is based on the hybrid model of pre-equilibrium reaction plus evaporation model; assumptions which may not be particularly suited for this nucleus below several tens MeV.

In Japan, a group of material scientists has proposed the ESNIT (Energy Selective Neutron Irradiation Test Facility) project to investigate the damage properties of various materials for the candidates of structural materials of D-T fusion reactors[3]. This facility produces neutrons based on the $^7Li(d,n)$ reaction, with maximum energy around 50 MeV. From this point of view, it was required to produce the evaluated data up to 50 MeV as accurately as possible. The present evaluation has been carried out mainly to fulfill the request from the ESNIT group. Therefore, the upper energy was set to be 50 MeV. On the other hand, the lower energy was set to be 20 MeV, below which the data in JENDL-3 can be utilized.

In the present evaluation, the total cross section was evaluated based on the generalized least-squares method by taking account of the available experimental data. Unfortunately, experimental data are not sufficient for other quantities to perform the evaluation based only on experimental information. Therefore, the evaluation had to rely partly on the theoretical calculations. The microscopic spherical optical model and DWBA were used to evaluate the discrete cross sections, and the Monte-Carlo method was employed to evaluate the double-differential cross sections (DDX). The evaluation of DDX was carried out by the SCINFUL/DDX program[4,5,6] which was specifically developed to calculate the neutron cross sections of ^{12}C.

2. Outline of the Evaluation Methods

The evaluation was divided into two parts, i.e., 1) the discrete part, and 2) the continuum part. The discrete part involves the evaluations for total, reaction, elastic scattering cross sections, inelastic scattering cross section to the first 2^+ state and capture cross section. The double-differential data are evaluated in the continuum part as continuous particle production cross sections.

3. Discrete Part Evaluation

3.1. Total Cross Section

The total cross section was evaluated based on the generalized least-squares method. In the present work, the following three sets of (relatively new) experimental data were taken into consideration;

Authors	Energy Range (MeV)	Neutron Source	Time resolution (ns/m)
Kellie et al.[7]	18.1 - 40.1	90-MeV e on W + Be	0.025
Cierjacks et al.[8]	18.0 - 32.0	50-MeV d on U	0.005
Larson[9]	18.1 - 80.9	140-MeV e on Ta	0.038

No clear explanation was given in these references on the numerical value of the systematic errors. Therefore, a 1-% systematic error was subjectively assigned to the data of Kellie et al. and Larson, which agree well each other in the overlapping energy region. However, the data measured by Cierjacks et al. are systematically higher than these data above 20 MeV by several %. This is probably due to the low S/N ratio of the measurement of Cierjacks et al. in this energy region; a result of the characteristics of the d-U neutron source which has a rapid fall of neutron intensity above around 20 MeV[10]. On the other hand, the data measured by Cierjacks et al. has the highest resolution. Therefore, it was decided not to abandon this data, but to give a rather large (5%) systematic error. By this assumption, the data of Cierjacks et al. was taken into account effectively as a "shape" data.

The analysis was carried out by the GMA code system[11,12]. The flow chart of this process is shown in **Fig. 1**. The experimental data were retrieved from NESTOR-2, and the format was converted to that of the GMA code system. Then, the systematic errors, determined above, are assigned, and the values at specified grid energy points are generated. The prior data are required for this procedure, and were taken from the spherical optical model calculation as described below. The GMA combines these three sets of data, and generates the evaluated data at the grid points. The weight was taken to be prior times %-error of each data[12]. This process was repeated once, replacing the prior data by the result of GMA code. The final value of the error enhancement factor (square-root of chi-square divided by number of freedom) was 1.37; statistically acceptable value.

The evaluated data are compared with the experimental data in **Fig. 2**. The three solid lines show the presently evaluated data; the upper and lower curves showing the $\pm 1\sigma$ range. The error varies from about 1 % at 20 MeV and 3 % at 50 MeV. In the energy range from 20 to 30 MeV, the present evaluation has a pronounced structure which reflects the high resolution data of Cierjacks et al. However, the magnitude is closer to the data of Kellie et al. and Larson which were considered to be more accurate in absolute sense; showing a clear benefit of employing the generalized least-squares method with full covariance information. Above 30 MeV, the present results exhibits a smoother energy dependence. **Fig. 3** shows the

error−correlation matrix of the presently evaluated total cross section. The "wall" at the furthest face corresponds to the diagonal unity components. The data have a strong correlation below 30 MeV. This is tribute to the presence of the data of Cierjacks et al. for which we gave a large systematic error, thus dominating the "shape" of the cross section in this energy range. The correlation becomes smaller and smaller with increasing energy, and the 50−MeV data has only about 10% correlation with other data.

3.2 Optical Model Calculation

Except for the total cross section, unfortunately, the data is scarce above 20 MeV. Therefore, the present evaluation was carried out by combining the available few experimental information with the spherical optical model calculation.

In the energy region of the present work, only a few work has been carried out on the systematics of the optical model potential(OMP). There is an old work of Watson et al.[13], which gives a global OMP for 1−p shell nuclei. This OMP, however, is based mainly on the (p,p) data, and quality of the fit to experimental values are not particularly excellent. On the other hand, Winfield et al.[14], Meigooni et al.[15], Olsson et al.[16] and Yamanouti et al.[17] have made coupled−channels analyses of the measured (n,n) and (n,n') angular distributions below 29 MeV and at 40.3 MeV. However, no clear energy dependence of the optical potential parameters could be drawn as required for evaluation purpose.

In the present evaluation, the OMP was determined in a more fundamental way. The density−dependent effective interaction calculated by Jeukenne−Lejeunne−Mahaux (JLM) theory[18] was used with the nucleon density distribution obtained by the Skyrme−Hartree−Fock (SHF) theory[19]. The real and imaginary central parts of the OMP, V and W, respectively, were calculated as Eq. (1),

$$V(E,r) + iW(E,r) = \lambda_V \cdot Re(U(E,r)) + i \cdot \lambda_W \cdot Im(U(E,r))$$
$$U(E,r) \equiv \int \rho(r') \cdot t_{eff}(E,r,r') d^3r' \qquad (1)$$

where E denotes the incident neutron energy, $\rho(r')$ the SHF density distribution of ^{12}C, and $t_{eff}(E,r',r)$ the density dependent effective interaction of JLM obtained from the "improved" local density approximation. The Skyrme−III force[20] was used in the SHF calculation, and λ_v and λ_w were fixed to be 1.0 and 0.8 as obtained by Hansen et al.[21] By adopting these globally determined values, there is effectively no adjustable parameters in this calculation. The spin−orbit potential was taken from the work of Walter and Guss[22]. The real OMP is similar to the usual Woods−Saxon form. On the contrary, the imaginary OMP was found to have rather complicated forms. The volume integral per nucleon of the V and W are compared with the phenomenological values determined by Winfield et al. The present potential reproduces the global feature well without any adjustable parameters.

The total and reaction cross sections were calculated by using the JLM potential with ECIS79 code[23]. The calculated total cross section agrees well with the result of the previous section except for the energy region below 30 MeV where fluctuation of the cross section is noticeable. The calculated reaction cross section was slightly normalized to give the same value as JENDL−3 at 20 MeV. The reaction cross section is compared with experimental information in **Fig. 4**. Agreement with the data of MacGregor et al.[24] and Zanelli et al.[25] is satisfactory.

3.3 Elastic and Inelastic Scattering Cross Sections

The elastic scattering cross section was obtained by subtracting the reaction cross section from the total cross section, and the result is given in **Fig. 5**. The result is again quite in

good accord with the data measured by Meigooni et al. and Olsson et al. below 26 MeV. The data of Dimbylow[26], which is a result of an optical model calculation, is also in good agreement with the present evaluation. The total, reaction and elastic scattering cross sections evaluated in this work were thus proved to be consistent each other. The angular distribution of elastically scattered neutrons were determined from a Legendre fit to the data of Meigooni et al. below 26 MeV. Above this energy, the result of the spherical optical model was adopted. The present evaluation reproduces the angular distribution data at 40.3 MeV measured by Winfield et al.

The inelastic scattering cross section to the first excited 2^+ state (Ex=4.44 MeV) were calculated by the DWBA with DWUCK-4 program[27]. The JLM OMP was employed to calculate the distorted wave, while the coupling potential was obtained from the concept of "collective model" as

$$V_{couple} = \frac{d}{dr}(V+iW) \qquad (2)$$

and the result was normalized to the data measured by Olsson et al. at 22 MeV. The result, given in **Fig. 6**, shows that the present calculation reproduces the rather steep slope of this cross section below 22 MeV. The angular distribution was also calculated by DWBA. Below 22 MeV, however, the angular distribution data were replaced by a Legendre fit to the data of Olsson et al.

3.4. Capture Cross Section

The capture cross section was calculated by EXIFON program[28], and was normalized to the data of JENDL-3 at 20 MeV.

4. Continuum Part Evaluation

The double-differential cross sections (DDX) for production of n, p, d, t, ^{3}He and α were evaluated by the Monte-Carlo method with SCINFUL/DDX program, which is a modified version of ORNL SCINFUL program, as well as the DDX of recoil particles. Starting from the following primary reactions,

$^{12}C + n \rightarrow n' + 3\alpha$
$\rightarrow 2n + {}^{11}C$
$\rightarrow p + {}^{12}B$
$\rightarrow d + {}^{11}B$
$\rightarrow t + {}^{10}B$
$\rightarrow {}^3He + {}^{10}Be$
$\rightarrow \alpha + {}^{9}Be$

decays of the each unstable nucleus was traced on the assumption of sequential two-body break-up model up to 5 subsequent steps. Angular distributions of these primary reactions are taken from experimental information if available, while those of the subsequent two-body decays are assumed to be isotropic with respect to the center-of-mass of the decaying nucleus. The kinematics are treated in the relativistic way, and the final results are obtained in the laboratory frame. By this modeling, the DDXs of recoiled particles, e.g., ^{6}Li, ^{7}Li, ^{9}Be, ^{10}B, ^{11}B, etc., are obtained as well as those of light particles. The DDX of charged particles are also calculated below 20 MeV, because these quantities are not given in JENDL-3. At

each incident energy, 500,000 histories were taken. More details on this program are found in Refs. 4, 5 and 6.

In **Figs. 7** and **8**, examples of the DDX of p and α at 39.7 MeV are compared with experimental data measured by Subramanian et al.[29]. Agreement with the data is satisfactory.

5. Concluding Summary

Evaluation of neutron cross sections of ^{12}C was carried out in the energy region of 20 to 50 MeV. The total cross section was evaluated on the basis of generalized least−squares method. Other quantities are evaluated with the aid of theoretical calculations. In the present evaluation, characteristic feature of ^{12}C was taken into account as the nucleon density distribution specific to ^{12}C which was used to calculate the optical model potential in a microscopic way. The DDX was evaluated also by using the SCINFUL/DDX program which was developed to calculate the neutron cross section of ^{12}C. The present evaluation gives a good description of the available experimental data.

Unfortunately, the high−precision total cross section data of Finlay et al.[30] was not available in the numerical form at the time of evaluation. When it becomes available, a re−evaluation of the total cross section might be carried out.

References

1) Shibata, K., Nakagawa, T., Asami, T., Fukahori, T., Narita, T., Chiba, S., Mizumoto, M., Hasegawa, A., Kikuchi, Y., Nakajima, Y. and Igarasi S., "Japanese Evaluated Nuclear Data Library, Version−3, JENDL−3", JAERI 1319 (1990).
2) Pearlstein, S., "Methods Used to Produce Nuclear Data Files for 0 − 10 GeV Incident Neutrons and Protons", Presented at Symposium on Nuclear Data Evaluation Methodology, 12−16 October, 1992, BNL, U.S.A.
3) Sugimoto, M., Noda, K., Kato, Y., Ohno, H. and Kondo, T., "Overview of ESNIT and Nuclear Data", JAERI−M 92−027, p.58(1992).
4) Kashimoto, H., Koyama, Y., Shinohara, H., Watanabe, Y. and Chiba, S., "Study of the ^{12}C Breakup Process and Carbon Kerma Factor", JAERI−M 93−046, p.287(1993).
5) Dickens, J.K., "SCINFUL: A Monte Carlo Based Computer Program to Determine a Scintillator Full Energy Response to Neutron Detection for En Between 0.1 and 80 MeV: User's Manual and FORTRAN Program Listing", ORNL−6462 (1988).
6) Dickens, J.K., "SCINFUL: A Monte Carlo Based Computer Program to Determine a Scintillator Full Energy Response to Neutron Detection for En Between 0.1 and 80 MeV: Program Development and Comparisons of Program Predictions with Experimental Data", ORNL−6463 (1988).
7) Kellie, J.D., Lamaze, G.P. and Schwartz, R.B., "TOTAL CROSS SECTION MEASUREMENT OF ^{6}Li, ^{7}Li AND C FROM 3 TO 40 MeV", Proc. of Int. Conv. on Nuclear Data for Technology, 22−26 Oct. 1979, Knoxvill, U.S.A., p.48(1980).
8) Cierjacks, S., Hinterberger, F., Schmalz, G., Erbe, D., Rossen, P.v. and Leugers, B., Nucl. Instr. Meth. 169, 185(1980).
9) Larson, D.C., "ORELA MEASUREMENTS TO MEET FUSION ENERGY NEUTRON CROSS SECTION NEEDS", Proc. of Symposium on Neutron Cross Sections from 10−50 MeV, 12−14 May, 1980, BNL, U.S.A., p.277(1981).
10) Cierjacks, S., "ACCELERATOR−BASED PULSED WHITE NEUTRON SOURCES", in Neutron Sources For Basic Physics and Applications, An OECD/NEA Report, Pergamon Press, p.81 (1983).

11) Poenitz, W.P., "DATA INTERPRETATION, OBJECTIVE EVALUATION PROCEDURES AND MATHEMATICAL TECHNIQUES FOR THE EVALUATION OF ENERGY-DEPENDENT RATIO, SHAPE AND CROSS SECTION DATA", Proc. of the Conf. on Nuclear Data Evaluation Methods and Procedures, BNL-NCS-51363, p.249(1981).
12) Chiba, S. and Smith, D.L., "A SUGGESTED PROCEDURE FOR RESOLVING AN ANOMALY IN LEAST-SQUARES DATA ANALYSIS KNOWN AS "PEELLE7S PERTINENT PUZZLE" AND THE GENERAL IMPLICATIONS FOR NUCLEAR DATA EVALUATION", ANL/NDM-121 (1991).
13) Watson, B.A., Singh, P.P. and Segel, R.E., Phys. Rev. 182, 977(1969).
14) Winfield,, J.S., Austin, S.J., DeVito,, R.P., Berg, U.E., Chen, Z. and Sterrenburg, W., Phys. Rev. C33, 1(1986).
15) Meigooni, A.S., Finlay, R.W., Petler, J.S. and Delaroche, J.P., Nucl. Phys. A445, 304(1985).
16) Olsson, N., Trostell, B. and Ramström, E., "CROSS SECTIONS AND PARTIAL KERMA FACTORS FOR ELASTIC AND INELASTIC NEUTRON SCATTERING FROM CARBON IN THE ENERGY RANGE 16.5 - 22.0 MeV", Proc. of Int. Conf. on Nuclear Data for Science and Technology, 30 May - 3 June, 1988, Mito, Japan, p.1945 (1989).
17) Yamanouti, Y., Sugimoto, M., Chiba, S., Mizumoto, M. and Hasegawa, K., "SCATTERING OF 28.2 MeV NEUTRONS FROM ^{12}C AND 18.5 MeV NEUTRONS FROM ^{52}Cr AND ^{60}Ni", Proc. of the Int. Conf. on Nuclear Data for Science and Technology, 13-17 May, 1991, Jülich, Germany, p.717 (1992).
18) Jeukenne, J.P., Lejeune, A. and Mahaux, C., Phys. Rev. 16, 80(1977).
19) Reinhard, P.G., "The Skyrme-Hartree-Fock Model of the Nuclear Ground State", Computational Nuclear Physics 1, p.28(1991), Springer-Verlag.
20) Beiner, M., Flocard, H., Giai, N.V. and Quentin, P., Nucl. Phys. A238, 29(1975).
21) Hansen, L.F., "Neutron scattering analysis with microscopic optical model potentials", Proc. of Beijing International Symposium on FAST NEUTRON PHYSICS, 9-13 September, 1991, Beijing, China, p.213 (1992).
22) Walter, R.L. and Guss, P.P., "A global optical potential model for neutron scattering for A>53 and 10 MeV < E < 80 MeV", Proc. Int. Conf. Nuclear Data for Basic and Applied Science, Santa Fe, New Mexico, p.1079(1985).
23) Raynal, J., "Notes on ECIS79", unpublished.
24) Mac Gregor, M.H., Gregor, W.P. and Booth, R., Phys. Rev. 111, 1155(1958).
25) Zenelli, C., Urone, P., Romero, J., Brady, F., Johnson, M., Needham, G., Ullmann, J. and Johnson, D., Phys. Rev. C23, 1015(1981).
26) Dimbylow, P., Physics in Medicine and Biology, 25, 637(1980).
27) Kunz, P.D., "Program DWUCK-4", unpublished.
28) Kakla, H., "STATISTICAL MULTISTEP REACTIONS", Proc. of Workshop on "Computation and Analysis of Nuclear Data Relevant to Nuclear Energy and Safety", 10 February - 13 March, 1992.
29) Subramanian, T.S., Romero, J.L., Brady, F.P., Watson, J.W., Fitzgerald, D.H., Garrett, R., Needham, G.A., Ullmann, J.L. and Zaneli, C.I., Phys. Rev. C28, 521(1983).
30) Finlay, R.W., "Precision total cross sections and the optical model at intermediate energy", Proc. of Beijing International Symposium on FAST NEUTRON PHYSICS, 9-13 September, 1991, Beijing, China, p.299 (1992).

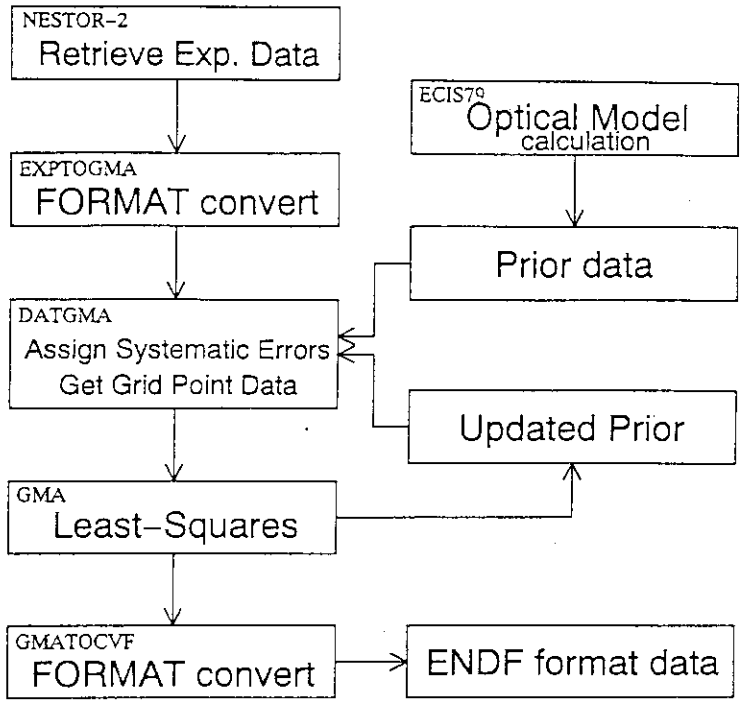

Fig. 1 Flow chart of GMA code system. The small characters at the upper left corner of the boxes denote the name of the programs

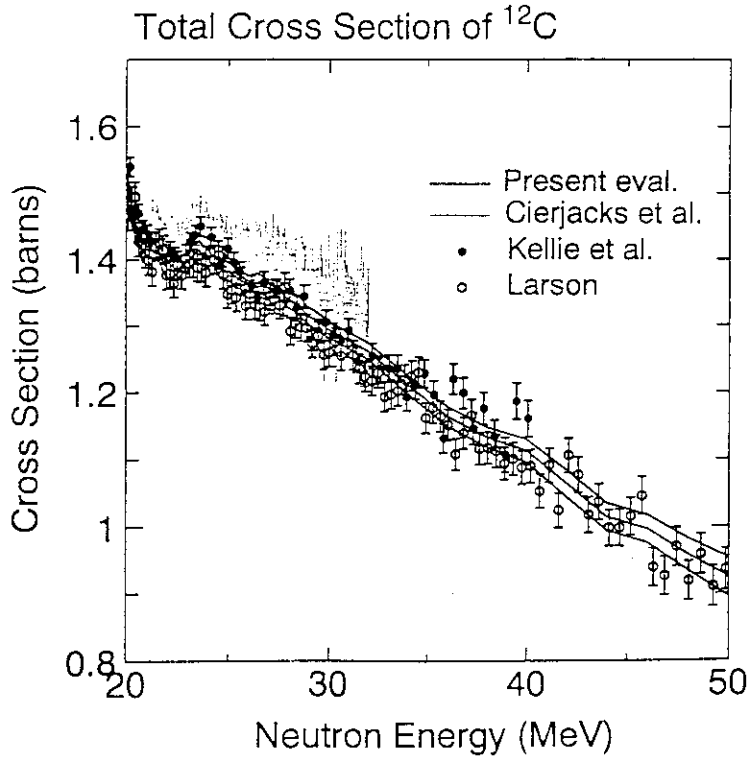

Fig. 2 Total cross section of ^{12}C from 20 to 50 MeV

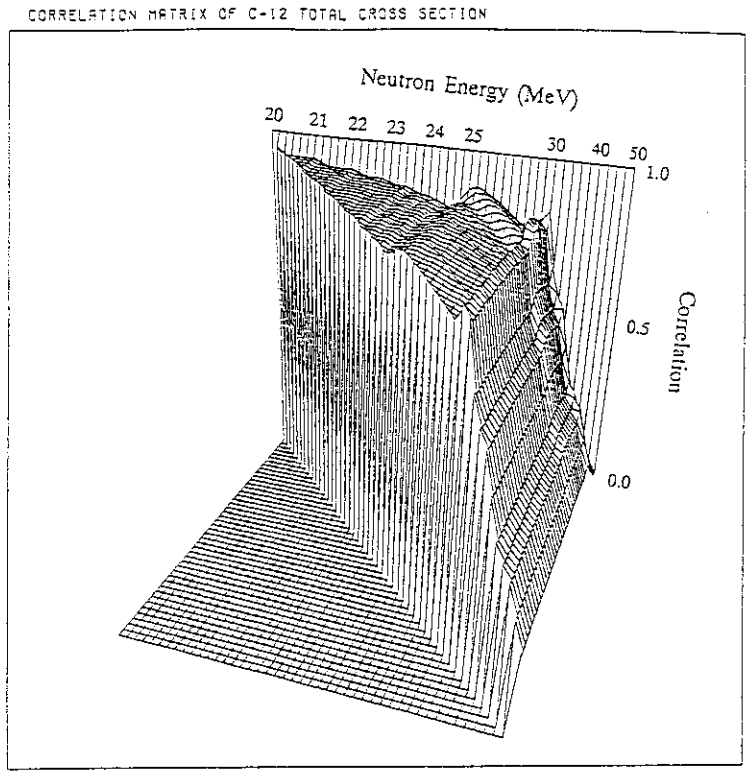

Fig. 3 Error-correction matrix of presently evaluated total cross section of ^{12}C

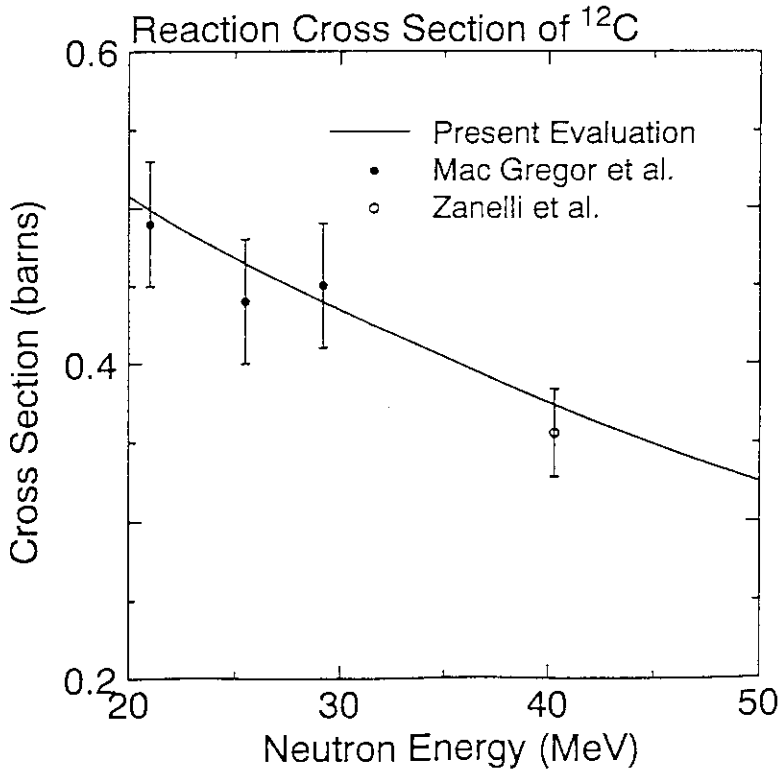

Fig. 4 Reaction cross section of ^{12}C

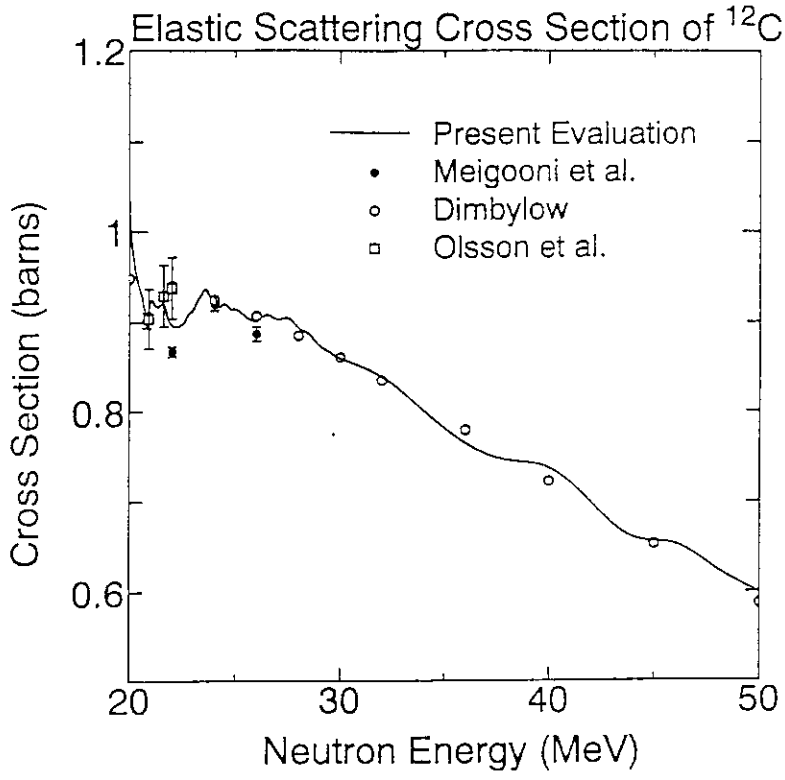

Fig. 5 Elastic scattering cross section of ^{12}C

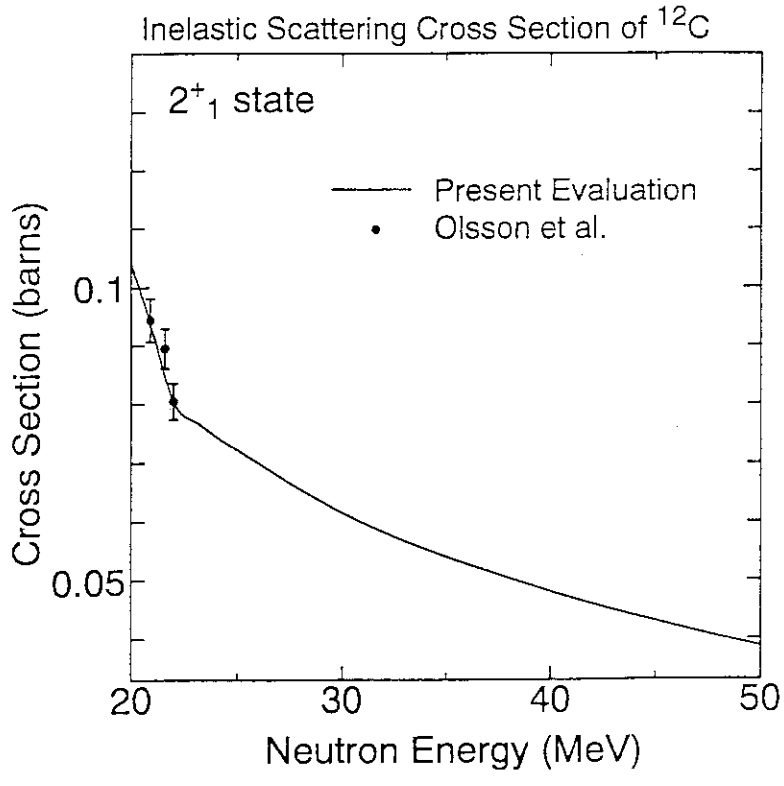

Fig. 6 Inelastic scattering cross section to the first excited 2^+ state of ^{12}C

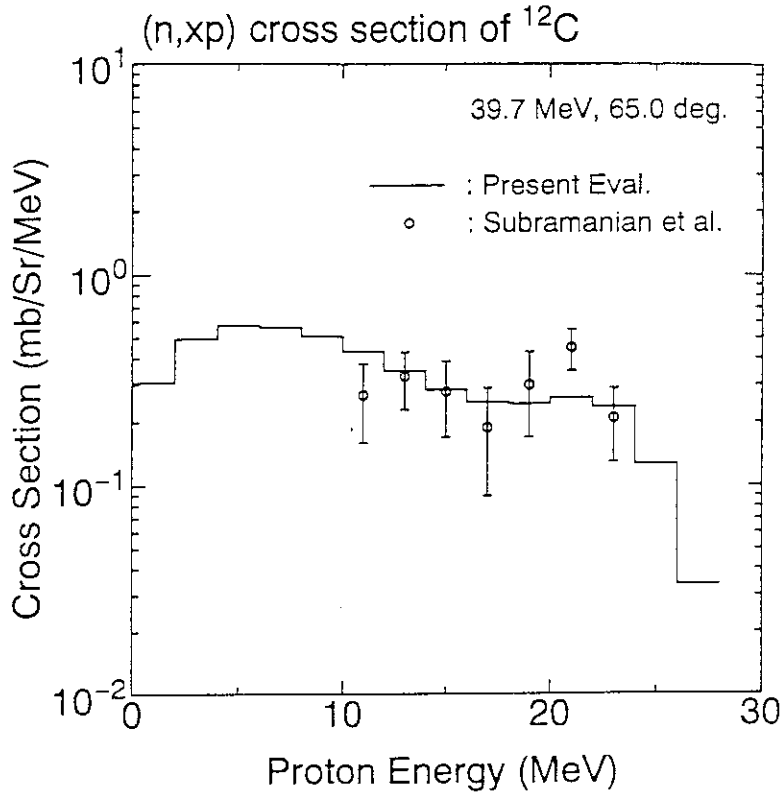

Fig. 7 Double-differential ^{12}C(n,xp) cross section at 39.7 MeV

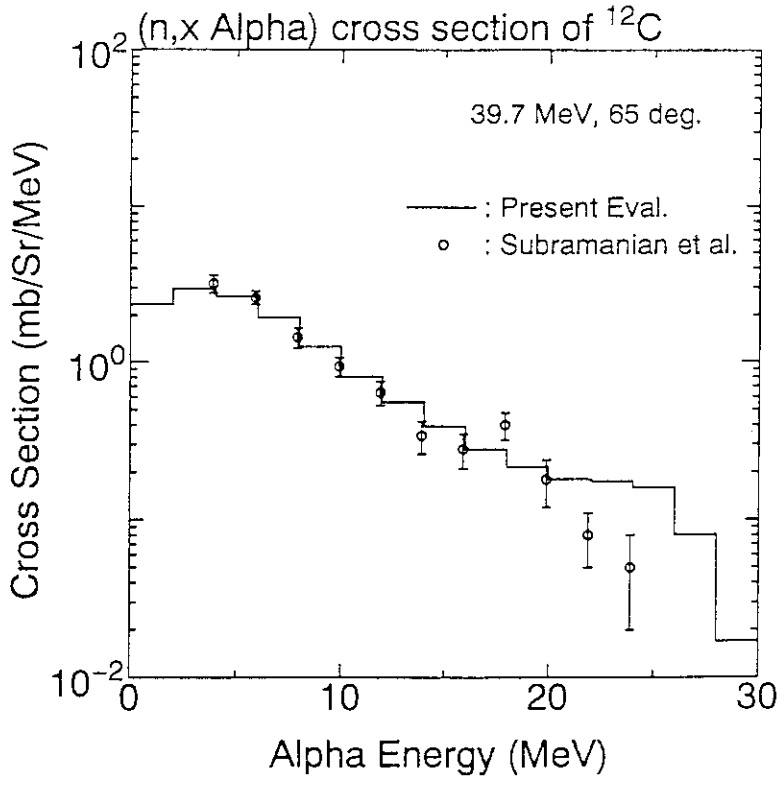

Fig. 8 Double-differential ^{12}C(n,xα) cross section at 39.7 MeV

5.16 Evaluation of Neutron Dosimetry Cross Sections of ^{59}Co and ^{197}Au up to 50 MeV

Naoteru ODANO* and Shin IWASAKI**

* *Tokai Brunch, Ship Research Institute, Ministry of Transport, Tokai, Naka－gun, Ibaraki 319－11, JAPAN*

** *Department of Nuclear Engineering, Tohoku University, Aramaki－Aza－Aoba, Aoba－ku, Sendai 980, JAPAN*

Abstract

Dosimetry cross sections of ^{59}Co and ^{197}Au were evaluated based on the nuclear model calculation from threshold to 50 MeV for the application in accelerator based high energy neutron filed provided by ESNIT at JAERI, etc. For the ^{59}Co, the $(n,2n)$, $(n,3n)$, $(n,4n)$, (n,p), (n,α) and $(n,2n\alpha)$ cross sections were evaluated and compared with available experimental data. The helium accumulation dosimetry cross section was also evaluated. For the ^{197}Au, the $(n,2n)$, $(n,3n)$, $(n,4n)$ and helium production cross section were evaluated. Weak activation cross sections, (n,p) and (n,α), were also evaluated.

1. Introduction

In Japan, it is scheduled to develop a high energy neutron source, ESNIT (Energy Selective Neutron Irradiation Test Facility at JAERI[1]), which is based on a high current deuteron linear accelerator using the Li+d reaction on liquid metal target, similar to the FMIT facility[2]. This facility is expected to provide neutrons of high intensity primarily with 14 MeV peak for the material irradiation test of the fusion energy development. To satisfy the energy selective requirement of the ESNIT, the beam energy varies from 10 to 40 MeV corresponding to the neutron peak energies from 5 to 14 MeV. The ESNIT spectra are not monoenergetic and have a large amount of component above its peak energy, called high energy tail up to 50 MeV.

In order to operate such irradiation facilities efficiently, neutron dosimetry is one of the key technologies to characterize the neutron source. Important issues on the neutron dosimetry have already been discussed[3,4] in conjunction with the FMIT facility. In the discussion, it was pointed out that among the activation dosimetry candidate reactions, the reactions on cobalt and gold were of primary importance because they were mono－isotopic

elements, and almost all activation products were radioactive, and their activities could be measured by a relatively simple technique; furthermore the sensitive regions of these multiple reactions covered the entire energy range of the neutron spectrum up to 50 MeV.

Young and Arthur have already evaluated the cross sections of ^{59}Co from 3 to 50 MeV[5], and for ^{197}Au from threshold to 30 MeV[6] mainly based on the theoretical model calculations by GNASH code[7]. It is, however, valuable to re-evaluate the cross sections regarding their evaluation as the starting points and taking into account a large body of experimental data obtained after the evaluations below 20 MeV, and a few but very recently measured experimental data above 20 MeV, too.

2. Evaluation Method

In this study, a theoretical model code system, SINCROS-II[8], was used to calculate the cross sections. The main part of the system consists of a modified version of the GNASH code. A simplified version of a optical model code, ELIESE-3[9], provides a set of particle transmission coefficients for the GNASH with spherical optical model potential parameters (OMP's). The direct inelastic scattering to the low-lying states of the target nuclides was taking into account for the ^{59}Co calculation using DWUCKY[10], a modified version of DWUCK[11]. In the system, a data base is provided for the OMP for neutron and charged particle, level density related data, and discrete level structure data of the medium and medium-heavy weight nuclei as the default ones.

In the present study, important model parameters (OMP and level density parameters) were modified from the data base values or replaced by other parameter sets to reproduce as well as possible the existing cross sections mainly below 20 MeV, but not with the data above 20 MeV because only a few experimental data with large uncertainties exist. The suitable neutron OMP set was selected by applying a criterion, SPRT test by Delaroche *et al.*[12] using CASTHY[13] and the ELIESE-3 codes.

The consistency of the calculated cross sections was discussed by comparing with experimental data in the whole energy range. Recently valuable activation cross section data for several elements have been measured in the higher energy range using the SF cyclotron facility of Institute for Nuclear Study, University of Tokyo[14,15,16]. These data were very valuable information to validate the present evaluation.

3. Calculation of ^{59}Co Cross Section

Five candidate of the neutron OMP: the system default set, *i.e.*, the modified Walter

and Guss set by Yamamuro[8], Wilmore and Hodgson set[17], Uhl *et al.*'s set[18], Watanabe's set[19], and Arthur *et al.*'s set[5] were tested by the S, R, and T values of the SPRT criterion (P not available); finally the OMP set by Arthur *et al.*'s set was selected[20]. The default proton OMP of Perey[21] was replaced by one of Mani[22] chosen among three explored sets including one by Menet[23]. The validity of the proton OMP was checked through the comparison of the calculated cross sections of ^{59}Co(n,p) and ^{57}Fe(p,n)^{57}Co with the experimental data. The α-particle OMP set has been unchanged from the default set: a modified Lemos's set by Arthur and Young[24].

We chose the six level density parameters for ^{58,59,60}Co, ^{58,59}Fe, and ^{56}Mn, and F2 (the Kalbach constant[25] divided by 100) as the adjustable ones due to their appreciable sensitivities to the objective cross sections(($n,2n$),(n,α) and (n,p)) of the fitting. The parameter adjustment was performed using the general least-squares method[26]. Above 20 MeV, level density parameters for ^{55,54,53}Mn were adjusted to reproduce recent experimental data of ($n,2n\alpha$) reaction by Uwamino *et al.*[16] We determined the decay channels of compound nuclei as shown in Fig.1 considering that our concerned cross sections were those of the reactions that would lead to the unstable nuclides and α-production cross section.

Figure 2 shows trends of the principal cross sections in the present calculation. Figure 3 compares ($n,2n$), ($n,3n$) and ($n,4n$) reaction cross sections with the experimental data, showing consistency with the data by Uno *et al.* above 20 MeV. The (n,xnp) cross sections are compared in Fig.4 with the experimental data below 20 MeV. The calculated (n,p) cross section reproduces relatively well with the data. Among the reactions shown in Fig.4, only the (n,p) reaction can be used in the dosimetry, because the other channels lead to stable or too long lived residual nuclides. Figure 5 illustrates the cross sections for the ($n,xn\alpha$) reactions as well as α-production cross section. Below 20 MeV, the present (n,α) cross section agrees well with the large body of the experimental data. The ^{56}Mn production cross section consists mainly of the (n,α) below 35 MeV; it is however, interesting that ($n,2n2p$) reaction may appreciably contribute to this cross section above 35 MeV. Main contributor to ^{54}Mn ($T_{1/2}$ = 312 d) production cross section is ($n,2n\alpha$) reaction and others might be negligible. This reaction can be a new dosimetry reaction for the long term irradiation purpose in the energy range between 30 and 50 MeV, because the decay data of ^{54}Mn are very well known, and the estimated maximum cross section is large enough (about 100 mb). In the present evaluation of the ($n,2n\alpha$) reaction, the shape of the cross section could not be reproduced completely. Further theoretical analyses must

therefore be necessary to assure the accuracy of the evaluation.

4. Calculation of Gold Cross Sections

We tested the following four neutron-OMP sets mainly with respect to the total cross section: the modified Walter and Guss set, Delaroche's OMP[27] which had been adopted in the analysis by Arthur and Young, Joly's set[28], and Yamakoshi's set[29]. Finally we chose the Delaroche's spherical OMP[27]. The comparison of the calculated total cross section with deformed and spherical OMPs in ref.(27), however, showed remarkable difference below 5 MeV, where the inelastic scattering reaction dominated, and the difference was quite small above this energy. For this reason, we assumed that the spherical OMP would be usable to calculate the threshold cross sections in the higher energy range.

Figure 6 shows the calculated cross section for the $(n,2n)$ reaction together with the experimental data and the evaluated cross section curves taken from IRDF-90[30] and ENDF/B-VI[31]. The IRDF-90 cross section has been validated by the present authors using the activation rate ratio to the standard cross section of $^{27}Al(n,\alpha)^{24}Na$ reaction from 12 to 20 MeV. The IRDF-90 curve shows relatively flat trend at the maximum. This shape can not be reproduced by ENDF/B-VI nor by the present calculation. In the $(n,3n)$ cross section data given in Fig.7, there are two clearly different trends; lower cross section group by Veeser *et al.*[33] and by Iwasaki *et al.*[34], and higher one by Bayhurst *et al.*[35] The present result passes along the lower data group. As shown in the same figure, Bayhurst *et al.* measured $(n,4n)$ cross section only at two energies just above the threshold energy. Uwamino *et al.*[14] gave a smaller excitation function from threshold to 40 MeV than the Bayhurst *et al.* and Uno *et al.* nor those of Uwamino *et al.*[14]

In Fig.8, both (n,p) and (n,α) reaction cross sections are shown with the experimental data. There have been very few measurements on these reactions. In the Young and Arthur's evaluation, they adopted the experimental data of Bayhurst and Prestwood[36] and extrapolated with smooth curves to 30 MeV. The present calculations overestimate by about twice for the (n,p), whereas reproduce well the (n,α) cross sections of Bayhurst et al.'s data above 16 MeV. The (n,α) cross section at 14.7 MeV is consistent with the α-spectrum data by Kneff *et al.*[37] It cannot definitely be concluded, however, whether if the present gold evaluation gave good cross sections of these reactions or not, because the available data are too old.

6. Conclusion

All activation cross sections and α-production cross section have been evaluated for cobalt up to 50 MeV and for gold up to 40 MeV based on the theoretical model calculations. As for the cobalt, the present calculations have successfully reproduced the almost available cross sections not only in the lower energy region below 20 MeV, but also the data above this energy. The $(n,2n\alpha)$ reaction can be a new candidate of the high energy dosimetry reaction. In the gold cross section evaluation, we have obtained a moderately acceptable cross section set, while we found some difficulties of the reproduction of the cross sections. Present evaluations provide a useful basis for the future evaluations of higher energy dosimetry cross sections covering the energy range of spallation neutron sources.

It is strongly recommended that precise and detailed cross section measurements should be carried out for important elements including cobalt and gold above 16 MeV in order to establish the high energy dosimetry cross sections. In particular, the gold data base is very poor except for the $(n,2n)$ reaction.

Acknowledgement

The authors would like to express their sincere thanks to Dr.Y.Uwamino of Institute for Nuclear Study, Univ. of Tokyo, for providing the experimental data before publication.

References

1) Sugimoto, M., *et al.*: *Proc. of 1991 Symp. on Nucl. Data, JAERI－M* 92－027, p.58 (1992).
2) Opperman, E.K.: *HEDL－TME* 81－45(1981).
3) Gold, R., *et al.*: *Proc. of Symp. on Neutron Cross－Sections from 10 to 50 MeV, May 12－14, 1980, Upton, New York, BNL－NCS－*51245, p.553 (1980).
4) Mann, F.M.: *Workshop report of session IV on Fusion Materials Irradiation Test (FMIT) Facility Related Problems － Shielding and Materials Damage Studies*, p.31 (1980).
5) Arthur, E.D., *et al.*: *ibid.*, p.752 (1980).
6) Young, P.G., and Arthur, E.D.: *LA*－10288－PR (1985).
7) Young, P.G., and Arthur, E.D.: *LA*－6947 (1977).
8) Yamamuro, N.: *JAERI－M* 90－006, (1990).
9) Igarasi, S.: *JAERI* 1224, (1972).

10) Yamamuro, N.: *JAERI－M* 88-140, (1988) [in Japanese].

11) Kunz, P.D.: "*DWUCK － A Distorted－Wave Born Approximation Program*", unpublished.

12) Delaroche, J.P., *et al.*: *Proc. Consultant's Meeting on the Use of Nuclear Theory in Neutron Nuclear Data Evaluation, IAEA*－190, Vol.I, p.251, (1979).

13) Igarasi, S. and Fukahori, T.: *JAERI* 1321, (1991).

14) Uwamino, Y., *et al.*: *Nucl. Sci. Eng.*, **111**, 391 (1992).

15) Uno, Y., *et al.*: *Proc. of 1992 Symp. on Nucl. Data, JAERI－M* 93-046, p.247 (1993)

16) Uwamino, Y., *et al.*: private communication.

17) Wilmore, D. and Hodgson, P.E.: *Nucl. Phys.*, **55**, 673 (1964).

18) Uhl, M., *et al.*: *Proc. Int. Conf. on Nuclear Data for Science and Technology, 1991, Jülich*, p.924, (1992).

19) Shibata, K., *et al.*, *JAERI* 1319, (1990).

20) Odano, N., *et al.*: *J. Nucl. Sci. Technolo.*, **30**, 1030 (1993).

21) Perey, F.G.: *Phys. Rev.*, **131**, 754 (1963).

22) Mani, G.S.: *Nucl. Phys.*, **A165**, 225 (1977).

23) Menet, J.J.H.: *Phys. Rev.*, **C4**, 1114 (1971).

24) Arthur, E.D., and Young, P.G.: Ref.(3), p.731.

25) Kalbach, C.: *Z. Phys.*, **A283**, 401 (1977).

26) Iwasaki, S., *et al.*: *Ann. Nucl. Energy*, **21**, 97 (1994).

27) Delaroche, J.P.: *Proc. Int. Conf. on Neutron Physics and Nuclear Data for Reactors and Other Applied Purposes, Harwell*, p.366, (1978).

28) Joly, S.: *Nucl. Sci. Eng.*, **94**, 94 (1986).

29) Yamakoshi, H.: *Proc. Int. Conf. on Nuclear Data for Science and Technology, May 30 － June 3, 1988, Mito, Japan*, p.561, (1988).

30) Kocherov, N.P., and Voncah, H.: *Proc. of the 7th ASTM－EURATOM Symp. on Reactor Dosimetry, Aug. 27－31, 1990, Strasbourg, France*, (1992).

31) Rose, P.F., (Ed.): *BNL－NCS*－17541 (ENDF－201), (1991).

32) Iwasaki, S., *et al.*: *Prog. Nucl. Energy*, **26**, 231 (1991).

33) Veeser, L.R., *et al.*: *Phys. Rev.*, **C16**, 1972 (1977).

34) Iwasaki, S., *et al.*: Ref.(15), p.247.

35) Bayhuest, B.P., *et al.*: *Phys. Rev.*, **C12**, 451 (1975).

36) Bayhurst, B.P., and Prestwood, R.J.: *J. Inorg. Nucl. Chem.*, **23**, 173 (1961).

37) Kneff, D.W., *et al.*: Ref.(3), p.289.

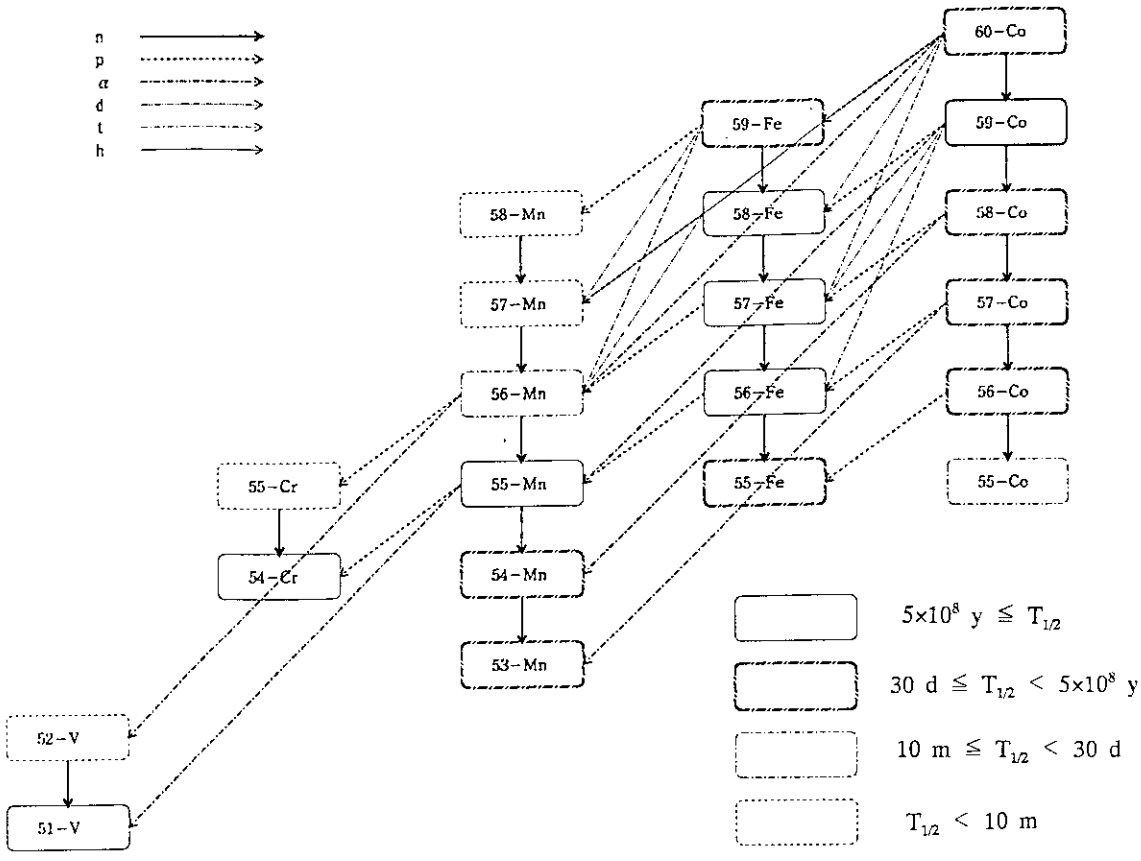

Fig. 1 Reaction chain for calculations of neutron induced reaction on ^{59}Co.

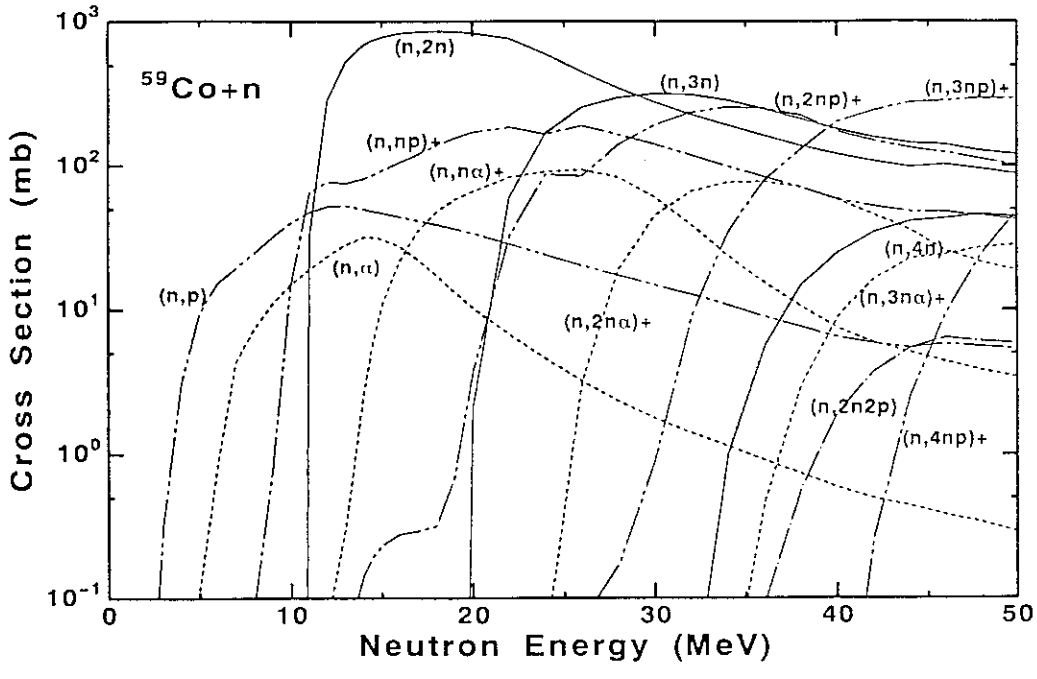

Fig. 2 Trends of principal evaluated cross sections of ^{59}Co+n from 1 to 50 MeV. For instance, (n,np)+ means (n,np)+(n,pn)+(n,d).

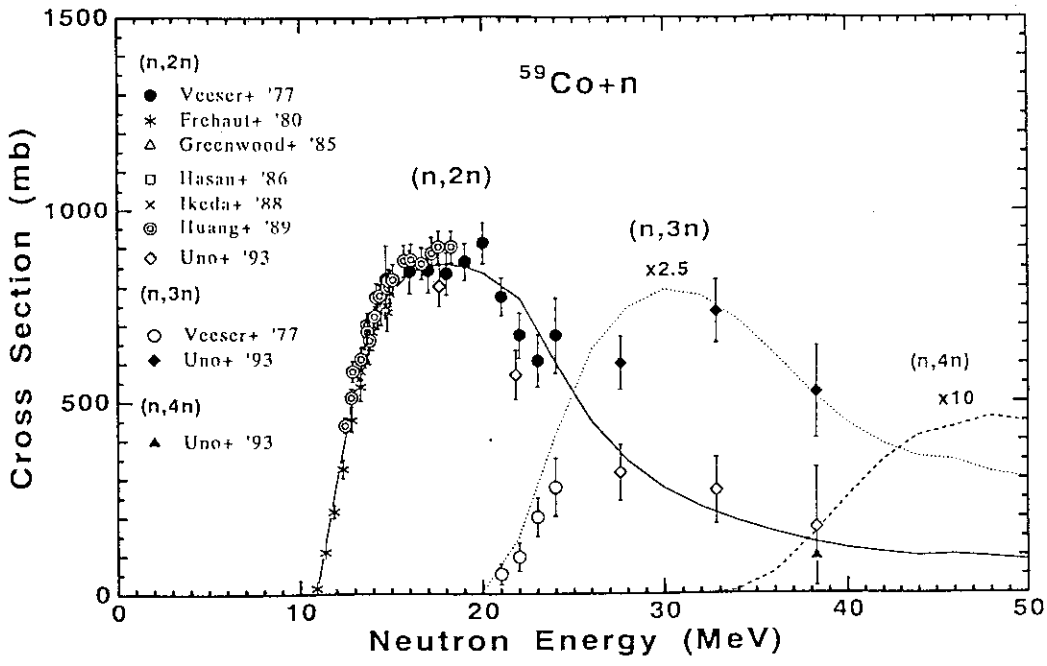

Fig. 3 Comparison of the evaluated cross sections for ^{59}Co(n,xn) reactions with selected experimental data. Note, the cross sections for (n,3n) and (n,4n) are multiplied by 2.5 and 10, respectively.

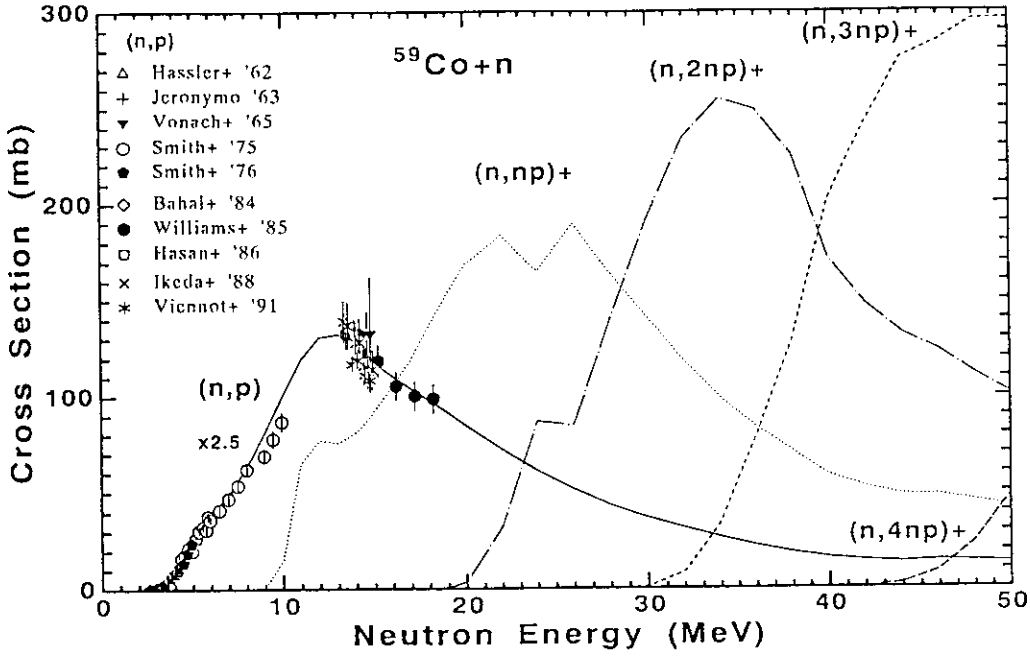

Fig. 4 Cross sections for ^{59}Co(n,pxn) reactions. The (n,p) is compared with the selected experimental data. These are multiplied by 2.5.

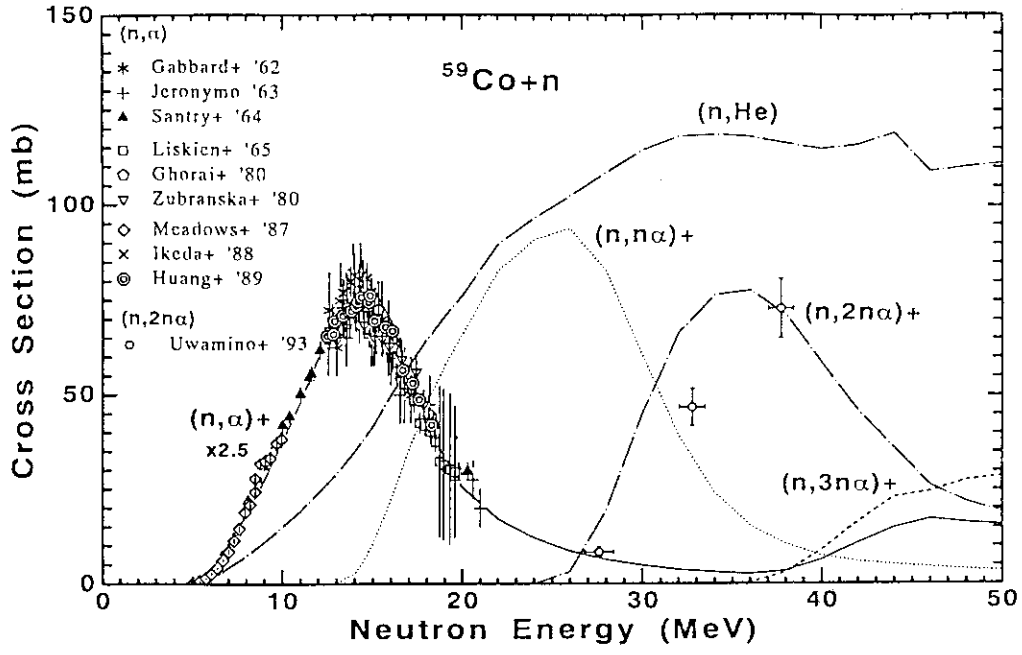

Fig. 5 Cross sections for $^{59}Co(n,\alpha xn)$ reactions as well as the (n,He). The (n,α) is compared with the selected experimental data, and includes (n,2n2p) cross section above 35 MeV. These are multiplied by 2.5.

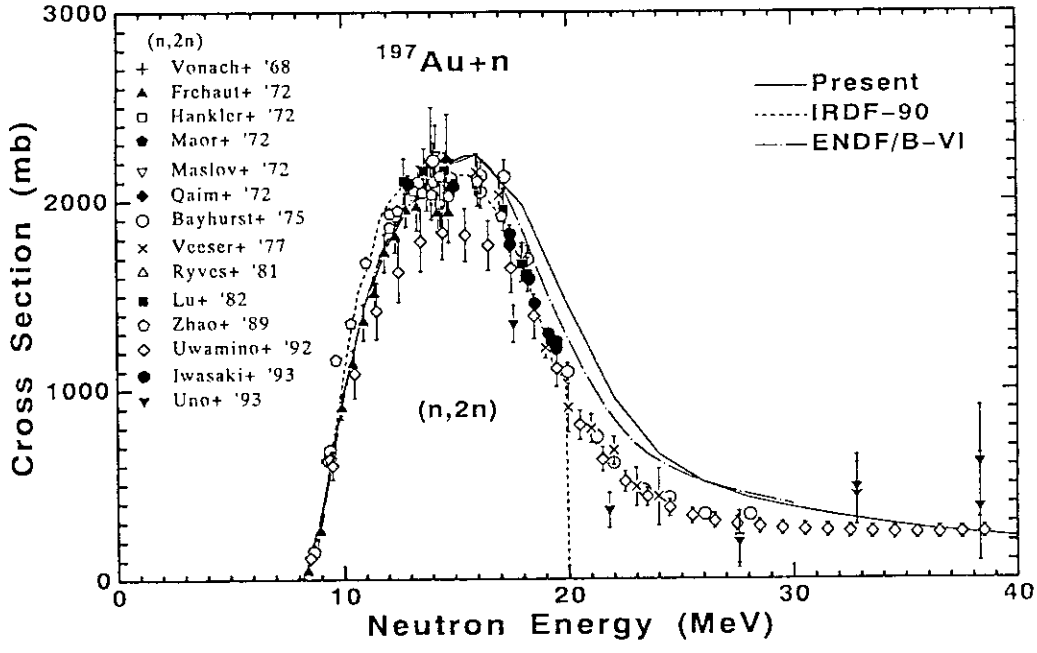

Fig. 6 Comparison of the evaluated cross sections for (n,2n) reactions on ^{197}Au with selected experimental data.

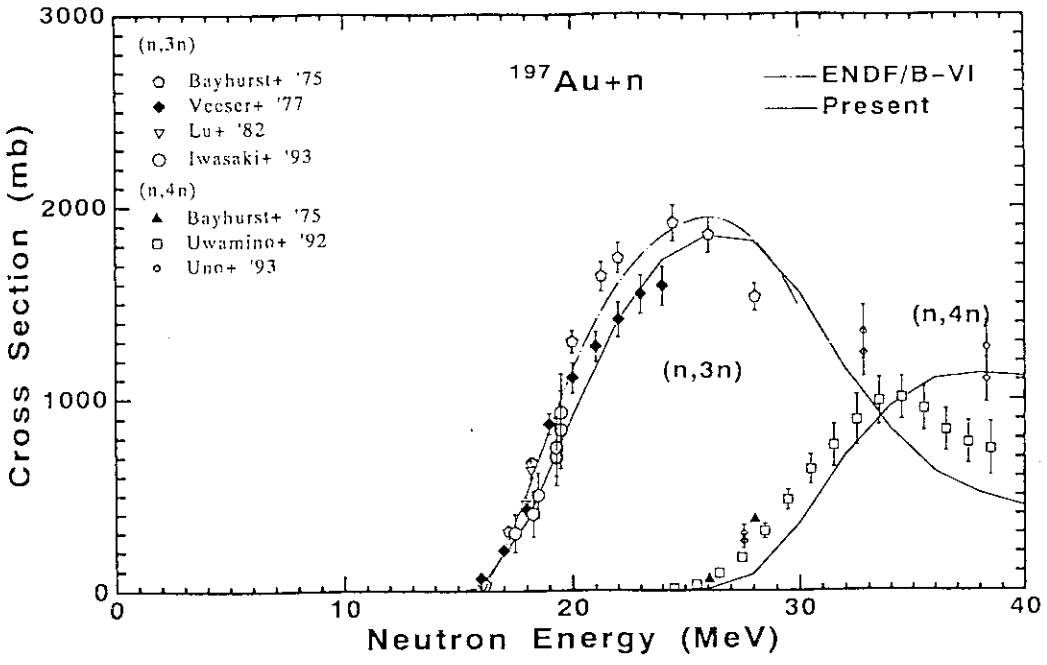

Fig. 7 Comparison of the evaluated cross sections for (n,3n) and (n,4n) reactions on ^{197}Au with experimental data.

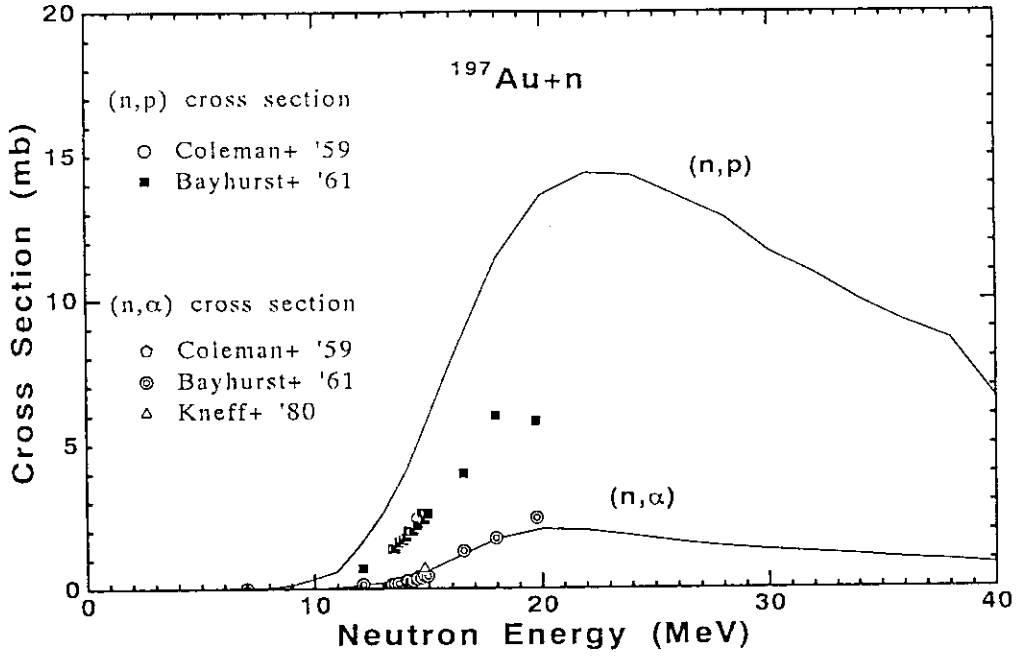

Fig. 8 Comparison of the evaluated cross sections for (n,p) and (n,α) reaction on ^{197}Au with experimental data.

5.17 Dosimetry Cross−section Evaluation by Cubic−B Spline Fitting

S. IWASAKI

Department of Nuclear Engineering
Tohoku University
Aramaki-Aza-Aoba, Sendai 980, Japan

ABSTRACT

Several threshold dosimetry cross-sections have been re-evaluated on the basis of experimental data for the upgrade version of JENDL DOSIMETRY FILE. In the evaluation, the experimental data selections from the data base have been done with the aide of a pattern clustering method on the available data. Then the selected data were fitted by a set of cubic B-spline functions using the least-squares method. In the fitting, the selection of number of knots and their positions was important. A suitable guide for this selection was introduced in order to avoid unnecessary oscillation of the fitted curves. The covariance data were simultaneously produced using the estimated correlation data with respect to each data set. The following five dosimetry cross sections have been re-evaluated: $^{23}Na(n,2n)^{22}Na$, $^{54}Mn(n,2n)^{54}Mn$, $^{59}Co(n,2n)^{58}Co$, $^{60}Ni(n,p)^{60}Co$, and $^{93}Nb(n,2n)^{92m}Nb$.

1.Introduction

Neutron dosimetry cross sections is one of the most significant nuclear data in the fission and fusion energy development. The first neutron dosimetry cross section file in Japan, JENDL DOSIMETRY FILE[1] (hereafter JDF) has been released. The features of this file are listed as follows: adoption of common data to the general purpose file, JENDL-3[2], inclusion of many reactions to be used in future especially fusion reactors, validation for major reactions using several integral experimental data, and generally high reliability. One drawback of this file to be pointed out, however, is loan of the covariance file from IRDF-85[3]; this does not match to the philosophy of the dosimetry evaluation methodology. Also, the most of the evaluated cross sections were based on the theoretical model calculation; a few cross sections have been done based on the experimental data, whereas there is no detailed description of the evaluation process. Review on JDF has been made in the working group of Integral Test for the Dosimetry File under JNDC this year, and it is recommended that re-evaluations should be made on some reactions on the basis of the experimental data together with the covariance matrix.

In this regard, the author has been continuing a development work of a new evaluation paradigm for the dosimetry cross sections. In this paradigm, consistent dosimetry cross sections would be obtained with their covariance data simultaneously based on the experimental data in the framework of the general least-squares method[4]. The flow diagram of the new paradigm under development is shown in Fig. 1. Left hand side of the diagram corresponds to the initial phase of the evaluation where the evaluation is performed by the fitting with the cubic spline functions to the collected experimental data. In the fitting, the conventional least-squares method is adopted. When a new, reliable set of differential or integral experimental data will appear in future, successive evaluation will be made using the general least-squares method

using the initial evaluation as the prior values, as shown in the right hand side of the diagram. In the present paper, we describe the fitting method of a set of cubic spline functions to the experimental data.

2. Evaluation Method by Cubic B-Spline Fitting

2.1 Selection of Experimental Data

The first step in the initial phase evaluation is collection of data with their documentation, and selection of proper data sets from the overall data base under some criteria. We have incorporated the pattern classifying method[5] with heuristic process. In the method, data set reported by one experimental group in a literature is treated as a unit data group called 'basic (data) cluster'. For a given reaction, all existing basic clusters would be grouped into one or at most two plus other minor ones according to a similarity criterion between clusters. A similarity measure like Maharanobis distance in the pattern clustering technique is defined. The minor clusters would be finally rejected because of their inconsistency with the main one(s).

Additional selection heuristic are also introduced. The first principle is minimum adoption of data clusters reported before '70 because generally less reliable data are easily included in the data base if they are included. The present method does not require the large number of the experimental data as done in the statistically averaging methods, as briefly described below. The methods and apparatus employed in the measurements before '70 were generally poor compared with the recent ones. Also, some reference standard nuclear data and decay data of the produces had not been well established. If a small number of data since '70 is available for given reaction, only reliable data before '70 would be added. The second principle is minimum renormalization process of the old data because the traceability of the data processing in the original analysis described in the literature is usually not sufficient. Only changing of the standard cross sections for the flux determination may be corrected afterward.

2.2 Choice of Cubic B-Spline Fitting

There have been two representative evaluation methods for the dosimetry cross sections: the first one is the GMA method by Poenitz[6], ANL and the second the method by the group[7] of IRK (Institute for Radiumforshungs und Kern, University of Wien). In the former method, the data values at selected grid energies are estimated by the interpolation with assumed energy dependency from the neighboring experimental data, and are averaged at each energy with the weights using the covariance data; the IRK group obtains the averaged cross section data in a set of energy bins with the estimated covariance data as a group cross section. Both methods assumed the existence of sufficient number of experimental data for the given reaction, and they collect the experimental data exhaustivel. They of course review the experimental method and analysis in detail, and correct the reported data or their error values to the updated ones. The fundamental philosophy of these methods is as follows; even if a few wrong data or overlooked data are included in the data base, the final values are considered to be reliable by the statistical averaging. The supposition of the existence of sufficient number of data is not always satisfied except for the neutron energies around 14 MeV. In the IRK method, the energy bin width should be made wider if only small number of data is given in the bin. This may introduce unnatural behavior in the cross section curve especially in the threshold region.

In the present work, therefore, we have adopted a fitting method using cubic B-spline functions, where the sufficiency of the number of data is desirable, but less important than the

above two methods.The fitting method also make us free from the prior knowledge on the energy dependency of the cross section as in GMA. Recently Badikov, et al.[8] proposed a method of Padé rational function fitting for the BROND dosimetry file. This method is similar to the present one.

2.3 B-spline Functions

A function of x, S(x) (x∈ [a,b]) can be expressed by sum of B-spline functions $N_{mi}(x)$[9] as,

$$S(x)=\sum_{i=1}^{n+m} c_i^* M_{mi}(x)=\sum_{i=1}^{n+m} c_i N_{mi}(x) \tag{2.1}$$

where $M_{mi}(x)$ is B-spline function of rank m (m-1th order) defined between knots ξ_{i-m} and ξ_i, i.e., $M_m(x)>0$: $\xi_{i-m} < x < \xi_i$; $M_m(x)=0$: $x\leq\xi_{i-m}$ or $x\geq \xi_i$; $N_{mi}(x)$, normalized B-spline function is given as,

$$N_{mi}(x)=(\xi_i-\xi_{i-m})M_{mi}(x). \tag{2.2}$$

Totally necessary knots are ξ_{i-m}, ..., ξ_{n+m} (ξ_1, ..., ξ_n called inner knots between a and b), and they can be chosen as $a=\xi_{1-m}=\ldots=\xi_0<\xi_1\leq\ldots\leq\xi_n<\xi_{n+1}=\ldots=\xi_{n+m}=b$, where $\xi_{i-m}<\xi_i$ (i=1,2,...,n+m) should be satisfied. A condition called 'Schoenberg-Whitney (S-W) condition' of the B-spline function demands that there should exist at least one B-spline function which supports the data $y_k(x_k)$. As far as the condition of S-W is satisfied, the position and number of knots are arbitrary. The coefficients c_i (i=1,2,...,n+m) of the eq. (2.1) are determined by the least-squares method taking account the covariance data of the experimental data y_k.

2.4 Some Criteria for the Fitting

The maximum order of the B-spline functions, m is usually four (thus m-1=3, i.e., the cubic spline functions) [9] to fit the commonly observed data. The feature of this functions smooth behavior and significantly less oscillatory behavior than the rational function fitting. The selection of knot's number and their positions, however, are very important to get the satisfactory fitting results. A heuristic for knots selection is introduced by Ichida et al.[10] called 'successive division method'. In this method the choice of the first knot is at the mid point which equally divides the total number of the data in the whole range. The next knots are again at the higher and lower mid points of the previously divided halves, respectively. Thus, usually the number of the inner knots are three is enough to fit the cross section data given in the present study.

Even in a few cases, the initial fitted curves showed slightly oscillating behavior. This seemed to be unnatural as the cross section curve although the magnitude of the oscillation was not large, less than the data uncertainties. This behavior was quite sensitive to the position of the knots. In order to avoid this, the good position was searched within a nearby region from the original mid points.

3. Application

Above mentioned processes have been applied to the given five dosimetry reactions, which will be described in the following. The covariance matrices have been estimated using the quoted error values by the respective authors and roughly estimated correlations within a set of experimental data.

3.1 ^{23}Na(n,2n)^{22}Na Reaction

This reaction is one of the important high threshold and long-lived (2.6y) dosimeter. This is also important activation reaction of sodium in fast reactors and for low activation material development in fusion reactor due to possible multi-step reactions with aluminum and magnesium producing the activity of ^{22}Na, i.e., ^{27}Al(n,nα)^{23}Na(n,2n)^{22}Na(2.6y), and ^{23}Mg(n,np)^{23}Na(n,2n)^{22}Na.

In the data base of the experimental data, there existed two apparently discrepant data groups together with one isolated data by sight and the clustering technique. JDF and IRDF-85 [3] adopted lower cross section group, while the ENDF/B-VI dosimetry file[11] took the higher cross section group, and they differ by about a factor of two. An integral test by Dumais et al.[12] employing the high energy neutron field provided by the Li+d reaction on thick target showed that JDF and IRDF-85 were clearly more preferable than that of ENDF/B-VI, but the JDF data were a bit smaller. After JDF evaluation, new experimental data sets by Xu, et al.[13], by Lu, et al.[14], by Strohmaier et al.[15], and by Sakuma, et al.[16] have been reported. Only Xu et al's data supported the higher cross section group whose main contributor is the measured one by Paulsen, et al[17], while the latter three data gave a little higher cross section values than the JDF. Strohmaier et al. [18] ascribed the high value of the Xu's data to the measurement of annihilation radiations.

In this paper we adopted the lower cross section group including the above three data sets as shown in Fig.2 with the fitted curve and other dosimetry files' data. The estimated errors (one standard deviations) are also plotted along with the fitted curve. Thus, the entirely new evaluated curve is obtained, and is consistent with the integral test by Dumais, et al.

3.2 ^{55}Mn(n,2n)^{54}Mn Reaction

This cross section is also a high threshold reaction about 10MeV. The manganese cross sections have been evaluated by Shibata[2], originally for ENDF/B-VI general purpose file on the basis of the theoretical model and transferred to JENDL-3. The data of this reaction in ENDF/B-VI have been then adopted in IRDF-90[20], and also in JDF. Thus, three dosimetry file's data are the same. The theoretical curve follows well the trend of the experimental data including the recent data by Sakuma, et al's[16], but runs along the lower cross section values of the main cluster between 14 and 17 MeV as seen in Fig. 3. The data by Paulsen, et al's[17] have been rejected by the clustering. In the present fit, the Shibata's theoretical values together with the estimated error values of about 30% below 12 MeV were also adopted because no available data exists.

3.3 ^{59}Co(n,2n)^{58}Co Reaction

This reaction has been regarded as one of the most important high threshold dosimeters

having relatively reliable cross section below 20 MeV. The evaluated cross section by IRK group (Wagner, et al[7]) was adopted as the new entry of NEA/NDC standard cross section file[20]. In addition, cobalt is one of the important mono-isotopic element dosimeter in the field of high energy neutrons up to 50 MeV, which has also been discussed by the other paper[21] and also presented in this symposium by Odano and Iwasaki. In Fig. 4, available cross section data and evaluated data are shown. Below 15MeV, all evaluations are consistent, but not above this energy except for the present and JDF by Yamamuro[22]. It can be pointed out that the cross section of this reaction is still not established as that of $^{93}Nb(n,2n)^{92m}Nb$ reaction does (see Sec. 3.6). Further differential cross section measurements and integral test aiming above 15 MeV are necessary to establish this reaction as the standard one.

3.4 $^{60}Ni(n,p)^{60}Co$ Reaction

This reaction has relatively low threshold energy of about 3MeV comparable to that of $^{58}Ni(n,p)^{58}Co$, and leaves a long-lived (5.7y) residual nucleus, ^{60}Co. These are desirable characteristic for the long-term reactor dosimetry. The experimental study for this reaction, however, has been very poor. Only one data set by Paulsen, et al.[17] was available except for the 14 MeV neutron energy region before the evaluations for all existing dosimetry files. Further, the Paulsen's data showed odd behavior below 12 MeV, being inconsistent with the theoretical model estimation[22]. However, some reliable experimental data have recently been reported[23,24] in this energy region, using H(t,p) and D(d,n) neutron sources, respectively; these data are almost consistent with each other, and could resolve the anomalous behavior of the Paulsen's data. In addition, the recent measured data around 14 MeV by FNS group of JAERI [25] are also taken into account. At this moment, only one data set by Paulsen in the energy range exists between 16 and 20 MeV. Therefore, in the present evaluation those data is adopted in this energy region with enlarged error values by about three times. An entirely new evaluation curve is obtained as shown in Fig. 5.

3.5 $^{93}Nb(n,2n)^{92m}Nb$ Reaction

Almost flat and reliable cross section above 12 MeV enable us to use this reaction as a flux monitor for the activation cross section measurements in this energy range, as pointed out by Winkler[26] and Iwasaki. et al.[27]. The evaluation by IRK group (Wagner, et al.[28]) was also a new entry of NEA/NDC standard cross section file[29]. The cross section curve of JDF was given by the theoretical model calculation by Yamamuro[22] for the calculation of activation cross section. In the present calculation, following new experimental data have been added to the data base of this cross section; the cross sections calculated from the ratio data by Iwasaki, et al.'s[27] between 12 and 20MeV measured at FNL of Tohoku University, measured by Ikeda, et al[30] around 14 MeV(A) using the associated particle method at FNS, and also by Ikeda, et al.(B)[31] from 9 to 12 MeV using the $H(^{11}B,n)^{11}C$ neutron source at Tandem Facility of JAERI. Almost consistent data having been obtained with the previous evaluations of IRDF-90 and Badikov, et al.[8] as compared in Fig. 6.

4. Conclusions

The first phase of the new evaluation paradigm for the dosimetry cross sections have been described. Preliminary results of this phase for the five dosimetry reactions were satisfactory.

The present evaluated cross section should be tested again by the integral experimental data as performed prior the release of the first version of JDF. The implementation of the second phase block in the system is ongoing. The new experimental data for the last two reactions $^{59}Co(n,2n)^{58}Co$, $^{60}Ni(n,p)^{60}Co$ relative to the cross section of the $^{93}Nb(n,2n)^{92m}Nb$ have been measured by the present authors between 12 and 20 MeV measured at Tohoku University Dynamitron facility this year and will be reported soon. These will be used in the second phase of the evaluation and resolve the ambiguity of the present cross section curves of these reactions. The extension of the system is also planned; the evaluation in the paradigm is based not only on the differential cross section data but also on the integral data with the covariances in the phases of the first and successive evaluations.

Acknowledgements

The members of the working group on Integral Test for Dosimetry Cross Sections are appreciated for their valuable discussion.

References

1. Nakazawa M., et al. : "JENDL Dosimetry File", JAERI 1325 (1991).
2. Shibata K., et al: JAERI 1319 (1990).
3. Cullen D.E., et al. :IAEA-NDS-41/R, rev.0 (1982).
4. Froener, F.H. Proc. Symp. on Nucl. Data Eval. Method, BNL, p209 World Scientific Pub., Co. Ltd., (Singapore, 1993).
5. Iwasaki S.: JAERI-M 93-046, p211 (JAERI, 1993).
6. Poenitz W.P. : Proc. Conf. Nucl. Data Eval. Methods and Procedures, p249, BNL-NCS-51363 (1981).
7. e.g., M. Wagner, et al.: Physics Data, No. 13-5, Fachinformationszentrum, Karlsruhe (1990).
8. Badikov S.A. and Zolotarev K.I.: Proc.8th ASTM-EURATOM Symposium on Reactor Dosimetry, Aug.29-Sep.3, 1993, Vail, Colorado, USA, to be published.
9. 吉本富士市、市田浩三 (Yoshimoto F and Ichida K) "スプライン関数とその応用 (Spline function and its application) ", 教育出版 (Kyo-iku Pub. Co. Ltd.) (1979) (in Japanese).
10. Ichida K., et al.: Computing, 16 (1976), pp. 329-338.
11. BNL/National Nuclear Data Center: ENDF/B-VI (1990).
12. Dumais J.R., et al.:, Proc. Int. Conf., Jülich, p202 Springer-Verlag, (1992).
13. Xu Z., et al..: Proc. Int. Conf., Jülich, p666, Springer-Verlag (1992).
14. Lu H, Zhao W., and Yu W. Chin. J. Nucl. Phys. **14**, 83 (1992),
15. Strohmaier B.,et al.:Proc. Int. Conf., Jülich, p663, Springer-Verlag (1992).
16. Sakuma M., et al.: JAERI-M 92-027, p.278 (1992).
17. Paulsen A.: Nukleonik **10**, 91 (1967).
18. Strohmaier B.:Ann. Nucl. Energy, **20**, pp.533-545 (1993).
19. Kocherov N.P. and McLaughlin P.K.: IAEA-NDS-141 (1990).
20. Vonach H.: NEANDC-311 "U", INDC(SEC)-101, NEA/OECD (1992),pp.80-82.
21. Iwasaki S. and Odano N. :Proc.8th ASTM-EURATOM Symposium on Reactor Dosimetry, Aug.29-Sep.3, 1993, Vail, Colorado, USA, to be published.
22. Yamamuro N.: JAERI-M 90-006 (1990).
23. Wagner, et al.: Nucl. Data for Science and Tech., Proc. Int. Conf., Jülich, 1991, S.M.

Qaim (Ed.), pp.358-360, Springer-Verlag (1992).
24. Sudár S. et al. : Nuclear Data for Science and Tech., Proc. Int. Conf., Jülich, 1991, S.M. Qaim (Ed.), pp. 291-293, Springer-Verlag (1992).
25. Konno C., et al.: JAERI 1329 (1993).
26. Winker G.: Nucl. Data for Science and Tech, Proc. Int. Conf., Jülich, p401, Springer-Verlag (1992),
27. Iwasaki S., et al.: Prog. of Nucl. Energy, 26 (1991), pp231.
28. Wagner M.: INDC(AUS)-014, IAEA (1991).
29. Vonach H. :NEANDC-311 "U", INDC(SEC)-101, NEA/OECD (1992), pp.78.
30. Ikeda Y., et al.: J. Nucl.Sci. and Tech., **3**, pp.870-880 (1993).
31. Ikeda Y.,et al.: JAERI-M 93-181 (1993).

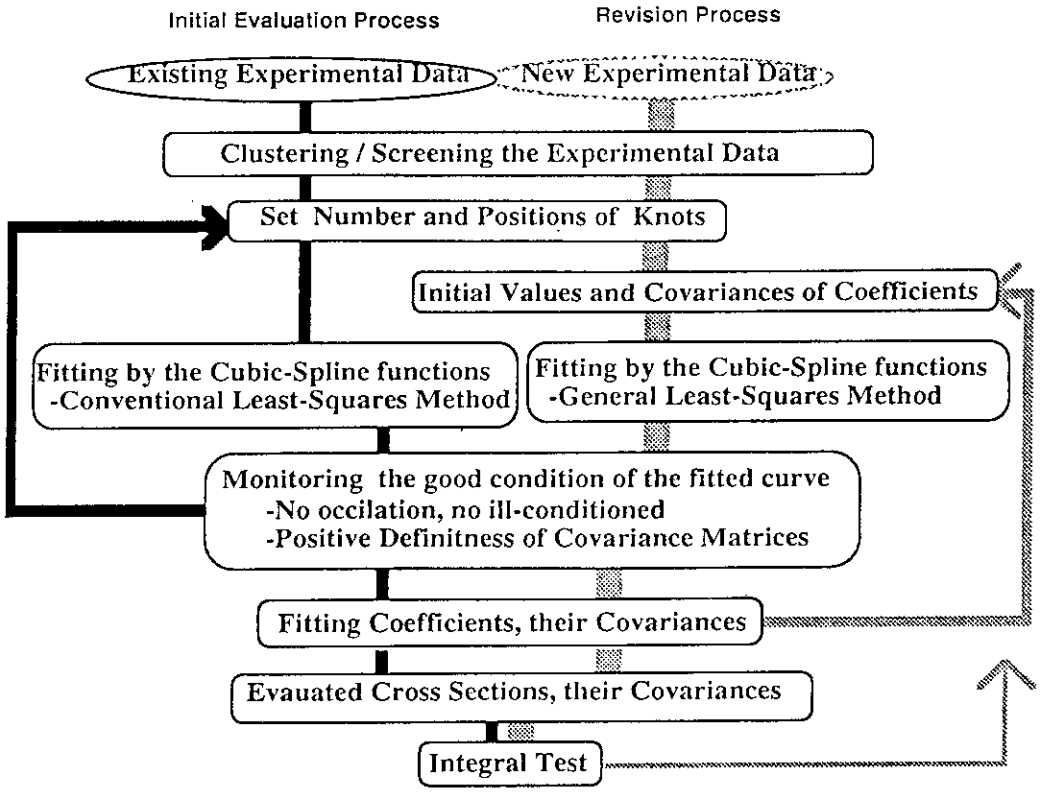

Fig. 1 New paradigm for the evaluation of dosimetry cross sections.

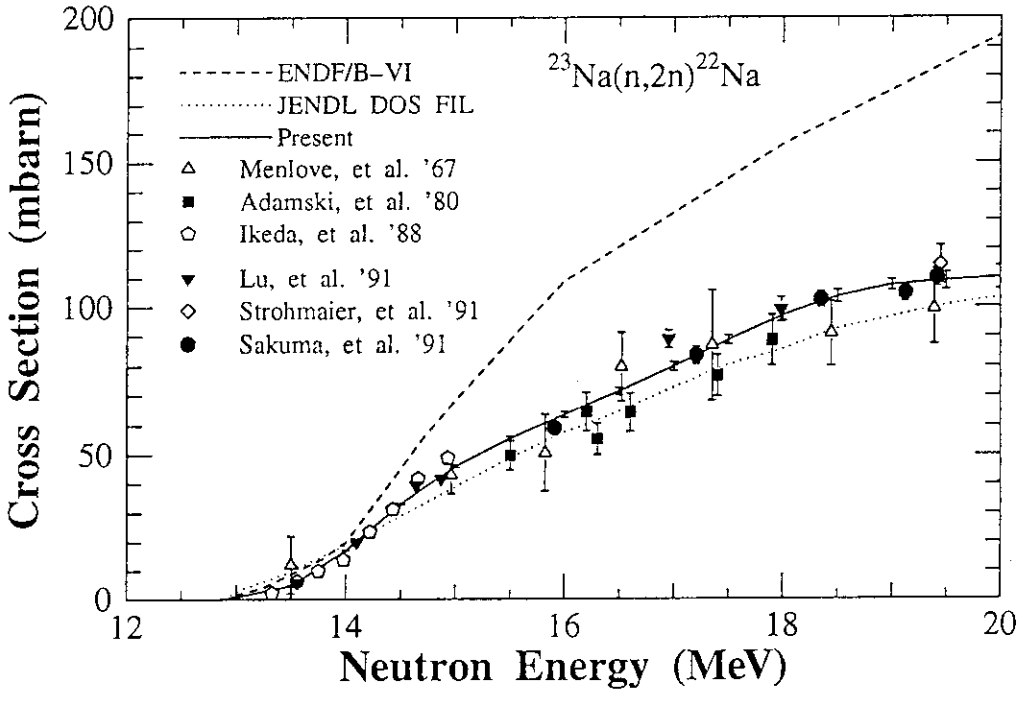

Fig. 2 Comparison of the evaluated cross sections for ^{23}Na(n,2n)^{22}Na with the experimental data

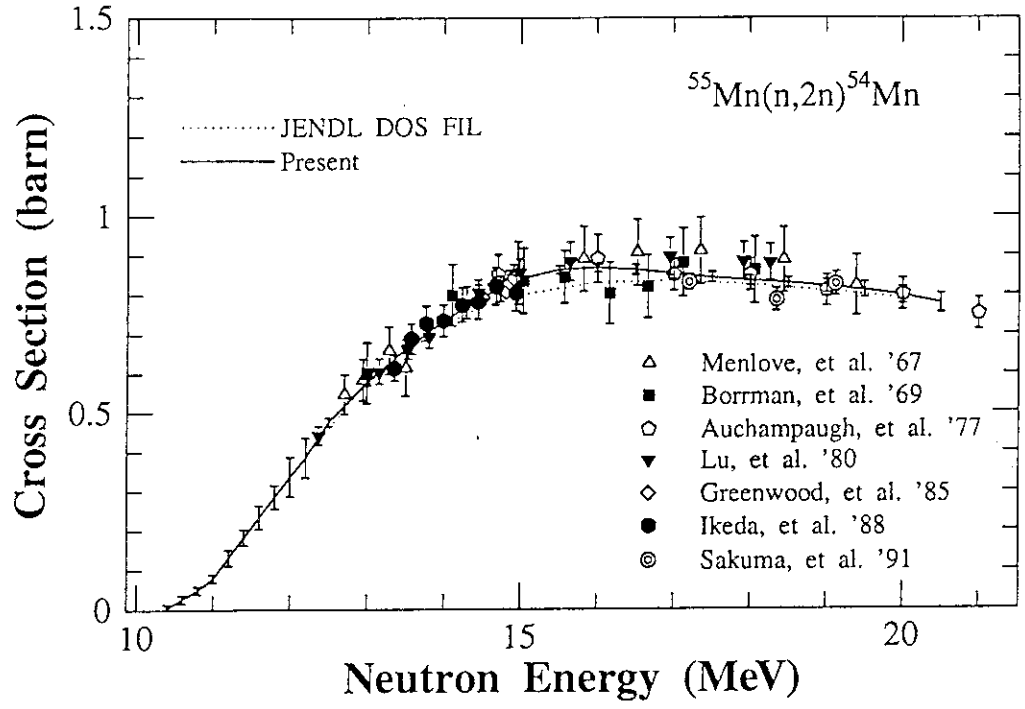

Fig. 3 Comparison of the evaluated cross sections for ^{55}Mn(n,2n)^{54}Mn with the experimental data.

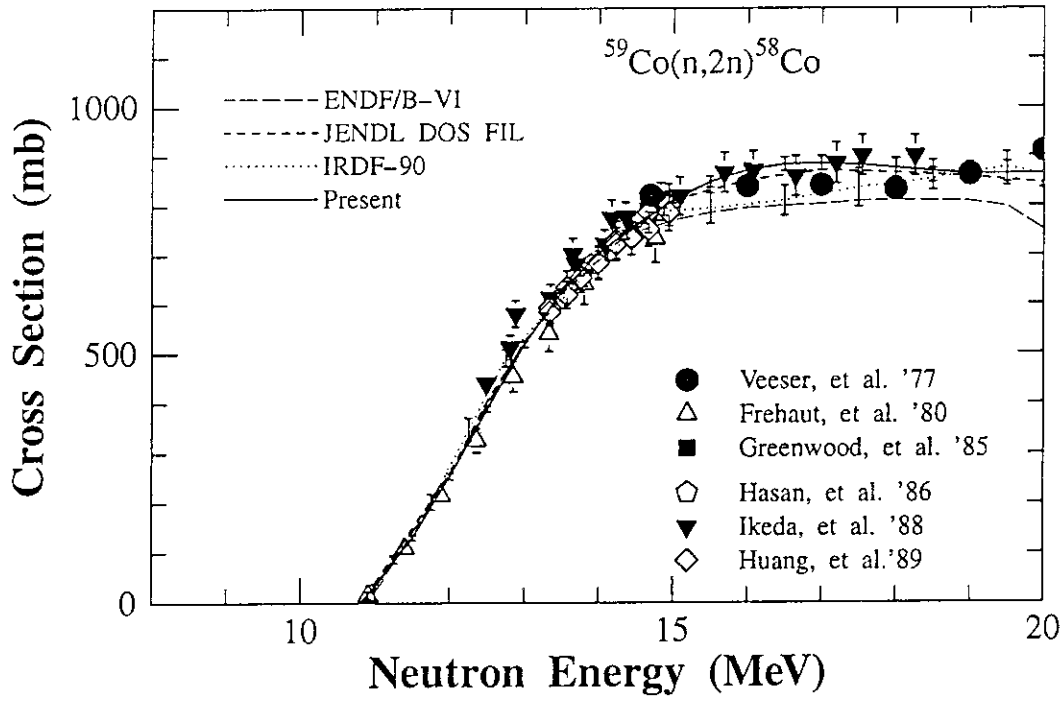

Fig. 4 Comparison of the evaluated cross sections for ^{59}Co(n,2n)^{58}Co with the experimental data.

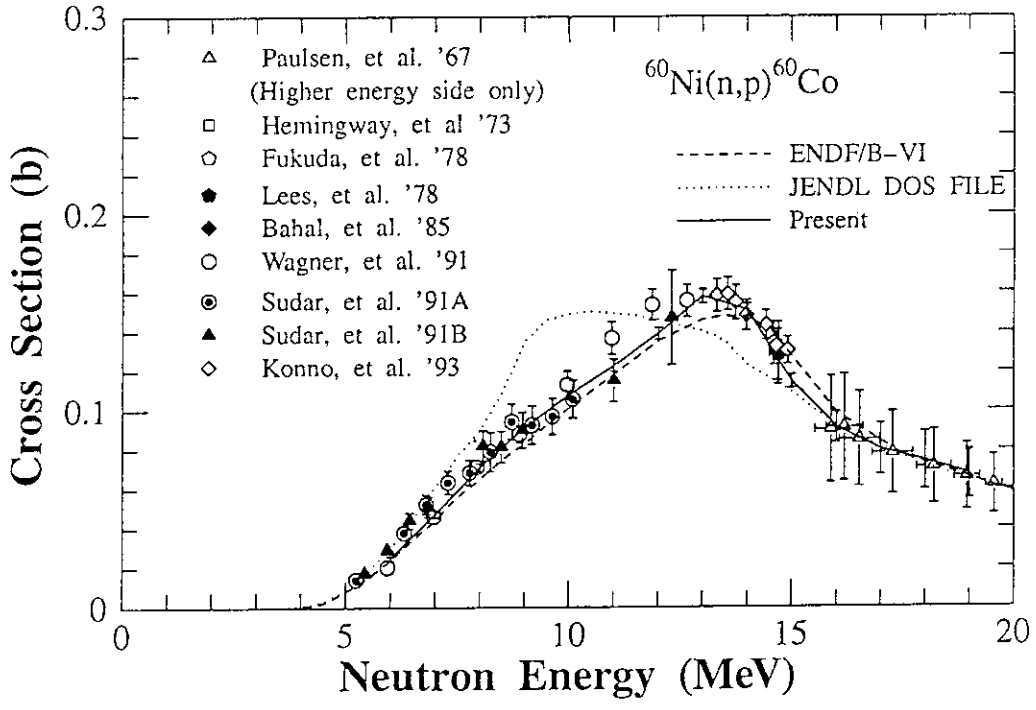

Fig. 5 Comparison of the evaluated cross sections for ^{60}Ni(n,2n)^{60}Co with the experimental data.

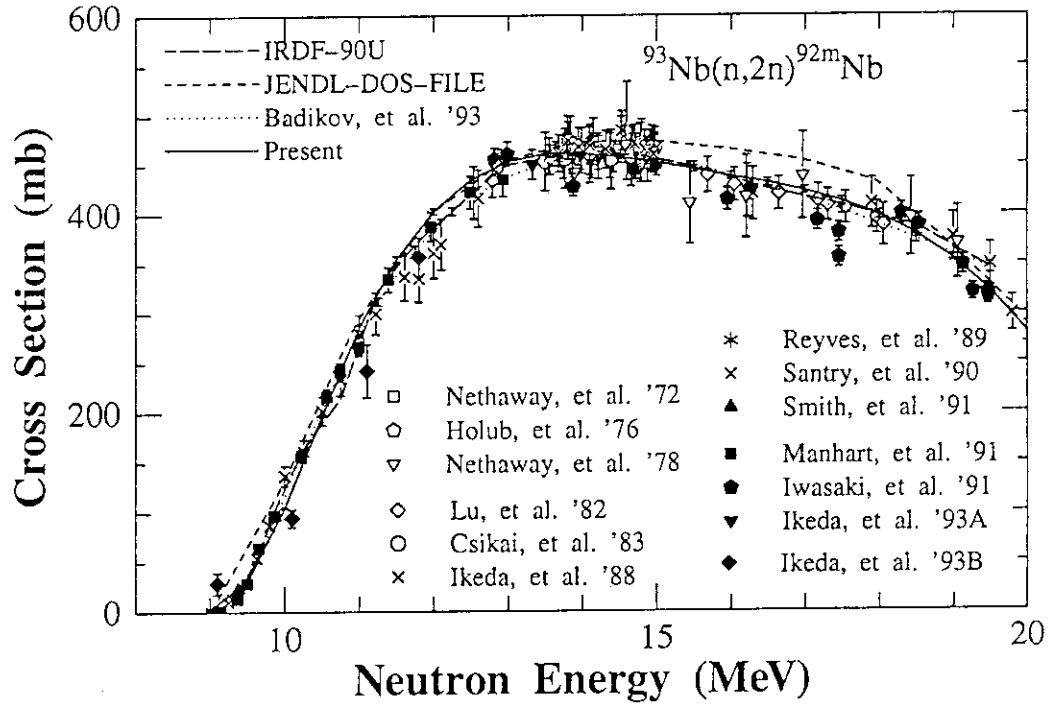

Fig. 6 Comparison of the evaluated cross sections for ^{93}Nb(n,2n)^{92m}Nb with the experimental data.

5.18 Evaluation of the D(γ, n) Reaction Cross Section

T.Murata

Nippon Nuclear Fuel Development Co.
Oarai-Machi,Ibaraki-Ken. 311-13, Japan

Evaluation was performed for the cross section of photo-disintegration of Deuteron in the photon energy range between the threshold energy of the reaction (2.224 MeV) and pion production threshold (140 MeV). Angular distributions of the emitted neutrons were also evaluated.

1. Theory for the evaluation

There are many theoretical and experimental works on the reaction. Partovi/1/ formulated the transition amplitude of the process including multipoles up to the octupole interaction and gave the calculated cross sections and simple angular distribution formula with several coefficients above photon energies higher than 10 MeV. Below 10 Mev, experimental cross sections were well reproduced with formulae given by Marshall and Guth/2/. The magnetic dipole absorption has significant effect in the energy region near threshold, and its cross section formula is given in the text book of Segre/3/. The angular distributions were calculated with the formulae given by Partovi and by Marshall and Guth in the respective energy regions. For the magnetic dipole process, isotropic angular distribution was added to the angular distribution below 10 MeV.

The cross section calculation formulae are summarized as follows,

Inc.Photon Energy : E < 10 MeV

$$\sigma(E\gamma) = \sigma_{ed} + \sigma_{eq} + \sigma_{md} + \sigma_{mq}$$

$\sigma_{ed}, \sigma_{eq}, \sigma_{mq}$: given by Marshall & Guth/2/

$$\sigma_{ed} = \sigma_b F_1^2/(1-\alpha\rho)$$

$$\sigma_{eq} = [(E-\varepsilon)/5Mc^2]\sigma_b F_2^2/(1-\alpha\rho)$$

$$\sigma_b = 8\pi e^2\hbar[\varepsilon(E-\varepsilon)^3]^{1/2}/3McE^3,$$

ε =2.224 MeV (binding energy of deuteron)

M : mean mass of neutron and proton

---

* Work performed as a part of evaluation program of the Working Group on Photo-Reaction Nuclear Data Evaluation of JNDC

For Hulthen potential:

$F_1=1-[(\alpha^2+k^2)/(\beta^2+k^2)]^2$, $F_2=1-[(\alpha^2+k^2)/(\beta^2+k^2)]^3$

$k^2=(M/\hbar^2)(E-\varepsilon)$

$\alpha=2.31\times10^{12}$ 1/cm, $\beta=1.41\times10^{13}$ 1/cm, $\rho=1.73\times10^{-13}$ cm

For simplified model: $F_1=1$, $F_2=1$

$\sigma_{mq}=[(\mu_p-\mu_n)^2E^2/6(Mc^2)^2]\sigma_{ed}$

μ_p, μ_n= magnetic moments of proton and neutron

σ_{md} : given in Segre's Text Book/3/

$$\sigma_{md}=\frac{2\pi e^2\hbar(\mu_p-\mu_n)^2[\varepsilon(E-\varepsilon)]^{1/2}(\varepsilon^{1/2}+W_0^{1/2})^2}{3M^2c^3E(E-\varepsilon+W_0)}$$

$W_0=0.0738$ MeV

Angular Distribution (CM system):Marshall&Guth + M1-term

$\sigma(\theta)=[3\sin^2\theta/8\pi][\sigma_{ed}+2(5\sigma_{eq}\sigma_{ed})^{1/2}\cos\theta+5\sigma_{eq}\cos^2\theta]$

$+[3\sigma_{mq}\cos^2\theta+\sigma_{md}]/4\pi$

Inc.Photon Energy : E >= 10 MeV

Theoretical calculation by Partovi/1/

$\sigma(E)$= sum of electric and magnetic transitions up to octupole calculated using wave functions with Hamada-Johnston's potential

Angular Distribution (CM system,for protons):

$\sigma(\theta)=a+b\cdot\sin^2\theta+c\cdot\cos\theta+d\cdot\sin^2\theta\cos\theta+e\cdot\sin^4\theta$

Table 1 Calculated D(γ,n)H cross sections and D(γ,p) angular distribution coefficients by Partovi/1/

Energy (MeV)	σ_t (μb)	a (μb/sr)	b (μb/sr)	c (μb/sr)	d (μb/sr)	e (μb/sr)
10	1387.	4.623	162.0	0.3744	29.96	−4.230
20	588.2	5.387	65.50	0.7314	18.25	−4.223
40	224.2	6.236	19.14	0.9983	7.914	−2.164
60	126.6	6.101	7.209	1.001	4.452	−1.564
80	87.40	5.651	3.009	0.9420	2.774	−1.317
100	66.25	5.114	1.025	0.8808	1.812	−.9853
120	53.41	4.618	0.0653	0.8230	1.237	−.7715
140	44.53	4.156	−.4096	0.7737	0.8757	−.6367

2. Evaluation Method and Results

Partovi's calculation reproduce the experimental cross sections fairly well. So,the evaluation of the cross section was made to interpolate the values given in Table 1, in the energy region higher than 10 MeV. For the interpolation, spline fitting of the third order was applied at first. The results show some undulation and not satisfactory. Then,physical model of Marshall and Guth,described in section 1 was applied,but gave smaller values than Partovi's. It was found that the simlified Marshall-Guth model,which set F1=1 and F2=1 (see section 1),reproduces Patovi's results rather well. This simplified model was adopted for the interpolation and some correction ,smoothly energy dependent less than 10 %, was applied in the energy region between 40 MeV and 80 Mev to reproduce the Partovi's values more well.

In the low energy region below 10 MeV, the simplified model plus magnetic dipole cross section was applied successfully to reproduce the experimental cross sections.

Evaluated cross section is shown in Fig.1 along with the experimental cross sections/4/, Partovi's calculated values and calculated result of Marshall-Guth model. Figure 2 shows low energy region cross sections. Magnetic dipole contribution is also shown in the figure.

Angular distributions of the emitted neutrons in the center of mass system were calculated with the formulae given in section 1, and are shown in Fig.3 comparing with the experimental values/5/.

Angular distributions in the center of mass system were transformed to the laboratory system with the relativistic kinematics given by Dedrick/6/, and are shown in Fig.4. The emitted neutron energy was calculated also with the kinematics and is shown in Fig.5. The differential cross sections were fitted with the following Legendre polynomials and the coefficients are given in Table 2 as a summary.

$$d\sigma/d\Omega = \sigma/4\pi \left[1 + \Sigma_{L=1} A_L P_L (\cos\theta) \right]$$

3. Discussion and Conclusion

Though, many sophisticated models have been presented by many physicists for the photodisintegration of deuteron to investigate nucleon-nucleon interaction, these models give not so different cross section of the reaction and angular distributions of the emitted nucleons. So, simple models to reproduce the experimental data were adopted for the present evaluation of the practical use,such as reactor design and so on. In the photon energy region higher than 60 MeV, present evaluated cross section show somewhat lower tendency compared with the experimental data. Re-evaluation in these region is a subject for a future study waiting for the measurements of good accuracy.

The present result will be compiled into the first version of Japanese evaluated photo-reaction data file, which will be released in next year.

Thanks are due to the members of the Working Group on Photo-Reaction for valuable discussion.

References

/1/ Partovi,F. : Ann.Physics 27(1964)79
/2/ Marshall,J.F.and Guth,E : Phys.Rev.78(1950)738
/3/ Segre,E.:"Nuclei and Particles"(Benjamin/Cummings,1977)p.496
/4/ Allen,L.Jr.: Phys.Rev.98(1955)705, Alexandrov,I.A. et al.: Soviet Phys.JETP 6(1958)472, Whalin,B.A. et al.:Phys.Rev.101 (1956)377, Barns,J.H. et al.:Phys.Rev.86(1952)359, Galey,J.A. : Phys.Rev.117(1960)763, Phillips,J.A. et al.: Phys.Rev.80 (1950)326, Keck,J.C.,Tollestrup,A.V.:Phys.Rev.101(1956)360, Halpern,J.,Weinstock,E.V.:Phys.Rev.91(1953)934, Hough,P.V.C.: Phys.Rev.80(1950)1069, Bishop,G.R. et al.:Phys.Rev.80(1950) 211, Snell,A.H. et al.:Phys.Rev.80(1950)637, McMurray,W.R. and Collie,C.H.:Proc.Phys.Soc.68A(1955)181, Barnes,C.A. et al.:Phys.Rev.86(1952)359, Phillips,J.A. et al.:Phys.Rev.80 (1950)326, Waffler,H.,Younis,C.:Helv.Phys.Acta24(1951)483, Birenbaum,Y. et al.:Phys.Rev.C32(1985)1825, Moreh,R. et al. Phys.Rev.C39(1989)1247, Debevec,P.T. et al.:Phys.Rev.C45 (1992)904.
/5/ Smith,F.D.:Nucl.Phys.465(1987)429, Shin,Y.M.:Nucl.Phys.154 (1970)482, Alexandrov,I.A. et al:Soviet Phys.JETP 6(1958)472, Keck,J.C.,Tollestrup,A.V.:Phys.Rev.101(1956)360, Whalin,B.A. et al.:Phys.Rev.101(1956)377
/6/ Dedrick,K.G.: Rev.Mod.Phys.34(1962)429

Table 2 Summary of the present evaluation: D(γ,n) cross sections and the Legendre polynomial expansion coefficients of the neutron angular distributions in the laboratory system

$$d\sigma/d\Omega = \sigma/4\pi[1 + \Sigma_{L=1} A_L P_L(\cos\theta)]$$

Eg(MeV)	SIG(mb)	A1	A2	A3	A4
2.300E+00	6.581E-01	2.913E-01	-1.197E-01	-5.839E-02	-1.145E-02
2.600E+00	1.183E+00	2.439E-01	-6.531E-01	-1.992E-01	-3.074E-02
3.000E+00	1.828E+00	2.442E-01	-8.342E-01	-2.283E-01	-3.110E-02
3.500E+00	2.280E+00	2.381E-01	-8.969E-01	-2.298E-01	-2.831E-02
4.000E+00	2.454E+00	2.320E-01	-9.219E-01	-2.264E-01	-2.577E-02
4.500E+00	2.474E+00	2.267E-01	-9.352E-01	-2.224E-01	-2.361E-02
5.000E+00	2.416E+00	2.221E-01	-9.436E-01	-2.185E-01	-2.176E-02
5.500E+00	2.318E+00	2.180E-01	-9.494E-01	-2.150E-01	-2.012E-02
6.000E+00	2.205E+00	2.144E-01	-9.539E-01	-2.117E-01	-1.865E-02
8.000E+00	1.753E+00	2.027E-01	-9.647E-01	-2.008E-01	-1.378E-02
1.000E+01	1.373E+00	1.828E-01	-9.444E-01	-1.811E-01	-1.326E-02
1.500E+01	8.528E-01	1.674E-01	-9.215E-01	-1.653E-01	-1.070E-02
2.000E+01	5.882E-01	1.337E-01	-8.804E-01	-1.309E-01	-4.701E-03
2.500E+01	4.350E-01	1.076E-01	-8.265E-01	-1.028E-01	-1.029E-03
3.000E+01	3.376E-01	1.058E-01	-7.789E-01	-9.806E-02	-1.891E-03
3.500E+01	2.714E-01	9.728E-02	-7.278E-01	-8.531E-02	1.461E-03
4.000E+01	2.242E-01	7.603E-02	-6.655E-01	-5.799E-02	9.649E-03
4.500E+01	1.893E-01	5.481E-02	-5.980E-01	-2.882E-02	1.722E-02
5.000E+01	1.629E-01	4.063E-02	-5.333E-01	-5.326E-03	2.143E-02
5.500E+01	1.425E-01	3.487E-02	-4.769E-01	1.034E-02	2.202E-02
6.000E+01	1.264E-01	3.431E-02	-4.277E-01	2.108E-02	2.068E-02
7.000E+01	1.031E-01	3.028E-02	-3.282E-01	4.784E-02	2.032E-02
8.000E+01	8.744E-02	2.347E-02	-2.294E-01	7.963E-02	2.334E-02
9.000E+01	7.622E-02	2.308E-02	-1.469E-01	1.037E-01	2.627E-02
1.000E+02	6.764E-02	2.903E-02	-8.225E-02	1.194E-01	2.824E-02
1.200E+02	5.483E-02	4.261E-02	2.671E-02	1.481E-01	3.123E-02
1.400E+02	4.558E-02	5.666E-02	1.068E-01	1.706E-01	3.277E-02

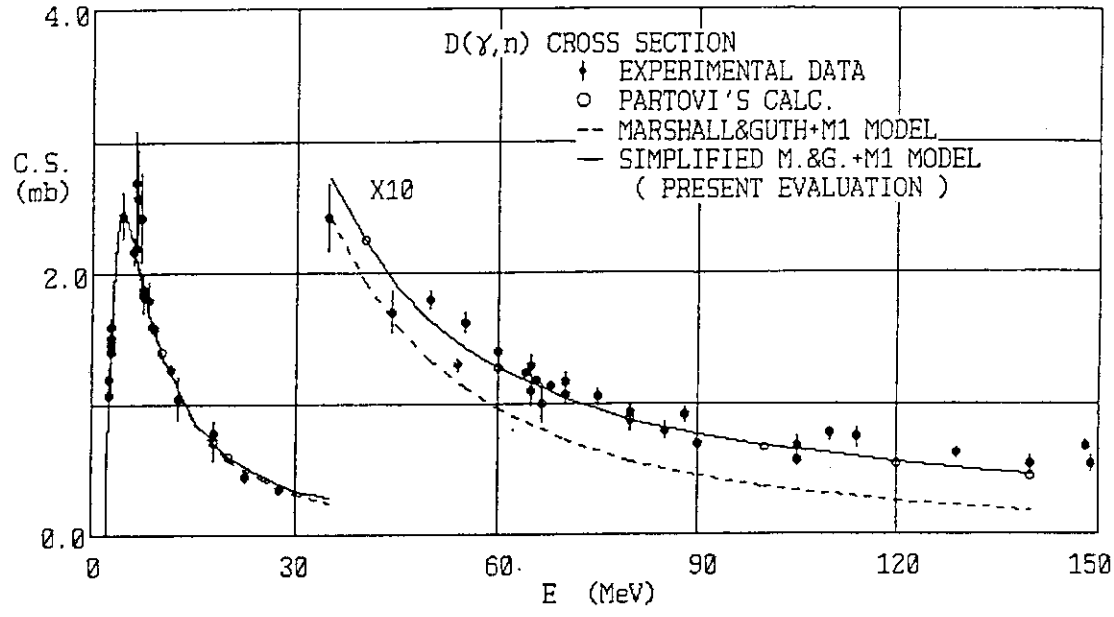

Fig. 1 D(γ,n)H evaluated cross section (solid line) compared with experimental cross sections/4/, Partovi's calculated values (circles) and calculated line (dashed) with the model of Marshall-Guth plus magnetic dipole component.

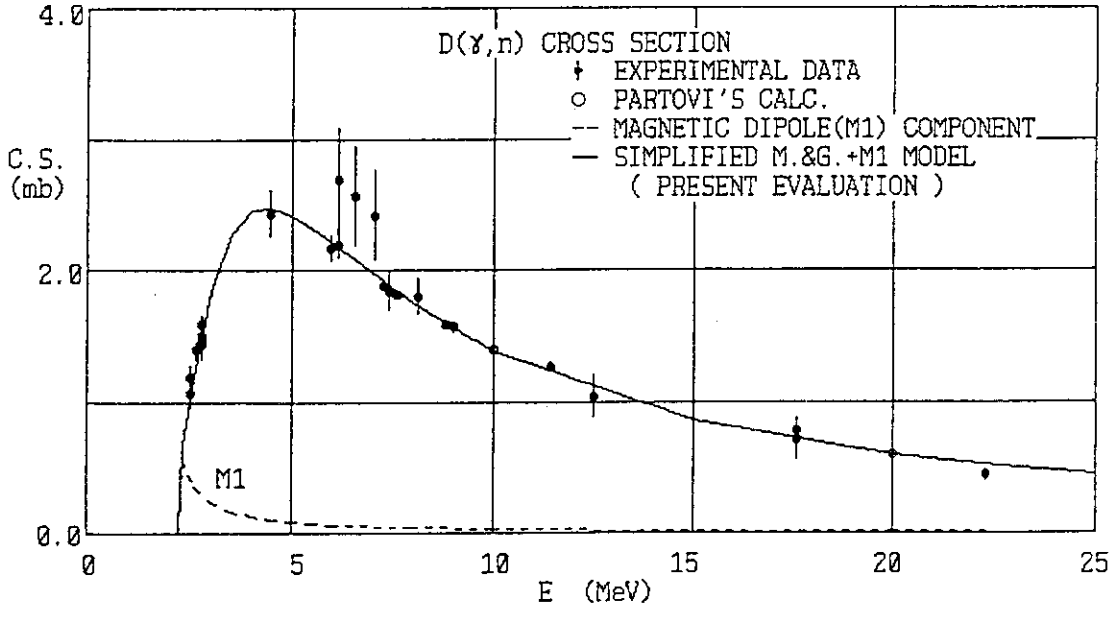

Fig. 2 D(γ,n)H evaluated cross section in the low energy region (solid line) compared with experimental cross sections/4/. Magnetic dipole contribution is shown by dashed line.

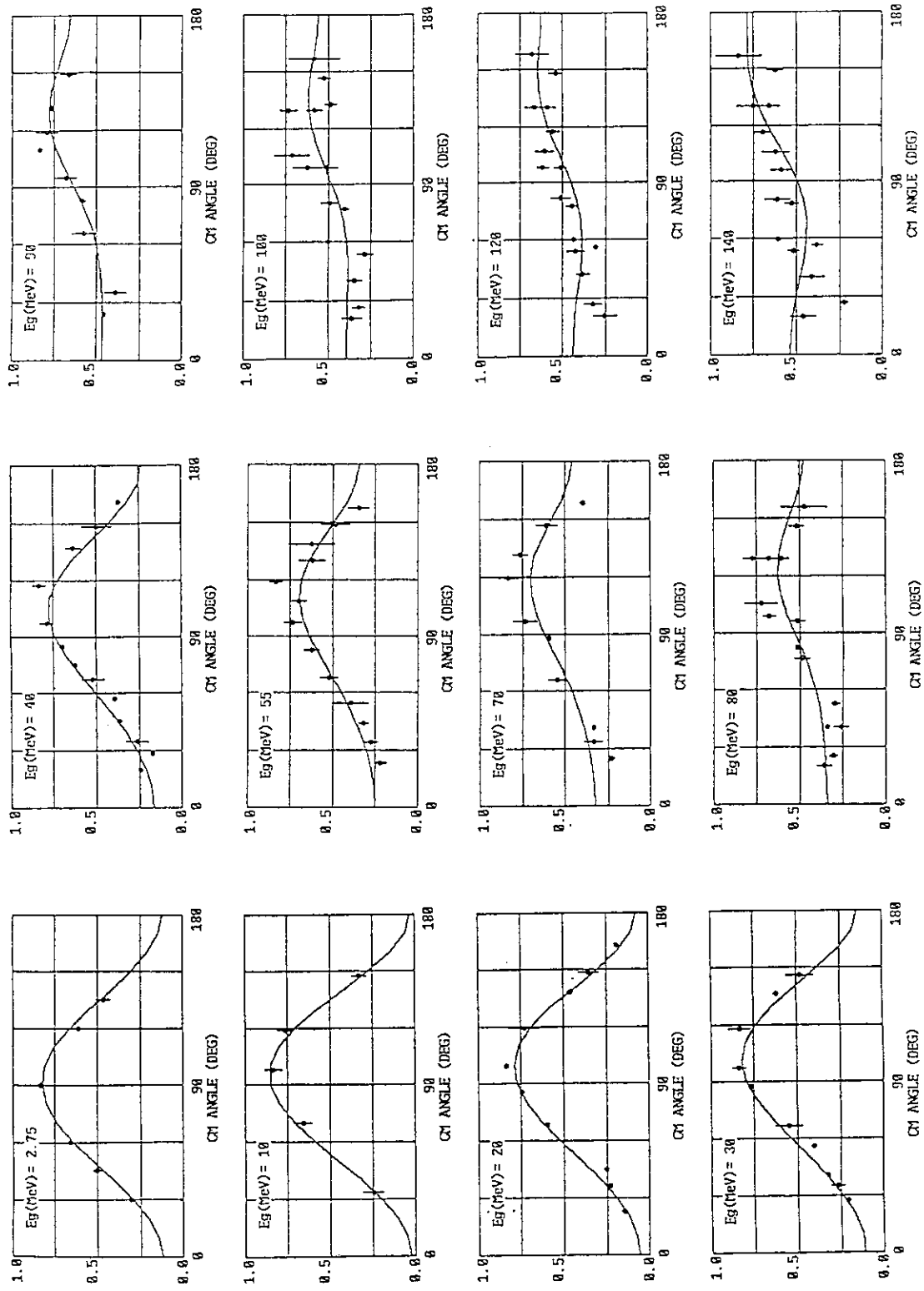

Fig. 3 Comparison of calculated angular distributions with experimental distributions/5/ of emitted neutrons by the D(γ,n) reaction in the center of mass system.

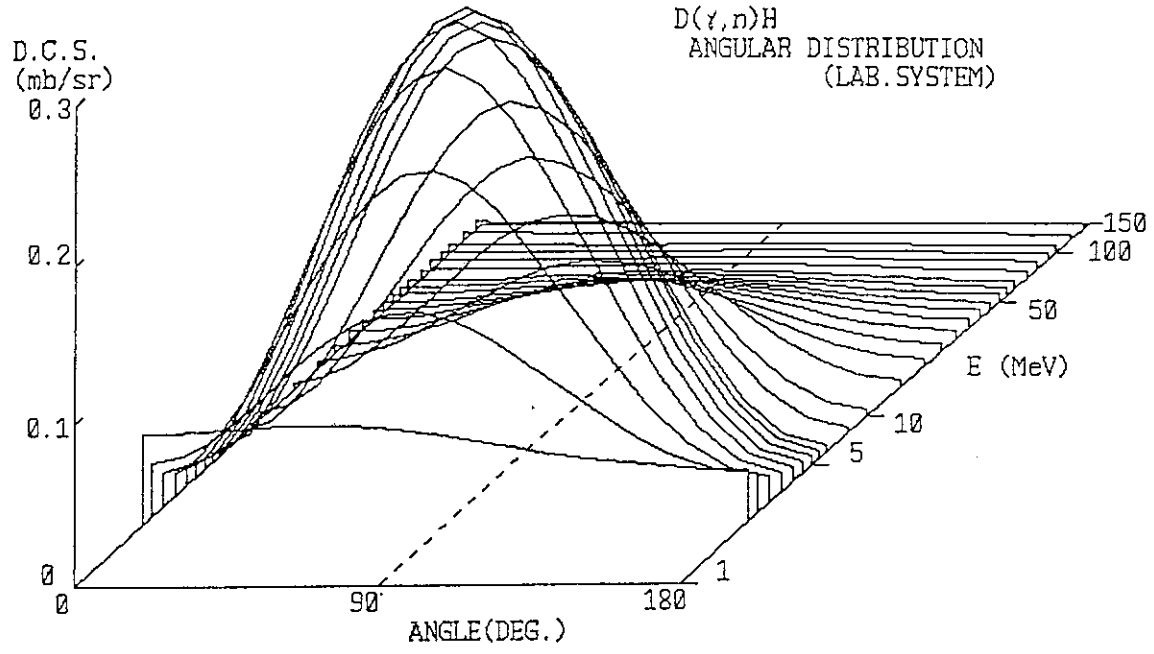

Fig. 4 Three dimensional plot of the evaluated differential cross sections of the D(γ,n)H reaction in the laboratory system.

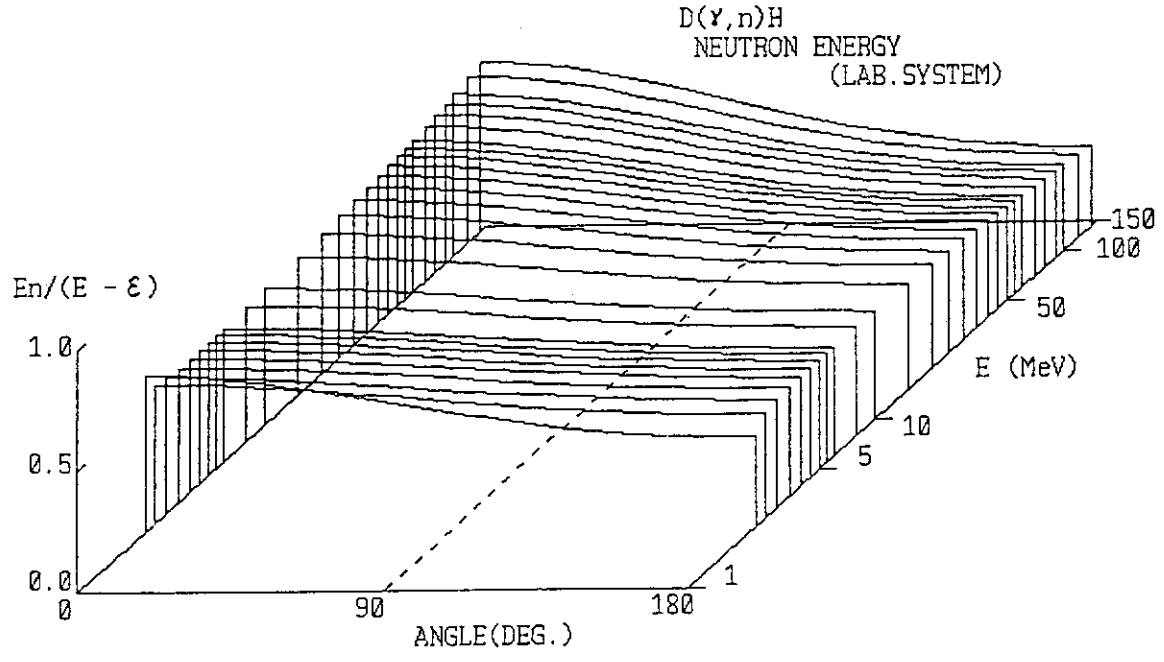

Fig. 5 Ratio of emitted neutron energy to released energy (E-ε) by the D(γ,n)H reaction (calculated with relativistic kinematics).

5.19 Nuclear Level Density Parameter Systematics Revisited : Nuclear Deformation Effects

Alberto Mengoni[#] and Yutaka Nakajima

Department of Reactor Engineering, Nuclear Data Center
Japan Atomic Energy Research Institute
319-11 Tokai-mura, Naka-gun, Ibaraki-ken

Introduction

The importance of the construction of a reliable systematics for nuclear level density parameters can be easily understood by considering that all the reaction cross section calculations, based on the statistical model theory, need the evaluation of nuclear level density. This quantity is available from experiment only in limited ranges of excitation energies and for a limited set of nuclei in the nuclide chart.

Of the models currently employed for the calculation of level density, the Fermi-gas model (FGM) is one of the most utilized example. In fact, for excitation energies of a few MeV up to several MeV, the FGM has proved to furnish reliable estimation of the density of nuclear states. As it is well known, the most important parameter which enters in the evaluation of nuclear level density based on the FGM is the parameter a. This parameter is related to the density of *single-particle* states at the Fermi energy. The purpose of the present contribution is to investigate the effect of nuclear deformation on the systematics of a.

The important fact to consider in the evaluation/calculation of a is that for a wide class of nuclei, the density of nuclear levels at excitation energies corresponding to the neutron binding energy (8 MeV or so) can be evaluated experimentally by measuring the spacing of neutron resonances (usually s-wave resonances). In fact, the level density parameter a enters in the FGM level density formula and the following relation can be used to derived it

$$< D >_{I=0} = \frac{1}{\sum_{J_0} \rho_{FGM}(U, J_0)} . \qquad (1)$$

Here U is the excitation energy corresponding to the neutron binding, opportunely corrected for pairing correlation effects and J_0 takes the allowed values of the total angular momentum for the neutron s-wave resonances.

A systematics of the parameter a can be constructed if the average level spacing of neutron resonances is available for various nuclei. Of course this is the case and the systematics of the a parameter has been constructed several times in the past [1]. We have recently [2]

[#]Permanent address: ENEA, Ente per le Nuove tecnologie, l' Energia e l' Ambiente, Nuclear Data and Codes Laboratory, V.le G. B. Ercolani 8, 40138 Bologna, Italy.

re-evaluated the level density parameter a for all the nuclei whose neutron resonance data are contained in the most recent compilation [3].

In order to obtain a good systematics it is essential to make the level density parameter a a slowly varying function of the mass number. To do this, various nuclear structure effects must be included in the evaluation of the level density parameters. Here, the effect of nuclear deformation will be considered in detail.

Nuclear structure effects

As it is well known, several nuclear structure effects manifest themselves on nuclear ground-state properties. For example, pairing correlation effects clearly show up in the systematics of mass differences. The same situation appears for shell effects which are evident when the residual energy δE, derived from the relation

$$M_{\mathrm{exp}} = M_d + \delta E \ , \tag{2}$$

is plotted as a function of the mass number A. Here, M_d is the "macroscopic" or "smooth"

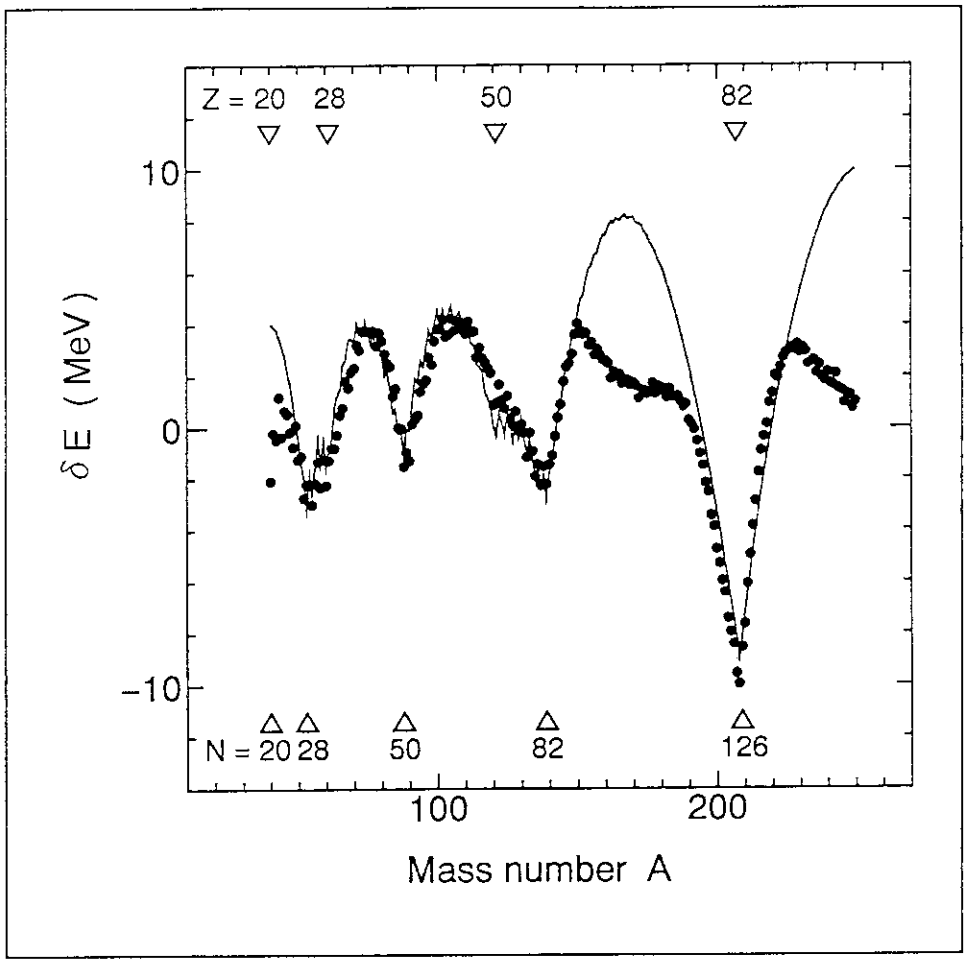

Figure 1: residual energy δE vs the mass number A. See the text for explanations.

part of the nuclear mass-formula, usually evaluated from liquid-drop or droplet models [4] and M_{exp} the experimental nuclear mass.

In Fig. 1 we show δE as derived from the experimental mass, M_{exp}. The droplet

model of Myers and Swiatecki [4] is used for the evaluation of M_d. In the same figure, a theoretical estimate of δE, evaluated following the prescription of Ref. [4], is given as solid line. It is important to note here that the evaluation of δE given in Fig. 1 as full dots, includes shell *and* deformation effects, whereas the theoretical calculation correspond to pure shell contribution which *does not* include deformation effects. It is in this way that we can discriminate the contribution of shell and deformation effects.

The question now arises: *are shell and deformation effects also present in excited nuclei?* The natural answer to this question is that yes, the nuclear structure effects, shell and deformation, are also present for excited nuclei at least as far as the excitation energy is not too high. Some evidence of this affirmation can be found examining nuclear properties derived, for example, from the analysis of giant resonances. We will show here that an alternative way to answer this question is to examine the systematics of the level density parameter a.

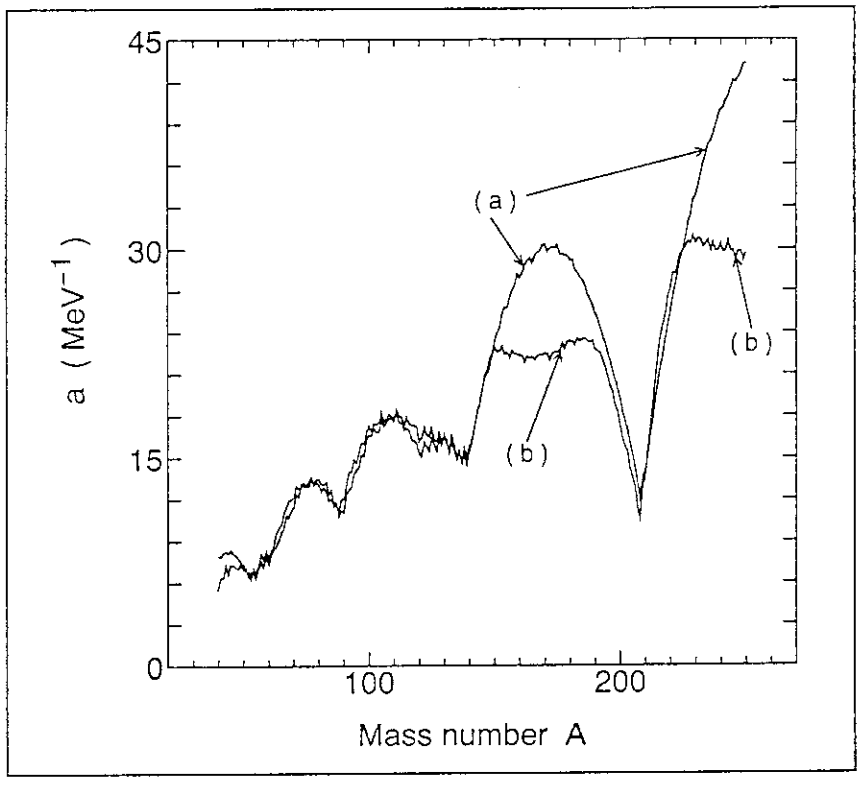

Figure 2: level density parameter a. The two curves are calculated as explained in the text.

Nuclear deformation effects on the level density parameters

It is well known that the systematics of a shows strong fluctuations due to shell effects. We are also in a position to correct for those effects. In fact, two approaches have been proposed for taking into account the shell structure. One method, proposed by Ramamurthy et al. [5] is based on considering shell inhomogeneities on the single-particle spectrum on which the nuclear excitations are built. Another approach has been proposed by Ignatyuk et al. [6] which is based on the generalized super-fluid model. In the latter case the FGM equations remain unchanged except for the parameter a which takes an energy-

dependent form

$$a(U) = a(*) \left[1 + \frac{E_{sh}}{U} \left(1 - e^{-\gamma U} \right) \right] \tag{3}$$

where $a(*)$ is the asymptotic level density parameter, E_{sh} is the shell correction energy and γ a damping parameter, usually taking the value $\gamma = 0.40\, A^{-1/3}$ MeV^{-1}.

The asymptotic parameter $a(*)$ shows a very smooth behavior when plotted as a function of the mass number A. In fact, the two parameters coincide when $U \rightarrow \infty$ and their physical meanings are equivalent provided that shell effects are removed.

We have constructed [2] the systematics of $a(*)$ and derived the following expression

$$a(*) = \alpha A \left(1 - \beta A^{-1/3} \right) \tag{4}$$

with the numerical parameters $\alpha = 0.05811$ MeV^{-1} and $\beta = -5.897$. Using these values and the equation (3) we can now calculate the level density parameter a as a function of the mass number. The results of this calculation are shown in Fig. 2. Here, the curve *(a)* shows the calculation made using $E_{sh} = \delta E$ with δE evaluated from the experimental mass differences. The curve *(b)* is calculated using the theoretical [4] shell energy *without* the inclusion of deformation effects.

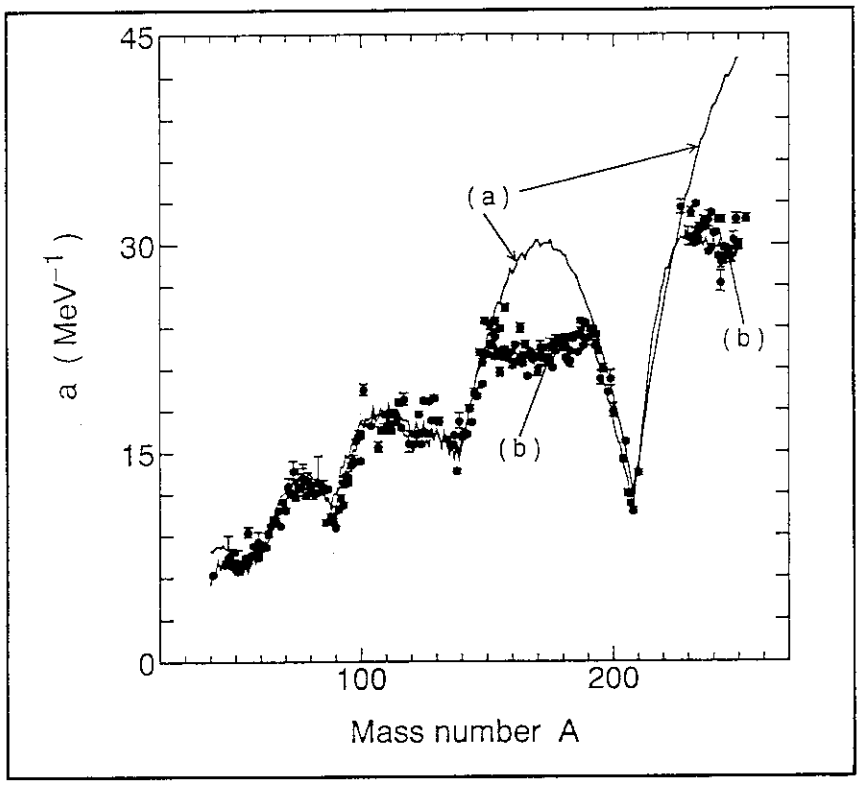

Figure 3: level density parameter a. The curves are calculated as explained in the text and are the same as those of Fig. 2. The dots are derived from the experimental level spacings.

To confirm the importance of deformation effects on the level density parameter a, we have superimposed to the calculations of Fig. 2, the values of this parameter as derived

from the experimental level spacings. The result is shown in Fig. 3. It can be seen that the experimentally derived level density parameters a are in a very good agreement with the values calculated using equation (3), with the shell correction energy evaluated including nuclear deformation effects (curve *(b)*). It can be also noticed that the effect of deformation is greatest in the mass region $150 < A < 190$ and for the actinides. Those are the same regions where the nuclear deformation plays a fundamental role in establishing ground-state properties.

Conclusions

We have investigated the level density parameter systematics in a wide region of the nuclide chart. We have shown that the systematics of a shows deformation effects very much in the same way as the residual energy in nuclear ground states.

Acknowledgements

This work has been partially supported by the Japan Atomic Energy Research Institute, JAERI, under the JAERI Foreign Researcher Inviting Program.

References

[1] Erba E., Facchini U. and Saetta-Menichella E.: *Nuovo Cimento*, **22**, 1237 (1961); Lynn J. E.: *The theory of neutron resonance reactions*, Clarendon Press, Oxford, (1968); Dilig W., Schantl W., Vonach H., and Uhl M.: *Nucl. Phys.* A **217**, 269 (1973).

[2] Mengoni A., and Nakajima Y.: *J. Nucl. Sci. Tech.*, in press, (1994); Mengoni A., and Nakajima Y.: JAERI-M 93-177 (1993).

[3] Mughabghab S. F., Divadeenam M. and Holden N. E.: *Neutron Resonance Parameters and Thermal Cross Sections, Part A*, Academic, New York, (1981); Mughabghab S. F.: *ibid.*, Part B, Academic, New York, (1984).

[4] Myers W. D. and Swiatecki W. J.: *Nucl. Phys.*, **81**, 1 (1966).

[5] Ramamurthy V. S., Kataria S. K. and Kapoor S. S.: *Proceedings of the IAEA Advisory Group Meeting on Basic and Applied Problems of Nuclear Level Densities*, Brookhaven National Laboratory Report BNL-NCS-51694, 187 (1983).

[6] Ignatyuk A. V., Istekov K. K. and Smirenkin G. N.: *Sov. J. Nucl. Phys.*, **29**, 450 (1979). For a recent review on the Generalized Superfluid Model see Rastopchin E. M., Svirin M. I. and Smirenkin G. I.: *ibid.*, **52**, 799 (1991); Ignatyuk A. V., Weil J. L., Raman S. and Kahane S.: *Phys. Rev.*, C **47**, 1504 (1993).

5.20 Shell−pairing Correlations of Nuclear Level Density

H.Nakamura, Fuji Electric Co., Ltd
1-1 Tanabe-Shinden, Kawasaki 210

ABSTRACT: For the purpose of preparing the systematics of the level density parameters, a revision to the KRK formula [1] has been made. The new formula, similar to the previous one, is based on the analytical expression of the single-particle state density, introducing, in particular, shell-pairing correlation (SPC) terms on it. The systematics of parameters consist of those for the ground states and for the excited states. For the former, the main advantage of present systematics is no direct use of experimental shell and pairing correction energy tables; The mean difference between the empirical and the computed mass exceses is ΔM = 0.252MeV for existing 1925 mass data. The results of preliminary analyses for the resonance spacing data are presented.

1. Introduction

Among the simple semiempirical models which account for the energy-dependent shell and pairing effects of the nuclear level density, the KRK model [1] is considered. This model relates the shell effects of the level density to the ground-state shell correction

$$Es = Mexp - Mdrop \tag{1}$$

defined as the difference of the experimental mass Mexp and the liquid drop mass Mdrop (gross term). However, the above shell correction Es does not take the unique contents but depends on the different mass formula, from which the shell and the pairing corrections, and the shell-pairing correlation terms are available. Separation of those correction terms on the systematics of level density parameters is not clear in literatures.

The purpose of the present work is to make those contents of correction clear on the level density parameters. In the present model, an analytical expression for the single-particle state density, similar to the previous KRK model, but introducing the shell-pairing correlation terms, so we call it SPC-model. The main advantage of the present model is its analytic form of systematics with about 60 parameters for the ground state, about 3 parameters for the excited states, and thus no use of the shell and pairing energy tables for individual nuclei on the statistical theory analysis for a large number of nuclear reactions.

In the next section, the brief description of the level density formulation is presented. In the Section 3 the systematics of parameters for the present model are given. The predictions of the present model are compared with the resonance data [2] fitted by using the KRK model in the Section 4. The last section is the concluding remarks.

2. Semiempirical Level Density Formula

Level density formula is reduced by using the traditional stasistical procedure as followings ;

Fourier expansion of single-particle state density ;

$$g(E) = g[1+f\cdot\cos\{Q(E-Ex)\}][1-\cos\{q(E-Fx)\}] \tag{2}$$

$Q = 2\pi/\hbar W$: related to the main-shell spacing.
$q = 2\pi/\hbar w$: related to the pairing energy.
$Fx = Ex+\hbar W(X+1/2)$: Fermi level.

X : occupied fraction of x-th shell.
x : stand for proton(=z) or neutron(=n) shell.
g : average single-particle state density .

Grand partition function ;

$$G = \int dE g(E)[1+2\exp\{B(Fx-E)\}+\exp\{2B(Fx-E)\}] \quad (3)$$

Saddle-point approximation for level density ;

$$R(E,J) = (1/2)W(J)R(U), \quad (4)$$

$$W(J) = \frac{2J+1}{2(2\pi)^{1/2}\sigma^3}\exp[-\frac{(J+1/2)^2}{2\sigma^2}], \quad J : \text{total spin}$$

$$R(U) = \frac{1}{(2\pi)^{3/2} D^{1/2}}\exp(S), \quad E \text{ Fexcitation energy}$$

$$D = (18/\pi^4)a^{1/2}U^{5/2}, \quad U : \text{excitation energy.}$$

$\sigma^2 = I t$, spin cut-off factor,

I : moment of inertia of nucleus.
t : thermodynamic temperature.

$S = 2at$: entropy.

$$a = \bar{a} + (1/2)t^{-2}[Es\cdot h1(T)\{h2(T)-1\} - P\cdot h1(Tp)\{h2(Tp)-1\}] \quad (5)$$

$Es = Cs\cdot f\cdot\cos(2X)$: shell correction energy.
$P = Cp\,\delta[1-Fp\cdot Es/Cs]$: pairing energy.

h1(T) = Tcosech(T),
h2(T) = Tcoth(T),
$T = \pi\sqrt{at}$, $Tp = \pi\sqrt{qt}$,
$\bar{a}$: asymptotic leveldensity parameter.
X : occupied fraction of the proton or neutron shell

= (n-M)/N, n : occupied particle number¤
M : magic number,
N : fully occupied number.
δ : = 1(even-n), = 0(odd-n)

$$U = at^2 + Es[h1(T)h2(T)-1] - P[h1(Tp)h2(Tp)-1] \quad (6)$$

$$I = Ir[1-h1(Tp) + (Es/Cs)\{h1(T)-h1(Tp)\}], \quad (7)$$
: for even-particle shell

$Ir = 0.015A^{5/3}$: Fermi-gas moment of inertia
A : mass number.

3. Systematics of Level Density Parameters

free parameters ;

Cs : shell correction energy const.
Ci : shell correction energy consts (i=1,6).
Cp : pairing energy const.
Fp : amplitude for shell-pairing correlation.

$\bar{a} = A0 \cdot A$: asymptotic level density parameter.
$W = W0 \cdot A^{1/3}$: related to the main-shell spacings.
$q = q0 \cdot A^{1/2}$: related to the pairing energy.
(A0,W0,q0) :parameters to be fixed.

fitting formula to the experimental mass excess data ;

$$[Es]exp = \{-Cs \cdot \cos(2\pi X) - C1 \cdot X - C2\} \cdot FF - Ci \cdot \{\sin(2\pi X)\}$$

: for odd-proton and -neutron shells.

C3 : for (X<0.5), C4 : for (X>0.5)

$FF = \exp\{-C5 \cdot X(1-X) + C6\}$: for deformed nuclei,
56<Z<76, Z>90
94<N<118, N>138.

FF = 1.0 Ffor for spherical nuclei.

$[P]exp = Cp \cdot [1 + Fp\ (Es/Cs)]$: for even-proton and -neutron shells

[Es]exp, [P]exp :

experimental shell and pairing energies adjusted by using, as the first guess, those (constant shell terms and the gross term) of Reference [3], and experimental mass excess data of Reference [4].

The resulting values for free parameters (mass excess fitting) are shown in Table 1 with the mean error. For a large range of mass number, the single-particle levels are grouped to coupled proton- and neutron-shells, as the proton 28- and the neutron 50-shells. For total 1925 nuclei, the mean difference ΔM between the empirical masses and the computed ones is,

$$\Delta M = 0.252\text{MeV}.$$

To the experimental error of the mass table an error of 0.3 MeV only for (28,28)-shell has been added quadratically, and reciprocal of this sum of two error has been used as weight.

4. Predictions for Resonance Data

Slow neutron resonance spacings and proton resonance spacings data have been analyzed by using the existing level density models in the previous study [2]. For the test of the present model some of those data are used for the present work, and the results are compared with the previous ones. For this analysis, the shell and pairing energies are derived from the preesent mass-formula. The predictions of the KRK and the SPC models are presented in Table 2. As shown there the present model predicts Dobs as well as the KRK. At the present study the search for systematics related to parameters ($\bar{a}$, W, q) is not sufficient.

5. Concluding Remarks

Semiempirical level density formula with the simple data-set for parameter systematics, compared with the previous ones, is presented. On the application for a wide range of nuclei, further studies will be needed for the well definded systematics of parameters ($\bar{a}$, W, q).

References;

[1] S.K.Kataria,V.S.Ramamurthy and S.S.Kapoor: Phys.Rev.,C18,549(1978).
[2] H.Vonach,et al: Phys.Rev.,C38,2541(1988).
[3] Y.Ando,M.Uno and M.Yamada: JAERI-M 83-025(1983).
[4] A.H.Wapstra and Audi: A.D.N.D.Tables (1985).

Table 1 Values for parameters of shell and pairing correction terms

shells		(1,1)	(1,2)	(2,2)	(2,3)	(3,3)	(3,4)	(4,4)	(4,5)
C1	-Z	0.408	1.174	1.743	1.743	-0.878	-4.231	0.000	0.000
	-N	0.961	0.521	1.508	1.555	-1.535	5.21I	5.257	0.000
C2	-Z	-1.433	-1.147	-0.824	-0.799	-0.725	-3.488	-10.884	-8.439
	-N	-1.304	-0.591	-1.618	-1.457	-0.601	-3.950	-3.962	-4.555
Cs	-Z	0.837	0.460	1.608	1.582	3.426	9.554	12.427	10.271
	-N	1.020	1.840	1.929	4.150	3.376	4.862	4.873	9.896
C3	-Z	-0.369	-0.753	-1.393	-2.121	-0.176	-0.849	-1.273	-2.054
	-N	0.488	-0.600	-0.071	-1.331	-1.320	-2.632	-2.634	-2.291
C4	-Z	-0.043	-0.714	-0.157	-1.349	-1.296	0.890	0.000	0.000
	-N	-1.079	-1.632	-1.300	-3.047	-1.571	-0.871	-1.296	0.000
C5	-Z					80.00	54.80	269.28	271.16
	-N						717.17	-2066.5	-445.5
C6	-Z					0.351	-1.433	-0.151	0.104
	-N						-0.860	-1.576	-2.800
Cp	-Z	1.738	1.802	1.445	1.481	1.209	0.946	0.852	0.508
	-N	1.958	1.559	1.757	1.189	1.171	0.898	0.994	0.580
Fp	-Z	0.009	-0.010	-0.012	-0.054	-0.058	2.451	1.623	1.458
	-N	-0.066	-0.078	-0.057	0.114	0.120	0.351	0.587	-0.089
ΔM(MeV)		0.402	0.071	0.095	0.323	0.120	0.491	0.197	0.809

mean error for 1925 experimental masses, ΔM = 0.252 MeV.

shell-1 (14 - 28), shell-2 (- 50), shell-3 (- 82),
shell-4 (-126), shell-5 (-184)

Table 2 Level density calculations (KRK and SPC-model)

A	Z	N	Es	Ep	U	t	$\tilde{a}$	S	SIG2	Dobs	D(SPC)	D(KRK)
Cr55	24	31	1.34	1.76	6.25	0.861	7.54	13.07	12.83	54.4	56.18	59.83
Fe55	26	29	-0.78	1.75	9.30	1.024	7.54	14.59	12.33	18.0	18.78	11.73
Mn55	25	30	0.27	1.45	8.07	0.981	7.54	14.48	10.34	7.1	13.65	15.32
Fe59	26	33	2.10	1.75	6.58	0.861	8.08	14.58	11.42	25.4	11.45	24.47
Ni59	28	31	-0.24	1.74	9.00	0.981	8.08	15.26	10.48	12.5	7.45	7.90
Co59	27	32	0.86	1.43	7.37	0.912	8.08	14.75	12.16	4.3	12.12	14.72

parameters ; (KRK) A0 = 0.137 (SPC) A0 = 0.137
W0 = 0.170 W0 = 0.30
q0 = 0.22

5.21 Comments on ENSDF —from the Evaluator to Dear Bitter Users

Kensuke KITAO
JNDC - ENSDF group*
and
Data Engineering, Inc.

Evaluated Nuclear Structure Data File (ENSDF) is a data base derived from only published experimental research papers. Some incomplete parts still exist in the file as pointed out by users, but it is unavoidable according to present policies for preparation of the file. About 96% of decay data sets in ENSDF have the normalization factor (that to give the intensity per 100 disintegration of parent nucleus). For lack of experimental data, the accuracy of these factors is still a problem. In ENSDF, about nine-hundred radionuclides of decay data sets contain unplaced gamma-rays. The number of such gamma-rays is amount of about 16800, and the one-hundred twelve isomers have not established excited energy.

Introduction

ENSDF (Evaluated Nuclear Structure Data File) is a computer data base file, maintained by the National Nuclear Data Center as well as NSRF (Nuclear Structure Reference File). It is consist of evaluated experimental data on nuclear level properties, radiations, radioactive decay, and reaction data for $1 \leq A \leq 266$, where A is the mass number. We can see the contents of ENSDF on a journal, Nuclear Data Sheets, and also access directly the ENSDF via computer network, i.e., Internet, Hepnet, Physnet, Esnet. (See page *iv* on each issue of Nuclear Data Sheets.)

Recently, there has frequently been querulous voices or bitter criticism on ENSDF from users. They say that the evaluator must give spin-parity value to each adopted level in ENSDF, and if possible it must be unique one. Why are decay data sets without normalization factor (to calculate particles or photons per 100 disintegration of the radionuclide) in the file? Why is total beta- and total gamma-energy following the decay of each nuclide not agree the decay energy of the nuclide? They also point out that there are levels to have not decided excited energies or spin-parity values in the adopted levels. In other words, they say that is ENSDF the "evaluated" data? It is naturally to raise these questions from users. We, as evaluator, take in part to prepare a part of the file. Therefore, it may be presumptuous that we explain the policies ([1]) of ENSDF. To afford a better understanding on the file by users, we should like to introduce some policies of the preparation of data sets and

* Japanese Nuclear Data committee - ENSDF group, c/o Y. Kikuchi, Nuclear Data Center, Japan Atomic Energy Research Institute, Tokai-mura, Naka-gun, Ibaraki-ken 319-11, Japan.

adopted levels and radiations, as well as the degree of completeness of the file.

1. ENSDF rejects speculation

For each nuclear species, ENSDF presents most reliable information to users on the adopted properties of the nucleus, and on the evaluated result, as the data set, of single type of experiment, such as a radioactive decay, a single nuclear reaction, and an in-beam spectroscopy. In the preparation of the data set, evaluators are limited or not allowed to use any speculation. For example, when we have only an experimental result, we are allowed to plot a point on graph sheet but can not overlap the curve obtained from a theoretical calculation, on the point.

2. Excitation energies and spin-parity of levels.

Evaluator evaluates experimental results for ENSDF but adds not the data not given by experiments. Adopted levels are those connected by gamma transitions and those as final states of reactions. The excitation energies of levels connected by gamma transitions are from a least squares fit to the adopted gamma energy. In general, observed kinetic energies of particles emitted in the nuclear reactions is less accurate compared with gamma-ray energies. Thus, a level from reaction data may be overlap on several levels determined by gamma-ray energies. Former level is not the same as a specific one of later levels, unless they have the same spin-parity or overlap each other. Column XREF in table of the adopted level in Nuclear Data Sheets, or XREF flags in ENSDF , denotes corresponding relations between levels on "Adopted levels, gammas" data set and ones on individual data sets.

There are levels without established excitation energy in ENSDF. Of course, existence of these levels has been confirmed through measurements of the half-life, band structures, and so on. See Fig. 1 for such example. Positions of such levels may be possible to estimate by aid of a theoretical calculation or systematics of neighboring isotopes or isotones with similar structure, but such prediction will be not accepted in general. Nuclides with such level are about 400 in the file. We show nuclides having isomeric state not established excitation energy or ones not established the order of ground and isomeric states in the table 1.

Values of spin are given from direct measurements but such measurement very limited. In general, angular momentum in particle transfer reaction, multipolarity of gamma-transition, and logft value given from constructed decay scheme perform the important role in the assignment of spin-parity values. Evaluators work according the rules of ENSDF itself on the assignment ([2]). Thus, needed information from published papers is not spin-parity values given by authors but experimental results to be useful for arguments of assignment.

3. Normalization of gamma-ray and decay energy

Some users have interest to calculate radiation exposure from radionuclides, decay heat of nuclear

reactors after shut-down. They need absolute intensities of radiations emitted from radionuclides, i.e., particles or photons per 100 disintegrations of the nuclide. ENSDF has prepare the normalization factor for each radionuclide, then user can obtain the absolute intensity using with the factor. However, some decay data sets containing in the file have not the factor. The number of the data set without normalization factor is 96% of about 3100 decay data sets. Moreover, although decay scheme established and normalization is given, it is likely that accuracy of the factor is very bad. It rises from lacking beta-spectra measurements, especially that of beta-rays to ground state of daughter, missing gamma-rays from higher energy states, existing gamma-rays observed but placed in decay scheme. For example, the number of unplaced gamma-rays in ENSDF amounts to about 16800 ([4]).

Concluding remarks

Problems as pointed out by users exist in ENSDF but it is unavoidable under present policies for preparing of the file. It seemed users to seek a complete data base in itself on decay and level structure data. Such data base must be constructed by different policies from that of the current ENSDF. For the data base, ENSDF can supply materials, so to speak the most refined materials. ENSDF is always revising by new experimental facts. However, the revision of ENSDF is not simultaneously done for all data. It is possible that the data sets of a isobars are not revised since 1982. This may be some confusion between users utilizing files as ENDF or JENDL.

In spite of many reports published, lack of data for evaluation becomes still an obstacle in completeness of ENSDF. Trend seen in recent papers on in-beam spectroscopy experiments is parted with measured gamma-ray energy and intensity. We expect researchers to inform us these eliminated data for submit to journal.

References

1) General Policies, pp.ⅷ -ⅷ, first issue of each year of Nuclear Data Sheets.
2) Summary of bases for spin and parity assignments, pp.ⅸ-ⅹ, ibid.
3) K. Kitao and M. Oshima: Nuclear Data Sheets for A=127 (to be published).
4) T. Narita and K. Kitao: Catalog of Gamma-rays unplaced in Radioactive Decay Schemes, JAERI-M 91-037 (1991).

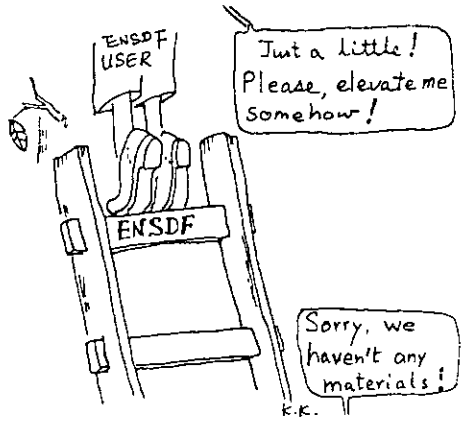

Table 1 Isomeric states without established exciting energy.

$^{70}Br^{m}$	$^{102}Y^{m,g}$	$^{119}Ag^{m,g}$	$+^{132}I^{m}$	$^{148}Tb^{m}$	$^{158}Tm^{m}$	$^{189}Hg^{m}$
$^{74}Br^{m}$	$^{102}Nb^{m,g}$	$^{119}Cs^{m}$	$^{133}Ce^{m}$	$^{148}Ho^{m}$	$^{160}Ho^{m}$	$^{189}Tl^{m}$
$^{78}Rb^{m}$	$^{102}Tc^{m}$	$^{120}Sb^{m}$	$^{133}Nd^{m}$	$^{149}Ho^{m,g}$	$^{160}Lu^{m}$	$^{190}Re^{m}$
$^{82}As^{m}$	$^{102}Sn^{m}$	$^{120}I^{m}$	$^{134}Sb^{m,g}$	$^{150}Tb^{m,g}$	$+^{162}Ho^{m}$	$^{190}Tl^{m}$
$^{84}As^{m}$	$^{108}Rh^{m,g}$	$^{122}Ag^{m}$	$^{135}Nd^{m,g}$	$^{150}Ho^{m,g}$	$^{162}Tm^{m}$	$^{190}Bi^{m}$
$+^{84}Y^{m}$	$^{110}Rh^{m,g}$	$^{122}In^{m}$	$^{136}La^{m}$	$^{151}Tm^{m,g}$	$^{165}Lu^{m}$	$^{191}Ir^{m}$
$^{87}Nb^{m}$	$^{112}Rhm,g$	$^{122}Cs^{m}$	$^{136}Pm^{m,g}$	$^{151}Yb^{m,g}$	$^{168}Re^{m}$	$^{192}Tl^{m,g}$
$^{88}Nb^{m}$	$^{113}Pd^{m}$	$+^{126}In^{m}$	$^{138}Pm^{m}$	$^{152}Pm^{m}$	$^{172}Re^{m}$	$^{192}Bi^{m}$
$^{89}Nb^{m,g}$	$^{114}Rh^{m}$	$+^{127}In^{m}$	$^{140}Pm^{m}$	$^{152}Tm^{m}$	$^{173}W^{m,g}$	$^{193}Tl^{m}$
$^{91}Ru^{m}$	$^{116}Rh^{m,g}$	$^{127}La^{m}$	$^{141}Tb^{m}$	$+^{153}Ho^{m}$	$^{182}Re^{m}$	$^{194}Ir^{m}$
$^{94}Rh^{m,g}$	$^{116}I^{m}$	$^{128}Sb^{m}$	$^{142}Eu^{m}$	$^{154}Pm^{m}$	$+^{183}Tl^{m}$	$^{194}Bi^{m}$
$+^{98}Rb^{m}$	$^{116}Cs^{m,g}$	$+^{128}In^{m}$	$^{143}Tb^{m}$	$+^{154}Eu^{m}$	$^{185}Au^{m}$	$+^{200}At^{m}$
$^{98}Y^{m}$	$^{117}Te^{m}$	$^{129}Ce^{m,g}$	$^{145}Tb^{m}$	$^{154}Tb^{m}$	$^{186}Ir^{m}$	$+^{217}PA^{m}$
$^{98}Rh^{m}$	$^{117}Cs^{m,g}$	$^{130}Sb^{m}$	$^{146}La^{m}$	$^{154}Ho^{m}$	$^{187}Hg^{m}$	$^{222}Ac^{m}$
$^{100}Nb^{m,g}$	$+^{118}In^{m}$	$^{131}Ce^{m}$	$^{146}Tb^{m}$	$^{156}Tb^{m}$	$^{187}Pb^{m,g}$	$^{247}Fm^{m,g}$
$^{102}Rb^{m}$	$^{118}Cs^{m,g}$	$^{132}Sb^{m}$	$^{147}Er^{m}$	$^{156}Tm^{m}$	$^{188}Tl^{m,g}$	

m: isomer

m,g: not established the order of ground and isomeric states

+: isomeric states given approximate values for excitation energies

^{127}La Levels

Cross Reference (XREF) Flags

A ^{127}Ce β$^+$ Decay
B (HI,xnγ)

E(level)§	Jπ	XREF	$T_{1/2}$	Comments
0.0	(3/2+)	AB	3.8 min *5*	Jπ: from syst of odd-La isotopes. $T_{1/2}$: from 63Pr02. Other: 3.5 min *5* (63Ya05).
0.0+x†	(11/2−)@	B	5.0 min *5*	Jπ: from syst of isomers in odd-La isotopes. E(level): the transition between the 5-min state (11/2−) and the 3.8-min (g.s.) has not been observed. $T_{1/2}$: from 73Le09.
58.4# *5*		A		
73.0+x?		B		
173.2# *7*		A		
235.5# *7*		A		
252.4+x†	(15/2−)@	B	59 ps *9*	$T_{1/2}$: from 85Sm07 (RDM).
426.2# *9*		A		
622.0+x?		B		
711.0+x†	(19/2−)@	B	9.4 ps *9*	$T_{1/2}$: from 85Sm07 (DSAM).
1026.0+x?		B		
1202.0+x?		B		
1341.9+x†	(23/2−)@	B	2.8 ps *14*	$T_{1/2}$: from 85Sm07 (RDM,DSAM).
1702.0+x‡	(21/2+)&	B		
2122.2+x†	(27/2−)@	B	1.01 ps *12*	$T_{1/2}$: from 85Sm07 (DSAM).
2145.9+x‡	(25/2+)&	B		Jπ: (E1) γ to (23/2−).
2722.9+x‡	(29/2+)&	B		
3030.2+x†	(31/2−)@	B	0.78 ps *11*	$T_{1/2}$: from 85Sm07 (DSAM).
3424.9+x‡	(33/2+)&	B		
4033.2+x†	(35/2−)@	B		
4237.9+x‡	(37/2+)&	B		
5032.2+x†	(39/2−)@	B	0.62 ps *10*	$T_{1/2}$: from 85Sm07 (DSAM).
5153.9+x‡	(41/2+)&	B		
6045.2+x†	(43/2−)@	B		
6150.9+x‡	(45/2+)&	B		
7147.2+x†	(47/2−)@	B		
7168.9+x‡	(49/2+)&	B		

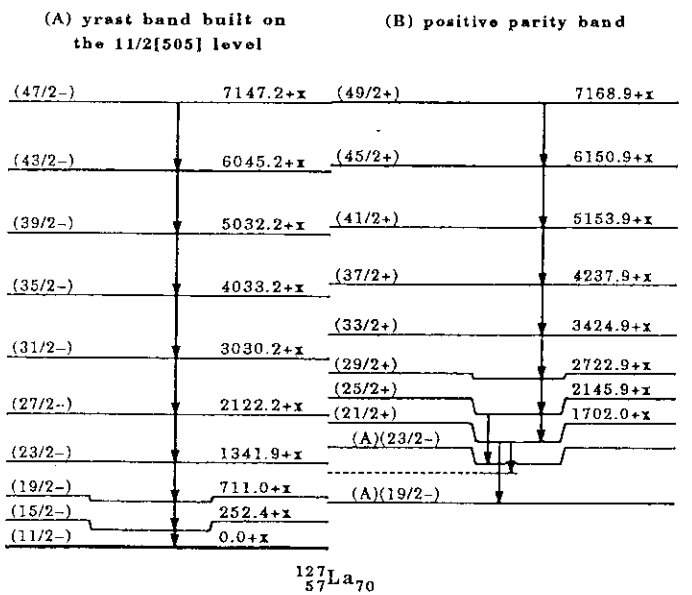

† Yrast band built on the 11/2[505] level.
‡ Positive parity band.
§ From (HI,xnγ), except as noted.
# From ^{127}Ce β$^+$ decay.
@ From stretched E2 cascades to (11/2−) and expected band structure.
& From existing a stretched E1 transition to a member of the negative parity band and expected band structure.

Fig. 1 An example of nuclide with levels not established excitation energies[3] in ENSDF.

5.22 Systematics of the Fragmentation Cross Section for Incident Proton Energies up to 3 GeV

Nobuhiro SHIGYO, Kenji ISHIBASHI, Yoshihisa WAKUTA

Department of Nuclear Engineering, Kyushu University
Hakozaki, Fukuoka-shi 812

We study the systematics of fragmentation reaction by the liquid-gas phase transition model, for incident proton energies up to 3 GeV. The formula based on the thermal droplet model is adopted for representing the experimental kinetic energy spectra. In addition, a simpler formula is successfully introduced for the spectra in this study. The relationship between parameters of two formulas is obtained quantitatively. The same nuclear temperature common to both kinetic energy spectra and mass yields of fragments in useful for describing the fragmentation phenomena. The present systematics are suited for incorporation as a subroutine set into the High Energy Transport Code.

1. Introduction

A spallation reaction is caused by bombarding a target with a particle having energy above a few hundred MeV. This reaction produces a great number of neutrons, and is applicable to producing an intense spallation neutron source or transmuting long-lived radioactive wastes. With increasing proton energy, the fragmentation process emits intermediate mass fragments like Na and Mg, which are never released by the cascade and the evaporation processes. Since accumulation of the spallation data is poor, such computer codes as High Energy Transport Code (HETC) and Nucleon Meson Transport Code (NMTC) are used for engineering purposes. However, the fragmentation process is not included in these codes. To incorporate this process into HETC, it is necessary to know the systematics of kinetic energy spectra and mass yields of the fragments.

On the basis of the liquid-gas phase transition model[1], we have investigated the systematics of the fragmentation reaction for incident proton energies up to 3 GeV. Some preliminary results were already reported[2]. In the present study, we attempt to represent the kinetic energy spectra of the fragments by using two types of formulas. One is the formula composed of the double integration form based on the thermal droplet model[3-4]. The other is the simpler form of the former without use of any integration. The relationship between parameters of two types of formulas is studied.

The present systematics are easily incorporated as a subroutine set into HETC. The use of the systematics will consume much less computation time than Quantum Molecular Dynamics (QMD), and reproduce the kinetic energy spectra to a reasonable degree. The simpler formula for the kinetic energy spectra is expected to be suited for this incorporation.

2. Model of Fragmentation

2.1 Experimental Data

About the proton induced fragmentation reaction, we are interested in the cross sections for the mass yields and the energy spectra of the fragments. We used the data of the mass distribution measured for incident proton energies of 0.48[5], 1.0[6], 4.9[7] on Ag, 1 GeV on Ni[6]. We also adopted the data of the energy spectra experimentally obtained for incident proton energies of 0.48 GeV on Ag[5], and 1.6, 2.3 and 3.1 GeV on Xe[4].

2.2 Liquid-Gas Phase Transition Model

The liquid-gas phase transition takes place in a Van der Waals field. We consider this kind of the phase transition in a highly excited nuclei[8]. In this model, a nucleus stays in liquid phase in an initial state. When an incident proton deposits its energy on the target nucleus and makes it in a highly excited state, the nuclear phase changes from the liquid to the gas phase. The gas phase region appearing in the nucleus may extend into the liquid region, and this extension leads to break up of the nucleus.

Panagiotou et al.[1] has proposed the probability for the fragment formation by simplifying the liquid-gas phase transition model. This probability is described by

$$P(A) \approx A^{-k} \exp\left\{\left[-F_S(T)A^{2/3} - F_B(T)A + \mu(T)A\right]/T\right\}, \tag{1}$$

where k is the critical exponent that is independent of T and A, F_S is the surface free energy per particle, F_B is the volume free energy per particle, μ is the chemical potential per particle and T is the nuclear temperature. We found the shape of the equation that reasonably represent the fragment mass yields for the incident proton energies concerned. Eq. (1) can be changed as

$$P(A) = \alpha A^{-2.0} \exp\left[-18\left(1 - \frac{T}{15}\right)^{1/2} A^{2/3}/T\right], \tag{2}$$

where α is the normalization constant, and is given by fitting the fragment mass yields. The nuclear temperature T is also considered as an adjustable parameter.

The fragment mass yields are fitted by Eq. (2). TABLE I lists the parameter sets of the fragment mass yields. Fig. 1 shows the results of the fragment mass distributions. In the cases other than the proton energy of 0.48 GeV, the results by this formula well agree with the experimental data, and Eq. (2) is valid for reproducing these data. For the proton energy of 0.48 GeV, the experimental yields have a bump at mass number of 6 to 25. Nevertheless, this formula reproduces such experimental data on an average.

3. Fragment Kinetic Energy Spectra

3.1 Double Integral Form

A moving source model is useful for representing the fragment angular and kinetic energy spectra[2]. This model assumes that a moving source has some velocity and emits a particle isotropically. The kinetic energy spectra of emitted particles are given by this model as

$$\frac{d^2\sigma}{dEd\Omega} = G\left(\frac{E_f}{E^*}\right)^{1/2}\exp\left(-\frac{E^*}{T}\right), \tag{3}$$

$$E^* = \frac{m + E_f - p\beta_s\cos\theta}{\sqrt{1-\beta_s^2}} - m, \tag{4}$$

$$p = \sqrt{2mE_f + E_f^2}, \tag{5}$$

where G is the normalization constant, T is the nuclear temperature, E_f is the kinetic energy of emitted particles in the laboratory system, E^* is the kinetic energy in the moving system, β_s is the velocity of the moving source, p is the momentum of the emitted particle, m is the mass of the emitted particle and θ is the emission angle in the laboratory system.

One can see that this approach lacks the effects of Coulomb barriers and excitation energy of fragments. Hirsch et al.[3] described kinetic energy spectra as

$$\frac{\mathrm{d}^2\sigma}{\mathrm{d}E_f\mathrm{d}\Omega} = N\left(\frac{E_f}{E^*}\right)^{1/2}\int_0^{E^*} P(B)\mathrm{d}B$$

$$\times\int_0^{E^*}\varepsilon^{1/2}\left(E^*-B-\varepsilon\right)^{1/2}\exp\left\{-\left[\varepsilon/T_\varepsilon-\left(E^*-B-\varepsilon\right)/T\right]\nu\right\}\mathrm{d}\varepsilon, \tag{6}$$

where

$$P(B)\mathrm{d}B = \sqrt{B}\exp\left[-\frac{\left(B-B_0\right)^2}{2\sigma^2}\right]\mathrm{d}B, \tag{7}$$

$$\nu = 1 - \frac{A_f}{A_r} \tag{8}$$

In these equations, N is the normalization constant, ε is the excitation energy of the fragment, T_ε is the nuclear temperature of the excited fragment. In this study, T_ε was assumed to be 3 MeV according to reference 3. B_0 is the most probable Coulomb barrier, σ is the variance of the Coulomb barrier, ν is the recoil correction factor, A_f is the mass number of the fragment and A_r is the mass number of the remnant.

The formulas in Eqs. (6) - (8) include 5 adjustable parameters of N, β_s, T, B_0 and σ. The values of these parameters were determined by the program SALS[9]. This program optimizes the adjustable parameters by the root mean square method. TABLE II shows the parameter sets obtained.

The solid curves in Fig. 2 show the kinetic energy spectra of fragments by Eqs. (6) - (8). The formulas reproduce the kinetic energy spectra well in wide incident proton energies.

Values of B_0 and σ are related to the maximum Coulomb barrier height B_{max}. This barrier is described within the scope of the thermal droplet model[3] by

$$B_{max} = \frac{Z_r Z_f e^2}{R_r^3 \nu^2}\left(R_{max}^3 + 3R_{max} R_f\right), \tag{9}$$

where Z_f is the charge of the fragment, Z_r is the charge of the remnant, R_f is the nuclear radius of the fragment, R_r is the radius of the remnant and R_{max} is the distance between the centers of the fragment and the remnant nucleus. TABLE III shows the ratios of B_0 and σ to B_{max}. These ratios depend dominantly on the incident proton energy.

3.2 Simpler Form without Integration

A simpler functional form is devised for describing the kinetic energy spectra. This form is given by

$$\frac{d^2\sigma}{dE_f d\Omega} = \frac{K}{2}\left(\frac{E_f}{E^*}\right)^{1/2}\left[1 - \tanh\left(-\frac{E^* - C}{D}\right)\right]\exp\left(-\frac{E^*}{T/\nu}\right), \tag{10}$$

where C and D are the quantities corresponding to the most probable Coulomb barrier B_0, and the variance of Coulomb barrier σ, respectively, and K is the normalization constant.

This formula also has 5 adjustable parameters K, β_s, T, C and D. These parameters were also determined by SALS. TABLE IV lists the results of the parameter sets. The dash curves in Fig. 2 indicate the calculation results. This formula reproduces the kinetic energy spectra of the fragments to a reasonable degree in a wide energy range. Since being free from the double integral, this formula will be easier to be incorporated into HETC than Eq. (6).

The relationship between parameters for Eqs. (6) and (10) is found by the results of fitting parameters. The results are plotted in Fig. 3 and the relation is written by

$$C = 0.86B_0 + 16, \tag{11}$$

$$D = 0.25\sigma + 7.0. \tag{12}$$

These approximate expressions are practically valid for the use of the simpler equation.

For the effect of the Coulomb barrier in the functions for Eqs. (6) and (10), the key function are considered, respectively, as

$$F_G(E^*) = \int_0^{E^*} \sqrt{B}\exp\left[-\frac{(B - B_0)^2}{2\sigma^2}\right]dB, \tag{13}$$

$$F_T(E^*) = \frac{1}{2}\left[1 - \tanh\left(-\frac{E^* - C}{D}\right)\right]. \tag{14}$$

The relationship of parameters in the above equations were obtained:

$$C = B_0 + \frac{\sigma^2}{20}, \tag{15}$$

$$D = \sigma + \frac{B_0}{20}. \tag{16}$$

The values of Eqs. (13) and (14) are plotted in Fig. 4 by the use of this relationship. Three types of curves are in good agreement. The deviation of Eqs. (11) - (12) from (15) - (16) is ascribed to the fact that Eqs. (11) - (12) include implicitly the effects of fragment excitation energy and the detailed probability distribution of the Coulomb barrier.

4. Common Nuclear Temperature

In sections 2 and 3, we used the individual nuclear temperatures for representing the mass yields and the kinetic energy spectra of the fragments. The nuclear temperatures obtained from the mass yields are close to those from the kinetic energy spectra. In principle, both the mass yields and kinetic energy spectra of the fragments take place from one phenomenon with a common nuclear temperature. Then, the nuclear temperatures obtained for the mass yields and the kinetic energy spectra are averaged to be the same value for the specified incident proton energy. Figs. 5 and 6 show the mass yields and the kinetic energy spectra of the fragments by the use of the same temperatures, respectively. These figures indicate that the common temperatures represent the mass yields and the kinetic energy spectra of the fragments reasonably. Fig. 7 shows the common nuclear temperatures as a function of the incident proton energies. The use of the common temperature is important to incorporate the fragmentation reaction in HETC.

5. Summary

On the basis of the liquid-gas phase transition model, the systematics of the fragmentation cross section were found for incident proton energies up to 3 GeV. The fragment mass yields were described by this model. To reproduce the kinetic energy of fragments, two types of formulas were used. One is the double-integration formula derived from the thermal droplet model. The other is the simpler formula without integral. The same temperature characterized the kinetic energy spectra and the mass yields of the fragments. These systematics cover the wide range of the incident proton energies and are useful for calculating the fragmentation reaction by HETC.

Acknowledgment

We would like to thank S. Sakaguchi of Agency of Science and Technology for his useful suggestion.

References

1) Panagiotou A.D. et al.: Phys. Rev., C31, 55 (1985).
2) Sakaguchi S. et al.: JAERI-M 92-027, 237 (1992).

3) Porile N.T. et al.: Phys. Rev., C39, 1914 (1989).
4) Hirsch A.S. et al.: Phys. Rev., C29, 508 (1984).
5) Green R.E.L. et al.: Phys. Rev., C29, 1806 (1984).
6) Andronenko L.N. et al.: Phys. Lett. B174, 18 (1986).
7) Westfall G.D. et al.: Phys. Rev., C17, 1368 (1978).
8) Bondorf J.P. et al.: Nucl. Phys., A443, 321 (1985).
9) Nakagawa T. et al.: "Program System SALS for Nonlinear Least-Squares Fitting in Experimental Science, in Recent Holland Publishing Company (1980).

Table I Parameter sets for fragment mass yields

Incident Proton energy	Target	α	T(MeV)
0.48GeV	Ag	1.0×10^2	7.8
1.0GeV	Ni	1.4×10^2	14
	Ag	3.0×10^2	15
1.6GeV	Xe	4.2×10^2	14
2.3GeV	Xe	8.4×10^2	14
3.1GeV	Xe	1.5×10^3	15
4.9GeV	Ag	7.2×10^4	15

Table II Parameter sets for double-integral formula for fragment energy spectra

Incident Proton Energy	Target	Fragment	N	T(MeV)	β_s	B_0(MeV)	σ(MeV)
0.48GeV	Ag	C	22	8.7	0.0072	15	2.6
		N	7.1	8.2	0.0062	16	4.6
		Na	5.8	9.4	0.0046	18	5.4
1.6GeV	Xe	Be	65	13	0.0044	8.4	7.4
		C	41	14	0.0044	11	7.4
		N	24	13	0.0044	12	8.2
		O	13	15	0.0044	16	7.0
2.3GeV	Xe	N	59	15	0.0059	5.4	9.0
3.1GeV	Xe	Be	270	15	0.0055	5.6	5.7
		C	130	13	0.0055	10	10
		N	79	13	0.0055	11	10
		O	45	14	0.0055	12	11

Table III Parameters B_0 and σ normalized by B_{max}

Incident Proton Energy	Target	Fragment	B_0(MeV)	B_{max}(MeV)	B_0/B_{max}	σ(MeV)	σ/B_{max}
0.48GeV	Ag	C	15	57	0.26	2.6	0.045
		N	16	60	0.27	4.6	0.077
		Na	18	69	0.26	5.4	0.078
1.6GeV	Xe	Be	8.4	47	0.23	7.4	0.16
		C	11	66	0.18	7.4	0.11
		N	12	73	0.22	8.2	0.11
		O	16	79	0.20	7.0	0.087
2.3GeV	Xe	N	5.4	73	0.074	9.0	0.12
3.1GeV	Xe	Be	5.6	47	0.12	5.7	0.12
		C	10	66	0.15	10	0.15
		N	11	73	0.15	10	0.14
		O	12	79	0.15	11	0.14

Table IV Parameter sets for the simpler formula for fragment energy spectra

Incident Proton Energy	Target	Fragment	K	T(MeV)	β_s	C (MeV)	D (MeV)
0.48GeV	Ag	C	6.5×10^4	9.1	0.0072	28	7.7
		N	5.9×10^4	8.5	0.0062	29	8.2
		Na	4.6×10^3	11	0.0045	31	8.4
1.6GeV	Xe	Be	6.5×10^4	16	0.0044	23	8.9
		C	6.1×10^4	16	0.0044	25	8.9
		N	4.7×10^4	15	0.0044	26	9.1
		O	2.4×10^4	18	0.0044	29	8.8
2.3GeV	Xe	N	4.0×10^4	20	0.0059	20	9.3
3.1GeV	Xe	Be	1.2×10^5	18	0.0055	20	8.5
		C	1.2×10^5	18	0.0055	24	9.6
		N	8.8×10^4	18	0.0055	25	9.6
		O	6.7×10^4	18	0.0055	26	9.8

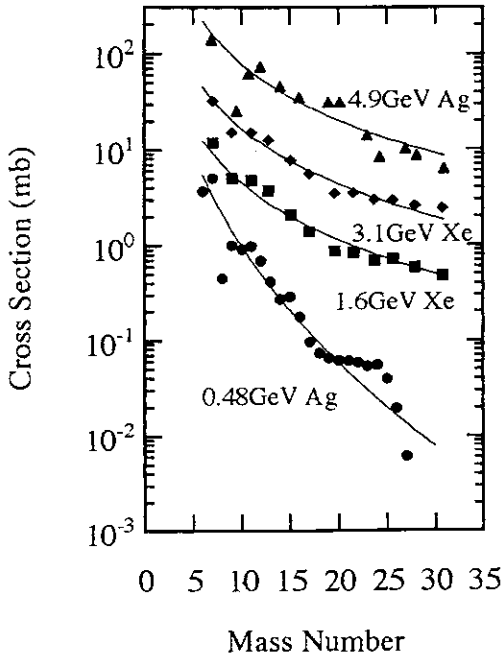

Fig. 1 Fragment mass yields

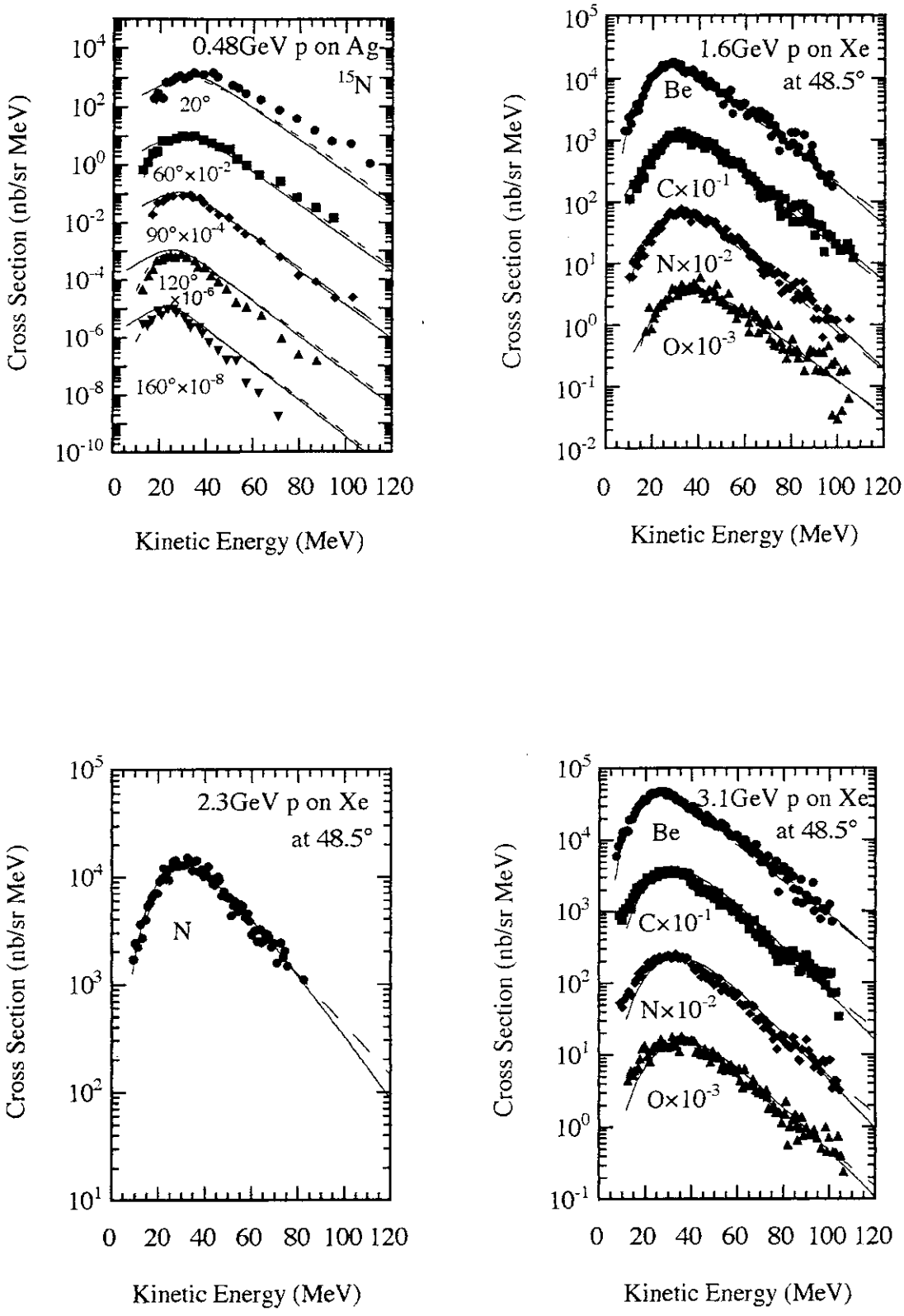

Fig. 2 Kinetic energy spectra for fragments
— Double-integral formula --- Simpler formula

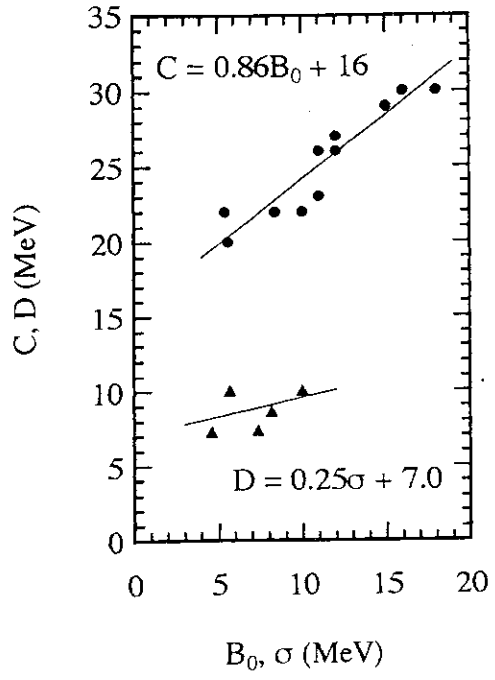

Fig. 3 Parameters C and D as functions of B_0 and σ, respectively

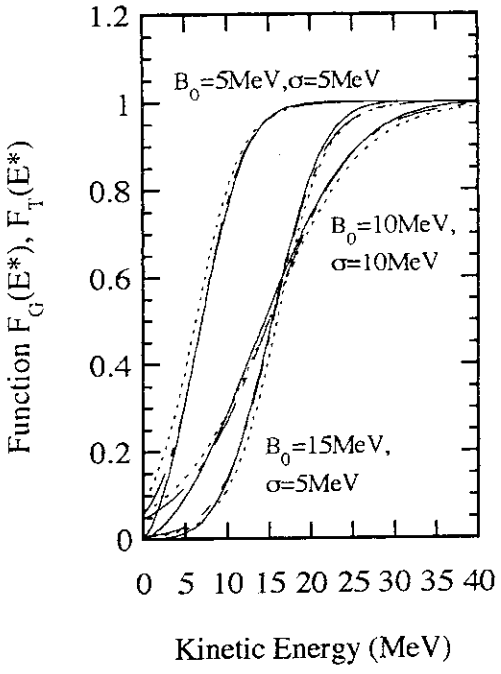

Fig. 4 Relation of $F_G(E^*)$ and $F_T(E^*)$
——— $F_G(E^*)$
····· $F_T(E^*)$ by Eqs. (15) and (16)
—— - $F_T(E^*)$ by best fitting

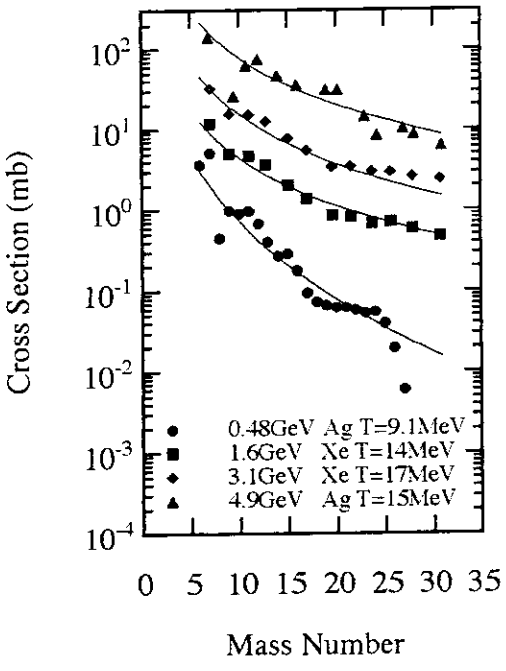

Fig. 5 Fragment mass yields by temperatures common to kinetic energy spectra

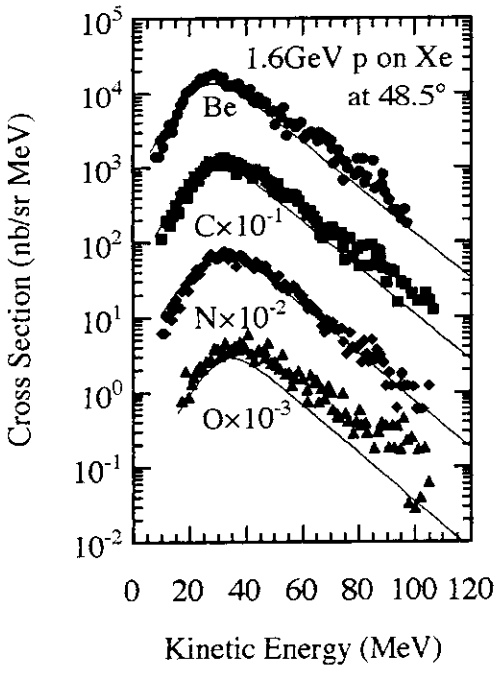

Fig. 6 Kinetic energy spectra of fragments by temperature common to mass yields

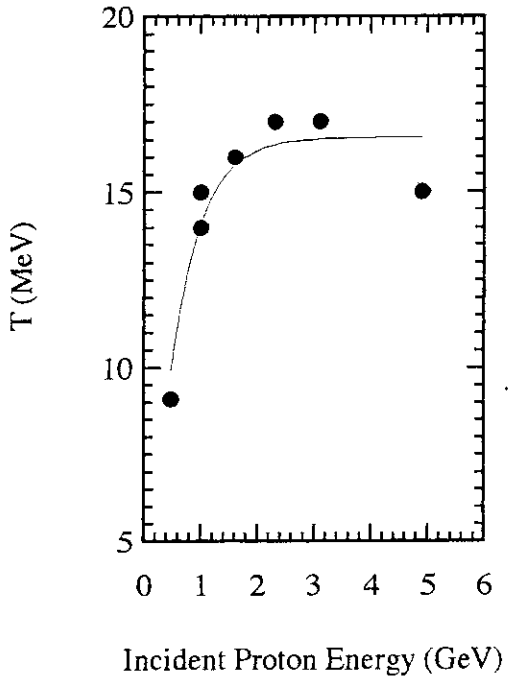

Fig. 7 Common nuclear temperature as a function of incident proton energy

5.23 Integral Test of Secondary Gamma-ray Production Cross Sections of Iron in JENDL-3 with Continuous Energy Monte Carlo Analysis

Kohtaro UEKI, Atsuto OHASHI, and Naoki YAMANO*

Ship Research Institute,
Shinkawa, Mitaka, Tokyo 181, Japan

*Sumitomo Atomic Energy Industries, Ltd.,
Kajiya-cho Kanda, Chuo-ku, Tokyo 101, Japan

Integral test of secondary gamma-ray production cross sections of iron in JENDL-3 was carried out with the continuous energy Monte Carlo analysis for the K&K iron secondary gamma-ray benchmark experiment. In the present analysis the 0.847 MeV peak was investigated in detail. At the peak, the large discrepancy was observed between the results with JENDL-3 and ENDF/B-IV data. The peak could not reproduced and an incomprehensive peak was appeared around 0.7 MeV with JENDL-3 data. Taking advantage of the Monte Carlo results, the iron secondary gamma-ray production cross sections were revised and the new data was proposed to JENDL-3.2.

Consequently, the Sn calculations with the revised iron cross sections reproduced the 0.847 MeV peak quite well as with ENDF/B-IV data. However, the peak around 8 MeV was disappeared completely with the revised data.

1. Introduction

In order to test the secondary gamma-ray production cross sections of iron in JENDL-3[1], the Monte Carlo was carried out for the K&K iron secondary gamma-ray benchmark experiment[2] by the continuous energy Monte Carlo code MCNP[3].

In the K&K benchmark experiment, the ^{252}Cf fission neutron-induced secondary gamma-ray leakage spectra from iron spheres of 25 cm and 35 cm diameters were measured with the Si (Li) Compton spectrometer in the energy range from 0.3 to 3 MeV. The 0.847 MeV peak, which is caused by inelastic scattering with iron was observed clearly but the peak around 8 MeV, which is produced by thermal-neutron capture was out of the measured spectra.

Accordingly, the 0.847 MeV peak was investigated in detail. The inelastic scattering peak could not reproduced by the Monte Carlo calculations with JENDL-3 data but reproduced completely with ENDF/B-IV[4] data. Taking advantage of the Monte Carlo results, the iron secondary gamma-ray production cross sections were revised to add the discrete gamma-rays for natural nuclides. Consecutively, the one-dimensional Sn code

DIAC[5] calculations were carried out with the revised cross sections and the 0.847 MeV peak was reproduced quit well as with ENDF/B－IV data.

2. MCNP calculations

The K&K neutron－induced secondary gamma－ray leakage spectra from iron sphere of 35 cm diameter was analyzed by the continuous energy Monte Carlo code with the NESX (Next Event Surface Crossing) estimation[6]. The NESX estimation was built in the particle scoring subroutine.

The configuration of the iron sphere experiment could be simplified as shown in Fig. 1. The ^{252}Cf source was set at the center of the sphere, and air of 100 cm thick was followed around the iron sphere in the Monte Carlo calculations. The ^{252}Cf source neutron and gamma－ray spectra are given in Table 1[8]. As summarized in Table 1, the ^{252}Cf source generates 5.44 times of source gamma－rays than neutrons. Accordingly, the magnitude of the contribution from source gamma rays must be multiplied by a factor of 5.44 and added to the neutron－induced secondary gamma rays at the calculation point. At the iron surface of the 35 cm diameter, the contribution of the source gamma ray was approximately within 20%, i.e, more than 80% was from the secondary gamma rays through the calculated gamma－ray energy range.

The MCNP calculated results are shown in Fig. 2. The FSDs are within 0.05(5%) in all the energy bins and the computation time was 15 min by the HITAC M880H computer at University of Tokyo.

At the glance, the large discrepancy is observed at the 0.847 MeV peak, which is caused by inelastic scattering with iron, between the results with JENDL－3 and ENDF/B－IV data. The peak is reproduced quite well with ENDF/B－IV data but is not reproduced completely and an incomprehensive gentle peak is appeared around 0.7 MeV. Except the peak, the MCNP calculations with JENDL－3 data agree quite well with the measured gamma－ray leakage spectrum and there is no essential difference between the JENDL－3 and the ENDF/B－IV results. Furthermore, the peak around 8 MeV, which is caused by thermal neutron capture of iron, is observed clearly by the calculations with those data.

Taking advantage of the MCNP calculations, the iron secondary gamma－ray production cross sections were revised to add the discrete gamma rays for natural nuclides. The new revised iron cross sections are proposed to JENDL－3.2 library. Consecutively, the analysis was carried out by the one－dimensional Sn code DIAC with the revised cross sections.

3. DIAC Calculations

The benchmark experiment was also analyzed by the one－dimensional Sn code DIAC with revised iron secondary gamma－ray production cross sections for JENDL－3.2. The

group constants for DIAC were produced by the RADHEAT－V4 code system[7] and gamma－ray cross sections were by the PHOTOX－V2 code. The source neutron spectrum of ^{252}Cf was given by the follow equation[8].

$$S(E) \sim \exp(-0.88E)\sinh\left(\sqrt{2E}\right) \qquad (1)$$

where, E is neutron energy in MeV.

The fission gamma－ray spectrum of ^{252}Cf was by Eq.(2)

$$\begin{aligned} \Gamma(E) &= 6.6 && (0.1 \le E < 0.6) \\ &= 20.2\exp(-1.78E) && (0.6 \le E < 1.5) \\ &= 7.2\exp(-1.09E) && (1.5 \le E < 10.5) \\ & \quad (photons\ /\ fission\ /\ MeV) \end{aligned} \qquad (2)$$

were, E is photon energy in MeV.

The ratio of photons/ neutrons (p/n) was set as 5.44 for the ^{252}Cf source.

In the DIAC calculations, the source region was within a radius of 0.88 cm of the iron spheres. The radii of the spheres were 12.5 cm and 17.5 cm. Air of 100 cm thick was followed the iron spheres. The special meshes were 0.5 cm width in it, and the material compositions were employed in Ref.(2).

The calculated results are summarized in Figs. 3 and 4. The comparison of secondary gamma－ray energy spectra with the experiments show that the 0.847 MeV peak, which is caused by inelastic scattering with iron, is well reproduced by the calculations with ENDF/B－IV as well as with the new cross sections for JENDL－3.2. The results for the inelastic scattering peak is improved distinctly by the new cross sections as compared with JENDL－3. However, in detail discussion, the results with the new cross sections have been remaining still some discrepancy with the experiments at the left side of the peak (around 0.7 MeV) : the ENDF/B－IV results indicate better agreement than those cross sections. Furthermore, the peak of thermal－neutron capture around 8 MeV is disappeared completely by the revised iron cross sections for JENDL－3.2.

4. Conclusions

As compared with the calculations to the measured leakage gamma－ray energy spectrum from the iron sphere of 35 cm diameter, the following remarks are obtained.

1. Except the 0.847 MeV peak, the calculations by the MCNP and the DIAC with both JENDL－3 and ENDF/B－IV data agree quite well with the measured gamma－ray leakage spectrum.

2. At the 0.847 MeV peak, the large discrepancy is observed between the results with

JENDL-3 and ENDF/B-IV by both the MCNP and the DIAC calculations. The peak cannot be reproduced, and an incomprehensive gentle peak is appeared around 0.7 MeV with JENDL-3 data. On the contrary, the peak is reproduced completely with ENDF/B-IV data.

3. The DIAC calculation with the new iron data, which is processed the revised cross sections by using the RADHEAT-V4 code system, the peak can be reproduced quite well as ENDF/B-IV data and the incomprehensive peak is disappeared.

4. However, the peak around 8 MeV, which is caused by thermal-neutron capture, is disappeared completely by using the revised iron cross sections.
The reason is under investigation on now.

References

1) K.Shibata, et al., JAERI 1319 (1990).
2) S.H. Jiang and H. Wherle, Nucl. Sci. Eng., 66, 354 (1978).
3) J.F. Briesmeister, ed., LA-7396-M, Rev. 2, (1986).
4) ENDF/B, Summary Documentation, BNL-NCS-17541 (ENDF-201), (2nd ed.), compiled by D. Garber, (1975).
5) N. Yamano, et al., J. Nucl. Sci. Tecnol., 16, 919 (1979).
6) K. Ueki, et al., J. Nucl. Sci. Technol., 30, 339 (1993).
7) N. Yamano, et al., JAERI 1316 (1989).
8) A.E. Profio, RADIATION SHIELDING AND DOSIMETRY, JOHN WILEY & SONS, 24～25 (1979).

Table 1 Neutron and photon intensity of ^{252}Cf.
$N(E) \sim \exp(-0.88E) \sinh (2.0E)^{1/2}$

Neutrons

Energy (MeV)	Neutrons/s-g
0.0 to 0.5	2.8×10^{11}
0.5 to 1.0	3.7×10^{11}
1.0 to 2.0	7.6×10^{11}
2.0 to 3.0	4.6×10^{11}
3.0 to 4.0	2.8×10^{11}
4.0 to 5.0	1.6×10^{11}
5.0 to 6.0	5.6×10^{10}
6.0 to 7.0	4.0×10^{10}
7.0 to 8.0	1.3×10^{10}
8.0 to 10.0	9.9×10^{9}
10.0 to 13.0	2.2×10^{9}
Total	2.43×10^{12}

γ Rays (photons/s-g)

Energy (MeV)	Prompt Fission	Fission Product	Total
0.0 to 0.5	3.3×10^{12}	1.3×10^{12}	4.6×10^{12}
0.5 to 1.0	1.7×10^{12}	4.0×10^{12}	5.7×10^{12}
1.0 to 1.5	7.7×10^{11}	9.1×10^{11}	1.7×10^{12}
1.5 to 2.0	4.2×10^{11}	3.5×10^{11}	7.7×10^{11}
2.0 to 2.5	2.2×10^{11}		
2.5 to 3.0	1.1×10^{11}		
3.0 to 3.5	5.6×10^{10}		
3.5 to 4.0	3.0×10^{10}		
4.0 to 4.5	1.7×10^{10}		
4.5 to 5.0	8.2×10^{9}		
5.0 to 5.5	4.9×10^{9}		
5.5 to 6.0	1.8×10^{9}		
6.0 to 6.5	1.0×10^{9}		
		Total	1.32×10^{13}

$n : \gamma = 2.431 \times 10^{12}$(n/s-g) : 1.322×10^{13}(p/s-g) = 1 : 5.44

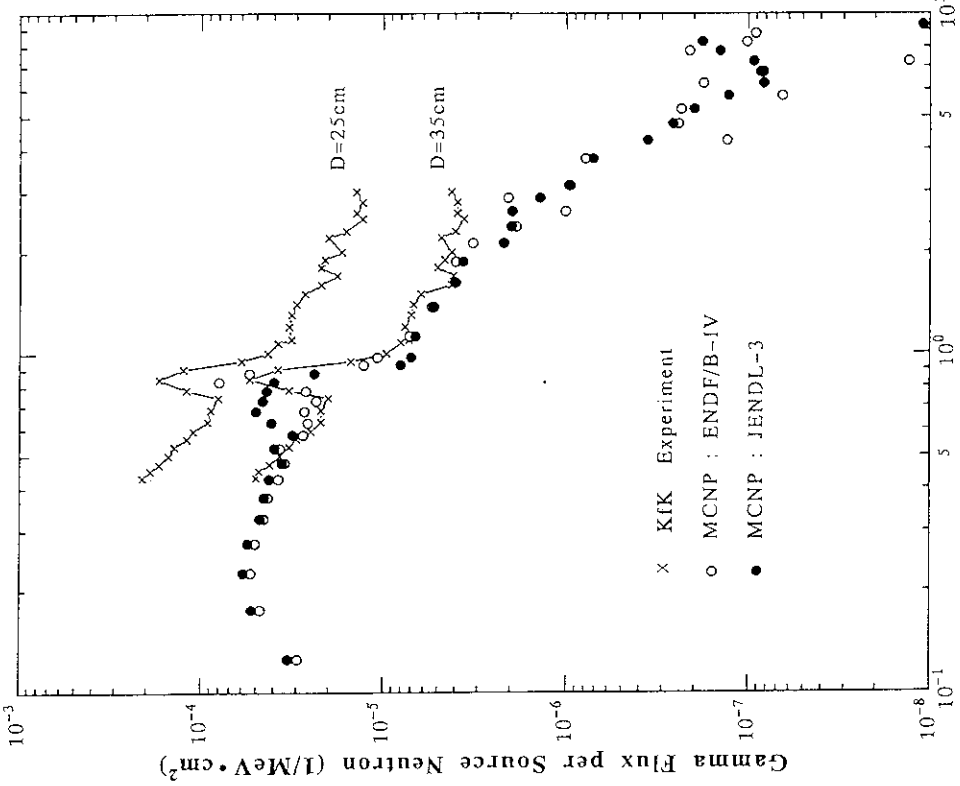

Fig. 2 Comparison of MCNP calculated and measured gamma-ray leakage spectra from iron spheres with a ^{252}Cf neutron source in the center (where D is the sphere diameter).

Fig. 1 Calculation model of the KfK iron secondary gamma-ray benchmark experiment.

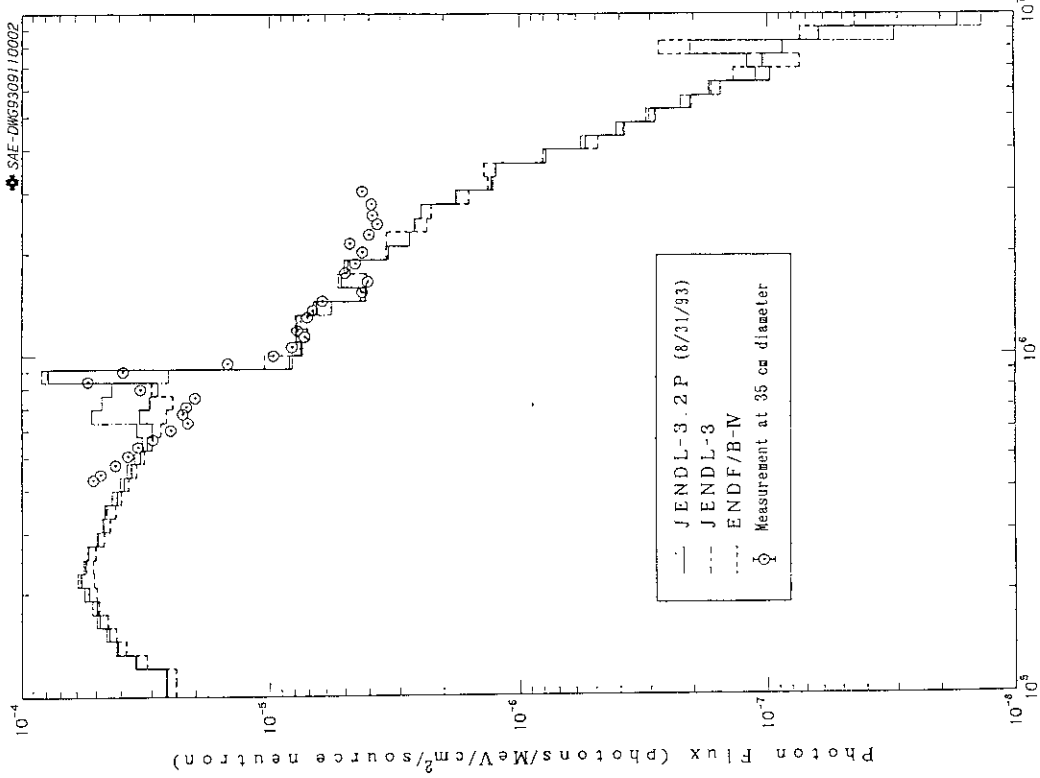

Fig. 4 Comparison of DIAC calculated and measured gamma-ray leakage spectra from iron shpere pf 35 cm diameter with a ^{252}Cf neutron source in the center.

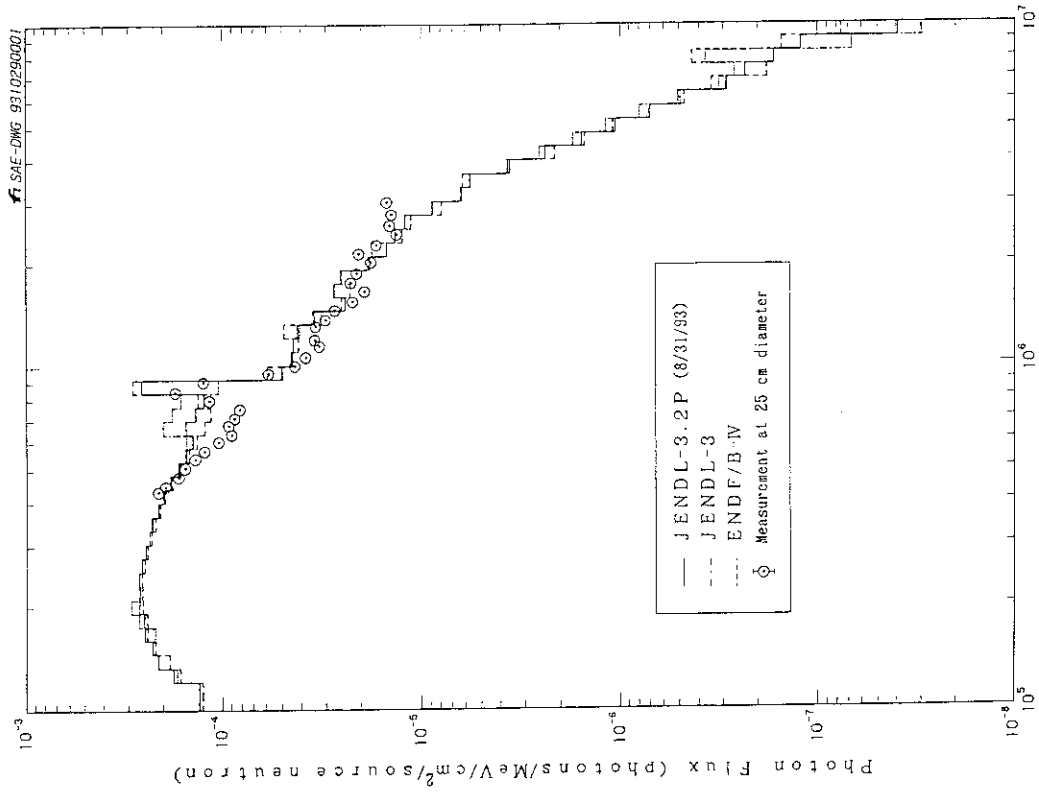

Fig. 3 Comparison of DIAC calculated and measured gamma-ray leakage spectra from iron sphere of 25 cm diameter with a ^{252}Cf neutron source in the center.

5.24 Techniques of Integral Experiment and Methods for Validation of Evaluated Nuclear Data Libraries for Secondary Gamma-ray Data under D-T Neutron Field

Fujio MAEKAWA and Yukio OYAMA

Japan Atomic Energy Research Institute
Tokai-mura, Naka-gun, Ibaraki-ken 319-11

In order to verify secondary gamma-ray data in evaluated nuclear data libraries, several experimental and analytical methods were proposed. Techniques of in-situ gamma-ray spectrum measurement for fusion neutronics experiments have been established by using a special scintillation detector and pulsed neutrons. An analytical method which can assist identification of error sources in data libraries is attempted. Another method is also proposed to experimentally examine energy valance of secondary gamma-ray data.

1. Introduction

Secondary gamma-ray data have been involved in the JENDL library since the version-3. Before using the data practically, it is strongly requested to examine validity of the data by means of integral experiments. However, there has not been many integral experiments about secondary gamma-ray under D-T neutron fields. Measurements of gamma-ray spectra which can be fed back to the nuclear data are conducted only at OKTAVIAN [1),(2)] and LLNL[3]. Both experiments are series of the pulse sphere program, and leakage gamma-ray spectra from spheres of various kinds of materials are measured. The experiments are suitable to examine secondary gamma-ray data associated with threshold reactions with D-T neutrons. But gamma-rays generated by neutron capture reactions with low energy neutrons are not included in the measured spectra because the time-of-flight technique is adopted to separate gamma-rays and neutrons.

To verify the secondary gamma-ray data for both threshold and radiative neutron capture reactions, integral experiments with thick assemblies measuring gamma-ray spectrum in the steady state are very helpful. Thus we have conducted such integral experiments for several materials, and techniques for measurement of gamma-ray spectrum in the experimental assemblies have been established.

2. Features of Benchmark Experiment at FNS

At the Fusion Neutronics Source (FNS) facility in Japan Atomic Energy Research Institute, a series of clean benchmark experiments [4)-(11)] have been performed using a D-T

neutron source and cylindrical experimental assemblies. For iron [11], copper [12], tungsten [11] and type 316 stainless steel [13],[14], gamma-ray spectrum and heating rate are measured in the assemblies along with neutron spectrum, reaction rate, and so on. Because gamma-rays are measured without any time cutoff, gamma-rays generated by various neutron reactions, not only threshold reactions with 14 MeV neutrons but also capture reactions with low energy neutrons, were measured. As for neutrons, low energy spectrum down to 3 keV for copper and tungsten and down to thermal energy for iron and SS316 are measured. Reaction rates for low energy neutrons, such as $^{197}Au(n,\gamma)$ and $^{235}U(n,f)$, are also measured. Hence examination of validation for secondary gamma-ray data, especially for gamma-rays from neutron capture reactions, is possible by analyses of the experiments.

Figure 1 illustrates the typical experimental arrangement. Some measurement points are set in the experimental assembly. The plural measurement points provide various fields of different neutron spectra. Neutrons of 14 MeV are dominant near the D-T source, and low energy neutrons are main in deeper positions. Thus it is possible to examine gamma-ray production data for various neutron fields, i.e., for various gamma-ray production reactions, changing the measurement points.

3. Technique of In-Situ Gamma-Ray Spectrum Measurement

Technique for the in-situ gamma-ray spectrum measurement has been recently established. The technique is based on the conventional method using liquid organic scintillator and unfolding technique. But special attentions are paid to fabrication of the gamma-ray spectrometer and rejection of decay gamma-rays.

At the first trial, an usual NE213 liquid organic scintillator in a Pyrex glass cell was used as the gamma-ray spectrometer. It was found that measured gamma-ray spectra was disturbed by gamma-rays which were generated by the following two neutron interaction of the detector itself.

$^{10}B(n,\alpha\gamma)^{7}Li$ ($E\gamma = 0.478$ MeV)
$^{1}H(n,\gamma)^{2}D$ ($E\gamma = 2.225$ MeV)

Boron-10 is contained in Pyrex glass (boric-silicic-glass) and hydrogen is in NE213. To eliminate those gamma-rays, a new detector replaced by deuterated organic scintillator (C_6D_6, BICRON BC-537) in a quartz glass cell has been introduced. The C_6D_6 scintillator has a similar capability [15] of the pulse shape discrimination to the NE213. Measured gamma-ray spectra by the old and new spectrometer are compared in Fig. 2. It is clearly seen that both parasitic gamma-rays by the old scintillator are eliminated in the new scintillator.

Gamma-rays can be roughly classified into two components; prompt and decay gamma-rays. The prompt gamma-ray is emitted immediately after the reaction occur. Decay gamma-ray

usually follows a disintegration of an activated nucleus. Since secondary gamma-ray data in nuclear data libraries does not correspond to decay gamma-rays but prompt ones, decay gamma-rays must be eliminated in gamma-ray measurement for the present purpose. But it is not easy because amount of decay gamma-rays depends on a history of irradiations of the experimental assembly. As illustrate in Fig. 3 (a), it is very difficult to know amount of decay gamma-rays with high accuracy during prompt gamma-ray measurement when it is measured before or after the measurement of prompt ones. To eliminate decay gamma-rays from prompt gamma-ray spectrum, a method with pulsed neutrons is adopted. The pulse width is about 1 ms and it corresponds to the slowing down time of 14 MeV neutrons down to thermal energy. Foreground and background gates are set up as shown in Fig. 3 (b). Prompt gamma-rays are observed only during the foreground gate. Only decay gamma-rays can be measured during the background gate. Trough the period of the gates, typically 1 ms, amount of decay gamma-rays can be regarded as constant because most of half lives of decay gamma-rays are more than a second. According to the method, amount of decay gamma-rays during a measurement of prompt gamma-ray spectrum can be subtracted exactly. Figure 4 shows typical pulse height spectra for the foreground and background gates.

4. Identification of Gamma-ray Production

In order to examine from which nucleus and reaction a gamma-ray was generated, Monte Carlo calculations were performed with the MCNP [16] transport code. Each generated gamma-ray was flagged in the calculations and classified in the calculated spectrum according to the kinds of nucleus and reaction.

Figures 5 and 6 show examples of calculated spectra in an experimental assembly of SS316. In the figures, not only usual spectra indicated as "Total" but also classified spectra for each nuclei and reaction are given. In the spectra at a shallower position of the assembly, most part of the spectrum is formed by non-elastic reactions (MT=3) as shown in Fig. 5. A difference of peaks around 0.85 MeV between experiment and calculation implies that the data for iron is not adequate at that peak. A peak around 1.4 MeV, which is formed by gamma-rays of non-elastic reactions of iron, chromium and nickel, seems to be good. The spectra at a deeper position of the assembly is nearly formed by only neutron capture reaction (MT=102) as shown in Fig. 6. Molybdenum is contained in the SS316 only 1.2 % in the atomic density. However, since it is remarkable that the contribution of molybdenum to the spectrum below 5 MeV is largest among consisting materials, careful attentions should be paid in evaluations of molybdenum though it is not the main structural material.

Owing to this method, calculated spectra can be closely connected to the original evaluated library without sensitivity analysis, and feedback to the evaluated data have become easy.

5. Experimental Examination of Energy Valance for Secondary Gamma-Ray Data

All errors in neutron transport, gamma-ray production and gamma-ray transport cross sections are accumulated in a calculated gamma-ray spectrum as illustrated in Fig. 7. Uncertainty of the gamma-ray transport cross section such as Compton scattering cross section is assumed to be small. But accuracy of neutron transport cross section is not always satisfactory. Accuracy of gamma-ray calculation, especially for gamma-rays associated with neutron capture reactions with multiply scattered low energy neutrons, considerably affected by accuracy of neutron transport cross sections. From a viewpoint of engineering, verification of gamma-ray production cross sections can be replaced by examination of energy valance of the reactions. Because most of design parameters relevant to gamma-rays, such as nuclear heating, are connected with deposited energy to a medium, and the deposited energy has a strong relation with the released energy by neutron reactions. Therefore a quantity in proportion to the released energy by one gamma-ray production reaction should be examined experimentally.

In a case of SS316, for example, a ratio of gamma-ray heating rate to fission rate of ^{235}U can be an good index of the gamma-released energy arisen by one neutron capture reaction at the measurement points where low energy neutrons are dominant instead of 14 MeV neutrons. Because the fission rate of ^{235}U is in proportion to neutron capture reaction rate of SS316 within ± 3 % and the following equation stands up.

$$\frac{\text{Released } \gamma\text{-Ray Energy}}{\text{by one } (n,\gamma) \text{ Reaction}} \propto \frac{\gamma\text{-Ray Heating Rate}}{\text{SS316}(n,\gamma) \text{ Rate}} \propto \frac{\gamma\text{-Ray Heating Rate}}{^{235}U(n,f) \text{ Rate}}$$

Since the index of energy valance, the ratio of the right side of the equation, can be determined by both experiment and analysis, experimental verification of energy valance in gamma-ray production data of the neutron capture reaction is possible for SS316.

Figure 8 shows an example of examination of energy valance for SS316 experiment in the calculated to measured value ratios (C/Es) for gamma-ray heating rate, fission rate of ^{235}U and the index of energy valance. Calculations were performed with the continuous energy Monte Carlo code MCNP and two-dimensional Sn code DOT3.5 [17] using the FSXLIB-J3 [18] library for MCNP and two different libraries for DOT; FUSION-J3 [19] without self-shielding correction of cross section and JSSTDL [20] with the correction, respectively. All the libraries were retrieved from JENDL-3.1.

Since calculations with MCNP and DOT+JSSTDL agree with the experiments for all the C/Es, both neutron cross sections and secondary gamma-ray production cross sections seems to be good in the libraries. As for the DOT+FUSION-J3 calculation, both the gamma-ray heating rate and the fission rate of ^{235}U disagree with the experiments. According to the disagreement only of gamma-ray heating rate, it can not be concluded that the secondary gamma-ray data in FUSION-J3 is not appropriate, because low energy neutrons, which

generate capture gamma-rays by nuclei of SS316, are not also in good agreement between the experiment and the calculation. On the other hand, according to the index of energy valance, it is clearly seen that the released gamma-ray energy is calculated about 40 % larger when FUSION-J3 is used for DOT due to neglect of the self-shielding correction.

6. Summary

Through the present studies, several experimental and analytical methodologies were attempted to verify secondary gamma-ray data in evaluated nuclear data libraries. These methodologies were very helpful to improve the secondary gamma-ray data so far.

References

1) YAMAMOTO J., KANAOKA T., MURATA I., TAKAHASHI A. AND SUMITA K.: "Gamma-Ray Emission Spectra from Spheres with 14 MeV Neutron Source," Proc. of the 1988 Seminar on Nucl. Data, JAERI-M 89-026, pp. 232-242 (1989).
2) YAMAMOTO J.: "Integral experiment on Gamma-Ray Production at OKTAVIAN," Proc. Second Specialists' Meeting on Nucl. Data for Fusion Reactors, JAERI-M 91-062, pp. 118-125 (1991).
3) GOLDBERG E., et al.: Nucl. Sci. Eng., **105**, pp. 319-340 (1990).
4) MAEKAWA H., et al.: "Fusion Blanket Benchmark Experiments on a 60 cm-thick Lithium-Oxide Cylindrical Assembly," JAERI-M 86-182 (1986).
5) MAEKAWA H., et al.: Fusion Technol. **19**, pp. 1949-1954 (1991).
6) MAEKAWA H., et al.: "Benchmark Experiments on a 60 cm-thick Graphite Cylindrical Assembly," JAERI-M 88-034 (1988).
7) OISHI K., IKEDA Y., MAEKAWA H. AND NAKAMURA T.: Nucl. Sci. Eng., **103**, pp. 46-58 (1989).
8) OISHI K., IKEDA Y., KONNO C. AND NAKAMURA T.: "Measurement and Analysis of Neutron Spectra in a Large Cylindrical Iron Assembly Irradiated by 14 MeV Neutrons," Proc. 7th Int. Conf. on Radiation Shielding, Bournemouth, pp. 331-340 (1988).
9) KONNO C., et al.: Fusion Eng. Des., **18**, pp. 297-303 (1991).
10) IKEDA Y., OISHI K., KONNO C. AND NAKAMURA T.: ibid., pp. 309-315 (1991).
11) OYAMA Y.: "Experiments of Nuclear Heating by Gamma-Rays at FNS," JAERI-M 91-062, pp. 106-117 (1991).
12) MAEKAWA F., et al.: to be published in a JAERI-M report.
13) KONNO C., et al.: Fusion Technol. **21**, pp. 2169-2173 (1992).
14) MAEKAWA F., et al.: Fusion Technol. **21**, pp. 2107-2111 (1992).
15) BOVET E, BOSCHUNG P. AND ROSSEL J.: Nucl. Instrum. Meth., **101**, 315-319 (1972).

16) BRIESMEISTER J. F. (editor): "MCNP - A General Monte Carlo Code for Neutron and Photon Transport, Version 3B," RSIC/CCC-200 (1988).
17) RHOADES W. A., MYNATT W. A.: "The DOT III Tow-Dimensional Discrete Ordinates Transport Code," ORNL/TM-4280 (1973).
18) KOSAKO K., et aL, "FSXLIB-J3: MCNP Continuous Energy Cross Section Library Based on JENDL-3, " JAERI-M 91-187 (1991, in Japanese).
19) MAKI K., et al.: "Nuclear Group Constant Set FUSION-J3 for Fusion Reactor Nuclear Calculations based on JENDL-3," JAERI-M 91-072 (1991, in Japanese).
20) HASEGAWA A.: "Development of a Common Nuclear Group Constants Library System: JSSTDL-295n-104γ Based on JENDL-3 Nuclear Data Library," Proc. Int. Conf. on Nucl. Data, Jülich, Germany, pp. 232-234 (1991).

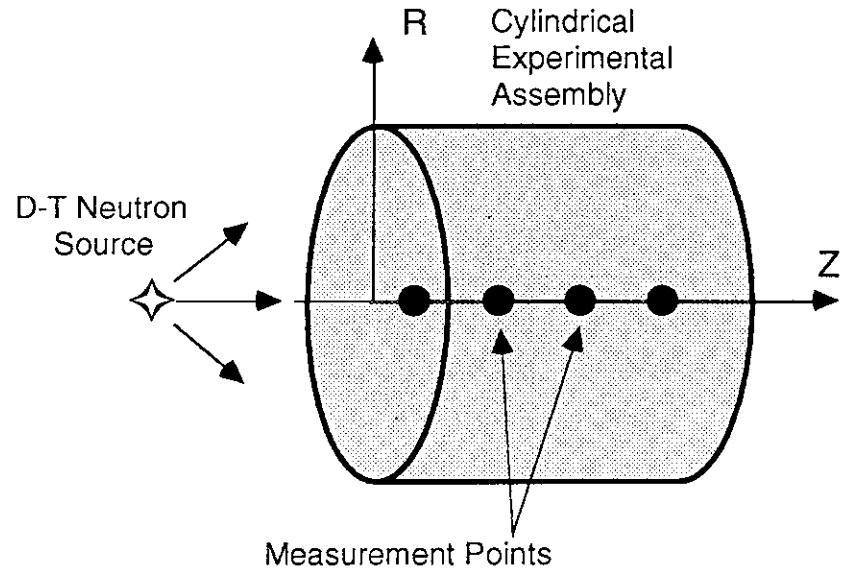

Fig. 1 Configuration of FNS clean benchmark experiments.

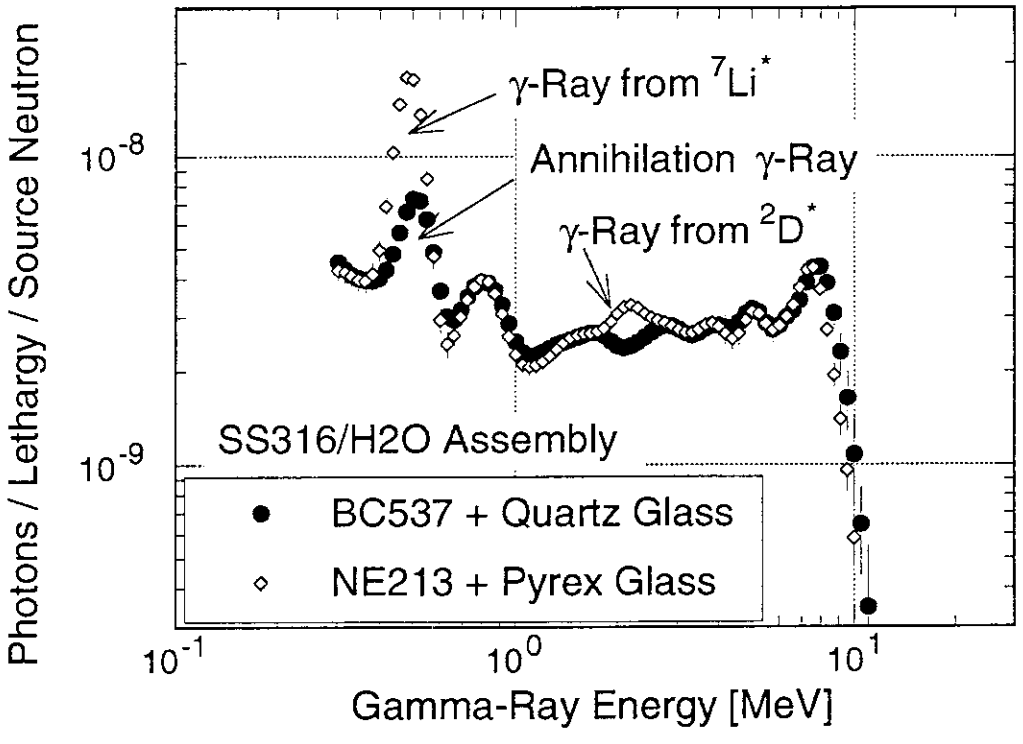

Fig. 2 Improvement of gamma-ray spectrum measurement by using a C_6D_6 (BC537) scintillator in a quartz glass cell.

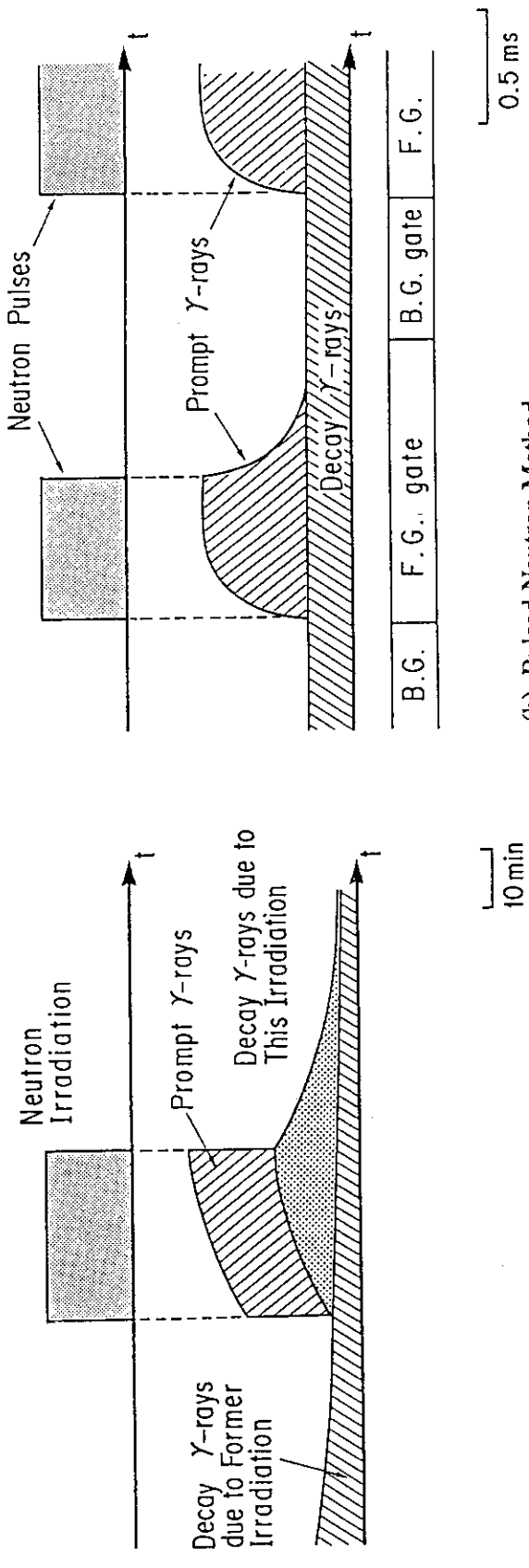

Fig. 3 Explanation for rejection of decay gamma-rays. Amount of decay gamma-rays can not be determined accurately with (a) usual method but with (b) pulsed neutron method.

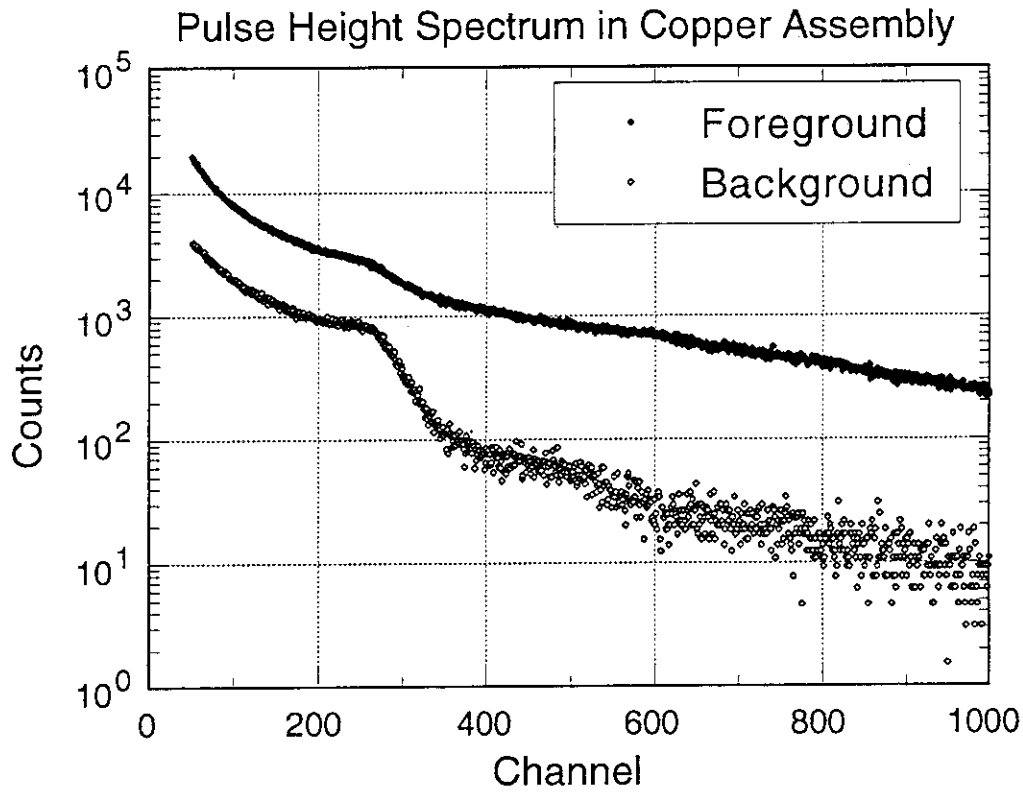

Fig. 4 Typical pulse height spectra for the foreground and the background gates of pulsed neutron method.

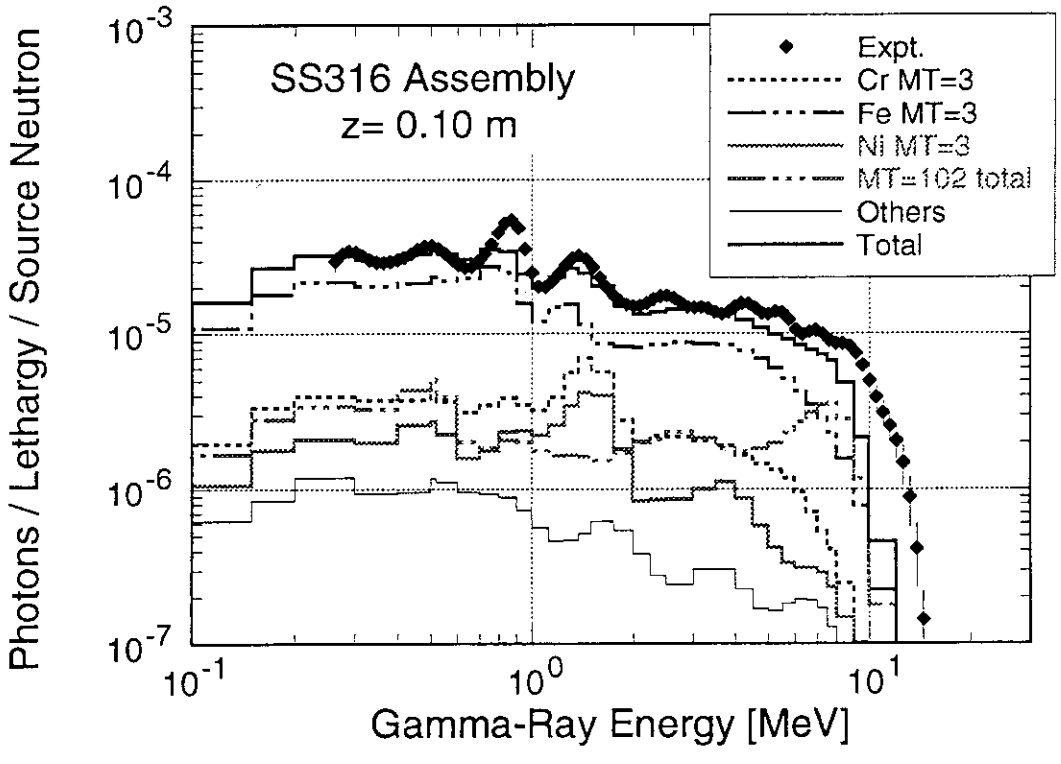

Fig. 5 Measured and calculated gamma-ray spectra at 0.10 m depth in a SS316 assembly. Calculated spectra were classified according to the kinds of nucleus or reaction.

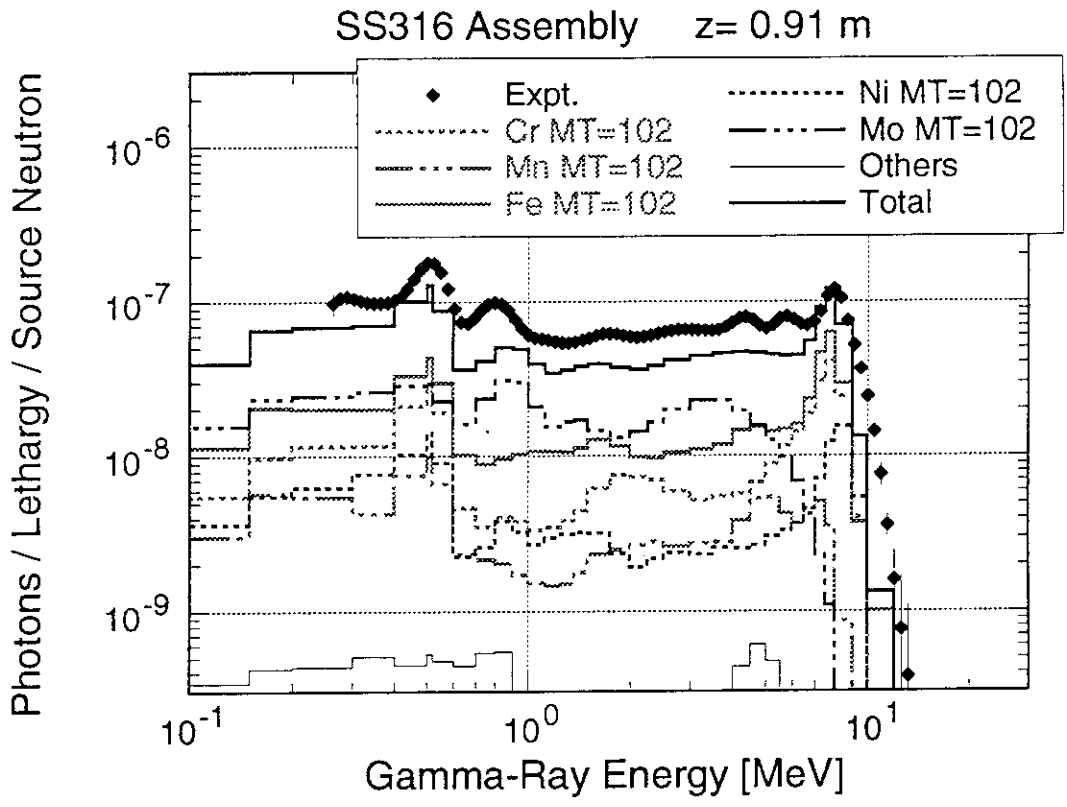

Fig. 6 Measured and calculated gamma-ray spectra at 0.91 m depth in a SS316 assembly. Calculated spectra were classified according to the kinds of nucleus or reaction.

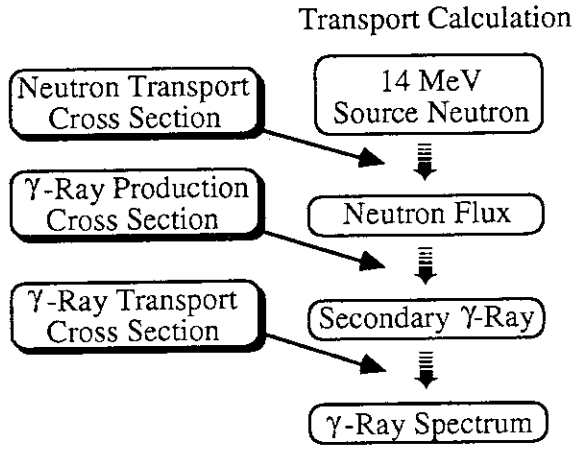

Fig. 7 Flow of transport calculation and the associated data bases.

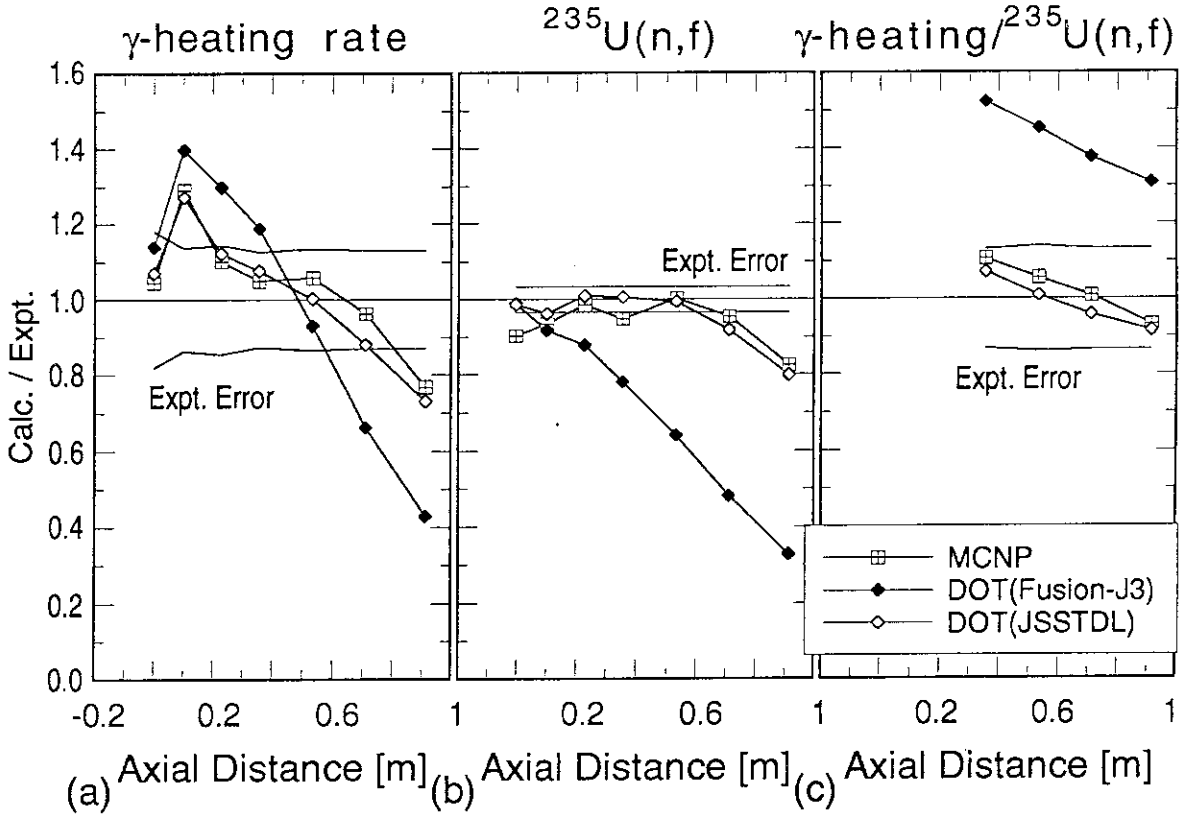

Fig. 8 Measured to calculated value ratios for gamma-ray heating, $^{235}U(n,f)$ and the ratio of gamma-ray heating to $^{235}U(n,f)$ rate.

5.25 An Index Database of Charged–particle Nuclear Reaction Data

Masaki CHIBA*
Faculty of Social Information, Sapporo Gakuin University

and

Kiyoshi KATŌ*
Deparment of Physics, Hokkaido University

Abstract:

We give a brief explanation of a retrieval system for the index information of Charged-Particle Nuclear Reaction Data, which has been installed in Hokkaido University Computing Center. For the installation of these data, the ORION Information Retrieval System has been used. The main purpose of the new system is to open a way for researchers to get benefits from utilizing the Charged-Particle Reaction Data in NRDF and EXFOR systems.

1. Introduction

We have made a database system of Charged-Particle Nuclear Reaction Data, which is called NRDF, and compiled many data so far. Those data have also been translated into the international data exchange format, called EXFOR. Therefore, we can now utilize the charge-particle nuclear reaction data in NRDF and EXFOR.

The retrieval system of NRDF data has been already available in several computer systems. However, we have no convenient systems for EXFOR data in Japan. In order to allow many researchers to use those data, we have tried to install them in the National Center for Science Information System (NACSIS). The contents of

*Japan Charged-Particle Nuclear Reaction Data group

NRDF and EXFOR databases consist of the data of index information and numerical results. However, in the present situation, it is not supported to install numerical data in NACSIS.

The present EXFOR data which we have received from IAEA reach to an amount 30 MB including about 1,500 entries. To take our responsibility for EXFOR data in Japan, we constructed a new database of index information of EXFOR data. This report is a brief explanation of the index information retrieval system.

By using this system, we can find the EXFOR entries or subentries of the desired data. This system has been constructed and available in Hokkaido University Computing Center. We have a plan to install the system in NACSIS-IR(Information Retrieval Service of the National Center for Science Information System).

2. Content of the Database

2.1 Record definitions

The content of the database consists of some index information of Charged-Particle Nuclear Reaction Data storaged in the EXFOR Library. We utilized the programe XNISPR [1] to prepare index information records. Information items of the record are shown in Table-1, which are same as in of XNISPR. A program called "input processor" was developed in order to load the index data records to the ORION database management system. The input processor reads the data which are made by the XNISPIR and transforms them so as to match data definitions in ORION.

Table-1 shows all the basic field items of a index data record. Table-2 shows compound fields defined for a set of fields of Table-1. They can be used as a parameter of the ORION commands to recieve the result of the search.

2.2 Indexings of a filed

Table-1 also showes the fields for which inverted indexes are made in the ORION Database Management System. Each no blank value of the "Index-Field & its Prefix" column in the Table-1 designates that inverted index is made for the field. Inverted indexing is made either for the whole value of the field or for the part of it. The latter is called partial indexing. For a given field, more than one inverted indexing may be made. This case is called multi indexing. Table-3 shows the fields

for which partial indexing or multi indexing are made.

3. Searching the Database

When searching the Index Database of Nuclear Reaction Data, we have to refer Tabel-1, Tabel-2 or Table-3, and consult the ORION online user guide[3]. In the following, we briefly explain how to search the Database. Fig.-1 shows an example of retrieval operation.

3.1 Beginning and ending online searching

To begin online searching of the Database, we have to key-in a starting command, "CPND" in HOkkaido University Computing Center. After keying "CPND" at TSS session, we can enter an ORION retrieval session. Then we can submit any ORION commands to search CPND entries or subentries compiled in EXFOR.

"QUIT" command terminates ORION session and returns to TSS session.

3.2 Index search facilities

Index search is performed by "FIND" comman. The "FIND" command provides several search facilitites using inverted indexes. We specify a search term or a conbination of search terms with logical operators as an option of the command. If the command is performed, a set of records containing the term(s) is made and a set number is assighned to the result.

At any time during a search, we can choose to display the relevant part of the inverted index terms by keying "LOOK" command specifying the term or fragment of interest.

(a) Index term search:

When a single word or term is specified with the field prefix on "FIND" command option, the word or term is matched to the inverted index relevant to the prefix.

An example of specifying index search option :

```
TGT:082
```

(b) Range search :

The search bounded by two terms is performed, if an option of "FIND" command is specified as follows;

```
index-term1/index-term2
```

(c) Left-hand match search or right-hand match search :

The search beginning with stem or ending with stem is performed, if a search term truncated as follows;

prifix:stem*	or	prifix:*stem

Here, "stem" is a character string which is a part of some word or term, and the asterisk * designats a wild card.

3.4 Display of retrieval results

We can see the results of retrieval by "DISPLAY" command. This command has optins such as a record set number, field names or a number of records to be displayed. We can also choose any items among the names listed in the Field Identifier of Table-1 or in the Compound Field Name of Table-2 for the "DISPLY" command.

4. Concluding remarks

The Database currently contains the index data for the Charged-Particle Nuclear Reaction Data compiled only in the EXFOR Library. We will also add index data for those in the NRDF Library to the Database. Then the reserchers will get benefit of the Database through the National Center for Science Information System and Hokkaido University Computing Center in the near future.

Acknowledgement

This work was carried out under the support for database development of the Hokkaido University Computing Center.

Reference:

[1] P.M. Attree, P.M. Smith:SYSTEM SPECIFICATION for the NDS DATA INDEX SYSTEM, 1979, IAEA-NDS-6.

[2] HITAC Program product VOS3
Information Retrieval System ORION Database Administrator's Guide

[3] HITAC Program Product VOS3 Information Retrieval System
ORION Online-User's Guide

Table 1 Database record definitions

Field Identifier	Field Label	Indexed-Field & its Prefix	content
ACN	ACCESSION-NO	ACN:	EXFOR Accession Number
PNT	POINTER		
LNM	LIB-NAME		
LFM	LIB-FORMAT	LIB:	
PSN	POSITION		
CNE	CONECTOR		
KYF	KEYWORD-FLAG		
LOC	LOCATION		
RTYP	RCT-TYPE		Reaction Type
RCD	RCT-CODE		Reaction Code
TGT	TARGET	TGT:	Charge & Mass Number of Target
PRJ	PROJECTILE	PRJ:	Projectile
PRCSP	PROCESS-PRTS	PRCSP:	Process Parts
PRCS	PROCESS		Reaction process
PRDUCT	RCT-PRODUCT		Reaction Product
PRDUCTS	PRODUCT-STATE		Product State
BRNCH	BRANCH		Branch
PRM	PARAMETER	PRM:	Parameter
PRTCL	PRTCL-CONSDRD		Particle Considered
MOD	MODIFIER		Modifier
DTYP	DATA-TYPE	DTYP:	Data type
MINF	EN-FLAG		Flag of Incident Energy
EMIN	EN-MIN		Minimum Value of Incident Energy
EMAXF	EN-FLAG		Flag of Incident Energy
EMAX	EN-MAX		Maximum Value of Incident Energy
YR	EXP-YEAR	YR:	Year of Experiment Performed
IN	INSTITUTE	IN:	Institute Experiment Performed
AU	AUTHOR	AU:	Name of First Author
RE	REFERENCE	RE:	
DTP	DATA-LINES		Data Points in Data-Table
VDT	VERSION-DATE	VDT:	
EDT	F-ENT-DATE	EDT:	File Entry Date
CHG	CHANGE-FLAG	CHG:	
ST	STATUS	ST:	
OAC	ORION-ACC		Record Id Number in ORION

Table 2 Compound field

Compound Field Name	
EN	(MINF, EMIN, MAXF, EMAX)
LIB	(LNF, LFM)
RCT	(TGT, PRJ, PRCSP, PRCS, PRDUCT, PRDUCTS, BRANCHPRM, PRTCL, MOD, DTYP)

Table 3 Partial indexing and multi-valued indexing field

Field Name	
ACN	Partial(1:5)
TGT	Partial(1:6), Partial(1:3)
PRCSP	Multi
IN	Multi
ST	Multi

Fig. 1 Example of retrieval

```
READY
CPND
 ORION  05-03
 ENTER YOUR REQUEST
    1/ FIND PRJ:P AND TGT:016
 *   13326     1/  PRJ:P
 *     128     2/  TGT:016
 *      45     3/  PRJ:P AND TGT:016
    4/ LOOK TGT:016*

   .ITEMS.     TERMS
 A      128  TGT:016
 B       20  TGT:016000
 C       92  TGT:016032
 D        6  TGT:016033
 E       10  TGT:016034
 END OF TERMS WITH YOUR STEM
 PICK LETTERS TO COMBINE
    4/ D
       6 ITEMS SAVED AS SET 4
 CONTINUE PICKS OR REQUESTS
    5/ FIND 3 AND 4
 *       6     5/  3 AND 4
    6/ DISPLAY =5 ACN RCD EMIN EMAX FOR ALL

 ITEM 1
   10.  ACCESSION-NO C0252023
  110.  RCT-CODE     16-S-33(P,X)9-F-18,,SIG
  260.  EN-MIN        0.30000E+09 EV
  280.  EN-MAX        0.40000E+09 EV

 ITEM 2
   10.  ACCESSION-NO C0252024
  110.  RCT-CODE     16-S-33(P,X)11-NA-22,,SIG
                 .
                 .
                 .
 ITEM 6
   10.  ACCESSION-NO C0252025
  110.  RCT-CODE     16-S-33(P,X)11-NA-24,,SIG
  260.  EN-MIN        0.30000E+09 EV
  280.  EN-MAX        0.40000E+09 EV

    6/ QUIT
 GOODBYE
READY
```

* Keyined strings are underlined

5.26 Sensitivities of Nuclear Data to the Nuclear Equilibrium State

Hiroki Nakamura and Hiroshi Sekimoto

Research Laboratory for Nuclear Reactors,
Tokyo Institute of Technology,
O-okayama, Meguro-ku, Tokyo 152, Japan

As a part of our study on the future society in nuclear equilibrium, sensitivity coefficients of one-group constants were calculated to the infinite multiplication factor and to the nuclide number densities in the reactor using perturbation method. In this calculation four types of reactor which have typical neutron spectrum were considered.

I. Introduction

Our society is still growing but should be in an equilibrium state in the future from the finiteness of the earth. In the equilibrium society the total consumption rate of energy will be a fixed value, and when nuclear power is used to sustain such society for a long period producing constant energy, the nuclear system will also be in a certain equilibrium state. We have named this state the "nuclear equilibrium", and been studying the nuclear energy system in the future society in such state, which can be considered as a goal of the present nuclear system.

Our study is just on the initial stage of this long-life and extensive work and we treat only four types of reactors distinguished by typical neutron spectrum shown in **Figure 1** to know the general information about the nuclear system in the nuclear equilibrium state.

In the previous works, one-group constants were generated for each reference spectrum with JENDL-3. Using these constants, we have estimated the criticality of reactor, the amounts and toxicities of radioactive wastes for various systems. From these analyses, we have obtained some general characteristics of the nuclear system in the future equilibrium society.

But these results contain uncertainties originated from the uncertainties included in both nuclear data and process to get one-group constants. In the present work, sensitivities of one-group constants to the criticality of reactor and nuclide number density were calculated using perturbation method.

II. Nuclear system in the nuclear equilibrium sate

From the point of view of radioactive wastes accumulation, we employ the closed cycle

system shown in **Figure 2**. In this model, natural uranium or thorium is supplied into the system in continuous process. All of the actinides are recycled into the reactor. Other heavy-isotopes and fission products are discharged to the repository and cooled down there until disposal.

Using this model, the equilibrium number density of i-th isotope in the reactor, n_i ,is represented by the following material balance equation :

$$\frac{dn_i}{dt} = -\left(\lambda_i + \sigma_{a,i}\phi + \lambda_d\right)n_i + \sum_j n_j\lambda_{j\to i} + \sum_k n_k\sigma_{k\to i}\phi + s_i = 0 \quad ,$$

where

λ_i : Decay constants of i-th isotope

$\sigma_{a,i}$: Absorption cross section of i-th isotope

ϕ : Neutron flux

λ_d : Discharge constant

$\lambda_{j\to i}$: Decay constants of j-th isotope to produce i-th isotope

$\sigma_{k\to i}$: Production cross section of i-th isotope from k-th isotope.

For heavy nuclide, s_i is supply rate from external source. For fission products, s_i is production rate from fission and written as follows

$$s_i = \sum_l^{HM} \gamma_{l\to i} n_l \sigma_{f,l}\phi \quad ,$$

where

$\gamma_{l\to i}$: Fission yield of i-th isotope from l-th isotope

$\sigma_{f,l}$: Fission cross section of l-th isotope.

These equations can be written in the matrix form

$$\mathbf{Mn} = \mathbf{s} \quad , \qquad \cdots(1)$$

where

M : Transfer matrix of nuclides in the reactor

n : Nuclide density vector

s : External source vector.

Number density in the nuclear equilibrium state can be obtained from this equation and using **n**

the infinite multiplication factor, k_∞ ,is written as

$$k_\infty = \frac{\nu\Sigma_f}{\Sigma_a} = \frac{(\nu\sigma_f\ ,\ \mathbf{n})}{(\sigma_a\ ,\ \mathbf{n})} \quad ,$$

where (,) means inner product and

σ_a : Absorption cross section vector

$\nu\sigma_f$: ν-value and fission cross section vector

III. Sensitivity Coefficient

Sensitivity coefficient of input parameter α (cross sections and another parameters) to the response R is defined as

$$S = \frac{\partial R/R}{\partial\alpha/\alpha} \approx \frac{\Delta R/R}{\Delta\alpha/\alpha} \quad .$$

This can be obtained by calculating ΔR with changed input parameter α' (= $\alpha + \Delta\alpha$). But we treat about 1,500 nuclides in our study and it is difficult to examine all of the input parameters using this method. In this work, perturbation method is employed to reduce the computer time.

III.a Sensitivity coefficient to the infinite multiplication factor

Sensitivity coefficient of input parameter α to the infinite multiplication factor is written as

$$S_{k_\infty} = \frac{\partial k_\infty / k_\infty}{\partial\alpha/\alpha} = \frac{(\sigma_a\ ,\ \mathbf{n})\frac{\partial}{\partial\alpha}(\nu\sigma_f\ ,\ \mathbf{n}) - (\nu\sigma_f\ ,\ \mathbf{n})\frac{\partial}{\partial\alpha}(\sigma_a\ ,\ \mathbf{n})}{(\sigma_a\ ,\ \mathbf{n})^2} \cdot \frac{(\sigma_a\ ,\ \mathbf{n})}{(\nu\sigma_f\ ,\ \mathbf{n})} \cdot \alpha$$

$$= \left[\left(\frac{1}{(\nu\sigma_f\ ,\ \mathbf{n})} \frac{\partial\nu\sigma_f}{\partial\alpha} - \frac{1}{(\sigma_a\ ,\ \mathbf{n})} \frac{\partial\sigma_a}{\partial\alpha}\ ,\ \mathbf{n} \right) \right.$$

$$\left. + \left(\frac{\nu\sigma_f}{(\nu\sigma_f\ ,\ \mathbf{n})} - \frac{\sigma_a}{(\sigma_a\ ,\ \mathbf{n})}\ ,\ \frac{\partial\mathbf{n}}{\partial\alpha} \right) \right] \cdot \alpha \quad . \qquad \cdots(2)$$

When the adjoint equation to eq. (1) is written as

$$\mathbf{M}^* \mathbf{n}^* = \mathbf{s}^* \quad , \qquad \cdots(3)$$

taking $\mathbf{s}^*$ as

$$\mathbf{s}^* = \frac{\nu\sigma_f}{(\nu\sigma_f\ ,\ \mathbf{n})} - \frac{\sigma_a}{(\sigma_a\ ,\ \mathbf{n})} \quad ,$$

eq. (2) can be rewritten as

$$S_{k_\infty} = \left[\frac{1}{(\nu\sigma_f\ ,\ \mathbf{n})}\left(\frac{\partial\nu\sigma_f}{\partial\alpha}\ ,\ \mathbf{n}\right) - \frac{1}{(\sigma_a\ ,\ \mathbf{n})}\left(\frac{\partial\sigma_a}{\partial\alpha}\ ,\ \mathbf{n}\right) - \left(\mathbf{n}^*\ ,\ \frac{\partial\mathbf{M}}{\partial\alpha}\mathbf{n}\right)\right]\cdot\alpha$$

III.b Sensitivity coefficient to the number density in the reactor

Using the unit vector **h** whose i-th element is 1, the number density of i-th isotope can be written as

$$n_i = (\mathbf{h}\ ,\ \mathbf{n}) \quad .$$

Then, sensitivity coefficient to the number density is written as

$$S_{n_i} = \frac{\partial n_i / n_i}{\partial\alpha/\alpha} = \left(\mathbf{h}\ ,\ \frac{\partial\mathbf{n}}{\partial\alpha}\right)\cdot\frac{\alpha}{n_i} \quad .$$

Taking vector **h** as $\mathbf{s}^*$ of eq. (3), this equation becomes

$$S_{n_i} = \left(\mathbf{s}^*\ ,\ \frac{\partial\mathbf{n}}{\partial\alpha}\right)\cdot\frac{\alpha}{n_i} = \left(\mathbf{M}^*\mathbf{n}^*\ ,\ \frac{\partial\mathbf{n}}{\partial\alpha}\right)\cdot\frac{\alpha}{n_i} = -\left(\mathbf{n}^*\ ,\ \frac{\partial\mathbf{M}}{\partial\alpha}\mathbf{n}\right)\cdot\frac{\alpha}{n_i} \quad .$$

IV. Calculated results

Calculations were performed for simple one-reactor-type and one-fuel-element systems. Their reactor design parameters and examined input parameters are shown in **Table 1** and **Table 2**, respectively. Generally sensitivity of (n,γ*) , (n,2n*) , (n,3n) and (n,p) , (n,α) cross sections are very small and negligible. **Fig. 3** shows absolute values of sensitivities to the infinite multiplication factor for uranium fueled soft spectrum fast reactor system. ^{239}Pu, ^{241}Pu, ^{238}U and ^{240}Pu are especially sensitive. Nu-value has large sensitivity. Some fission products can not be ignored. **Figs. 4 - 8** show absolute values of sensitivities to the number densities of long-life fission products ^{99}Tc, ^{129}I and ^{239}Pu, ^{241}Am, ^{244}Cm, which have large and long time contribution to the toxicity of spent fuel also for uranium fueled soft spectrum fast reactor system (the symbol ∇ in the figures indicates negative value). For fission products, fission yields are most important.

References

1. H. Sekimoto and N. Takagi, "Preliminary Study on Future Society in Nuclear Quasi-Equilibrium," J. Nucl. Sci. Technol., 28, 941(1991)

2. N. Takagi and H. Sekimoto, "Feasibility of Fast Fission System Confining Long-Lived Nuclides," J. Nucl. Sci. Technol., 29, 276(1992)

3. N. Takagi, Doctoral thesis, Tokyo Institute of Technology, 1992

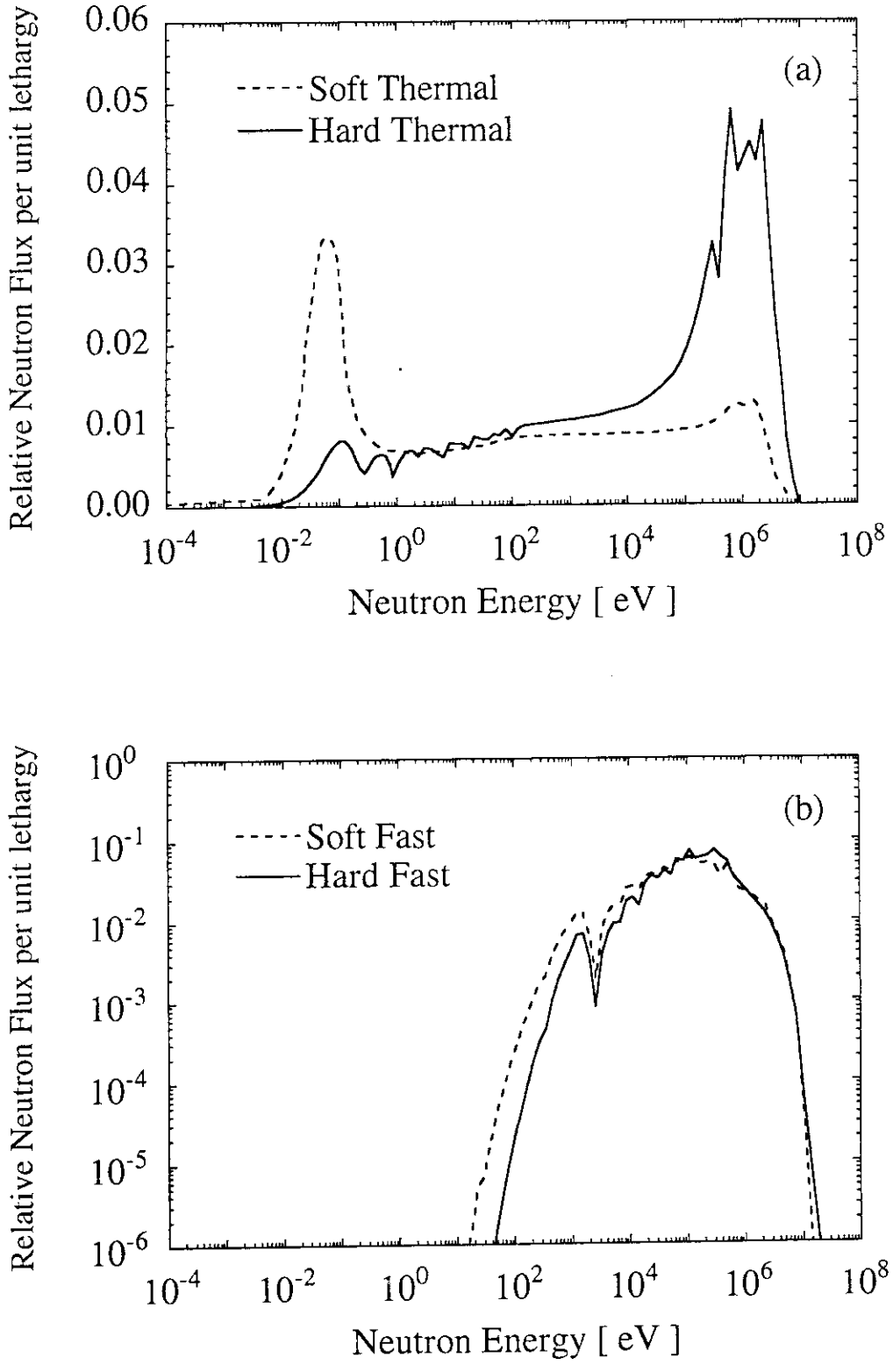

Fig. 1 Neutron spectra for (a) two types of thermal reactors and (b) two types of fast reactors employed referenced in the present study.

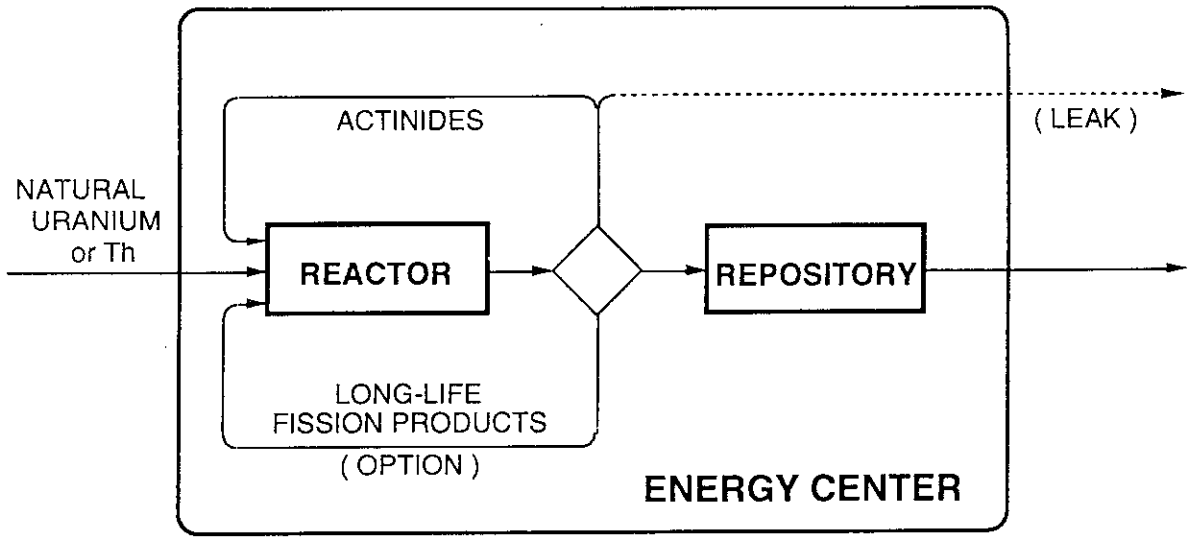

Fig. 2 Equilibrium nuclear fuel cycle in the future. The natural uranium or thorium is charged to the reactor in the energy center. The whole actinides produced in the reactor are incinerated in the reactor. The whole stable fission products produced in the reactor are taken out from the energy center. The short-life fission products and ^{90}Sr and ^{137}Cs and ^{151}Sm are also taken out from the energy center after decaying out. The treatment for each long-life fission product, ^{79}Se, ^{126}Sn, ^{99}Tc, ^{93}Zr, ^{135}Cs, ^{107}Pd and ^{129}I, is optional whether to be incinerated in the reactor with/without isotope separation or simply to be taken out from the energy center.

Table 1 Reactor design parameters

	Thermal reactors	Fast Reactors
Thermal power output	3 GWt	3 GWt
Power density	50 W/cc	300 W/cc
Discharge constant	0.347 $year^{-1}$	0.347 $year^{-1}$

Table 2 Examined parameters

	Input parameters
Heavy Nuclide	(n,f) , (n,γ) , (n,γ*) , (n,2n) (n,2n*) , (n,3n) , ν -value
Fission product	(n,f) , (n,γ) , (n,γ*) , (n,2n) (n,p) , (n,α) , fission yield

* Residual nuclide in excited state

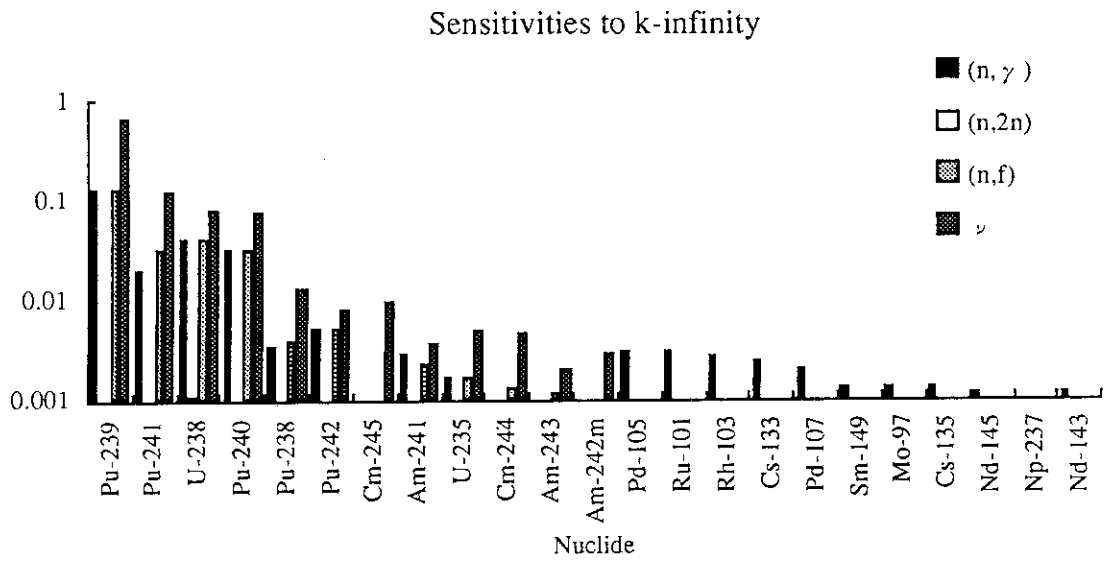

Fig. 3 Sensitivities to the infinite multiplication factor for uranium fueled soft spectrum fast reactor.

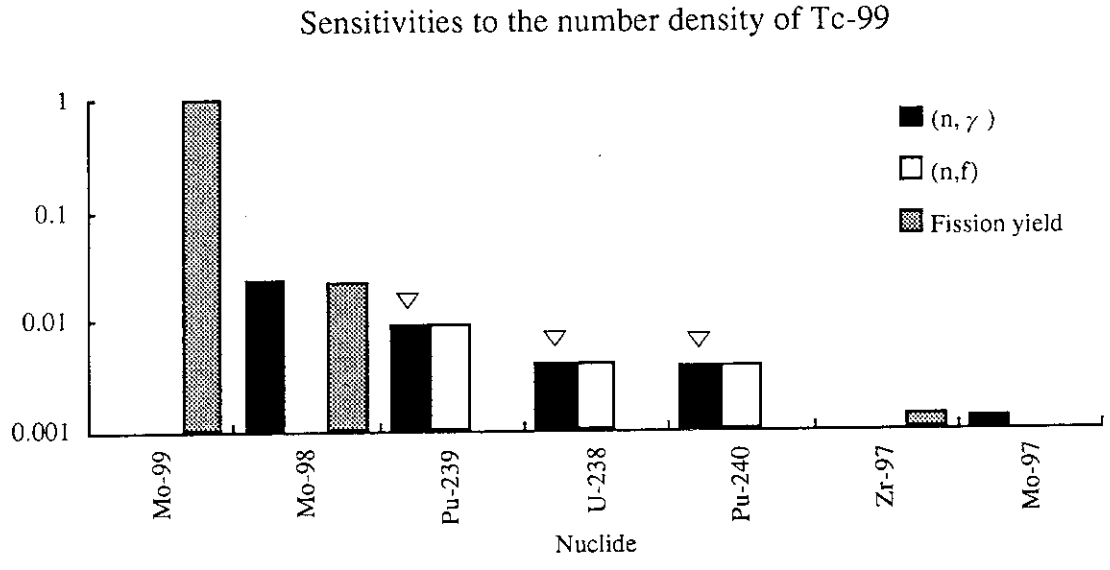

Fig. 4 Sensitivities to the number density of ^{99}Tc for uranium fueled soft spectrum fast reactor.

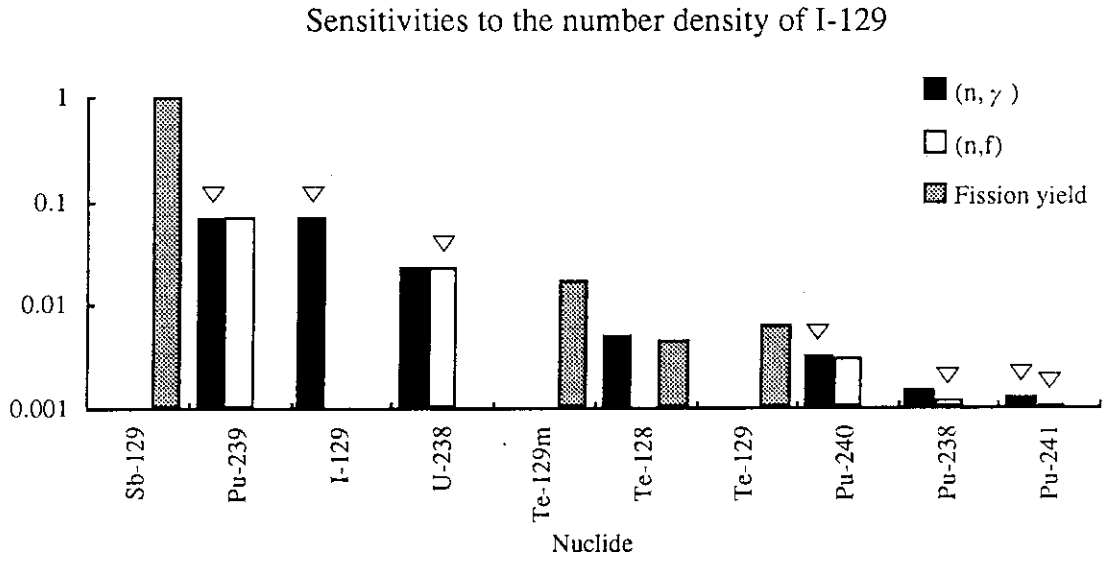

Fig. 5 Sensitivities to the number density of ^{129}I for uranium fueled soft spectrum fast reactor.

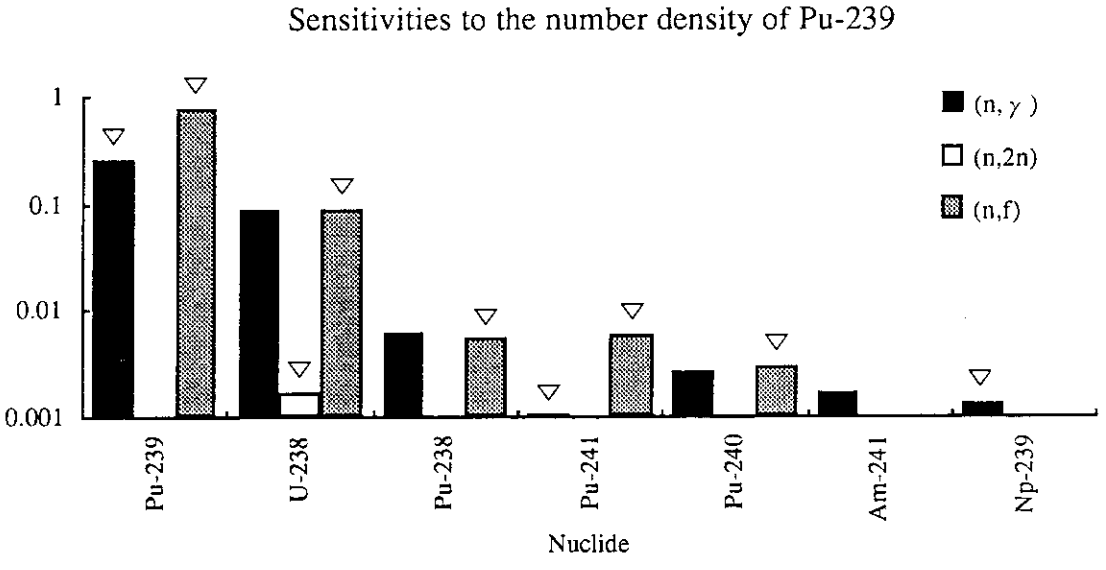

Fig. 6 Sensitivities to the number density of ^{239}Pu for uranium fueled soft spectrum fast reactor.

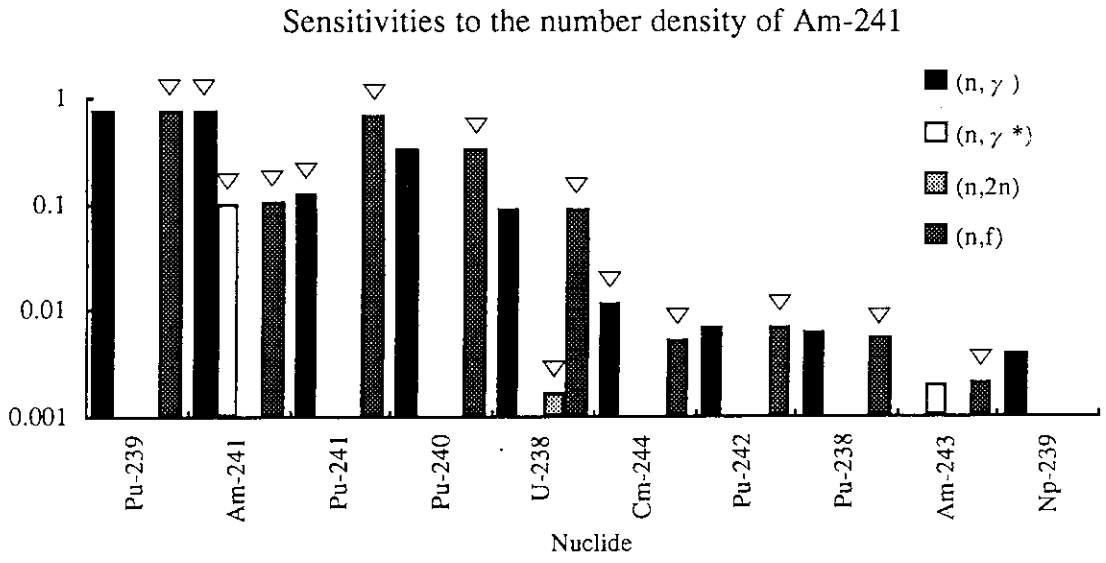

Fig. 7 Sensitivities to the number density of ^{241}Am for uranium fueled soft spectrum fast reactor.

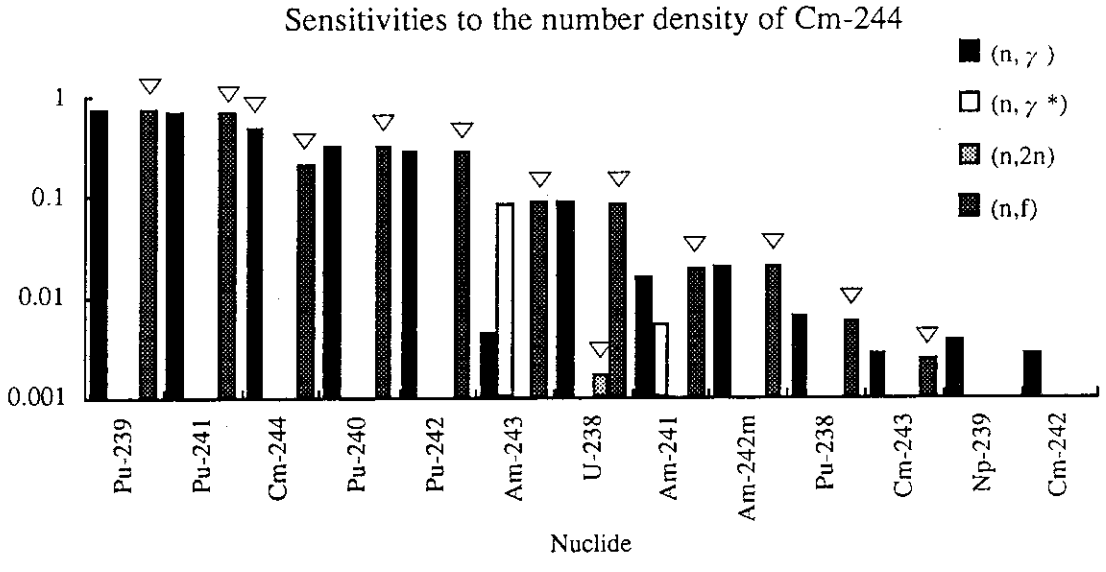

Fig. 8 Sensitivities to the number density of ^{244}Cm for uranium fueled soft spectrum fast reactor.

5.27 Some Subjects in ICF Reactors Requiring Nuclear Data in the Medium Energy Region

Y.Nakao and A.Oda
Department of Nuclear Engineering, Kyushu University,
Hakozaki, Fukuoka 812, Japan
H.Nakashima
Department of Energy Conversion Engineering, Kyushu University,
Kasuga, Fukuoka 816, Japan

Abstract

The neutrons bursting from ICF burning pellets contain not only moderated components (14MeV) but also fast populations whose maximum energy reaches more than 20MeV. By considering these neutron spectra and using nuclear data for incident neutron energies up to 20MeV, we evaluate the tritium breeding ratio for conceptual ICF reactor designs.

1. Introduction

Usual neutronic calculations for fusion reactors use neutron cross-section data in the energy region below 15MeV. Such a data would suffice as far as magnetic confinement D-T fusion is concerned.

In inertial confinement fusion (ICF) scheme, however, fusion reactions occur during rapid expansion of the compressed and ignited fuel pellets. If a D-T neutron is emitted in the same direction as the medium expansion velocity, the birth energy observed in the rest frame can be fairy larger than 14MeV. (The situation is schematically shown in **Fig.1**.) As a result, the neutrons bursting from ICF burning D-T pellets contain not only moderated components (<14MeV) but also fast populations whose maximum energy reaches more than 20MeV. Nuclear design calculations for ICF reactors (*e.g.* calculations of tritium breeding, nuclear heating, etc.) hence require (a) reliable information about source neutron spectrum, and (b) neutron cross-section set covering the energy range up to about 25MeV.

In this paper we show the burst neutron spectrum from a typical D-T burning pellet, and then examine the tritium breeding in conceptual ICF reactor designs.

2. Burst Neutron Spectrum from ICF Pellet

Recently, the present authors made coupled neutronic/hydrodynamic calculations for

isobarically compressed D−T pellet models to investigate the effect of neutron heating on the thermonuclear burning.[1] From these calculations, the energy spectra of neutrons bursting from D−T burning pellets were also derived.

Figure 2 represents for a typical pellet (compressed ρR = 6 g/cm^2) the energy spectrum that is integrated over the pellet burn time. A fairly broadened spectrum is observed, although the distribution peak around 14−MeV energy still stands out. Because of rapid pellet expansion, the burst neutrons contain fast components whose maximum energy exceeds 20MeV. The fraction of population above 14−MeV energy is about 20% of the total population. The low energy components result mainly from collisions with the pellet matters. The average kinetic energy of these burst neutrons is about 10MeV.

We also evaluated the tritium production in the pellet T_P (T−atoms per D−T reaction) and the neutron multiplication k_n, the latter being due to D(n,2n)p. When the initial (*i.e.* compressed) ρR = 6 g/cm^2, for example,

T_P = 0.03 (mainly from D−D reaction),

k_n = 1.10.

3. Neutronic Calculation for Breeding Blanket

By considering the energy spectrum of neutrons incident on the blanket, we made tritium breeding calculations for conceptual ICF reactor designs, SENRI−1[2] and KOYO.[3]

3.1. Blanket models and Method of Calculation

Figure 3 illustrates the configuration and composition of the blanket models. In SENRI−1 blanket, two regions are used for tritium breeding. Both regions are composed of natural liquid metal Li. The inner 64−cm thick layer flows from top to bottom along the inner surface of the spherical stainless−steel chamber. In KOYO model, both blankets I (inner) and II (outer) are composed of SiC and $Li_{17}Pb_{83}$. The volume fractions of SiC and $Li_{17}Pb_{83}$ in the blanket I are respectively 7.8 and 70.7 %, the rest being the void. The corresponding values for blanket II are 2.3 and 57.7 %. Natural lithium is used for Li in $Li_{17}Pb_{83}$.

The neutron fluxes in the blanket were obtained using steady−state transport code ANISN[4] with the P_3−S_8 approximation. A spherical geometry was assumed. As for neutron cross−sections, we used a multigroup constant set JSSTDL,[5] which covers the incident neutron energies up to 20 MeV. The source neutrons above 20−MeV energy were excluded from the present ANISN calculation.

Three kinds of neutron spectrum are used as input sources: (1) the "actual" spectrum

resulting from the burning pellet, (2) the moderated spectrum obtained from "stationary" pellet, and (3) monochromatic 14–MeV source.

3.2. Results and Discussion

Table 1 summarizes the results of ANISN calculation, *i.e.* the tritium production in the blanket per unit source neutron. The ^{7}Li contribution is relatively large in the SENRI–1 model (fast blanket), whereas in the KOYO model (thermal blanket) the contribution from ^{6}Li is dominant.

From these results we can evaluate the tritium breeding ratio (TBR) in the ICF system as follows:

$$\mathrm{TBR} = T_P + k_n T_B,$$

where T_P is the contribution from the D–D reaction, k_n the neutron multiplication in the pellet, and T_B the contribution from the blanket as given in Table 1. The values of T_P and k_n are shown in Sec.2.

In the SENRI–1 blanket case, the total TBR for "actual" source is estimated to be 1.48, whereas it is 1.56 for monochromatic source, being larger than for "actual" source by about 5%. The source component around several MeV is considerably less for "actual" source, which leads to the decrease of TBR from ^{7}Li$(n,n'\alpha)$T.

The value of TBR estimated for moderated source is 1.45, being almost the same as that for the "actual" source. The neutron with energy of over 10 MeV has a largest contribution to the total TBR. The difference in the number of neutrons in that energy range is very small between the "actual" and moderated sources.

As for the KOYO blanket, the similar tendency is observed in the estimated values of TBR. The total TBR is 1.29 for the "actual" source; it is 1.47 for the monochromatic source, being larger by about 15%. The value of TBR estimated for the moderated source is almost the same as that "actual" source.

4. Concluding Remarks

We have shown that because of the rapid pellet expansion, the neutrons bursting from ICF burning pellets contain fast populations with energies of more than 20 MeV in addition to moderated components.

Using the realistic source neutron spectrum, we also evaluated the tritium breeding in the conceptual ICF blanket designs. The use of monochromatic 14–MeV source overestimates the TBR by 5–15%. If one adopts the spectrum obtained from the "stationary" pellet, the TBR value is almost the same as that obtained from the realistic

source spectrum. This is because the number of high-energy neutrons (*e.g.* over 10MeV) that has a large contribution to the total TBR are not so different between the two spectra.

One of the interesting issues other than tritium breeding is nuclear heating. For an accurate calculation of the nuclear heating rate as well as TBR, we need an evaluated neutron cross-section set that covers the energy range up to 25MeV.

Acknowledgment

The authors are grateful to Dr. A.Hasegawa of JAERI who kindly offered us his multigroup constants, JSSTDL.

References

(1) Y.Nakao, *et al.*, to be published in *J.Nucl. Sci. Technol.*, **30**, No.12(1993).
(2) H.Oomura, *et al.*, *J.Fusion Energy*, 4(1985)289.
(3) Y.Kitagawa, *et al.*, presented at 7th Int. Conf. Emerging Nuclear Energy Systems, Chiba, September, 1993.
(4) W.W.Engel,Jr., ORNL K-1963(1967).
(5) A.Hasegawa, Proc. Int. Conf. Nuclear Data for Science and Technology, Jülich, May, 1991.

Table 1 Tritium production in the blanket per unit source neutron, T_B

(a) SENRI-1

Source neutron spectrum	T6 inner	T6 outer	T7 inner	T7 outer	Total
Calculated*	0.763 (0.760)	0.106 (0.105)	0.440 (0.448)	0.008 (0.007)	1.318 (1.320)
Monochromatic 14MeV	0.754	0.117	0.679	0.014	1.563

(b) KOYO

Source neutron spectrum	T6 inner	T6 outer	T7 inner	T7 outer	Total
Calculated*	0.057 (0.060)	1.068 (1.086)	0.005 (0.006)	0.016 (0.012)	1.141 (1.164)
Monochromatic 14MeV	0.074	1.369	0.007	0.017	1.466

* $(\rho R)_{comp}$ = 6g/cm². The values in ( ) result from the calculation assuming a source neutron spectrum from "stationary" pellet.

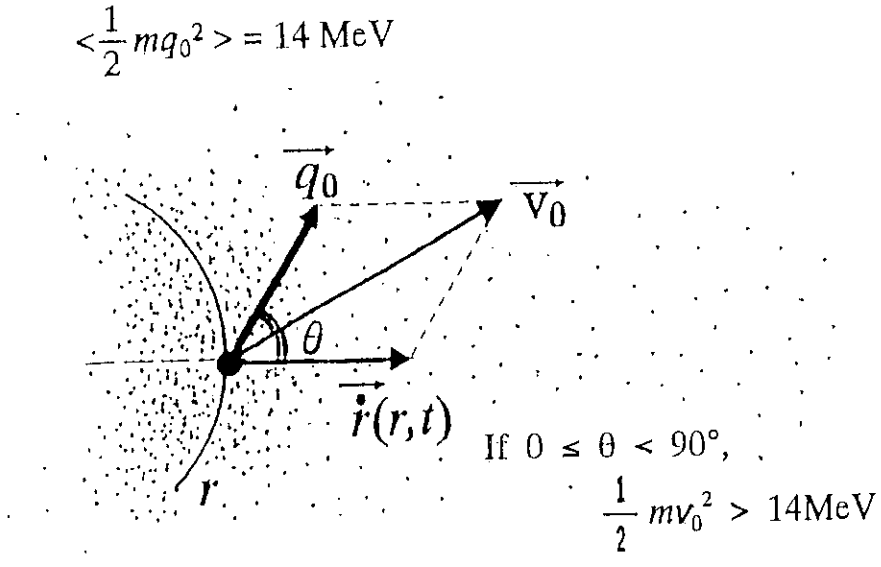

Fig. 1 Neutron generation in ICF burning plasma
Here, v_0 is the velocity of fusion-produced neutrons in the rest frame.

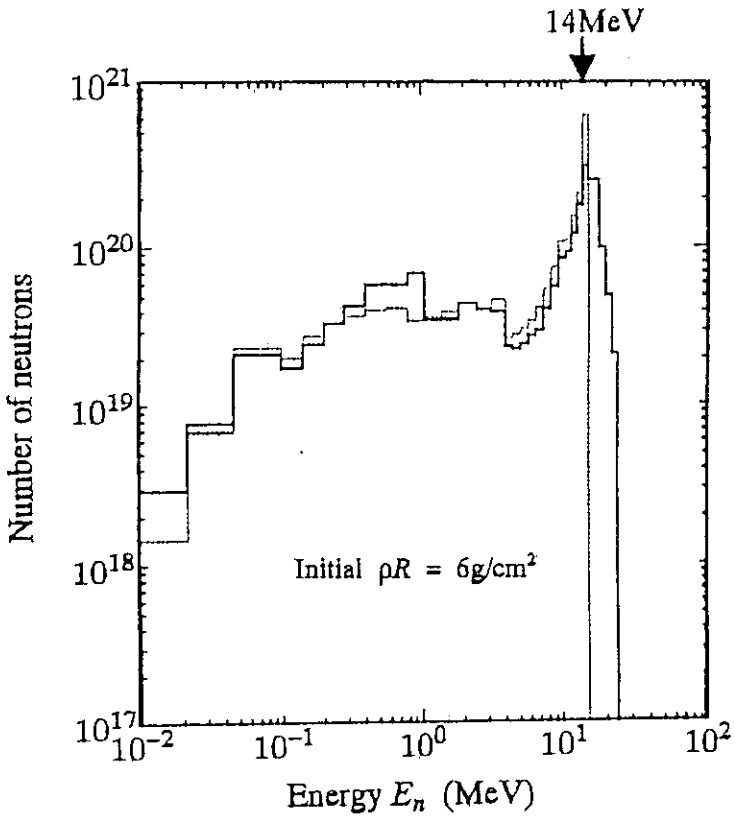

Fig. 2 Time-integrated energy spectrum of neutrons bursting from a D-T burning pellet (compressed ρR=6g/cm^2)
The dotted line indicates the spectrum of neutrons from a "stationary" pellet.

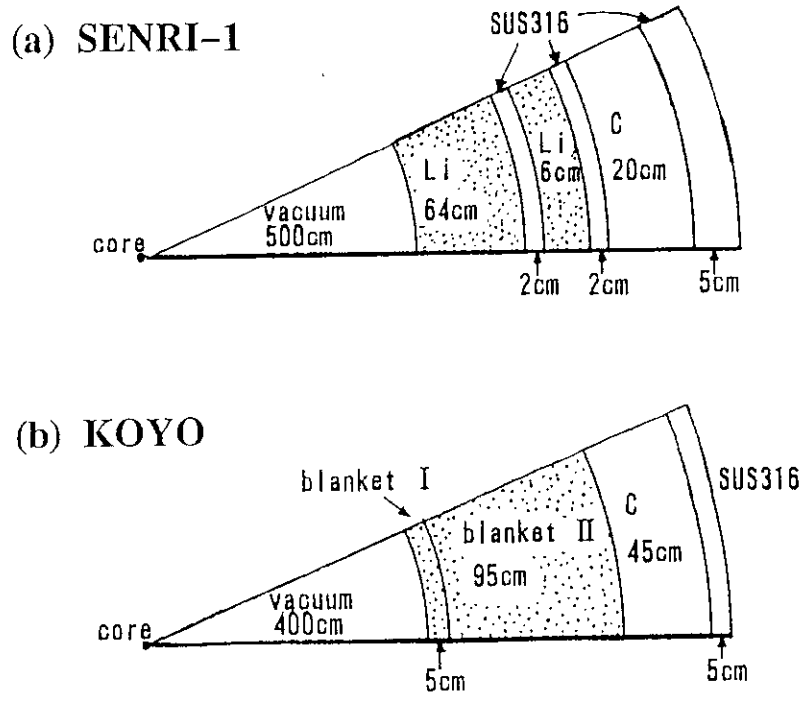

Fig. 3 Blanket models derived from conceptual ICF reactor designs
(a) SENRI-1, (b) KOYO

5.28 Measurement of the Neutron Capture Cross Section of ^{99}Tc

Toshio KATOH*, Yoshimune OGATA**, Hideo HARADA***
and Shoji NAKAMURA***

* Department of Nuclear Engineering, Nagoya University
Furo-cho, Chikusa-ku, Nagoya, 464-01
** Radioisotope Research Center, Nagoya University
Furo-cho, Chikusa-ku, Nagoya, 464-01
*** Power Reactor and Nuclear Fuel Development Corporation
Tokai-mura, Ibaraki-ken, 319-11

ABSTRACT

The thermal neutron cross section of the ^{99}Tc(n, γ)^{100}Tc reaction has been measured by means of an activation method for the purpose to obtain fundamental data for the research of the transmutation of nuclear waste.

Targets containing about 370 kBq of ^{99}Tc were irradiated for 2 m with reactor neutrons. Activation detectors of Co/Al and Au/Al alloy wires were irradiated to monitor the neutron flux and the Westcott's epithermal index $r(T/T_o)^{1/2}$.

Spectra of γ-rays from the irradiated Tc samples were measured with a high purity Ge detector. Decay of the 540-keV and the 591-keV γ-rays were followed. A half-life of the decay of the γ-rays was 15.56 $\pm$ 0.30 s and in good agreement with the half-life of ^{100}Tc.

The amount of the produced ^{100}Tc was obtained from the intensities of the 540-keV and the 591-keV γ-rays.

The specific activity of ^{99}Tc in the targets were obtained by measuring the specific β-activity of sample solution by the liquid scintillation counting method. Then, the amount of ^{99}Tc in the targets were determined. A cross section of the ^{99}Tc(n, γ)^{100}Tc reaction was determined from the number of ^{99}Tc atoms of the target, the activity of the produced ^{100}Tc and the neutron flux data. The cross section obtained is 18 $\pm$ 2 b and is almost same as the value reported in references. The resonance integral was also measured by a Cd-ratio method.

I. INTRODUCTION

The nuclide ^{99}Tc is one of the most important fission products in the radioactive waste management. The accurate cross section of the thermal neutron capture reaction of ^{99}Tc is necessary for the research of neutron utilized transmutation. There have been only two measurements[1),2)] of the cross section of the $^{99}Tc(n, \gamma)^{100}Tc$ reaction.

The present paper describes a result of a recent cross section measurement taking advantage of a highly efficient Ge detector and a fast electronic circuit.

II. MEASUREMENT OF THE THERMAL NEUTRON CROSS SECTION

Targets containing about 370 kBq of ^{99}Tc were irradiated with reactor neutrons of Rikkyo University for the measurement of the thermal neutron capture cross section of ^{99}Tc. The specific activity of ^{99}Tc target solutions was obtained by measuring the specific β-activity by the liquid scintillation counting method, and 460.62 kBq/g. The amount of activity(number of atoms) of each sample was estimated from the weight of each sample and the specific activity. Six samples were prepared and four of them were used for the experiment.

Activation detectors of Co/Al and Au/Al alloy wires were irradiated to monitor the neutron flux and the Westcott's epithermal index $r(T/T_0)^{1/2}$. The irradiation position is characterized with a thermal neutron flux of $(4.19 \pm 0.12) \times 10^{11}$ n/cm^{2}s and the epithermal index of 0.037.

Gamma-ray spectra of irradiated ^{99}Tc samples were measured immediately after the irradiation. A HPGe detector of 90% efficiency combined with a fast electronic circuit was used for the measurement. The system of the measurement was same as used in the measurement of the neutron cross section of ^{137}Cs[3)].

Fig. 1(a) and (b) show gamma-ray spectra of ^{99}Tc samples irradiated without a Cd shield and with a Cd shield. In the spectra, γ-ray peaks are seen at the energies of 540 and 591 keV as well as γ-peaks at higher energies.

The decay of these peaks were followed and results are shown in Fig.(2). The decay curves in Fig.(2) show that these γ-peaks decay with a half-life of about 15 s.

The weighted average value of half-life was 15.56 ± 0.30 s and in good agreement with a half-life of ^{100}Tc[4)].

This means the 540-keV and the 591-keV γ-rays are emitted from ^{100}Tc produced through the the neutron capture reaction

of ^{99}Tc.

The reaction rate(R) of the neutron capture reaction of ^{99}Tc was deduced from the number of atoms of the target and the intensity of the γ-rays of produced ^{100}Tc.

The neutron fluxes were determined by using the monitor wires for the irradiation without a Cd shield and the irradiation with a Cd shield. Obtained reaction rate(R) of the monitors were analyzed with the following equations as was done in the case of ^{137}Cs[3].

$$R/\sigma_0 = \phi_1 + \phi_2 s_0 G_{epi} \quad (1)$$

for irradiation without a Cd shield,

$$R'/\sigma_0 = \phi'_1 + \phi'_2 s_0 G_{epi} \quad (2)$$

for irradiation with a Cd shield,

where σ_0 is the reaction cross section of each monitor, ϕ_1(') and ϕ_2(') are parameters determined by the flux monitors; ϕ_1 and ϕ_2 are approximately the thermal and the epithermal neutron fluxes in case of no Cd, respectively, and ϕ'_1 and ϕ'_2 the thermal and the epithermal fluxes with a Cd shield.

The s_0 and the G_{epi} are parameters[3] determined for each monitor, and s_0 is 1.83 for the present Co/Al wire and 17.02 for Au/Al. The value of G_{epi} was 1.00 for both monitors in the present experiment. Obtained relation between R/σ_0 and s_0 is shown in Fig.(3). From this relation, ϕ's in the equations were detemined and then the thermal neutron cross section(σ_0: for 2200 m/s neutrons) and the resonance integral I_0(including the 1/v part) can be deduced[3].

III. RESULTS

Results obtained at present are $\sigma_0 = 18 \pm 2$ barn and $I_0 = 296 \pm 60$ barn. The result of σ_0 is almost same as the value in the references. More precise measurements are in progress.

REFERENCES:

(1) Lucas, M., Hagemann, R., Naudet, R., Renson, C., Chevalier, C.: IAEA-TC-119/14
(2) Ovechkin, B. B., et al: INIS-mf-1543(Conf. on Neutron Physics at Kiev) 2, 131 (1973)
(3) Sekine, T., Hatsukawa, Y., Kobayashi, K., Harada, H., Watanabe, H., Katoh, T.: J. Nucl. Sci. Technol. 30(11) 1099 (1993)
(4) Berzins, G., Bunker, M. E., Starner, J. W.: Phys. Rev. 187(4) 1619 (1969)

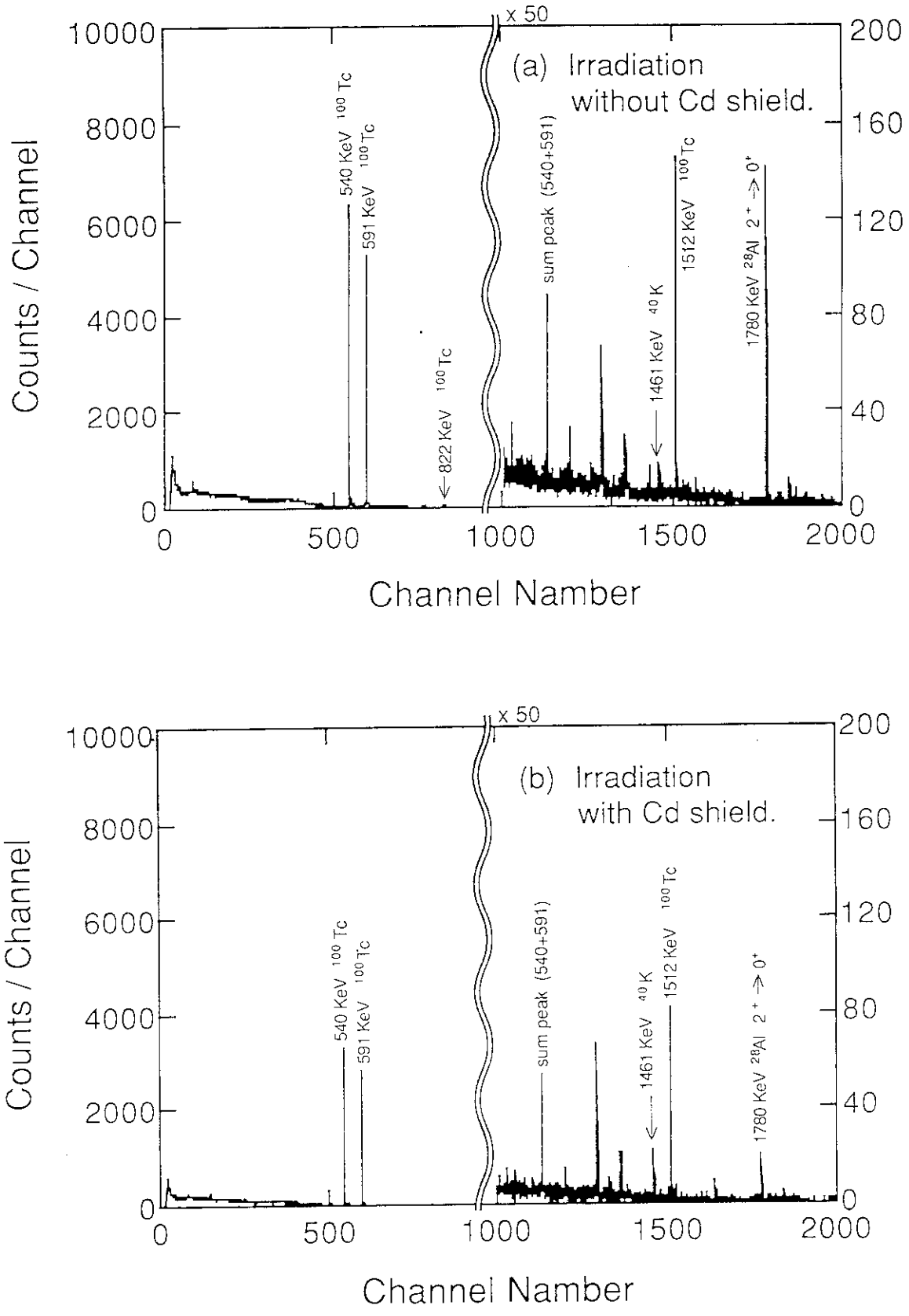

Fig. 1 Gamma-ray spectra of ^{99}Tc samples irradiated without and with a Cd shield.

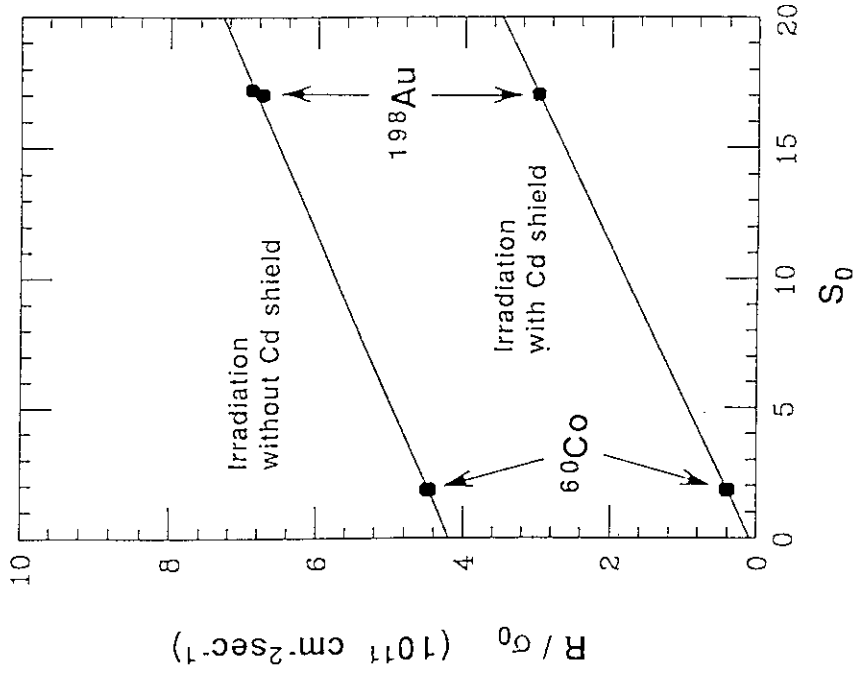

Fig. 3 Plot of R/σ_0 against s_0 for neutron flux monitors irradiated without and with a Cd shield.

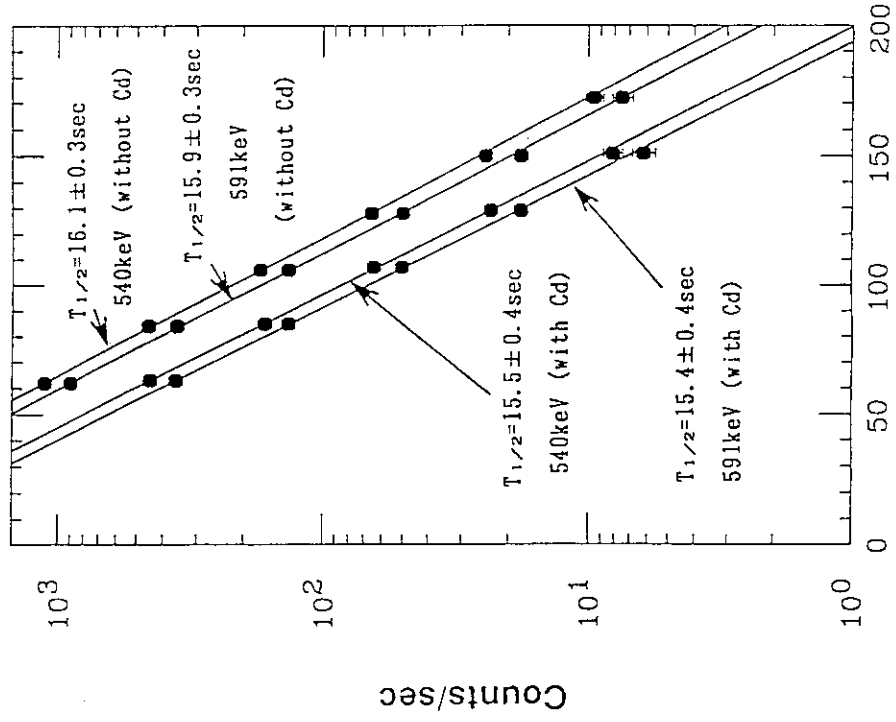

Fig. 2 Decay curves of the 540-keV and 591-keV γ-peaks.

5.29 Nuclear Data Activities in Hungary*

J. Csikai

Institute of Experimental Physics, Kossuth University
4001 Debrecen, Pf. 105, Hungary

Abstract: The review outlines the present status of nuclear data activities in Hungary in collaboration with a number of research groups abroad. Measurements and calculations are devoted mainly to the determinations of the excitation functions of neutrons and charged particles induced reactions from threshold up to 30 MeV. Some typical fields of the recent activities are discussed only.

1. Introduction

Nuclear data are investigated for testing nuclear reaction models, design of fusion reactors, unfolding the neutron fields, production of medically used isotopes as well as nuclear astrophysics and cosmochemistry.

2. Experimental

Neutrons and charged particles are produced by variable energy cyclotrons MGC-20 (Debrecen), CV28 (KFA Jülich), U-120M (Rez, Prague), low voltage (150-200 kV) neutron generators (Debrecen) and proton accelerators 100-400 kV (Univ. Bochum). The irradiation time is between a few minutes and about 300 h.

The measurements are based mainly on activation method using in same cases the radiochemical separation technique and the high resolution gamma spectrometry. The spectra are analyzed by the MAESTRO I, MAESTRO II and the AccuSpec programs. The excitation functions of charged particle reactions are measured by the stacked-foil technique. Activation cross sections for the generation of very long-lived radionuclides is determined by accelerator mass

*This work was partly supported by the International Atomic Energy Agency, Vienna (Contract No.: 6971/RB, No.4882/CF), Hungarian Research Foundation (Contract No. 1734/91) and the German-Hungarian bilateral agreement [No.13(x237.1)].

spectrometry (AMS). The alpha particles emitted in low energy charged particle reactions is detected by SB Si detector. Activation foils are used as neutron fluence and energy monitors.

Results and discussion

A) Neutron induced reactions

1) Excitation functions and isomeric cross section ratios were measured for the $^{63}Cu(n,\alpha)^{60}Co^{m,g}$, $^{65}Cu(n,\alpha)^{62}Co^{m,g}$ and $^{60}Ni(n,p)^{60}Co^{m,g}$ reactions between 6 and 15 MeV. Results were compared with the calculated data using the STAPRE code with $|M|^2 = FM\,A^{-3}\,E^{-1}$ and $\eta = \theta_{eff}/\theta_{rig}$, where FM = 300 while η = 1.0 and 0.5. Some results are shown in Figs. 1-4 [1].

2) The (n,α) and (n,p) cross sections have been determined for a number of nuclei with high precision at E_n = 14.6 MeV to improve the (N-Z)/A systematics. Results are summarized in Tables 1 and 2. Further measurements are needed to obtain any nuclear structure effects in the $\sigma_{n,\alpha}$ and $\sigma_{n,p}$ data. The gross trends prove the presence of the (N-Z)/A asymmetry parameter and isotope effects in the data (see.Figs. 5, 6 7, and 8) [2, 3].

3) High purity C, Al, $KHCO_3$, Zn, Cu, Ni, Mo, Si_3N_4 and SiO_2 samples were irradiated with 14.6 MeV neutron fluence of about 10^{13} n/cm^2 in Debrecen to produce long-lived radionuclides (^{10}Be, ^{26}Al, ^{14}C, ^{36}Cl, ^{40}K, ^{59}Ni, ^{93}Mo, ^{93}Zr, etc.) in fast neutron induced reactions important for cosmochemistry. The determinations of the reaction products are in progress by using either the radiochemical separation method or the classical and accelerator mass spectrometry in collaboration with KFA Jülich. Cologne and Hannover Universities. Reactions and methods are given in Table 3. In addition, measurements and calculations using the EXIFON code were carried out for some reactions producing long-lived isotopes. Results are summarized in Table 4 [4-7].

B) Charged particle reactions

1) Excitation functions and isomeric cross section ratios were measured for the $^{61}Ni(p,\alpha)^{58}Co^{m,g}$ reaction from threshold up to 18.6 MeV. As shown in Figs 9, and 10 the measured and calculated data are sensitive for the accepted model parameters [8].

2) Cross section curves of p, d, ^{3}He, ^{4}He induced reactions have been studied up to 30 MeV proton energy in the context of routine production of medically used isotopes. The monitor reactions were produced on natural Ni, Ti, Cu, Fe metals. As can be seen in Table 5 both enriched isotopes and natural elements were used as target materials. A typical excitation function is shown in Fig. 11 [9-17].

3) The S(E) factor for the $^{10}B(p,\alpha)^{7}Be$ and $^{11}B(p,\alpha)^{8}Be$ were determined over the $15 \leq E_p \leq 134$ keV c.m. energy range. Results are indicated in Fig. 12 [18].

References

[1] F. Cserpák, S. Sudár, J. Csikai and S.M. Qaim, Phys.Rev., in press.

[2] Á. Grallert, J. Csikai and Cs.M. Buczkó, I. Shaddad, IAEA RCM on Activation Cross Sections, Del Mar (USA) 29-30 April, 1993

[3] J.Csikai, First IAEA RCM on Helium Production Data, Debrecen, 17-19 November 1992.

[4] J. Csikai, IAEA RCM on Activation Cross Section, Del Mar (USA) 29-30 April, 1993.

[5] J. Csikai, Cs.M. Buczkó, R. Pepelnik, H.M. Agrawal, Ann. nucl. Energy 18(1) (1991)1.

[6] J. Csikai, INDC(NDS)-263, IAEA, Vienna (1992) p. 33.

[7] U. Herpers, R. Michel et al., (to be published)

[8] S. Sudár, F. Szelecsényi and S.M. Qaim, (in press)

[9] A.Fenyvesi, F. Tárkányi, F. Szelecsényi, S. Takács, Z. Szűcs, T. Molnár and I. Mahunka, (to be published)

[10] F. Tárkányi, S. Takács, Z. Kovács, (to be published)

[11] F.Ditrói, A.Fenyvesi, S.Takács, F.Tárkányi, J.Bergman, S-J. Heselius, O. Solin, (to be published)

[12] F.Szelecsényi, T.E. Boothe, S.Takács, Z.Szűcs, F.Tárkányi, (to be published)

[13] T.E. Boothe, S. Takács, T. Molnár, F. Tárkányi, (to be published)

[14] F.Tárkányi, F. Szelecsényi, P.Kopeczky, T.Molnár, L. Andó, P. Mikecz, Gy. Tóth, A. Rydl, ATOMKI Annual Report, 1992.

[15] I. Mahunka, L. Andó, P. Mikecz, A.M. Tcheltsov, I.A. Suvorov, ATOMKI Annual Report, 1992.

[16] I. Mahunka, P. Mikecz, T. Ido, M. Kawamura, L.Andó, Z. Kovács, ATOMKI Annual Report, 1992.

[17] F.Tárkányi, Z. Kovács, S.M. Qaim, Appl. Radiat. Isot. Vol. 44, No.8, 44(8) (1993) 1105.

[18] C.Angulo, S. Engster, C. Rolfs, W.H. Schultz, E. Somorjai, ATOMKI, Annual Report, 1992.

Table 1 Recent measured and evaluated data for some (n,α) reaction cross sections at around 14.6MeV.

Reaction	Forrest	Ikeda et al.	present
$^{45}Sc(n,\alpha)^{42}K$	56 ± 3	53.3 ± 4.3	53.7 ± 2.6
$^{50}Ti(n,\alpha)^{47}Ca$	8.75 ± 0.8	9.31 ± 0.78	8.6 ± 0.6
$^{51}V(n,\alpha)^{48}Sc$	16.15 ± 0.75	16.94 ± 0.87	17 ± 1
$^{51}V(n,n\alpha)^{47}Sc$			0.09 ± 0.005
$^{54}Cr(n,\alpha)^{51}Ti$	12.6 ± 1.5		10.8 ± 2.1
$^{55}Mn(n,\alpha)^{52}Cr$	27.5 ± 4		22 ± 1.6
$^{54}Fe(n,\alpha)^{51}Cr$	88.5 ± 6	84.5 ± 6	86 ± 5
$^{59}Co(n,\alpha)^{56}Mn$	30.0 ± 1		31 ± 1
$^{78}Se(n,\alpha)^{75m}Ge$			4.5 ± 0.7
$^{78}Se(n,\alpha)^{75}Ge$	5.5 ± 2		6.4 ± 1.2
$^{80}Se(n,\alpha)^{77m}Ge$			1.1 ± 0.2
$^{80}Se(n,\alpha)^{77}Ge$	17.0 ± 6		3.6 ± 0.3
$^{89}Y(n,\alpha)^{86}Rb$	5.5 ± 0.5		5.4 ± 0.6
$^{90}Zr(n,\alpha)^{87m}Sr$		3.65 ± 0.22	3.8 ± 0.2
$^{94}Zr(n,\alpha)^{91}Sr$	4.3 ± 0.6	4.9 ± 0.42	4.7 ± 0.3
$^{92}Mo(n,\alpha)^{89}Zr$	27.3 ± 1.5	24.5 ± 1.2	26.2 ± 1.2
$^{98}Mo(n,\alpha)^{95}Zr$	5.8 ± 0.35	6.45 ± 0.49	5.9 ± 0.3
$^{100}Mo(n,\alpha)^{97}Zr$	3.19 ± 0.25	2.81 ± 0.2	3.2 ± 0.2
$^{114}Cd(n,\alpha)^{111m}Pd$			0.3 ± 0.03
$^{115}In(n,\alpha)^{112}Ag$	2.4 ± 0.3		2.3 ± 0.2
$^{118}Sn(n,\alpha)^{115g}Cd$			0.9 ± 0.08
$^{120}Sn(n,\alpha)^{117m}Cd$		0.183 ± 0.07	0.21 ± 0.09
$^{120}Sn(n,\alpha)^{117g}Cd$		0.227 ± 0.079	0.26 ± 0.03

Table 1 (cont.)

Reaction	Forrest	Ikeda et al.	present
$^{142}Nd(n,\alpha)^{139}Ce$	6.8 ± 1.5		5.5 ± 0.4
$^{144}Nd(n,\alpha)^{141}Ce$	4.7 ± 1.5		4.0 ± 0.3
$^{146}Nd(n,\alpha)^{143}Ce$	3.1 ± 0.5		3.5 ± 0.3
$^{184}W(n,\alpha)^{181}Hf$	1.15 ± 0.15		0.85 ± 0.09
$^{186}W(n,\alpha)^{183}Hf$	0.55 ± 0.07	0.6 ± 0.11	0.54 ± 0.05
$^{203}Tl(n,\alpha)^{200g}Au$			0.37 ± 0.06
$^{206}Pb(n,\alpha)^{203}Hg$	2.0 ± 1.0		0.57 ± 0.04

Table 2 Recent measured and evaluated data for some (n,p) reaction cross sections at 14.6MeV.

Reaction	Forrest	Ikeda et al.	present
$^{48}Ti(n,p)^{48}Sc$	67 ± 8	60.4 ± 2.9	67 ± 4
$^{54}Fe(n,p)^{54}Mn$	315 ± 10	287 ± 13	309 ± 17
$^{74}Se(n,p)^{74}As$	135 ± 15		112 ± 7
$^{76}Se(n,p)^{76}As$	70 ± 10		49 ± 3
$^{78}Se(n,p)^{78}As$	18 ± 4		19 ± 1.1
$^{90}Zr(n,p)^{90m}Y$		13.28 ± 0.89	13.3 ± 0.7
$^{91}Zr(n,p)^{91m}Y$		18.3 ± 1.0	24 ± 1.2
$^{92}Zr(n,p)^{92}Y$	19.2 ± 2	22.2 ± 2.3	20 ± 1.0
$^{94}Zr(n,p)^{94}Y$	10 ± 1	8.91 ± 0.72	7.3 ± 0.8
$^{92}Mo(n,p)^{92m}Nb$		63.6 ± 3.1	41 ± 2.1
$^{95}Mo(n,p)^{95m}Nb$		7.79 ± 0.74	8.2 ± 0.6
$^{96}Mo(n,p)^{96}Nb$	21 ± 2	24 ± 1.2	25 ± 1.3
$^{98}Mo(n,p)^{98m}Nb$		6.25 ± 0.4	5.2 ± 0.24
$^{110}Cd(n,p)^{110m}Ag$			10.8 ± 1.4
$^{111}Cd(n,p)^{111}Ag$	50 ± 15		29 ± 2.1
$^{112}Cd(n,p)^{112}Ag$	16 ± 3		16 ± 1.2
$^{113}Cd(n,p)^{113m}Ag$			17 ± 1.0
$^{115}In(n,p)^{115g}Cd$			4.0 ± 0.25
$^{115}In(n,p)^{115m}Cd$			7.4 ± 2.95
$^{116}Sn(n,p)^{116m}In$		10.68 ± 0.83	10.8 ± 0.7
$^{117}Sn(n,p)^{117}In$	13 ± 2	14.01 ± 1.18	20 ± 1.2
$^{118}Sn(n,p)^{118}In$	7 ± 2		6.2 ± 0.46
$^{142}Nd(n,p)^{142}Pr$	13.8 ± 1.1		13.6 ± 0.9
$^{146}Nd(n,p)^{146}Pr$	4.5 ± 0.7		4.1 ± 0.4
$^{182}W(n,p)^{182}Ta$	5.9 ± 0.5		6.5 ± 0.5
$^{183}W(n,p)^{183}Ta$	4.1 ± 0.5		5.0 ± 0.4
$^{184}W(n,p)^{184}Ta$	3 ± 0.4		3.2 ± 0.2

Table 3 Reactions and methods considered to use for cross section measurements

Reaction	Half life	Decay E_γ(keV)	Method
$^{13}C(n,\alpha)^{10}Be$	1.62×10^{6} y	β^-	AMS
$^{14}N(n,p)^{14}C$ $^{17}O(n,\alpha)^{14}C$ $^{18}O(n,n\alpha)^{14}C$	5730 y	β^-	BC, RC
$^{27}Al(n,2n)^{26}Al$	6.345 s 7.2×10^{5} y	ε 1808.6	GS, AMS
$^{39}K(n,p)^{39}Ar$	269 y	β^-	CMS, BC
$^{39}K(n,\alpha)^{36}Cl$	3×10^{5} y	ε, β^-	AMS
$^{40}Ca(n,p)^{40}K$	1.28×10^{9} y	ε, β^-	AMS
$^{58}Ni(n,\alpha)^{55}Fe$	2.73 y	ε	XR
$^{60}Ni(n,p)^{60}Co$	10.47 m 5.27 y	IT, β^- 1173.2 1332.5	GS
$^{60}Ni(n,2n)^{59}Ni$	7.5×10^{4} y	ε	AMS
$^{66}Zn(n,\alpha)^{63}Ni$ $^{63}Cu(n,p)^{63}Ni$	100.1 y	β^-	RC+BC, AMS
$^{92}Mo(n,p)^{92}Nb$	10.150d 3.6×10^{7} y	ε 934.5 561.1	GS RC+AMS, RC+GS
$^{94}Mo(n,p)^{94}Nb$ $^{95}Mo(n,d)^{94}Nb$	6.26 m 2×10^{4} y	IT, β^- 702.6 871.1	AMS, RC+GS
$^{96}Mo(n,\alpha)^{93}Zr$ $^{97}Mo(n,n\alpha)^{93}Zr$	1.5×10^{6} y	β^-	AMS

Table 4 Cross sections for the generation of long-lived isotopes

Reaction	$T_{1/2}$	σ(mb) meas. (13.4-15.0 MeV)	σ(mb) calc. (13.4-15.0 MeV) (EXIFON)
$^{39}K(n,p)^{39}Ar$	269 y	195, 162, 314, 356	108.9 - 114.3
$^{39}K(n,\alpha)^{36}Cl$	3×10^{5} y	110, 120, 109	310.4 - 308.5
$^{139}La(n,2n)^{138}La$	1.1×10^{11} y	-	1496.7 - 1700.2
$^{92}Mo(n,p)^{92}Nb$	1.7×10^{8} y	60, 64	197 - 206.4
$^{94}Mo(n,p)^{94}Nb$	2×10^{4} y	55	45.8 - 55.7
$^{14}N(n,p)^{15}C$	5736 y	77, 38	18.9 - 24.4
$^{93}Nb(n,p)^{93}Zr$	1.5×10^{6} y	51, 42	23 - 30
$^{60}Ni(n,2n)^{59}Ni$	7.5×10^{4} y	352, 391, 104	246.3 - 557.5
$^{64}Ni(n,2n)^{63}Ni$	125 y	958	916 - 1120.2
$^{17}O(n,\alpha)^{14}C$	5736 y	-	154.4 - 155.4
$^{141}Pr(n,\alpha)^{138}La$	1.3×10^{11} y	3, 3	0.6 - 1.1
$^{80}Se(n,2n)^{79}Se$	7×10^{4} y	-	855 - 1133.9
$^{116}Sn(n,\alpha)^{113}Cd$	9×10^{15} y 14.6 y	-	2.2 - 4.4
$^{99}Tc(n,2n)^{98}Tc$	1.5×10^{6} y	1227	1231.5 - 1368.3
$^{51}V(n,2n)^{50}V$	4.8×10^{14} y	-	388.9 - 751.4
$^{180}W(n,p)^{180}Ta$	2×10^{13}y	1	5.6 - 6.7
$^{66}Zn(n,\alpha)^{63}Ni$	100 y	-	18.4 - 27.7

Table 4 (cont.)

Reaction	$T_{1/2}$	σ(mb) meas. (13.4-15.0 MeV)	σ(mb) calc. (13.4-15.0 MeV) (EXIFON)
$^{93}Zr(n,\alpha)^{90}Sr$	29 y	-	12 - 13.1
$^{94}Zr(n,2n)^{93}Zr$	$9x10^5$ y	-	1459.3 - 1501.8
$^{109}Ag(n,2n)^{108m}Ag$	418 y	724, 757, 671	-
	433 y	716 - 44*, 677 - 82*	
$^{27}Al(n,2n)^{26}Al$	$7.5x10^6$	0.62	0 - 75.2
$^{134}Ba(n,2n)^{133}Ba$	10.54 y	1556 + 95*	-
$^{134}Ba(n,p)^{134}Cs$	2.06 y	6 + 2*	-
$^{137}Ba(n,p)^{137}Cs$	30 y	5 + 1*	8.2 - 13.3
$^{209}Bi(n,2n)^{208}Bi$	$3x10^4$ y	2197, 2147, 2750, 1800, 2250, 2420, 2520, 2250, 2260	2118.2 - 2159.9
$^{79}Br(n,p)^{79}Se$	$6.5x10^4$ y	-	40.7 - 42.8
$^{40}Ca(n,p)^{40}K$	$1.28x10^9$ y	470, 492, 471	485 - 456
$^{42}Ca(n,\alpha)^{39}Ar$	269 y	90	138.1 - 147.9
$^{63}Cu(n,p)^{63}Ni$	100 y	54	78.4 - 87.4
$^{63}Cu(n,\alpha)^{60}Co$	5.27 y	51, 45 - 2*	61.4 - 73
$^{50}Cr(n,p)^{50}V$	$0.25x10^{14}$ y	830, 357	521.6 - 496.4
$^{113}In(n,p)^{113}Cd$	$9x10^{15}$ y	-	9.1 - 12.1
	14.6 y		

*Present experiment

Table 5 Reactions for the production of medical isotopes

Target	Beam	Isotope	Collaboration
^{66}Zn, ^{67}Zn, ^{68}Zn	p	^{66}Ga, ^{67}Ga	
^{111}Cd, ^{112}Cd	p	^{111}In	Rez
^{82}Kr, ^{83}Kr	^{3}He, α	$^{82}Sr(^{82}Rb)$	Jülich
^{82}Kr, ^{83}Kr	p	$^{81}Rb(^{81}Kr)$, ^{81}Rb ^{82m}Rb	Jülich
^{38}Cl	α	^{38}K	Turku
^{38}Ar	p	^{38}K	Jülich
^{nat}Ar	α	^{43}K	
^{123}Te	p	^{123}I	Moscow
^{124}Xe	p	^{123}I, ^{122}I	Jülich
^{nat}Cd	p	^{110}In	
^{38}Ar	α	^{42}K, ^{43}K	
^{16}O	^{3}He	^{18}F	Turku
^{78}Kr	p	^{75}Br, ^{77}Br	Jülich
^{10}B	p	^{7}Be	Turku
^{122}Te	p,d	^{122}I, ^{123}I	
^{nat}Te	p,d	^{123}I, ^{124}I	
^{nat}Sb	α, ^{3}He	^{123}I, ^{124}I	
^{nat}B	p	^{7}Be	

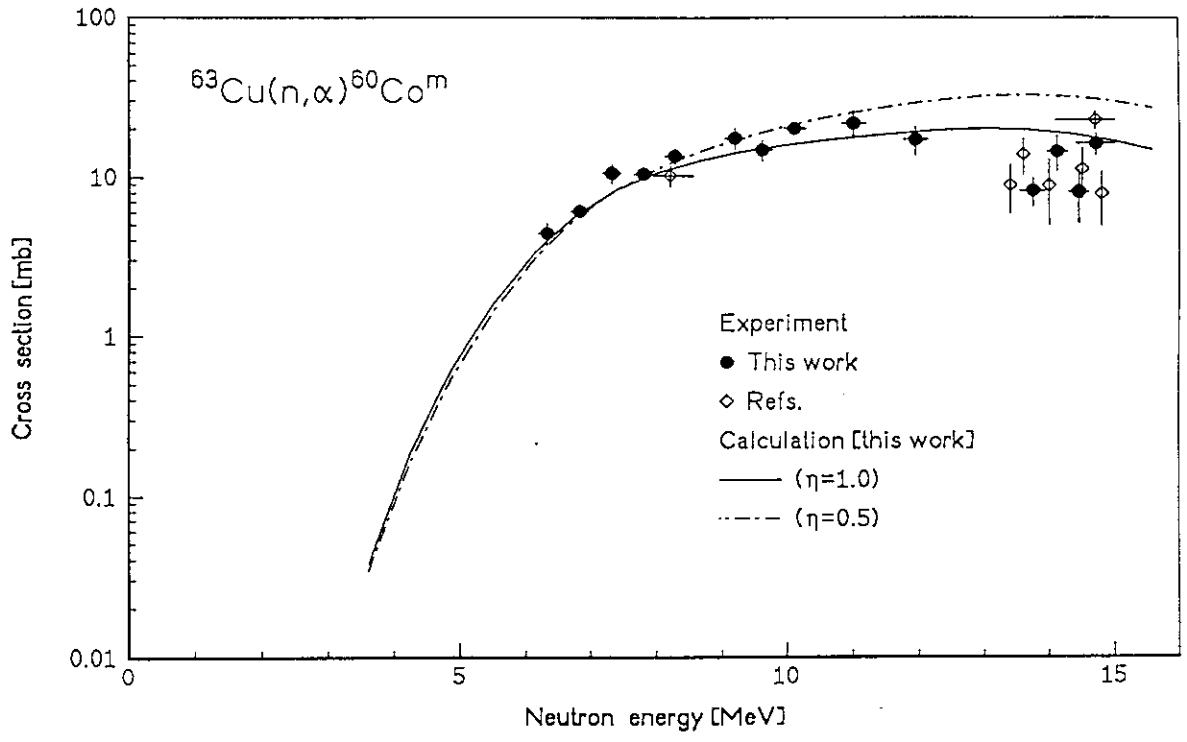

Fig. 1 Excitation function of the $^{63}Cu(n,\alpha)^{60}Co^{m}$ ($T_{1/2}$ = 10.5 min) reaction.

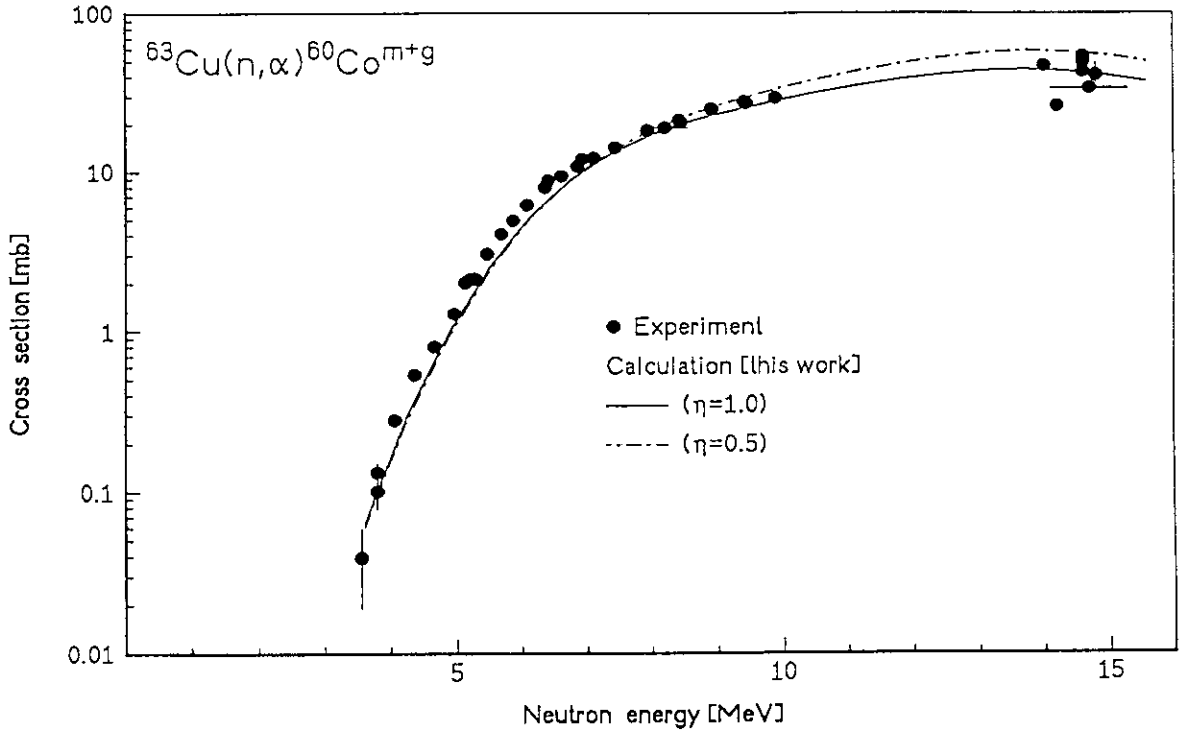

Fig. 2 Excitation function of the $^{63}Cu(n,\alpha)^{60}Co^{m+g}$ ($T_{1/2}$ = 5.27 y) process.

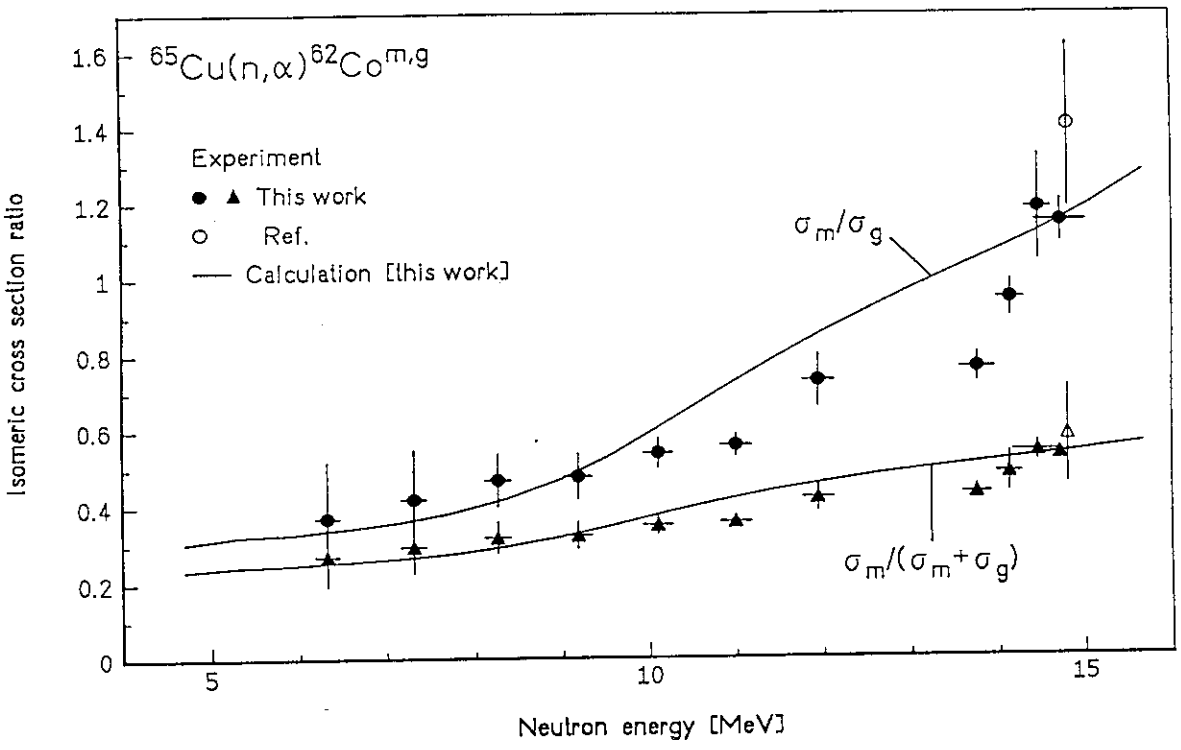

Fig. 3 Isomeric cross section ratio for the isomeric pair $^{62}Co^{m,g}$ formed via (n,α) reaction on ^{65}Cu, plotted as a function of incident neutron energy. The metastable state has a spin of 5^+ and the ground state 2^+.

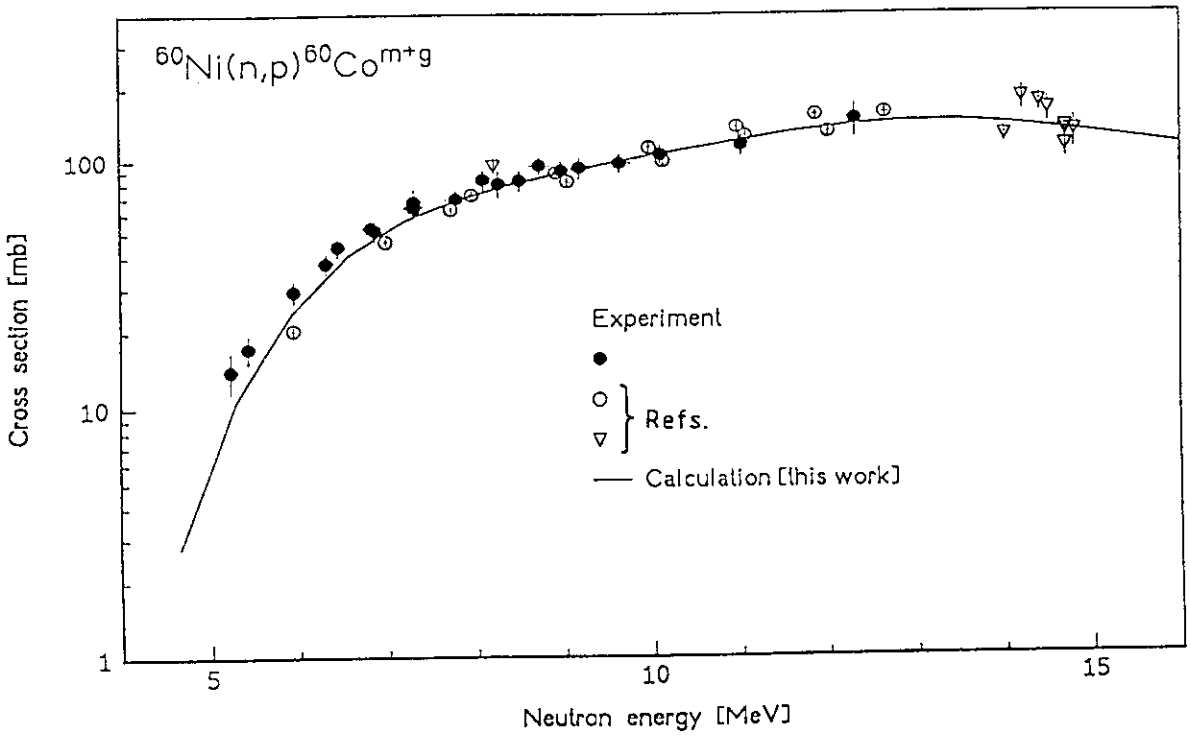

Fig. 4 Excitation function of the $^{60}Ni(n,p)^{60}Co^{m+g}$ ($T_{1/2}$ = 5.27 y) process.

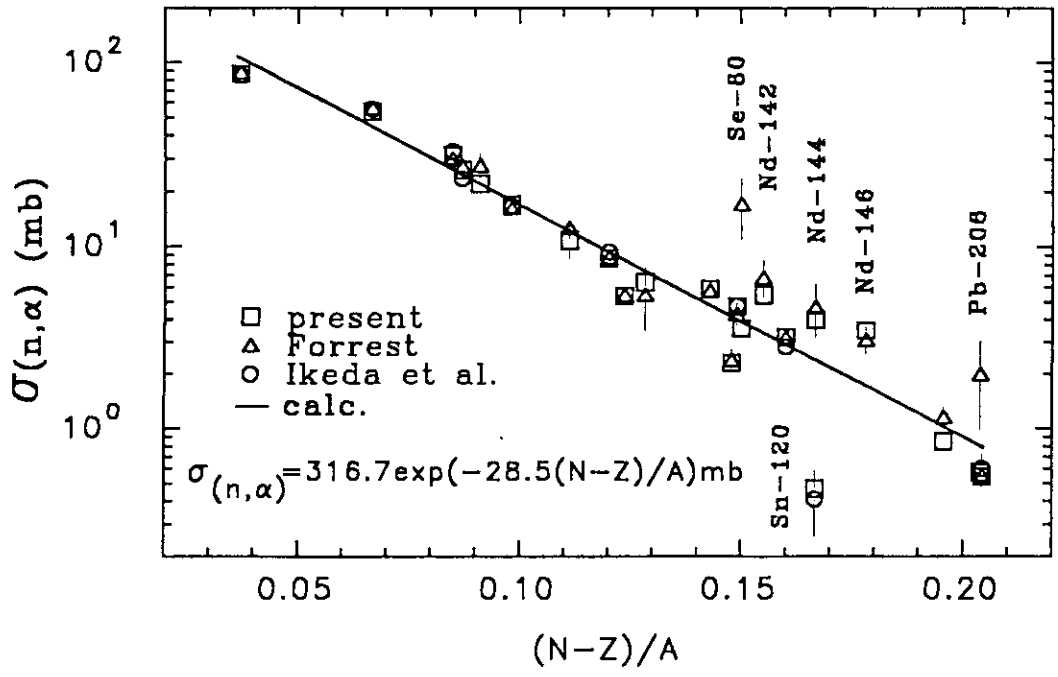

Fig. 5 Dependence of (n,α) cross sections on (N-Z)/A asymmetry parameter.

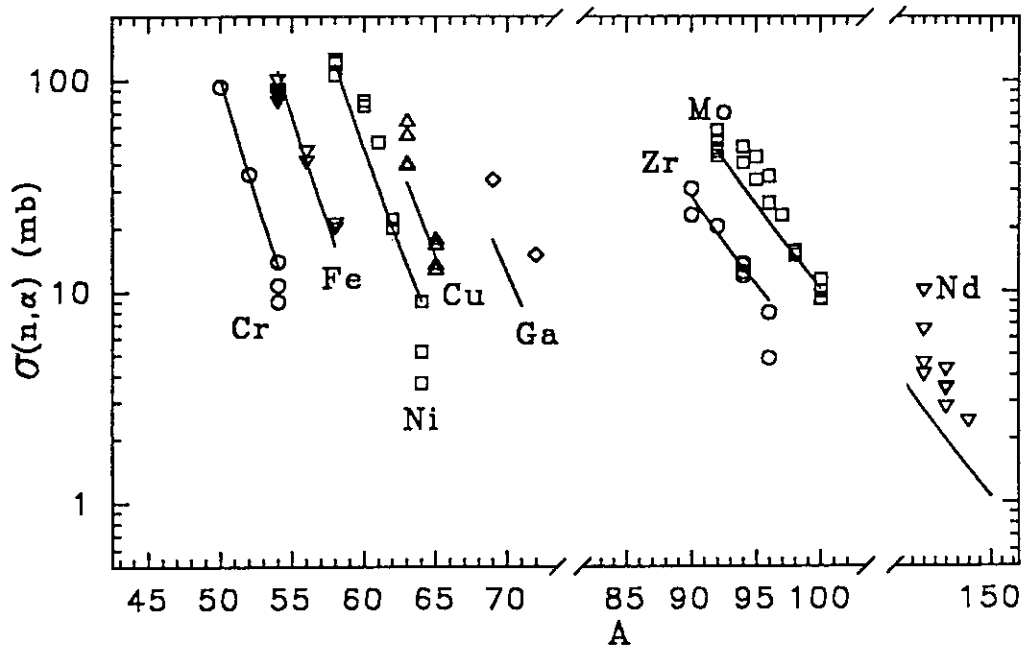

Fig. 6 The (n,α) cross sections for isotopes taking the data from Qaim, Forrest, Ikeda et al. and our experiment. Solid lines in Figs. 5 and 6 are calculated by eq. given in the Fig. 5 using Forrest's adopted data.

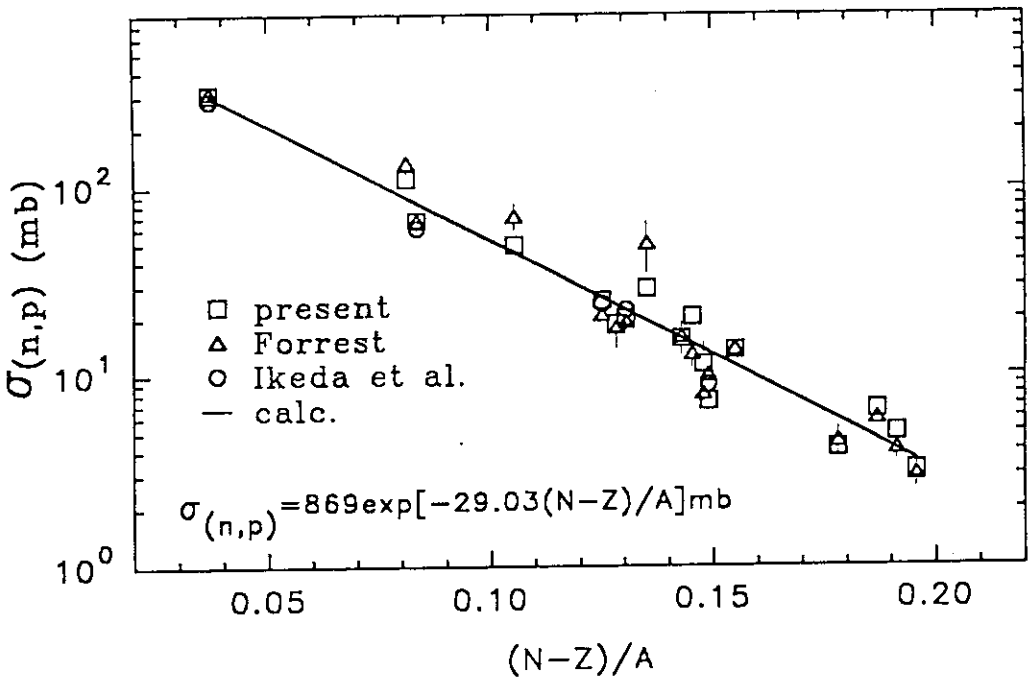

Fig. 7 Dependence of (n,p) cross sections on (N-Z)/A.

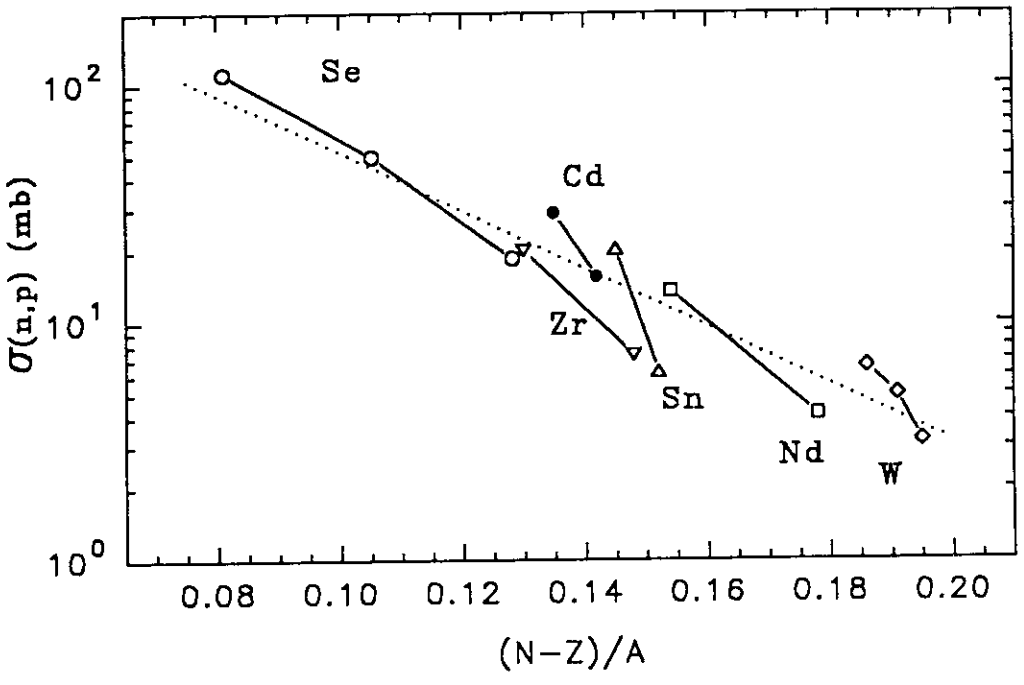

Fig. 8 The (n,p) cross sections for isotopes taking the data from Qaim, Forrest, Ikeda et al. and our experiment. Solid lines in Figs. 7 and 8 are calculated by eq. given in the Fig. 7 using Forrest's adopted data.

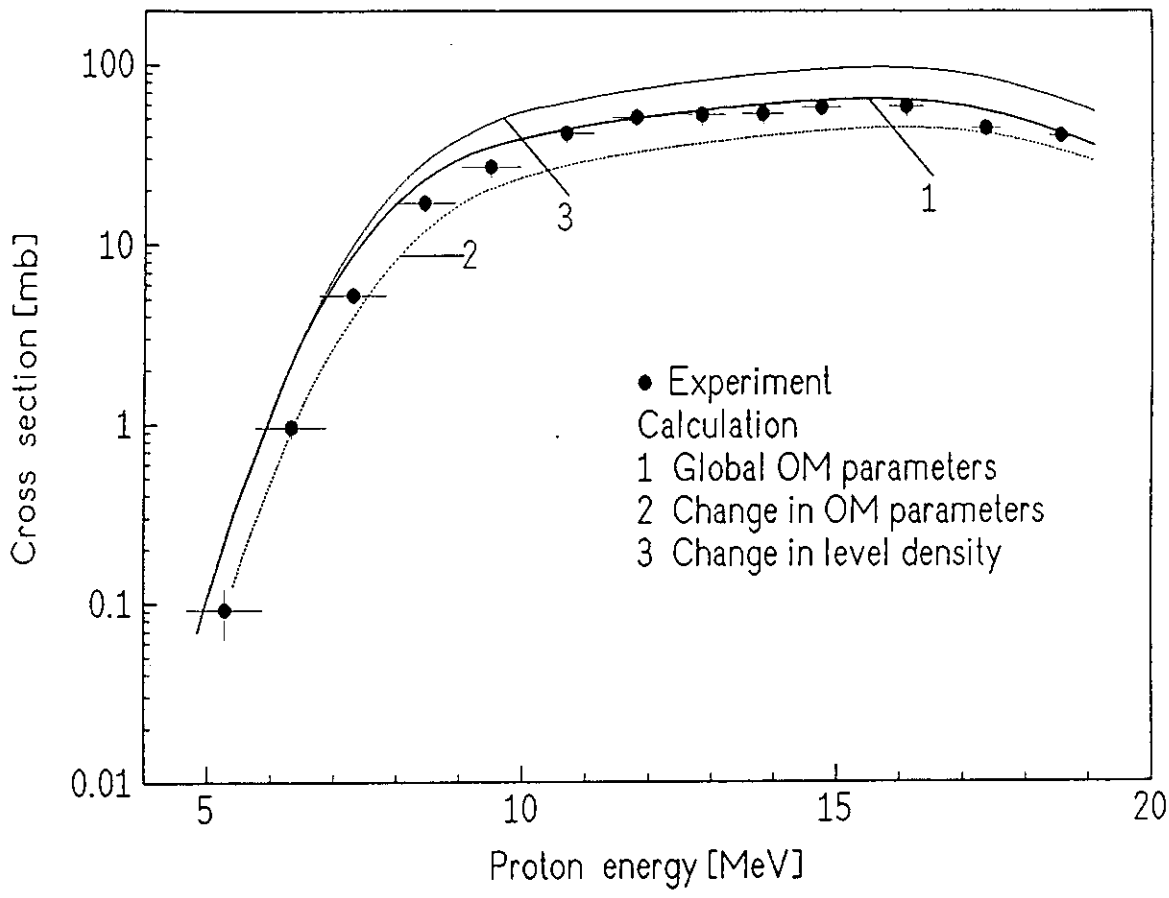

Fig. 9 Measured and calculated cross sections for the $^{61}Ni(p,\alpha)^{58}Co^{m+g}$ process.

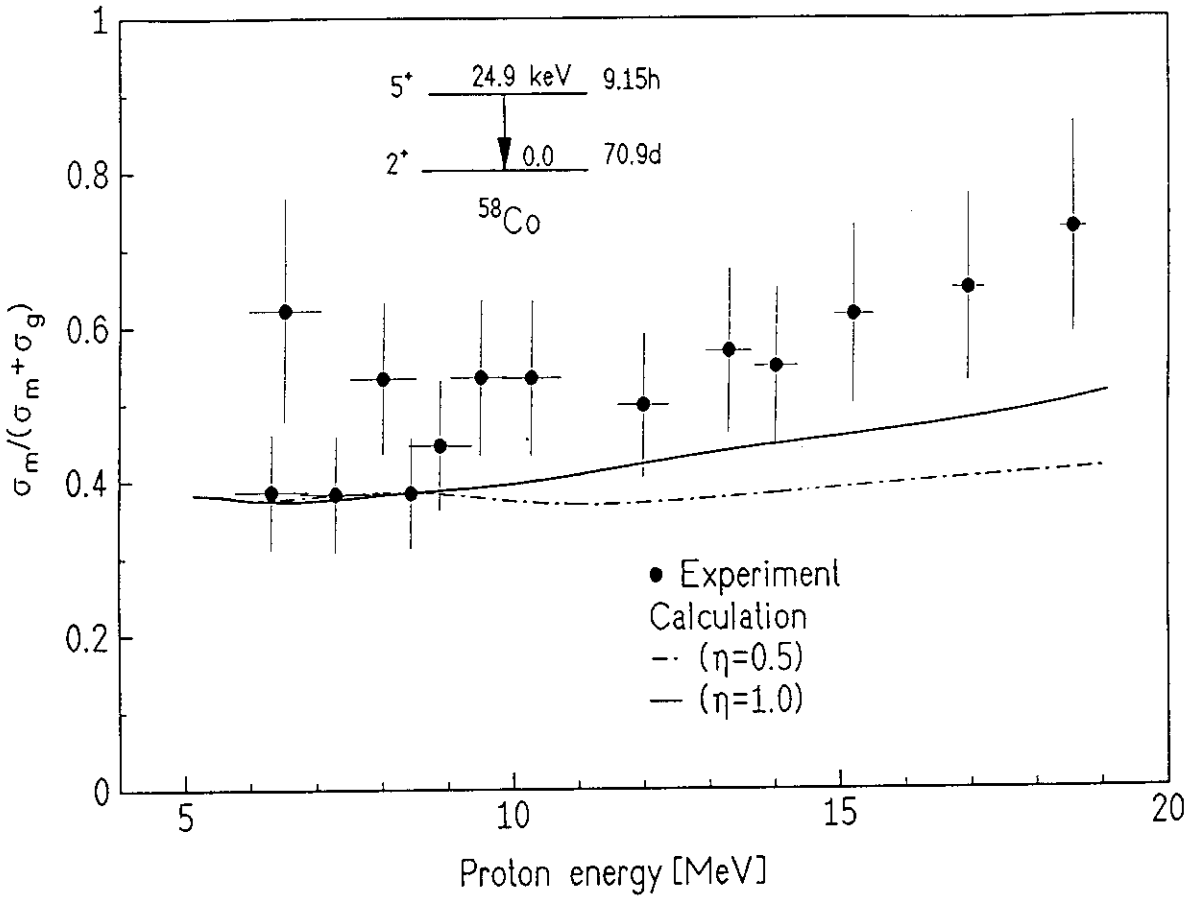

Fig. 10 Measured and calculated isomeric cross section ratios (σ_m/σ_{m+g}) for the $^{61}Ni(p,\alpha)^{58}Co^{m,g}$ process as a function of proton energy. The spin and parities of the two isomeric levels concerned are shown.

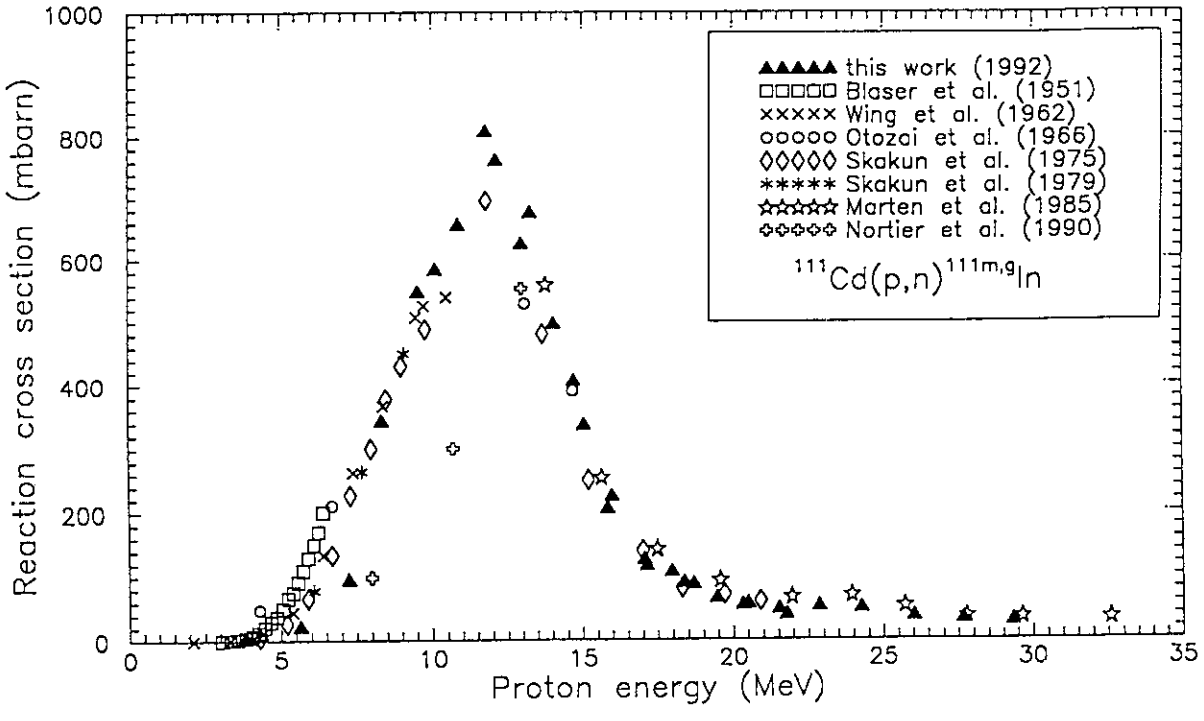

Fig. 11 Excitation functions for $^{111}Cd(p,n)^{111}In^{m,g}$ reaction.

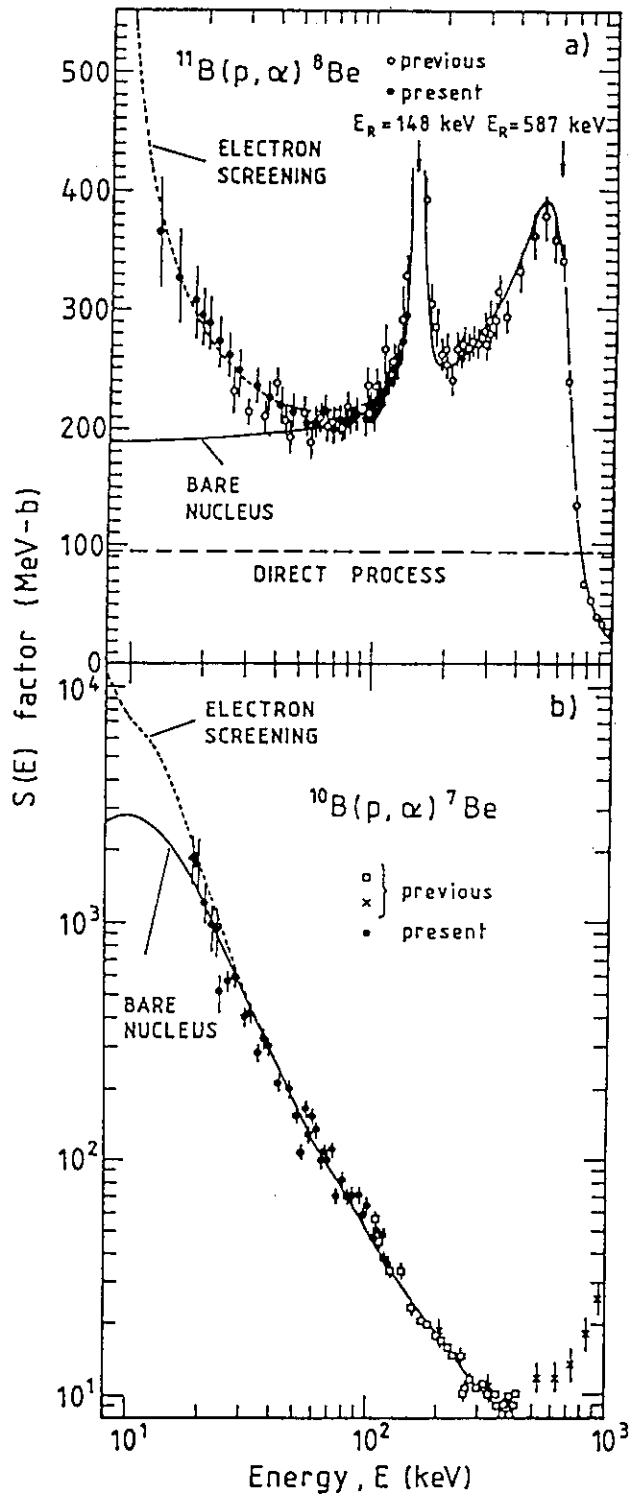

Fig. 12 Absolute S(E) factor for $^{11}B(p,\alpha)$ and $^{10}B(p,\alpha)$ reactions.